Lawrence Berkeley National Laboratory

Title
MATHEMATICAL MODELING OF LITHIUM (ALLOY) , IRON SULFIDE CELLS AND THE ELECTROCHEMICAL PRECIPITATION OF NICKEL HYDROXIDE

Permalink
https://escholarship.org/uc/item/31n3x2w6

Author
Bernardi, D.

Publication Date
1986

Lawrence Berkeley Laboratory

UNIVERSITY OF CALIFORNIA

Materials & Molecular Research Division

MATHEMATICAL MODELING OF LITHIUM(ALLOY),
IRON SULFIDE CELLS AND THE ELECTROCHEMICAL
PRECIPITATION OF NICKEL HYDROXIDE

D. Bernardi
(Ph.D. Thesis)

January 1986

DISCLAIMER

Mathematical Modeling of Lithium(alloy), Iron Sulfide Cells
and
The Electrochemical Precipitation of Nickel Hydroxide

Dawn Bernardi

Ph.D. Thesis

Department of Chemical Engineering
and Lawrence Berkeley Laboratory
University of California
Berkeley, California 94720

February 1986

Mathematical Modeling of Lithium(alloy), Iron Sulfide Cells
and
The Electrochemical Precipitation of Nickel Hydroxide

Dawn Bernardi

Ph.D. Thesis

Department of Chemical Engineering
and Lawrence Berkeley Laboratory
University of California
Berkeley, California 94720

February 1986

Abstract

Part A

Mathematical Modeling of Lithium(alloy), Iron Sulfide Cells

Computer programs simulating the behavior of LiAl/FeS and $Li(Si)/FeS_2$ high temperature molten salt cells have been developed. The models predict the cell voltage, temperature, and heat-generation rate during cell operation. Position-dependent behavior such as reaction-rates and concentrations within the cell are also calculated. The models predict operational characteristics and determine the influence of changes in design parameters on the performance of the cells. The effects of state-of-discharge, initial electrolyte composition, temperature, and discharge current density on cell behavior are investigated. Factors that can limit a cell during operation are identified. The cell discharge behavior is compared with available experimental data. The models clarify our understanding of the battery systems and help guide experimental research.

Part B

The Electrochemical Precipitation of Nickel Hydroxide

The objective of this research is to develop a fundamental understanding of the precipitation of nickel hydroxide from acidic nickel nitrate solutions. This chemical process occurs in the fabrication of nickel battery electrodes. A mathematical model that simulates the formation and growth of a nickel hydroxide film on a rotating disk electrode has been developed and used to study the system. Experimental investigations of the system are also conducted with a rotating disk electrode apparatus. A mechanism for the nitrate-reduction reaction has been proposed. Experimental studies are conducted, along with theoretical efforts, in order to verify the proposed reaction sequence.

Acknowledgments

There are many people that are responsible for making my stay in Berkeley a happy one. I have a lot of fond memories and many friends who have helped form them. I wish to express my utmost thanks to Professor John Newman for his advise and also for being my very good friend. He provided a learning environment that allowed me freedom to explore on my own, yet he was always available when I needed his guidance. I can't begin to express in words how much I have learned from him, but I can hope to continue to build my technical career in the spirit of his philosophies.

I wish to also thank Professor Scott Lynn, Professor Richard Andersen, and Mark Verbrugge for reading this thesis and providing many valuable comments. Thanks are also due to Karen Tomasu and Eric Wong for their contributions to the work presented in Part B of the thesis.

I appreciate my parents for putting up with a daughter that seemed to be a perpetual student and for giving me support when I needed it most. I wish to close with acknowledgment of my husband Mark, the most important part of my life.

Contents

Introduction

This dissertation addresses two major topics and is composed of two parts. The first, Part A, presents theoretical work on lithium-alloy, iron sulfide cells. The second, Part B, concerns the electrochemical precipitation of nickel hydroxide, which is a processing step in the fabrication of nickel battery electrodes. The two parts of the thesis are presented and discussed separately. Part A is composed of Chapters 1 through 5; Chapters 6 and 7 constitute Part B of the dissertation.

Part A. Mathematical Modeling of the Lithium(alloy), Iron Sulfide Cell

Secondary, high-temperature batteries employing molten-salt electrolytes based on lithium as the negative electrode and sulfur as the positive electrode were conceived for electric vehicle propulsion and energy storage applications. The melting point of the electrolyte in these cells usually restricts the operating temperatures to above 400°C. The stationary energy storage applications include off-peak storage for electric utility systems (also referred to as load leveling) and the storage of energy produced by wind or the sun.[1] The incentive for the development of these systems is the extremely high theoretical energy density and thermodynamic, open-circuit potential of the Li/S couple (2.23 V and 2602 W-hr/kg, respectively).[2] The Li/S cell, which was invented in 1968 at Argonne National Laboratory,[1] posed several engineering difficulties associated with the high lithium and sulfur activities. The advantages of using a molten-salt electrolyte over an aqueous electrolyte include reducing electrolyte decomposition, ohmic resistance, and mass-transfer limitations. High temperature operation also promotes relatively fast electrode reactions compared to cells operated at lower temperatures. The disadvantages to operating at high temperatures are increased corrosion of cell components and increased

volatility and solubility of active material. In Li/S cells, these same disadvantages are aggravated by the high lithium and sulfur activities, and the liquid lithium electrode is difficult to contain. In 1973, these problems were lessened by substituting solid, $\alpha-\beta$ LiAl alloy for the lithium in the negative electrode and FeS for the sulfur in the positive electrode at the expense of a lower cell voltage and energy density.[2] Later, the Li(Si)/FeS$_2$ couple was proposed as a higher voltage and higher power alternative to the LiAl/FeS cell. However, the Li(Si)/FeS$_2$ cells share some of the disadvantages of the Li/S system associated with the increased activities of lithium and sulfur relative to LiAl/FeS cells. The lithium alloys and iron sulfides are both solid materials that form porous structures that can be filled with electrolyte. In terms of engineering development, the LiAl/FeS cell is currently the most technically advanced system of this type. An extensive compilation of state-of-the-art LiAl/FeS cell design, construction, and performance has been published by Gay *et al*.[1]

Currently, lithium(alloy), iron sulfide batteries require further development in order to reach commercial acceptability. We believe that theoretical efforts combined with experimental investigations provide the most efficient methods of development. Modeling these cells can aid in design and development by identifying system limitations and investigating the influence of changing operating parameters on cell performance. Mathematical models also contribute to a more fundamental understanding of battery systems. The comparison of model to experimental results can help substantiate our understanding of the systems.

A mathematical model of the LiAl/LiCl-KCl/FeS cell was developed by Pollard and Newman[3,4,5] in 1979. Much of their work was done in conjunction with experimental investigations at Argonne National Laboratory. Pollard and Newman predicted regions of bipolarity within the electrodes under certain operating conditions. The understanding of bipolar regions observed in experimental

LiAl electrodes[6] was facilitated by Pollard and Newman's model results.[7] Pollard and Newman predict LiCl precipitation in the LiAl electrode and KCl precipitation in the FeS electrode during discharge under certain operating conditions. Precipitation is also observed experimentally during discharge.[6,8] Pollard and Newman's model predicts that the clogging of pores by KCl precipitation is the primary capacity-limiting mechanism of these cells. At the current state of development, the major problems with experimental LiAl/FeS cells are cell failure by shorting, electrode swelling and extrusion, and agglomeration of the negative electrode on extended cycling.[2]

During the discharge of an FeS electrode in LiCl-KCl electrolyte, investigators[8] have identified two intermediate sulfide phases, X-phase (Li_2FeS_2) and J-phase ($LiK_6Fe_{24}S_{26}Cl$). The thermodynamic behavior of LiAl/FeS cells in LiCl-KCl electrolyte involves these intermediates and is investigated in Chapter 1.

The results of the modeling work for the LiAl/FeS cell subsequent to the original work of Pollard and Newman are presented in Chapter 2. The galvanostatic discharge behavior of the cell constitutes the main emphasis of this work. The model developed by Pollard and Newman incorporates only the X-phase intermediate. In Chapter 2, the results of a model that includes the J-phase intermediate are presented, and the effects of KCl precipitation on positive-electrode utilization are examined. The formation of J-phase during discharge is undesirable because of the lack of reversibility of reactions involving J-phase.[8]

In Chapter 3, a general energy balance for battery systems is derived and applied to the LiAl/FeS cell model and the lead-acid cell.

The thermodynamic behavior of the lithium(alloy)/FeS_2 cell is examined in Chapter 4, and a mathematical model of the cell is presented in Chapter 5.

Part B. The Electrochemical Precipitation of Nickel Hydroxide

Part B of this dissertation presents fundamental investigations of the electrochemical precipitation of nickel hydroxide, the positive-electrode active material in several alkaline, secondary batteries. Electrochemical precipitation is a method of impregnating nickel hydroxide active material directly into the pores of the battery electrode by cathodic reduction of nickel nitrate solution. We have studied electrochemical precipitation of nickel hydroxide with a rotating disk electrode to obtain a more fundamental understanding of the mechanism of the process.

Secondary batteries that use the nickel hydroxide electrode employ alkaline electrolyte and operate at ambient temperature. Some examples of these batteries are: zinc-nickel oxide ($Zn/NiOOH$), iron-nickel oxide ($Fe/NiOOH$), cadmium-nickel oxide ($Cd/NiOOH$), and hydrogen-nickel oxide ($H_2/NiOOH$). During discharge of these cells, the nickelic oxyhydroxide ($NiOOH$) is converted to nickel hydroxide ($Ni(OH)_2$) in the positive electrode. For near-term electric-vehicle applications, the zinc-nickel oxide and iron-nickel oxide batteries are being considered, whereas lithium(alloy), iron sulfide high-temperature batteries are being considered in the longer term.[3] The cadmium-nickel oxide cells are used extensively by the military in aircraft and communication applications. The hydrogen-nickel oxide battery is used primarily in the aerospace industry and is a possible candidate for load-leveling applications. The success of these batteries is very dependent on the development of a low cost, improved nickel hydroxide electrode. Landgreb et al.[42] discuss the state of development of the nickel-hydroxide electrode.

Several preparation methods of the nickel-hydroxide electrode have been developed. Each method incorporates $Ni(OH)_2$ in to a porous, conducting medium in a different way. The electrochemical precipitation method is regarded as the most promising. For example, Miller[43] reports that

electrochemically produced electrodes are fabricated in one-third the time and exhibit greater stability than electrodes produced by a chemical method.

The idea of preparing battery electrodes by the precipitation of nickel hydroxide from the reduction of nickel nitrate solutions was proposed independently and almost simultaneously by Pozin[44] and Briggs et al.[45] in 1962. McHenry[46] was one of the first to investigate the engineering aspects of the electrode development; in 1968 MacArthur[47] was the first to propose a mechanism for the nitrate reduction reaction.

The electrochemical precipitation of nickel hydroxide is still subject to many unanswered questions and, work is continuing to complete our understanding of the process. We have chosen to study the process with a simplified system, the rotating disk electrode, rather than a porous electrode. We have also chosen to study the system with aqueous, acidic nickel nitrate solution, rather than the alcohol and water solutions containing other nitrate salts or nickel salts often used in electrode preparation.[48] In Chapter 6, we develop a mathematical model for the electrochemical precipitation of a porous nickel-hydroxide film on a rotating disk electrode and discuss experimental results. In Chapter 7, experimental results at conditions in which a $Ni(OH)_2$ layer is not present on the electrode surface and a mechanism for the nitrate reduction reaction that is consistent with our experimental observations and literature results are presented.

Part A

Mathematical Modeling of Lithium(alloy), Iron Sulfide Cells

Chapter 1

Thermodynamic Behavior of LiAl/FeS Cells

1.1. Introduction

An understanding of the thermodynamic behavior of LiAl/FeS cells can aid in the development and design of these cells. A large research effort has been directed toward the understanding of the chemistry of the FeS electrode in molten-salt electrolytes. This successful endeavor is reviewed extensively by Selman and Saboungi.[8] Much of the success of this research may be attributed to the work done at Argonne National Laboratory.

Tomczuk *et al.*[9] present a thermodynamic analysis of the FeS electrode with broad scope, utilizing a number of experimental techniques. The researchers combined EMF and cyclic voltammetric measurements with metallography and x-ray diffraction results to characterize the electrode. Photomicrographs of coexisting electrode phases are shown, and the complex reaction sequences are identified. The authors also discuss the chemical reactions that can occur if regions of an electrode are not equilibrated.

Most of the developmental work on the FeS electrode has concentrated on its behavior in LiCl-KCl electrolyte at temperatures between 400 and 500°C. We also concentrate on this electrolyte, mainly because it is well studied and thermodynamic data are available. In Section 1.3.2 we try to extrapolate our work to LiCl-KCl-LiF electrolyte.

The LiAl electrode material in LiAl/FeS cells is a two-phase alloy and is well understood. The lithium activity of lithium-aluminum is constant between approximately 8 and 49 atom percent lithium, where the two phases, α and β coexist.[2] The potential of the LiAl electrode in LiCl-KCl electrolyte at 400°C is

approximately 300 mV more positive than that of liquid lithium. The compositions of β-LiAl and α-LiAl are 47.5 and 10 atom percent lithium, respectively. The electrode reaction is

$$LiAl(\beta - phase) \longrightarrow Li^+ + Al(\alpha - phase) + e^-$$
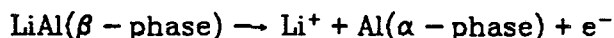
In this chapter, we summarize and extend some of the important findings of the work of Tomczuk *et al*. With the results of Tomczuk *et al*., the thermodynamic behavior of a LiAl/FeS cell that is operated in an infinite amount of electrolyte can be determined. We have extended their analysis to give the behavior of a cell with a finite amount of electrolyte at any initial composition. In the last section of this chapter, we compare our predicted open-circuit cell potentials with literature results of experimental cells.

1.2. The Regions of Stability of FeS in LiCl-KCl Electrolyte

There are five compounds that have been identified during the discharge of an FeS electrode. These compounds are: FeS, Li_2S, Fe, Li_2FeS_2 (X-phase), and $LiK_6Fe_{24}S_{26}Cl$ (J-phase). FeS is the original electrode material, and Li_2S and Fe are the products of complete discharge. The intermediate phases formed during discharge are referred to as J-phase and X-phase. Three independent electrochemical reactions can be written for this system. Table 1-1 gives five electrochemical reactions that we use to describe the FeS electrode.

Table 1-1.

Electrochemical Reactions of the FeS electrode

---

1. $26FeS + Li^+ + Cl^- + 6K^+ + 6e^- \rightarrow LiK_6Fe_{24}S_{26}Cl + 2Fe$

    (J-phase)

2. $J + 25Li^+ + 20e^- \rightarrow 13Li_2FeS_2 + 11Fe + 6K^+ + Cl^-$

    (X-phase)

3. $2FeS + 2Li^+ + 2e^- \rightarrow Li_2FeS_2 + Fe$

4. $Li_2FeS_2 + 2Li^+ + 2e^- \rightarrow 2Li_2S + Fe$

5. $J + 51Li^+ + 46e^- \rightarrow 26Li_2S + 24Fe + 6K^+ + Cl^-$
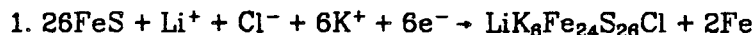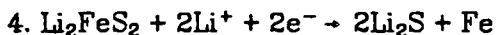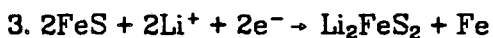
Each reaction involves two sulfide phases and Fe. The Gibbs phase rule can be applied at a given temperature and shows that there is only one degree of freedom for reactions 3 and 4, and two degrees of freedom for reactions 1, 2, and 5. In other words, electrode reactions 3 and 4 are characterized by constant open-circuit potentials relative to the $(\alpha-\beta)$ LiAl reference electrode (at constant temperature and pressure), and reactions 1, 2, and 5 have potentials that vary with electrolyte composition. In the next two sections, we discuss the primary data needed to describe the thermodynamic behavior of this system. In Section 1.2.3, the possible reaction sequences during the discharge of a LiAl/FeS cell are discussed.

1.2.1. Primary Data

The thermodynamic, open-circuit potential data at a single electrolyte composition (eutectic in this case) and electrolyte activity coefficient data for a

range of compositions are what we call primary data. We can use these primary data to calculate the thermodynamic, open-circuit potential for a range of compositions. The primary open-circuit potential data are given for the eutectic composition of the electrolyte as a reference condition and are of the form

$$U_{i,out} = a_i + b_i T .$$

(1-1)

The fourth and fifth columns of Table 1-2 give the literature data for the coefficients in this equation, corresponding to the five reactions in Table 1-1. Equation 1-1 yields the potential in volts and requires the temperature in kelvins. All the electrode reaction potentials are given relative to the two-phase (α, β) LiAl alloy reference electrode.

Table 1-2.

Coefficients for the Open-Circuit Potential

Reaction	a_i [V]	$b_i \times 10^3$ [V/K]	a_i [V]	$b_i \times 10^3$ [V/K]
1.	1.8328	-0.5267	1.9547[9]	-0.68[9]
2.	1.19072[9]	-0.1753[9]	1.19072[9]	-0.1753[9]
3.	1.3389[10]	0.0133[10]	1.3389[10]	0.0133[10]
4.	1.43211[10]	-0.147[10]	1.43211[10]	-0.147[10]
5.	1.3272	-0.0068696	1.33978[9]	-0.02445[9]

The poor reversibility of the electrochemical reactions of J-phase lead to large uncertainties in the determination of their thermodynamic properties.[9] As we mentioned earlier, only three of the reactions are independent, so the thermodynamic data for reactions 1 and 5 are calculated from data for reactions 2, 3, and 4. The second and third columns of data have the parameters for reactions 1 and 5 calculated in this manner. The difference between the calculated and the experimental data for reactions 1 and 5 indicates that the data in the fourth and fifth columns are thermodynamically inconsistent. The data in the second and third columns are used in our thermodynamic calculations. The primary data in this table are for eutectic composition of electrolyte; however, the open-circuit potential of reactions 4 and 5 (relative to (α, β) LiAl) are independent of electrolyte composition. Appendix A-3 gives the equation that fits electrolyte activity coefficient data as a function of composition.[11] These activity-coefficient data were obtained from Reference 12.

1.2.2. Working Equations

The theoretical open-circuit potential for reaction l as a function of electrolyte composition, relative to a reference electrode in the same solution is written as

$$U_l = U_l^o - U_{RE}^o + \frac{RT}{n_{RE}F} \sum_i s_{i,RE} \ln(a_i) - \frac{RT}{n_l F} \sum_i s_{i,l} \ln(a_i). \qquad (1\text{-}2)$$

The stoichiometric coefficients are defined in accordance with Equation 3-6. The electrolyte species (i) are Li^+, K^+, and Cl^-. For the case of the LiAl/FeS cell, it is convenient that the negative electrode is the same material as the reference electrode. Equation 1-2 can be applied to the FeS electrode in LiCl-KCl electrolyte to relate $U_{l,eut}$ to U_l:

$$U_l = U_{l,out} - \frac{RT}{F}\ln\left[\left[\frac{a_{LiCl}}{a_{LiCl}^{eut}}\right]^{\frac{s_{Li^+,l}}{n_l}}\left[\frac{a_{LiCl}}{a_{LiCl}^{eut}}\right]^{\frac{-s_{Li^+,RE}}{n_{RE}}}\left[\frac{a_{KCl}}{a_{KCl}^{eut}}\right]^{\frac{s_{K^+,l}}{n_l}}\right],\qquad(1\text{-}3)$$

where the activities of LiCl and KCl are written without regard for their dissociation ($a_{LiCl} = a_{Li^+}a_{Cl^-}$). The open-circuit potentials of reactions 1, 2, and 5 can be written easily in terms of electrolyte activity to yield potentials at any composition with this equation. As an example, the substitution of primary data into Equation 1-3 for reaction 1 will be described. The stoichiometric coefficients for reaction 1, a_1 and b_1, from Table 1-2, and the activity at eutectic composition ($x_{LiCl}^{eut} = 0.58$) can be substituted into Equation 1-3 to give

$$U_1 = 2.0178 - 0.6444 \times 10^{-3}T -$$

$$\frac{RT}{F}\left[\frac{5}{6}\ln\left(x_{LiCl}\gamma_{LiCl}\right) - \ln\left(x_{KCl}\gamma_{KCl}\right)\right],\qquad(1\text{-}4)$$

where the relative activities of LiCl and KCl are defined as $x_{LiCl}\gamma_{LiCl}$ and $x_{KCl}\gamma_{KCl}$, respectively.

Material balances can be written to relate the electrolyte composition to the state-of-discharge. We define two parameters of importance: the initial composition of electrolyte x_{LiCl}^o and the initial number of moles of electrolyte per mole of FeS, n_e^o. Appendix A-1 gives the computer program that is used to calculate the results of Figures 1-1, 1-2, 1-3, and 1-5.

1.2.3. Reaction Sequences During Equilibrium Discharge

Figure 1-1 gives a plot of the temperature versus state-of-discharge showing the regions in which the reactions 1 through 5 occur. The state-of-discharge is put in terms of utilization of FeS. Utilization is defined as the ratio of charged passed to the total charge available in the positive electrode if it were discharged to Li_2S and Fe. For example, Equation 5-9 gives an expression
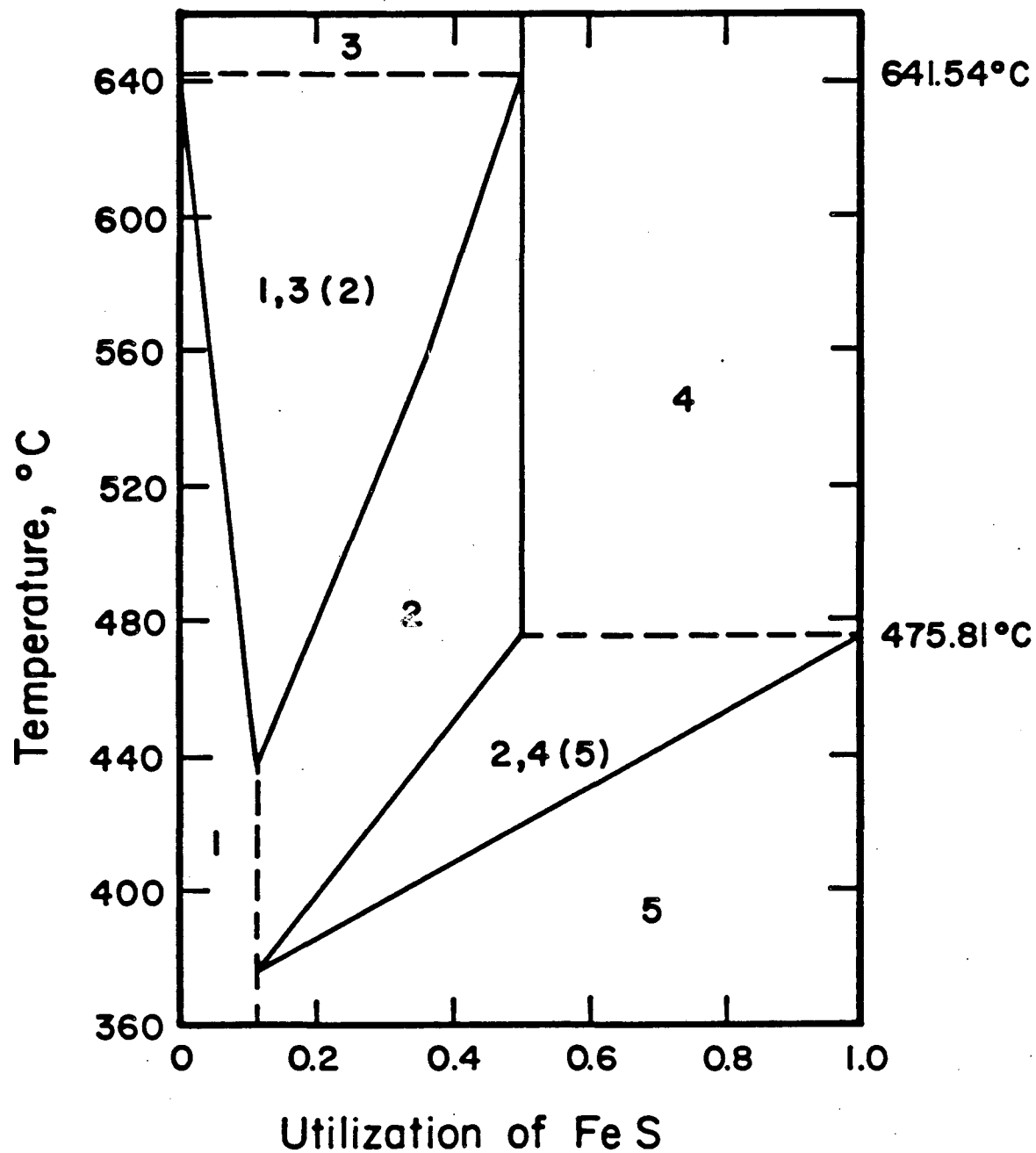
Figure 1-1. Reaction regions as a function of temperature and utilization for a cell with $x_{LiCl}^0 = 0.58$ and $n_s^0 = 1.0$. The numbers refer to the reactions in Table 1-1, and parenthesis indicate that the reaction can be obtained from the other two reactions.

for the percent utilization of an FeS$_2$ electrode.

The computer program mentioned in the previous section yields the information shown in Figure 1-1. This type of plot can give insight into the different discharge mechanisms that are possible during the operation of a LiAl/FeS cell. The initial conditions are for a cell being discharged with a eutectic composition of electrolyte and an electrolyte to FeS ratio of 1.0. The numbers within the designated regions refer to the reactions that are thermodynamically possible. First let us describe this figure in the context of an isothermal cell discharge. As discharge proceeds at a temperature below 641.5°C, the first reaction (FeS to J-phase) causes the electrolyte composition to shift by depleting the KCl species. Reaction 1 alone occurs to a utilization that is defined by the boundary of the region of reaction 1, and is less than 11.5%. If the temperature is greater than 440°C, the upper triangular region is entered as discharge continues. Five phases are equilibrated in this region: FeS, J-phase, X-phase, Fe, and the electrolyte phase. Upon entering this region, X-phase begins to form (reaction 2), and the electrolyte composition stabilizes until the FeS is exhausted. One could say that reaction 3 alone occurs in this region (reaction 1 plus reaction 2), since this reaction leaves the composition stationary. The exhaustion of FeS is marked by the utilization at the right side of the upper triangle, and is less than 50%.

After exhaustion of FeS, reaction 2 occurs (J-phase to X-phase), and this shifts the composition back toward eutectic. If the temperature is below 475.8°C and greater than about 377°C, the lower triangular region is entered as discharge proceeds. In this region, five phases (J-phase, X-phase, Li$_2$S, Fe, and the electrolyte) are equilibrated. X-phase reacts to Li$_2$S (reaction 4), and the composition will remain constant until X-phase is exhausted. The X-phase is exhausted at the utilization defining the right side of the lower triangular region. In the final region of discharge, the remaining J-phase reacts to Li$_2$S

and Fe (reaction 5), and the composition will continue its downward shift toward eutectic.

If the temperature is greater than 475.8°C, the lower triangular region is not entered during discharge. Instead, the region in which reaction 2 occurs is entered, and the J-phase is exhausted at 50% utilization. Reaction 4 begins at 50% utilization, and X-phase reacts to Li_2S and Fe. In this final region of discharge, three phases are equilibrated: X-phase, Li_2S, and Fe.

If the temperature is greater than 641.5°C, J-phase never becomes stable. FeS reacts to X-phase (reaction 3) from 0 to 50% utilization, and from 50 to 100% utilization, X-phase reacts to Li_2S (reaction 4). We call this the X-phase mechanism.

If the temperature is below about 377°C, X-phase will not form, and the reaction sequence is FeS to J-phase (reaction 1) from 0 to 11.5% utilization followed by J-phase to Li_2S and Fe (reaction 5) from 11.5 to 100% utilization. We call this the J-phase mechanism. The X-phase and J-phase mechanisms are simple compared to the reaction sequences that are possible in the temperature range from 641.5 to 377°C for the conditions of Figure 1-1. Mathematical model results with these two mechanisms are presented in Chapters 2 and 3.

The boundaries designated in Figure 1-1, which define the reaction sequences, are a function of the initial composition and the amount of electrolyte. Increasing the amount of electrolyte will decrease the size of the two triangular shaped regions. The dashed sides of the triangles will remain in place. The bottom tips of the triangles will remain at 11.5% utilization, but tips of the upper and lower triangles will shift toward 641.5 and 475.8°C, respectively. As the amount of electrolyte approaches infinity, the triangles become infinitely thin. In this limiting case, there are only three possible reaction sequences: the X-phase mechanism, the J-phase mechanism, and three reaction sequence

of FeS to J-phase, J-phase to X-phase, and X-phase to Li_2S (reactions 1, 2, and 4).

If the initial concentration of LiCl, x^0_{LiCl}, is increased, the two temperatures marked by the dashed lines will shift downward, bringing the regions of X-phase stability to lower temperatures, or making J-phase unstable at high temperatures.

1.3. The Thermodynamic, Open-Circuit Potential Behavior

The thermodynamic, open circuit-potential behavior of a LiAl/LiCl-KCl/FeS cell is discussed in this section. In Section 1.2.3, the regions in which the reactions given in Table 1-1 can occur are discussed. The rectangular regions, in which reactions 3 or 4 occur alone, are three-phase regions. If we apply the Gibb's phase rule at constant temperature and pressure, we see that these two regions correspond to regions of constant potential during equilibrium discharge. The two triangular regions shown in Figure 1-1 are regions in which five phases are in equilibrium. These triangular regions are also regions of constant potential (at a given temperature), because the electrolyte is not involved in the overall reaction. The regions in which reactions 1, 2, or 5 occur alone are four-phase regions, and have an open-circuit potential (relative to α-β LiAl) that varies with electrolyte composition.

The computer program mentioned in Section 1.2.2 can generate the information given in Figure 1-2. This figure gives the open-circuit potential behavior as a function of state-of-discharge for the same conditions as Figure 1-1: initial eutectic composition and one mole of electrolyte per mole of FeS. This type of plot can give insight into the potential-time profile for the reversible operation of a LiAl/FeS cell. The different lines refer to different percent utilizations during the discharge of a cell. The occurrence of reactions 1, 2, or 5 causes the electrolyte composition to vary with utilization. For example, the bands marked 0%, 1%, 5%, and 9% utilization reflect the dependence of the open-

Figure 1-2. The open-circuit potential behavior as a function of temperature at different percent utilization for a cell with $x_{LiCl}^0 = 0.58$ and $n_s^0 = 1.0$.

circuit potential on electrolyte composition for reaction 1. Similarly, the bands marked 12%, 23%, and 37% reflect the composition dependence of the potential of reaction 2, and the nearly horizontal bands are associated with reaction 5. The results shown in Figure 1-1 can be applied to the results in Figure 1-2 to determine the different reactions occurring for a given open-circuit potential as a function of utilization and temperature.

1.3.1. The Effects of Changing n_e^o and x_{LiCl}^o

Figure 1-3 shows the open-circuit potential behavior for the same initial electrolyte composition as in Figure 1-2 (eutectic) and a larger electrolyte to FeS ratio ($n_e^o = 2.55$). These values of n_e^o and x_{LiCl}^o are the values used in the mathematical models presented in Chapters 2 and 3.

A larger value of n_e^o simply means that the cell in Figure 1-3 has more electrolyte than the cell in Figure 1-2. At a given state-of-discharge, the cell with $n_e^o = 2.55$ will be closer to the initial composition than the cell with $n_e^o = 1.0$. Comparing Figures 1-2 and 1-3, we can see that the bands representing the open-circuit potentials for reaction 1 (labeled 0%-9% utilization) shift toward the 0% utilization line with larger values of n_e^o. The intercepts, not the slopes, of the lines change. In the limit that n_e^o approaches infinity, the electrolyte composition will not change during discharge, and the series of bands shown for different utilization in the figures will converge to a single line. This is the situation discussed by Tomczuk et al.[9]

An increase in x_{LiCl}^o will shift the wedge shaped region of J-phase stability to lower temperatures. This can be seen by examining the equation for U_l for reactions 1, 2, and 5. For example, as can be seen from Equation 1-4 (for reaction 1), increasing x_{LiCl}^o will only slightly change the slope in this equation; the intercept will be changed much more. This effect is illustrated and discussed in Reference 9 for increasing x_{LiCl}^o from 0.58 to 0.67 with a value of n_e^o of infinity.
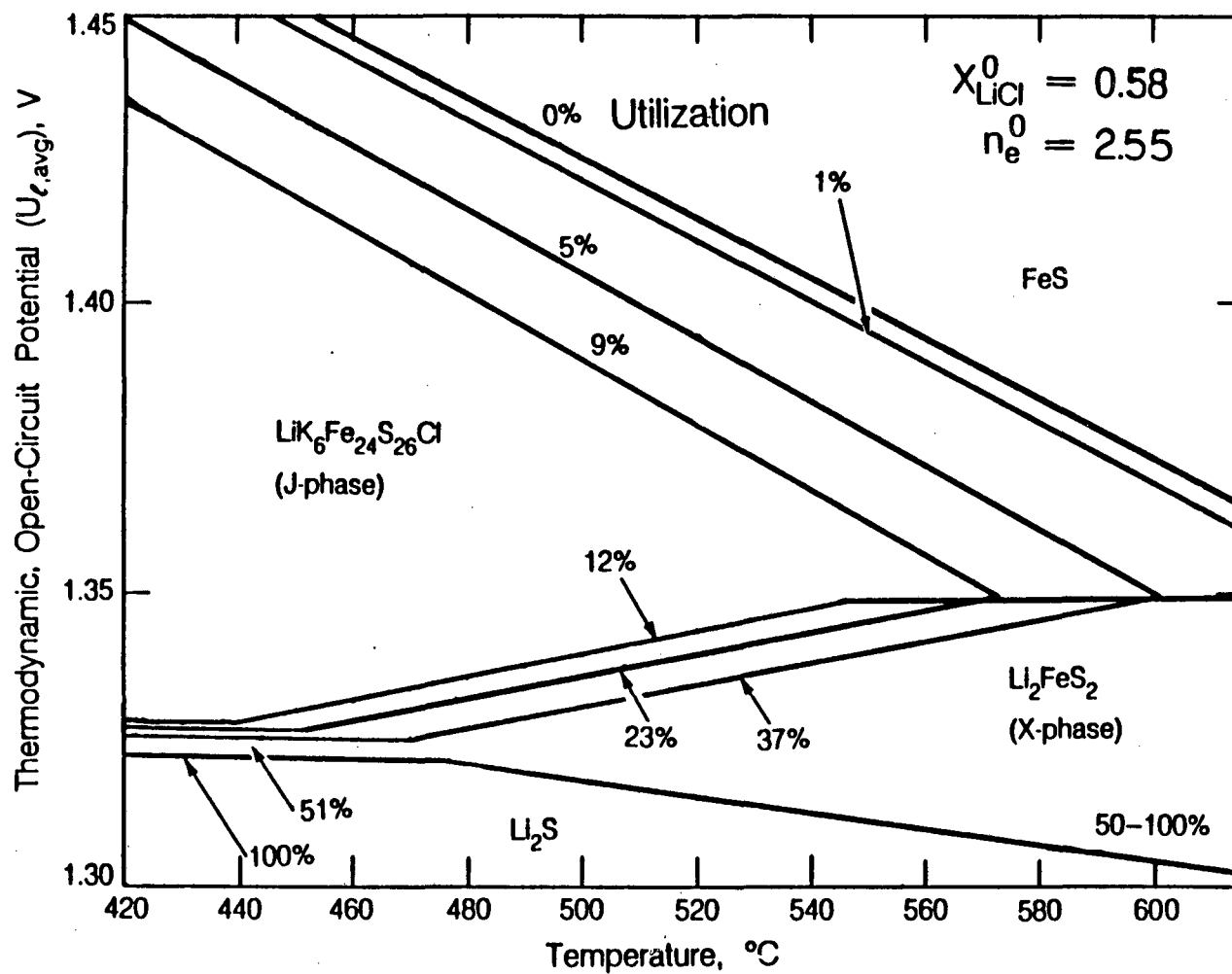
Figure 1-3. Calculated open-circuit potential behavior as a function of temperature at different percent utilizations for a cell with $x^0_{LiCl} = 0.58$ and $n^0_e = 2.55$.

The authors discuss how this increase is known to be sufficient to suppress the harmful effects of the J-phase on electrode performance in experimental cells.

1.3.2. Effects of Diluting the Electrolyte; Comparison with
Experimental Results

Figure 1-4 shows potential as a function of temperature with state-of-discharge as a parameter for an experimental cell employing a 61.63% LiCl, 7.05% LiF, and 31.32% KCl electrolyte and $n_s^0 = 3.7$.[13] Activity-coefficient data for this ternary system are not available. We can extrapolate the available primary data for the LiAl/LiCl-KCl/FeS and try to predict the thermodynamic properties of a LiAl/LiCl-KCl-LiF/FeS cell. We assume that no new reactions occur in the electrolyte with LiF. As a first approximation we assume that LiF is inert and does not dissociate; LiF serves only to dilute the LiCl and KCl. We also assume that the activity coefficients in the ternary electrolyte may be calculated from the equations for the binary electrolyte with the compositions x_{LiCl} and x_{KCl} (where $x_{LiCl} + x_{KCl} + x_{LiF} = 1$). This approximation is good for small x_{LiF}. With these assumptions, we can calculate the results of Figure 1-5.

In comparing the results of Figure 1-4 and 1-5, we see that there is a pronounced discrepancy at 0% utilization; however, the first experimental data point given in Reference 13 at 479.1°C is in agreement with the calculated results. The last experimental data point taken at 0% utilization (417.9°C) appears more in accordance with what we would expect with a lower electrolyte composition of 0.50 at 9% utilization. In other words, this experimental data point at 417.9°C intersects the 9% utilization line (reaction 1) in Figure 1-5. In these experiments, several days elapsed between data points. We do not feel that we can give a definite reason for the discrepancy between Figures 1-4 and 1-5. There are, however, several possibilities that can be examined. The previous discussion leads to the possible explanation of self-discharge or current
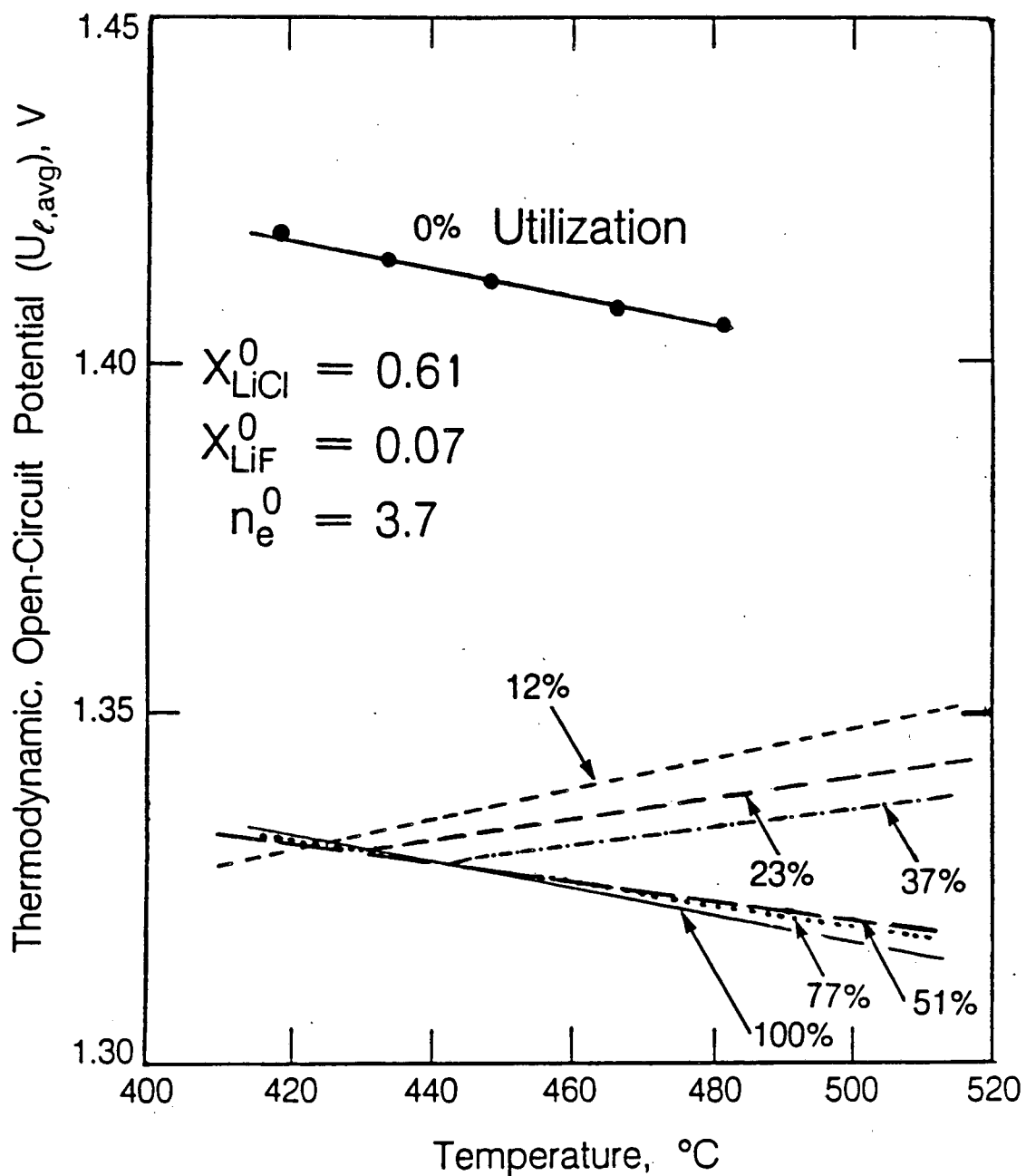
Figure 1-4. The open-circuit potential behavior as a function of temperature at different percent utilizations for an experimental cell[13] with $x^0_{LiCl} = 0.61$, $x^0_{LiF} = 0.07$, and $n^0_e = 3.7$.
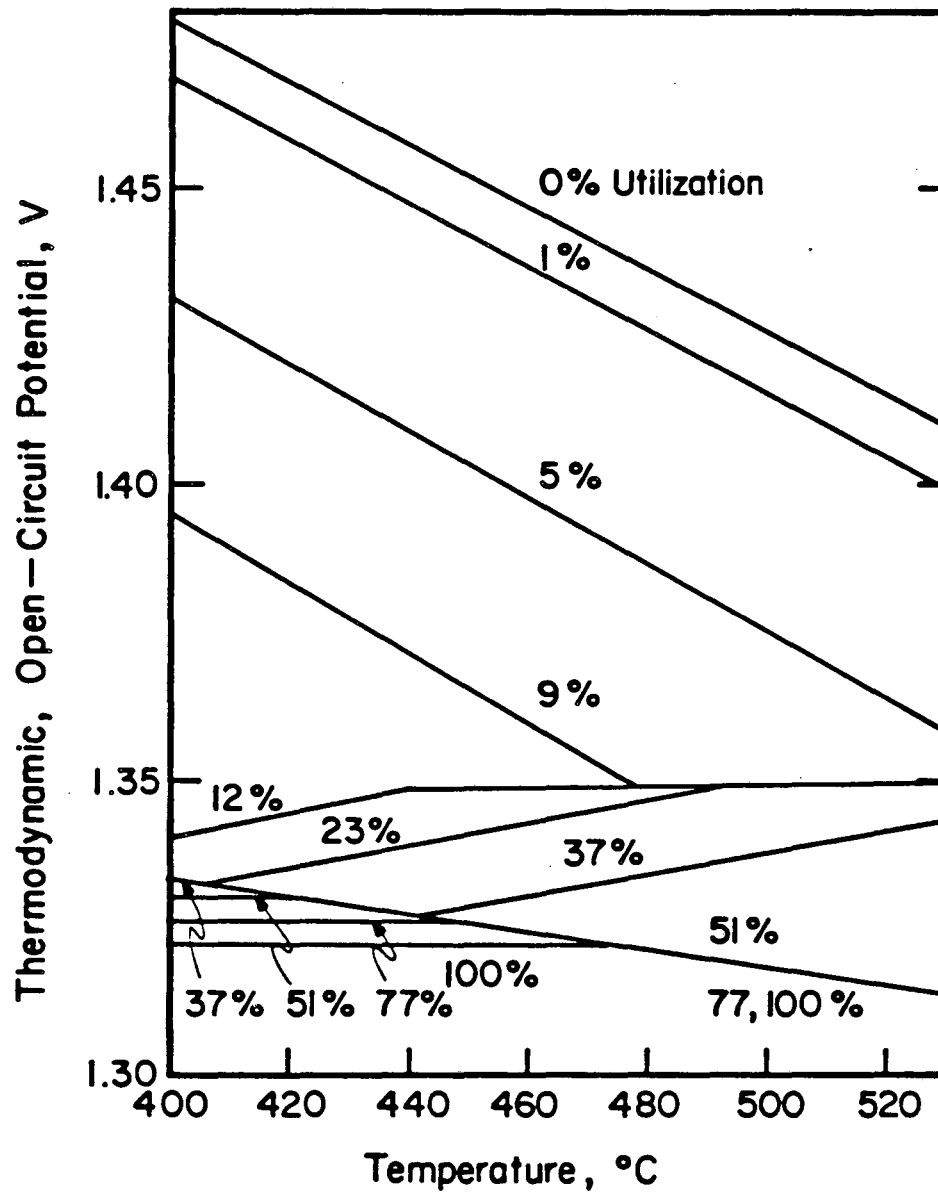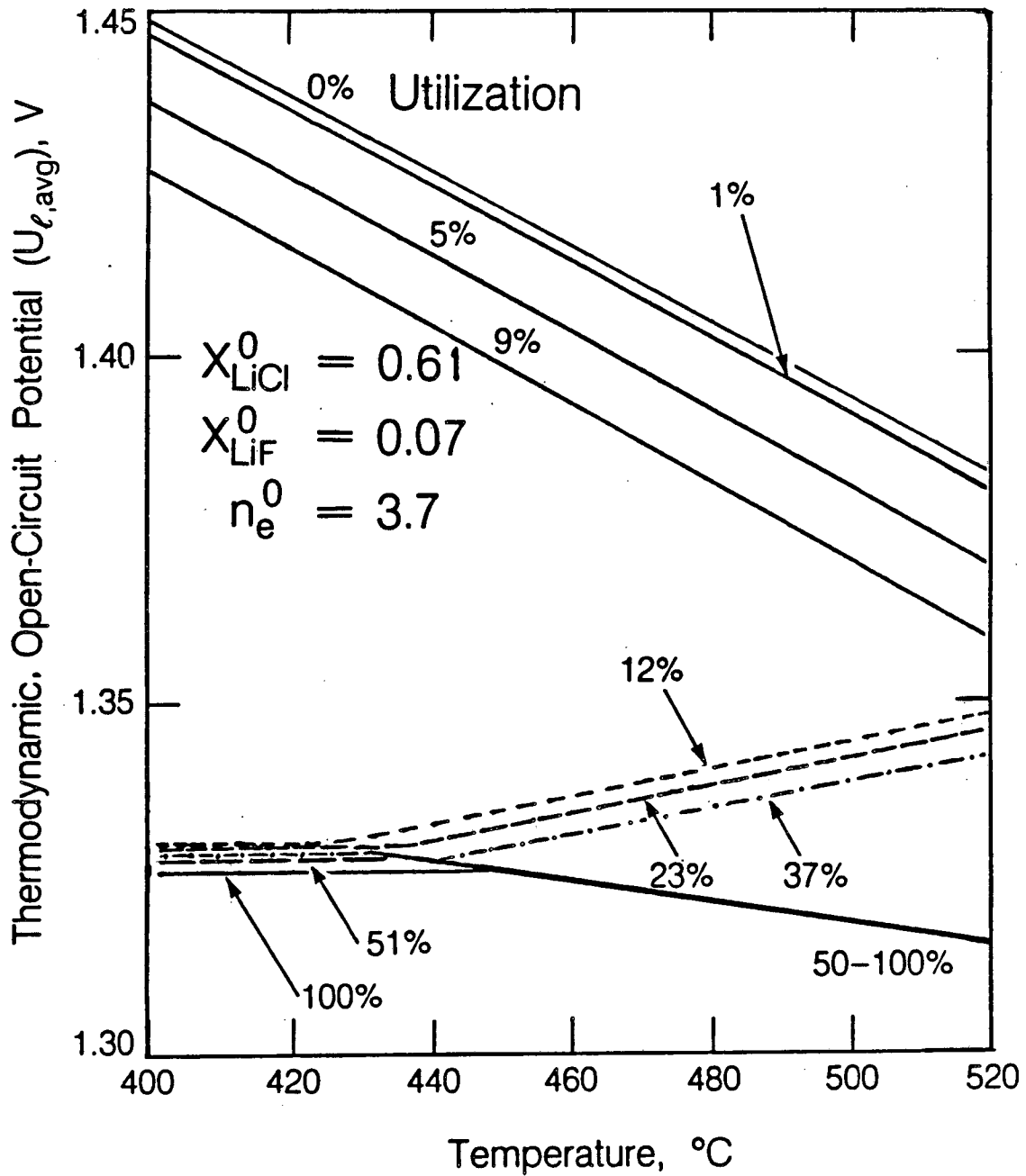
Figure 1-5. Calculated open-circuit potential behavior as a function of temperature at different percent utilization for a cell with $x_{LiCl}^0 = 0.61$, $x_{LiF}^0 = 0.07$, and $n_e^0 = 3.7$.

leakage. We would then expect the reported 12% utilization line in Figure 1-4 actually to be greater than 21% utilization, and discharge greater than 91% utilization should not be possible. The researchers, however, obtain several data points at 100% utilization. Also the results at 100% utilization agree well with the results in Figure 1-5. Another possible explanation for the discrepancy may be found in the examination of Equation 1-3. One may ask the questions: What term in this equation is responsible for the slope (dU/dT)? and, Could this temperature coefficient be incorrect? Equation 1-3 has two terms that determine the slope. The temperature coefficient in one term is a constant, 0.644, and the other is dependent on the composition. The activity coefficient term is constant with respect to temperature because of the form of the activity coefficient expression that we have chosen. It is possible that this expression may not adequately describe this electrolyte. The composition-dependent term is very small for $x^0_{LiCl} = 0.61$ and approaches more positive values for more lithium lean electrolytes.

A more rigorous method of extrapolating the primary data for the LiAl/LiCl-KCl/FeS cell to predict the thermodynamic properties of a LiAl/LiCl-KCl-LiF/FeS cell is to include the Li^+ from LiF in x_{Li^+}. Equation 1-3 may be written in terms of ionic mole fractions;

$$U_l = U_{l,eut} - \frac{RT}{F}\ln\left[\left[\frac{x_{Li^+}\gamma_{LiCl}}{x^{eut}_{Li^+}\gamma_{LiCl}}\right]^{\frac{s_{Li^+,l}}{n_l} - \frac{s_{Li^+,RE}}{n_{RE}}}\left[\frac{x_{Cl^-}}{x^{eut}_{Cl^-}}\right]^{\frac{-s_{Cl^-}}{n_l}}\left[\frac{x_{K^+}\gamma_{KCl}}{x^{eut}_{K^+}\gamma_{KCl}}\right]^{\frac{s_{K^+,l}}{n_l}}\right] \quad (1\text{-}5)$$

For the LiCl-KCl electrolyte, Equations 1-3 and 1-5 yield the same open-circuit potentials. For LiCl-KCl-LiF electrolyte, the equations do not give identical results. For the ternary electrolyte with dissociated LiF, we substitute $x_{Li^+} = \frac{1}{2}(x_{LiCl} + x_{LiF})$, $x_{K^+} = \frac{1}{2}(x_{KCl})$, and $x_{Cl^-} = \frac{1}{2}(x_{LiCl} + x_{KCl})$ into Equation 1-5. Equation 1-5 is rigorous and would yield the correct open-circuit potential if

γ_{LiCl} and γ_{KCl} for the LiCl-KCl-LiF system were known. We may assume that the activity coefficient terms in Equation 1-5 and 1-3 are equivalent at the same state-of-discharge. The differences in open-circuit potential between Equation 1-5 and Equation 1-3 are small. For example, at 450°C and 12% utilization (reaction 2) the difference is 1.7 mV.

1.4. Conclusions

We have discussed the thermodynamic, open-circuit potential behavior of the LiAl/FeS cell as a function of state-of-discharge and temperature. This thermodynamic information is derived from the primary data (activity coefficients as a function of electrolyte composition and open-circuit potential data at a single composition) available in the literature. We use the primary data with the least uncertainty and formulate a consistent set of thermodynamic data for the FeS electrode reactions. Calculations of the open-circuit potential are compared to results of experimental cells and reasonable agreement is obtained. The composition dependence of the open-circuit potential is completely determined if the activity coefficient behavior of the electrolyte species is known. It is important that primary data are available for thermodynamic analysis of this system.

In agreement with other studies,[1,9] lithium-rich electrolyte and low operating temperatures should suppress the formation of J-phase and improve LiAl/LiCl-KCl/FeS cell performance. The use of electrolytes that do not contain potassium would eliminate the problems associated with J-phase. More research is needed to identify and characterize suitable new electrolytes. FeS_2 electrodes do not exhibit the problems associated with J-phase and may be considered as an alternative electrode for use in LiCl-KCl electrolyte. During discharge of the FeS_2 electrode, FeS does not form, and FeS_2 does not appear to react with potassium.[14]

Chapter 2

Mathematical Modeling of LiAl/FeS Cells

2.1. Introduction

The mathematical model of the LiAl/LiCl-KCl/FeS cell was originally developed by Pollard and Newman.[3,4,5] This model has been further developed by Pawlikowski[11] and this author. The results of the modeling work for the LiAl/FeS cell subsequent to the original work of Pollard and Newman are presented in this chapter. The galvanostatic discharge behavior of the cell is the main emphasis of this work. Pollard and Newman investigated the charge and relaxation behavior[3,5] along with the galvanostatic discharge behavior[3,4] in their work. We present behavior for two different positive-electrode discharge mechanisms. These mechanisms, referred to as X-phase and J-phase, are described in Chapter 1 (Section 1.2.3). The thermodynamic, open-circuit potential behavior of the cells that are modeled in this chapter is given in Figure 1-3. This figure shows that if a cell is discharged reversibly, we can expect the J-phase mechanism to occur for temperatures less than 440°C and the X-phase mechanism to occur for temperatures greater than approximately 640°C.

In Section 2.2, we briefly describe the mathematical model and the modifications that have been made to the original work of Pollard and Newman.[3,4] In Section 2.3, results are presented for the LiAl/FeS cell discharged with the J-phase mechanism. The effects of KCl precipitation on positive-

electrode utilization are discussed in Section 2.4.

2.2. Mathematical Model Description

A cross section of the cell sandwich is shown schematically in Figure 2-1. The model is one dimensional and consists of a porous negative electrode (shown on the left) and a porous positive electrode (shown on the right) with a reservoir and porous separator in between. The hatched area in the electrodes refers to the cell's active material (also called the matrix phase). The clear area refers to the molten LiCl-KCl electrolyte that fills the pores within the cell. The fundamental equations in the model are material balance equations for species in the electrolyte phase and matrix phase, an Ohm's law equation, a current balance equation, and electrochemical kinetic equations. In the next section we give these equations. This set of governing equations was originally developed by Pollard and Newman,[3,4] and we refer the reader to their work for the development of the equations and boundary conditions. These equations are cast into finite difference form along with the appropriate boundary conditions and solved iteratively by the method of Newman(BAND).[15] In the next section, the governing equations will be discussed in greater detail. The model calculates time-dependent behavior such as the cell voltage and temperature. The model also calculates position- and time-dependent behavior such as distributions of electrolyte composition, reaction rates, and porosity.

2.2.1. Discussion of Governing Equations

In this section, we list the governing equations for the LiAl/LiCl-KCl/FeS cell model. We refer the reader to the work of Pollard and Newman[3,4] for boundary conditions and the development of the equations. The material balances for the LiCl and KCl electrolyte species, including the effects of diffusion, migration and convection, are given by

LiAl/LiCl-KCl/FeS cell

$$LiAl \rightarrow Li^+ + e^- + Al \qquad\qquad 2FeS + 2Li^+ + 2e^- \rightarrow Li_2 FeS_2 + Fe$$
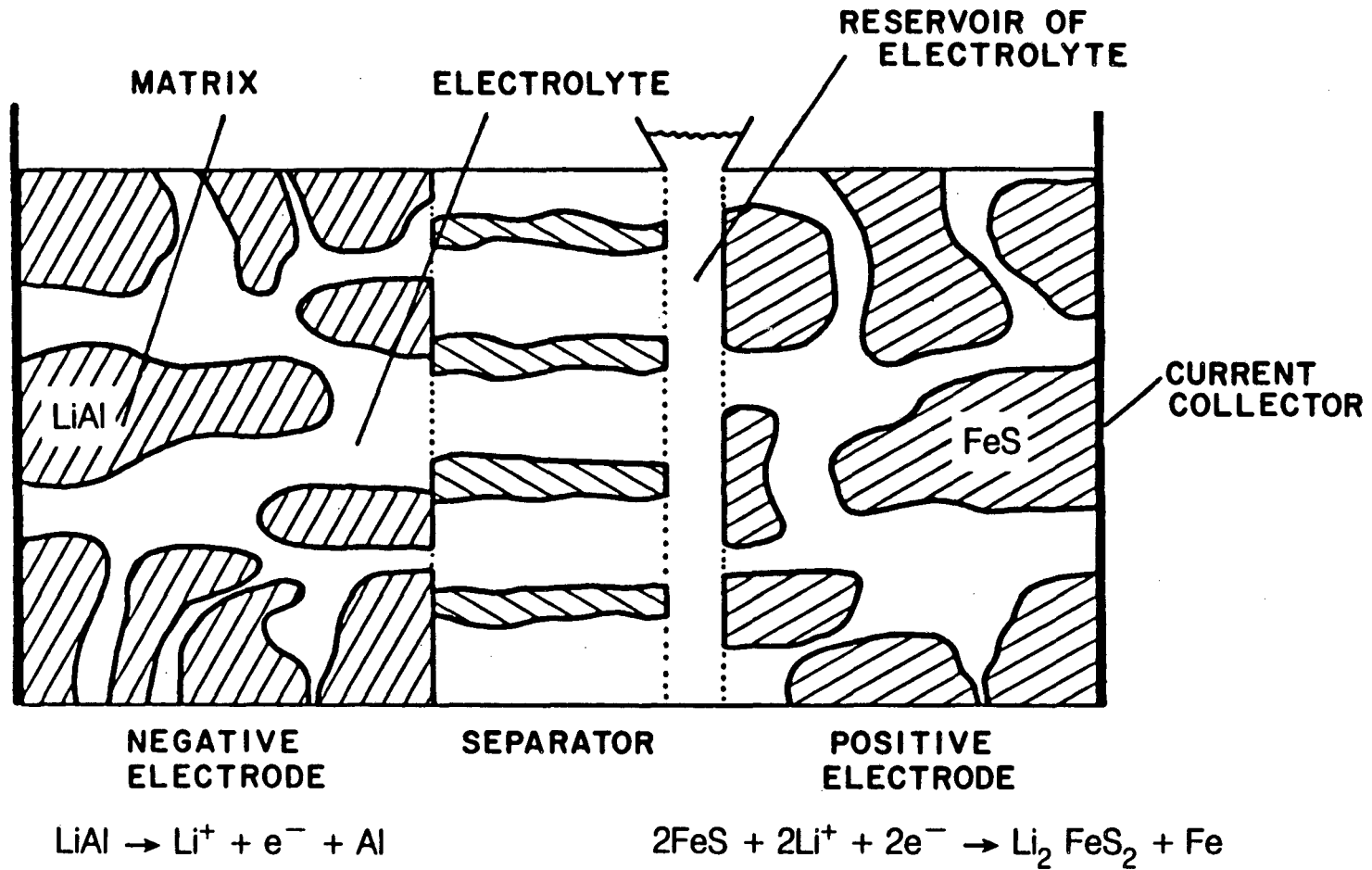
XBL 849-8736

Figure 2-1. Schematic diagram of the LiAl/FeS cell.

$$\frac{\partial(\epsilon x_{LiCl}/\tilde{V}_e)}{\partial t} + \nabla \cdot (x_{LiCl}\mathbf{g} - \frac{\epsilon D}{\tilde{V}_e}\nabla x_{LiCl}) = -\sum_l \frac{s_{Li^+,l}}{n_l F}j_l - \frac{1}{\tilde{V}_{LiCl,s}}\frac{\partial \epsilon_{LiCl,s}}{\partial t} \quad (2\text{-}1)$$

and

$$\frac{\partial(\epsilon x_{KCl}/\tilde{V}_e)}{\partial t} + \nabla \cdot (x_{KCl}\mathbf{g} - \frac{\epsilon D}{\tilde{V}_e}\nabla x_{KCl}) = -\sum_l \frac{s_{K^+,l}}{n_l F}j_l - \frac{1}{\tilde{V}_{KCl,s}}\frac{\partial \epsilon_{KCl,s}}{\partial t}, \quad (2\text{-}2)$$

respectively. Where

$$\mathbf{g} = \mathbf{v}^\circ / \tilde{V}_e + \frac{\mathbf{i}_{pore}}{2F}. \quad (2\text{-}3)$$

The overall material balance on the solid phases,

$$\frac{\partial(\epsilon + \epsilon_p)}{\partial t} = \sum_l \sum_{i,solid} \frac{s_{i,l}\tilde{V}_i}{n_l F}j_l. \quad (2\text{-}4)$$

describes how the electrode porosity changes with the extent of reaction at each location within the electrode. A current balance equation,

$$\sum_l j_l = \nabla \cdot \mathbf{i}_{pore}. \quad (2\text{-}5)$$

relates the divergence of the solution current to the total transfer current. Ohm's law is applied to the matrix and the electrolyte phases and then combined to yield

$$\nabla \eta = \left(\frac{1}{\kappa} + \frac{1}{\sigma}\right)\mathbf{i}_{pore} - \frac{I}{\sigma} - \frac{RT}{Fx_{LiCl}}\left(1 + \frac{d \ln\gamma_{LiCl}}{d \ln x_{LiCl}}\right)\left(1 - \frac{s_{Cl^-,RE}x_{LiCl}}{n_{RE}x_{KCl}}\right)\nabla x_{LiCl} \quad (2\text{-}6)$$

for the overpotential distribution. The overpotential is defined as

$$\eta = \Phi_{matrix} - \Phi_{pore}. \quad (2\text{-}7)$$

A kinetic equation of the form

$$j = \sum_l j_l = \sum_l ai_{o,l} \left(e^{\alpha_{a,l} F \eta_{s_l}/RT} - e^{-\alpha_{c,l} F \eta_{s_l}/RT} \right) \qquad (2\text{-}8)$$

relates the transfer current to the local surface overpotential for each reaction ($\eta_{s_l} = \eta - U_{l,o}$). We can eliminate Equation 2-8 and the transfer current variable, j, from this set of equations. Equations 2-1, 2-2, 2-4, 2-5, and 2-6 are solved simultaneously, subject to the appropriate boundary conditions, for the local variables x_{LiCl}, ϵ, i_{pore}, g, and η. The modifications that have been made to the original model will be discussed in the next section.

Following the solution of these equations, we can calculate other characteristics of the cell. As examples, a voltage balance gives the cell voltage, and an energy balance gives the cell temperature (assumed to be uniform throughout) and heat-generation rate. The kinetic equation for each reaction will give j_l, and individual material balances on the solid phase species yield the volume fractions, $\epsilon_{i,solid}$.

2.2.2. Modifications to Pollard and Newman's Original Model[3,4]

In this section, we discuss the modifications to the model of Pollard and Newman.[3,4] The first major development is the incorporation of the J-phase mechanism (see Chapter 1) by Pawlikowski and Newman.[11] The method is discussed in Section 2.2.2.2, and we present results of the model in Section 2.3. In an effort to reduce capacity limitations by KCl precipitation, the kinetic equations were modified. This development is discussed in Section 2.4. The energy balance as been modified to include heat effects due to simultaneous electrode reactions and electrolyte mixing. A general energy balance equation is developed in Chapter 3, and the results of applying it to the LiAl/FeS cell discharged with the X-phase and J-phase mechanisms are presented. In Chapter 5, we discuss the modifications required for the simulation of a Li(Si)/FeS$_2$ cell and present results of this model. In the next section, we discuss the modification of the original matrix conductivity equation.

2.2.2.1. Positive-Electrode Matrix Conductivity

Pollard and Newman observed that their model predicts the positive-electrode resistance to be about six times lower than experimental observations[3,4] and that the resistance of the matrix phase is negligible ($\sigma_{eff} \approx 10^4$ (Ω-cm)$^{-1}$). One possible explanation for this is the model's calculation of the positive-electrode matrix conductivity. Measurements of the conductivity of X-phase have been published recently,[16] and it appears that the value used in the original model ($\sigma_X = 500$ (Ω-cm)$^{-1}$) is too large by a factor of 100. Changing the value of the conductivity of X-phase would only affect the resistance of the electrode when the second reaction of the X-phase mechanism occurs to an appreciable extent. The model does not predict the second reaction to occur to an appreciable extent before the cutoff voltage is reached. Therefore, changing σ_X to 6.3 (Ω-cm)$^{-1}$ could not explain the observed discrepancy.

The original model assumed parallel conduction paths in the electrode and combined the conductivities of the solid phases in the electrode matrix by

$$\sigma_{matrix} = \sum_{i,solid} \sigma_i \, \epsilon_i^{1.5} . \tag{2-9}$$

Photomicrographs of coexisting phases of an FeS electrode indicate that the iron phase formed during discharge appears as discrete iron particles.[9] Iron is extremely conductive ($\sigma_{Fe} \approx 10^4$ (Ω-cm)$^{-1}$), and assuming a parallel conduction path for such a highly conductive material can give a very large matrix conductivity. For example, we can apply Maxwell's model[17] for solid phase conductivity to this system. With Maxwell's model, there is assumed to be a continuous phase and several discrete phases. We apply this model in the following manner. We assume that the discrete phases are Fe and voids. All other electrode phases are lumped together and called the continuous phase with the conductivity given by

$$\sigma_{continuous} = \frac{\epsilon_X \, \sigma_X + \epsilon_{Li_2S} \, \sigma_{Li_2S} + \epsilon_{Fe} \, \sigma_{Fe}}{\epsilon_X + \epsilon_{Li_2S} + \epsilon_{FeS}} . \qquad (2\text{-}10)$$

We can then apply Maxwell's equation in this manner to give the matrix conductivity.

$$\frac{\sigma_{matrix}/\sigma_{continuous} - 1}{2 \, \sigma_{matrix}/\sigma_{continuous} + 1} = \left(\frac{\sigma_{Fe}/\sigma_{continuous} - 1}{2 \, \sigma_{Fe}/\sigma_{continuous} + 1} \right) \epsilon_{Fe} - \epsilon . \qquad (2\text{-}11)$$

We shall compare the effective conductivities of the positive electrode calculated with Equations 2-9 and 2-11. After exhaustion of FeS, for the base case operating conditions in Table 2-3, $\epsilon_X = 0.55447$, $\epsilon_{Fe} = 0.08522$, and $\epsilon = 0.36030$. We calculate $\sigma_{eff} = 2050$ $(\Omega\text{-cm})^{-1}$ and 2.62 $(\Omega\text{-cm})^{-1}$ from Equations 2-9 and 2-11, respectively. If we assume, as an extreme case, that all the current is going to the second reaction, then the potential differences across the matrix phase are 3×10^{-3} mV and 3 mV for Equations 2-9 and 2-11, respectively. This does not explain, however, the ≈ 40 mV discrepancy that is discussed by Pollard and Newman.[3,4]

To summarize, Equation 2-11 is an improvement in the estimation of the matrix conductivity over Equation 2-9. However, the discrepancy between model and experimental electrode resistances is not fully explained and requires further investigation.

Equations 2-9, 2-10, and 2-11 and the appropriate derivatives required for the linearization of the Ohm's law equation are included in the computer code in a subroutine called MCOND (see Appendix A-2).

2.2.2.2. Incorporation of the J-phase Mechanism

The incorporation of the J-phase mechanism into Pollard and Newman's original computer model of the LiAl/FeS cell[3,4,5] was accomplished by Pawli-kowski.[11] This work involved a considerable reprogramming effort. The J-

phase mechanism is discussed in Chapter 1 (reactions 1 and 3) and is written as

$$26FeS + Li^+ + Cl^- + 6e^- \rightarrow J + 2Fe$$

and

$$J + 51Li^+ + 46e^- \rightarrow 26Li_2S + 24Fe + 6K^+ + Cl^- .$$
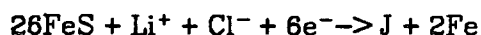
The open-circuit potentials are given by Equations 1-2 and 1-3 with the coefficients for reactions 1 and 3 in Table 1-2. As discussed in Chapter 1, the open-circuit potentials of the reactions in the J-phase mechanism relative to the LiAl electrode are dependent on electrolyte composition and temperature. In contrast, the open-circuit potentials of the reactions in the X-phase mechanism are only functions of temperature. Consequently, the surface overpotentials, $\eta_{s_l} = \eta - U_{l,o}$, for the above reactions have an additional dependence on the electrolyte composition variable, x_{LiCl}. Pawlikowski[11] also developed a more convenient electrolyte activity coefficient expression than the original expression given in Pollard and Newman's work.[3,4] This expression is given in Appendix A-3.

The voltage gap between the potential plateaus for the reactions of the X-phase mechanism does not vary with temperature as much as the potential gap for the J-phase mechanism (see Figure 1-3). Consequently, with the X-phase mechanism we assume that the gap is constant at 0.0326 V [3,4] (see $U_{1,o}$ in Table 2-1). Since the cell temperature will typically rise only about 10°C during discharge at the base case operating conditions (see Figure 3-2), this is not a bad approximation. For the J-phase mechanism, the temperature rise may be 30 to 40°C. The variation of this potential gap with temperature must be included in the model.

2.2.3. Operating Parameters

In Sections 2.3 and 2.4 we present model results for the discharge of a LiAl/LiCl-KCl/FeS cell operating with X-phase and J-phase positive-electrode mechanisms. Many of the operating parameters are the same parameters that were used in Pollard and Newman's original work.[3,4] For example, the negative electrode operating variables are unchanged, and we refer the reader to Pollard and Newman's work for these values (Figure 9 of Reference 4). Formulas for the dependency of κ, t_+^*, $\tilde{V}$, D, x_{KCl}^{sat}, and x_{LiCl}^{sat} on electrolyte composition and temperature are given in the Appendix of Pollard and Newman's work.[3,4] We give the positive-electrode kinetic parameters in Table 2-1 and the physical parameters in Table 2-2. Table 2-3 provides the operating parameters for a base case corresponding to the conditions of Figure 9 in Reference 4. Deviations from these values are noted in the figure captions. In these tables, subscripts 1 and 2 refer to the first and second reaction in the mechanism (X-phase or J-phase), respectively.

Pollard and Newman[3,4] discuss the effects of increasing the discharge current density, the initial temperature, and the electrolyte composition from a base case. Increasing T_o, x_{LiCl}^o, and decreasing i tend to decrease capacity limitations by KCl precipitation, hence increasing the utilization of the cell's active material.

2.3. Mathematical Modeling of the LiAl, FeS Cell
with the J-phase Intermediate

In this section, we discuss the results of modeling the LiAl/FeS cell with the J-phase mechanism as the positive electrode reactions. Despite the undesirability of the presence of J-phase, it is important to understand the effects that it has on cell behavior. This understanding helps us to define which factors are likely to improve the performance of the FeS electrode. The pres-

Table 2-1

Positive-Electrode Kinetic Parameters used in Models

Parameter	J-phase Mechanism Value	X-phase Mechanism Value
$\alpha_{a,l} = \alpha_{c,l}$	1.0	1.0
n_1	6.0	2.0
n_2	46.0	2.0
$s_{Li^+,1}$	-1.0	-2.0
$s_{Li^+,2}$	-51.0	-2.0
$s_{K^+,1}$	-6.0	0.0
$s_{K^+,2}$	6.0	0.0
$s_{Cl^-,1}$	-1.0	0.0
$s_{Cl^-,2}$	1.0	0.0
$(ai_o)_l$	2000. A/cm^3	2000. A/cm^3
$U_{1,o}$	-	0.0326 V
$U_{2,o}$	-	0.0 V
U_2	-	1.34 V
a_1	1.9547 V	1.3671 V
a_2	1.3398 V	1.4544 V
b_1	-6.8×10^{-4} V/K	-2.2×10^{-5} V/K
b_2	-2.4×10^{-5} V/K	-1.78×10^{-4} V/K

Table 2-2

Physical Parameters Used in Analysis

Parameter	J-phase Mechanism Value	X-phase Mechanism Value
$\tilde{V}_{LiCl}$	20.5 cm^3/mole	20.5 cm^3/mole
$\tilde{V}_{KCl}$	37.58 cm^3/mole	37.58 cm^3/mole
$\tilde{V}_{FeS}$	18.55 cm^3/mole	18.55 cm^3/mole
$\tilde{V}_{Fe}$	7.1056 cm^3/mole	7.1056 cm^3/mole
$\tilde{V}_J$, $\tilde{V}_X$	669.69 cm^3/mole	46.23 cm^3/mole
$\tilde{V}_{Li_2S}$	27.677 cm^3/mole	27.677 cm^3/mole
σ_{Fe}	8.23×10^4 (Ω-cm)$^{-1}$	8.23×10^4 (Ω-cm)$^{-1}$
σ_{FeS}	1.9×10^3 Ω-cm)$^{-1}$	1.9×10^3 (Ω-cm)$^{-1}$
σ_{Li_2S}	0 (Ω-cm)$^{-1}$	0 (Ω-cm)$^{-1}$
σ_J , σ_X	500 (Ω-cm)$^{-1}$	6.3 (Ω-cm)$^{-1}$

Table 2-3

Base Case Input Data

Quantity	Value	Quantity	Value
x_{LiCl}^0	0.58(eutectic)	$M\hat{C}_p^m/A$	1.89 J/cm²-K
$\Delta \tilde{H}_{KCl_f}^o$	26530. J/mol	i	0.0416 A/cm²
h	8.25 × 10⁻⁶ W/cm²-K	V_R^o/A	0.03 cm
T_o	743.15 K	T_A	298.15 K
Q_+	4630 C/cm³	ϵ_{FeS}^o	0.445
Q_-	2800 C/cm³	ϵ_+^o	0.555
L_+	0.18 cm	ϵ_-^o	0.39
L_-	0.32 cm	ϵ_s^o	0.75
L_s	0.16 cm	p	∞

ence of J-phase in experimental cells is believed to be undesirable because the reactions involving this phase are slow, which causes difficulties in cell charging.[8]

The model of the LiAl/FeS cell with the J-phase mechanism was developed by Pawlikowski[11] from Pollard and Newman's[3,4] model with the X-phase mechanism. There are several aspects that make the model with the J-phase mechanism more complicated than the model with the X-phase mechanism. These aspects are discussed in Section 2.2.2.1. The thermodynamics of the FeS electrode reactions are discussed in Chapter 1.

2.3.1. Electrolyte Composition Changes During Discharge

Figure 2-2 shows the mixing-cup average composition of LiCl within a cell for the case with $x^0_{LiCl} = 0.58$ and $n^0_s = 2.55$, ignoring electrolyte freezing. The cell is discharged at a constant current density of 0.0416 A/cm^2. The average composition of LiCl is calculated from the current fractions and stoichiometry of the electrode reactions and is used in the energy balance calculation (Chapter 3). The onset of the second reaction following the exhaustion of FeS is responsible for the change of slope at 11.5% utilization. The two portions of the curve are not linear, although they appear to be. The formation of J-phase by the first reaction requires potassium and results in the increasing mole fraction of LiCl prior to 11.5% utilization. Potassium ion is a product of the second reaction and results in the decrease in x^{avg}_{LiCl} from 11.5% to 100% utilization. The analogous curve for the X-phase mechanism would be a horizontal line at $x^0_{LiCl} = 0.58$.

In the simulations, the effects of diffusion, migration, convection, and nonuniform reaction distribution result in a spatial variation of electrolyte throughout the cell sandwich. The contribution of convection arises primarily from the squeezing of the electrolyte as the porosity changes. Figure 2-3 shows model calculations of composition profiles across the cell at several states-of-discharge. The values of x^{avg}_{LiCl} and n^0_s are the same as in Figure 2-2. The mathematical model predicts that the reactions do not occur simultaneously. That is, FeS is completely exhausted by the first reaction (at 11.5% utilization), before the second reaction occurs. Prior to the onset of the second reaction, the mole fraction profiles exhibit a maximum at the position of the first reaction front. In Figure 2-3, the maximum is at $y/L_{tot} = 0.88$ and 1.00 for 8% and 11.5% utilization, respectively. The composition profiles given by Pollard and Newman for the X-phase mechanism exhibit a minimum at the position of the first reaction front (Figure 2 of Reference 4). At 11.5% utilization, x_{LiCl} is high
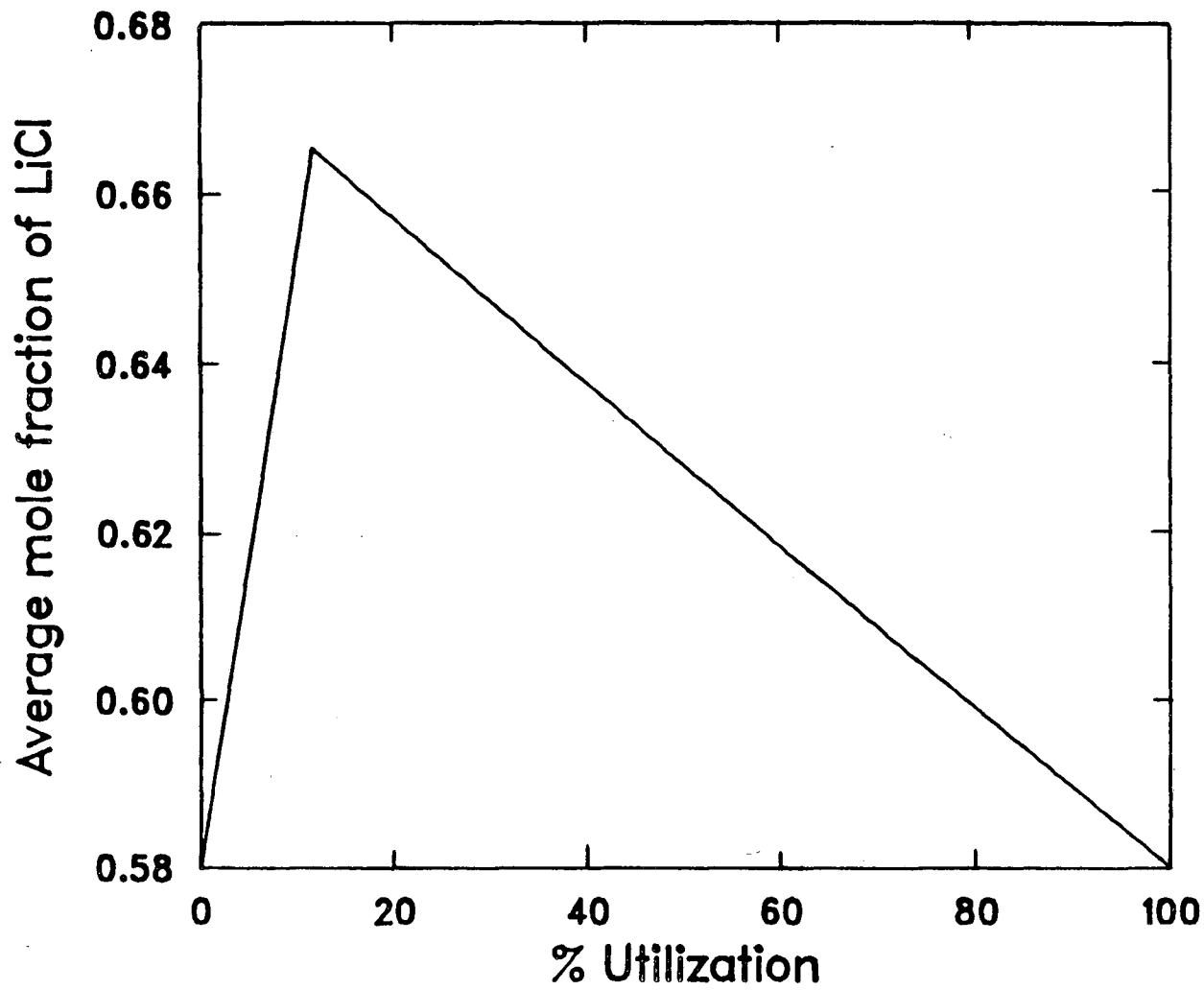
Figure 2-2. The average composition of LiCl as a function of positive electrode utilization for the J-phase mechanism (ignoring electrolyte freezing) for $x^0_{LiCl} = 0.58$ and $n^0_a = 2.55$.
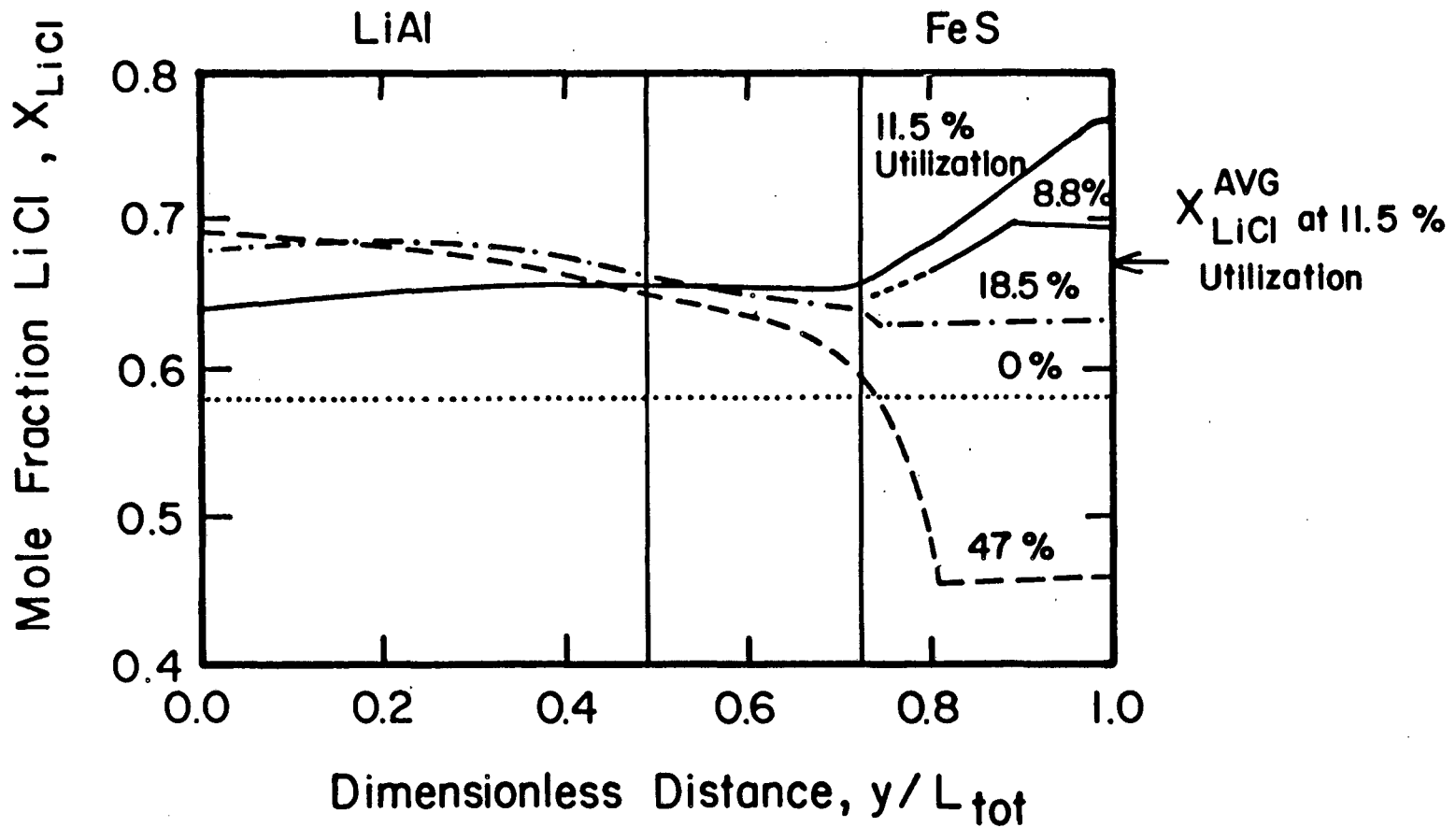
Figure 2-3. Position dependence of the mole fraction of LiCl at different states-of-discharge for the J-phase mechanism. Simulation parameters are for the base case (Tables 2-1, 2-2, and 2-3).

enough at the back of the electrode ($y/L_{tot} = 1.00$) that the second reaction begins there. Soon after 12% utilization, x_{LiCl} has decreased enough that the position of the second reaction front moves to the electrode-reservoir interface. In Figure 2-3 the position of the second reaction front is at the minimum in the composition profile for 18% and for 47% utilization. At 47% utilization the cutoff voltage is reached. The capacity-limiting mechanism for the cell is the clogging of pores by KCl precipitation in the positive electrode. For the same operating conditions, simulation of discharge behavior with the X-phase mechanism results in a much lower maximum utilization ($< 40\%$). The switching of the position of the second reaction front from the back to the front the electrode with the J-phase mechanism allows for more uniform utilization of active material and is one of the reasons for the longer cell discharge time. Even at isothermal operating conditions (all other conditions the same) the cell with the J-phase mechanism yields 45% utilization.

2.3.2. Cell Voltage Behavior

Figure 2-4 shows the cell voltage as a function of utilization, and Figure 3-1 shows the temperature behavior for the cell discussed above. In the region from 0% to 11.5% utilization, the open-circuit potential decreases because x_{LiCl} increases and the cell temperature increases. The decline of the open-circuit potential is partially responsible for the observed voltage drop in this region.

As explained in Chapter 1, we expect the J-phase mechanism to be observed in experimental cells at relatively low temperatures. For cells with a large excess of electrolyte, we would expect the J-phase mechanism to occur for temperatures less than 475.8°C. For more electrolyte-starved cells, the J-phase mechanism would occur for temperatures less than 440°C and 377°C for $n_e^o = 2.55$ and 1.0, respectively (see Figures 1-1 and 1-2). Figure 2-5 shows the voltage behavior of an experimental cell at a low enough temperature that a pure J-phase discharge mechanism should occur.[9] As mentioned previously,
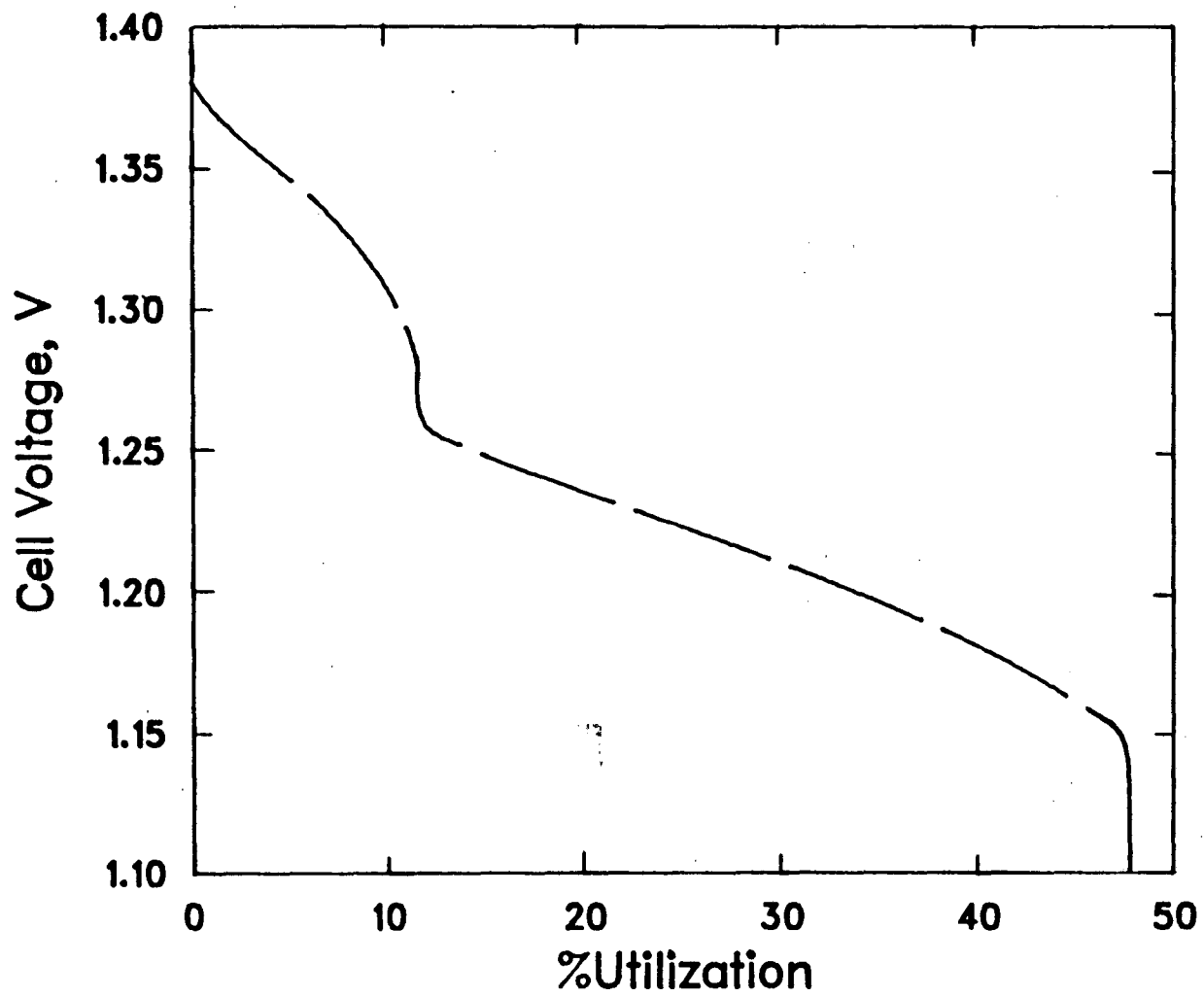
Figure 2-4. Cell voltage as a function of positive electrode utilization for the J-phase mechanism. Parameters as in Figure 2-3.
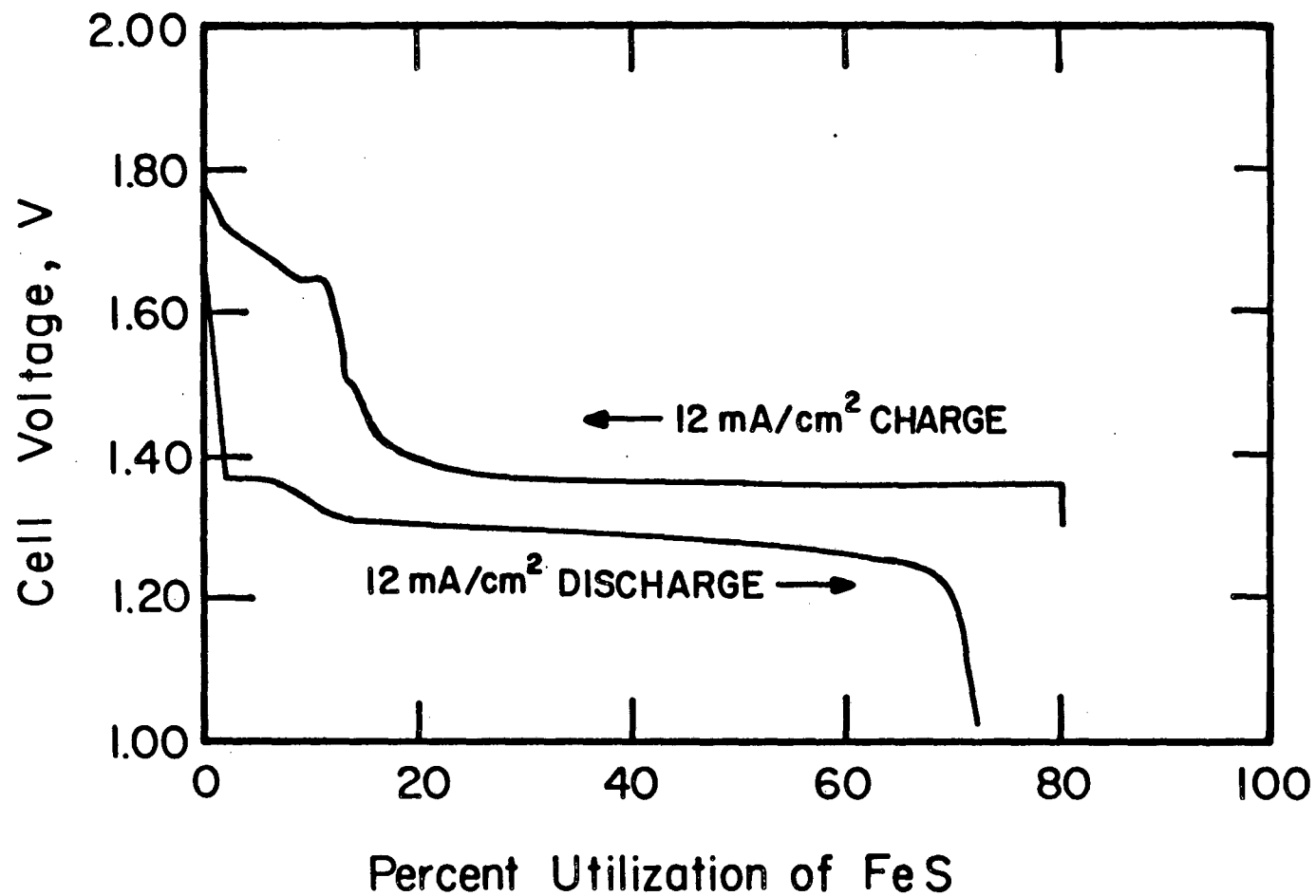
Figure 2-5. Experimental cell voltage as a function of positive electrode utiliza-
tion at 443°C using electrolyte of eutectic composition.[9]

the presence of J-phase in experimental cells is believed to be undesirable because the reactions involving this phase are slow.[8] The charge and discharge voltage behaviors are asymmetric in experimental cells that operate with the J-phase mechanism and are more symmetric with the X-phase mechanism. In other words, the cells operating with the J-phase mechanism are difficult to charge. The cell was charged to 1.78 V; consequently, the the initial high voltage during discharge may be due to over-charging. The following two plateaus during discharge correspond to each reaction in the J-phase mechanism. A maximum utilization of 73% is observed. At these operating temperatures and the conditions of Figure 2-4, our mathematical model would predict the cutoff voltage to be reached before 47% utilization. The capacity limitations, which are caused in the model by KCl precipitation, are discussed in Section 2.4.

Although the model is not capable of simulating the other possible reactions along with the J-phase mechanism, it is interesting to examine whether the occurrence of these other reactions becomes thermodynamically possible. The model predicts that the overpotential within the positive electrode is not great enough for the conversion of FeS to X-phase to occur. This is in harmony with experimental observations at these operating conditions. In the model, we assume that J-phase is directly converted to Li_2S and Fe in a single reaction, and the onset of this reaction is predicted to occur at 11.5% utilization. The J-phase to X-phase transition would occur at this utilization if the model had the capability of simulating this reaction. Then, the reactions of J-phase and X-phase being converted to Li_2S and Fe would occur as the overpotentials within the electrode became greater. A mathematical model including the five possible positive electrode reactions may predict a larger maximum utilization than the models with only the J-phase mechanism and the X-phase mechanism. The incorporation of more reactions will allow more uniform utilization of active

material. This will tend to delay the precipitation of KCl in the positive electrode and increase the maximum utilization of the cell.

2.4. The Effects of KCl Precipitation on
Positive-Electrode Utilization

2.4.1. Capacity-Limiting Mechanisms

The principal capacity-limiting mechanism predicted by the mathematical models is the plugging of the porous positive electrode with KCl precipitate. This causes the cell voltage to drop sharply to the cutoff point at relatively low utilization (< 60%). In contrast, experimental cells operating under similar conditions exhibit much longer lifetimes (> 80% utilization) and smoother voltage declines to the cutoff point. Crystals of KCl have been observed in experimental cells discharged at approximately 430°C.[8] It appears, however, that the models either severely overestimate the effects of precipitation or predict the precipitation prematurely. There are many possible explanations for the discrepancy between theoretical and experimental results, and Pollard and Newman[3,4] examine them in their work. The authors conclude that mixing by natural convection, supersaturation, and local heat effects are unlikely explanations for the discrepancy. Other possible reasons are electrode expansion, precipitate morphology and its effects on the reaction distribution, modification of the solubility limit by impurities, and possible conductivity of the KCl precipitate. The first two reasons will be discussed in Sections 2.3.2 and 2.3.4. The last two reasons will be addressed in the following discussion.

Figure 2-6 shows the predicted cell voltage behavior for a cell with the solubility limit modified such that precipitation does not occur at all during discharge. The results of Figure 2-6 are discussed by Pollard and Newman (Figure 9 of Reference 4) and are more representative of the behavior that is
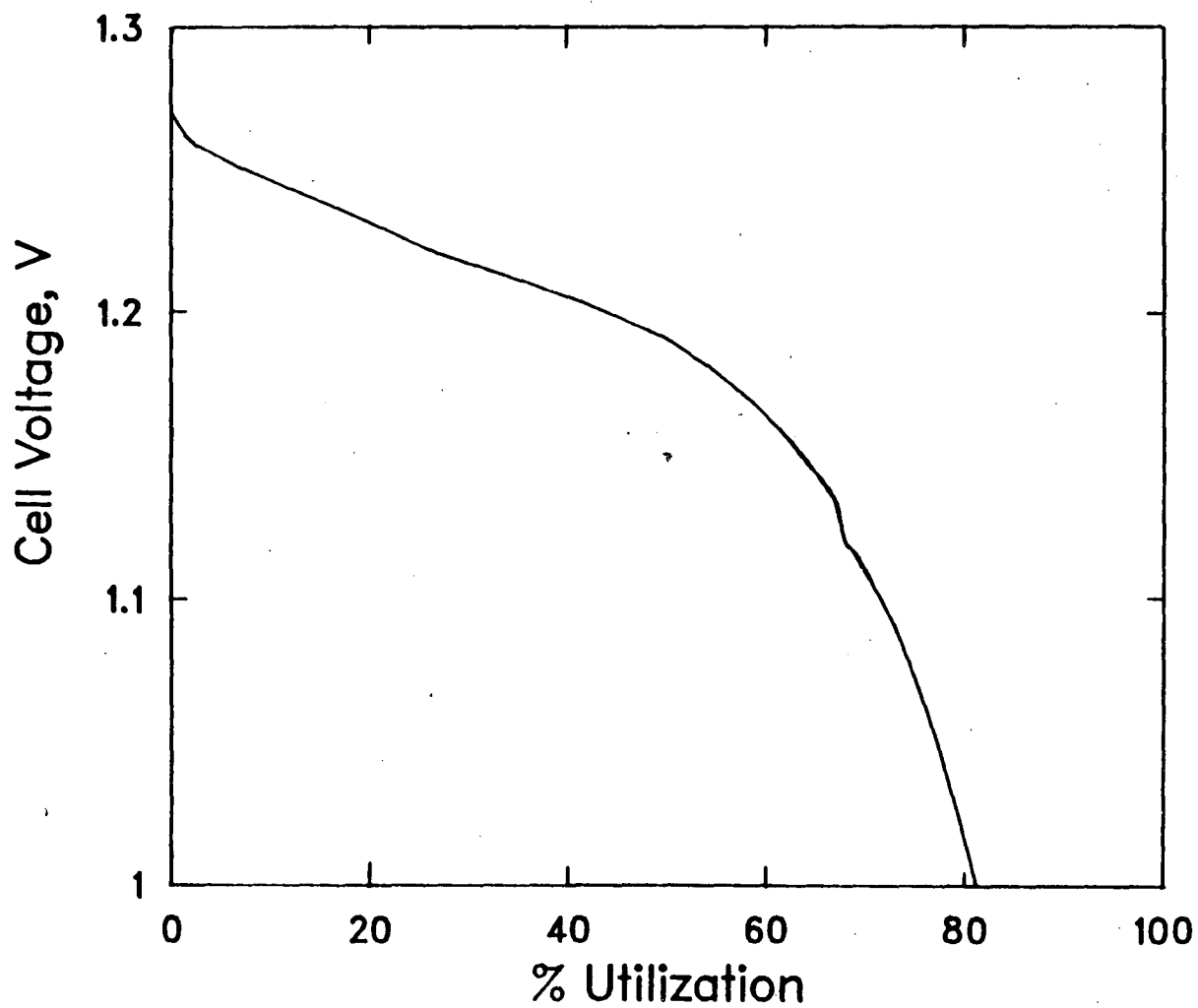
Figure 2-6. Cell voltage as a function of positive electrode utilization for the X-phase mechanism without KCl precipitation. Simulation parameters are for the base case except x_{KCl}^{sat} (Tables 2-1, 2-2, and 2-3).

observed in experimental cells than model results with precipitation. As shown by Pollard and Newman, the model results are in excellent agreement with experimental results from 40% to 70% utilization. The discrepancy from 0% to 40% utilization may in part be explained by the occurrence of reactions 1 and 2 of Table 1-1 which are not included in the X-phase mechanism. This may be seen by examining Figure 1-3. It is possible that the experimental cell exhibited capacity limitations by KCl precipitation at ≈ 70% utilization. This may explain the sharp voltage decline, relative to the model results, from 70% utilization to the cutoff point at 74% utilization. Increasing the x_{KCl}^{sat} by about a factor of 1.2 throughout discharge would predict capacity limitations by precipitation at ≈ 70% utilization. At 70% utilization the maximum x_{KCl} is 0.65; the saturation mole fraction of KCl is 0.55.

One other point to consider is relaxing the assumption that the KCl precipitate is completely insulating. If the precipitate were about as conductive as the electrolyte, we would expect the cell voltage behavior to be similar to the results in Figure 2-6. However, the transference number of lithium should be zero in the precipitate.

For the simulation shown in Figure 2-6, KCl precipitation would normally be observed at 28.3% utilization, and the second reaction begins at 28.4% utilization. In a simulation at the same conditions except the cell is discharged isothermally, precipitation occurs sooner, at 24.7% utilization. The discontinuity observed at 66% utilization is where the FeS is fully exhausted. At this point, the amount of current going to the second reaction goes from 65% to 100%. After this, the cell voltage continuously decreases to the cutoff voltage at 81% utilization. In this case, the capacity-limiting mechanism is the increasing ohmic limitation caused by the increasing thickness of the fully reacted region. The region is composed of Li_2S and Fe and has a relatively low porosity of 0.166.

2.4.2. The Precipitation Parameter

The precipitation of LiCl or KCl salts may affect the rates of the electrochemical reactions occurring within the pores of the electrode. This is accounted for by assuming that the exchange current density for an electrode reaction is related to the amount of precipitate by the expression,

$$i'_{o,l} = i_{o,l} \left[1 - \left(\frac{\epsilon_p}{\epsilon + \epsilon_p} \right) m \right],$$

where m is an adjustable parameter. Notice that the exchange current density is decreased with an increase in the amount of precipitate. The morphology of the precipitate is reflected by the value of m. For instance, if m is zero, then a passivating film-type precipitate is implied, and the electrode reactions cannot occur in the region of precipitation. The reaction rates are not affected by precipitation if m is very large. This may describe the case of a passivating salt that forms a very thin, needle-like precipitate. We would expect more utilization of active material as the value of m is decreased from infinity. For example, for the X-phase mechanism, when m is decreased from infinity to 1.0 to 0.5, the maximum utilization increases from 52.1 to 53.6% to 55.4%. For very small values of m, however, the maximum utilization of the cell decreases; in the limit of $m = 0$, utilization of active material halts in the region of precipitation. We have not investigated results with m smaller than 1/3.

The high temperatures and high values of $i_{o,l}$ for this system cause rapid, localized reactions to occur within the electrode. As a result, a highly nonuniform reaction distribution results. Figure 2-7 shows a smoothed plot of the transfer current distribution for the first reaction of the X-phase mechanism for two values of m. A reaction front gradually moves through the electrode as active material is consumed. KCl will precipitate in the region of highest transfer current. If the precipitate is allowed to inhibit the electrode reaction,
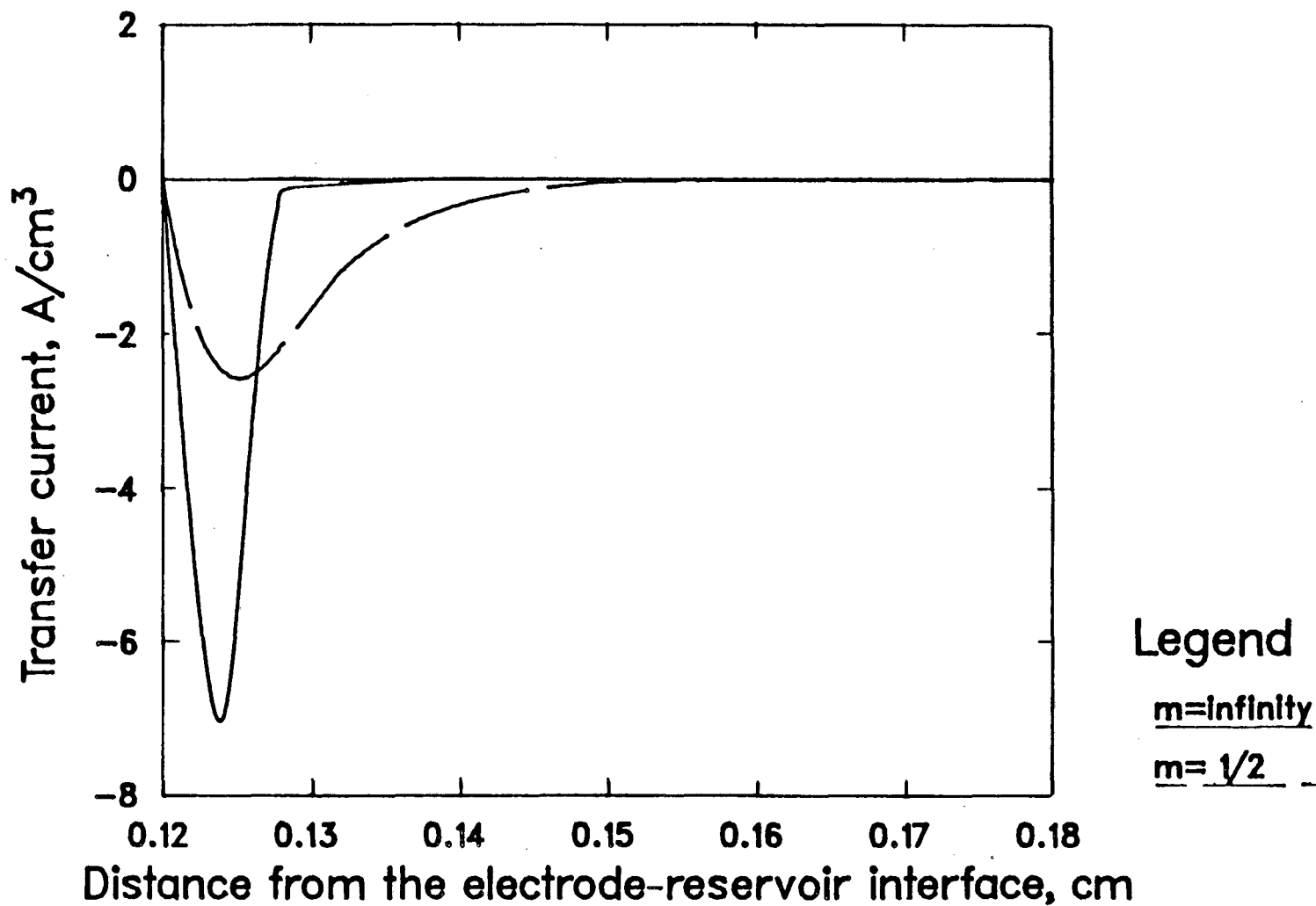
Figure 2-7. Transfer current distribution in the positive electrode for the first reaction of the X-phase mechanism for two values of m. Simulation parameters are for the base case except m.

then we would expect the reaction front to be more spread out within the electrode. In other words, by decreasing m a reaction will be more uniformly distributed. As shown in Figure 2-7, the reaction front is thicker for the case of $m = 0.5$ than for $m = \infty$. The precipitated regions correspond approximately to the thickness of the fronts. The thicker reaction front has precipitate distributed more uniformly and the porosity is larger than the case with the thin reaction front. For the case of $m = \infty$, the transfer current is actually slightly positive in back of the reaction front (~0.14 cm). This phenomenon of bipolarity is not observed at this utilization for the case of $m = 0.5$. At this degree of utilization (38.2%), the reaction front is at the same position for both cases, and the first reaction uses approximately 60% of the current.

Figure 2-8 shows the position of the first reaction front as a function of utilization. Prior to the onset of precipitation at 26.0% utilization, the reaction distributions are identical. In both cases, the bending downward of the curves (slowing down of the front), indicates the occurrence of the second reaction. In the region from 28% to 38% utilization, we see that the reaction front for the case of $m = \infty$ moves slightly faster through the electrode than for the case of $m = 0.5$. We expect this because the smaller value of m should allow more uniform utilization of the active material, and the second reaction has not yet occurred to an appreciable extent. Later in the discharge, the precipitation of KCl and the simultaneous reactions in the positive electrode interact to cause oscillatory behavior. This will be discussed in Section 2.4.4. At approximately 38% utilization, the reaction front with the large m value slows down, halts at 47.4% utilization, and reaches the cutoff voltage (1.0 V) at 52.1% utilization. The same capacity-limiting mechanism usually occurs for the smaller value of m; however, a greater depth of discharge is achieved (55.4% for $m = 0.5$ versus 52.1% for $m = \infty$) before the cutoff voltage is reached. The more uniform reaction distribution is responsible for the longer discharge-time of this cell.
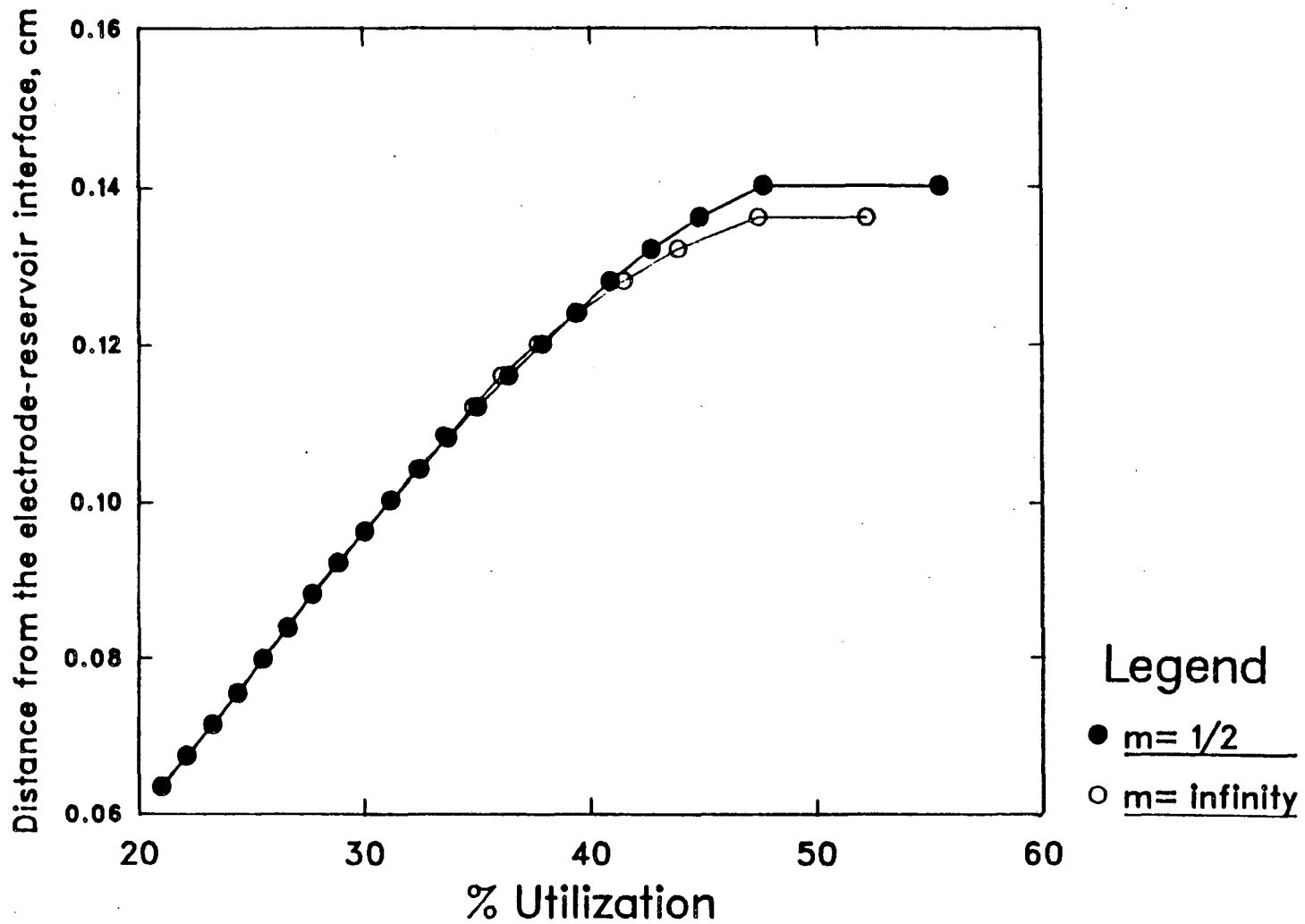
Figure 2-8. Position of the reaction front in the positive electrode for the first reaction of the X-phase mechanism as a function of percent utilization of FeS. Simulation parameters are for the base case except m.

Figure 2-9 shows the cell voltage behavior for the J-phase mechanism and two values of m. When m is decreased from infinity to 0.5, the maximum utilization increases from 47% to 51%. The point where the two curves diverge corresponds to the onset of precipitation. It should be noted that there is a large temperature excursion during discharge at these operating conditions. Figure 3-1 gives the temperature profile for the case of $m = \infty$. The temperature profile for the case of $m = 0.5$ is identical to the case of $m = \infty$ up to 47% utilization. With an initial porosity of 0.60, the maximum utilization increases from 58.8% to 60.0% when m is decreased from infinity to 0.5.

2.4.3. The Initial Porosity of the FeS Electrode

The results of modeling both the X-phase and J-phase mechanisms show that increasing the initial porosity of the FeS electrode gives an increase in the cell utilization. One reason for this is that the increased pore volume allows more precipitation before the pores are blocked and the cell voltage drops to the cutoff point. The electrolyte concentration profile and reaction distributions throughout the electrode are also affected. In practice, highly porous electrodes with good mechanical stability are difficult to construct. Electrode expansion is observed experimentally and is not accounted for in the models. Later, we will relate the results of varying the initial porosity to the expansion phenomenon.

2.4.3.1. Results for the X-phase Mechanism

Figure 2-10 shows the cell voltage versus utilization for three values of the initial porosity of the FeS electrode (X-phase mechanism). All three cells have the same positive-electrode capacity (833.3 C/cm^2) so that an increased porosity corresponds to a thicker electrode. For a given utilization, the case with the largest ϵ_0^s gives the highest cell voltage. This is primarily an ohmic resistance effect in the electrolyte phase (which is more resistant to current flow than the
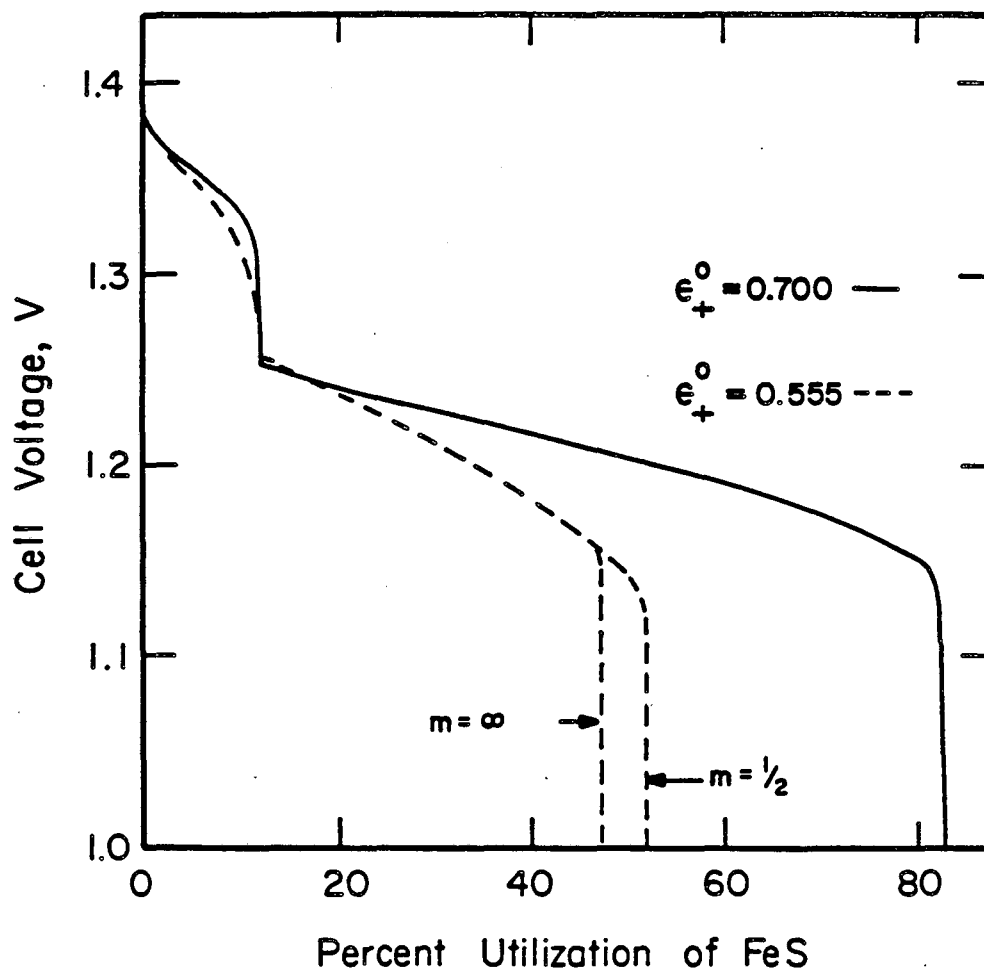
Figure 2-9. Cell voltage as a function of positive electrode utilization for the J-phase mechanism for two values of m and ϵ_+^o. Simulation parameters are for the base case except m and ϵ_+^o.
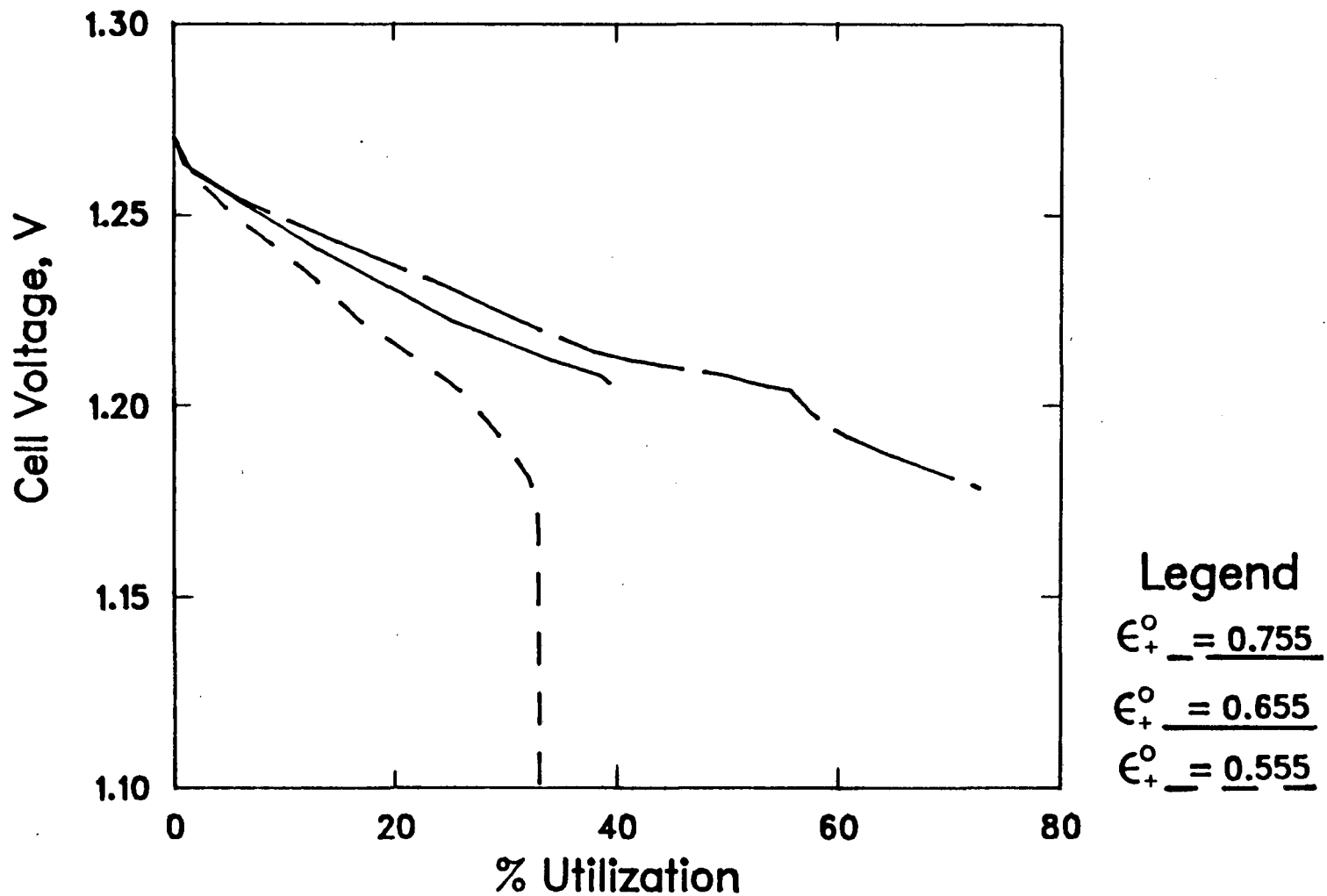
Figure 2-10. Total cell voltage as a function of positive electrode utilization for the X-phase mechanism for three values of ϵ_+^o. Simulation parameters are for the base case except for ϵ_+^o, L_+, and $\tilde{V}_X$. $\tilde{V}_X$ = 56.24 cm^3/mole and, L_+ = 0.232 and 0.328 cm for ϵ_+^o = 0.655 and 0.755, respectively. Heat transfer characteristics have been modified and allow for slightly more cooling than the base case.

matrix phase); the current in the pores must follow a more tortuous path for the case with $\epsilon_+^o = 0.555$ than for the case with $\epsilon_+^o = 0.755$.

The onset of the second reaction occurs at 18%, 28%, and 35% utilization for the cases with $\epsilon_+^o = 0.555$, 0.655, and 0.755, respectively. For the reversible cell discharge discussed previously, the second reaction begins at 50% utilization. For the case of $\epsilon_+^o = 0.555$, the onset of the second reaction occurs at the time of KCl precipitation. Figure 2-11 shows the porosity distribution throughout the cell for various states of discharge. The drop in porosity is due to the large molar volume of the X-phase intermediate in this simulation. Eventually, two areas of precipitation form, one at each reaction front, and by 33% utilization the cutoff voltage is reached. The two spikes downward in Figure 2-11 represent these two areas of precipitation. Precipitation is delayed in a more porous electrode because KCl can more easily diffuse from regions of high to low concentrations, resulting in a more uniform concentration profile. The onset of precipitation is observed at 28% and 41% utilization for the cases of $\epsilon_+^o = 0.655$ and 0.755, respectively. The porosity of the electrode also affects the reaction distribution. At 10% utilization, the transfer current at the position of the reaction front is four times larger for the case of $\epsilon_+^o = 0.655$ than for the case of $\epsilon_+^o = 0.755$. This lowering of the transfer current also works to delay precipitation. The discontinuity in slope observed at 56% utilization on Figure 2-10 for the case of $\epsilon_+^o = 0.755$ corresponds to FeS exhaustion. At this point, the amount of current going to the second reaction changes from 42% to 100%. Again, this would occur at 50% utilization if the cell were discharged reversibly. The highly exothermic second reaction increases the cell temperature enough from this point on so that all the precipitate melts. The temperature of the cell at 72% utilization is 486°C. The initial temperature of the cell is 470°C. This simulation was not carried out to the 1.0 V cutoff; however, it appears that KCl precipitation may not be the capacity-limiting mechanism.

Negative Electrode   **Separator**   **Positive Electrode**

0 % Utilization

11.5 %

33 %
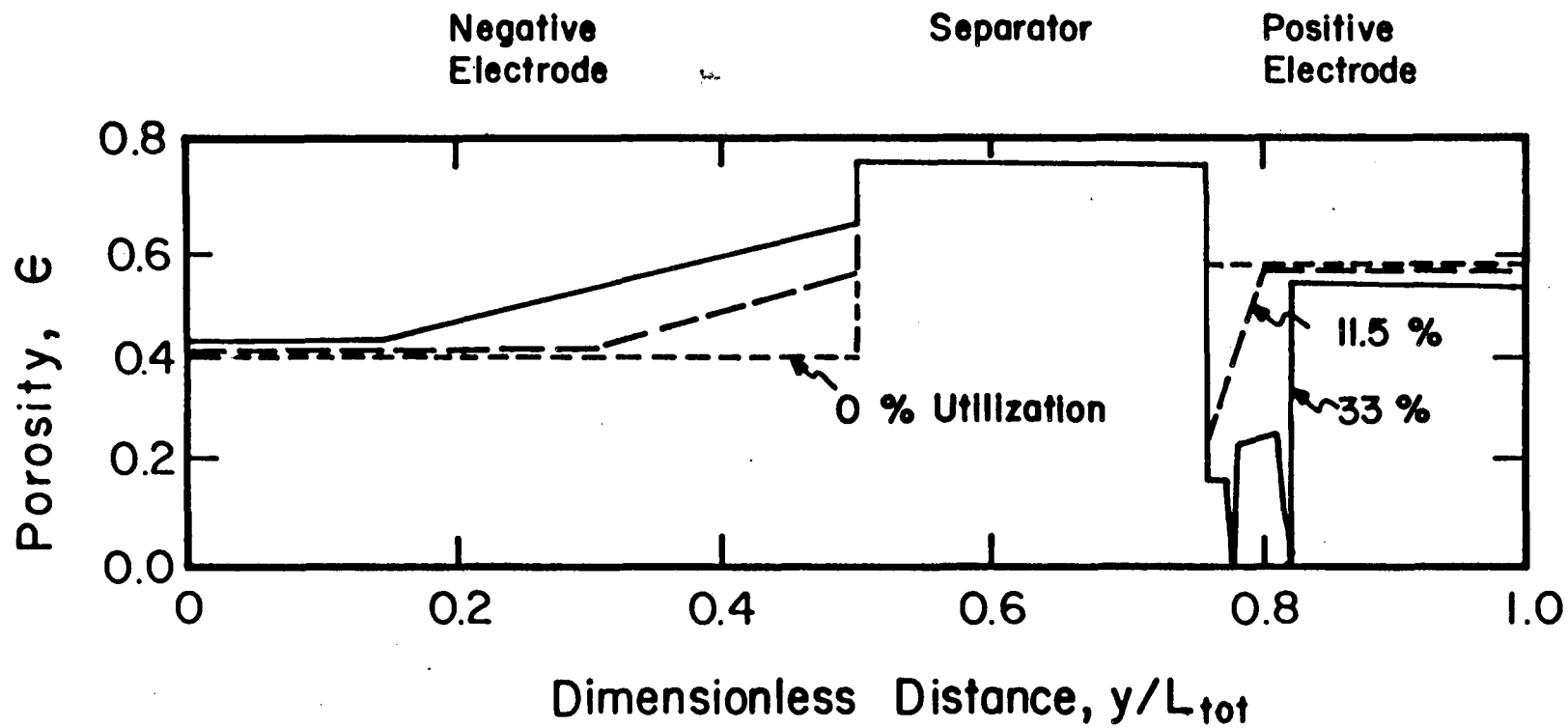
Figure 2-11. Position dependence of porosity at different states-of-discharge for the X-phase mechanism. Simulation parameters as in Figure 2-10 with $\epsilon_+^0 = 0.555$.

2.4.3.2. Results for the J-Phase Mechanism

Figure 2-9 shows the cell voltage versus utilization for the J-phase mechanism and two values of ϵ_+^0 ($m = \infty$). We see that an increase in the initial porosity of the positive electrode from 0.555 to 0.700 increases the cell utilization from 47% to 83%. The capacity-limiting mechanism in both cases is the blockage of pores by KCl precipitate in the positive electrode. The precipitation of KCl occurs at 45% and 75% utilization for the case of $\epsilon_+^0 = 0.555$ and 0.700, respectively. Unlike the results for the X-phase mechanism, the cell reaches the cut-off voltage just after the onset of precipitation. Two considerations lead to an explanation as to why the precipitation has such a drastic effect with the J-phase mechanism relative to the X-phase mechanism results. Unlike the X-phase mechanism, the first reaction of the J-phase mechanism is more exothermic than the second. Figure 3-1 shows the temperature profile for the simulation of the J-phase mechanism with $\epsilon_+^0 = 0.555$ ($m = \infty$). Furthermore, KCl is a product of the second reaction.

We will now investigate the results of varying ϵ_+^0, which can help aid in the understanding of the effect that positive-electrode expansion has on experimental cells. Our mathematical model does not account for electrode swelling during discharge. The model assumes that as the solid phase expands during discharge, the positive electrode becomes less porous. Similarly, the negative electrode's active material shrinks during discharge, and the electrode becomes more porous (see Figure 2-11). The model predictions of lower utilization than is observed experimentally can, in part, be explained by expansion of the positive electrode. Pollard and Newman[3,4] use the value of $\epsilon_+^0 = 0.555$ for their model in their comparison to experimental cell discharge behavior. This initial porosity corresponds to a capacity density of 1.286 A-hr/cm^3 ($\epsilon_{eS}^\beta = 0.445$) and can be compared to the value of 1.4 A-hr/cm^3 ($\epsilon_{eS}^\beta = 0.484$, $\epsilon_+^0 = 0.516$) that is used in the construction of the experimental cells.[1] Pollard and

Newman used the slightly larger initial porosity in an attempt to account for the swelling of the positive electrode. More recently, experimental measurements of the positive electrode expansion have been made; it appears that the expansion is greater than originally assumed.

In experimental cells, the phase changes that occur during discharge-charge cycles subject the active-material solids to forces that tend to cause an electrode to expand and disperse particles out of the electrode boundary. This extrusion of material may cause bridging of the electrodes and short circuit. Short circuit has been a primary mode of failure in experimental cells, but it can be circumvented by improved mechanical construction of the electrodes.[1] Experimental cells are usually constrained at the faces and edges in an attempt to prevent expansion. Cells that are examined after discharge-charge cycles usually exhibit expansion of both the positive and negative electrodes, relative to the size of the as-fabricated electrodes.[1] Elliott and Cooper[18] studied the change in thickness of a cell sandwich (assembled in the fully charged state) over eight discharge-charge cycles. The cell exhibited a large initial, permanent expansion during the first three discharge-charge cycles which is ascribed to expansion of the positive electrode. From the third to the eighth cycle, a cyclic expansion-contraction discharge-charge pattern was observed. It seems reasonable to conclude from these results that positive electrodes in experimental cells expand most in the first few cycles and maintain a steady average thickness for the remainder of cycle life. This may explain why the maximum utilization during discharge is usually low for the first cycle, increases during the break-in cycles, and is relatively constant thereafter.[1] We can define the percent expansion of the positive electrode during n cycles as the percent increase in thickness over the original thickness:

$$\% \text{ Expansion} = 100 \, \frac{L_+^n - L_+^1}{L_+^1}.$$

L_+^T refers to the total electrode thickness in a cell like the one that is mathematically modeled or the half thickness of the electrode in a bicell (two outer negative electrodes with a positive electrode in between). We can define the percent expansion in terms of porosity in the charged state ϵ_+^o from the relationships: $\epsilon_{FeS}^{o,1} L_+^{o,1} = \epsilon_{FeS}^{o,n} L_+^{o,n}$ (the theoretical capacity remains constant) and $1 - \epsilon_{FeS}^{o} = \epsilon_+^o$. The superscript o implies that the porosity is that of an electrode in the fully charged state.

Quantitative measurements of positive electrode expansion at the end of cycle life are available.[1] Positive electrodes that were assembled with 0.155 cm half-thicknesses and $\epsilon_+^{o,1}$=0.53 were observed to expand 16, 23, and 29% after 804, 1031, and 559 cycles, respectively. We calculate: $\epsilon_+^{o,804} = 0.60$, $\epsilon_+^{o,1031} = 0.62$, and $\epsilon_+^{o,559} = 0.64$. With this information, we can speculate that well-cycled cells really operate with charged state porosities between 60 and 65% even though the as-fabricated porosity is only 53%. Experimental data of the positive electrode expansion within a cycle is also available and will be discussed later.

Figure 2-12 gives mathematical model predictions for the maximum utilization of a cell discharged through the J-phase positive-electrode mechanism versus the initial porosity of the positive electrode. All the simulations have the same capacity, heat-transfer characteristics, and capacity-limiting mechanism (KCl precipitation). At first we will concentrate on the 0% expansion line. We have assumed that in this range there is a linear relationship between the maximum utilization and ϵ_+^o as shown by the solid dots on the figure. There are data available for positive electrodes in bicells with half-thicknesses of 0.155 cm. These cells were fabricated with an initial porosity of $\epsilon_+^{o,1} = 0.53$ which corresponds to a capacity density of 1.358 A-hr/cm^3 (4889 C/cm^3) and capacity per unit area of 757.9 C/cm^2. As a first example, we can use Figure 2-12 to estimate 41.6% for the maximum utilization of this cell.
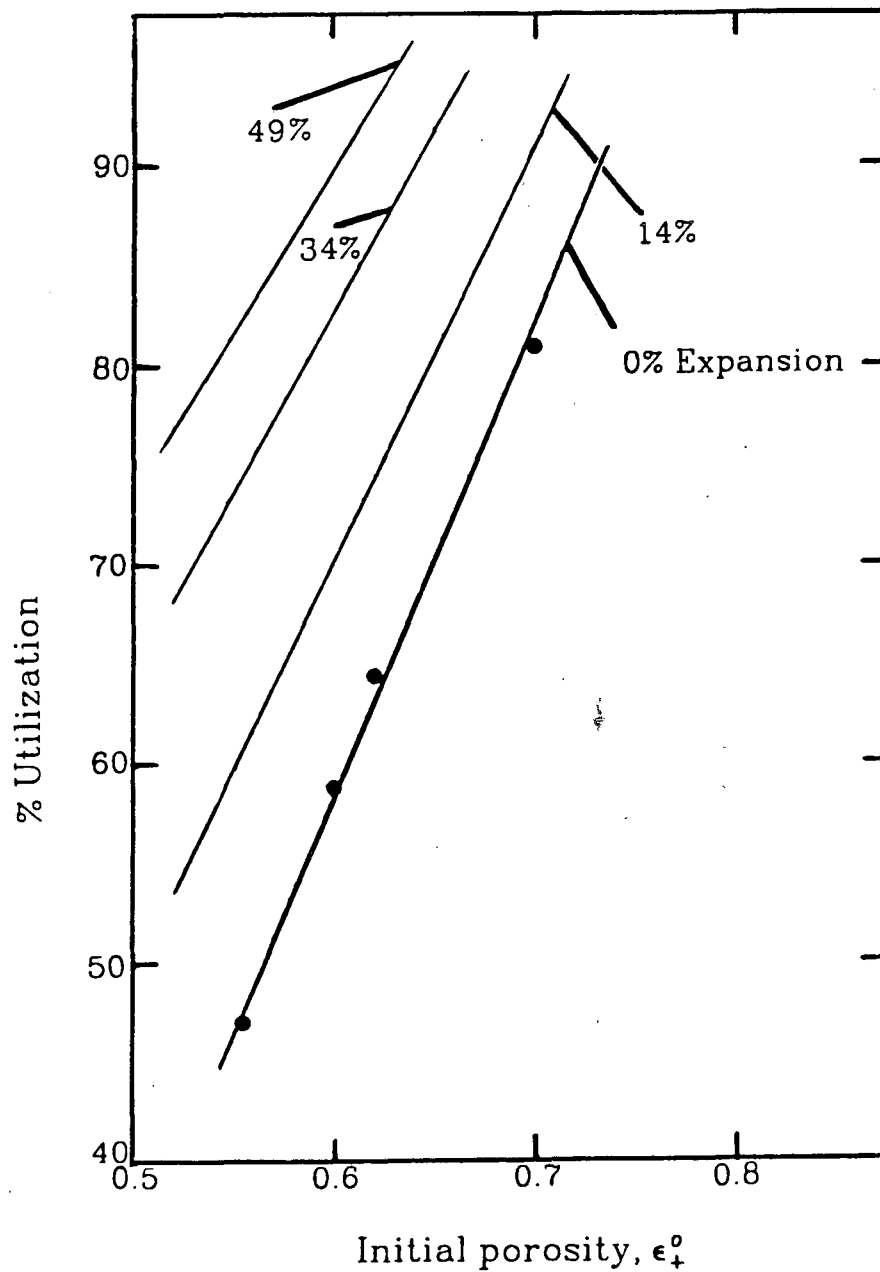
Figure 2-12. Maximum positive electrode utilization as a function of ϵ_+^0. The points are simulation results.

Now let us assume that the cell was observed in the fully charged state after 130 cycles, and the positive electrode had expanded 14% from the as-fabricated electrode. That is, the electrode half thickness was measured as 0.1767 cm, and the capacity density decreased to 1.191 A-hr/cm^3 (4289 C/cm^3). Of course, the capacity per unit area remained constant at 757.9 C/cm^2. The porosity $\epsilon_p^{.131} = 0.5877$ allows us to predict the cell to achieve 55% utilization on the 131st discharge. In the preceding development, we have tried to account for the permanent expansion of the positive electrode. In the next few paragraphs we will try to account for the expansion of the positive electrode that is cyclic, not permanent.

Figure 2-13 presents graphically the average percent expansion during discharge and charge of a series of experimental cells.[1] All of the cells are well-cycled and exhibit a steady expansion-contraction pattern during discharge-charge cycles. The figure shows that the average positive electrode exhibits a permanent expansion of 14% (in the fully charged state) over the as-fabricated electrode (also in the fully charged state). The average cell has expanded 49% at the end of discharge.

The information in Figure 2-13 can be used to interpret the information in Figure 2-12 more liberally. One may predict the maximum utilization of a cell accounting for expansion of the positive electrode during a discharge. In the previous discussion, we saw that, relative to the as-fabricated electrode, a well-cycled electrode is 14% expanded in the fully charged state and 49% expanded in the discharged state. We might expect that the simulation of well-cycled LiAl/FeS cells should allow for expansion somewhere in the range of 14 to 49%. If 14% expansion is assumed, Figure 2-12 yields the underestimated prediction of 55% utilization, and if 49% expansion is assumed we would expect an overestimated prediction of the maximum utilization. If we assume 49% expansion from the as-fabricated electrode, the electrode half thickness would be 0.2310
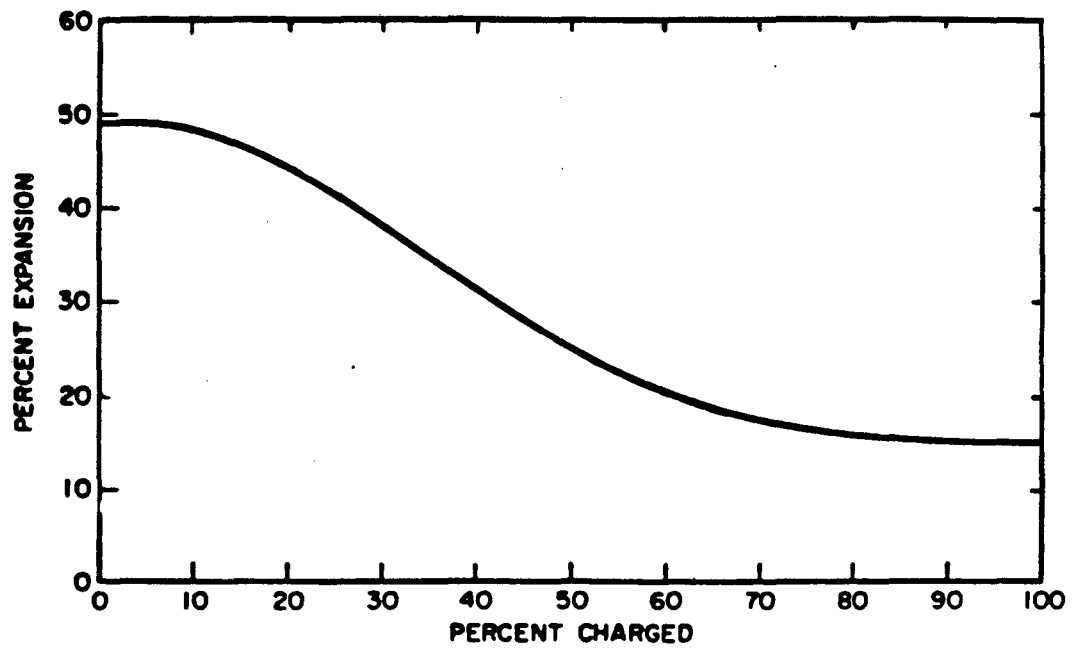
Figure 2-13. Average positive-electrode expansion of a series of experimental cells as a function of state-of-charge.[1]

cm, and the capacity density would have decreased to 0.912 A-hr/cm^3 (3281 C/cm^3). Of course, the capacity per unit area remains constant at 757.9 C/cm^2. The porosity $\epsilon_+^{0,131} = 0.6846$ allows us to predict the cell to achieve 78.3% utilization on the 131st discharge.

A compromise value of expansion, between 14 and 49%, would yield the predicted maximum utilization between 55% and 78.3%. We may speculate that the compromise expansion value should lie closer to the value of 49% than 14% because KCl causes limitations of utilization in the latter stage of discharge. The choice of a compromise of 34% expansion corresponds to a positive electrode half thickness of 0.2077 cm and a capacity density of 1.014 A-hr/cm^3 (3649 C/cm^3). For this example, we can calculate $\epsilon_+^{0,n} = 0.6493$, and the value of 69.8% utilization of FeS is predicted. The lines for various values of percent expansion in Figure 2-12 have been added as a convenience.

As mentioned earlier, experimental cells typically achieve 80% utilization of FeS during discharge. Our mathematical model results (Figure 2-12) give 80% utilization of FeS with $\epsilon_+^{0,n} = 0.69$, or an electrode that has expanded 51.6% from the as-fabricated electrode. Since this degree of expansion is not in the range of 15 to 49%, we should conclude that we have not fully accounted for the discrepancy in maximum utilization between experimental and theoretical results with expansion. The precipitation parameter (Section 2.4.2) may account for the remaining discrepancy. Recall that the model used in plotting Figure 2-12 had the precipitation parameter $m = \infty$. The results of Figure 2-9 show that for the case of $m = \frac{1}{2}$, the model gives a larger maximum utilization of the positive electrode than the case with $m = \infty$. We can conclude that the simulation of well-cycled LiAl/FeS cells should allow for expansion by using values of ϵ_+^0 between 0.59 and 0.68 and a compromise value of 0.65 is recommended.

Future modeling efforts should account for the variations in positive and negative electrode thicknesses during discharge. Experimental data of the electrode thickness as a function of time[1] could be incorporated into the model.

2.4.4. Capacity-limiting Mechanisms and Oscillatory Behavior

The primary capacity-limiting mechanism predicted by the mathematical models is the clogging of pores by KCl precipitate in the positive electrode. In the case of the X-phase mechanism, precipitation effects along with the simultaneous reactions in the positive electrode can cause oscillatory behavior. Figure 2-14 shows the current density for the first reaction of the X-phase mechanism as a function of utilization for a cell being discharged isothermally at 470°C. The points represent time steps; the cell current is 0.0416 A/cm^2. Precipitation and the second reaction are first observed at 31.5% utilization and 35.1% utilization, respectively. Precipitation is localized in the region of the first reaction zone. The ohmic limitations caused by the local porosity reduction allow the second reaction to occur (represented by the approach to a minimum in Figure 2-14) in a reaction front located near the electrode-reservoir interface. This gives time for the precipitate to melt, opening the pores and allowing the first reaction to resume again (represented by the approach to a maximum in Figure 2-14). This process is repeated and results in the oscillatory behavior. At times, the current maxima are greater than the overall cell current because of a bipolar electrode effect wherein the second reaction operates anodically near the electrode-reservoir interface. The oscillatory behavior is more complicated if the cell is discharged nonisothermally (moderately well-insulated). The second reaction has a relatively large heat effect and causes the cell temperature to oscillate along with the partial current of the second reaction. The cell voltage oscillates over a few millivolts also, with the same frequency as the partial current oscillations.
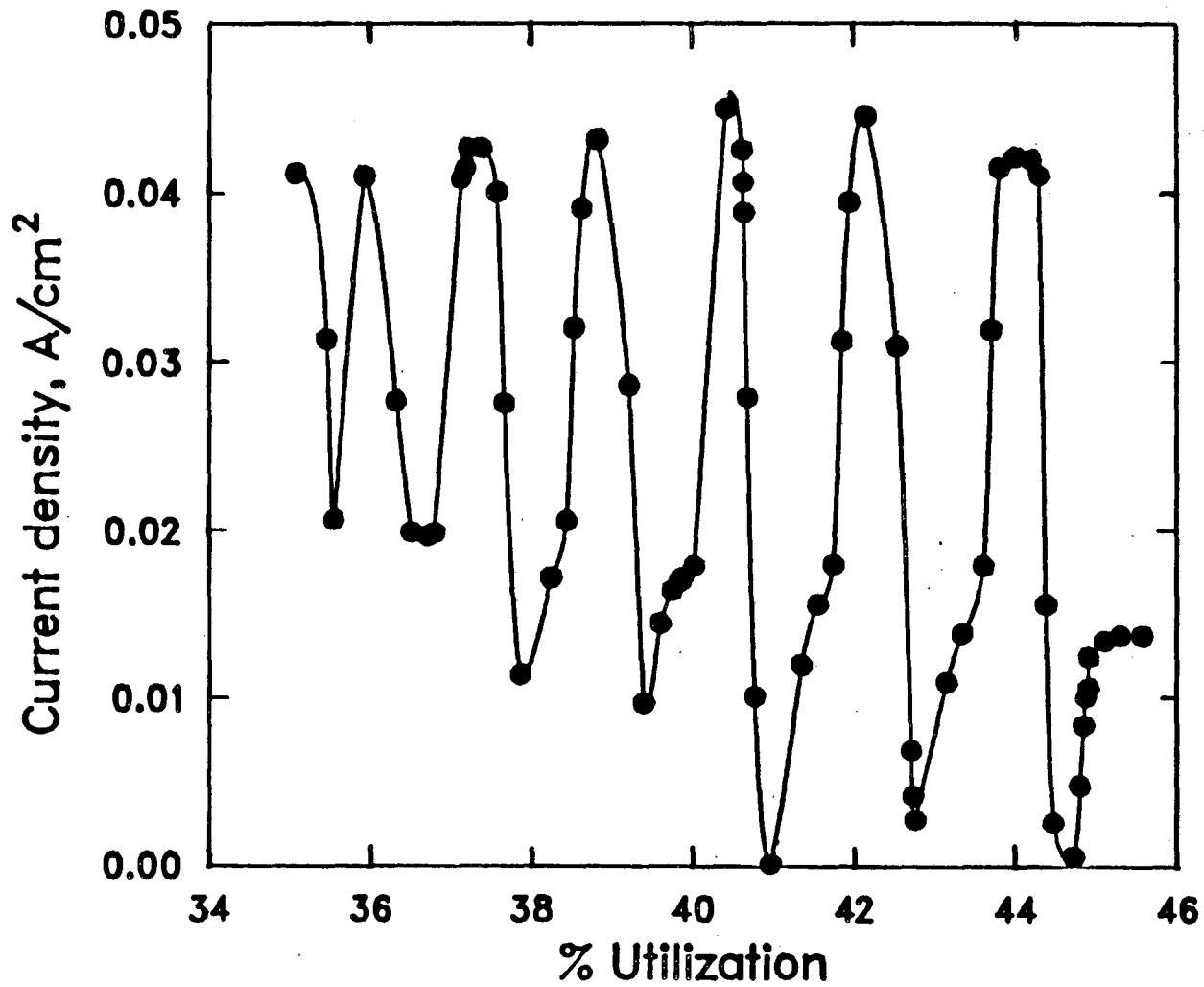
Figure 2-14. Partial current density for the first reaction of the X-phase mechanism as a function of positive-electrode utilization. Simulation parameters are for the base case except that the cell is operated isothermally at 470°C, $m = 1/3$, and $\epsilon_+^0 = 0.655$.

The oscillatory behavior is not observed when the cell is discharged without precipitation (see Figure 2-6). The behavior is also not observed with the J-phase mechanism because FeS is exhausted by the first reaction prior to the onset of precipitation. The involvement of potassium in the first reaction works to delay precipitation, and the voltage plateaus for the J-phase mechanism are more widely separated than those for the X-phase mechanism so the reactions do not occur simultaneously.

The oscillations predicted by the X-phase model are probably not observed experimentally for the same reasons that the models overestimate the effect of precipitation in general. Doubling the number of mesh points in the positive electrode results in essentially the same behavior. It is interesting that the heat-generation rate is particularly sensitive to the oscillations, as shown in Figure 2-15.

2.5. Conclusions

Mathematical models that describe the LiAl/LiCl-KCl/FeS cell with two possible discharge mechanisms have been developed. The models can predict time-dependent behavior such as the cell voltage, temperature, and heat-generation rate during galvanostatic discharge. Position- and time-dependent behavior such as electrolyte composition profiles, reaction-rate distributions and variations in volume fractions of individual phases are also calculated by the models. The results of the theoretical analysis show many of the general trends in discharge behavior that are observed experimentally. The models help identify the factors that can limit a battery during operation and determine the influence of changes in design parameters on the performance of the cells.

The simulated cell voltage behavior with the J-phase mechanism shows reasonable agreement with the behavior of an experimental cell at conditions in which we would expect the positive electrode to discharge through the J-
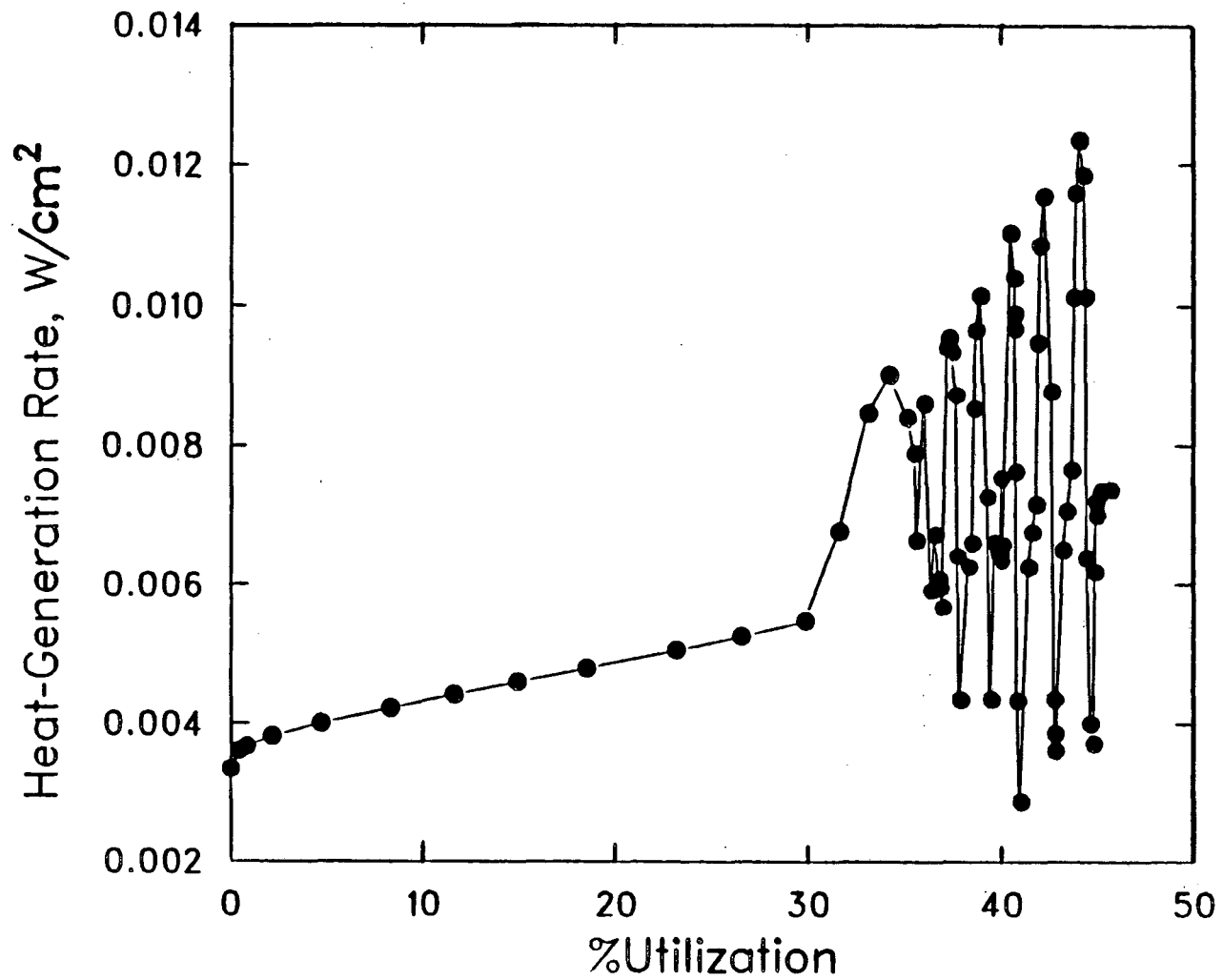
Figure 2-15. Heat-generation rate as a function of positive-electrode utilization for the X-phase mechanism. Parameters as in Figure 2-13.

phase mechanism. The main capacity-limiting mechanism predicted by the mathematical models (for both the X-phase and J-phase mechanisms) is the clogging of pores by KCl precipitation in the positive electrode. KCl precipitation in experimental cells may be a capacity-limiting mechanism; however, it appears to limit utilization at a much larger depth of discharge, if at all.

The main failure mechanism in experimental cells is the expansion and extrusion of active material, which eventually leads to short circuit. Positive electrode expansion is a problem during the discharge of experimental cells; however, it may be responsible for eliminating or lessening the KCl precipitation problem in these cells. Fabricating electrodes with larger initial porosities may help reduce the problem of electrode swelling. It has been proposed that assembling the positive electrode in the fully discharged state (Li_2S and Fe) will reduce electrode expansion and increase cell performance.[1] Our models predict that the KCl precipitation problem is lessened by increasing the initial porosity of the positive electrode.

Our mathematical models predict that increasing the initial porosity of the positive electrode increases the cell voltage; this is because the solid electrode material is taken to be more conductive than the electrolyte in the pores.

The thermodynamic analysis presented in Chapter 1 indicates that lower operating temperatures and LiCl concentrations will enhance the reactions involving J-phase. Decreasing cell operating temperature and LiCl concentration are also predicted by the models to decrease positive-electrode utilization if KCl precipitation in the positive electrode is the capacity-limiting mechanism. Perhaps the low electrode utilization observed in the discharge of experimental cells with the J-phase mechanism is due in part to the detrimental effects of KCl precipitation that may be present at low operating temperature or high KCl concentrations.

The exchange current densities and transfer coefficients for all the electrode reactions and all of the properties of J-phase used in the models are not based on experimental data. There is a great need for the determination of kinetic data for the reactions as well as physico-chemical properties of the electrode phases in the modeling of the iron sulfide electrodes.

Chapter 3

A General Energy Balance for Battery Systems

3.1. Introduction

Energy balance calculations are required for the design and thermal management of battery systems. A proper cell energy balance will give reliable predictions of thermal characteristics such as heat generation and temperature-time profiles. In this chapter, we present a general energy balance equation for battery systems. This equation includes energy contributions from mixing, phase changes, and simultaneous electrochemical reactions with composition dependent open-circuit potentials.

The problem of determining heat effects with simultaneous electrochemical reactions was first addressed by Sherfey and Brenner in 1958.[19] The authors presented an equation for the rate of thermal energy generation in terms of the current fraction, the entropy change, and the overpotential for each reaction. Later, Gross[20] presented essentially the same equation; however, he introduced a quantity for each reaction called the enthalpy voltage. The enthalpy voltage is the enthalpy of reaction per coulomb of charge, and it may be derived from the overpotential and the entropy change terms in Sherfey and Brenner's equation. These treatments are restricted in their application to cell reactions in which every reactant is present in a single, pure phase. Gibbard[21] discussed the calculation of thermodynamic properties of battery systems when some of the reactants are dissolved in solution; however, his treatment of the energy balance considers the case of a single reaction without mixing effects.

Numerous researchers [13,19,20,22-25] have adopted experimental approaches and used calorimetry to determine heat output directly. Dibrov and Bykov [23] used calorimetric data along with enthalpy voltages to determine current fractions of the reactions of cadmium-silver oxide and zinc-silver oxide cells.

The formulation of a general energy balance is useful in developing a fundamental understanding of the processes involved in cell heat generation. However, in its most rigorous form, the energy balance presented is difficult to apply without a detailed mathematical model because instantaneous composition profiles and current fractions are required. For example, Tiedemann and Newman [26] have developed such a model for the lead-acid cell. A model for the lithium-aluminum, iron sulfide battery was presented by Pollard and Newman. [3,4,5] These models do provide the necessary information to calculate the thermal characteristics from an energy balance such as the one presented in this work; however, these works utilize a relatively simple energy equation in which mixing effects are ignored and a single cell reaction occurs. Pollard's model calculates current fractions of the two simultaneously occurring reactions, but the fractions are not utilized in the energy balance. In practice, it is difficult to obtain concentration profiles and to predict the partitioning of current among possible reactions. However, applying an energy equation that includes the effects of simultaneous reactions to experimental measurements will allow the calculation of the current fractions.

The energy balance is derived in the next section, and the terms in the equation are discussed in Section 3.3. Simplifications and special cases of the general energy equation are also discussed in these sections. The results of applying the energy balance to a mathematical model of the LiAl/LiCl-KCl/FeS cell are given as examples in Section 3.4. The relative contributions corresponding to the terms in the equation are examined in Section 3.4.2. In Section 3.5, we draw conclusions from the work presented.

3.2. Derivation of the Energy Balance

In this section, the general energy balance for a battery system will be derived. The temperature of the battery is assumed to be uniform throughout and changes with time as determined by the following processes:

(1) reactions.

(2) changes in the heat capacity of the system.

(3) phase changes.

(4) mixing.

(5) electrical work.

(6) heat transfer with the surroundings.

A battery may be thought of as a composite of many discrete phases that are changing in energy content. It is assumed that these phases are interacting by way of electrochemical reactions, phase changes, and mixing processes. The first law of thermodynamics may be written as

$$\frac{dH_{tot}}{dt} = q - IV,$$

(3-1)

where H_{tot} is the sum of the enthalpies of the phases expressed as

$$H_{tot} = \sum_j \int_{v_j} \left[\sum_i c_{i,j} \, \overline{H}_{i,j} \right] dv_j .$$

(3-2)

and i and j denote the individual species and phase, respectively. The term q represents the rate of heat transfer with the surroundings, and IV is the electrical work. It is convenient to define an average composition for each of these phases and write $\frac{dH_{tot}}{dt}$ as

$$\frac{dH_{tot}}{dt} = \frac{d}{dt} \sum_j \sum_i \left[n_{i,j} \, \overline{H}_{i,j}^{avg} + \int_{v_j} c_{i,j} \, (\overline{H}_{i,j} - \overline{H}_{i,j}^{avg}) \, dv_j \right].$$

(3-3)

The first term on the right side of Equation 3-3 represents the rate of change of the enthalpy of the cell if all species are present at their average composition. The second term is a correction accounting for composition variations. In the development that follows, the first term in Equation 3-3 will be split into three separate terms. Applying the product rule for differentiation and recalling that

$$\left(\frac{\partial \overline{H}_{i,j}^{avg}}{\partial T} \right)_p = \overline{C}_{P,j}^{avg} ,$$
(3-4)

we obtain

$$\sum_j \sum_i \frac{d}{dt} (n_{i,j} \, \overline{H}_{i,j}^{avg}) = \sum_j \sum_i \left[n_{i,j} \, \overline{C}_{P,j}^{avg} \frac{dT}{dt} + \overline{H}_{i,j}^{avg} \frac{dn_{i,j}}{dt} \right] ,$$
(3-5)

for the first term in Equation 3-3.

It is assumed that there are several simultaneous electrode reactions of the form

$$\sum_i s_{i,l} \, M_i^{z_i} = n_l \, e^-$$
(3-6)

occurring within the battery. The reactions are written so that species i is always in a specified phase m, having a certain secondary reference state. For example, in a LiCl-KCl molten salt cell, all the electrode reactions are written so that the ionic lithium species is always present in the molten electrolyte phase and any precipitation of LiCl is accounted for separately.

A species balance may be written as

$$\frac{dn_{i,m}}{dt} = \sum_l \frac{s_{i,l} \, I_l}{n_l \, F} - \sum_{j,j \neq m} \frac{dn_{i,j}}{dt} .$$
(3-7)

The first term on the right side of Equation 3-7 represents the amount of i that is produced or consumed by electrode reactions. The partial current I_l is positive for a cathodic reaction and negative for an anodic reaction. The second term accounts for phase changes such as the LiCl precipitation mentioned

above. Integration of Equation 3-7 yields

$$n_{i,m} = n_{i,m}^o - \sum_{j,j \ne m} (n_{i,j} - n_{i,j}^o) + \sum_l \frac{s_{i,l}}{n_l F} \int_0^t I_l \, dt \; .$$

<div align="right">(3-8)</div>

We may express partial molar enthalpies in the form

$$\overline{H}_{i,m}^{avg} = \overline{H}_{i,m}^o - R \, T^2 \frac{d}{dT} \ln(a_{i,m}^{avg}) \; .$$

<div align="right">(3-9)</div>

The theoretical, open-circuit potential for reaction l at the average composition, relative to a reference electrode in the same solution is given by

$$U_{l,avg} = U_l^o - U_{RE}^o + \frac{RT}{n_{RE} F} \sum_i s_{i,RE} \ln(a_{i,m}^{avg}) - \frac{RT}{n_l F} \sum_i s_{i,l} \ln(a_{i,m}^{avg}).$$

<div align="right">(3-10)</div>

By utilizing the Gibbs-Helmholtz relation for each reaction, we may write the standard reaction enthalpy in terms of the standard cell potential,

$$\sum_i \frac{s_{i,l}}{n_l F} \overline{H}_{i,m}^o = T^2 \frac{d}{dT} \left(\frac{U_l^o}{T} \right) \; .$$

<div align="right">(3-11)</div>

Looking at Equations 3-5 and 3-7, we can see that the contribution to the rate of enthalpy change associated with the electrode reactions may be written as

$$\sum_i \overline{H}_{i,m}^{avg} \sum_l \frac{s_{i,l} I_l}{n_l F} = \sum_l \frac{I_l}{n_l F} \sum_i \overline{H}_{i,m}^{avg} s_{i,l} \; .$$

<div align="right">(3-12)</div>

Using Equations 3-9 and 3-11, we may write this contribution in terms of the electrode reaction potentials,

$$\sum_l \frac{I_l}{n_l F} \sum_i \overline{H}_{i,m}^{avg} s_{i,l} = \sum_l I_l \left[T^2 \frac{d \frac{U_l^o}{T}}{dT} - \frac{R \, T^2}{n_l F} \sum_i \frac{d}{dT} \ln(a_{i,m}^{avg})^{s_{i,l}} \right].$$

<div align="right">(3-13)</div>

Using Equation 3-10, we may write Equation 3-13 in terms of the theoretical, open-circuit potentials relative to a reference electrode in the same solution,

$$\sum_l I_l \sum_i \frac{\overline{H}_{i,m}^{avg} s_{i,l}}{n_l F} = \sum_l I_l \left[T^2 \frac{d \frac{U_{l,avg}}{T}}{dT} \right].$$

<div align="right">(3-14)</div>

The quantity multiplying l_l on the right side and the left side of Equation 3-14 is sometimes termed the enthalpy voltage of reaction l.

Substitution of Equations 3-7, 3-8, and 3-14 into Equation 3-5 and placing this result into Equation 3-3 results in the final form for $\dfrac{dH_{tot}}{dt}$. Equating this to $q - IV$ (Equation 3-1) gives the following form for the energy balance equation:

$$q - IV =$$

$$\sum_l \left[l_l\, T^2\, \frac{d\frac{U_{l,avg}}{T}}{dT} \right] \qquad \text{enthalpy} - \text{of} - \text{reaction}$$

$$- \sum_j \frac{d}{dt} \left[\int_{v_j} \sum_i c_{i,j} RT^2 \frac{\partial}{\partial T} \ln \left(\frac{\gamma_{i,j}}{\gamma_{i,j}^{avg}} \right) dv_j \right] \qquad \text{enthalpy} - \text{of} - \text{mixing}$$

$$- \sum_i \sum_{j,j \neq m} \left[\left(\Delta \overline{H}_{i,j-m}^o - RT^2 \frac{d}{dT} \ln \frac{\gamma_{i,m}^{avg}}{\gamma_{i,j}^{avg}} \right) \frac{dn_{i,j}}{dt} \right] \qquad \text{phase} - \text{change}$$

$$+ \frac{dT}{dt} \left[\sum_j \sum_i n_{i,j}^o\, \overline{C}_{p_{i,j}}^{avg} + \sum_l \frac{\int_0^t l_l\, dt}{n_l\, F} \Delta \overline{C}_{p_l} \qquad \text{heat} - \text{capacity} \right.$$

$$\left. + \sum_i \sum_{j,j \neq m} (\overline{C}_{p_{i,j}}^{avg} - \overline{C}_{p_{i,m}}^{avg})(n_{i,j} - n_{i,j}^o) \right] \qquad (3\text{-}15)$$

where

$$\Delta \overline{C}_{p_l} = \sum_i s_{i,l}\, \overline{C}_{p_{i,m}}^{avg} . \qquad (3\text{-}16)$$

and

$$\Delta \overline{H}_{i,j-m}^o = \overline{H}_{i,m}^o - \overline{H}_{i,j}^o . \qquad (3\text{-}17)$$

It should be recognized that all the composition dependence of Equation 3-15 may be expressed in terms of activity coefficients ($a_{i,j} = x_{i,j}\, \gamma_{i,j}$). This is a reflection of the fact that the composition dependence of any thermodynamic quantity is completely determined if the activity coefficient behavior of the species is known. This analysis does not include enthalpy changes associated with nonfaradaic reactions. However, reactions such as self-discharge or corrosion may be divided into anodic and cathodic components and included in the

enthalpy-of-reaction term (other reactions must be accounted for and included as an additional term). Also, the heat capacities of the battery support materials should be understood to be included in Equation 3-15. Actually, in most practical applications the heat capacity of a battery module does not change substantially during operation. In such cases, the heat capacity term may be replaced by some average value. Also, the rate of heat transfer q between the battery and surroundings may be expressed as

$$q = -hA(T - T_A),\qquad(3\text{-}18)$$

where the heat-transfer coefficient h is based on separator area and is estimated from the heat losses for a battery module.

As an example of how Equation 3-15 may be used, let us apply it to the LiAl/LiCl-KCl/FeS battery. We shall assume that any number of reactions may be occurring and that all the reacting phases are pure except the electrolyte. The molten LiCl-KCl electrolyte phase is considered to be a solution of varying composition throughout the battery. The species present are the Li^+, K^+, and Cl^- in the electrolyte and those corresponding to the pure reacting phases. The open-circuit potential data are considered to be given at the eutectic composition of the electrolyte as a reference condition and to be of the form $U_{i,\textit{out}} = a_i + b_i T$. All the electrode reaction potentials are given relative to the two phase (α,β) LiAl alloy reference electrode. It is convenient that this is also the negative electrode material. We may relate $U_{i,\textit{out}}$ to $U_{i,avg}$ by

$$U_{i,avg} = U_{i,\textit{out}} - \frac{RT}{F}\ln\left[\left[\frac{a_{LiCl}^{avg}}{a_{LiCl}^{out}}\right]^{\frac{s_{Li^+,i}}{n_i}}\left[\frac{a_{LiCl}^{avg}}{a_{LiCl}^{out}}\right]^{\frac{-s_{Li^+,RE}}{n_{RE}}}\left[\frac{a_{KCl}^{avg}}{a_{KCl}^{out}}\right]^{\frac{s_{K^+,i}}{n_i}}\right]\qquad(3\text{-}19)$$

The resulting equation will allow for precipitation of pure LiCl and pure KCl solid phases. With the above considerations, Equation 3-15 becomes

$$M\hat{C}_P^m \frac{dT}{dt} = -hA(T - T_A) - IV \tag{3-20}$$

$$+ \sum_l I_l \left[a_l + \frac{RT^2}{F} \frac{d}{dT} \ln \left[\left(\frac{\gamma_{LiCl}^{avg}}{\gamma_{LiCl}^{avg}} \right)^{\frac{s_{Li^+,l}}{n_l}} \left(\frac{\gamma_{LiCl}^{avg}}{\gamma_{LiCl}^{avg}} \right)^{\frac{-s_{Li^+,RE}}{n_{RE}}} \left(\frac{\gamma_{KCl}^{avg}}{\gamma_{KCl}^{avg}} \right)^{\frac{s_{K^+,l}}{n_l}} \right] \right]$$

$$+ \frac{d}{dt} \int_v \epsilon \, RT^2 \left[c_{LiCl} \frac{\partial}{\partial T} \ln \left(\frac{\gamma_{LiCl}}{\gamma_{LiCl}^{avg}} \right) + c_{KCl} \frac{\partial}{\partial T} \ln \left(\frac{\gamma_{KCl}}{\gamma_{KCl}^{avg}} \right) \right] dv$$

$$- \frac{dn_{LiCl_s}}{dt} \left[\Delta\tilde{H}_{LiCl_f}^o + RT^2 \frac{d\ln\gamma_{LiCl}^{avg}}{dT} \right] - \frac{dn_{KCl_s}}{dt} \left[\Delta\tilde{H}_{KCl_f}^o + RT^2 \frac{d\ln\gamma_{KCl}^{avg}}{dT} \right].$$

where $\dfrac{dn_{LiCl_s}}{dt}$ and $\dfrac{dn_{KCl_s}}{dt}$ are the crystalization rates of solid LiCl and KCl phases, respectively. There is a considerable amount of simplification involved in going from Equation 3-15 to Equation 3-20. For example, the ionic activity coefficients, ionic concentrations, and ionic partial molar enthalpies have been combined into neutral combinations that refer to undissociated LiCl and KCl. If the electrolytes were considered to be completely dissociated, then Equation 3-15 could be rearranged to contain mean ionic activity coefficients (neutral combinations of individual ionic activity coefficients).

In the next section each of the terms in Equation 3-15 will be discussed. Afterwards, Equation 3-20 will be applied more specifically to the LiAl/FeS cell.

3.3. Discussion of the Terms in the Energy Balance

3.3.1. The Enthalpy-of-Reaction Term

If we use an average heat capacity and do not consider enthalpy-of-mixing and phase-change terms then Equation 3-15 may be written as

$$q = IV + \sum_i I_i \left[T^2 d \frac{\frac{U_{i.avg}}{T}}{dT} \right] + M\hat{C}_p^m \frac{dT}{dt}. \tag{3-21}$$

During discharge, the chemical energy of the cell is directly converted into work in the form of electricity. The work that the cell delivers is a maximum when the cell operates reversibly. This reversible work, expressed as a rate, can be written as

$$IV_{rev} = \sum_i I_i \left[U_{i.avg} \right], \tag{3-22}$$

and is tucked into the enthalpy-of-reaction term. The difference between V_{rev} and V is the cell overpotential. The overpotential is indicative of irreversibilities such as ohmic losses, charge-transfer overpotentials, and mass-transfer limitations. The overpotential times the current is termed the polarization heat and is composed of the joule heating within the battery as well as the energy dissipated in electrode overpotentials.

Also housed in this enthalpy-of-reaction term is the entropic- heat,

$$q_{rev} = -\sum_i I_i \left[T \frac{d(U_{i.avg})}{dT} \right]. \tag{3-23}$$

Equations 3-22 and 3-23 represent the power and the heat generation that accompany reversible, isothermal cell operation, respectively. The reversible work is related to the change in Gibbs function of the cell's contents. The entropic-heat is related to the entropy change. We may write Equation 3-21 in terms of these contributions as

$$q = \left[IV - \sum_i I_i U_{i.avg} \right] + \sum_i I_i T d \frac{U_{i.avg}}{dT} + M\hat{C}_p^m \frac{dT}{dt}. \tag{3-24}$$

Equations 3-22 and 3-23 have allowed the enthalpy-of-reaction and electrical work terms in Equation 3-21 to be combined and restated as irreversible and reversible heat effects. This form is most convenient when dealing with reversi-

ble conditions since the polarization heat, $IV - \sum_l I_l \left[U_{l,avg} \right]$, is zero in that case. Furthermore, Equation 3-24 is the form of the energy balance that is most commonly encountered in the literature. The composition dependence of the open-circuit potential is contained in $U_{l,avg}$ (see Equation 3-10). The original form (Equation 3-21) has the advantage that a strong composition dependence of the two terms separately may partially cancel in the enthalpy voltage. Also, if the open-circuit potentials $U_{l,avg}$ are independent of composition and linearly related to temperature, then the enthalpy-of-reaction term becomes

$$-\sum_l I_l a_l \, . \tag{3-25}$$

Notice that the temperature coefficients, b_l, are not needed and the enthalpy voltage of reaction l is $- a_l$.

3.3.2. The Enthalpy-of-Mixing Term

The enthalpy-of-mixing term represents the heat effects associated with generation or relaxation of concentration profiles. For example, if we do not consider phase-change terms, then this term represents the rate of heat generation after current interruption of cell operation. First, the definition of the average composition will be discussed. Later, an estimate of the adiabatic temperature rise due to relaxation of concentration profiles in a lead-acid cell after full discharge will be made.

The enthalpy-of-mixing term is the only term in Equation 3-15 that is dependent on the spatial variation of composition. This term may be thought of as a correction because the other terms depend only on the average composition. The term is difficult to treat because it involves integrations of concentration profiles. Consequently, it is instructive to discuss the conditions under which it may be neglected. The definition of the average composition of species i is arbitrary. Therefore, if mixing effects are to be neglected then the average

composition should be chosen such that the value of this neglected term is minimized. For a binary phase, with components 1 and 2, it can be shown that the integral in the mixing term may be minimized if the average concentration is defined as

$$c_1^{avg} = \frac{\int_v c_1\, dv}{\int_v dv} \quad \text{or} \quad x_1^{avg} = \frac{\int_v c\, x_1\, dv}{\int_v c\, dv}, \tag{3-26}$$

where

$$c = c_1 + c_2.$$

This will be shown as follows. For a binary system, the integral in the mixing term in Equation 3-15 may be written as

$$\int_v c \left[\tilde{H} - (x_1 \overline{H}_1^{avg} + x_2 \overline{H}_2^{avg}) \right] dv, \tag{3-27}$$

where the molar enthalpy is defined as

$$\tilde{H} = x_1 \overline{H}_1 + x_2 \overline{H}_2.$$

and $\overline{H}_i^{avg}$ is the partial molar enthalpy of species i at the average composition. It should be recognized that in this development it is assumed that the spatial variation of composition is fixed and that Equation 3-27 is only a function of x_1^{avg}. By writing the mixing integral in this form, we may obtain a clearer interpretation of the mixing term. The sum subtracted from $\tilde{H}$ is the tangent line to the enthalpy-vs-composition ($\tilde{H} - x_1$) plot at the average composition. The integral may be considered to be a measure of the ability to approximate the $\tilde{H}$ curve with a tangent, in the range of composition variation throughout the cell. Therefore, if the enthalpy curve is linear in this range, then $\overline{H}_1$ and $\overline{H}_2$ are independent of composition, and the integral is zero regardless of the value of x_1^{avg}. Also, if the activity coefficients are independent of temperature (see

Equation 3-9) then mixing effects can be ignored. Different choices of the tangent, corresponding to different values of the average composition may give better or worse approximations of the enthalpy curve. Equation 3-27 may be minimized with respect to the average composition by solving the following equation for x_1^{qvg}:

$$\frac{d}{dx_1^{qvg}}\left[\int_v c\ (x_1\overline{H}_1^{avg} + x_2\overline{H}_2^{avg})\ dv\ \right] = 0 .$$

(3-28)

In formulating Equation 3-28, it was recognized that the composition profiles and enthalpy curve are independent of the choice of x_1^{qvg}. We may further simplify Equation 3-28 and write

$$\int_v c_1\ dv\ \frac{d\overline{H}_1^{avg}}{dx_1^{qvg}} + \int_v c_2\ dv\ \frac{d\overline{H}_2^{avg}}{dx_1^{qvg}} = 0 .$$

(3-29)

The Gibbs-Duhem equation,

$$x_1^{qvg}\frac{d\overline{H}_1^{avg}}{dx_1^{qvg}} + x_2^{qvg}\frac{d\overline{H}_2^{avg}}{dx_1^{qvg}} = 0 ,$$

(3-30)

may be applied, and Equation 3-29 may be solved for x_1^{qvg} as given in Equation 3-26. The corresponding development for multicomponent mixtures is given in Appendix A-3. Equation 3-26 is guaranteed to be the choice of the average composition that will minimize Equation 3-27 only if the integral has simple behavior. The behavior is said to be simple if the second derivative of the integral is non-zero for all possible values of x_1^{qvg} (in range of concentration variation throughout the cell). For example, if the integral has a point of inflection such that its value may be either positive or negative depending upon x_1^{qvg}, then x_1^{qvg} may be chosen so that the integral is zero. In this case, the best choice of the x_1^{qvg} is not necessarily defined by Equation 3-26. Regardless of the behavior of the integral, Equation 3-26 is the most convenient definition of the average composition. It has physical significance, and it is usually a simple

function of state-of-charge. It is the final uniform composition of a concentration profile that is allowed to relax, and the energy effect associated with this process, in this case, is proportional to the value of the integral for the initial profile.

It is useful to examine further the sign of the integral. The sign of Equation 3-27 will indicate such things as whether mixing effects will tend to heat, or cool, a cell during operation. It is convenient now to look at Equation 3-27 as a function of the mixing behavior and assume that that average composition is fixed. Equation 3-27 will be positive if

$$\tilde{H} > (x_1 \overline{H_1^{avg}} + x_2 \overline{H_2^{avg}}) . \tag{3-31}$$

The right side of Equation 3-31 is linear in x_1. If Equation 3-31 is differentiated twice with respect to x_1, we obtain

$$\frac{d^2 \tilde{H}}{dx_1^2} > 0 . \tag{3-32}$$

In other words, if, in the range of concentration variation throughout the cell, the enthalpy curve is always concave upward then the integral will be positive. Conversely, the integral will be negative if the enthalpy curve is everywhere concave downward. For example, in the lead-acid cell the sulfuric acid-water system has an enthalpy curve that is always concave upward. Consequently, the temperature of a well-insulated lead-acid cell will always increase after current interruption during operation due to relaxation of concentration profiles. To illustrate this, in Appendix A-3 Equation 3-15 is used to estimate this temperature rise. The temperature rise, after full discharge, is approximately 1.6 K. It is also important to investigate the consequence of neglecting mixing effects in thermal calculations. For the lead-acid cell, the temperature during operation (generation of concentration profiles) is overestimated if calculations are made by neglecting the mixing term. The situation is reversed for

a high-temperature cell employing LiCl-KCl electrolyte. In the range of concentration variation throughout this cell the enthalpy curve is always concave downward, and the cell temperature will decrease due to mixing effects after current interruption. Calculations that neglect mixing will give underestimations of temperature when concentration profiles are being generated (during cell operation). This will be investigated in greater detail later.

If the enthalpy curve, in the range of composition variation, may be concave upward or concave downward, then the sign of the integral depends on the choice of the average composition. Certain associated systems, such as ethanol and water, exhibit inflection points in their enthalpy curves.

3.3.3. Phase-Change Terms

In the enthalpy-of-reaction term of Equation 3-15, all the reactions have species i in the same phase m. For example, in Equation 3-20 LiCl is always present as a molten LiCl-KCl solution phase in all reactions. However, one of the phases present in the cell during operation may be pure solid LiCl. The purpose of the phase-change terms is to account for the enthalpy change due to crystallization of this solid phase. For example, ice crystals form during low temperature operation of aqueous batteries, and an energy balance such as Equation 3-23 would not correctly predict cell temperatures. If the m-phase types in the enthalpy-of-reaction contribution (Equation 3-15) are the only phases present in the cell during operation, then the phase-change terms are zero.

3.3.4. The Heat-Capacity

The quantities to the right of $\dfrac{dT}{dt}$ in the heat-capacity effects term of Equation 3-15 represent the heat capacity of the cell. This heat capacity changes with time because the composition of the cell changes due to electrochemical

reactions and phase changes. The first part of this heat capacity represents the initial heat capacity of the cell's reactive material. The heat capacity of the cell's inert supporting material should be included in this part. The second and third parts account for changes in the initial heat capacity as a result of electrochemical reactions and phase changes, respectively.

As mentioned earlier, the total heat capacity of a typical cell (including supporting material) is approximately constant so that this term usually reduces to a simple expression.

3.4. Application of the Energy Balance to the LiAl/FeS Cell Model

The results of applying Equation 3-15 to the model of the LiAl/LiCl,KCl/FeS cell will be given in this section. The purpose of these examples is to illustrate how the energy balance equation may be applied to a specific system and to examine the relative contributions corresponding to the terms in this equation. The use of Equation 3-15 is best illustrated by application to a mathematical model of a battery in which concentration profiles can be used to calculate energy contributions from mixing, and current fractions can be used to calculate energy contributions from simultaneous reactions. This model of the LiAl/FeS cell was originally developed by Pollard and Newman in 1981.[3,4,5] The development of the model and some model results are given in Chapter 2. Many of the details of the theoretical analysis can be found in Pollard and Newman's publications. The model gives the galvanostatic discharge behavior of a one-dimensional cell sandwich consisting of a porous LiAl negative electrode, porous FeS positive electrode, electrolyte reservoir, and separator. The model simulates the discharge processes in the positive by the two simultaneously occurring reactions given as mechanism 1 in Table 3-1. Pawlikowski[11] in 1982 developed a model of the cell with mechanism 2 as the positive electrode discharge reactions. Mechanisms 1 and 2 yield the same overall reaction and differ mainly in the intermediate phase (X-phase or J-phase).

Table 3-1.

Model discharge mechanisms in the FeS electrode

Reaction	a_i^* [V]	$b_i \times 10^{3*}$ [V/K]
Mechanism 1 (X-phase intermediate)		
1) $2FeS + 2Li^+ + 2e^- \rightarrow Li_2FeS_2 + Fe$ (X-phase)	1.367	-0.022
2) $Li_2FeS_2 + 2Li^+ + 2e^- \rightarrow 2Li_2S + Fe$	1.454	-0.178
Mechanism 2 (J-phase intermediate)		
3) $26FeS + Li^+ + Cl^- + 6K^+ + 6e^- \rightarrow LiK_6Fe_{24}S_{26}Cl + 2Fe$ (J-phase)	1.955	-0.680
4) $J + 51Li^+ + 46e^- \rightarrow 26Li_2S + 24Fe + 6K^+ + Cl^-$	1.340	-0.024

*a_i and b_i were obtained from Reference 9.

The electrochemistry of the FeS electrode is reasonably well understood. The actual discharge processes can be more complicated and like a mixture of the two proposed mechanisms along with simultaneously occurring chemical reactions (see Chapter 1). There is evidence, however, for the simple 2-reaction mechanisms under certain operating conditions.[9] In Chapter 1, the reactions of the FeS electrode in LiCl-KCl molten salt electrolyte are discussed in greater detail. The conditions under which we expect the X-phase and J-phase mechanism to occur and the temperature and composition dependence of the thermodynamic open-circuit potential are also examined in Chapter 1. The

thermodynamic data given in Chapter 1 are slightly different from the data given in Table 3-1. The data in Chapter 1 (Table 1-2, second and third columns) are probably the best data available at this time.

In practice, LiAl/FeS batteries are operated between 400°C and 500°C. Higher operating temperatures and LiCl concentrations tend to favor mechanism 1. Lower temperatures and LiCl concentrations favor mechanism 2. Discharge through the X-phase intermediate is preferred because of the poor reversibility of the J-phase reactions. For purposes of comparison, the simulations of the two mechanisms will use the same initial temperature and electrolyte composition.

The model discharges are meant to simulate a well insulated (but not adiabatic) battery operating in an ambient temperature environment with no external heating. The relevant input data and energy equation specific to each mechanism are given in Appendix A-3.

3.4.1. Results

Figure 3-1 gives the cell temperature as a function of utilization for both mechanisms. The dashed lines show the temperature profile for adiabatic and reversible discharge. Under these conditions the two mechanisms yield the same temperature at 100% depth of discharge because the overall reaction is the same. In both cases the reactions are exothermic, so that the cell temperature increases throughout discharge. Though the adiabatic-reversible profile of mechanism 1 appears linear, there is actually a slight amount of curvature due to the logarithmic dependence of the cell temperature. The composition dependencies associated with the J-phase reactions result in the more discernible curvature of each portion of the adiabatic-reversible profile of mechanism 2. The criterion of reversibility allows the stoichiometry of the reactions to yield the discontinuities in slope located at 50% and 12% for mechanism 1 and mechanism 2, respectively. For example, with mechanism 1 up to 50%
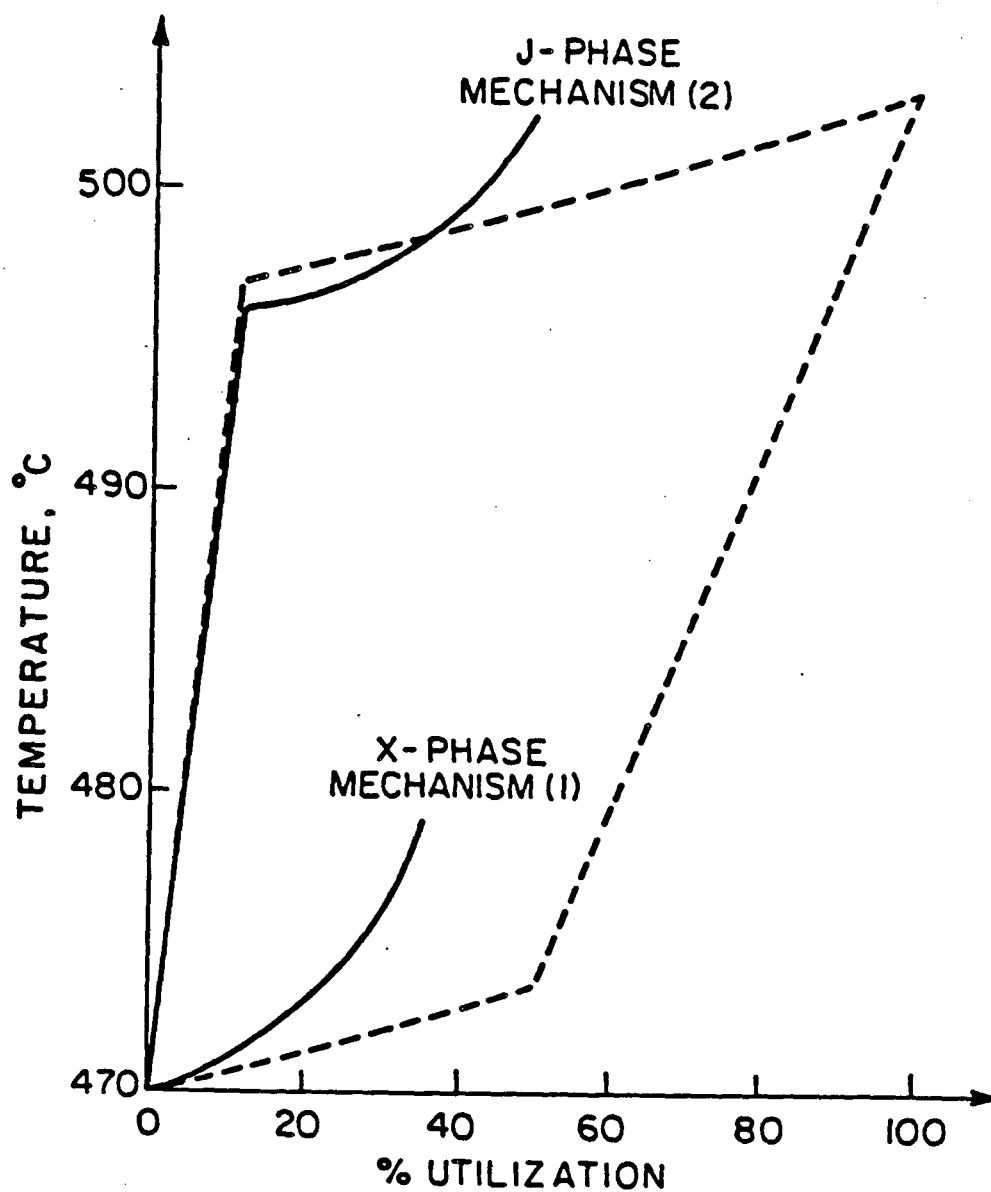
Figure 3-1. Cell temperature as a function of utilization for mechanisms 1 and 2. The dashed lines are for adiabatic-reversible discharge. The solid lines are the results of the mathematical model simulations. Cutoff voltages of 1.2 and 1.0 volts were used for mechanisms 1 and 2, respectively.

utilization only reaction 1 occurs, and after this point reaction 2 occurs. The dashed curve in Figure 3-2 is the heat generation rate for reaction 1. It is approximately constant because the temperature is not changing substantially, and this is responsible for the apparent linearity in Figure 3-1. With the J-phase reactions, the stoichiometry dictates the transition from reaction 3 to reaction 4 to occur at 12% utilization.

It is interesting to compare these results to the results of the more realistic simulations. The solid lines in Figure 3-1 are the results of the mathematical models. The relevant input data and energy equation specific to each mechanism are given in Appendix A-3. In these simulations, the irreversibilities associated with ohmic losses, migration effects, mass-transfer, and charge-transfer overpotentials cause electrode polarization. The onset of the second reaction of each mechanism may occur before the prediction based on reversibility because of the resulting potential distribution in the porous, positive electrode. Compared to the values of 50% and 12% utilization, the second reaction begins at 30% and 11% utilization for mechanisms 1 and 2, respectively. At these operating conditions, the reaction potential difference $U_{3,avg} - U_{4,avg}$ for the J-phase mechanism is always about four times larger than the difference $U_{1,avg} - U_{2,avg}$ for the X-phase mechanism; we see that the onset of the second reaction occurs closer to the reversible prediction in the case of the J-phase mechanism because a larger positive electrode polarization is required to promote the onset of the second reaction as compared with the X-phase mechanism.

The solid lines in Figure 3-2 are plots of the terms in Equation A-12 as functions of state of charge for the X-phase mechanism up to 30% utilization. The dashed line in Figure 3-2 is called the entropic-heat and has the value of $-i_1 b_1 T$. It would be the only term on the right side of Equation A-12 if the equation were written for the adiabatic-reversible case. The polarization-heat, $i_1(U_{1,avg} - V)$,
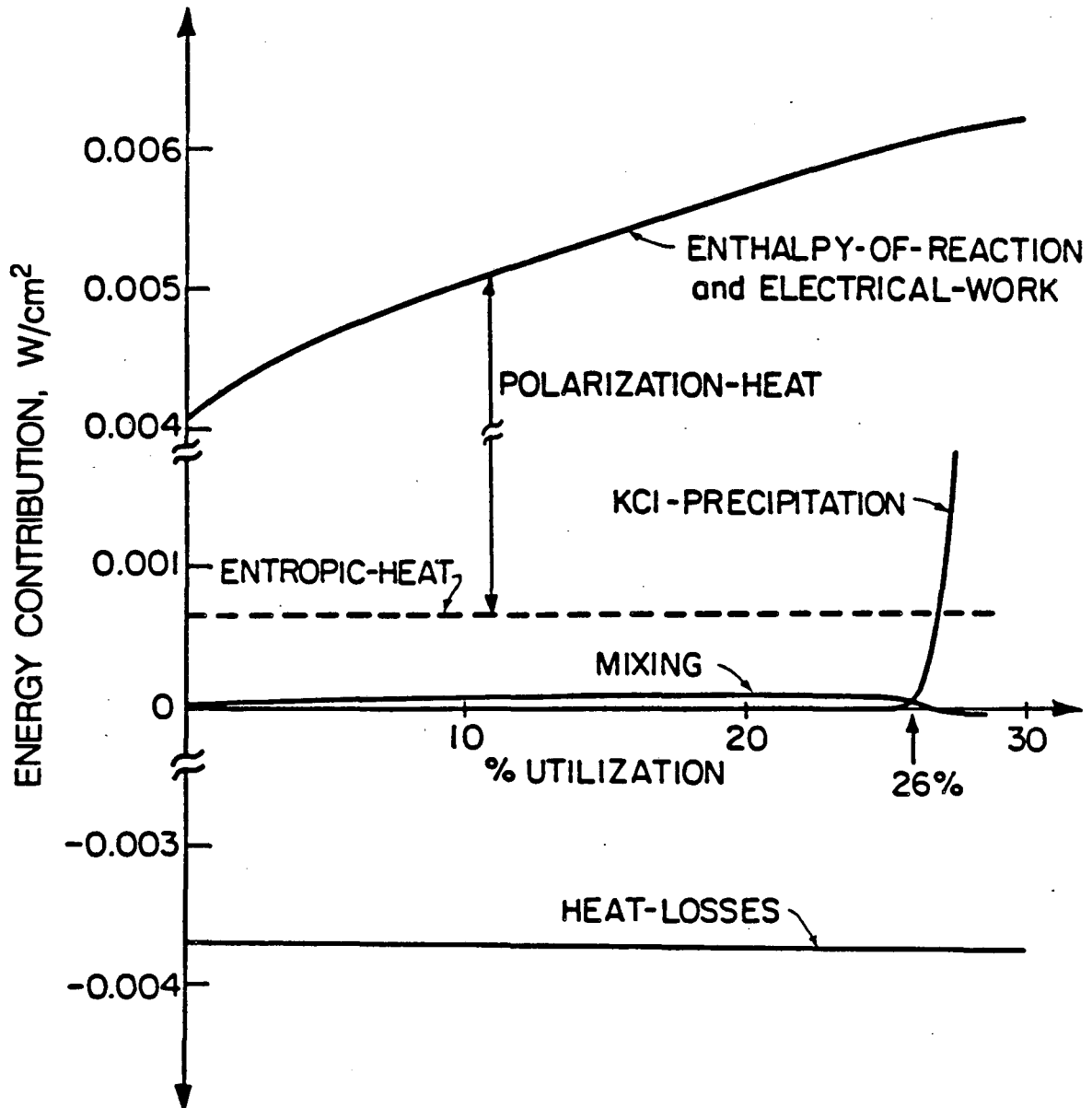
Figure 3-2. Terms comprising the energy balance for a LiAl/FeS cell (Equation A-12 in Appendix A-3) as a function of utilization.

and the entropic-heat add up to the enthalpy-of-reaction and electrical-work term. The heat-loss contribution does not change markedly because the cell is well insulated and the overall cell temperature does not change substantially. The profile for the X-phase mechanism in Figure 3-1 follows the adiabatic-reversible profile up to about 5% utilization because the heat-loss contribution tends to cancel the polarization-heat. The polarization-heat is mainly responsible for the increasing departure of the cell temperature from the reversible case throughout discharge. With increasing utilization, the polarization-heat increases because the open-circuit potential ($U_{1,avg}$) is approximately constant and the cell voltage drops.

These results can be contrasted to the results with the J-phase mechanism from 0% to 11% utilization. The average LiCl concentration increases, and the composition dependent $U_{3,avg}$ decreases accordingly (Equation 3-19). Actually, $U_{3,avg}$ decreases at about the same rate as the cell voltage, so that the polarization-heat remains relatively constant. Up to about 5% utilization, the heat-loss term approximately cancels the polarization-heat, and the temperature profile follows the adiabatic-reversible case. The cell temperature increases enough from 5% to 11% utilization so that the heat-loss term dominates, and the temperature remains below the adiabatic-reversible case. After 12% utilization, the heat losses and $U_{4,avg}$ stay approximately constant, so that the polarization-heat dominates, and by 36% utilization the profile lies above the adiabatic- reversible case.

Although the mixing term offers a negligible contribution to the energy balance, it is interesting to investigate the processes that determine its behavior. As we mentioned earlier, for the molten LiCl-KCl system, the value of the integral in Equation A-12 is always negative. Therefore, if the heat losses are made negligible, the cell temperature will decrease after current interruption. Prior to the onset of precipitation, this is entirely a mixing effect. At 25%

utilization in Figure 3-2, this temperature decline is only about 0.2 K. Before precipitation, the concentration of LiCl steadily decreases in the positive electrode and increases in the negative electrode, and the average composition, x_{LiCl}^{avg} = 0.58 (defined by Equation 3-26), is constant. The mixing term (the time derivative of the integral) also increases, and the cell temperature would be slightly underestimated if mixing effects were ignored. The concentration throughout the separator and reservoir volumes remains close to the average composition, so that their contributions to the integral are two orders of magnitude smaller than the contributions from integration through the electrodes. Figure 3-2 shows that the integral increases in magnitude to the point where the mixing term is zero (26.5% utilization). After this point the mixing term is slightly negative corresponding to a decrease in the magnitude of the integral with time. The mixing term decreases when KCl precipitates because in the region of precipitation the electrolyte composition is approximately constant at its saturation value. Following the onset of precipitation, the adiabatic temperature decline after current interruption is determined by the more complex processes of simultaneous melting of KCL and electrolyte mixing. We present the breakdown of contributions only up to 30% utilization because when the second reaction begins simultaneously, reaction heat effects and precipitation effects cause oscillatory behavior. The description and discussion of this phenomenon are given in Chapter 2 (Section 2.4.4). An example of the effect of this phenomenon on the heat-generation rate of a cell discharged isothermally (470°C) is shown in Figure 2-14.

3.4.2. Isothermal Behavior with the J-phase Mechanism

It is useful to examine the behavior of the heat-generation rate during isothermal cell operation. Figure 3-3 gives the calculated heat-generation rate and cell voltage as a function of utilization during the discharge of a LiAl/FeS cell. The mechanism of the positive electrode is the J-phase mechanism. The
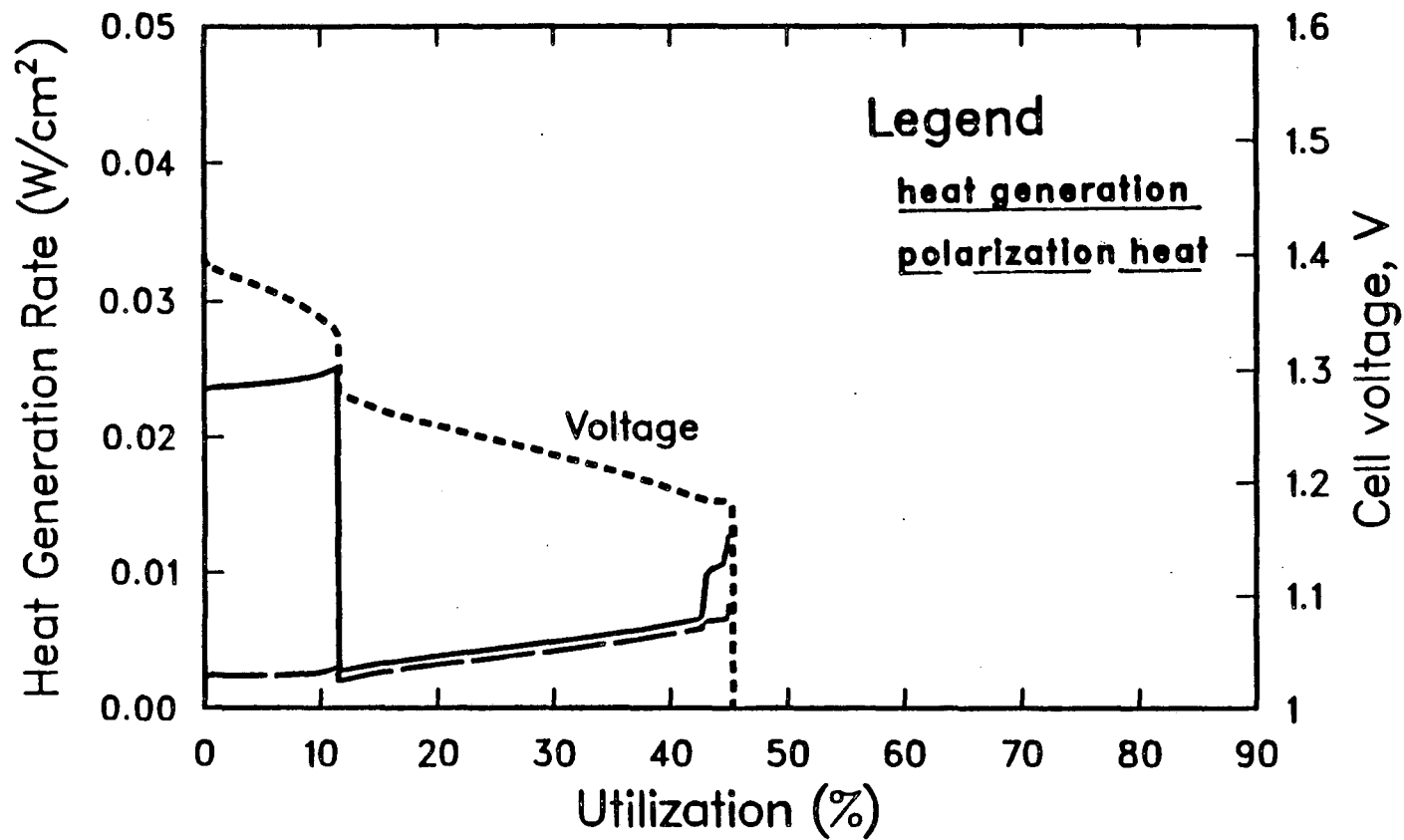
Figure 3-3. Model calculations of the cell heat-generation rate and voltage as a function of utilization. The cell is discharged isothermally (470°C) with the mechanism 2 for the positive electrode reaction sequence.

heat-generation rate is the sum of the entropic heat, the polarization heat, and the heat due to electrolyte mixing and precipitation; it is the quantity that would be measured experimentally with a calorimeter. The solid line in Figure 3-3 gives the heat-generation rate, and the large dashed line gives the polarization heat contribution. The difference between those two curves gives the entropic heat contribution. From 0 to 11.5% utilization, we see that the main contribution to the heat-generation rate is the entropic heat of the first reaction in the J-phase mechanism. The polarization heat is the main contribution to the heat generation rate after 11.5% utilization. The sharp increase in the heat-generation rate at 42% utilization marks the onset of KCl precipitation in the positive electrode. At 46% utilization, the cell voltage drops to its 1 V cutoff point because the KCl precipitate has clogged the pores of the positive electrode. Figure 3-4 gives experimental data for a cell discharged isothermally (410°C) and galvanostatically at 45 mA/cm^2.[13] The thermodynamic behavior of this experimental cell is discussed in Chapter 1. As we see in Figures 1-4 and 1-5, we expect the J-phase mechanism to be the reaction sequence of the positive electrode. A more qualitative than quantitative comparison of Figures 3-3 and 3-4 should be made because the operating conditions are different. The zero intercept of the experimentally measured heat-generation rate is probably an indication of the finite response time of the calorimeter. The agreement between model and experiment for the the maximum heat-generation rate and the heat-generation rate in the range of 15% to 40% utilization is fairly good. This is not surprising since the $i\,T$ product in the entropic contribution to the heat-generation rate (Equation 3-23) is approximately the same for model and experiment, and $dU_{i,avg}/dT$ is weakly dependent upon composition and temperature. The model predicts a steep drop in the heat-generation rate at 11.5% utilization when the FeS is exhausted and the second reaction of the J-phase mechanism begins. That is, the model does not predict the reactions of the J-phase mechanism to occur simultaneously within the electrode. The gradual
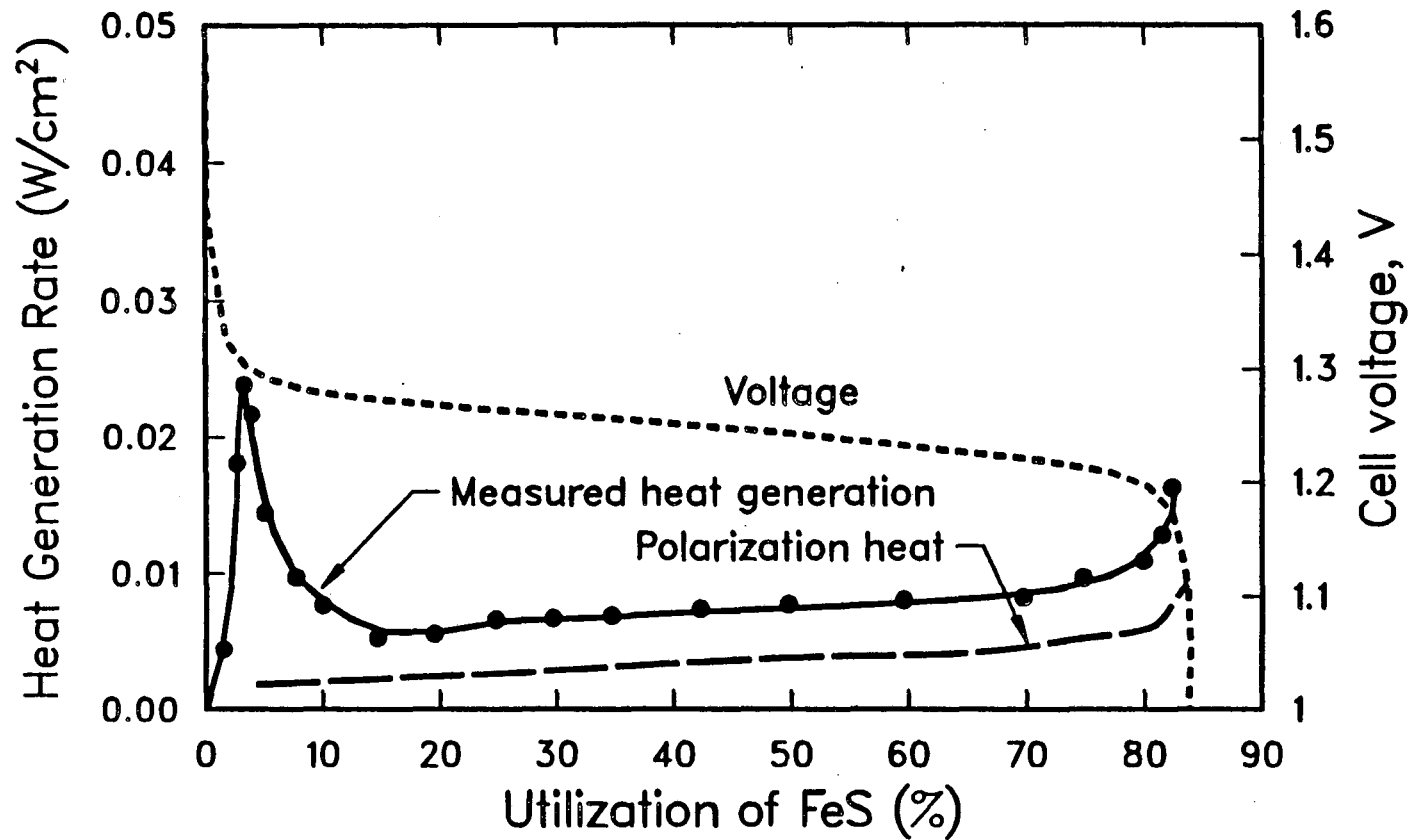
Figure 3-4. Experimentally measured cell heat-generation rate and voltage as a function of utilization.[13] The cell is discharged isothermally (410°C) at 45 mA/cm^2. The initial electrolyte composition is: x_{LiCl} = 0.6163, x_{KCl} = 0.3132, and x_{LiF} = 0.0705, and n_s^o = 3.7.

drop in the experimental heat-generation rate at approximately 10% utilization may indicate that the reactions occur simultaneously in the experimental cell. It is possible, however, that the response time of the calorimeter may not be fast enough to measure the transition in heat-generation rate that would occur if the reactions did not occur simultaneously.

3.5. Conclusions

The examples presented help to illustrate that the processes involved in cell heat generation may be complex and that the application of a sufficiently general energy equation is advantageous. Equation 3-24, written for a single cell reaction, is the energy equation most commonly used in battery applications. The use of this form of an energy balance is justified only if phase-change effects, mixing effects, and simultaneous reactions are not important. An energy equation including the effects mentioned above is of course most easily applied to modeling studies. However, applying an energy equation that includes the effects of simultaneous reactions to experimental measurements may help elucidate reaction mechanisms. For example, if heat generation rates and cell voltage measurements are made on LiAl/FeS cells under isothermal operating conditions, an energy equation may be fit to the experimental data to determine the current fractions of simultaneously occurring reactions. The experiments performed under truly isothermal conditions have the advantage that an estimate of the mean cell heat capacity is not required. However, if experimental cells are not maintained isothermal, then heat capacity effects or the effects of non-uniform temperature may obscure the relationship of the experimental results to the energy balance.

A reversible-isothermal model is relatively easy to construct from knowledge of the stoichiometry of the probable cell reactions and the temperature dependence of their open-circuit potentials. The comparison of such a model with experimental results may also aid in the understanding of the

system, just as the adiabatic-reversible model was used to aid in the interpreta-
tion of the simulation of the well-insulated cell in the examples. Regardless of
the application, understanding the fundamental processes involved in cell heat
generation will aid in our ability to design and develop more efficient and reli-
able battery systems.

Chapter 4

Thermodynamic Behavior of Li(Si)/FeS$_2$ Cells

4.1. Introduction

The description of the thermodynamic behavior of Li(alloy)/FeS$_2$ cells can aid in the understanding, development, and design of these cells. There has been considerably less research directed toward the chemistry of the FeS$_2$ electrode than the FeS electrode. In the search for a high energy density, high power cell, the LiAl/FeS couple was developed. We discussed the thermodynamic behavior of this cell in Chapter 1. The Li(Si)/FeS$_2$ cell was later considered as a higher voltage, higher power alternative to the LiAl/FeS cell. It should be noted, however, that the theoretical specific energy of a Li(Si)/FeS$_2$ cell operating on the uppermost FeS$_2$ voltage plateau only (and the relevant plateaus of the Li(Si) electrode) is 434.5 W-hr/kg, while the theoretical specific energy of a LiAl/FeS system (with the negative electrode operating over a composition range which allows a fair comparison) is 436.4 W-hr/kg. The higher potential of the Li(alloy)/FeS$_2$ cell does, however, reduce the number of cells per battery and increase the maximum power achievable relative to the LiAl/FeS cell. It should also be recognized that the sulfur activity of the FeS$_2$ electrode is higher than that of the FeS electrode, and this leads to high corrosion rates and long-term instability. These problems are discussed in the Introduction and in Chapter 5.

The intermediate phases of the FeS$_2$ electrode are the subject of some controversy. Tomczuk et al.[14] at Argonne National Laboratory have accomplished some of the most recent work with this electrode. In their work, the authors summarize the controversy, and we feel that they also resolve a great deal of it.

We make use of their work in the construction of the Li(alloy)/FeS$_2$ cell model presented in Chapter 5. The researchers combined metallography and x-ray diffraction methods. Photomicrographs of coexisting electrode phases were examined, and the complex reaction sequences were identified. Recently, another controversy has evolved over the FeS$_2$ electrode. The work of Schmidt and Weppner[28] contradicts Argonne's work. This controversy has not been discussed in the literature.

The compositions of the intermediate phases in the Li-Si system have also been subject to some controversy. We believe that the work of Wen and Huggins[29] resolves this disagreement. These researchers use the equilibrium coulometric titration technique in the determination of the composition dependence of the Li(Si) electrode potential and X-ray diffraction analyses to characterize the intermediate phases.

In Section 4.2 we summarize some of the important findings of Argonne's work[14] and compare their work with Schmidt and Weppner's[28] results. We discuss Wen and Huggins'[29] work on the thermodynamic behavior of the Li(Si) electrode in Section 4.3. The thermodynamic data on the FeS$_2$ electrode and the Li(Si) electrode are combined in the examination of the open-circuit potential behavior for reversible-isothermal discharge of a Li(Si)/FeS$_2$ cell in Section 4.4.

4.2. The Li-Fe-S Phase Diagram

Figure 4-1 gives the phase diagram for the Li-Fe-S system that is in accordance with Argonne's[14] data. Some of the details of the diagram (minor single-phase and two-phase regions that are not involved in FeS$_2$ discharge) have been omitted. In Section 4.2.2, some of the omitted details are discussed. Table 4-1 shows the reactions for the four regions of discharge of an FeS$_2$ electrode. (Electrochemical reactions are written for the three-phase regions of
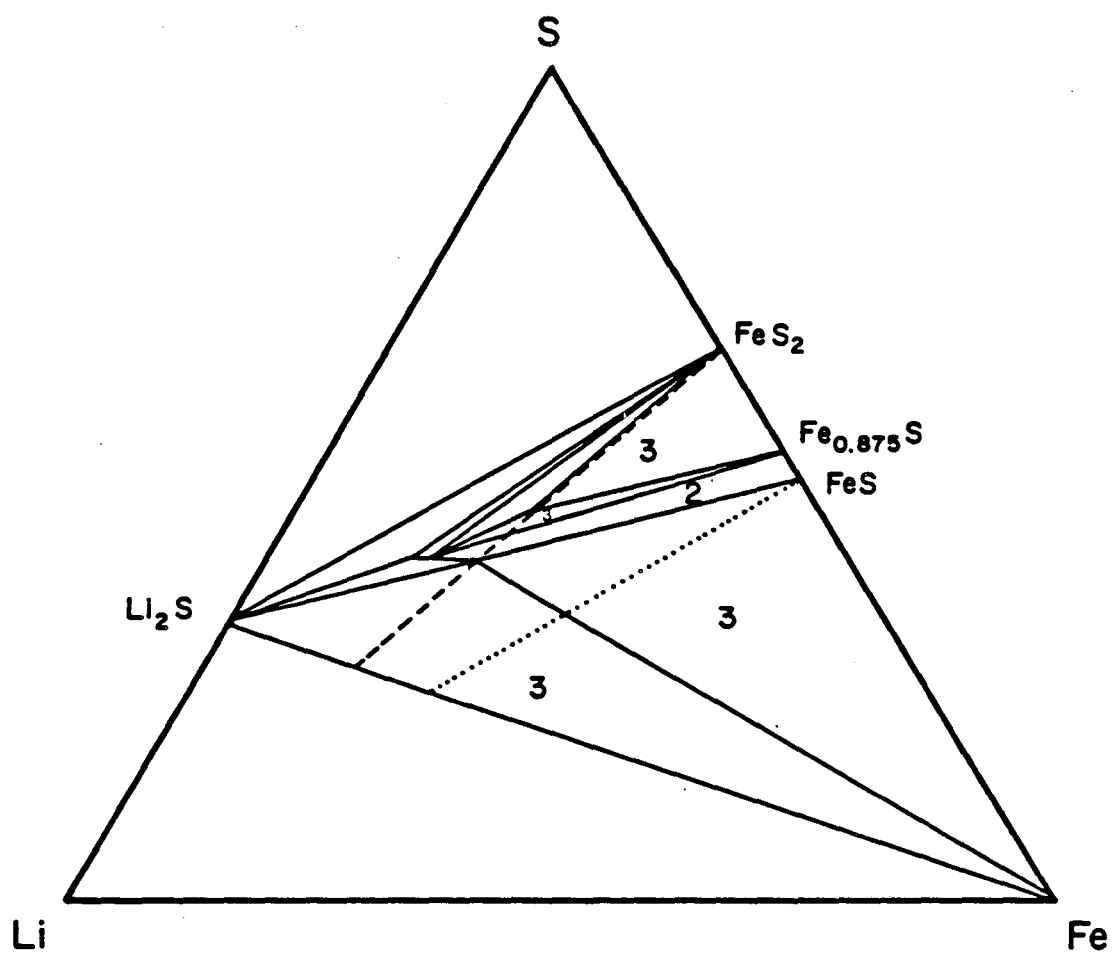
Figure 4-1. Ternary phase diagram for the Li-Fe-S system as given by Tomczuk et al.[14] The numbers are in regions of particular interest and indicate the number of phases in equilibrium.

discharge, and the two-phase region will be discussed later). In contrast to the FeS electrode (Chapter 1), the overall cell reactions do not involve the electrolyte phase. The regions are conveniently shown on a ternary phase diagram, and the open-circuit potentials relative to a Li, a LiAl, or a Li(Si) reference electrode are independent of the amount and composition of the electrolyte. The numbers on the phase diagram refer to the number of solid phases of the positive electrode in equilibrium when the overall composition of the system is within that region. The addition of lithium to an Fe-S system corresponds to moving along a line connecting the Fe-S composition to the pure lithium corner of the triangle. Therefore, the reversible discharge of an FeS_2 electrode corresponds to moving along the dashed line in Figure 4-1. The dashed line passes through four regions. The regions correspond to regions a through d in Table 4-1. It is helpful to think of the dashed line as beginning just below pure FeS_2. That is, beginning with a minor amount of the $Fe_{0.875}S$ phase. The reason for this will be discussed in Section 4.2.2. Region a is within the FeS_2-$Li_3Fe_2S_4$-$Fe_{0.875}S$ triangle. Region b is the thin triangle representing the $Li_3Fe_2S_4$-$Fe_{0.875}S$–$Li_{2.2}Fe_{0.8}S_2$ equilibrium. Region c is a two-phase region. At the beginning of this region, $Fe_{0.875}S$ and $Li_{2.2}Fe_{0.8}S_2$ are in equilibrium. Within the two phase region, the phases $Fe_{1-x}S$ and $Li_{2+x'}Fe_{1-x'}S_2$ are in equilibrium. At the end of region c, virtually all the $Fe_{1-x}S$ has disappeared, and only Li_2FeS_2 remains. In passing through the two-phase region, the composition variables x and x' range from 0.2 to 0 and 0.125 to 0, respectively. The final region of discharge, region d, is the Li_2FeS_2-Li_2S-Fe three-phase triangle. Li_2S and Fe are the final products of the complete discharge of an FeS_2 electrode. The potentials of the FeS_2 electrode in regions a and d are frequently called the upper-upper and lower voltage plateau, respectively. The voltage behavior in regions a, b, and c are sometimes lumped together and referred to as the upper voltage plateau.

We can compare the FeS_2 electrode discharge sequence with the discharge of an FeS electrode. The dotted line in Figure 4-1 represents the discharge of the FeS electrode. There are two regions of discharge shown for this electrode. The first region is the FeS-Li_2FeS_2-Fe phase triangle. The second region is the same as region d of FeS_2 discharge. Discharge of the FeS electrode through this final region occurs with a larger iron content than the discharge of the FeS_2 electrode through the same region. In actuality, this simple two reaction sequence (the X-phase mechanism) would occur at a much higher temperature ($> 641.5°C$). As we discussed in Chapter 1, at 450°C the J-phase intermediate (along with the X-phase intermediate) is a stable discharge product of the FeS electrode.

We will not include any potassium containing compounds in our treatment of the FeS_2 electrode. Experimental measurements indicate, however, that for the equilibrium discharge of an FeS_2 electrode in eutectic electrolyte, minor amounts of $LiK_6Fe_{24}S_{26}Cl$ (J-phase) are formed in region d.[14] Tomczuk et al. postulate that the slow chemical conversion (see Section 1.2.2) of the electrochemically produced X-phase to J-phase accounts for this. In Section 4.2.2, we discuss the evolution of sulfur vapor, which can also lead to the formation of J-phase via the reaction of FeS with the electrolyte. Tomczuk et al. also indicate the presence of the potassium containing compound $KFeS_2$ in the nonequilibrium discharge of the FeS_2 electrode.

4.2.1. Thermodynamic Open-Circuit Potential Data

The Gibbs phase rule can be applied to the FeS_2 electrode (at a constant temperature and pressure) and shows that there is only one degree of freedom for region c, and zero degrees of freedom for regions a, b, and d. In other words, reactions a, b, and d in Table 4-1 are characterized by potential plateaus and region c has an open-circuit potential that varies with utilization of the electrode. In this two-phase region, the solid phases change composition as the

electrode is discharged.

We describe the temperature dependence of the open-circuit potential in the three-phase regions with an equation of the form

$$U_l = a_l + b_l T .$$
(4-1)

Table 4-2 gives the literature data for the coefficients in this equation corresponding to reactions a, b, and d in Table 4-1. These coefficients and temperature in kelvins will give the potential in volts. All the electrode reaction potentials are given relative to a two-phase (α, β) LiAl alloy reference electrode.

Table 4-1

Electrochemical Reactions of the FeS_2 electrode

at 450°C [14]

Region

a. $2FeS_2 + 3Li^+ + 3e^- \rightarrow Li_3Fe_2S_4$

b. $Li_3Fe_2S_4 + 0.47Li^+ + 0.47e^- \rightarrow 1.58Li_{2.2}Fe_{0.8}S_2 + 0.84Fe_{0.875}S$

c. $Fe_{1-x}S$ and $Li_{2+x}Fe_{1-x}S_2$ produce Li_2FeS_2

d. $Li_2FeS_2 + 2Li^+ + 2e^- \rightarrow 2Li_2S + Fe$

The data in this table are for eutectic composition of electrolyte; however, the open-circuit potentials of all the reactions relative to the (α, β) LiAl reference electrode should be independent of electrolyte composition.

The reaction sequences described above are for the temperature of 450°C. The phase diagram in Figure 4-1 and the reaction stoichiometries shown in Table 4-1 are dependent on the temperature. The temperature dependency of the Fe-S system is well characterized.[32] The length of the single-phase portion of the Fe-S leg ($Fe_{1-x}S$ phase) will increase as the temperature is increased (up to 1015 K). The solid-solution phase $Li_{2+x}Fe_{1-x}S_2$ is not observed at room temperature. It is believed that this compound decomposes on cooling to $Li_{2.33}Fe_{0.67}S_2$ and Li_2FeS_2.[14]

The solid line in Figure 4-2 is a plot of the thermodynamic open-circuit potential of the $LiAl/FeS_2$ cell as a function of positive electrode utilization at

Table 4-2

Coefficients for the Open-Circuit Potential

of the FeS_2 Electrode

Region	a_i [V]	$b_i \times 10^3$ [V/K]
a.[*]	1.4251	0.4785
b.[†]	1.208771	0.65142
d.	1.43211	-0.147

[*]a_a and b_a were obtained from Reference 30.
[†]a_b and b_b were obtained from Reference 31.
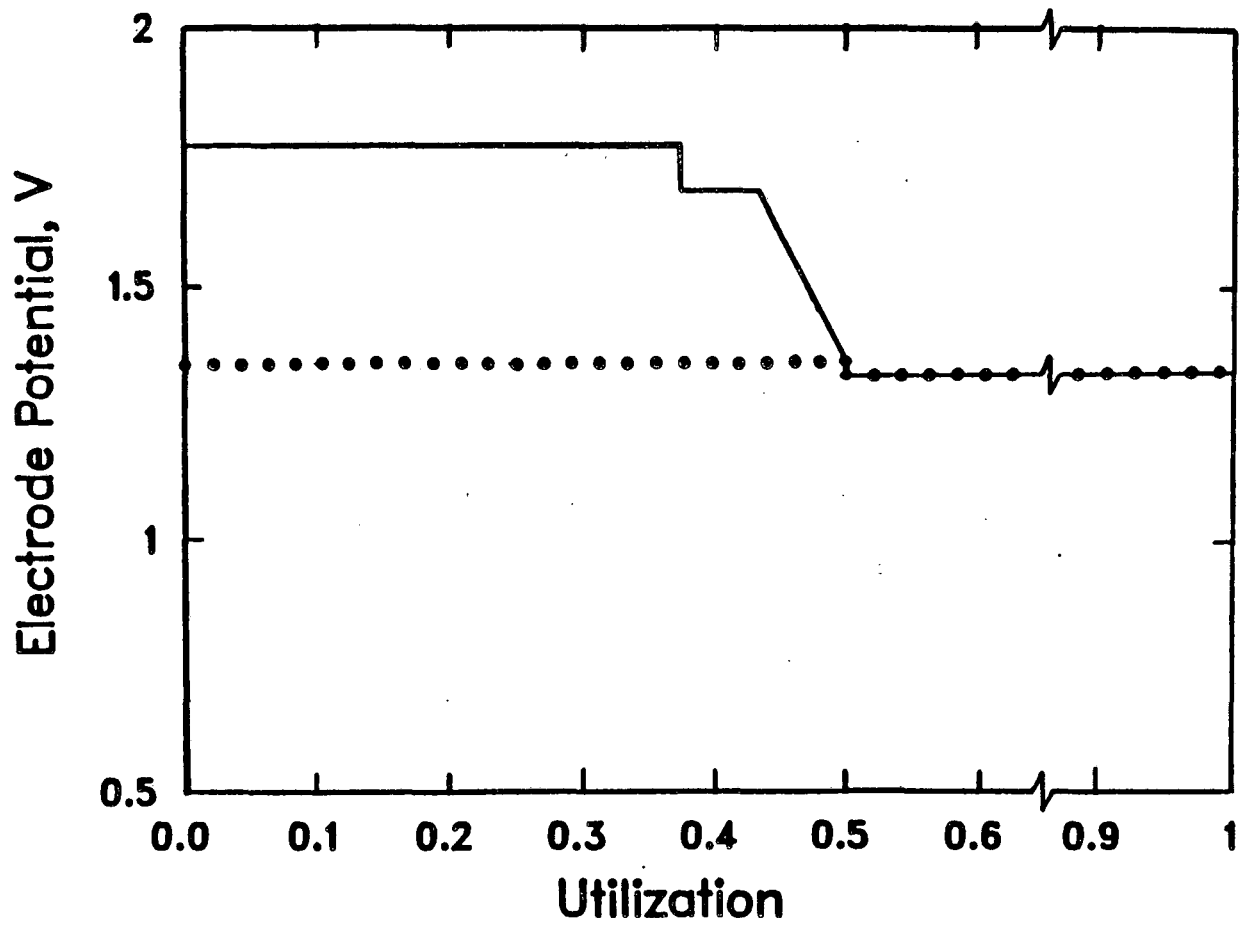
Figure 4-2. Thermodynamic, open-circuit potential as a function of positive electrode utilization at 450°C. The solid line is for a LiAl/FeS$_2$ cell. The dotted line is for a LiAl/FeS cell (X-phase mechanism).

450°C. The dotted line is for a LiAl/FeS cell discharged through the X-phase mechanism. This plot was constructed with the information given in Tables 4-1 and 4-2, and with the assumption of a linear potential variation through the two-phase region c. The thermodynamic, open-circuit potential behavior in region c has not been investigated by Tomczuk *et al.*[14] This lack of experimental data leads us to assume a linear potential variation in this region. The open-circuit potential at each end of this region is well characterized. The potential at the upper end of the region is given by the data for region b in Table 4-2. The potential at the lower end is given by the data for reaction three in Table 1-2. As shown in Figure 4-2, this is also the potential of the first plateau for discharge of the FeS electrode through the X-phase mechanism. The data for the two end points of region c can be combined to give

$$U_c = U_b + \frac{(a_3 - a_b) + T(b_3 - b_b)}{1 - (2.2(4x'_o - 2)/(2x'_o - 0.8) - 3)} \left[\frac{q_c \, 2 \, \tilde{V}_{FeS_2}}{\epsilon_{FeS_2}^\beta F} \right]. \qquad (4\text{-}2)$$

for the open-circuit potential behavior as a function of temperature and state-of-discharge q_c (the number of coulombs of charge passed for reaction c per unit volume of the electrode, see Equation 5-4). As we discussed earlier, the value of x'_o (0.875 at 450°C) is a function of temperature. The data for the Fe-S system[32] can be used, and we can estimate x'_o to have the following linear temperature dependence:

$$x'_o = -9.240 \times 10^{-5} \, T + 0.91658. \qquad (4\text{-}3)$$

The numbers 2.2 and 0.8 in Equation 4-2 arise from the formula of the compound $Li_{2.2}Fe_{0.8}S_2$ phase, which is assumed to be independent of temperature.

In Figure 4-2, region a of discharge terminates at 37.5%, utilization and region b terminates at approximately 42% utilization. The sloping potential region, region c, terminates at 50% utilization of FeS_2. One may actually consider the FeS_2 electrode to have yet another region of discharge with a small

capacity within the FeS-Li_2FeS_2-Fe triangle, which is responsible for the vertical drop in potential at the end of region c. As shown in Figure 4-2, this potential drop is equivalent to the gap in plateau voltages for the LiAl/FeS cell. It arises because the dashed line in Figure 4-1 touches the corner of the Li_2FeS_2–FeS–Fe three-phase triangle. The width of the region would increase with increases in the ratio of $Fe_{0.875}S$ to FeS_2 at the beginning of discharge. In this work we will assume that there is always an infinitesimally small amount of the $Fe_{0.875}S$ at the beginning of discharge to avoid discharge along the boundary in region a.

4.2.2. Additional Details Concerning the Li-Fe-S Phase Diagram

In this section, we will discuss some of the details of the Li-Fe-S phase diagram that were omitted from the discussion in the beginning of Section 4.2. The first subject to be discussed is the constant FeS_2 electrode potential that is obtained with discharge along the FeS_2–$Li_3Fe_2S_4$ boundary of the FeS_2–$Li_3Fe_2S_4$–$Fe_{0.875}S$ triangle (Figure 4-1) in experimental cells. These experimental cells utilize stoichiometric FeS_2 as the starting material. The potential during discharge, exactly along the boundary, is unstable. There are at least two explanations for this observed constant potential. The first possibility is the loss of sulfur due to the evolution of sulfur vapor. The dashed line in Figure 4-1 does not describe the discharge of an FeS_2 electrode with sulfur evolution. The discharge line would be shifted downward (away from the S corner) and perhaps develop curvature depending on the sulfur content at each point during the discharge. As discussed in the beginning of Section 4.2, $Fe_{0.875}S$ would then be a product of the first reaction, and capacity in the FeS–Li_2FeS_2–Fe region would appear during discharge. Since FeS may electrochemically react to form J-phase, this may explain the presence of J-phase in experimental cells as discussed in Section 4.2.1.

A second possible explanation is that the boundary may actually be a narrow two-phase region. For example, the compound $Li_3Fe_2S_4$ may have some

range of iron and sulfur composition. Thus, $Li_3Fe_2S_4$ would be represented by a corner of a two-phase triangle within the phase diagram. The discharge along this two-phase, FeS_2-$Li_3Fe_2S_4$ boundary would give a stable, constant potential. On the diagram then, another two-phase triangle would also exist between the boundary of the first two-phase region and the $Li_{2.2}Fe_{0.8}S_2$ phase.

The solubility of lithium in $Fe_{1-x}S$ is another detail of the Li-Fe-S phase diagram to be discussed. During discharge through region c, minor amounts of lithium are detected in the $Fe_{1-x}S$ phase.[31] That is, this single-phase portion has some width in lithium composition. Consequently, the FeS_2–$Fe_{0.875}S$ two-phase field would also have some width.

The Li_2S–FeS_2–S region of Figure 4-1 was not investigated by Tomczuk *et al*. The potential in this region can be calculated from the Gibbs free energies of the components.[33] The calculations give 1.88 V versus the LiAl reference electrode. This value agrees with the data of Schmidt and Weppner[28] that are discussed in the next section.

The final topic of discussion is an anomalous voltage spike that is observed in experimental cells. The voltage spike shown in Figure 4-3 at the beginning of discharge is a typical experimental observation (see also Figure 5-8). We can formulate three possible explanations for this behavior. One explanation is the presence of a highly reactive impurity. Secondly, the spike may be due to the reaction of liquid sulfur formed by over-charging the electrode. Another possibility is that the Li-Fe-S phase diagram may not be complete. For example, FeS_2 may exhibit some degree of nonstoichiometry, and the point on the diagram may actually be part of a single-phase segment. This region would not have much lithium capacity and would give rise to a sharp voltage drop on discharge.
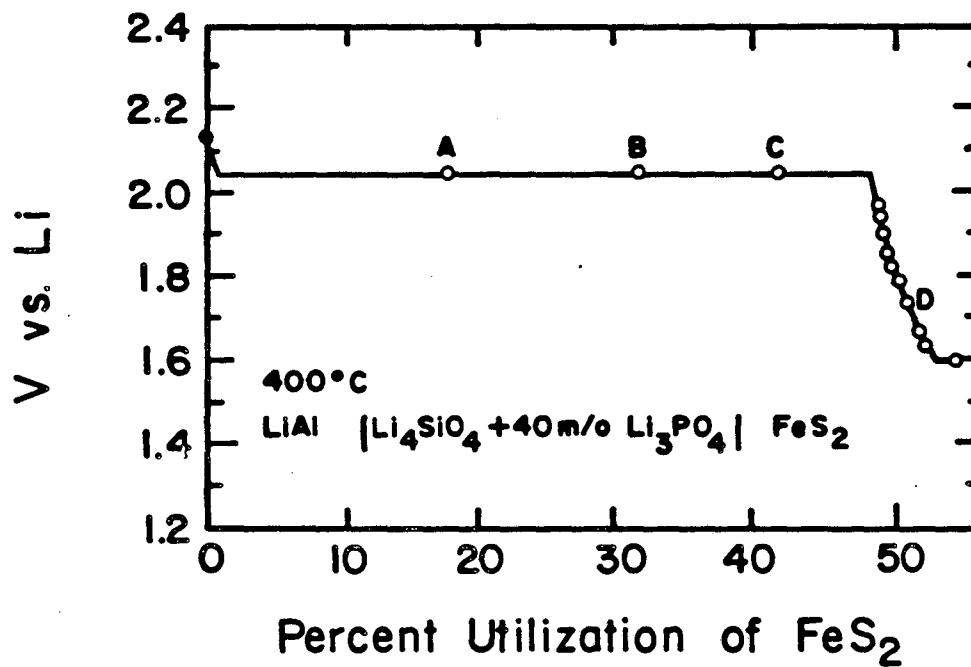
Figure 4-3. Measured potential as a function of composition for the discharge of an FeS_2 electrode as given by Schmidt and Weppner.[28]

4.2.3. Comparison of the Work of Schmidt and Weppner[28] and Tomczuk et al.[14]

The discussion in Section 4.2 concerned only the work of Tomczuk et al. from Argonne National Laboratories. We use their work to calculate the results shown in this chapter and in the mathematical model presented in Chapter 5. In this section, we compare the results of their work with the results of Schmidt and Weppner.[28] Schmidt and Weppner studied the potential and phase behavior of the FeS_2 electrode from 0 to about 40% lithium content at 400°C. They used both solid-state, $Li_4SiO_4 - Li_3PO_4$ and molten LiCl-KCl electrolytes. The use of the solid electrolyte was claimed to reduce the observed reaction with the molten salt electrolyte in the first part of discharge.[28] However, the solid electrolyte permitted the loss of sulfur vapor within the $S-FeS_2-Li_2S$ three-phase region; this did not occur when the molten salt electrolyte was employed. Some of their data are shown in Figure 4-3. The samples at the points labeled A, B, C, and D were prepared at the defined compositions. All other points had the lithium content varied by coulometric titration from the composition at point D (Li_2FeS_2). One major conclusion in their work contradicts the work of Tomczuk et al., namely, that Li_2FeS_2 is the only ternary compound in the Li-Fe-S phase diagram. They claim that this compound has a wide range of non-stoichiometry, indicated by the sloping potential region in Figure 4-3. They show a 10% variation in lithium content about Li_2FeS_2. The stoichiometry given by Tomczuk et al. shows a 20% variation in lithium content from $Li_3Fe_2S_4$ to Li_2FeS_2 (through region c). Schmidt and Weppner did not titrate through a wide enough range to conclude that 10% is the maximum variation in lithium content throughout the sloping potential region. To summarize, the two studies agree that an FeS_2 electrode would encounter a sloping potential region on discharge. However, the position and width of the region are not in agreement. It should be noted that Tomczuk et al. did their experimentation at a temperature 50°C higher than Schmidt et al. It is possible that

the range and position of the sloping potential region are functions of temperature.

Schmidt and Weppner do not agree with the existence of the $Li_3Fe_2S_4$ phase. They consider the plateau from 0 to 42% utilization to be the reaction of FeS_2 to Li_2FeS_2. It is unfortunate that they did not have another data point in the range of 42 to 48% utilization that could support this conclusion. Experimental cells distinctly show a second voltage plateau at 37% utilization, which supports the existence of the $Li_3Fe_2S_4$ phase.

Schmidt and Weppner are in good agreement (within 1%) with Tomczuk et al.[1] on the potential in region a (0-35% lithium) and in the $FeS-Fe-Li_2FeS_2$ three-phase region (> 43% lithium) at 400°C with 4 data points and 2 data points, respectively.

Schmidt and Weppner are also in good agreement with our calculated potential (see Section 4.3.2) for the $S-FeS_2-Li_2S$ region. It is confusing that they claim their 20% Li - 65 %S - 15% Fe measurement to be in the $S-FeS_2-Li_2FeS_2$ three-phase region, which does not exist. Perhaps, this is a misprint. They have one data point in this region. As mentioned earlier, this measurement could only be obtained with the molten salt electrolyte.

Schmidt and Weppner's data are 45 mV lower for the potential in the $Fe-Li_2S-Li_2FeS_2$ region than the data of Tomczuk et al. It should be noted that Schmidt et al. report only one data point in this region.

Schmidt and Weppner[34] have also investigated the non-equilibrium discharge behavior of FeS_2. They observed a drop in voltage at a lower lithium concentration than they expected. The voltage drops until a 79 mV lower plateau voltage is reached. They explain these observations by the formation of a metastable Li_2S_2 phase. One may argue that the second plateau is due to the onset of reaction b in Table 4-2. The data of Tomczuk et al., however, predict

the second plateau to be 100 mV lower than the first plateau when the temperature is 400°C. More research is required to resolve the discrepancies in the two pieces of work.

4.3. The Phase Behavior of Li(Si) at 450°C

Figure 4-4 gives a plot of the potential of a Li(Si) electrode relative to a two-phase LiAl reference electrode as given by a Wen and Huggins.[29] Table 4-3 gives the corresponding electrochemical reactions and coefficients for the form of the open-circuit potential given in Equation 4-1. The potential is given in volts, and the temperature is in kelvins. Sharma and Seefurth[35] give the temperature dependence of the potential plateaus. The reactions are written according to the phase compositions given by Wen and Huggins.

Table 4-3

Reactions and Coefficients for the

Open-Circuit Potential of the Li(Si) Electrode

Reaction		a_i^* [V]	$b_i \times 10^{3*}$ [V/K]
I	$Li_{3.25}Si \rightarrow Li_{2.33}Si + 0.92Li^+ + 0.92e^-$	-0.187529	0.0731
II	$Li_{2.33}Si \rightarrow Li_{1.71}Si + 0.62Li^+ + 0.62e^-$	-0.088097	0.1122
III	$Li_{1.71}Si \rightarrow Si + 1.71Li^+ + 1.71e^-$	-0.0345	0.1056

*a_i and b_i were obtained from Reference 35.
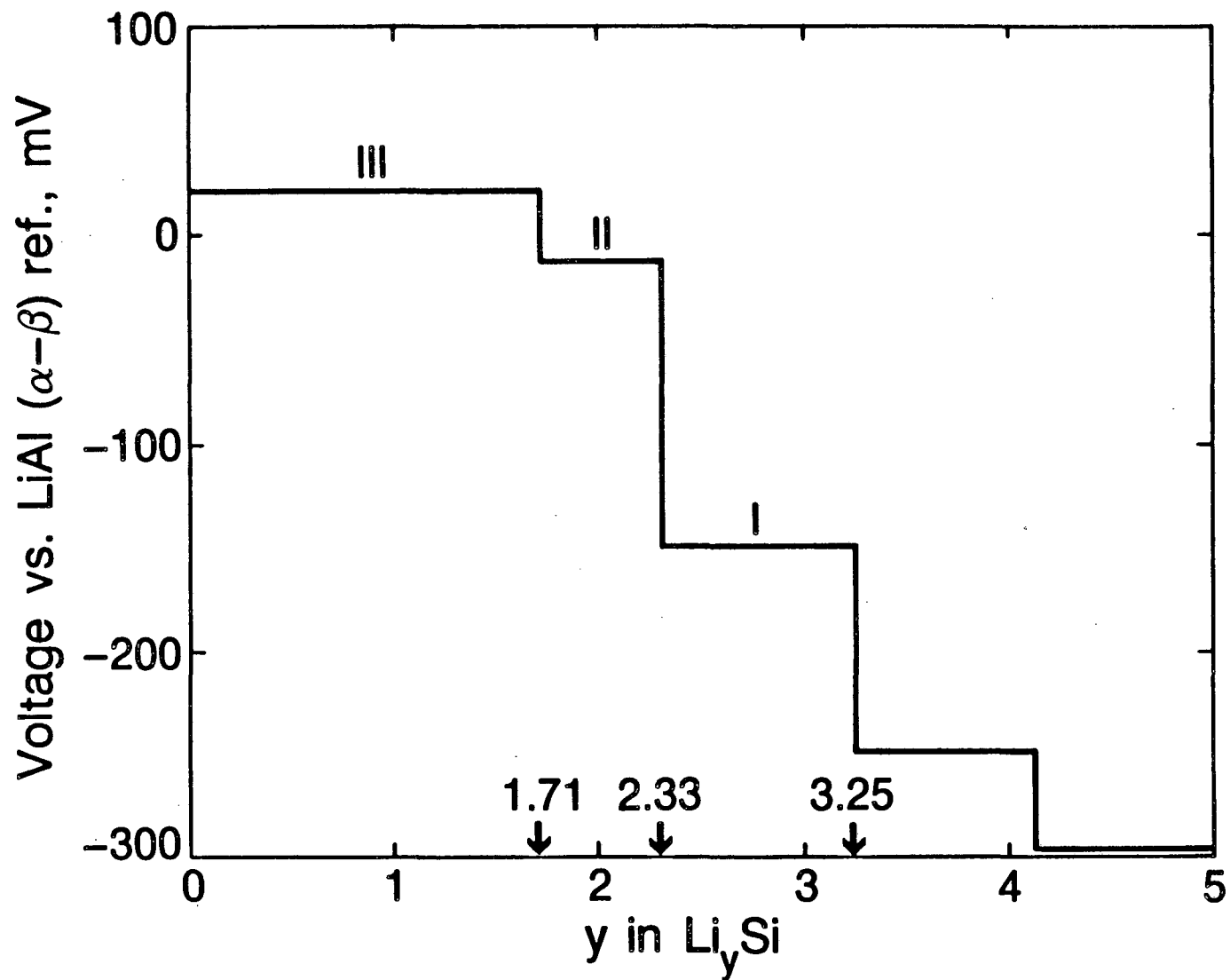
Figure 4-4. Coulometric titration curve providing potential as a function of Li(Si) electrode composition at 400°C.[28]

The equilibrium discharge of a Li(Si) electrode is shown by moving to the left in Figure 4-4 from a chosen starting material. We have designated three regions of discharge. Each region is a two phase region and is characterized by a potential plateau (at constant temperature and pressure). For example, starting with the $Li_{3.25}Si$ alloy, the removal of lithium on discharge will form the $Li_{2.33}Si$ phase. When the starting material is exhausted, potential plateau II is reached. If more lithium is removed from the $Li_{2.33}Si$ phase, the $Li_{1.71}Si$ phase is formed. The exhaustion of the $Li_{2.33}Si$ allows the potential to rise to plateau III. In this region, the $Li_{1.71}Si$ is in equilibrium with essentially pure silicon.

There are several aspects that should be considered in the design of a Li(Si) electrode. The $Li_{4.4}Si$ alloy is not a desirable starting material because it is unstable and cannot be handled effectively in a dry room. Also, discharge through region III should be avoided because the electrode has a high specific resistance is this region.[36]

In Figure 4-4 the potential appears to rise vertically between plateaus. The vertical portions on this figure, however, are actually narrow single-phase regions. Wen and Huggins investigate these narrow regions of non-stoichiometry and give the chemical diffusion coefficients of lithium in the alloy. The width of the $Li_{3.25}Si$, $Li_{2.33}Si$, and $Li_{1.75}Si$ single-phase regions corresponds to $\Delta y = 0.028$, 0.06, and 0.008, respectively. In our work with the Li(Si) electrode, we ignore the width of the single-phase regions.

4.4. The Open-Circuit Potential Behavior of Li(Si)/FeS$_2$ Cells

The computer program given in Appendix A-4 combines the data in Tables 4-1 and 4-2 and Equations 4-2 and 4-3 to yield the open-circuit potential behavior of a Li(Si)/FeS$_2$ cell. All of the results are presented for a cell with the capacity limited by the FeS$_2$ electrode. Figure 4-5 illustrates the open-circuit potential behavior as a function of positive electrode utilization. The cell is
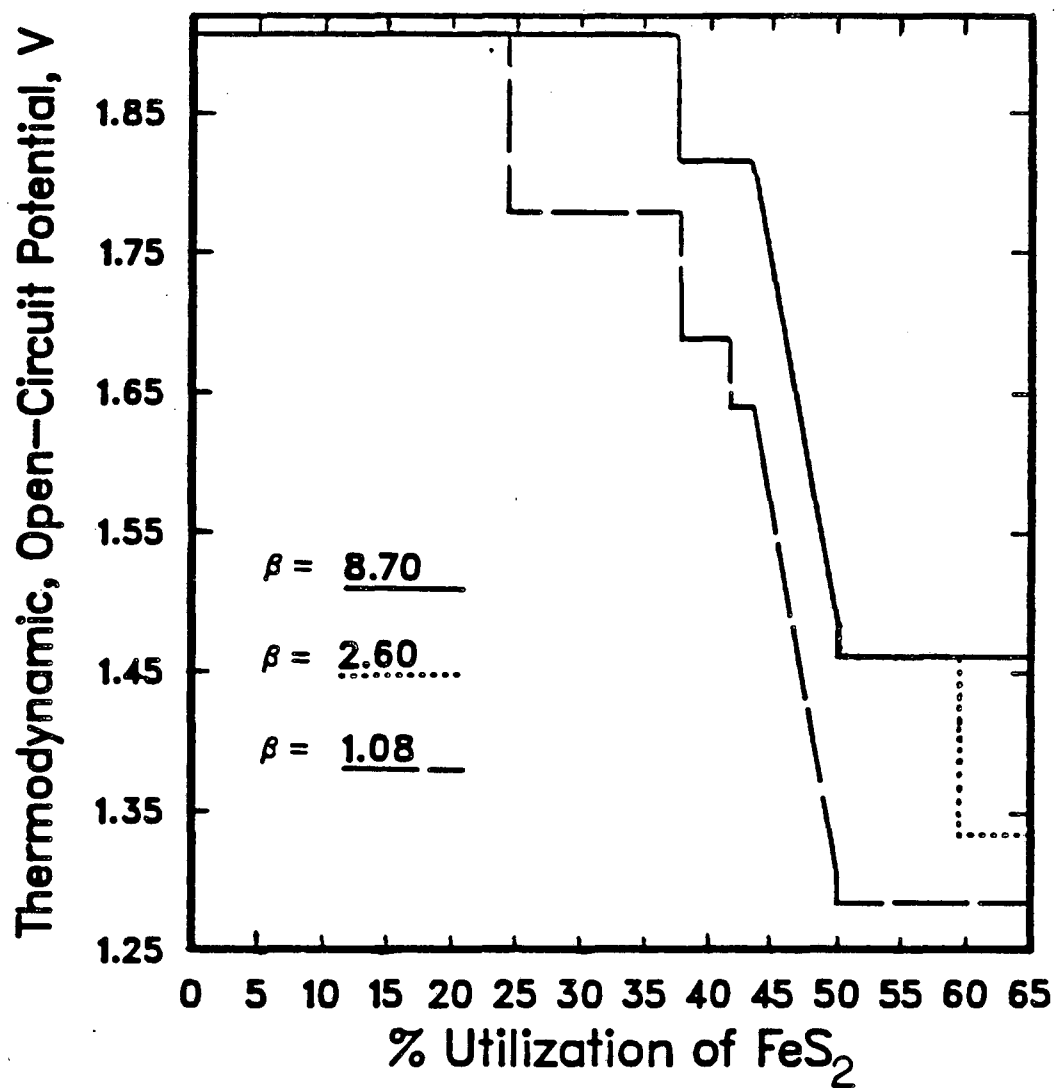
Figure 4-5. Calculated open-circuit potential behavior as a function of positive electrode utilization for a Li(Si)/FeS₂ cell at 725 K. In each curve, the ratio of negative to positive electrode starting material β is varied.

discharged reversibly and isothermally at 450°C for different values of the parameter β, the mole ratio of $Li_{3.25}Si$ to FeS_2. For a large value of β, we would expect to see the positive electrode behavior reflected in the discharge of a $Li(Si)/FeS_2$ cell. This is the case in Figure 4-5 for $\beta = 8.7$. As the value of β is decreased we would expect to see more of the negative-electrode behavior during discharge.

In Figure 4-5 for the case of $\beta = 8.7$, the first drop in potential at 37.5% utilization is caused by the positive electrode going from region a to region b. The sloping potential region reflects the positive electrode going through region c (the two-phase region). At 50% utilization, the positive electrode reaches region d, the final plateau. Discharge with $\beta = 2.6$ is similar to the case with $\beta = 8.7$ except for the extra potential drop at 60% utilization. This potential drop reflects the behavior of the negative electrode going from region I to region II. For the case of $\beta = 1.08$, the corresponding potential drop occurs much earlier in the discharge (at 22% utilization). The second potential drop stems from the positive electrode going from region a to region b, the third potential drop marks the negative electrode entering region III, and the remainder of discharge reflects the behavior of the positive electrode. For the case with $\beta = 1.08$, the capacity of the negative electrode almost matches the capacity of the positive electrode. As we mentioned in Section 4.3, entering region III of the Li(Si) electrode during discharge is undesirable. One may reject the design of this cell based on the results of Figure 4-5 alone.

Figure 4-6 gives the thermodynamic, open-circuit potential as a function of positive electrode utilization for two different temperatures and $\beta = 1.08$. If the temperature is increased from 650 K to 725 K, then the open-circuit potentials for the first four plateaus are increased. The final plateau in this figure reflects region d of the FeS_2 electrode. The positive electrode reaction in this region is exothermic, and the open-circuit potential decreases with increasing tempera-
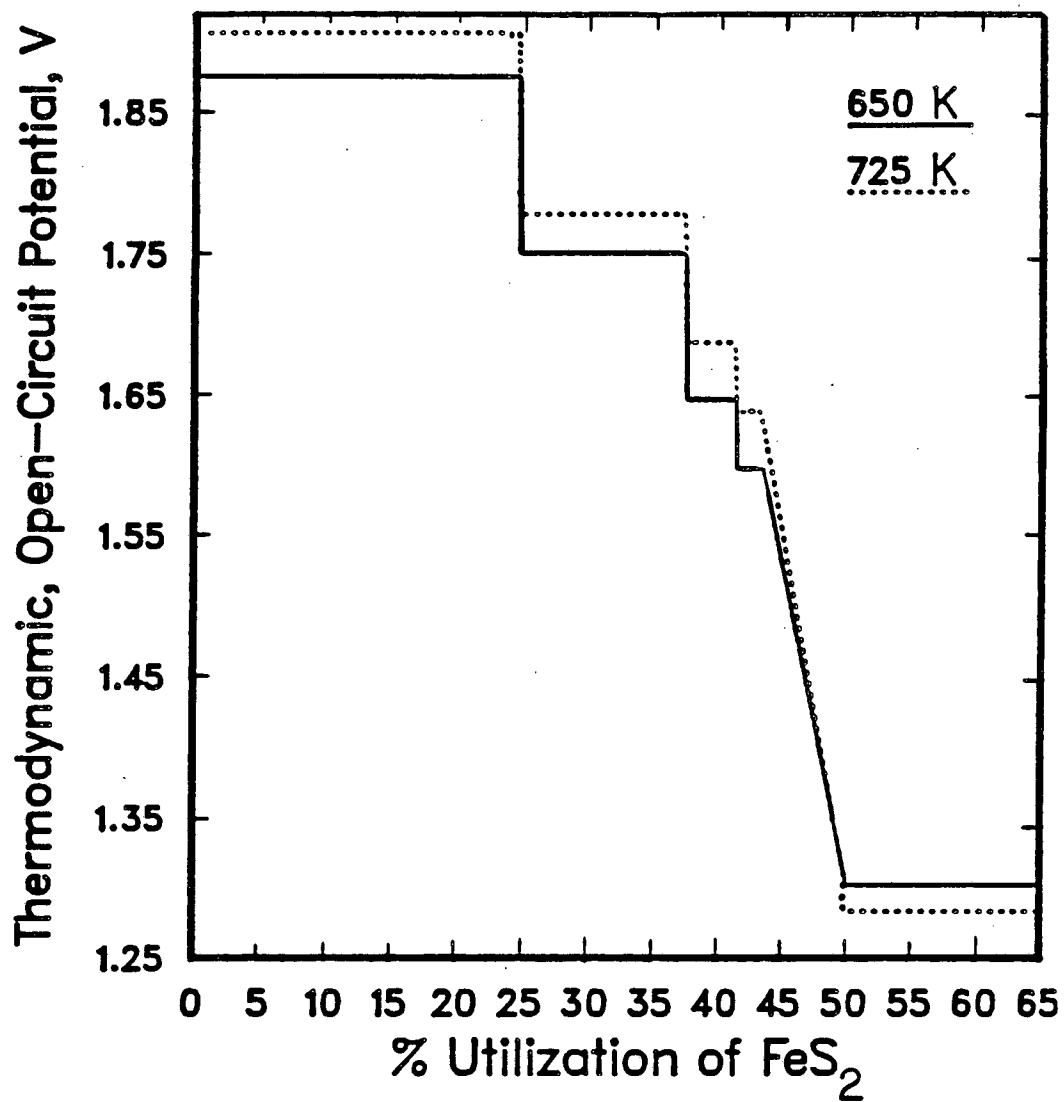
Figure 4-6. Calculated open-circuit potential behavior as a function of positive electrode utilization for a Li(Si)/FeS$_2$ cell at two different temperatures.

ture.

With these thermodynamic data, we can examine the heat-generation rate for the reversible isothermal discharge of a Li(Si)/FeS_2 cell. This can give insight into the heating or cooling that may be required to maintain isothermal operation of a cell. This is an important aspect of cell design. In Figure 5-9 we show the mathematical model result for the temperature decrease of a well-insulated (but not adiabatic) LiAl/FeS_2 cell during discharge on the upper-upper plateau of the FeS_2 electrode.

4.5. Conclusions

We have discussed the thermodynamic, open-circuit potential behavior of the Li(Si)/FeS_2 cell as a function of state-of-discharge, temperature, and negative-to-positive capacity ratio. This thermodynamic information is derived from the primary data on the open-circuit electrode potentials relative to LiAl available in the literature.

There are four regions in the discharge of an FeS_2 electrode and three regions in the discharge of a Li(Si) electrode. Consequently, the equilibrium voltage behavior of a Li(Si)/FeS_2 cell exhibits many regions (up to six) and can vary as much as 0.6 V during discharge. This must be considered in the design of these cells because there may be applications that will not tolerate the large voltage drop during discharge.

All of the regions in the discharge of a Li(Si)/FeS_2 cell are endothermic except the region in which reaction d of the FeS_2 electrode occurs. Therefore, to maintain isothermal operation, a Li(Si)/FeS_2 cell discharged reversibly would require external heating, up to 50% utilization of FeS_2, and cooling after 50% utilization.

Chapter 5

Mathematical Modeling of Li(alloy)/FeS$_2$ Cells

5.1. Introduction

A mathematical model of the Li(alloy)/LiCl-KCl/FeS$_2$ cell is described in this chapter. The model is developed from Pollard and Newman's model[3,4,5] for the LiAl/LiCl-KCl/FeS cell. The thermodynamic behavior of the Li(alloy)/FeS$_2$ cell is addressed in Chapter 4. An understanding of the thermodynamic behavior of the cell is essential to developing the mathematical model. It is our hope that modeling the Li(alloy)/FeS$_2$ cell will aid in its design, help guide experimental research, and contribute to a more fundamental understanding of the system.

The interest in high temperature molten salt batteries was originally focused on the LiAl/FeS cell and has more recently broadened to Li(Si)/FeS$_2$ couples. The thermodynamic behavior of the LiAl/FeS cell is discussed in Chapter 1, and some model results are given in Chapter 2. The Li(Si)/FeS$_2$ cell has a higher operating voltage than the LiAl/FeS cell, and the Li(Si) electrode has more usable lithium content than the LiAl electrode.

The galvanostatic discharge behavior of the Li(alloy)/FeS$_2$ cell constitutes the main emphasis of this chapter. In Section 5.2, we describe the mathematical model and the modifications that have been made to the original work of Pollard and Newman.[3,4] In Section 5.3, we give model results for the Li(alloy)/FeS$_2$ cell and make comparisons with experimental results available in the literature.

5.2. Mathematical Model Development

A cross section of a cell sandwich is shown schematically in Figure 2-1. In order for this figure to correspond to the model developed in this chapter, the negative electrode can be either LiAl or Li(Si), and the positive electrode can be either FeS or FeS_2. The description of Figure 2-1 given in Section 2.2, except for the incorporation of the J-phase mechanism, applies to the Li(alloy)/FeS_2 model. The fundamental equations, presented in Section 2.2.1, are material balance equations for species in the electrolyte phase and electrode matrix phase, an Ohm's law equation, a current balance equation, and kinetic equations. The equations are cast into finite difference form along with the appropriate boundary conditions and solved iteratively by the method of Newman (BAND).[15] The Fortran computer code for the cell model (BATRY) is given in Appendix A-2. In the next section, the incorporation of the FeS_2 electrode behavior into the cell model is discussed. The incorporation of the Li(Si) electrode into the model is presented in Section 5.2.2. The computer code is discussed in Section 5.2.3 along with a flow chart of the program.

5.2.1. Incorporation of the FeS_2 Electrode Behavior

The reactions of the FeS_2 electrode and thermodynamic data are given in Chapter 4. We distinguish four regions of behavior in the discharge of the FeS_2 electrode. The four regions are denoted as a, b, c, and d. If the electrode is discharged reversibly, then a single electrode reaction occurs within each region, corresponding to the reactions given in Table 4-1. The irreversible discharge of the electrode allows the reactions to occur simultaneously.

5.2.1.1. Kinetic Behavior

We shall first discuss the incorporation of the kinetic expressions for the reactions of the FeS_2 electrode. A polarization equation of the form

$$j_l = a i_{o,l} \left(e^{a_{a,l} F \eta_{s_l}/RT} - e^{-a_{c,l} F \eta_{s_l}/RT} \right) \tag{5-1}$$

is used, where

$$\eta_{s_l} = \eta - U_{l,o} . \tag{5-2}$$

is the local surface overpotential, and η is the electrode potential minus the electrolyte potential (Equation 2-7). The quantity $U_{l,o}$ is the theoretical open-circuit cell potential for reaction l, relative to a reference electrode of the same kind as reaction b shown in Table 4-1, at the composition prevailing locally. As we discussed in Chapter 4, the thermodynamic, open-circuit potentials of the overall cell reactions are not dependent on electrolyte composition; however, the open-circuit potential for the reaction in region c has a dependency on the local composition of the electrode's active material. It follows that η_{s_l} is $\eta - (U_a - U_b)$, η, and $\eta - (U_d - U_b)$ for the reactions in regions a, b, and d, respectively. The values of U_l are given by Equation 4-1 along with the coefficients given in Table 4-2.

The kinetic equation for the reaction in region c is more complicated than the other reactions because the surface overpotential is dependent on the extent to which the reaction has occurred. The surface overpotential is given by

$$\eta_{s_c} = \eta - (U_c - U_b). \tag{5-3}$$

where, U_c is defined by Equation 4-2 and

$$q_c = \int_0^t j_c \, dt . \tag{5-4}$$

5.2.1.2. Solid Phase Behavior

The behavior of the intermediate phases in the discharge of an FeS_2 electrode is fairly complex. The phase transitions that occur during the reversible discharge of the electrode are discussed in Section 4.2. In the mathematical

model, we simplify the phase transitions considerably. Equation 2-4 is the material balance on the solid electrode material. We assume that the phase transitions that occur as a result of the transfer currents j_b and j_c are approximated by the single transition

$$Li_3Fe_2S_4 + Li^+ + e^- \rightarrow 2\,Li_2FeS_2 \,. \tag{5-5}$$

The volume fraction of Li_2FeS_2 (X-phase) is calculated at each time step. One can think of this phase as being a lumped phase composed of the solid solution phases $Fe_{1-x}S$ and $Li_{2+x}Fe_{1-x}S_2$. (The composition variables x and x' are discussed in Section 4.2.) The molar volume of the lumped phase is assumed to be that of Li_2FeS_2 (X-phase). The approximation becomes accurate as reactions b and c approach completion. At this point, the amount of $Fe_{1-x}S$ approaches zero and the $Li_{2+x}Fe_{1-x}S_2$ phase has the composition Li_2FeS_2 (x = 0). We do not have molar volume data for the $Li_{2+x}Fe_{1-x}S_2$ compound as function of the composition variable x.

We use the same argument for the calculation of the matrix conductivity; the conductivity of the lumped phase is assumed to be that of Li_2FeS_2.

5.2.2. Incorporation of the Li(Si) Electrode Behavior

The thermodynamic behavior the Li(Si) electrode is described in Chapter 4. In Section 4.3, we distinguish three regions in the discharge of a $Li_{3.25}Si$ electrode. The mathematical model simulates the first region; the region in which the reaction

$$Li_{3.25}Si \rightarrow Li_{2.33}Si + 0.92\,Li^+ + 0.92\,e^- \tag{5-5}$$
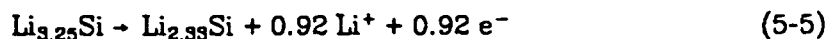
occurs. The simulation of the Li(Si) electrode is, therefore, virtually identical to the treatment of the LiAl electrode. The $Li_{3.25}Si$ alloy is analogous to β-LiAl, and the $Li_{2.33}Si$ alloy is analogous to α-Al. Initially, it is assumed that the negative electrode matrix consists of non-porous, spherical particles of $Li_{3.25}Si$. On

discharge, the outermost region of the particle reacts first, and a layer of $Li_{2.33}Si$ is formed which thickens gradually as the discharge proceeds. We refer the reader to the work of Pollard and Newman[3,4] for the mathematical description of this process.

A more complete description of the electrode behavior would include the reaction

$$Li_{2.33}Si \rightarrow Li_{1.71}Si + 0.62\, Li^+ + 0.62\, e^-, \qquad (5\text{-}6)$$
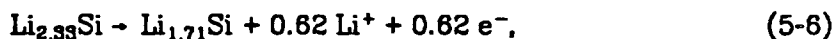
which occurs in the second region. The reaction in the third region should also be incorporated; however, the high resistivity of the pure silicon phase makes this reaction undesirable (Section 4.3). The Li(Si) electrode is twice as thick as the LiAl electrode in the mathematical model simulations.

5.2.3. Operating Parameters

In the next section, we present the model results for the galvanostatic discharge of the Li(alloy)/LiCl-KCl/FeS_2 cell. Many of the operating parameters for the LiAl/FeS_2 cell are not changed from those given in Chapter 2 for the LiAl/FeS model. In the model, the input parameter IPHASE is set to 0 or 1 to simulate the FeS_2 or FeS electrode behavior, respectively. We give some of the base case operating conditions and data required for the FeS_2 model in Table 5-1.

Deviations from the values in Table 5-1 will be noted in the figure captions. The operating parameters that are not given in this section can be found in Section 2.2.3 (Tables 2-1, 2-2, and 2-3). For example, the kinetic parameters, $i_{o,l}$, $\alpha_{a,l}$, $\alpha_{c,l}$, for the FeS and FeS_2 electrode reactions are the same. The thermodynamic data in Table 4-2 and Equation 4-2 are included in the model.

The molar volume data of some phases in the FeS_2 electrode are given in Table 5-2. The crystalographic data that are used to calculate the molar volumes are given in Reference 14.

Table 5-1

Physical Parameters and Base Case Input Data for the

LiAl/FeS$_2$ Cell Model

Quantity	Value	Quantity	Value
σ_{FeS_2}	100 $(\Omega\text{-cm})^{-1}$	i	0.0416 A/cm^2
L_+	0.21458 cm	T_o	743.15 K
$\epsilon^o_{FeS_2}$	0.245	$U_{a,o}$	0.0878 V
ϵ^o_+	0.755	$U_{b,o}$	0.0 V
$\epsilon_{ccp}\sigma_{ccp}$	2.1819 $(\Omega\text{-cm})^{-1}$	$U_{d,o}$	-0.37 V
p	1/3	U_b	1.6929 V

Table 5-2

Molar Volume Data for the Phases in the FeS_2 Electrode

Compound	M_i g/mol	crystal habit	unit cell volume $(\text{Å})^3$	formulas per unit cell	$\tilde{V}_i$ cm³/mol
FeS_2	119.975	cubic	158.956	4	23.93
$Li_3Fe_2S_4$	260.767	monoclinic	164.65	1	99.17
Li_2FeS_2	133.853	hexagonal	82.72	1	49.82
$Li_{2.33}Fe_{0.67}S_2$	117.713	hexagonal	249.55	4	37.58
$Fe_{0.875}S$	80.930	hexagonal	368.44	12	18.49
Li_2S	45.942	fcc	186.37	4	28.062

We assumed the values of 4 and 12 for the formulas per unit cell (given in the fifth column of Table 5-2) of the $Li_{2.33}Fe_{0.67}S_2$ and $Fe_{0.875}S$ compounds, respectively. Comparing the molar volumes of these compounds to that of Li_2FeS_2 and FeS (see Table 2-2), we see that our assumptions seem consistent. As we mentioned in Section 5.2.1.2, several simplifying assumptions have been made concerning the solid phase material balances. Due to these assumptions, the simulation of the FeS_2 electrode only requires the molar volume data for the FeS_2, $Li_3Fe_2S_4$ (Z-phase), Li_2FeS_2 (X-phase), Li_2S, and Fe phases.

The initial porosity of an FeS_2 electrode must be larger than the FeS electrode material because the FeS_2 electrode experiences a much larger volume increase upon full discharge than the FeS electrode. Researchers at General Motors build experimental FeS_2 cells with theoretical porosities of 0.30 to 0.50 when fully discharged (to Li_2S and Fe).[37,38] The data given in Table 5-2 for $\tilde{V}_{FeS_2}$ and $\tilde{V}_{Li_2S}$ and Table 2-2 for $\tilde{V}_{Fe}$ can be used to calculate ϵ_s^o from the theoretical

ϵ_+^{final}. For example, the theoretical final porosities of 0.30 and 0.50 correspond to initial porosities of 0.727 and 0.805, respectively. For our base case operating conditions, we use an initial porosity of 0.755.

The relevant Li(Si) electrode data are given in Table 2-3. The stoichiometric coefficients of the phases in the FeS_2 electrode that are needed for material balances are also given in this table. The molar volume data of pure Li and Si are for 20°C and obtained from Reference 39. The diffusion coefficients were obtained from Reference 28. We estimate the molar volumes

Table 5-3

Electrode Data

Li(Si) Electrode		FeS₂ Electrode	
Quantity	Value	Quantity	Value
$x_{Li}^{Li_{3.25}Si}$	0.7647	n_l	2.0
$x_{Si}^{Li_{3.25}Si}$	0.2352	$s_{Li^+,l}$	-2.0
$x_{Li}^{Li_{2.33}Si}$	0.6997	$s_{K^+,l}, s_{Cl^-,l}$	0.0
$x_{Si}^{Li_{2.33}Si}$	0.3003	$s_{FeS_2,a}$	-4/3
$\tilde{V}_{Li}$	13.093 cm³/mol	$s_{Z,a}$	2/3
$\tilde{V}_{Si}$	12.054 cm³/mol	$s_{Z,b(c)}$	-2
$D_{Li_{3.25}Si}$	7.9 × 10⁻⁵ cm²/s	$s_{X,b(c)}$	4
$D_{Li_{2.33}Si}$	4.9 × 10⁻⁵ cm²/s	$s_{X,d}$	-1
i_o	2.8 × 10⁻³ A/cm³	$s_{Li_2S,d}$	2
L_-	0.64 cm	$s_{Fe,d}$	1

of the lithium saturated $Li_{3.25}Si$ and $Li_{2.33}Si$ phases from

$$\rho_{Li_{3.25}Si} = \frac{\left(x_{Li}^{Li_{3.25}Si}M_{Li} + x_{Si}^{Li_{3.25}Si}M_{Si}\right)}{\left(x_{Li}^{Li_{3.25}Si}\tilde{V}_{Li} + x_{Si}^{Li_{3.25}Si}\tilde{V}_{Si}\right)} \tag{5-7}$$

and

$$\rho_{Li_{2.33}Si} = \frac{\left(x_{Li}^{Li_{2.33}Si}M_{Li} + x_{Si}^{Li_{2.33}Si}M_{Si}\right)}{\left(x_{Li}^{Li_{2.33}Si}\tilde{V}_{Li} + x_{Si}^{Li_{2.33}Si}\tilde{V}_{Si}\right)}. \tag{5-8}$$

respectively. In order to simulate the Li(Si) electrode behavior, the parameter IALLOY in the program is set to 0 (1 for LiAl), and the value for U_b must be changed. For example, for the base case condition of isothermal discharge at 743.15 K, U_b should be changed to 1.8261 V for operation with the Li(Si) negative electrode. The thermodynamic data for the first reaction of the Li(Si) electrode are given in Section 4.3.

5.2.4. Comments Concerning the Computer Code

The computer code for the Li(alloy)/FeS$_2$ cell is constructed from Pollard and Newman's code for the LiAl/FeS cell. The program has the ability to simulate FeS or FeS$_2$ positive electrode behavior and LiAl or Li(Si) negative electrode behavior. A flow chart of the program BATRY is shown in Figure 5-1, and the computer code is given in Appendix A-2. The major branch points within the main program are statement numbers 1 to 15. The program starts out with DELT = 0 at statement number 1. The following time steps branch from statement number 2, which is the beginning of the flowchart. At the beginning of the time-stepping loop, the time DEL for depletion of a reactant at each mesh point J is calculated with the previous current distribution. If a reactant is to be exhausted within the present time step, the time step is adjusted so the reactant is fully depleted within the time step. At statement number 3, the main iteration loop counter JCOUNT is initialized (before the first set of iterations the
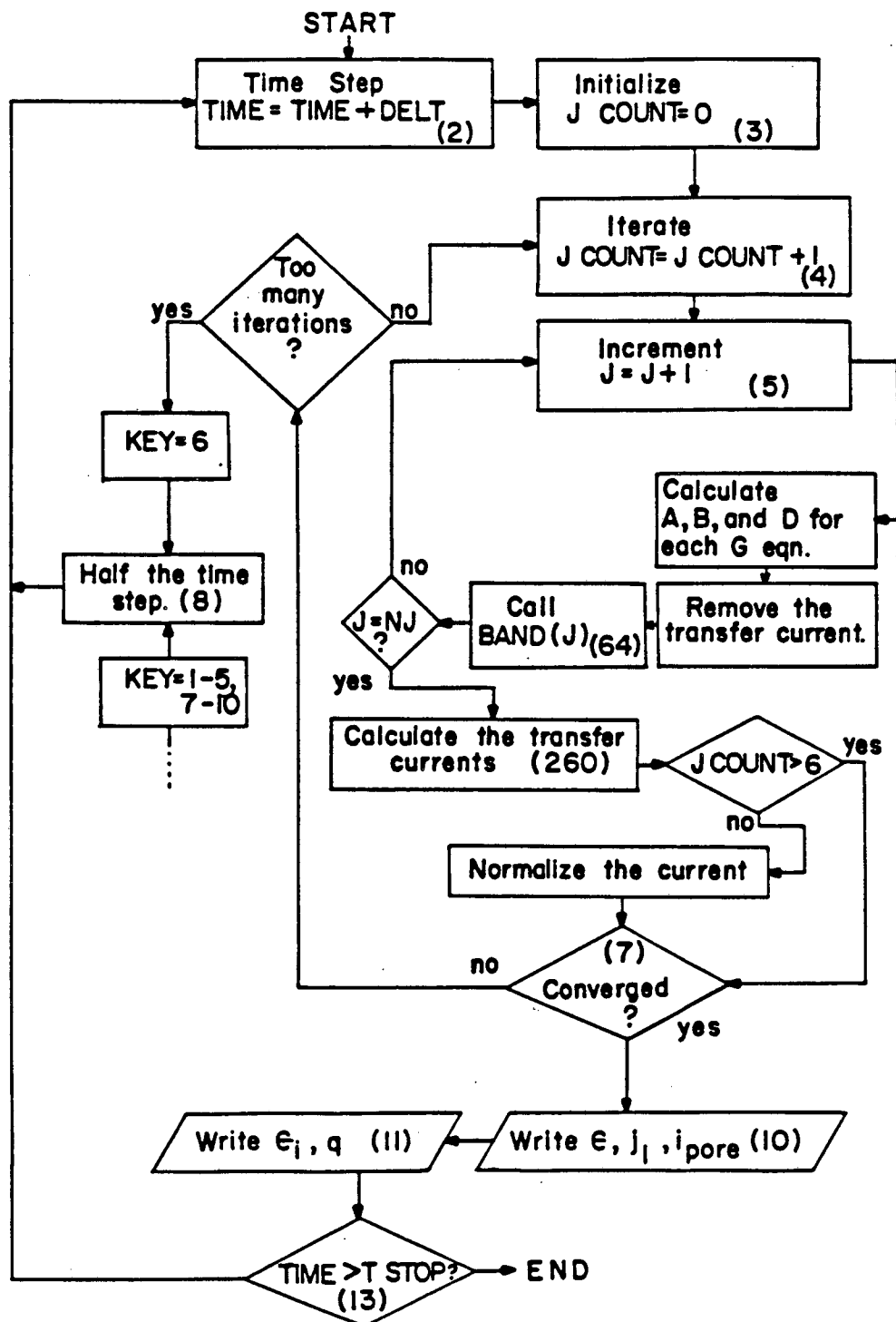
Figure 5-1. Flow chart for computer program BATRY (numbers in parenthesis refer to program-statement numbers).

program branches to statement number 260 for normalization of the current density and then back to statement number 4). The following iterations will branch from statement number 4. Statement number 5 increments the mesh point counter J. Within the J loop, the BAND coefficients, A, B, and D are calculated for each of the six equations G (see Section 2.2). The transfer-current variable and the kinetic equation are eliminated from the set of equations and unknowns also within this loop. At statement number 64, subroutine BAND is called for each mesh point. BAND uses the matrix inversion subroutine MATINV. After the loop has operated on all the mesh points, the deviation variables (current value minus most recent guess) are transformed to actual variables. At statement number 260, the current distribution in the positive electrode is normalized by shifting the potential distribution to give the correct total current density. The current distribution is renormalized only for the first six iterations. The program tests for convergence at statement number 7. If the convergence test is passed, the program begins printing results at statement numbers 10 and 11. At statement number 13, the program checks the time and number of time steps to see if it should stop.

In Section 5.3, we show results for reaction d in Figures 5-2 and 5-7. In order to conserve computer memory, the simulation of reaction d is accomplished by restarting the program with the appropriate data for reaction d substituted in for the first reaction. As the cell approaches 50% utilization, only reaction c occurs in the back of the positive electrode; FeS_2 has been exhausted, and reaction a does not occur. Specifically, U_d replaces U_a, and the X-phase, Li_2S, and Fe variables and data are put into storage locations for the FeS, X-phase, and Fe variables and data. For cases in which the FeS_2 is not exhausted before the onset of reaction d (as in Figure 5-3, 100 mA/cm^2) reprogramming and additional storage locations would be required in order to simulate region d.

5.3. Model Results for the Li(alloy)/FeS$_2$ Cell

In this section, we discuss the results of modeling the LiAl/FeS$_2$ cell. The thermodynamic behavior of Li(alloy)/FeS$_2$ cells is discussed in Chapter 4. An understanding of the thermodynamic behavior of iron-sulfide electrodes is essential to mathematical modeling. The Li-Fe-S ternary phase diagram indicates the different phase transitions that occur during the reversible discharge of an FeS$_2$ electrode.

The solid line in Figure 5-2 represents the reversible cell voltage for a LiAl/FeS$_2$ cell discharged at constant temperature. The utilization is defined as

$$\%\text{Utilization of FeS}_2 = \frac{100\, i\, t\, \tilde{V}_{FeS_2}}{L_+\, \epsilon^\beta_{FeS_2}\, 4\, F} \tag{5-9}$$

and may be thought of as a dimensionless time during discharge. The four regions of discharge of the FeS$_2$ electrode can be distinguished. Regions a, b, and d are potential plateaus; the cell potential in the intermediate region c varies with the state-of-discharge.

5.3.1. Discharge Behavior at 470°C and Eutectic Electrolyte Composition

The dashed line in Figure 5-2 gives the model result for the voltage of the FeS$_2$ electrode in a LiAl/FeS$_2$ cell, relative to a LiAl $(\alpha-\beta)$ reference electrode placed at the positive electrode-reservoir interface. Four regions of discharge of the FeS$_2$ electrode can be distinguished. The rounding of the discharge curve, relative to the solid curve is due to irreversibilities associated with ohmic losses, migration effects, mass-transfer, and reaction overpotentials.

At 92% utilization, we predict the 1 V cell cutoff voltage to be reached. This corresponds to approximately 6 hours of discharge. The cell voltage drops at this point because KCl precipitate has clogged the pores of the FeS$_2$ electrode. All the FeS$_2$ discharge reactions consume lithium ions, which causes the KCl
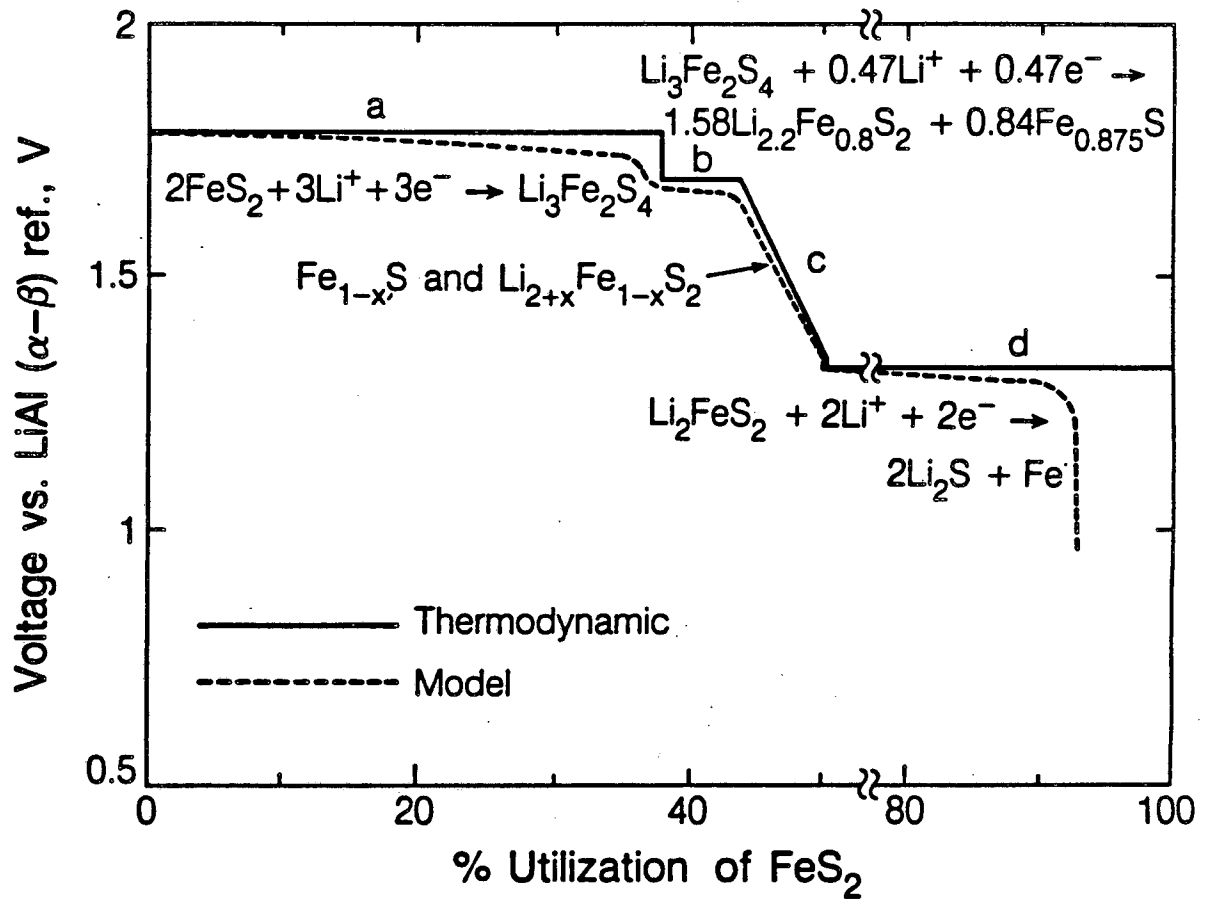
Figure 5-2. Calculated voltage of the FeS_2 electrode in a $LiAl/FeS_2$ cell relative to a LiAl (α, β) reference electrode placed at the electrode-reservoir interface. The solid curve is for a cell discharged reversibly at 470°C, and the dashed curve is the model result for a discharge current density of 41.6 mA/cm^2 (base case operating conditions).

concentration in the positive electrode to increase. If the KCl concentration increases above its saturation value, solid KCl precipitates within the electrode. The onset of KCl precipitation is predicted at 30% utilization; however, by 41.6% utilization the precipitate is not present because it was allowed to dissolve during the period that reaction c alone was occurring within the electrode, and the reaction distribution was nearly uniform. KCl precipitation is initiated a second time, on the final plateau, at 68.6% utilization. KCl precipitation has limited the electrode utilization to 92% utilization. At this point, the cell cutoff voltage is reached.

On the first plateau, reaction a is occurring, and the voltage drops at the end of the plateau. The onset of reactions b and c is marked by the voltage leveling, and the FeS_2 is exhausted at 39% utilization. Between these two points three reactions occur simultaneously within the positive electrode. Reactions b and c occur together at the same position within the electrode, and reaction a occurs in a region located more toward the back of the electrode. Reaction c begins simultaneously with reaction b in irreversible discharge, although it does not proceed rapidly until reaction b is completed at approximately 43.2% utilization.

The solid line in Figure 5-3 gives the FeS_2 electrode behavior when the discharge current density is increased to 100 mA/cm². The onset of the reactions b and c is initiated sooner (21.4% utilization) than for the case with the lower current density because of the increased overpotentials induced by the higher discharge current. The onset of KCl precipitation is predicted to occur at 17.6% utilization. In this case the FeS_2 is not exhausted before the cell cutoff voltage of 1.10 V is reached. The cell cutoff voltage is chosen to be the voltage just before the onset of reaction d since we cannot use the computer storage locations for reaction a to simulate reaction d in this case (see Section 5.2.4). The larger discharge current density means that at a given utilization a shorter
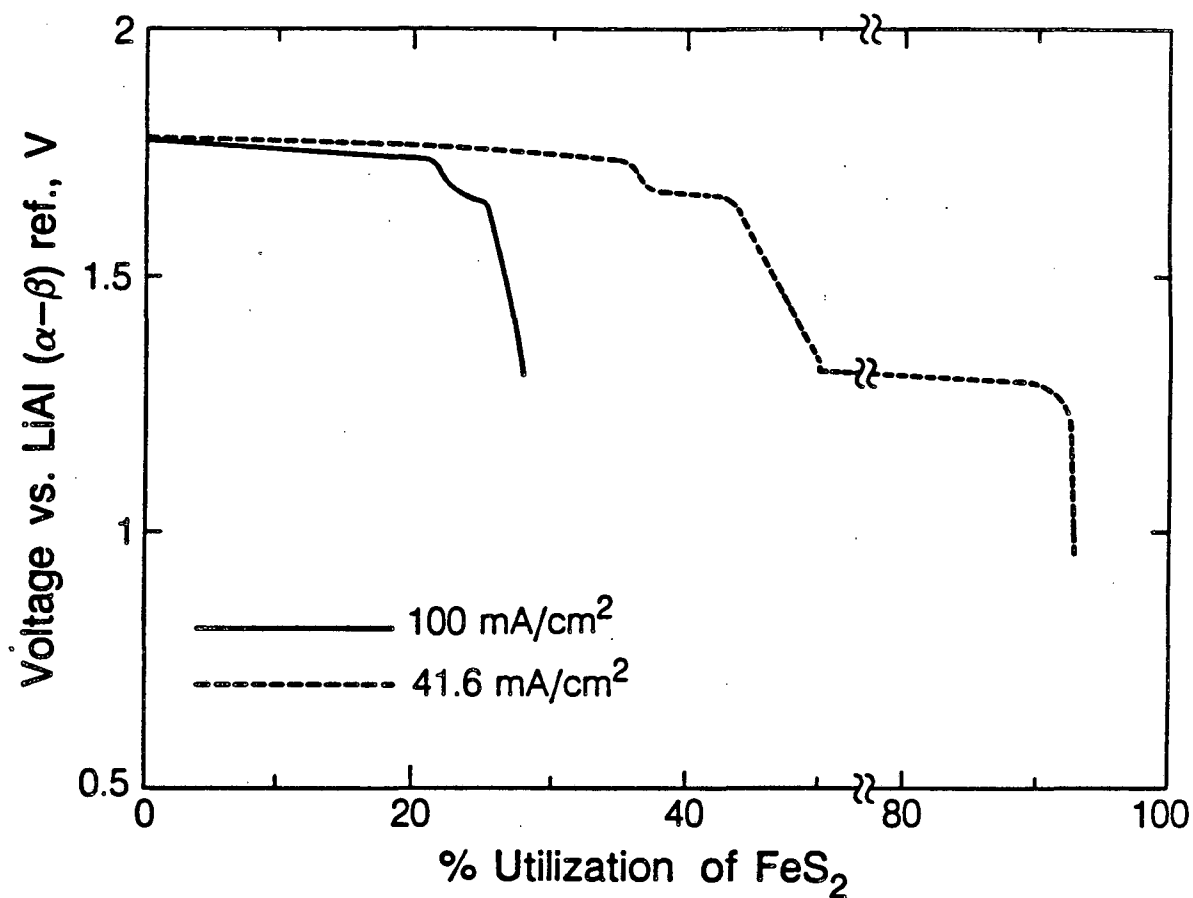
Figure 5-3. Model results for the voltage of the FeS$_2$ electrode in a LiAl/FeS$_2$ cell relative to a LiAl (α, β) reference electrode placed at the electrode-reservoir interface for two discharge current densities (base case operating conditions, except for i).

time period has elapsed. For example, the end of discharge for the 100 mA/cm^2 case (27.8% utilization) is reached after 0.65 hours. For the case with 41.6 mA/cm^2, 27.8% utilization is reached after 1.57 hours of discharge.

5.3.1.1. Reaction Distributions within the FeS$_2$ Electrode

The transfer-current density is equal to the divergence of the current density in the pores of the electrode with respect to distance (Equation 2-5). It is also proportional to the reaction rate per unit volume of the electrode. Figure 5-4 gives the distribution of the total transfer current at the onset of the b and c reactions. The behavior of the transfer current distribution is understood most easily be examining the potential distribution. The potential distribution is governed by the modified Ohm's law equation (Equation 2-6). We can non-dimensionalize this equation and define the different contributions to the potential gradient

$$\frac{\nabla \eta}{I\left(\frac{1}{\kappa}+\frac{1}{\sigma}\right)} = \frac{i_{pore}}{I}\frac{\frac{1}{\kappa}}{\left(\frac{1}{\kappa}+\frac{1}{\sigma}\right)} - \frac{i_{matrix}}{I}\frac{\frac{1}{\sigma}}{\left(\frac{1}{\kappa}+\frac{1}{\sigma}\right)} - \frac{RT}{Fx_{LiCl}}\frac{\left(1 + \frac{d\,\ln\gamma_{LiCl}}{d\,\ln x_{LiCl}}\right)\nabla x_{LiCl}}{I\left(\frac{1}{\kappa}+\frac{1}{\sigma}\right)}. \quad (5\text{-}10)$$

total = solution term + matrix term + concentration term

The solution term is proportional to the fraction of current flowing in the electrolyte and the electrolyte's fraction of the total electrode resistance at a given position within the electrode. Analogously, the matrix term is proportional to the fraction of current flowing in the matrix phase and the matrix's fraction of the total electrode resistance at a given point. In the absence of electrolyte concentration variations, these two terms determine the potential distribution. The concentration term accounts for concentration variations and is proportional to $\nabla(\ln x_{LiCl})$.

As shown in Figure 5-4, the solution current is transferred to the matrix phase at two main positions (mesh points). These two spikes mark the positions
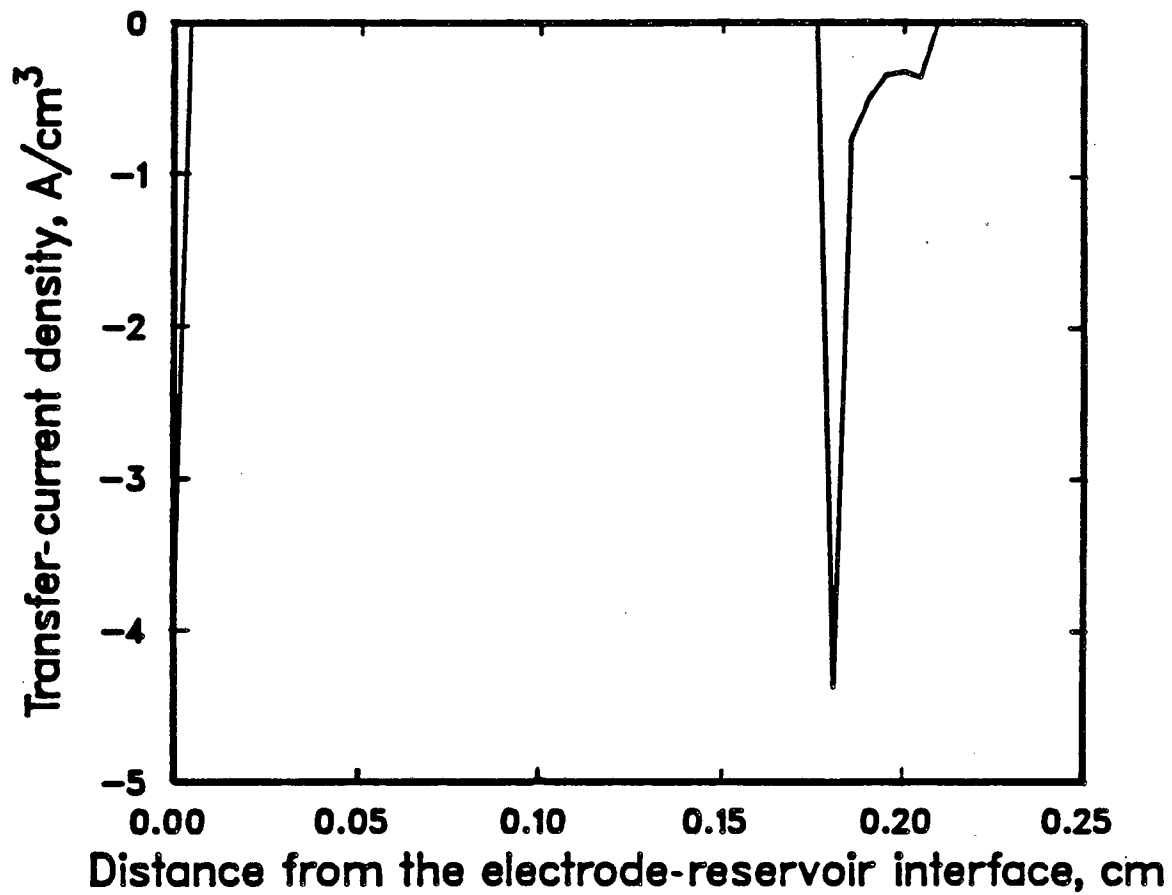
Figure 5-4. Transfer-current distribution within the FeS$_2$ electrode at the onset of reactions b and c (parameters as in Figure 5-3 for the 41.6 mA/cm^2 discharge).

of two reaction fronts. The position of the reaction front for reaction a is deep within the electrode, and electrode reactions do not occur in the region of the electrode between these two fronts. There is a minimum in j_a that is explained by the terms in the Ohm's law equation shown in Figure 5-5. The minimum in j_a is associated with the total potential gradient passing through zero. The behavior of the potential gradient appears to be dominated by the concentration term. KCl precipitate is present in the reaction zone of reaction a. The electrolyte concentration is constant in this region and is partially responsible for the zero in the gradient of the potential. The solution term also decreases after the position of the reaction front because the fraction of current density in the pore phase is decreasing as current is transferred to the matrix phase.

The reaction front for reactions b and c is at the front of the electrode. Most of the 41.6 mA/cm^2 of current density is transferred to the matrix phase by reaction a (i_a = 31.8 mA/cm^2). The remaining 9.8 mA/cm^2 of current density is transferred to the matrix phase by reactions b and c at a single mesh point. At the onset of reactions b and c, the surface potentials η_{s_b} and η_{s_c} are negative only at the front mesh point of the FeS$_2$ electrode. At the the front of the electrode j_b = 3.975 A/cm^3 and j_c = 0.131 A/cm^3. The transfer current for reaction c is smaller than reaction b due to the state-of-discharge dependent overpotential.

At 40% utilization, the FeS$_2$ is exhausted, and eventually the capacity in region b is also exhausted. After this point, reaction c is the only reaction occurring within the electrode.

As discharge proceeds, the reaction distribution becomes uniform, and at 49.77% utilization the transfer-current distribution is uniform throughout the electrode with a value of 0.195 A/cm^3. The dependency of the surface overpotential on the state-of-discharge forces the reaction zone to penetrate deep into the electrode, unlike the behavior of the reaction zone depicted in Figure
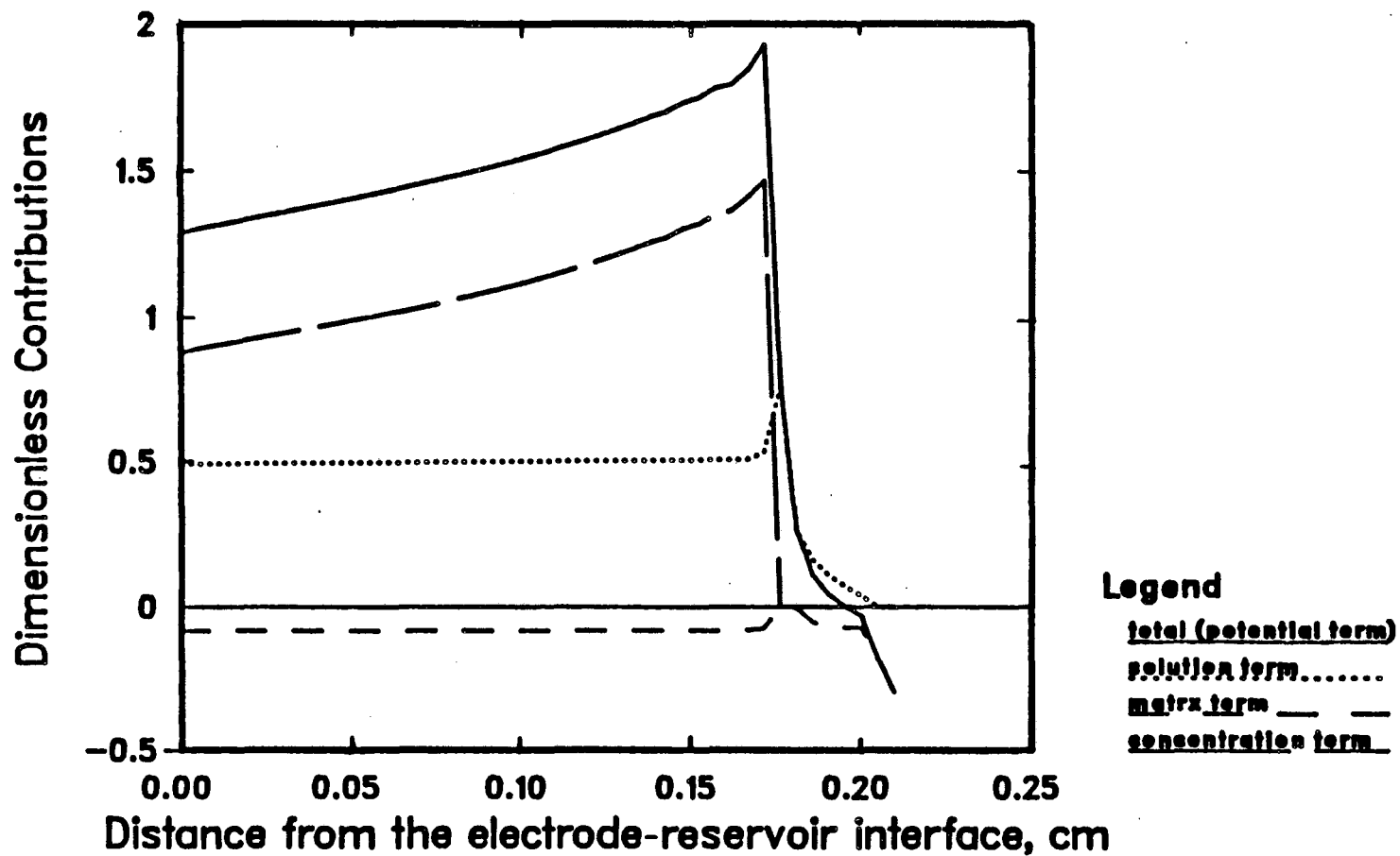
Figure 5-5. Contributions of terms in the Ohm's law equation (Equation 5-4) throughout the FeS$_2$ electrode (corresponding to the case depicted in Figure 5-5).

5-4. After 49.77% utilization, the capacity in region c becomes exhausted at the front of the electrode, and the exhausted area moves deeper into the electrode as discharge proceeds.

At 49.99% utilization, the surface overpotential η_{s_d} at the front of the electrode becomes negative, this marks the onset of reaction d. The behavior of the reaction zone for reaction d is similar to that of reaction a. It is a sharp zone that starts at the front of the electrode and moves through the electrode as X-phase is converted to Li_2S and Fe.

5.3.1.2. Comparison of the Behavior of the LiAl/FeS$_2$ Cell
to the Behavior of the Li(Si)/FeS$_2$ Cell

Figure 5-6 gives the model results for the voltages of electrodes relative to a two-phase LiAl $(\alpha-\beta)$ reference electrode placed at the positive electrode-reservoir interface. The upper dashed line gives the potential of the FeS$_2$ electrode in a LiAl/FeS$_2$ cell, relative to this reference electrode. The lower dashed line gives the potential of the LiAl negative electrode relative to this reference electrode; the difference between the two dashed curves, is the cell voltage.

The results of the of the Li(Si)/FeS$_2$ cell discharged only on the upper-upper plateau of the positive electrode are shown by the solid curves. The behavior of the FeS$_2$ electrode appears to be independent of the negative electrode. We presume that the potential of the positive electrode in the Li(Si)/FeS$_2$ cell would yield approximately the same potential as in the LiAl/FeS$_2$ cell if we chose to discharge to greater depths. As shown by this figure, a larger cell voltage is obtained with the cell with the Li(Si) electrode relative to the cell with LiAl as a negative electrode.

5.3.2. Discharge Behavior at 450°C and Lithium-Rich Electrolyte
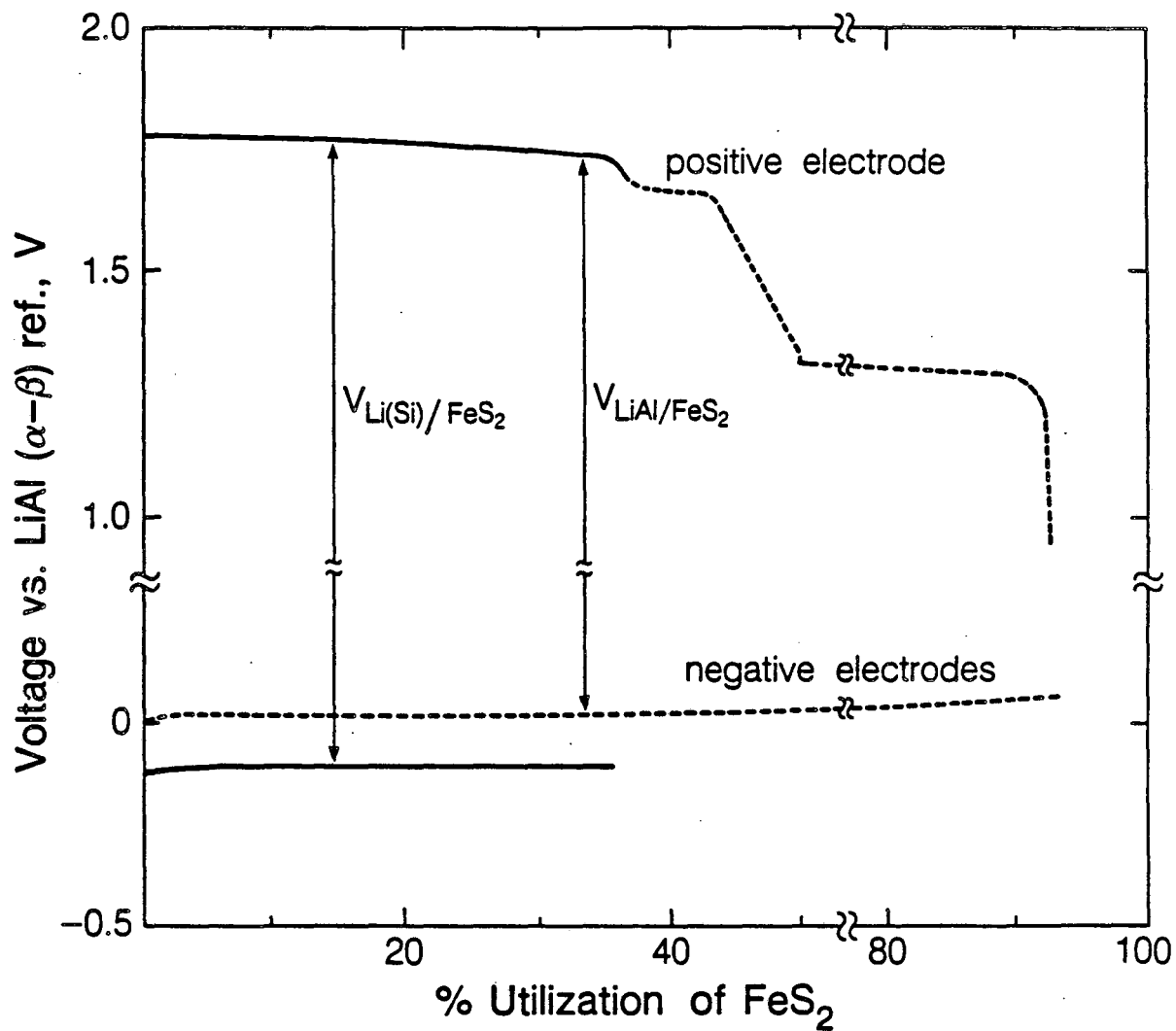
Figure 5-6. Model results for the potential of electrodes in a Li(alloy)/FeS$_2$ cell relative to a LiAl (α-β) reference electrode placed at the positive electrode-reservoir interface (base case operating conditions).

One of the most important aspects of modeling is to compare model results with experimental results. The more agreement that is seen, the more confident we are with our understanding of how a system works. Figure 5-7 compares model and experimental results[37] for the FeS_2 electrode behavior in a $LiAl/FeS_2$ cell at 450°C, 50 mA/cm², and 68% LiCl electrolyte. The reversible discharge behavior is also shown in this figure. The 4 regions of discharge of the FeS_2 electrode can be distinguished in the experimental curve. As we discuss in Chapter 4 (Section 4.2.3), there is some controversy in the literature[27] concerning different regions of discharge for the FeS_2 electrode. The results of Figure 5-7 give some credence to the "4-region" behavior of the FeS_2 electrode.

This spike at the beginning of discharge is a common observation in experimental FeS_2 cells, and we do not predict it with our mathematical model. We postulate three possible reasons for the initial voltage spike. A voltage spike at the start of discharge may indicate that the cell was overcharged. It is also possible that the spike is due to impurities in the FeS_2 electrode. Finally, as we discuss in Chapter 4 (Section 4.2.2), the spike may indicate the existence of another iron sulfide phase.

We can also contrast the start of region d in the model and experimental results. Region d begins at less than 50% utilization in the experimental cell, which indicates that some of the capacity of the electrode has been lost. We do not predict this capacity loss with our mathematical model. The capacity loss problem with experimental cells has been studied by several researchers. The weight loss of FeS_2 due to evolution of sulfur vapor in an argon atmosphere has been determined as a function of temperature.[40] The FeS_2 samples demonstrated stability at 300°C and severe weight loss at 450°C. The capacity loss of the electrode is also, however, dependent upon the electrolyte and potential. As we discussed in Section 4.2.3, Weppner et al.[27] were able to obtain a stable
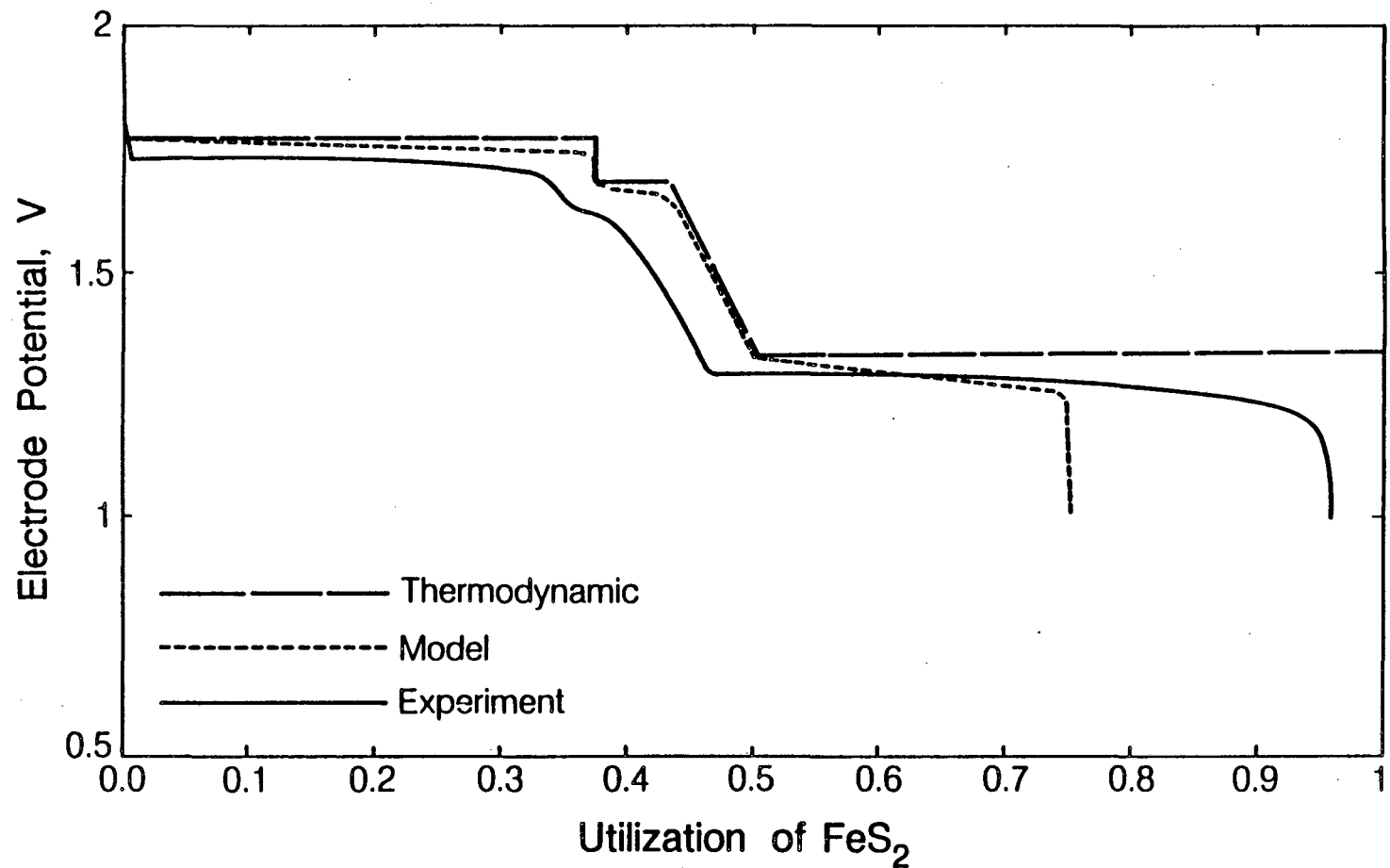
Figure 5-7. Comparison of model and experimental results[37] for the voltage of the FeS$_2$ electrode in a LiAl/FeS$_2$ cell, relative to a LiAl (α-β) reference electrode (450°C, 50 mA/cm^2, x^0_{LiCl} = 0.68). The model has the reference electrode placed at the electrode-reservoir interface, and the experiment has the reference electrode placed within the separator. The reversible, thermodynamic potential is also shown in order to display more clearly the losses of the system.

voltage reading in the $S-FeS_2-Li_2S$ region (see Figure 4-1) with molten, eutectic, LiCl-KCl electrolyte at 400°C, but not with solid-state $Li_4SiO_4 - Li_3PO_4$ electrolyte. Stable voltage readings were obtained for all other measurements with the solid-state electrolyte. Figure 5-8 demonstrates the capacity loss after 80 charge-discharge cycles observed by Dunning et al.[37] for a temperature of 450°C and lithium-rich electrolyte (68% LiCl). It was also observed that the rate of capacity loss is higher in the lithium rich than the eutectic electrolyte.

The voltage drop shown for the experimental cell in Figure 5-7 is probably due to the exhaustion of X-phase, since greater than 50% of the electrode's capacity in region d is not possible (region d spans from 45-95% utilization). The voltage drop to the cutoff point in the model result is due to the clogging of the pores with KCl precipitate. Under certain operating conditions, a loss of capacity in region d is observed experimentally[38] and may be explained by KCl precipitation. If the capacity loss in region d is caused by KCl precipitation, utilization in region d should increase with temperature, x_{LiCl}^0, and ϵ_+^0. All of these trends are observed experimentally.[38] It is appropriate here to recall that in Figure 5-3 (for the case of 100 mA/cm^2) the model predicted that KCl precipitation contributed to the apparent shortening of the upper plateau. The effects of KCl precipitation on the performance of the FeS electrode are discussed in Section 2.4.

At 13% utilization of FeS_2, LiCl precipitation is observed in the LiAl negative electrode; the precipitation of LiCl, however, does not limit the utilization of the electrode's active material.

Some of the more recent work directed toward the capacity loss problem in experimental cells should be mentioned. As we discuss above, the capacity loss of the FeS_2 electrode should decrease with decreasing temperature. Kaun[41] proposes an electrolyte with a lower melting point (310°C) and broader
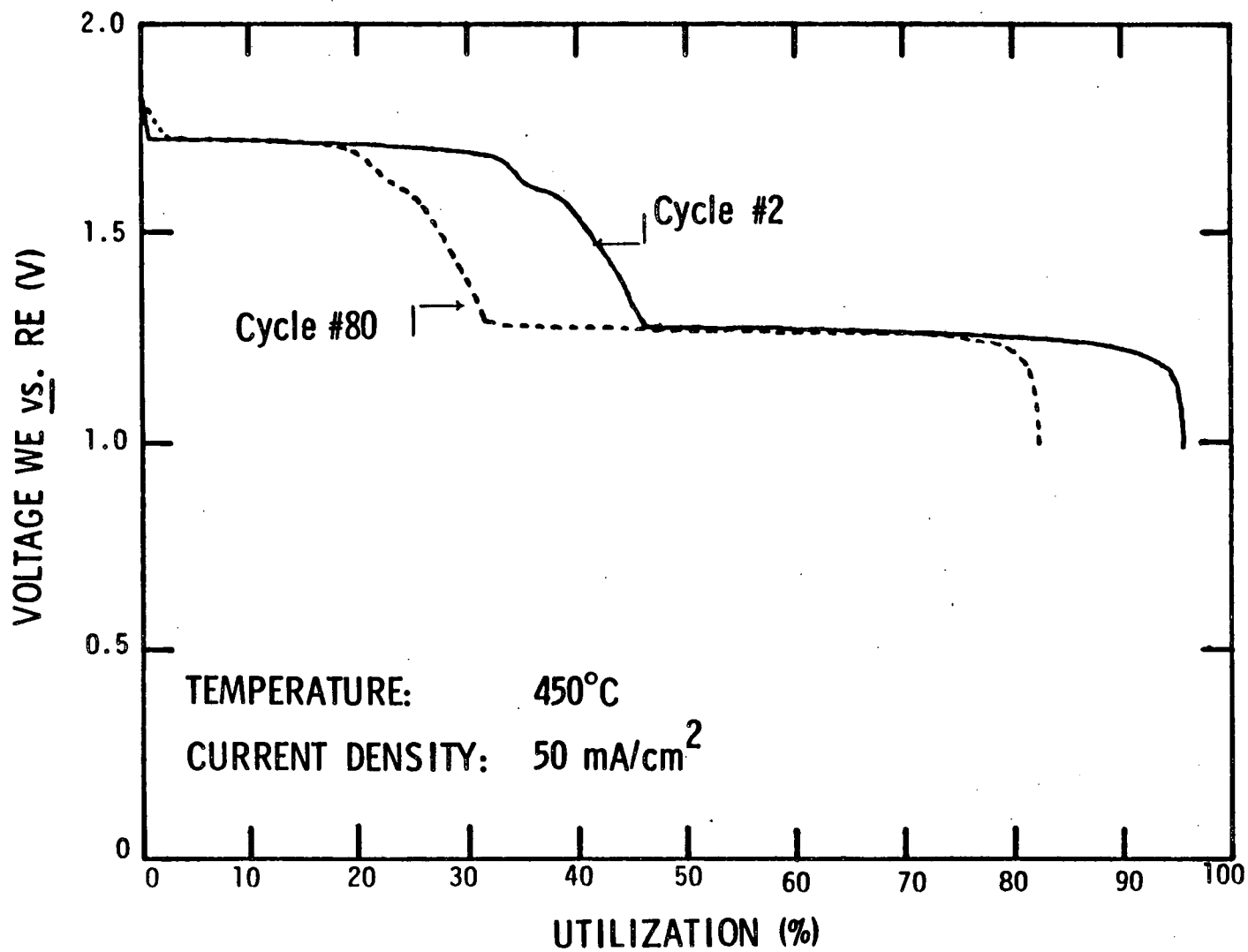
Figure 5-8. Experimental FeS_2 electrode potential after 2 cycles (also shown in Figure 5-7) and after 80 cycles in a $LiAl/FeS_2$ cell, relative to a reference electrode placed in the separator[37] (conditions are 450°C and 50 mA/cm²).

liquidus than LiCl-KCl electrolyte. His electrolyte, $x_{LiCl} = 0.25$, $x_{LiBr} = 0.38$, $x_{KBr} = 0.37$, allows lower cell operating temperatures of 390 to 400°C. Kaun operates LiAl/FeS$_2$ cells only on the upper plateau of the FeS$_2$ electrode (regions a, b, and c) where X-phase is the final discharge product. There is a much smaller volume change on discharge of this cell than in a cell that is discharged to Li$_2$S and Fe, so Kaun uses cells with dense positive electrodes (ϵ_+^0 = 0.5). The cell capacity remains constant through more than 300 cycles at 50 mA/cm^2 and a temperature of 397°C. This is a substantial improvement over the more conventional LiAl/FeS$_2$ cells (discharged to Li$_2$S and Fe) built in their laboratory. These conventional cells operate at 427°C with LiCl-KCl electrolyte and lose 30% of their capacity after 200 cycles (also see Figure 5-8).

As we discuss in the Introduction, there are other disadvantages to high operating temperatures than capacity loss of the FeS$_2$ electrode; for example, there are increases in corrosion of cell components at higher operating temperatures. Operating these cells at lower temperature may lessen the high-temperature problems. Also, operation only on the upper plateau of the FeS$_2$ electrode has the advantage of a relatively constant voltage throughout the cell discharge. This is important because there may be applications for these cells that could not tolerate the large voltage change between the upper-upper plateau (region a) and the lower plateau (region d) that occurs between 37.5 and 50% utilization. It would be interesting, however, to investigate experimentally a LiAl/FeS$_2$ cell discharged through the lower plateau with Kaun's electrolyte and the low operating temperature of 397°C.

5.3.3. Non-isothermal, Galvanostatic Discharge Behavior

As we discuss in Chapter 3, the temperature coefficients b_i of an electrode reaction (see Table 4-2) can be analyzed to give an indication of the temperature behavior of a cell during discharge. For example, b_a (relative to LiAl) for

the FeS_2 electrode is positive (0.4785×10^{-3} V/K), which indicates that the overall reaction is endothermic, and we would expect the temperature of an insulated cell to decrease during discharge. If the cell is operated isothermally, like the cells discussed in Section 5.3.1, external heating must be applied during discharge through region a in order to maintain a constant temperature. Figure 5-9 shows the modeled behavior of the temperature of a moderately-well insulated cell (solid line) discharged in an ambient temperature environment. This situation is compared with the temperature decline if the cell were discharged reversibly and adiabaticly. From 0 to 15% utilization, the cell temperature is lower than the temperature of the reversible, adiabatic cell. This is due to heat loss through the insulation, which is most important initially when the temperature of the cell is highest. The onset of KCl precipitation in the FeS_2 electrode occurs at 18% utilization, and the polarization heat (see Section 3.3.1.) becomes increasingly important as the reaction zone moves through the positive electrode. These two factors are responsible for the cell temperature being higher than the adiabatic, reversible case after 16% utilization.

Reactions b and c of the FeS_2 electrode are also endothermic, and reaction d is exothermic. The temperature coefficient for reaction c is positive and is given by differentiating Equation 4-2 with respect to temperature.

5.4. Conclusions

In conclusion, we wish to stress the importance of the electrode thermodynamics and mathematical models in analyzing battery systems. Thermodynamic data and analysis are essential to developing mathematical models and can help us understand experimental results as well as design cells. Mathematical models allow one to probe into the cell and examine reaction rate distributions and concentration distributions.
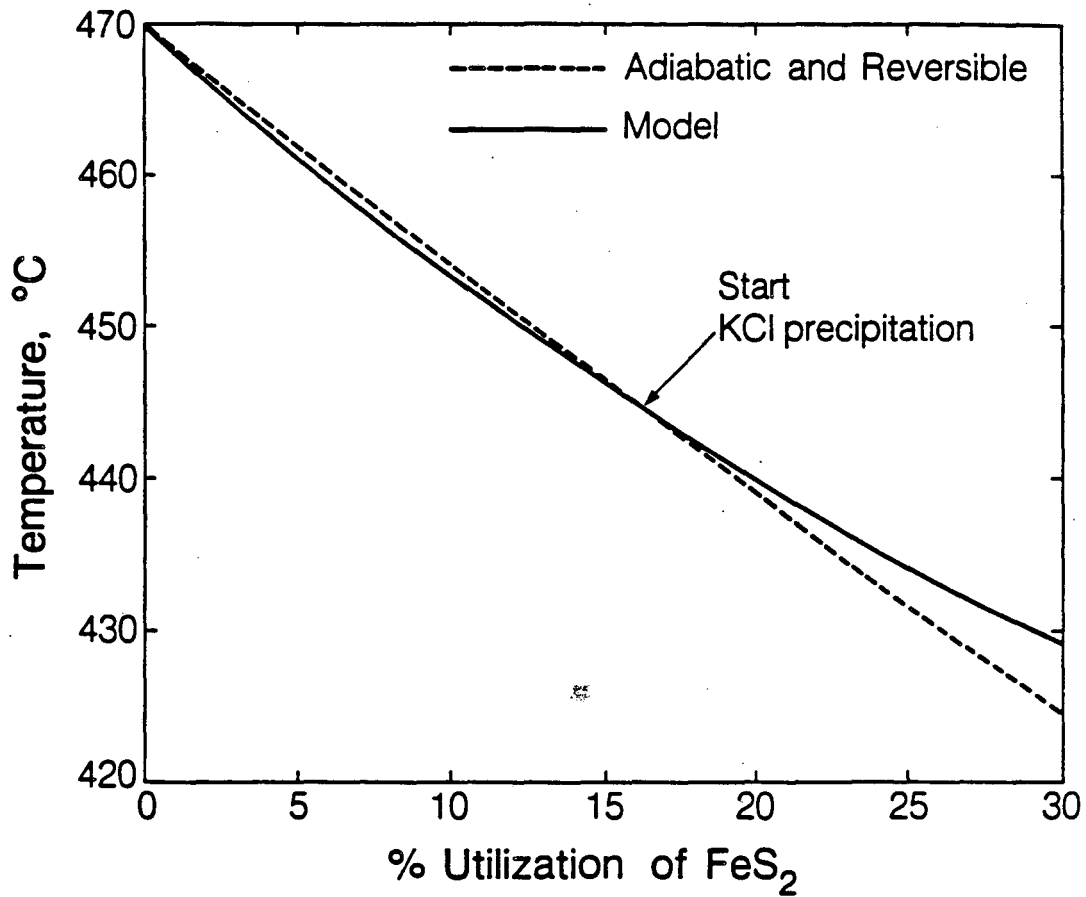
Figure 5-9. Comparison of the calculated temperature of a cell discharged reversibly and adiabatically to that of a well-insulated, although not adiabatic, cell (base case operating conditions except $\epsilon_s^o = 0.555$).

By comparing model results and experimental works, we can contribute to and help substantiate our understanding of battery systems. The agreement between the model and experimental results supports the "4-region" behavior of the FeS_2 electrode. The experimentally observed capacity loss problem on the upper voltage plateau during discharge must be solved if the system is to be practical. Our model predicts that KCl precipitation can limit the utilization of the FeS_2 electrode, usually on the lower voltage plateau. The capacity loss due to KCl precipitation should be decreased with increasing temperature, LiCl concentration in the electrolyte, and porosity of the electrode. For certain operating conditions, limitations on the utilization of the lower voltage plateau are observed experimentally and are probably due to KCl precipitation.

List of Symbols for Part A

a	interfacial area per unit electrode volume, cm^{-1}
$a_{i,j}$	activity of species i in phase j
A	separator area, cm^2
a_l	constant in the expression for the open circuit potential of reaction l, V
b_l	temperature coefficient in the expression for the open circuit potential of reaction l, V/K
$c_{i,j}$	concentration of species i in phase j, mol/cm^3
$\hat{C}_p^m$	mean heat capacity at constant pressure, J/g-K
$\overline{C}_{p_{i,j}}$	partial molar constant pressure heat capacity of species i in phase j, J/mol-K
D	diffusion coefficient, cm^2/sec
dv_j	differential volume element of phase j, cm^3
e^-	symbol for an electron
F	Faraday's constant, 96,487 C/equiv
g	variable defined by Equation 2-3
h	heat transfer coefficient, W/cm^2-K
H_{tot}	enthalpy, J
$\tilde{H}$	molar enthalpy, J/mol
$\overline{H}_{i,m}^0$	molar enthalpy or partial molar enthalpy of species i in the secondary reference state corresponding to phase m, J/mol
$\overline{H}_{i,j}$	partial molar enthalpy of species i in phase j, J/mol
i	current density, A/cm^2
$i_{o,l}$	exchange current density for reaction l, A/cm^2
i_l	partial current density of electrode reaction l, A/cm^2
I	cell current, A
I_l	partial current of electrode reaction l, A

j	transfer current density per unit volume of electrode, A/cm^3
K	constant in Equation A-7, mol
L	length of cell, cm
m	precipitation parameter
M	mass of the cell, g
M_i	molecular weight of species i
$\mathbf{M}_i$	symbol for the chemical formula of species i
n	number of discharge-charge cycles
n_e	number of moles of electrolyte per mole of FeS
n_l	number of electrons involved in reaction l
n_{RE}	number of electrons involved in the reference electrode reaction
$n_{i,j}$	moles of species i in phase j, moles
q	heat-transfer rate, W
q_l	capacity for reaction l (see Equation 5-4), C/cm^3
Q	capacity per unit volume of electrode, C/cm^3
R	universal gas constant, 8.3143 J/mol-K
$s_{i,l}$	stoichiometric coefficient of species i in reaction l
t	time, s
t_i^*	transference number of species i, relative to the molar average reference velocity
T	absolute temperature, K
$U_{l,avg}$	theoretical open-circuit potential for reaction l at the average composition, relative to a reference electrode, V
$U_{l,o}$	theoretical open-circuit potential for reaction l at the local composition within the electrode, relative to a reference electrode that is taken to be the same kind as the second reaction in the discharge mechanism, V
U_l^o	standard electrode potential for reaction l, V
U_{RE}^o	standard electrode potential for the reference electrode reaction, V

V_R^0	initial reservoir volume, cm^3
$\mathbf{v}^\bullet$	molar average velocity, cm/sec
v_j	see dv_j
$\tilde{V}$	molar volume, cm^3/mole
V	cell potential, V
x, x$^\bullet$	composition variables in non-stoichiometric compounds
$x_{i,j}$	mole fraction of species i in phase j
y	distance from electrode, cm
z_i	charge number of species i

Greek letters

α_a	transfer coefficient in the anodic direction
α_c	transfer coefficient in the cathodic direction
ϵ	porosity or electrolyte volume fraction
ϵ_i	volume fraction of species i
$\gamma_{i,j}$	activity coefficient of species i in phase j
η	overpotential defined by Equation 2-7, V
η_{s_l}	surface overpotential of reaction l, V
κ	effective ionic electrolyte conductivity, $(\Omega\text{-cm})^{-1}$
ρ	density, g/cm^3
σ	solid phase electrical conductivity, $(\Omega\text{-cm})^{-1}$
Φ	electric potential, V

Subscripts

A	ambient
continuous	refers to phases that form a continuum
ccp	current collector in the positive electrode
e	electrolyte
eff	effective

f	heat of fusion
i	refers to a species
j,m	refer to phases
l	refers to a reaction
matrix	refers to the solid electrode matrix
p	precipitate
pore	refers to the pores of an electrode
rev	reversible
RE	reference electrode reaction
s	refers to solid, surface, or separator
tot	total
+	positive electrode
—	negative electrode

Superscripts

avg	average
eut	eutectic composition
final	at end of discharge
m	mean
o	refers to secondary reference state or initial
RE	reference electrode composition

References for Part A

1. E. C. Gay, R. K. Steunenberg, W. E. Miller, J. E. Battles, T. D. Kaun, F. J. Martino, J. A. Smaga, and A. A. Chilenskas, in *Li-Alloy/FeS Cell Design and Analysis Report*, Argonne National Laboratory Report ANL-84-93, (July, 1985).

2. J. R. Selman, "Molten-Salt Battery Cells with Sulfur or Metal Sulfide Electrodes," R. P. Tischer, ed., *The Sulfur Electrode*, Academic Press, New York, New York, pp. 219-232 (1983).

3. R. Pollard, *Mathematical Modeling of the Lithium-Aluminum, Iron Sulfide Battery*, Dissertation, University of California, Berkeley (1979).

4. R. Pollard and J. Newman, "Mathematical Modeling of the Lithium-Aluminum, Iron Sulfide Battery, I. Galvanostatic Discharge Behavior," *Journal of the Electrochemical Society*, **128**, 491-502 (March, 1981).

5. R. Pollard and J. Newman, "Mathematical Modeling of the Lithium-Aluminum, Iron Sulfide Battery, II. The Influence of Relaxation Time on the Charging Characteristics," *Journal of the Electrochemical Society*, **128**, 503-507 (March, 1981).

6. C. E. Vallet, D. E. Heatherly, L. Heatherly, Jr., and J. Braunstein, in " Physical Chemistry of Molten Salt Batteries, Final Report for Period Oct. 1, 1981-Sept. 30, 1982," *LiCl Precipitation from LiCl-KCl Anolyte in Porous Li-Al Electrodes*, Oak Ridge National Laboratory Report ORNL/TM-8714, (May, 1983).

7. C. E. Vallet, Personal Communication, (1983).

8. J. R. Selman and M. L. Saboungi, "Electrochemistry of Sulfur in Halide Melts," R. P. Tischer, ed., *The Sulfur Electrode*, Academic Press, New York, NY, pp. 113-

127 (1983).

9. Z. Tomczuk, S. K. Preto, and M. F. Roche, "Reactions of FeS Electrodes in LiCl-KCl Electrolyte," *Journal of the Electrochemical Society,* **128,** 760-772 (April, 1981).

10. Z. Tomczuk, M. F. Roche, and D. R. Vissers, "Emf Measurements on the Li-Al/FeS Couple in LiF-LiCl-LiBr Electrolyte," *Journal of the Electrochemical Society,* **128,** 2255-2256 (October, 1981).

11. E. Pawlikowski, Postdoctoral research, unpublished. Department of Chemical Engineering, University of California, Berkeley (March, 1982).

12. J. Lumsden, *Thermodynamics of Molten Salt Mixtures,* Academic Press, New York (1966).

13. D. M. Chen and H. F. Gibbard, "Thermal Energy Generation of LiAl/FeS Cells," *Journal of the Electrochemical Society,* **130,** 1975-1979 (October, 1983).

14. Z. Tomczuk, B. Tani, N. C. Otto, M. F. Roche, and D. R. Vissers, "Phase Relationships in Positive Electrodes of High Temperature Li-Al/LiCl-KCl/FeS$_2$ Cells," *Journal of the Electrochemical Society,* **129,** 925-931 (May, 1982).

15. J. Newman, *Electrochemical Systems,* Prentice Hall, Englewood Cliffs, New Jersey (1973).

16. S. P. S. Badwal and R. J. Thorn, "Conductivities and Electronic Structures of Some Phases in the Lithium-Iron-Sulfur System," *Journal of Solid State Chemistry ,* **43,** 163-174 (July, 1982).

17. R. E. Meredith and C. W. Tobias, "Conduction in Heterogeneous Systems," *Advances in Electrochemistry and Electrochemical Engineering 2,* C. W. Tobias, ed., Interscience Publishers, New York, pp. 15-47 (1962).

18. R. C. Elliott and T. O. Cooper, in *High Performance Batteries for Off-Peak Energy Storage and Electric-Vehicle Propulsion*, Argonne National Laboratory Report ANL-75-1, pages 25-29 (July, 1975).

19. J. M. Sherfey and Abner Brenner, "Electrochemical Calorimetry," *Journal of the Electrochemical Society*, **105**, 865-672 (November, 1958).

20. Sidney Gross, "Heat Generation in Sealed Batteries," *Energy Conversion*, **9**, 55-62 (1969).

21. H. Frank Gibbard, "Thermal Properties of Battery Systems," *Journal of the Electrochemical Society*, **125**, 353-358 (March, 1978).

22. I. A. Dibrov and V. A. Bykov, *Elektrokhimiya*, **13**, 350-355 (March, 1977). (English translation: "Enthalpy Method of Analyzing Complex Electrochemical Processes Silver-cadmium and Silver-zinc Batteries," *Soviet Electrochemistry*, **13**, 298-302 (March, 1977)).

23. I. A. Dibrov and V. A. Bykov, *Zhurnal Prikladnoi Khimii*, **49**, 2023-2026 (September, 1976). (English translation: "Comparison of Different Methods for Calculating Heat Losses in Storage Cells, with Reference to the Silver-cadmium and Silver-zinc Systems," *Journal of Applied Chemistry of the U.S.S.R.*, **49**, 2025-2028 (September, 1977))

24. L. D. Hansen and R. M. Hart, "The Characterization of Internal Power Losses in Pacemaker Batteries by Calorimetry," *Journal of the Electrochemical Society*, **125**, 842-845 (June, 1978).

25. Frank B. Tudron, "Dynamic Microcalorimetry: Thermal Effects of Miniature Alkaline Cells under Load," *ibid.*, **128**, 516-520 (March, 1981).

26. William H. Tiedemann and John Newman, "Mathematical Modeling of the Lead-Acid Cell," *Proceedings of the Symposium on Battery Design and*

Optimization (The Electrochemical Society, volume 79-1, 1979), pp. 23-38.

27. Hans Bode, translated by R. J. Brodd and Karl V. Kordesch, *Lead-Acid Batteries*, (New York: Wiley-Interscience, 1977).

28. J. A. Schmidt and W. Weppner, "Phase Equilibria and Thermodynamics of Li - Fe - S," E.F. Bertaut *et al.*, Eds., *Proc. 7th Int. Conf. on Solid Compounds of Transition Elements*, Grenoble, France: I B 13 (1982).

29. C. J. Wen and R. A. Huggins, "Chemical Diffusion in Intermediate Phases in the Lithium-Silicon System," *Journal of Solid State Chemistry*, **37**, 271-278 (1981).

30. Z. Tomczuk and D. R. Vissers, in *Lithium/Iron Sulfide Batteries for Electric-Vehicle Propulsion and other Applications*, Argonne National Laboratory Report ANL-83-62, page 19 (1983).

31. Z. Tomczuk, Personal communication (1982).

32. H. Rau, "Energetics and Defect Formation and Interaction in Pyrrhotite $Fe_{1-x}S$ and its Homogeneity Range," *Journal of the Physics and Chemistry of Solids*, **37**, 425-429 (1976).

33. M. Roche, Personal communication (1982).

34. J. A. Schmidt and W. Weppner, "Kinetics of Compositional Variations in the Ternary System Li - Fe - S," The Electrochemical Society Extended Abstracts for the Montreal, Canada Meeting, Volume 82-1, Abstract 344, page 562 (May, 1982).

35. R. A. Sharma and R. N. Seefurth, "Thermodynamic Properties of the Lithium-Silicon System," *Journal of the Electrochemical Society*, **123**, 1763-1768 (December, 1976).

36. L. Redy and D. R. Vissers, in *Lithium/Iron Sulfide Batteries for Electric-*

Vehicle Propulsion and other Applications, Argonne National Laboratory Report ANL-83-62, page 8 (1983).

37. J. S. Dunning, in *Lithium/Iron Sulfide Batteries for Electric-Vehicle Propulsion and other Applications*, Argonne National Laboratory Report ANL-80-128, pages 190-198 (February, 1981).

38. J. S. Dunning, in *High Performance Batteries for Electric-Vehicle Propulsion and Stationary Energy Storage*, Argonne National Laboratory Report ANL-79-94, pages 61-67 (March, 1981).

39. R. C. Weast, *Handbook of Chemistry and Physics*, 48th Edition, CRC Press, Cleveland, Ohio (1967).

40. F. R. McLarnon, in "Technology Base Research Project for Electrochemical Energy Storage," Lawrence Berkeley Laboratory Report for the First Quarter of Fiscal Year 1985, Project status report titled *Investigation of the Mechanism for Capacity Decline in FeS_2 Electrodes in Lithium-Iron Sulfide High Temperature Batteries*, (January, 1985).

41. T. D. Kaun, "Li-Al/FeS_2 Cell with LiCl-LiBr-KBr Electrolyte," *Journal of the Electrochemical Society*, **132**, 12, 3063-3064 (December, 1985).

Part B

The Electrochemical Precipitation of Nickel Hydroxide

Chapter 6

Modeling the Precipitation of Ni(OH)$_2$ on a

Rotating Disk Electrode

6.1. Introduction

In this chapter we present a mathematical model that simulates the precipitation of Ni(OH)$_2$ from a nickel nitrate solution on a rotating disk electrode. The basic structure of the mathematical model was developed by Russell and Newman.[49,50] The Russell-Newman model simulates the active-passive transition and sustained current oscillations for the anodic dissolution of an iron rotating disk electrode in sulfuric acid. The high rate anodic dissolution of iron produces a porous film of FeSO$_4$ on the surface of the electrode. The pH in the solution at the film-electrode interface increases until the electrode passivates. Passivation blocks the flow of current and allows the pH to decrease again. This process is repeated and is responsible for current oscillations.

The problem addressed in this work is analogous only to the film-formation part of the Russell-Newman model. We consider the reduction of nitrate ion in acidic nickel nitrate solution. The reduction of nitrate ion causes a pH increase in the solution adjacent to the electrode surface. A sufficient increase in pH causes the precipitation of a Ni(OH)$_2$ film on the electrode surface.

The model presented is one-dimensional; only axial variations are considered. The equations are based on dilute-solution theory. This is an approximation for the transport of the Ni^{++} and NO$_3^-$ species due to the high concentration of nickel nitrate $(c_{Ni(NO_3)_2} = 2.56$ M$)$. Concentrated solution theory could be used if the transport properties were available. We consider a single-step

electrochemical reaction for the reduction of nitrate (see Equation 6-1a). This is an approximation to the actual behavior. The reduction of nitrate is more likely to be a complicated series of reaction steps involving adsorbed species and several possible reaction products. In Chapter 7, we investigate the mechanism of nitrate reduction in greater detail. There is, however, experimental evidence suggesting that HNO_2 is the principal reaction product in concentrated nickel nitrate solutions $(c_{Ni(NO_3)_2} > 2 \text{ M})$.[51]

In Section 6.2, we describe the mathematical model and the modifications that have been made to the Russell-Newman model. Model results with and without a sufficient pH increase to cause $Ni(OH)_2$ precipitation are given in Section 6.3. In Section 6.3, we also discuss our experimental observations of the current response to a potential step. Possible improvements to the model and further experiments are suggested in Section 6.4.

6.2. Mathematical Model Description

Figure 6-1 shows schematically the processes that are mathematically modeled. The following events lead to formation of $Ni(OH)_2$. Initially, the concentration profiles are uniform. The electrode potential, relative to a reference electrode, is stepped from the open-circuit potential to a constant value. A current begins to flow as the nitrate reduction reaction proceeds. We can write this reaction as producing hydroxide ions,

$$NO_3^- + 2H_2O + 2e^- \rightarrow HNO_2 + 3OH^-,$$
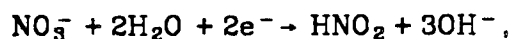
or consuming hydrogen ions

$$NO_3^- + 3H^+ + 2e^- \rightarrow HNO_2 + H_2O . \tag{6-1a}$$
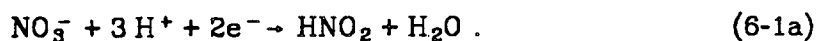
The consumption of hydrogen ions (or production of hydroxide ions) causes the hydroxide ion concentration to build up in the diffusion layer near the electrode surface. The surface concentration increases above the saturation con-
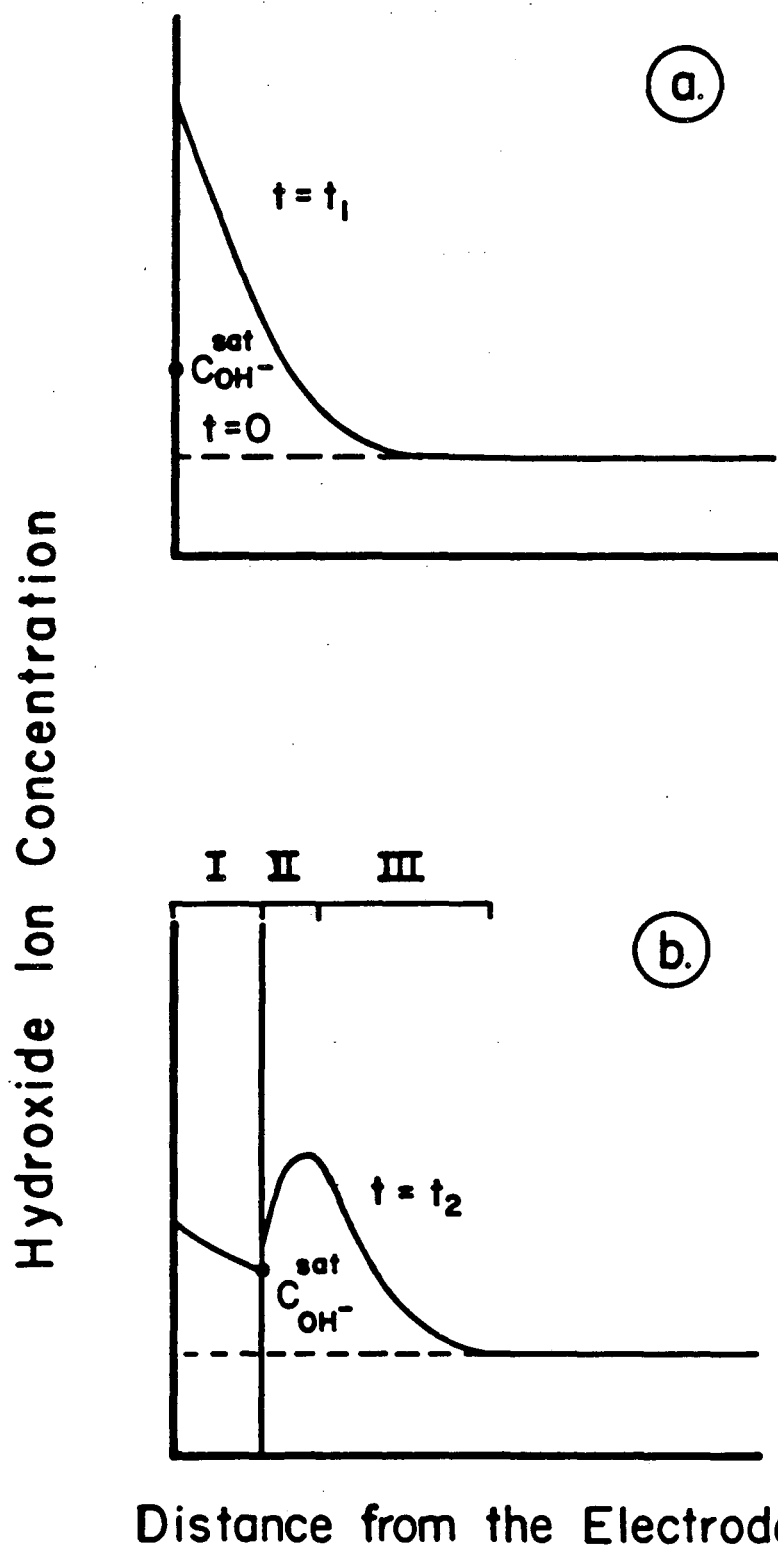
Figure 6-1. Schematic description of hydroxide ion concentration profiles $(0 < t_1 < t_2)$. a) The dotted line represents the uniform profile at $t = 0$. $t = t_1$ is just prior to the conditions of $Ni(OH)_2$ precipitation. b) $t = t_2$ is a little bit after the onset of precipitation. Region I is the film, region II is the diffusion layer, and the "long profiles" are in region III. Regions I and II are shown exaggerated in thickness.

centration of $Ni(OH)_2$ to a maximum supersaturation value (for example, 45 times the saturation concentration, see Section 6.2.3). The precipitation of nickel hydroxide, written as

$$Ni^{++} + 2OH^- \rightarrow Ni(OH)_2,$$

or

$$Ni^{++} + 2H_2O \rightarrow Ni(OH)_2 + 2H^+, \tag{6-1b}$$
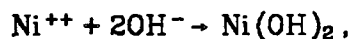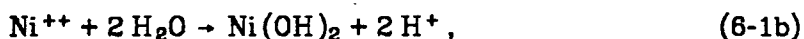
is initiated on the electrode when the hydroxide ion concentration reaches the maximum supersaturation value. This scenario is equivalent to assuming that the nucleation rate constant is a step function of the maximum supersaturation concentration. That is, the nucleation rate constant is large at the maximum supersaturation concentration and zero before that point. It is also assumed that, after nucleation, there is no resistance to crystallization. This implies that the solution at the solid-solution interface is saturated (not supersaturated) and that the growth of the film is determined by the mass-transfer rate of the film-forming species. In this model we consider only the axial transport of species within the pores of the film and neglect radial transport. We also assume that the solution within the pores can become supersaturated, but that the solution at the pore mouth is fixed at the saturated value. The curved line in Figure 6-1a indicates the hydroxide ion concentration just prior to precipitation. Figure 6-1b gives the profiles after the onset of precipitation. The steep concentration gradient results in a flux of nickel and hydroxide ions that provides material for film formation.

In Section 6.2.1.4 we relate the flux of nitrate ions to the flux of hydrogen and hydroxide ions by the water-dissociation equilibrium constraint. Also, the rate of $Ni(OH)_2$ precipitation is related to the hydroxide ion flux as well as the hydrogen and the nickel ion fluxes.

It is appropriate to mention here that we neglect the dissociation of HNO_2 in our mathematical model formulation. Incorporating the dissociation of HNO_2 into the mathematical model would require another equilibrium constraint and another material balance for the NO_2^- species. The incorporation of HNO_2 dissociation equilibrium would tend to keep the hydrogen ion concentration higher than if we neglect this homogeneous reaction. As we discuss in Section 6.3.1, this effect is observed with the water dissociation equilibrium. We also neglect the possible nickel hydrolysis products other than the solid hydrolysis product of interest, namely, $Ni(OH)_2$(solid). We would not expect significant quantities of hydrolysis products at low pH. We can estimate the relative amounts of the species from the relevant equilibrium constants. For example, $Ni(OH)_2$(aqueous), $Ni_4(OH)_4^{+4}$, and $NiOH^+$ species are the main hydrolysis products of nickel ions, and the equilibrium constants are 1×10^{-19} (mole/liter)^2, 1×10^{-27} (mole/liter)^4, and 1.38×10^{-10} mole/liter, respectively.[52] We estimate the ratio of the amount of one of these species to the total amount of nickel to be less than 20% for pH less than 9.3, 6.6, and 9.2 for the $NiOH^+$, $Ni_4(OH)_4^{+4}$, and $Ni(OH)_2$(aqueous) species, respectively. The effect of including these hydrolysis products would tend to decrease the nickel ion concentration and increase the hydrogen ion concentration. In other words, hydrolysis products compete with $Ni(OH)_2$(solid) for hydroxide ions.

The fundamental equations in the model are material-balance equations for species in the electrolyte, a current balance equation, an electrical neutrality equation, and an equilibrium relationship between the hydrogen and hydroxide ion species. As shown in Figure 6-1, the distance domain is separated into three regions: the porous film (I), the electrolyte solution near the film-solution interface with a steep hydroxide-ion concentration gradient (II), and the region extending to the bulk solution (III). The distance variable in each region is stretched appropriately. The governing equations are cast into finite difference

form along with the appropriate boundary conditions and solved iteratively by the method of Newman (BAND).[53] The governing equations are given in the next few sections, and we refer the reader to the the work of Russell and Newman[49,50] for certain aspects of the model development. The model calculates time-dependent behavior such as current and film thickness. The model also calculates distributions of species concentrations and electric potential within the pores of the film and in the diffusion layer.

6.2.1. Discussion of the Governing Equations

In this section, we give the differential equations and boundary conditions that govern the system and define the appropriate reduced variables in each of the regions described in the previous section. The initial variables in the model are four ionic species and the potential. The unknowns are numbered as

1	Ni^{++}	2	NO_3^-
3	OH^-	4	H^+
5	Φ		

for notational convenience.

The concentration of each ionic species i is governed by a material-balance equation,

$$\frac{\partial c_i}{\partial t^*} = -\nabla \cdot \mathbf{N}_i + R_i .$$

(6-2)

The flux of species $\mathbf{N}_i$ is defined as

$$\mathbf{N}_i = -z_i u_i F c_i \nabla \Phi - D_i \nabla c_i + \mathbf{v} c_i$$

(6-3)

and contains contributions due to migration, diffusion, and convection. The current is calculated at any position by summing the charge that is being transported by the individual species.

$$\mathbf{i} = F \sum_i z_i \mathbf{N}_i \, . \qquad (6\text{-}4)$$

Electroneutrality, mathematically expressed as

$$\sum_i z_i c_i = 0 \, , \qquad (6\text{-}5)$$

is maintained throughout the region where the mass-transport problem is solved.

Equations 6-2, with $i = 1$ to 4, along with Equation 6-5 are sufficient to solve for the five unknowns listed above, after we have dealt with the homogeneous reaction terms.

The equilibrium of water is represented by the homogeneous reaction

$$H_2O = H^+ + OH^- \, . \qquad (6\text{-}6)$$

It is assumed that equilibrium exists, and that it is represented by

$$K = c_{H^+} \, c_{OH^-} \, . \qquad (6\text{-}7)$$

Equation 6-6 indicates that $R_3 = -R_4$ (see Equation 6-2). Adding the material balance Equation 6-2 for the hydroxide species ($i = 3$) to that of the hydrogen species ($i = 4$) results in a combined equation that no longer contains the homogeneous reaction term explicitly.

$$\sum_{i=3}^{4} \frac{\partial c_i}{\partial t^*} = - \sum_{i=3}^{4} \nabla \cdot \mathbf{N}_i \, . \qquad (6\text{-}8)$$

Equations 6-7 and 6-8 replace Equation 6-2 for $i = 3$ and 4.

Conservation of charge implies that the current density must be independent of position

$$\nabla \cdot \mathbf{i} = F \sum_{i=1}^{4} z_i \nabla \cdot \mathbf{N}_i = 0 \, . \qquad (6\text{-}9)$$

Equation 6-9 replaces Equation 6-2 for $i = 2$.

Equations 6-5, 6-7 to 6-9, and Equation 6-2 with $i = 1$ are the five independent equations used to solve for the concentrations of the four ionic species and the potential.

In the presence of a film, the film thickness δ_y is an additional unknown. The film thickness is a function of time; however, δ_y is independent of distance. The equation,

$$\frac{d\,\delta_y}{dy} = 0 \,, \qquad (6\text{-}10)$$

is used as the governing equation for the film thickness. (This allows us to use the standard form of the BAND subroutine and does not require us to use a more efficient version that recognizes scalar unknowns, such as δ_y.)

6.2.1.1. Governing Equations in Terms of Reduced Variables

In this section, we give the governing equations in terms of the appropriate reduced variables for the region within the porous film and the region extending from the film to the bulk solution. This model considers variations only in the direction normal to the electrode surface. Radial variations are not included in the development. The velocity in the electrolyte is approximated by the first term of its power-series expansion in the axial distance y,

$$v_y = -a\Omega\left(\frac{\Omega}{\nu}\right)^{1/2} y^2 \,, \qquad (6\text{-}11)$$

where $a = 0.51023$. A dimensionless time and distance are defined as

$$t = \Omega\left(\frac{D_4}{\nu}\right)^{1/3}\left(\frac{a}{3}\right)^{2/3} t^\circ \qquad (6\text{-}12)$$

and

$$x = \left(\frac{a\,\nu}{3\,D_4}\right)^{1/3}\left(\frac{\Omega}{\nu}\right)^{1/2} y \,, \qquad (6\text{-}13)$$

respectively. A distance variable for the solution region outside the film is

chosen so that it always has a value of zero at the film-solution interface. This variable is stretched with the time variable.

$$\xi = \frac{x - \delta_x}{\sqrt{t}}, \qquad (6\text{-}14)$$

where δ_x is a dimensionless film thickness obtained by multiplying δ_y by the factor multiplying y in Equation 6-13. In the absence of a film, $\delta_x = 0$.

The hydrogen ion diffusion coefficient is chosen to nondimensionalize the variables in Equations 6-12 and 6-13, since the hydrogen ion has the largest diffusion coefficient. This will assure that the diffusion layers of all the species will be well within our distance domain ($0 < \xi < 6$).

At the onset of precipitation, t is reset to zero. For notational convenience, we define

$$\delta = \frac{\delta_x}{\sqrt{t}}. \qquad (6\text{-}15)$$

Substitution of these dimensionless variables into Equation 6-8 gives

$$\sum_{i=3}^{4} \left\{ t\left(\frac{\partial c_i}{\partial t}\right)_\xi - t\frac{d\delta}{dt}\frac{\partial c_i}{\partial \xi} \right\} = \sum_{i=3}^{4} \left\{ \frac{1}{2}(\xi + \delta)\frac{\partial c_i}{\partial \xi} + \frac{z_i u_i F}{D_4}\frac{\partial}{\partial \xi}\left(c_i \frac{\partial \Phi}{\partial \xi}\right) \right.$$
$$\left. + 3t^{3/2}\xi^2 \frac{\partial c_i}{\partial \xi} + \frac{D_i}{D_4}\frac{\partial^2 c_i}{\partial \xi^2} \right\} \qquad (6\text{-}16)$$

for the summation material balance of the H^+ and OH^- species. The material balance for Ni^{++}, Equation 6-2 with $i = 1$, becomes

$$t\left(\frac{\partial c_1}{\partial t}\right)_\xi - t\frac{d\delta}{dt}\frac{\partial c_1}{\partial \xi} = \frac{1}{2}(\xi + \delta)\frac{\partial c_1}{\partial \xi} + \frac{z_1 u_1 F}{D_4}\frac{\partial}{\partial \xi}\left(c_1 \frac{\partial \Phi}{\partial \xi}\right)$$
$$+ 3t^{3/2}\xi^2 \frac{\partial c_1}{\partial \xi} + \frac{D_1}{D_4}\frac{\partial^2 c_1}{\partial \xi^2}. \qquad (6\text{-}17)$$

and the charge conservation relationship (Equation 6-9) becomes

$$-F^2 \frac{\partial}{\partial \xi} \left(\frac{\partial \Phi}{\partial \xi} \sum_{i=1}^{4} z_i^2 u_i c_i \right) - F \sum_{i=1}^{4} z_i D_i \frac{\partial^2 c_i}{\partial \xi^2} = 0 \ . \tag{6-18}$$

The equilibrium and electroneutrality equations are applied directly. The governing equation for the film thickness becomes

$$\frac{d\delta}{d\xi} = 0 \ . \tag{6-19}$$

A reduced distance variable, η, within the film is defined by

$$\eta = \frac{x}{\delta_x} \ . \tag{6-20}$$

The electrode-film boundary is located at $\eta = 0$. The film-electrolyte boundary is located at $\eta = 1$.

Substitution of the appropriate reduced variables into Equations 6-8 and 6-2 gives

$$\sum_{i=3}^{4} \left\{ t\delta^2 \left[\frac{\partial c_i}{\partial t} \right]_\eta - \frac{\eta}{2} \frac{d(t\delta^2)}{dt} \frac{\partial c_i}{\partial \eta} \right\} = \sum_{i=3}^{4} \left\{ \frac{z_i u_i F}{D_4} \frac{\partial}{\partial \eta} \left(c_i \frac{\partial \Phi}{\partial \eta} \right) + \frac{D_i}{D_4} \frac{\partial^2 c_i}{\partial \eta^2} \right\}$$

$$\tag{6-21}$$

and

$$t\delta^2 \left[\frac{\partial c_1}{\partial t} \right]_\eta - \frac{\eta}{2} \frac{d(t\delta^2)}{dt} \frac{\partial c_1}{\partial \eta} = \frac{z_1 u_1 F}{D_4} \frac{\partial}{\partial \eta} \left(c_1 \frac{\partial \Phi}{\partial \eta} \right) + \frac{D_1}{D_4} \frac{\partial^2 c_1}{\partial \eta^2} \tag{6-22}$$

for the summation material balance and material balance for the Ni^{++} species, respectively.

The charge conservation relationship within the pores of the film has the same form as Equation 6-18 with ξ replaced by η. The porosity in the film, ϵ_f, is assumed to be a constant, independent of the position within the film. The velocity is assumed to be equal to zero in the pores of the film, so a convection term is not included in the above equations. The equilibrium and electroneutrality

equations are applied directly. The governing equation for the film thickness becomes

$$\frac{d\delta}{d\eta} = 0 .$$

(6-23)

6.2.1.2. Boundary Conditions at ξ_{max}

In the absence of a film, the boundary conditions at ξ_{max} are determined by the specified bulk concentration of nickel nitrate, the bulk pH, the water-dissociation equilibrium expression, and the electroneutrality equation. If $c_{Ni(NO_3)_2}^{\infty}$ is the bulk concentration of nickel nitrate and $c_{HNO_3}^{\infty}$ is the bulk concentration of nitric acid, then

$$c_4(\xi_{max}) = \frac{10^{pH^{\infty}}}{1000}$$

(6-24)

and

$$c_3(\xi_{max}) = \frac{K}{c_4(\xi_{max})} .$$

(6-25)

where K is the equilibrium constant in Equation 6-7. The other bulk concentrations become

$$c_1(\xi_{max}) = c_{Ni(NO_3)_2}^{\infty}$$

(6-26)

and

$$c_4(\xi_{max}) = 2c_1(\xi_{max}) - c_3(\xi_{max}) + c_2(\xi_{max}) .$$

(6-27)

The potential is set equal to zero at ξ_{max}. A normal hydrogen electrode (NHE) is used as the reference electrode.

$$\Phi(\xi_{max}) = 0 .$$

(6-28)

The boundary conditions at ξ_{max} in the presence of a film are established by calculating the corresponding position in terms of the variable x.

$$x_{\xi_{max}} = \sqrt{t} \, (\xi_{max} + \delta) .$$

(6-29)

The concentration profiles in region III of Figure 6-1 are termed the "long" profiles. The values of the long concentration profiles at $x = x_{\xi_{max}}$ are the values selected for the boundary conditions. In equation form,

$$c_i(\xi_{max}) = c_{long,i}(x = x_{\xi_{max}}); \quad i = 1 \text{ to } 4.$$ (6-30)

We refer the reader to the work of Russell and Newman[49,50] for a more complete description of this method.

6.2.1.3. Boundary Conditions at the Film-Solution Interface

The film-solution interfacial boundary conditions in terms of net flux expressions are presented in this section. We define the reduced flux of species i in the film as

$$N_i^f = \epsilon_f \left\{ -z_i u_i F c_i \left. \frac{\partial \Phi}{\partial \eta} \right|_{\eta = 1} - D_i \left. \frac{\partial c_i}{\partial \eta} \right|_{\eta = 1} \right\}$$ (6-31)

and the reduced flux of species i in the solution outside the film as

$$N_i^s = \delta \left\{ -z_i u_i F c_i \left. \frac{\partial \Phi}{\partial \xi} \right|_{\xi = 0} - D_i \left. \frac{\partial c_i}{\partial \xi} \right|_{\xi = 0} \right\}.$$ (6-32)

The net flux of any species at the film-solution interface is defined as the flux of species arriving from the pores of the film minus the flux moving into the solution outside the film,

$$N_i^{net} = N_i^f - N_i^s.$$ (6-33)

We can write

$$\sum_{i=1}^{4} z_i N_i^{net} = 0$$ (6-34)

at the film-solution interface. We also know that N_2^{net} is equal to zero at this point because the nitrate species does not contribute to film formation. Using

this relationship we can then relate the net flux of nickel ions to the net flux of hydrogen and hydroxide species,

$$2 N_1^{net} = N_3^{net} - N_4^{net} .$$ (6-35)

The charge conservation equation is applied directly at the film-solution interface. The current density flowing out of the film pores is equated to the current density flowing into the electrolyte.

The hydroxide ion concentration is fixed at the saturation concentration of nickel hydroxide at the interface.

$$c_3(\xi = 0) = c_{OH^-}^{sat} .$$ (6-36)

The value of $c_{OH^-}^{sat}$ is calculated from the solubility product K_{sp} and the bulk concentration of nickel species.

$$c_{OH^-}^{sat} = \left(\frac{K_{sp}}{c_{Ni^{++}}^{\infty}} \right)^{1/2} \times 1000^{-3/2} .$$ (6-37)

We use the value, $K_{sp} = 3.98 \times 10^{-15}$ (mole/liter)^3, given by Cherepkova et al.[54] The factor of 1000 raised to the -3/2 power arises because of the conversion from units of molarity to units of mol/cm^3. It is a good approximation to assume that the saturation concentration of hydroxide is independent of changes in the nickel ion concentration. The magnitude of the concentration of nickel ions changes negligibly relative to changes in the hydroxide ion concentration. This is illustrated in Section 6.3.

Equilibrium (Equation 6-7) and electroneutrality (Equation 6-5) are applied directly. The final relationship is a material balance on the nickel species that determines the change in the thickness of the film.

$$(1 - \epsilon_f) D_1 \rho_f (\sqrt{t} \delta) \frac{d(\sqrt{t} \delta)}{dt} = N_1^{net} .$$ (6-38)

6.2.1.4. Boundary Conditions at the Electrode Surface

The reduced flux of species i at the electrode-film interface, N_i^{sur}, is given by

$$N_i^{sur} = -z_i u_i F c_i \left.\frac{\partial \Phi}{\partial \xi}\right|_{\xi=0} - D_i \left.\frac{\partial c_i}{\partial \xi}\right|_{\xi=0},$$ (6-39)

without a film present. With a film present on the electrode surface, the same form of this equation applies if the equation is multiplied by ϵ_f and η is substituted for ξ.

The current must balance with the fluxes, and the flux of nitrate ions can also be related to the current,

$$\sum_{i=1}^{4} z_i N_i^{sur} = 2 N_2^{sur},$$ (6-40)

because the nitrate ion is not involved in other reactions. The flux of nickel ions must be zero at the electrode surface,

$$N_1^{sur} = 0.$$ (6-41)

These considerations lead to the following condition:

$$3 N_1^{sur} = N_2^{sur} - N_3^{sur}.$$ (6-42)

Equilibrium (Equation 6-7) and electroneutrality (Equation 6-5) are applied at the electrode surface (just outside the diffuse double-layer region). When a film is present, Equation 6-23 also applies.

The final boundary condition is a kinetic expression that determines the flux of nitrate ions due to electrochemical reaction. A Butler-Volmer relationship,

$$i = n F k_a \exp\left[\frac{\alpha_a F}{RT}\left(V - \Phi_o\right)\right] - n F k_c c_2 \exp\left[-\frac{\alpha_c F}{RT}\left(V - \Phi_o\right)\right],$$ (6-43)

is assumed. The kinetic constants and reaction orders are taken from the data

of Zhdanov *et al.*[55] These researchers measured the potentiostatic current response at various nickel nitrate concentrations and pH on a rotating nickel disk electrode. The data suggest that the electrochemical reduction of nitrate is pseudo-first order in nitrate ion and zero order in hydrogen ion. They give 110 mV/decade as the Tafel slope and 0.54 for the transfer coefficient. The reference electrode is chosen to be the NHE. We have estimated the ohmic correction and concentration overpotential to be negligible for their data. A value of k_c was chosen so that Equation 6-43 agrees closely with their data. The magnitude of k_a is calculated using k_c and the standard cell potential for the nitrate-reduction reaction. Figure 6-2 gives the comparison of Equation 6-43 (solid lines) with Zhdanov's data.[55] For the cases under consideration, the driving force for the electrochemical reaction is such that the backward (anodic) reaction rate is negligible and only the forward (cathodic) reaction rate is important.

In the presence of a film, the current density i in Equation 6-43 is replaced by $\frac{i}{\epsilon_f}$.

6.2.2. Modifications to the Russell-Newman Model [49,50]

Very few modifications to the original model of Russell and Newman for the anodic dissolution of iron in sulfuric acid are required to simulate the nickel nitrate system. The model for the reduction of $Ni(NO_3)_2$ and the formation of a $Ni(OH)_2$ film is simpler than the Russell-Newman model due to the absence of passivation.

The boundary conditions for the nickel nitrate system are described in Sections 6.2.1.2, 6.2.1.3, and 6.2.1.4.

The presence of a high concentration of nickel nitrate will give rise to numerical differencing errors in the calculation of the flux of nickel and nitrate
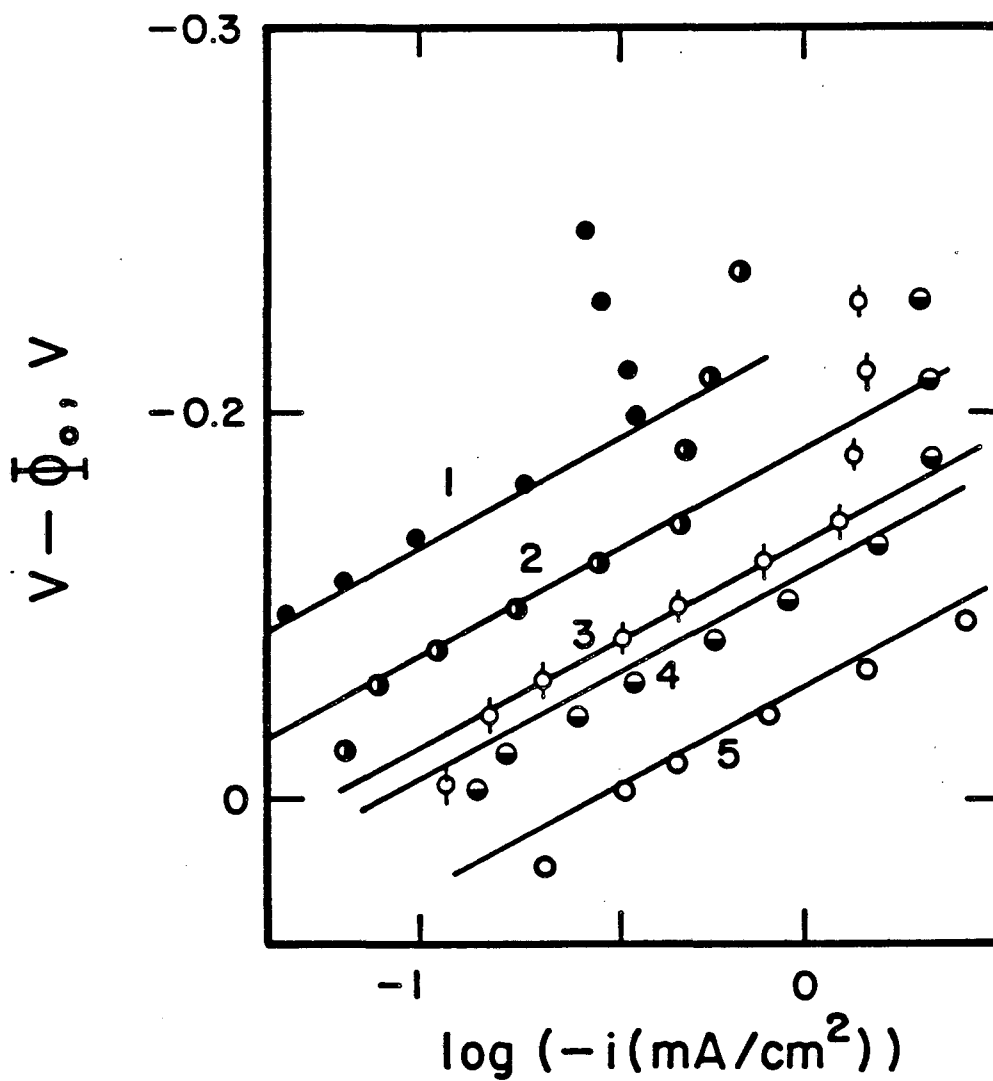
Figure 6-2.   Kinetic data given by Zhdanov *et al.*[55] for a rotating nickel disk electrode (Ω = 1010 rpm). The solid lines are the results of Equation 6-44 for the kinetic parameters given in Table 6-1. The background solution is 1.5 M $NiSO_4$ and 0.02 M H_2SO_4. $Ni(NO_3)_2$ concentration is 1) 0.03 M, 2) 0.1 M, 3) 0.3 M, 4) 0.4 M and 5) 1.5 M.

ions. This numerical difficulty is lessened by replacing the concentration variables for nickel and nitrate species by $(c_{Ni^{++}} - c_{Ni^{++}}^{\infty})$ and $(c_{NO_3^-} - c_{NO_3^-}^{\infty})$, respectively $(c_{Ni(NO_3)_2}^{\infty} = 2.56\ M)$.

Finally, the initial guesses required for the fluxes of the reacting species for a cathodic reaction (nitrate reduction) are of opposite sign than for an anodic reaction (iron dissolution). These initial guesses are required at the initial potential step and at the onset of precipitation.

6.2.3. Operating Parameters

The physical properties and other data used in the model are given in this section. Table 6-1 gives these data.

Table 6-1

Input data for mathematical model.

A. Transport properties

Species	$u_i \times 10^9$ cm^2–mol/J –s	$D_i \times 10^5$ cm^2/s	z_i
Ni^{++}	3.026	0.7500	2
NO$_3^-$	7.665	1.900	-1
OH$^-$	21.22	5.260	-1
H$^+$	37.57	9.312	1

B. Process parameters and physicochemical constants

Symbol	Value	Description	Dimensions
a	0.51023	Disk hydrodynamic constant	
$c_{OH^-}^{sat}$	3.94×10^{-11}	Saturation concentration	mol/cm^3
k_c	5.7×10^{-7}	Cathodic rate constant	cm/s
k_a	2.13×10^{-26}	Anodic rate constant	mol/cm^2-s
n	2	Equivalents per mole of NO$_3^-$	
r_o	0.382	Electrode radius	cm
R	8.3143	Universal gas constant	J/mol-K
T	298.15	Absolute temperature	K
α_a	1.0	Anodic transfer coefficient	
α_c	0.54	Cathodic transfer coefficient	
K	10^{-20}	Water equilibrium constant	(mol/cm^3)^2
κ	0.111	Electrolyte conductivity	Ω^{-1}–cm^{-1}
ν	0.00994	Kinematic viscosity	cm^2/s
ξ_{max}	6.0	Max. dimensionless distance	

ϵ_f	0.657	Film porosity	
ρ_f	$0.0223^{[56]}$	Film density	mol/cm^3

The values of mobilities and diffusivities in Table 6-1 are infinite dilution values.[53] The bulk solution conductivity is for 2.56 M $Ni(NO_3)_2$. We measured this value with a Wayne-Keers conductivity bridge. The value of the kinematic viscosity is estimated from the limiting-current data given by Zhdanov.[51]

The extent of supersaturation is required in the computer model and is not well characterized in the literature. Cherepkova *et al*[54] measured the pH of hydroxide formation at a stationary electrode and found the concentration of hydroxide ions to be 25 times higher than the saturation value. In general, the lower the solubility of a substance the greater the degree of supersaturation that can be observed. For example, the solubility of $FeSO_4$ is 1.88 M, and super-saturation values of 2 to 3 times the saturation concentration are typically observed.[57] Also, the solubility of O_2 is on the order of 10^{-3} M and supersatura-tion values of 70 to 100 times the saturation concentration are observed.[58] The saturation concentration of OH^- in 2.56 M Ni^{++} is 3.94×10^{-8} M. We have taken the degree of supersaturation in the mathematical model to be 45 times the saturation concentration of OH^-.

6.2.4. Method of Solution

In this section, we briefly describe the solution method; however, we refer the reader to the original work of Russell and Newman[49,50] for many important aspects. Russell and Newman explain the calculation of the driving force for the electrochemical reaction $(V - \Phi_0)$. The reference electrode is located in the bulk solution, essentially at infinity. The electrode potential, relative to the given reference electrode $(V - \Phi_{RE})$ must be corrected for variations in electrolyte conductivity within the film and the diffusion layer, the diffusion potential,

and ohmic drop in the bulk solution before it can be used in the kinetic equation.

Russell and Newman describe the perturbation technique that is used as a guide in setting up the equations describing initial film formation. The perturbation solution may also be used to estimate the order of magnitude of errors in the finite-difference formulations. We also refer the reader to the work of Russell and Newman for a description of the numerical treatment of the two distinct regions (ξ and η domains) with a moving boundary.

The governing equations and boundary conditions discussed in Section 6.2.1 are cast into finite-difference form and solved iteratively by the method of Newman (BAND).[53] The time steps are carried out with the Crank-Nicholson procedure.[59] The Fortran computer code for the model (NIFILM) is given in Appendix B-1.

The accuracy of the model is checked by comparison with an approximate analytic solution for the surface concentration of hydrogen ion. The time-stepping procedure is modified to obtain reasonable agreement with the analytic solution in the analytic solution's region of validity. This method is discussed in greater detail in Section 6.3.1.

6.3. Results of Modeling the Formation of a $Ni(OH)_2$ Film

The results of modeling the formation of a $Ni(OH)_2$ film on a rotating disk electrode in nickel nitrate solution are given in this section. In Section 6.3.4 our experimental observations are discussed. Our experimental methods and apparatus are discussed in Section 7.2.

6.3.1. Surface Concentration of H^+ as a Function of Time

In this section, we discuss the model prediction for the surface concentration of hydrogen ion as a function of time after the initial potential step. This

result is compared with an approximate analytic solution. The analytic solution is for the species surface concentration as a function of time for a current step, neglecting migration effects and homogeneous reactions. Figure 6-3 compares the model's calculation of the H^+ surface concentration as a function of time to this approximate analytic solution. The current density in the model is constant at 0.06876 mA/cm^2. The reduction of nitrate ion is assumed to be first order in nitrate ion concentration. The nitrate ion concentration at the surface does not change appreciably with time because it is at such a high concentration in the bulk. This explains why the current density is nearly constant in time. Modifying the kinetics to provide some dependence on hydrogen ion concentration would result in a larger current decrease in time than the case that the model considers. The model predicts the migration flux to be negligible compared to the diffusion flux for hydrogen. This is because the bulk concentration of hydrogen ion is so low (see Equation 6-3).

For short times, the hydrogen ion concentration at the disk surface can be estimated with the Sand equation,[60]

$$c_{H^+}^{sur} = -\left(\frac{t^{\bullet}}{\pi}D_{H^+}\right)^{1/2}\frac{3i}{F} + c_{H^+}^{\infty} \, . \tag{6-44}$$

For longer times, the hydrogen ion surface concentration can be approximated by Nisancioglu and Newman's analytic solution,[61]

$$c_{H^+}^{sur} = \frac{3il}{2FD_{H^+}}\left(\Gamma(4/3) - \sum_{n=0}^{\infty} B_n e^{-\lambda_n t^{\bullet} D_{H^+}/l^2}\right) + c_{H^+}^{\infty} \, . \tag{6-45}$$

The coefficients B_n and the eigenvalues λ_n are given in Reference 61. The diffusion-layer thickness l is given by

$$l = \left(\frac{3D_{H^+}}{\alpha \nu}\right)^{1/3}\left(\frac{\nu}{\Omega}\right)^{1/2} \, . \tag{6-46}$$
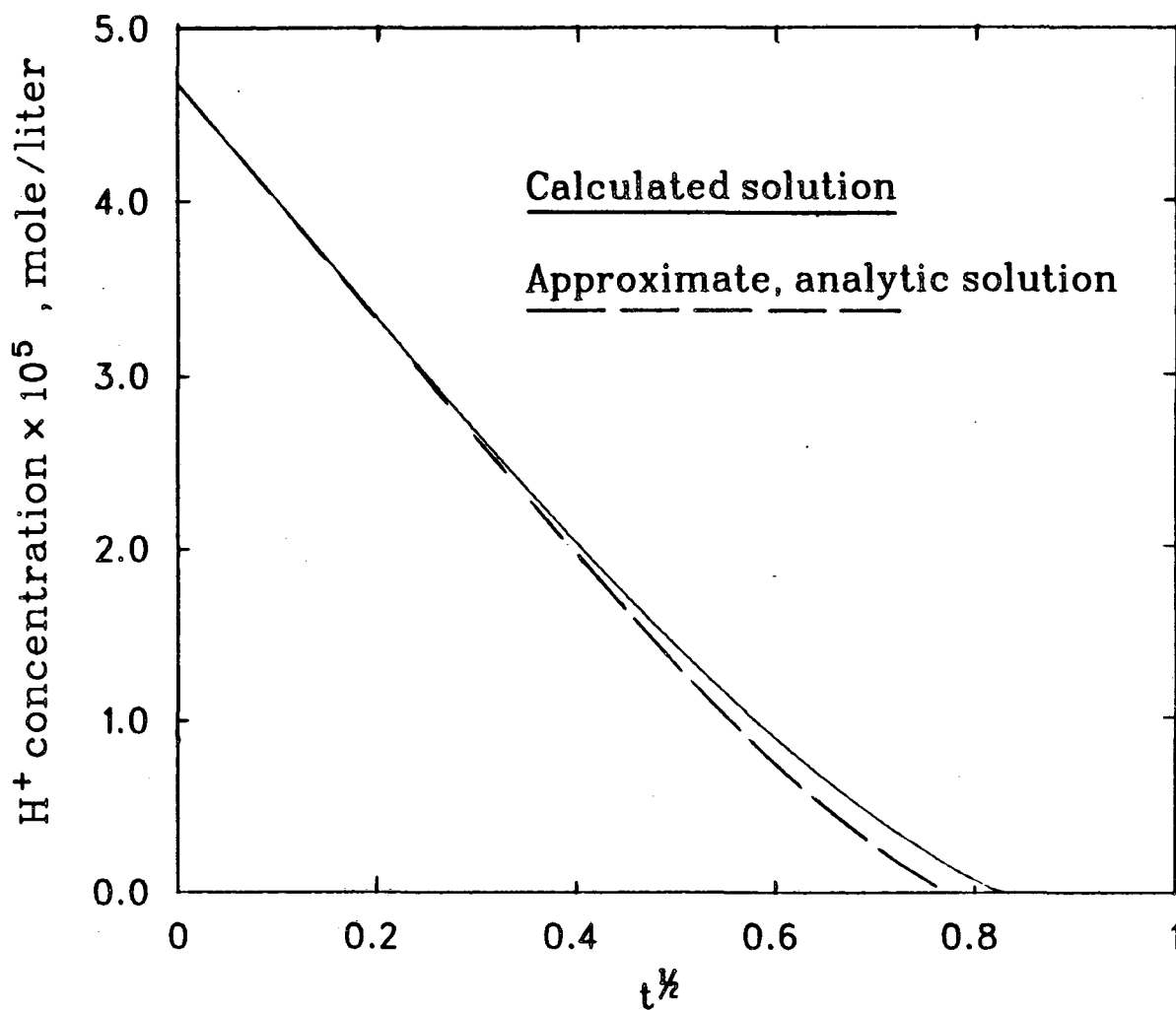
Figure 6-3. The surface concentration of hydrogen ion as a function of dimensionless time. 2.56 M $Ni(NO_3)_2$, 4.7 × 10^{-5} M HNO_3, Ω = 500 rpm, 0.1 V vs NHE. Other parameters are given in Table 6-1.

The series in Equation 6-45 converges rapidly for long times, and is used for $\sqrt{t}$ > 0.38.

In Figure 6-3, the difference between the model and Equations 6-44 and 6-45 for $\sqrt{t}$ > 0.4 is explained by the homogeneous reaction of H^+ and OH^-. In the model, the current is directly proportional to the flux of H^+ minus the flux of OH^- (see Section 6.2.1). In the approximate analytic solution, the current is proportional to the flux of H^+, and the migration flux is assumed to be zero. Initially, the flux of OH^- at the electrode surface is very small relative to the flux of H^+. For example, at $t = 0.2$ the fluxes of the hydrogen and hydroxide species are -1.069 $\times 10^{-9}$ and 2.04 $\times 10^{-14}$ mol/cm²-sec, respectively. For $\sqrt{t}$ > 0.4 the flux of OH^- becomes more and more significant, resulting in the observed discrepancy. As the H^+ ion concentration is depleted, the flux of OH^- ions must increase to maintain the concentration of OH^- required by the equilibrium constraint. At the onset of precipitation $(t = 0.7467)$, the fluxes of H^+ and OH^- at the electrode surface are -3.517 $\times 10^{-10}$ and 7.172 $\times 10^{-10}$ mol/cm²-s, respectively. The model predicts the migration fluxes of H^+ and OH^- to be negligible. At the onset of precipitation, the migration flux of H^+ is 4.42 $\times 10^{-20}$ mol/cm²-s.

The primary purpose of the comparison between the model and the approximate analytic solution is to check the model's time-stepping procedure. Time steps that are too large result in large errors. For example, in Figure 6-3 218 time steps are required in the range of $0 < \sqrt{t} < 0.3$. An initial time step of 10^{-6} is used. Initially, the time steps increase logarithmically. This results in less than 1.3 % difference between the model and Equation 6-44. If only 10 time steps are used in the range of $0 < \sqrt{t} < 0.3$, the error increases and reaches 8% at $\sqrt{t} = 0.3$. The initial time-stepping procedure is especially important because the errors propagate. For the results shown in Figure 6-3, 695 time steps are used between $t = 0$ and the onset of precipitation at $t = 0.7467$. At

approximately $t = 0.24$, the time steps are changed from being increased logarithmically to being increased linearly. Near the onset of precipitation $(\sqrt{t} \approx 0.6)$, the time steps are decreased in order to avoid overshooting $c_{OH^-}^{sat}$.

The approximate analytic solution cannot be used to calculate the nitrate ion concentration at the surface because the migration flux is significant. At the onset of precipitation, $c_{NO_3^-}^{\infty} - c_{NO_3^-}^{sur}$ is calculated as 4.5×10^{-4} M and 4.0×10^{-4} M by the model and Equation 6-45, respectively. The migration flux of NO_3^- contributes to the transport of nitrate ions toward the electrode surface. At the onset of precipitation, the migration flux and diffusion flux of nitrate ions at the electrode surface are -0.085×10^{-10} and 3.48×10^{-10} mol/cm^2-s, respectively. We discuss the potential profile and the direction of the migration flux of nitrate ion in the next section.

6.3.2. Concentration Profiles Just Prior to Ni(OH)$_2$ Precipitation

Figure 6-4 gives the concentration profiles for H^+, NO_3^-, and Ni^{++} species just prior to the onset of Ni(OH)$_2$ precipitation. The model predicts the conditions of precipitation to be reached 0.22 seconds after the potential step to 0.1 V vs. NHE. As we discussed in the previous section, the current remains approximately constant at -0.069 mA/cm^2 prior to film formation. The OH$^-$ concentration is inversely proportional to the H$^+$ concentration and is not shown; the OH$^-$ concentration is at the supersaturation value at this point in time. In this simulation, the supersaturation value is chosen to be 45 times the saturation concentration, $45 \times c_{OH^-}^{sat}$. In the next time step, which is infinitesimally small, a thin film of Ni(OH)$_2$ precipitate forms on the electrode surface, and at the film-solution interface, the OH$^-$ concentration falls to its saturation value. Figure 6-5 gives concentration profiles at the onset of precipitation. The three regions (see Figure 6-1) are not drawn to scale. The initial stages of Ni(OH)$_2$ film growth are discussed in more detail in the next section.
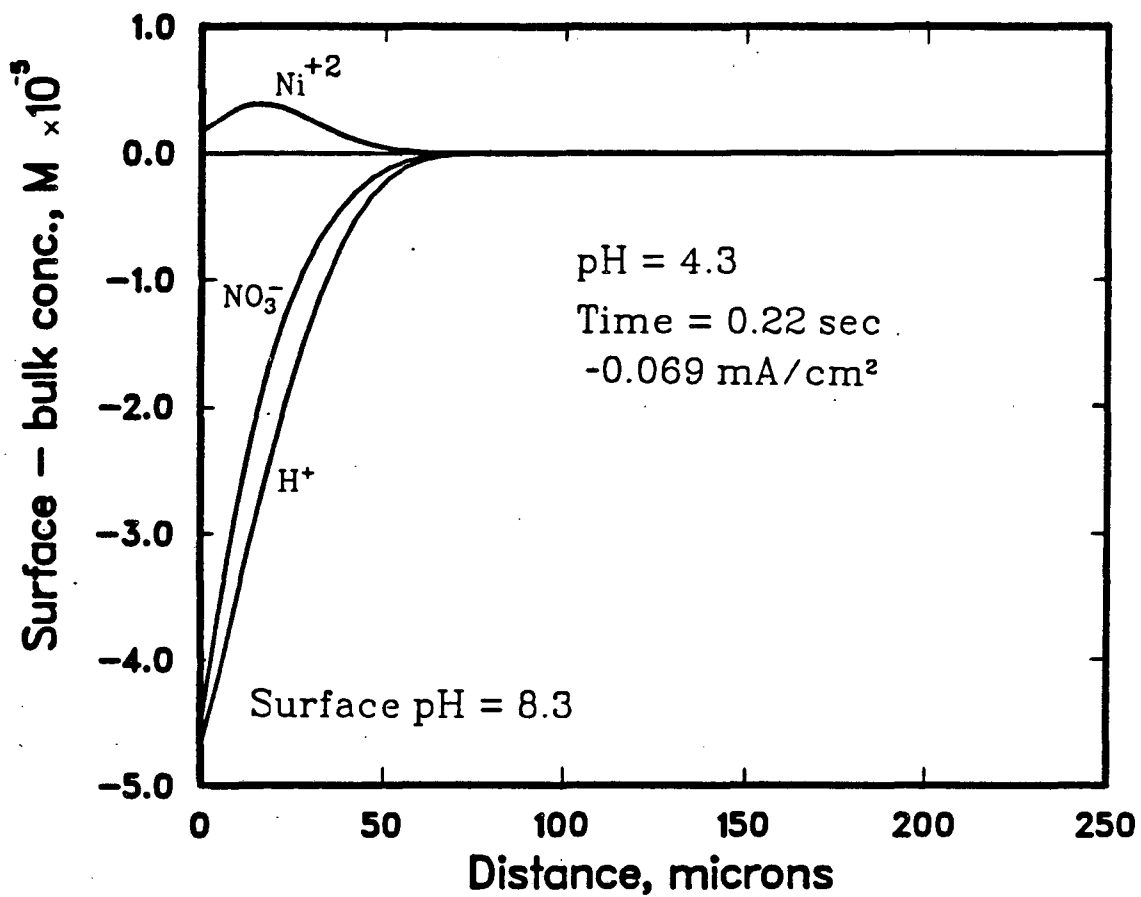
Figure 6-4. Concentration profiles just prior to Ni(OH)$_2$ precipitation (parameters as in Figure 6-3).
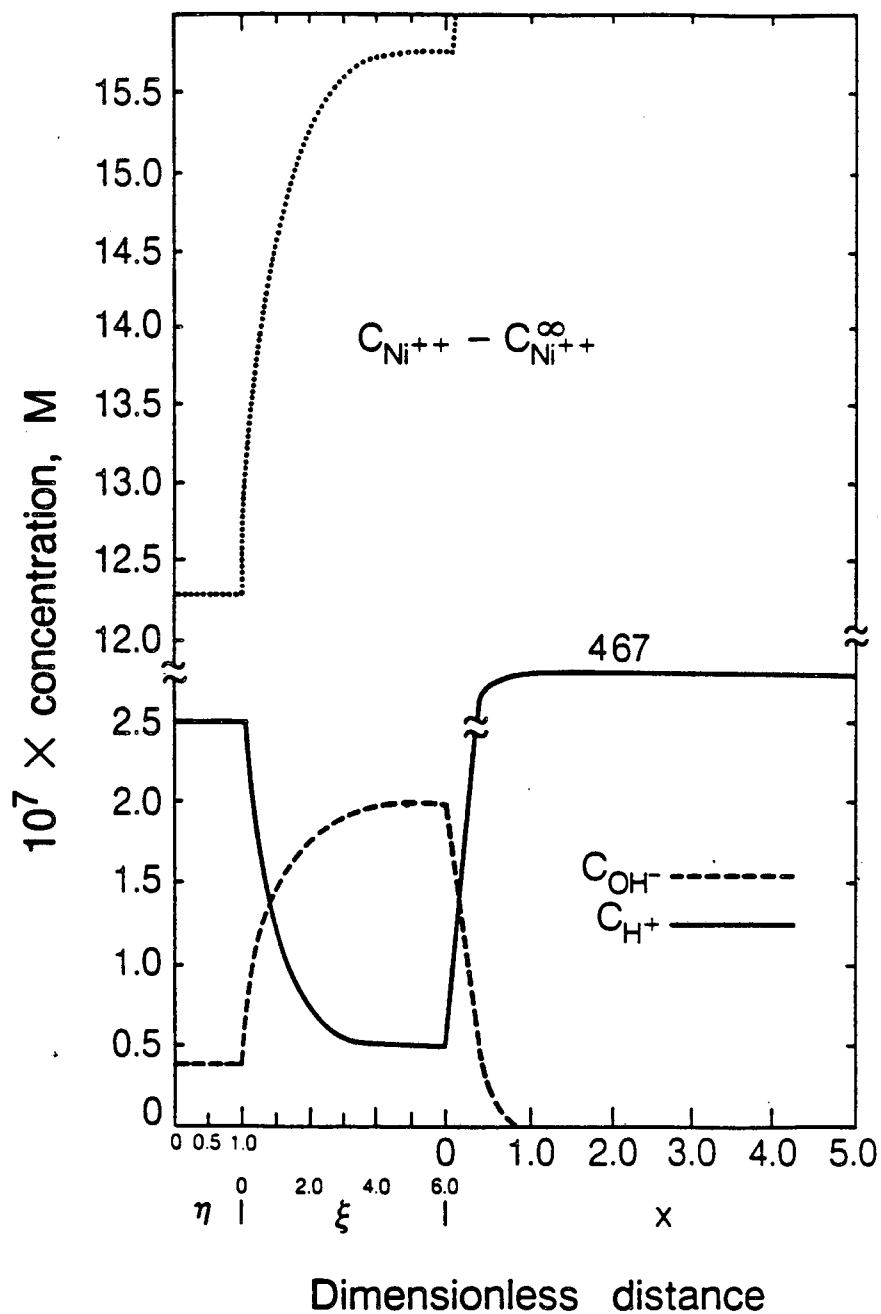
Figure 6-5.   Concentration profiles at the onset of precipitation. The abscissa
variable η is within the film (region I in Figure 6-1). The abscissa variable ξ
corresponds to region II in Figure 6-1. The profiles with the x abscissa are
termed the "long profiles" (region III of Figure 6-1). Parameters are given in
Table 6-1 except that a supersaturation factor of 5 is used.

Just prior to the onset of precipitation (Figure 6-4), the surface concentration of H^+ (5.43×10^{-9} M) has decreased several orders of magnitude relative to the bulk concentration (4.7×10^{-5} M). Similarly, the surface and bulk concentrations of OH^- are 1.84×10^{-6} M and 2.34×10^{-10} M, respectively. In contrast, the surface concentrations of Ni^{++} and NO_3^- are the same order of magnitude as their bulk concentrations ($c_{Ni(NO_3)_2}^{\infty} = 2.56$ M). For example, $c_{Ni^{++}}^{\infty} - c_{Ni^{++}}^{sur}$ is calculated as -1.70×10^{-6} M.

The direction of the migration flux of nitrate ions, at the electrode surface, may be contradictory to what is intuitively expected. The migration flux of nitrate ions contributes to the transport of NO_3^- toward the electrode surface. It may be expected that a negative ion should migrate away from a cathode. This conflict with intuition can be resolved by examining the potential profile given in Figure 6-6. This will also explain the maximum in the Ni^{++} concentration and the migration of Ni^{++} (at $y=0$) away from the electrode surface.

The potential is governed by

$$\nabla \Phi = -\frac{i}{\kappa} - \frac{F}{\kappa} \sum_i z_i \, D_i \nabla c_i \; . \qquad (6\text{-}47)$$

The first term represents the contribution to the potential gradient due to Ohm's law. The second term is the contribution to the potential gradient due to the diffusion potential. Notice that the diffusion potential term is zero if all the diffusion coefficients are equal. In this case, we expect the gradient of potential and the current to be of opposite sign. That is, for a cathode we would expect the potential gradient to be positive and, negatively charged species to migrate away from the electrode surface. There is a tendency for ions that diffuse easily to diffuse ahead of other ions. This results in a diffusion potential, which can exist even in the absence of current. For the reduction of nitrate ion in acidic, nickel nitrate solution, H^+ and NO_3^- are the major contributers to the
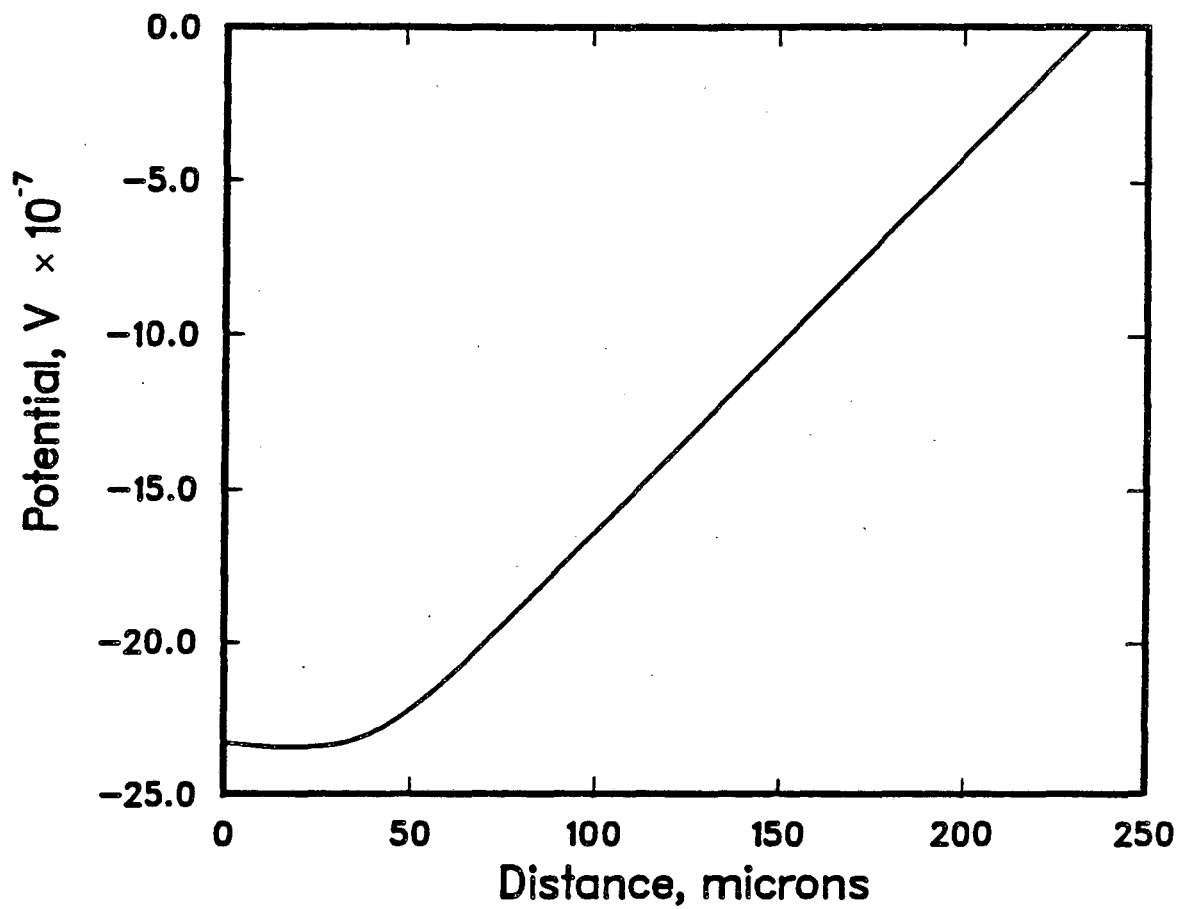
Figure 6-6. Potential profile corresponding to the conditions of Figure 6-4.

diffusion potential. At the electrode surface, the magnitude and direction of the potential gradient are dominated by the diffusion potential term in Equation 6-47. The ohmic term and the diffusion potential term cancel at approximately 20 microns from the electrode, resulting in the observed minimum in the electric potential. Farther into the solution, the potential gradient is determined by the Ohm's law term in Equation 6-47. At the edge of the diffusion layer, where the concentration gradients approach zero, the gradient of the diffusion potential approaches zero.

The maximum in the concentration profile of the nickel species is also explained by the behavior of the potential profile. In view of Equation 6-3, it should not be surprising that the concentration profile roughly follows the potential profile. The direction of the migration flux of Ni^{++} at the electrode surface is away from the electrode.

For the case shown in Figure 6-4, the model predicts that 0.22 second is required to reach the conditions of $Ni(OH)_2$ precipitation at the surface of the electrode. As the concentration of H^+ approaches zero, the OH^- concentration increases very rapidly. Consequently, the time to reach precipitation conditions is a weak function of the chosen supersaturation value. This time period increases with increasing acid concentration and decreasing current (increasing potential).

6.3.3. The Initial Stages of $Ni(OH)_2$ Film Growth

The model predicts that a thin film of precipitate forms on the electrode immediately after the situation depicted in Figure 6-4. The magnitude of the current density after initial film precipitation is a function of the film porosity and the ohmic potential drop in the solution. The current density also becomes a function of the ohmic potential drop in the film as the film grows thicker. The ohmic potential drop in the solution is small for the conditions of Figure 6-4.

Consequently, the initial current density after film precipitation is simply $i\epsilon_f$. For example, the cathodic current density is 0.069 mA/cm^2 in Figure 6-4, and it drops to 0.045 mA/cm^2 in Figure 6-5. Russell and Newman[49,50] discuss the effects of significant ohmic potential drop in the solution.

Figure 6-7 gives the dimensionless film thickness as function of the square root of dimensionless time for a supersaturation factor of 45. It should be noted that at 300 on the abscissa (2 microseconds) the film thickness is only a fraction of a monolayer (10^{-8} microns). The leveling of the curve is due to the small supersaturation factor used. A larger supersaturation factor will give a larger rate of film growth at a given time after film initiation, because the flux of film-forming species will remain larger for a longer period of time.

6.3.4. Comparison With Experimental Results

In this section, we discuss the model behavior in conjunction with our experimental observations. In the experimental investigations, we observe a fluctuating current response for conditions in which a film is present on the electrode surface. Figure 6-8 gives the current response to a potential step of -0.225 V vs. SCE. The electrode is a glassy carbon rotating disk. The bulk concentrations of species and disk rotation speed are the same as in Figure 6-4. An initial current spike is observed; however, the width of the spike is small enough that it cannot be distinguished from the axis. During the spike, the cathodic current density rises to a maximum of about 1 mA/cm^2 and then falls to a minimum of about 0.5 mA/cm^2, all within the first 0.5 second. After the spike, the current gradually increases to a maximum and a decreases to a steady average current after several minutes. We observe the magnitude of the initial current spike to be dependent on the acid concentration. In Chapter 7 (Section 7.4.2), the initial current spike is discussed in greater detail. Possible explanations for the maximum in the average current are also discussed in
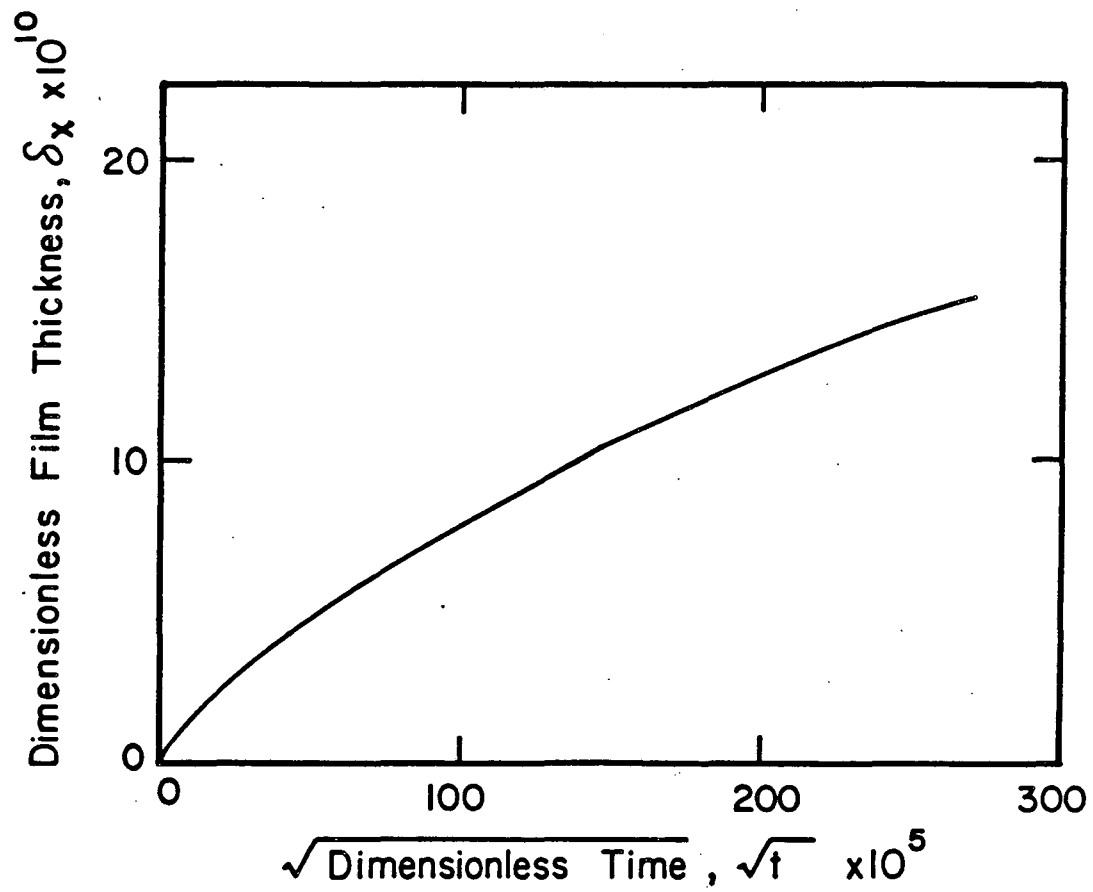
Figure 6-7.   Dimensionless film thickness, δ_x, as a function of the square root of dimensionless time $\sqrt{t}$ for the initial stages of film growth.
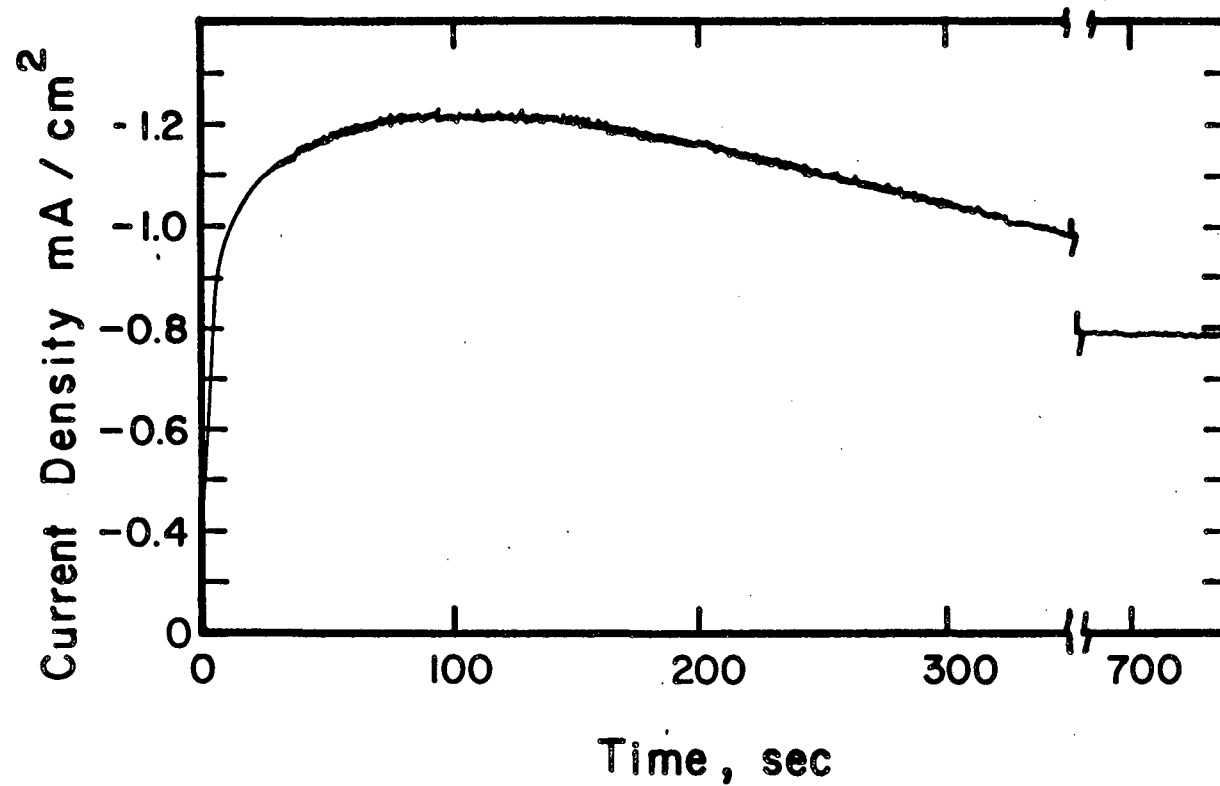
Figure 6-8. Experimental results for the current response to a potential step (-0.225 V vs SCE). 2.56 M Ni(NO$_3$)$_2$, 1 × 10^{-5} M HNO$_3$, Ω = 500 rpm.

Chapter 7. In this section, we address the observation of the fluctuating current. The experimentally observed fluctuating current response occurs at conditions in which the surface concentration of hydrogen is estimated to be very low, corresponding to conditions for $Ni(OH)_2$ precipitation. At large negative potentials (relative to the experimentally observed open-circuit potential), a film can be seen on the electrode *in situ*.

At the time of the potential step, the model predicts the current to rise instantaneously to a value that is primarily determined by the kinetics of the nitrate reduction reaction, and within a fraction of a second a $Ni(OH)_2$ precipitate forms on the electrode surface. The current decreases at the onset of precipitation to approximately $i\epsilon_f$. The mathematical model does not predict the experimentally observed current fluctuations.

Current fluctuations are frequently observed in nonpassivating systems. For example, Lee et al.[62] observe current oscillations in the electrodissolution of copper in acidic, chloride media. The authors interpret the observed oscillations in terms of the instability of a CuCl film that forms on the electrode surface. That is, a film periodically thickens when the film formation reaction is faster than the dissolution reaction and thins when the dissolution rate exceeds the film formation rate. The observed oscillations are believed to correspond to situations for which a balance between film formation and dissolution is unstable. An initially infinitesimal disturbance can grow and result in oscillations of finite amplitude. The same authors, Pearlstein et al.[63], performed a linear stability analysis and predicted conditions in which an unstable CuCl film is present on the electrode surface. Their predictions are in qualitative agreement with their experimental results. It is possible that the proposed mechanism may explain the observed current fluctuations in the reduction of nitrate ion in nickel nitrate solutions.

Figure 6-9 gives an example of the fluctuating current that is observed for a potential step to -0.6 V vs. SCE. A film is not visible on the electrode at these conditions; however, the solution in the vicinity of the electrode appears cloudy. At these conditions, the observed period and amplitude are approximately 20 μsec and 0.5 mA/cm^2, respectively. The steady, average-current density is approximately -29.5 mA/cm^2. It is interesting to note that steady, average-current densities are obtained sooner for more negative potential steps. That is, in contrast to the results of Figure 6-8 (-0.25 V vs. SCE), with a steady, average-current density of approximately -0.8 mA/cm^2 after 10 minutes, the steady, average-current density in Figure 6-9 was observed after approximately 1 minute. This observation is in accordance with our belief that the adsorption reactions proposed in Chapter 7 are relatively less important at more negative potentials.

The behavior of the experimentally observed fluctuating current response with varying rotation speed and potential should be addressed. Qualitatively, the frequency of the current fluctuations decreases with decreasing rotation rate, and the amplitude of the fluctuations increases with decreasing potential.

6.3.5. Conditions in Which Film Formation Does Not Occur

For certain operating variables, the conditions of precipitation are not met. For example, if the current is low enough, a steady-state surface pH is reached that is below the pH for $Ni(OH)_2$ precipitation. The same argument can be made for a high bulk concentration of acid. Figure 6-10 gives model results for operating conditions that do not result in the conditions of film formation. This figure gives the surface concentration of H^+ as a function of time for two electrode rotation speeds. The operating conditions are similar to the conditions of Figure 6-4, except for the bulk acid concentration (pH = 2.222), which is about two orders of magnitude higher. The steady-state surface conditions of pH = 2.231 and 2.228 are reached for 800 rpm and 1600 rpm, respectively. In the
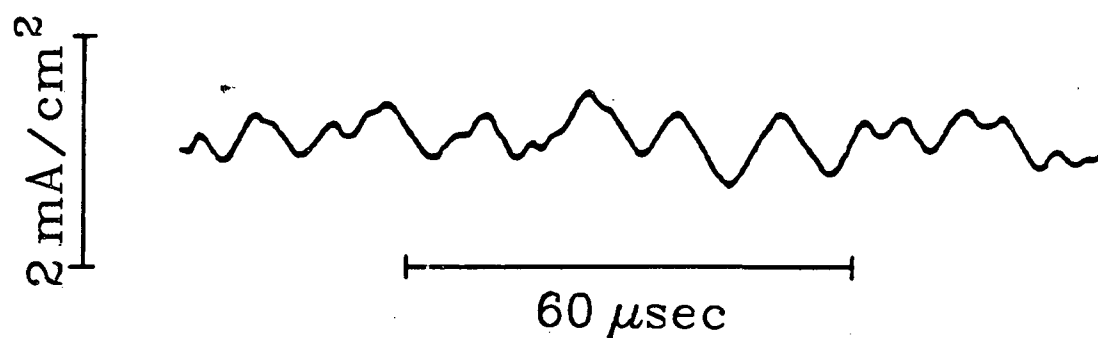
Average current density $= -29.5\,\text{mA/cm}^2$

800 rpm

$-0.6\,\text{V vs. SCE}$

Figure 6-9.   Experimentally recorded fluctuating current response (-0.6 V vs SCE, 2.56 M Ni$(NO_3)_2$, 0.006 M HNO$_3$, Ω=800 rpm).
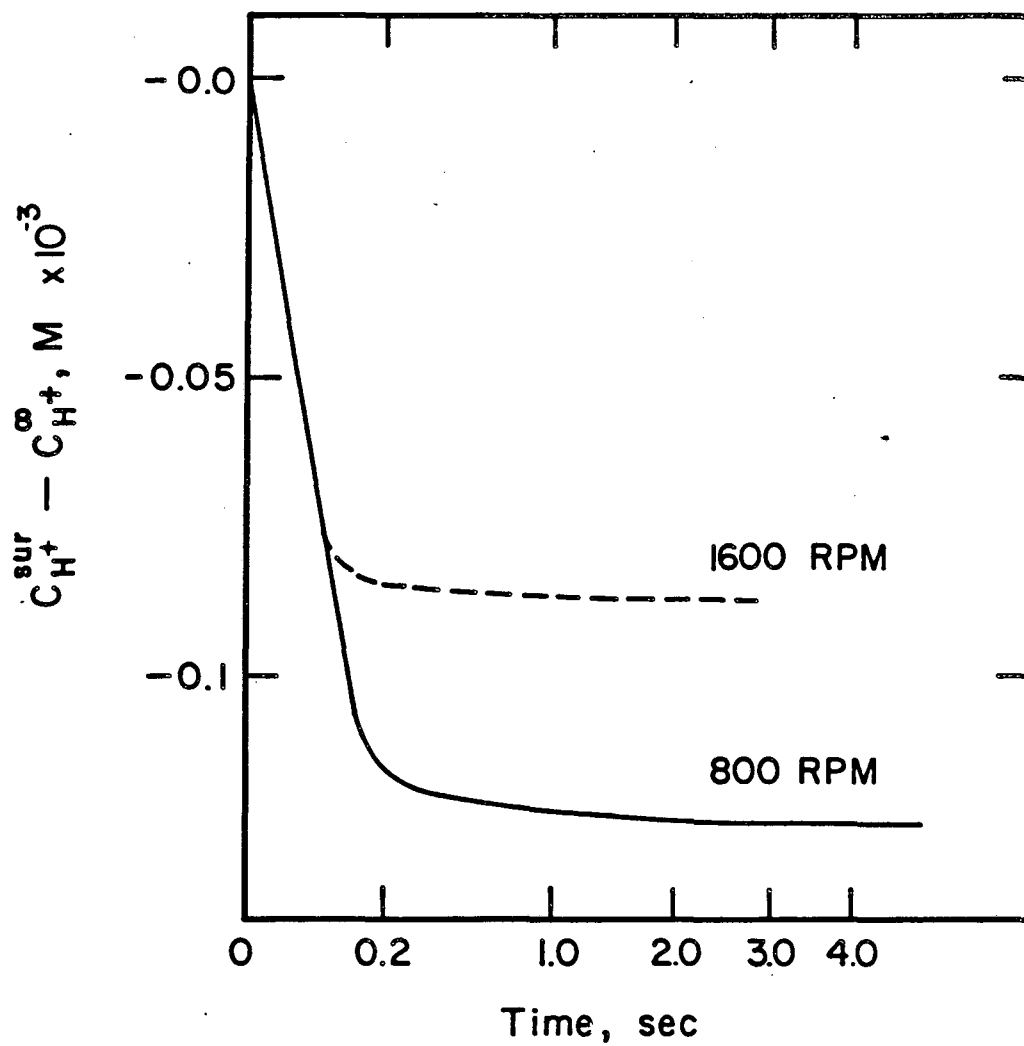
Figure 6-10. Model results for the surface concentration of hydrogen ion as a function of time (2.56 M Ni(NO$_3$)$_2$, 0.006 M HNO$_3$, 0.05 V vs NHE).

model, supersaturation, corresponding to a surface pH of 8.3, is required for film formation. As expected, the steady-state conditions are reached sooner for the higher rotation speed.

In Figure 6-10, a square-root scale is used for the abscissa in order to show the linear region (Equation 6-44). As we observed in Figure 6-4, the behavior in the linear region agrees with the approximate analytic result (Equation 6-44). In contrast to the results of Figure 6-4, the behavior in the logarithmic region ($t^* > 0.2$ s) agrees well with Equation 6-45. This good agreement is seen because at these conditions the hydroxide ion flux is small, relative to the hydrogen ion flux. For example, the steady-state condition for 800 rpm has a hydroxide ion flux of 4.96×10^{-19} mol/cm^2-s and a hydrogen ion flux of -3.03×10^{-9} mol/cm^2-s.

Figure 6-11 gives the concentration profiles in the solution adjacent to the electrode surface for the case of 800 rpm and 0.015 seconds after the potential step. Figure 6-12 gives the steady-state concentration profiles for this case ($t^* = 5.42$ s). As expected, the steady-state diffusion layers penetrate deeper into the solution than diffusion layers at 0.015 seconds. The steady-state potential profile is shown in Figure 6-13. We see that the observed maximum in the nickel ion concentration profile is not a transient affect.

Experimentally, conditions that do not result in film formation can be useful in the investigation of the mechanism of nitrate ion reduction. As we mentioned in the previous section, with a film on the electrode a fluctuating current response is observed. In Chapter 7, we take a closer look at the mechanism of nitrate ion reduction. Experimental operating conditions similar to those of Figure 6-10 are combined with potential sweep techniques. It appears that the mechanism of nitrate ion reduction is more complicated than the simple reaction in the model proposed in this chapter. At experimental conditions similar to those of Figure 6-10 (see Figure 7-2), we see an initial current spike, an increase to a maximum and a decrease to a steady-state (-0.1 mA/cm^2) after
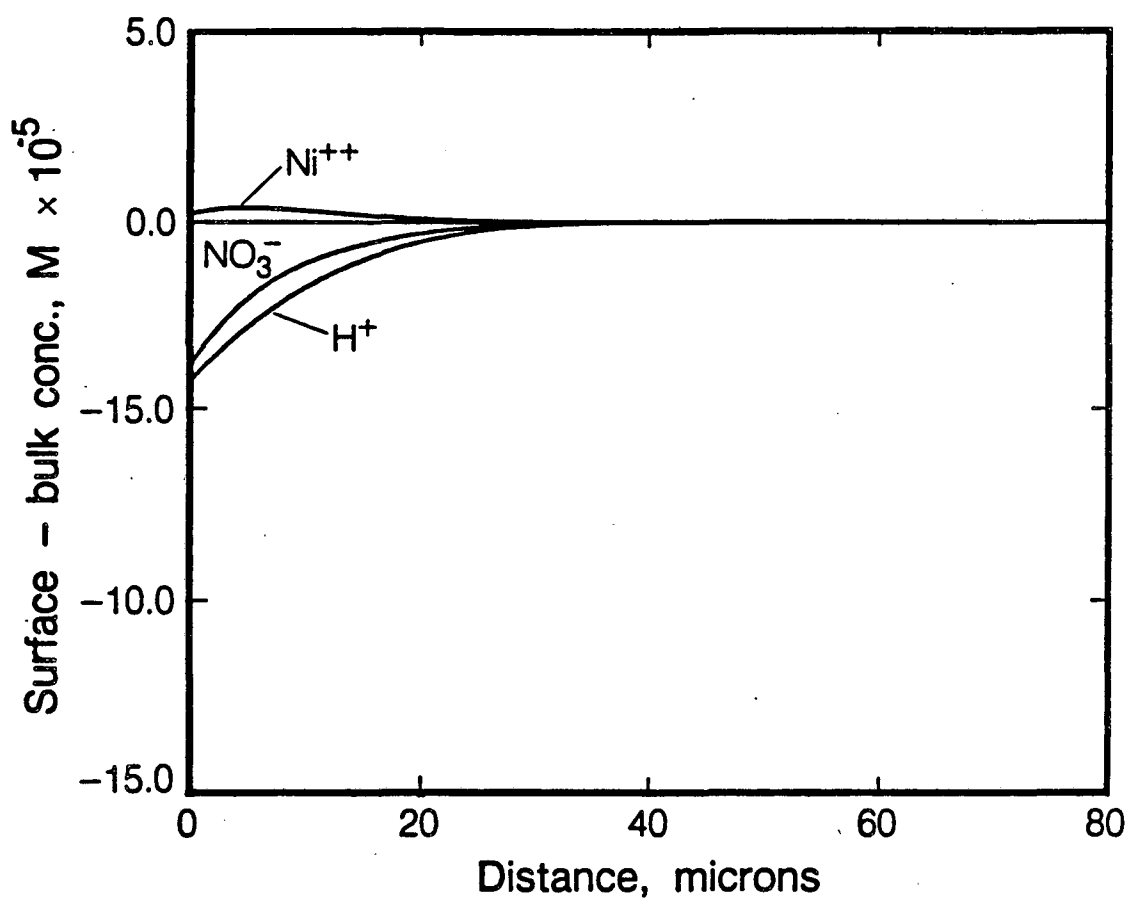
Figure 6-11. Concentration profiles for the conditions of Figure 6-10 (Ω = 800 rpm) at 0.015 seconds.
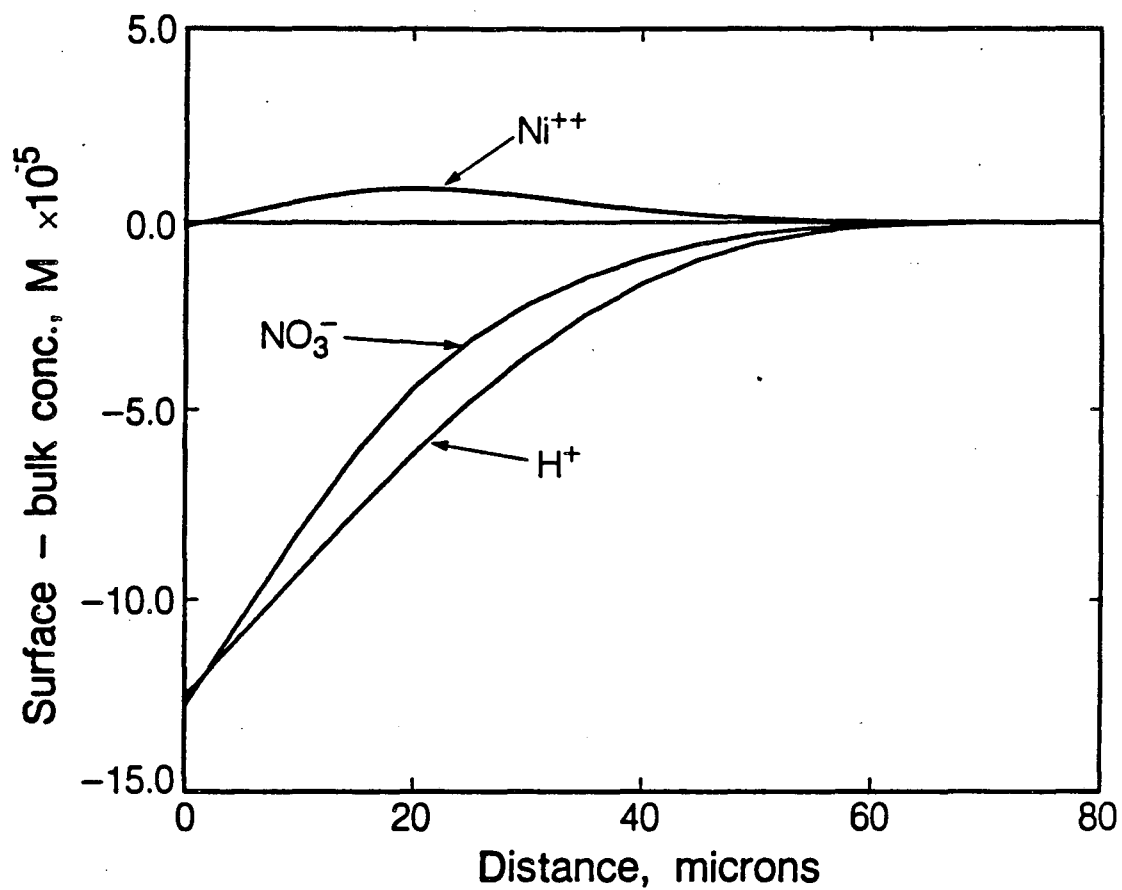
Figure 6-12. Steady state ($t = 5.4$ s) concentration profiles for the conditions of Figure 6-10.
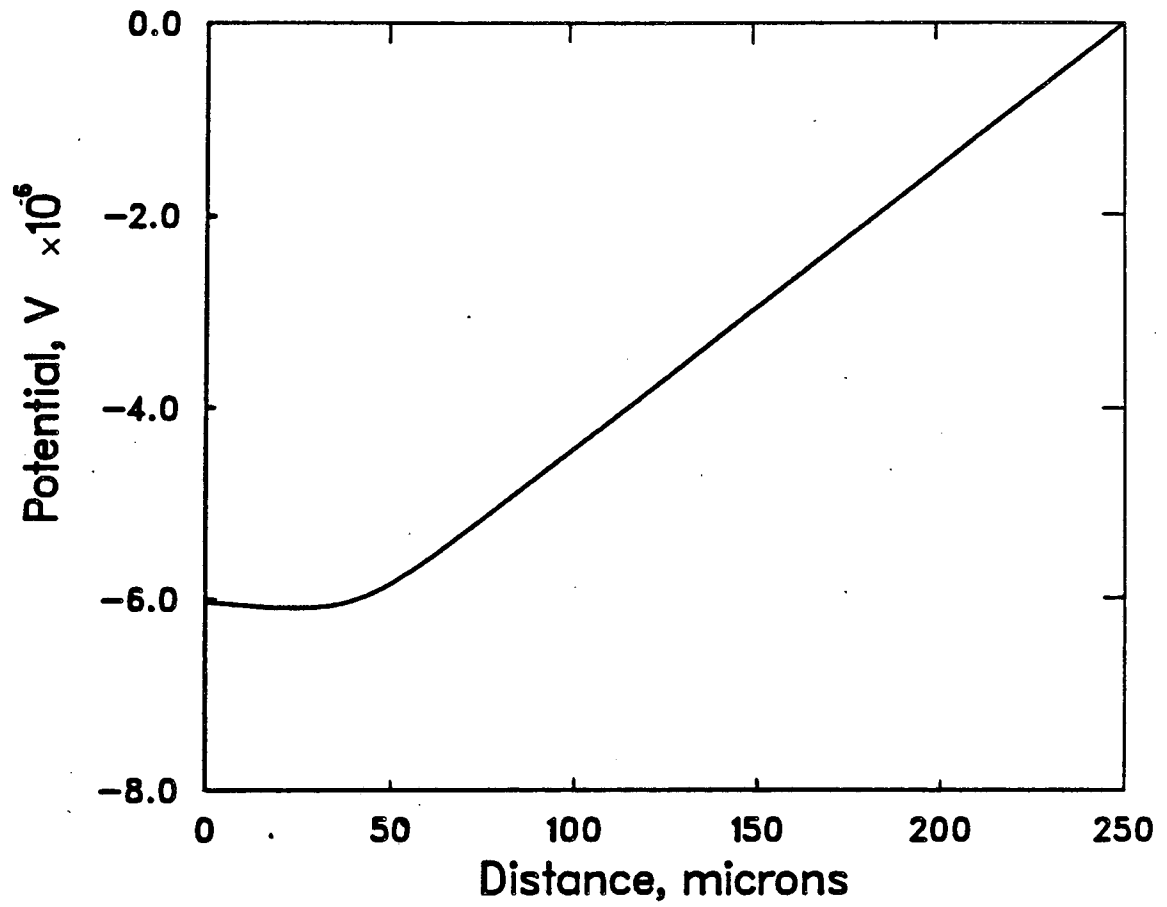
Figure 6-13. Steady-state potential profile for the conditions of Figure 6-10.

approximately 20 minutes. This is in contrast to the conditions depicted in Figure 6-10 which predict a nearly constant current (-0.195 mA/cm^2) and steady-state conditions after only 1 second. To summarize, we believe that the mechanism involves adsorbed hydrogen, intermediate adsorbed species, and further reduction to hydroxylamine. We might expect our steady-state model predictions to represent reality much more than the transient results. As we mentioned earlier, Zhdanov *et al.*[55] observe the steady-state results to be independent of pH and first order in nitrate concentration.

6.4. Conclusions and Further Work

We have theoretically investigated the electro-precipitation method with a mathematical model for the formation of a Ni(OH)$_2$ film on a rotating disk electrode. Our results show the conditions (current and nitric acid concentration) in which precipitation can be reached on a rotating disk electrode. Experimentally, if we strongly polarize the electrode, we can see a film on the electrode surface with the naked eye.

Even though the bulk solution is acidic, the transport of hydroxide ions must be taken into account because the solution adjacent to the electrode is basic at the conditions of precipitation. The comparison of our model to an analytic solution that neglects hydroxide ion transport shows that the surface pH is overestimated when the transport of hydroxide ions is neglected.

The model also demonstrates that the direction that a species migrates (due to the electric field gradient) may be contradictory to what is intuitively expected. The model predicts the positively charged nickel species (at the electrode surface) to migrate away from the cathodically-polarized electrode. The diffusion potential is responsible for this effect.

In light of the experimentally observed fluctuating current behavior (which is not predicted by the model), perhaps further work should include sta-

tionary electrode experiments. We do not observe a fluctuating current response for the conditions of Figure 6-9 when the disk is stationary. It is interesting to note that the stability analysis of Pearlstein et al.[69] predicts instability for stationary electrode situations.

Further modeling efforts should also shift to the stationary electrode conditions. Model improvements may include a more complicated kinetic mechanism including species adsorption. The nickel hydrolysis products discussed in Section 6.2 may affect the conditions of precipitation and should be included in the model. The inclusion of nucleation, precipitation, and dissolution kinetics may prove useful. Also, concentrated-solution theory for the nickel and nitrate species should replace the dilute-solution theory used in the present model.

List of Symbols for Chapter 6

a disk hydrodynamic constant, 0.51023

c_i concentration of species i, mol/cm^3

D_i diffusion coefficient for species i, cm^2/s

dt time step size

F Faraday's constant, 96487 C/equiv

i superficial current density, A/cm^2

K water equilibrium constant, (mol/cm^3)^2

K_{sp} solubility product of $Ni(OH)_2$, (mol/l)^3

k_c cathodic rate constant, cm/s

k_a anodic rate constant, mol/cm^2-s

l steady-state diffusion layer thickness, cm

$\mathbf{N}$ molar flux, mol/cm^2-s

N_i^f reduced flux of species i in the film, mol/cm-s

N_i^s reduced flux of species i in solution, mol/cm-s

N_i^{net} reduced net flux at film-solution interface, mol/cm-s

N_i^{sur} reduced flux at electrode surface, mol/cm-s

pH $-\log(1000\,c_{H^+})$

R universal gas constant, 8.3143 J/mol-K

R_i rate of homogeneous reaction, mol/cm^3-s

r_o radius of disk electrode, cm

T absolute temperature, K

t dimensionless time

t^* time, s

u_i ionic mobility, cm^2-mol/J-s

V electrode potential, V

v	velocity, cm/s
x	dimensionless distance from electrode
y	distance from electrode, cm
z_i	charge number

Greek letters

α_a	anodic charge-transfer coefficient
α_c	cathodic charge-transfer coefficient
δ	reduced film thickness ($\delta_x/\sqrt{t}$)
δ_x	dimensionless film thickness
δ_y	film thickness, cm
ϵ_f	film porosity
ϵ_s	surface porosity
η	reduced distance variable in the film
$\Gamma(4/3)$	the gamma function of 4/3, 0.89298
κ	conductivity, $(\Omega\text{-cm})^{-1}$
ν	kinematic viscosity, cm^2/s
π	3.14159...
ξ	stretched variable in the electrolyte
ρ_f	molar density of the film, mol/cm^3
Φ	potential in solution, V
Φ_o	potential just outside diffuse double layer, V
Ω	disk rotation speed, rad/s

Subscripts and Superscripts

i	species i
∞	far from the electrode surface
o	position just outside the diffuse double layer
max	in the bulk solution
RE	reference electrode

sat   saturation conditions

sur   at the electrode surface

Chapter 7

Investigation of the Mechanism of Nitrate Ion Reduction

7.1. Introduction

An experimental investigation of the cathodic behavior of nickel nitrate solutions with a rotating-disk electrode is presented in this chapter. The reduction of nitrate ion in nickel nitrate solutions is the electrode reaction in the electrochemical precipitation of nickel hydroxide. Nickel hydroxide is the active material in nickel battery electrodes. The reduction of nitrate ion causes a pH increase in the solution adjacent to the electrode; the precipitation of nickel hydroxide occurs with a sufficient increase in pH. In this work, the nitrate-ion-reduction mechanism is investigated in order to obtain a more fundamental understanding of the system.

In this chapter, however, we investigate the nickel nitrate system at conditions in which $Ni(OH)_2$ precipitation is not initiated. That is, the solution adjacent to the electrode is not sufficiently alkaline for precipitation of $Ni(OH)_2$ (or other basic nickel salts). In Chapter 6, a theoretical and experimental investigation of the system under conditions of precipitation is given. Our objectives and some background material are given in the next two sections. The experimental procedures are discussed in Section 7.2. Experimental results are discussed in Section 7.3, and a mechanism for the nitrate ion reduction reaction is proposed in Section 7.4. In Section 7.5, experimental results are discussed in conjunction with theory based on the mechanism proposed in Section 7.4. The results of this chapter are summarized in Section 7.6, and we suggest further work in Section 7.7.

7.1.1. Background

As early as the 1930's, the reduction of nitrate ion in aqueous solutions had captured the attention of researchers. Tokuoka *et al.*[64] observed that solutions of nitrate ions (0.0002 - 0.01 M) are readily reducible only in the presence of polyvalent cations, providing the reduction potential of the cation is more negative than the reduction potential of the anion. For the nickel nitrate system, the deposition potential of Ni^{++} is more negative than the reduction potential of NO_3^-. The researchers observed that the rate of nitrate ion reduction is increased with the concentration and valency of the cation. The researchers postulate that the presence of divalent cations, which collect at the negatively charged cathode, diminishes the electric field; hence, the approach of the nitrate anions to the cathode is facilitated.

The interest in nickel battery electrodes has helped focus nitrate ion reduction research on acidic, nickel nitrate solutions. Zhdanov *et al.*[55] studied the reduction of nickel nitrate solutions at various nitrate ion concentrations. A plot of their data, in the potential range of -0.25 to -0.55 V relative to a saturated calomel electrode (SCE), is given in Figure 7-1. The original data are given with reference to the hydrogen electrode. As shown in Figure 7-1, a current maximum is observed in the data recorded in the direction of decreasing potential. The maximum is not observed in the reverse direction. A qualitative explanation of the experimental results is given. The authors explain the current maximum by the desorption of NO_2^- ion. The NO_2^- ion, which is an intermediate reduction product, is believed to desorb near the potential of zero charge. The subsequent increase in current is assumed to be caused by the adsorption of hydrogen ions. The adsorbed hydrogen reacts with adsorbed NO_2^- to form adsorbed HNO_2, which is then cathodically reduced. A similar current maximum is also observed in our experimental investigations. We also believe that the current maximum may be explained by the adsorption and reaction of
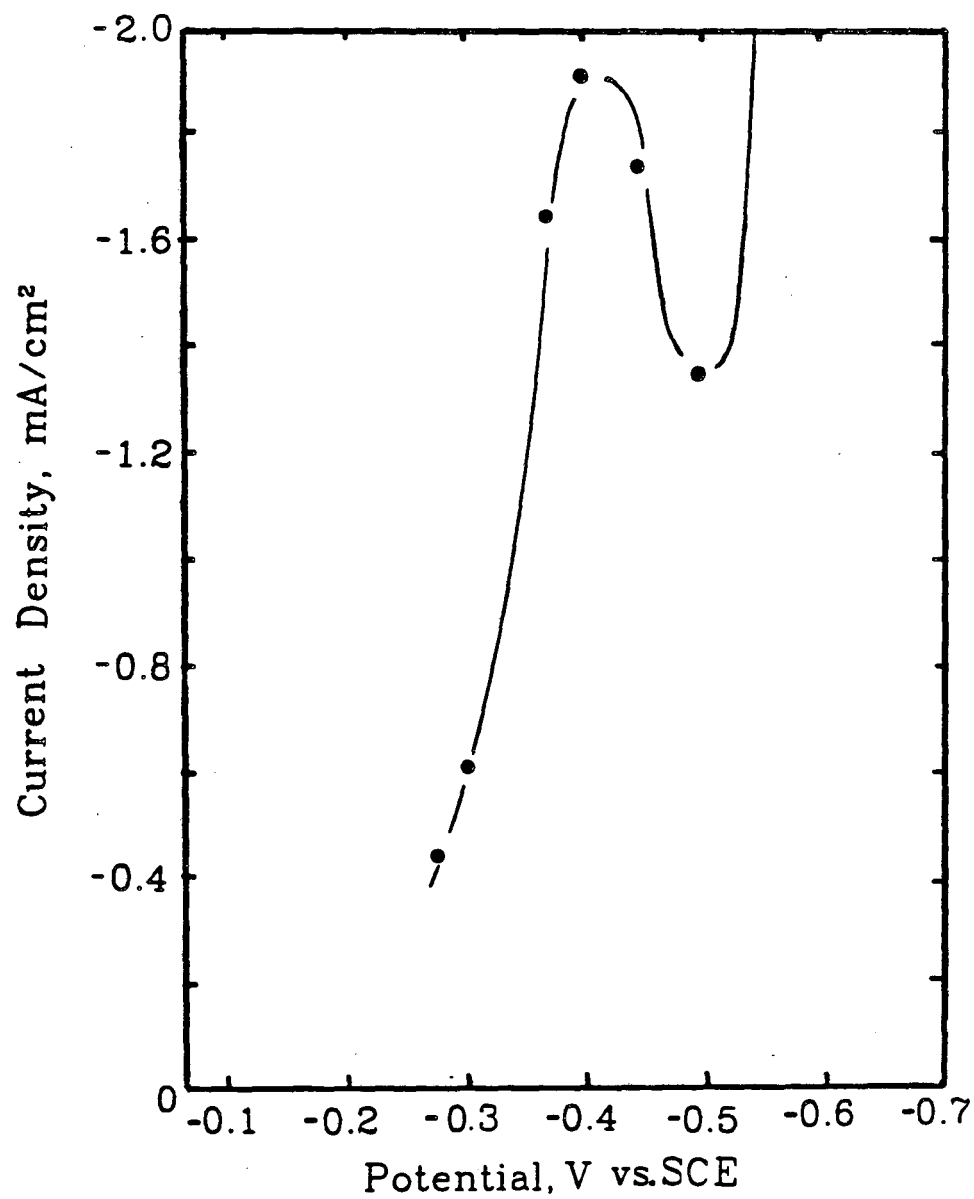
Figure 7-1. Experimental data given by Zhdanov *et al.*[55] for a rotating nickel disk electrode (1010 rpm, 0.5 M Ni(NO$_3$)$_2$, 0.02 M H$_2$SO$_4$, 1 M NiSO$_4$). The data are recorded in the direction of decreasing potential.

species. We propose a simple mechanism for the nitrate-ion-reduction reaction that can be used to calculate the current response to a potential step; the analytic solution is compared to experimental results. The scope of our research is discussed in the next section.

7.1.2. Scope of the Research

The goal of this research is to obtain a more fundamental understanding of the nitrate-ion-reduction reaction in acidic, nickel nitrate solutions. The behavior of the current response as a function of nitric acid and nickel nitrate concentrations is investigated. The results are compared with observations and theories available in the literature. A mechanism for the reduction of nitrate ion, which is consistent with our results and literature results, is proposed.

7.2. Experimental Procedure

All experiments were performed in an electrochemical cell with a rotating-disk electrode in acidic, nickel nitrate solution. A schematic diagram of the cell is given in Figure 7-2. The electrode pretreatment procedures are described in Section 7.2.2. The cell is made of pyrex glass and holds approximately 300 ml of solution. Separate counterelectrode and reference electrode compartments are located at opposite ends of the main compartment of the cell. A saturated calomel electrode was used as a reference electrode, and a platinum screen was used as the counterelectrode.

The 0.764-cm-diameter disk electrode is embedded in a Teflon®, insulating cylinder (2 cm diameter). The electrode and rotator were obtained from the Pine Instrument Company. Glassy carbon, gold, and platinum electrodes were used in the experiments; the glassy carbon electrode was used in most investigations. Both the glassy carbon and gold surfaces have high hydrogen overpotentials, which allowed us to study the nitrate reduction reaction in the

Sparger

RDE

Reference
Electrode

Counter
Electrode

Cell
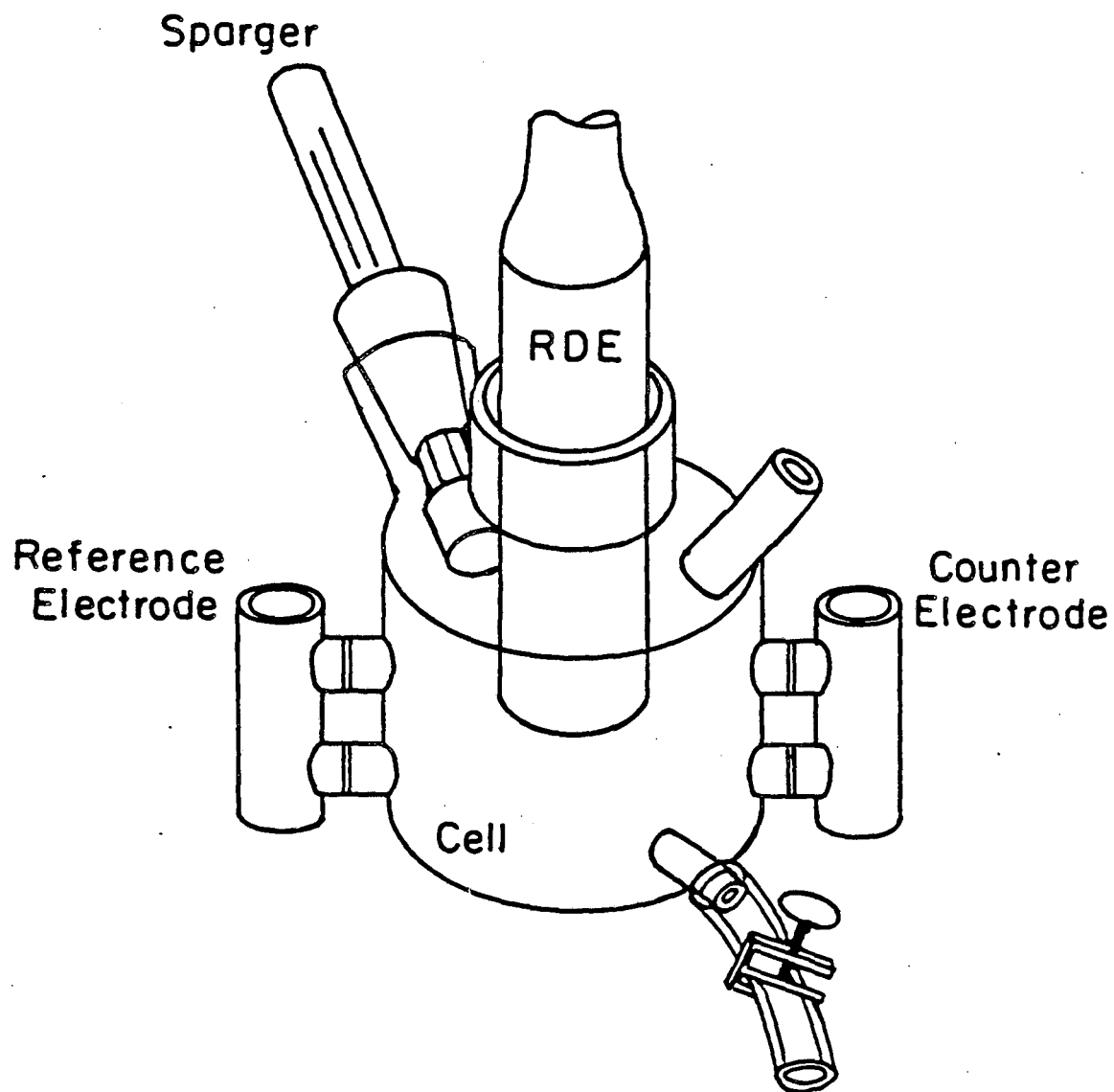
XBL 839-6452A

Figure 7-2. Schematic diagram of the experimental apparatus.

absence of H_2 evolution. Preliminary experiments with a platinum disk electrode gave a larger current response, in a given potential range, than those with the gold and glassy carbon electrodes. This is presumably due to the hydrogen-evolution reaction on the platinum electrode.

The potential between the the disk electrode and the reference electrode was controlled with a Stonehart model BC1200 potentiostat. For some experiments the potential was ramped at a constant rate with a Princeton Applied Research model 175 universal programmer. A Hewlett-Packard, model 7047A analog X-Y recorder and a Nicolet model 206 digital oscilloscope were used to record data.

7.2.1. Electrode Pretreatment

Before an experiment the disk electrode was polished three times with a Buehler Economet III grinder/polisher, first with 9-micron, followed by 3-micron and 1-micron diamond paste. The electrode was dipped for approximately 10 seconds in three solutions: 70% HNO_3, CCl_4, and 70 % HNO_3. After dipping in each solution, the electrode was rinsed with purified water. (After testing several solvents, we found that CCl_4 removed the polishing paste most effectively.) The electrode was then cycled at 1 V/s in a 1 M HNO_3 solution. After the electrode was cycled, it was rinsed and placed in the experimental cell.

In order to obtain reproducible results the electrode had to be dipped after each experimental run, and polished after no more than two experimental runs.

7.2.2. Solution Preparation

The electrolyte solution was prepared with nickel nitrate reagent, nitric acid, and purified water. The nickelous nitrate 6-hydrate reagent and nitric acid solution were obtained from the J.T. Baker Chemical Company. The water was purified using a SYBRON/Barnstead NANOpure distilling apparatus with

charcoal filters. The solution was de-aerated for at least two hours before each experiment with high-purity nitrogen. The solution was continuously sparged in the experimental cell. All experiments were carried out at room temperature.

Reproducible results were obtained if the solution was discarded after each experimental run. Experimental results with the 300 ml volume cell were essentially identical with the results of a 500 ml volume cell at the same conditions.

7.2.3. Characterizing the Acidity of Nickel Nitrate Solutions

The acidity of a solution may be characterized in several ways. Zhdanov et al.[51] use the potentiometric method to measure the hydrogen ion concentration in various nickel nitrate solutions. Most researchers of the nickel nitrate system characterize the acidity of their solutions by giving the electrometric pH measurement. This method is most useful when a measurement of the relative acidity is important. For a given nickel nitrate concentration, a pH measurement at various concentrations of nitric acid gives a good indication of the solution's acidity. However, one may be misled by using a pH measurement to compare the acidity of two solutions with very different concentrations of nickel nitrate.

One of the problems with using the pH measurement in concentrated nickel nitrate solutions is the time required for a measurement. In our experiments, for example, a 2.56 M $Ni(NO_3)_2$, 0.006 M HNO_3 solution gives a stable pH measurement (independent of stirring and time) after approximately one hour. The time required for a stable reading is smaller for less concentrated nickel nitrate solutions. Figure 7-3 gives a plot of the electrometric pH measurement as a function of the logarithm of the nitric acid concentration for various concentrations of nickel nitrate.
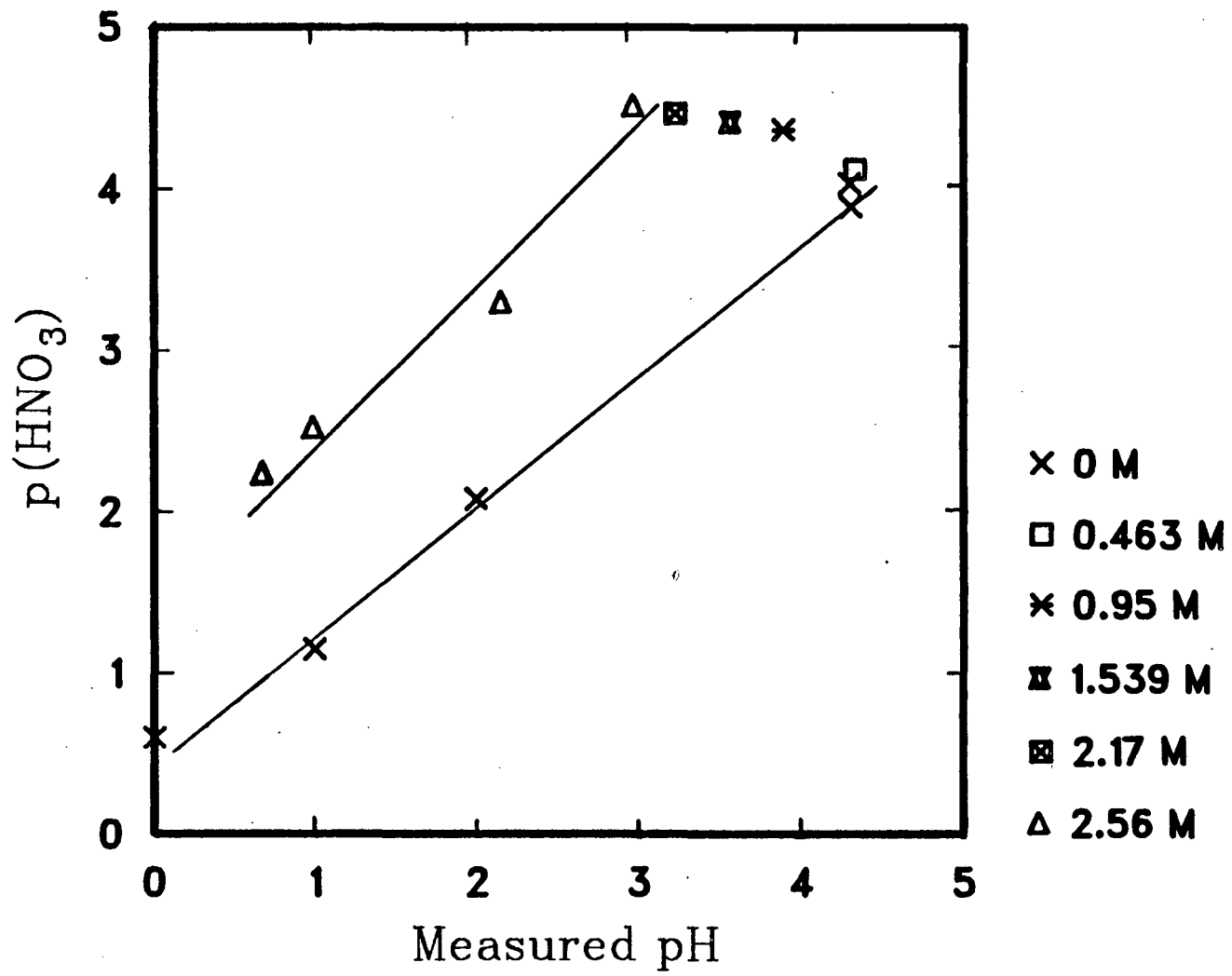
Figure 7-3. Electrometric pH measurement as a function of the logarithm of the molar nitric acid concentration at various concentrations of $Ni(NO_3)_2$.

The acidity of a nickel nitrate solution can also be characterized by speci‐
fying the quantity of acid that is added to the solution. This method is espe‐
cially useful in acidic, nickel nitrate solutions because of the absence of nickel
hydrolysis products. The hydrolysis products of nickel, however, are stable in
neutral and basic solutions.[52]

7.3. Experimental Results

The cathodic behavior of acidic, nickel nitrate solutions was investigated
with potential-sweep and potential-step experiments. Figure 7-4 gives the
current response to a slow potentiostatic sweep (1 mV/s). Two regions of
behavior can be distinguished. In the direction of decreasing potential, a max‐
imum is seen in the current response between -0.2 and -0.5 V versus SCE. Fig‐
ure 7-5 (1 mV/s) shows the behavior in this region more clearly. This chapter
focuses on the behavior of the system in this potential range. The sweep rate is
slow enough (1 mV/s) that the diffusion layers are well developed. For example,
in Figure 6-10 (800 rpm) a steady-state diffusion layer thickness is obtained
within 1 second at a current of -0.195 mA/cm^2, and the surface concentration of
hydrogen ion is 0.0059 M. We can estimate the surface concentration of hydro‐
gen ion for the currents in Figure 7-5, and the solution adjacent to the elec‐
trode is not sufficiently alkaline to cause the precipitation of $Ni(OH)_2$ (or other
basic nickel salts). As we mentioned in the previous section, Zhdanov *et al.*[55]
(Figure 7-1) also observe a current maximum in this type of experiment, and
their data contain a similar hysteresis effect; potential scans in the forward and
reverse directions do not coincide (except in the Tafel region shown in Figure
6-2). We believe that the behavior exhibited in Figure 7-5 reflects the kinetics of
the nitrate-ion-reduction mechanism.

For cathodic currents greater than about 5 mA/cm^2, the solution adjacent
to the electrode is alkaline enough for hydroxide precipitation. A second

Figure 7-4. Current density as a function of applied potential in a potential-sweep experiment with a glassy carbon, rotating disk electrode (800 rpm, 1 mV/s, 2.56 M Ni(NO$_3$)$_2$, 0.006 M HNO$_3$).

Figure 7-5. Cathodic current density as a function of applied potential in a potential-sweep experiment with a glassy carbon, rotating disk electrode for two different sweep rates (conditions as in Figure 7-4 except the sweep rate).

region, at potentials more negative than -0.6 V versus SCE, is distinguished by the fluctuating current behavior. The behavior in this region is discussed in Chapter 6. The fluctuating current response is probably indicative of the formation of a $Ni(OH)_2$ precipitate on the electrode surface. At approximately -0.8 V versus SCE during the sweep to more negative potentials, the solution in the vicinity of the electrode appears cloudy. For potentials more negative than -1.2 V versus SCE, a film is visible on the electrode surface.

The effects of acid concentration and nickel nitrate concentration on the current response in potential-sweep experiments are discussed in the next section. The current response to a potential step at various electrolyte compositions is given in Section 7.3.1.

7.3.1. Potential Sweep Experiments

As mentioned in the previous section, two regions of behavior can be distinguished in Figure 7-4. The behavior in the first region, shown in Figure 7-5 (1 mV/s), is the subject of this section. First, however, we will discuss the transition from this region to the region with the fluctuating current response. At a potential of approximately -0.7 V versus SCE, the cathodic current rises rapidly to 5.5 mA/cm^2. The current fluctuates and increases more slowly for potentials less than -0.7 V versus SCE. In this second region, the concentration of hydrogen ion at the electrode surface is low enough for $Ni(OH)_2$ precipitation. An increase in the bulk acid concentration should increase the current at which this transition in behavior occurs. The transition occurs at -5.5 mA/cm^2 in 0.006 M HNO$_3$ (Figure 7-4). The transition occurs at -17 mA/cm^2 when the bulk concentration of HNO$_3$ is increased to 0.025 M. If we assume Levich behavior (the limiting current being proportional to the bulk hydrogen ion concentration), we predict the transition to occur at -22 mA/cm^2 in 0.025 M HNO$_3$.

Zhdanov *et al.*[51] investigate the current response with a nickel rotating-disk electrode for various concentrations of Ni(NO$_3$)$_2$ and a bulk pH of 1.0. They describe their results as limiting-current behavior. Their limiting current is observed to be linearly dependent on the square root of the disk's rotation rate for a given concentration of Ni(NO$_3$)$_2$. The diffusion coefficient of hydrogen ion in 2.5 M Ni(NO$_3$)$_2$ is calculated to be 3.0 × 10^{-5} cm^2/s. If we assume that the limiting current corresponds to our transition current, we calculate the hydrogen-ion diffusion coefficient to be 5.2 × 10^{-5} cm^2/s and 3.1 × 10^{-5} cm^2/s for the 0.006 and 0.025 M HNO$_3$ (2.56 M Ni(NO$_3$)$_2$). The discrepancy in the value of the diffusion coefficient in 0.006 M HNO$_3$ may be due to differences in the estimation of the bulk concentration of HNO$_3$ or the concentration dependence of the diffusion coefficient. We assumed that the hydrogen ion concentration was given by the amount of nitric acid added to the solution. However, the formation of nickel hydrolysis products may result in a higher hydrogen ion concentration than expected. Hydrolysis is most significant at lower acid concentrations. Zhdanov *et al.* obtained the bulk concentration of hydrogen ion by the potentiometric method.

All of the experimental results given in this chapter were obtained with a glassy carbon disk electrode. We have, however, performed experiments with a gold disk electrode and observed behavior that is similar to the results obtained with the glassy carbon electrode; a maximum in the current is seen at approximately -0.4 V versus SCE with a gold electrode.

The effect of changing the acid concentration on the current response in a potential-sweep experiment is shown in Figure 7-6. Increasing the acid concentration, relative to the case depicted in Figure 7-5 (1 mV/s), causes an increase in the current maximum. It is interesting that Zhdanov *et al.*[55] do not observe the current response to be dependent on the solution's acidity for pH = 0.8 to 1.7 in potential range of -0.25 to -0.35 V versus SCE (0.5 M Ni(NO$_3$)$_2$, 1 M NiSO$_4$).
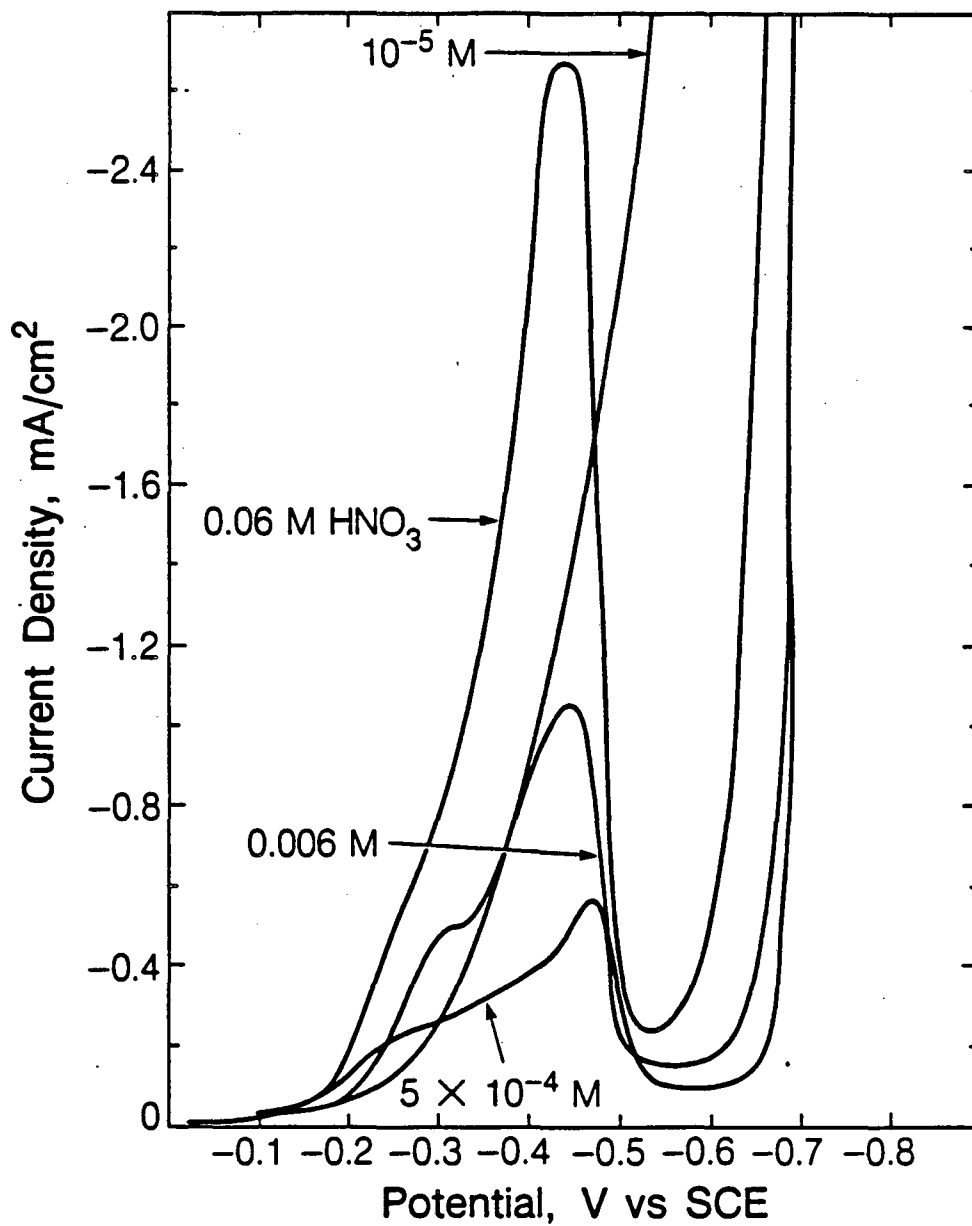
Figure 7-6. Cathodic current density as a function of applied potential in a potential-sweep experiment with a glassy carbon, rotating disk electrode for various concentrations of HNO_3 and 2.56 M $Ni(NO_3)_2$ (800 rpm, 1 mV/s).

XBL 861-9401

The researchers observe a first-order dependency on the $Ni(NO_3)_2$ concentration in this potential range (Figure 6-2).

A decrease in the acid concentration to 5×10^{-4} M HNO_3 from the case of Figure 7-5 yields a decrease in the maximum current; lowering the acid concentration further to 3×10^{-5} M HNO_3 eliminates the current maximum. We may suspect that the conditions for $Ni(OH)_2$ precipitation prevail in the solution adjacent to the disk electrode for the case with the lowest acid concentration (3×10^{-5} M HNO_3). In Chapter 6, a mathematical model predicted precipitation conditions to exist at similar conditions: 2.56 M $Ni(NO_3)_2$, 4.7×10^{-5} M HNO_3, -0.07 mA/cm^2, and 500 rpm. The model predicts that precipitation conditions are met for cathodic currents larger than 0.07 mA/cm^2 in the experiment.

As shown in Figure 7-4, a current maximum is not observed in the direction of increasing potential. A maximum in the current response in the direction of increasing potential is observed with higher bulk acid concentrations. For solutions of 0.025 M HNO_3, 2.56 M $Ni(NO_3)_2$ and 0.06 M HNO_3, 0.25 M $Ni(NO_3)_2$, a maximum in the direction of increasing potential is observed at approximately the same potential as the maximum in the scan in the other direction. The current maximum is approximately ten times larger than the maximum in the direction of decreasing potential.

Figure 7-7 shows the effect of decreasing the nickel nitrate concentration on the current response in a potential-sweep experiment. The effect of increasing the rate of the potential sweep is illustrated in Figure 7-5. This effect is interesting and may be contrasted to cyclic voltammetry experiments, which typically use much larger sweep rates (> 100 mV/s). Current maxima are often seen in cyclic voltammetry because of mass-transfer limitations, and in contrast to this work, the maxima are increased by increasing the potential sweep rate.[60]
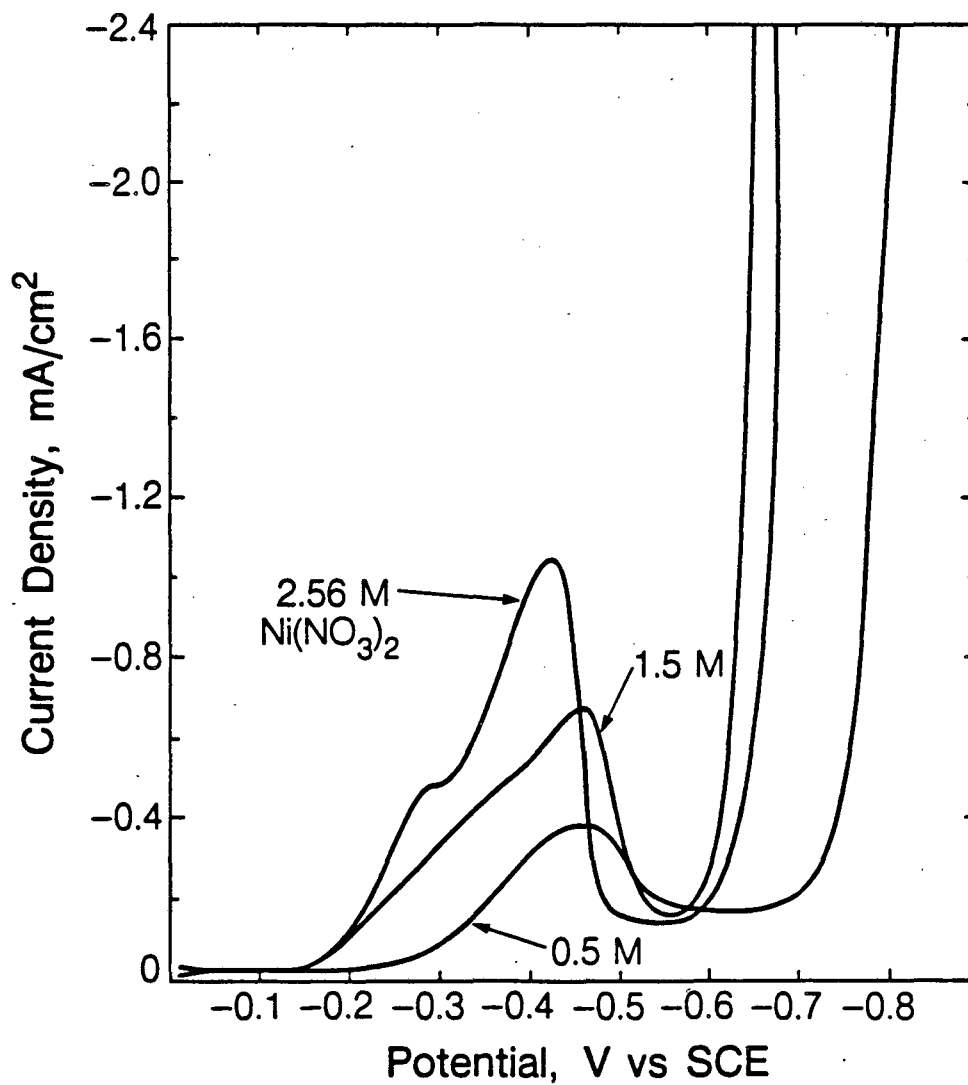
Figure 7-7. Cathodic current density as a function of applied potential in a potential-sweep experiment with a glassy carbon, rotating disk electrode for various concentrations of Ni $(NO_3)_2$ and 0.006 M HNO_3 (800 rpm, 1 mV/s).

Some mass-transfer resistance is present at these conditions, as shown in Figure 7-8. Higher rotation rates yield slightly higher current densities.

As we mentioned in Section 7.2.2, reproducible results were obtained if the solution was discarded after each experimental run. Figure 7-9 compares the results that are obtained with a clean solution to those which are obtained after the third use of the solution in an experiment. In general, the cathodic currents are higher for the more used solutions. This may be evidence for the production of reducible, intermediate products in the nitrate ion reduction sequence for these operating conditions.

We estimate that a very slow sweep rate (< 0.001 mV/s) would be required in order to obtain steady, potential sweep behavior. Since irreproducible results are obtained in "old solutions," we decided to collect the steady-state results of several potential-step experiments. Figure 7-10 compares the current response in a potential-sweep experiment to steady-state current responses of five potential-step experiments. It should be noted that the steady state currents in the potential-step experiments were not obtained until more than 800 seconds. It is interesting that current maxima are also obtained in the potential-step experiments. In Section 7.4.1, we propose a mechanism in order to explain the results of our potential-step experiments. A simple adsorption model is formulated from this mechanism, and in Section 7.4.2 we compare our experimental results with theory based on the adsorption model. The results of our potential-step experiments are given in the next section. The potential-step experiments are easier to quantify than the potential-sweep experiments because one does not have to address a transient potential source.

7.3.2. Potential-Step Experiments

Figure 7-11 (2.56 M Ni$(NO_3)_2$) gives the results of two potential-step experiments. The potential was stepped to -0.35 V versus SCE at initial time. The result is reproducible if the solution is fresh and the electrode is polished.
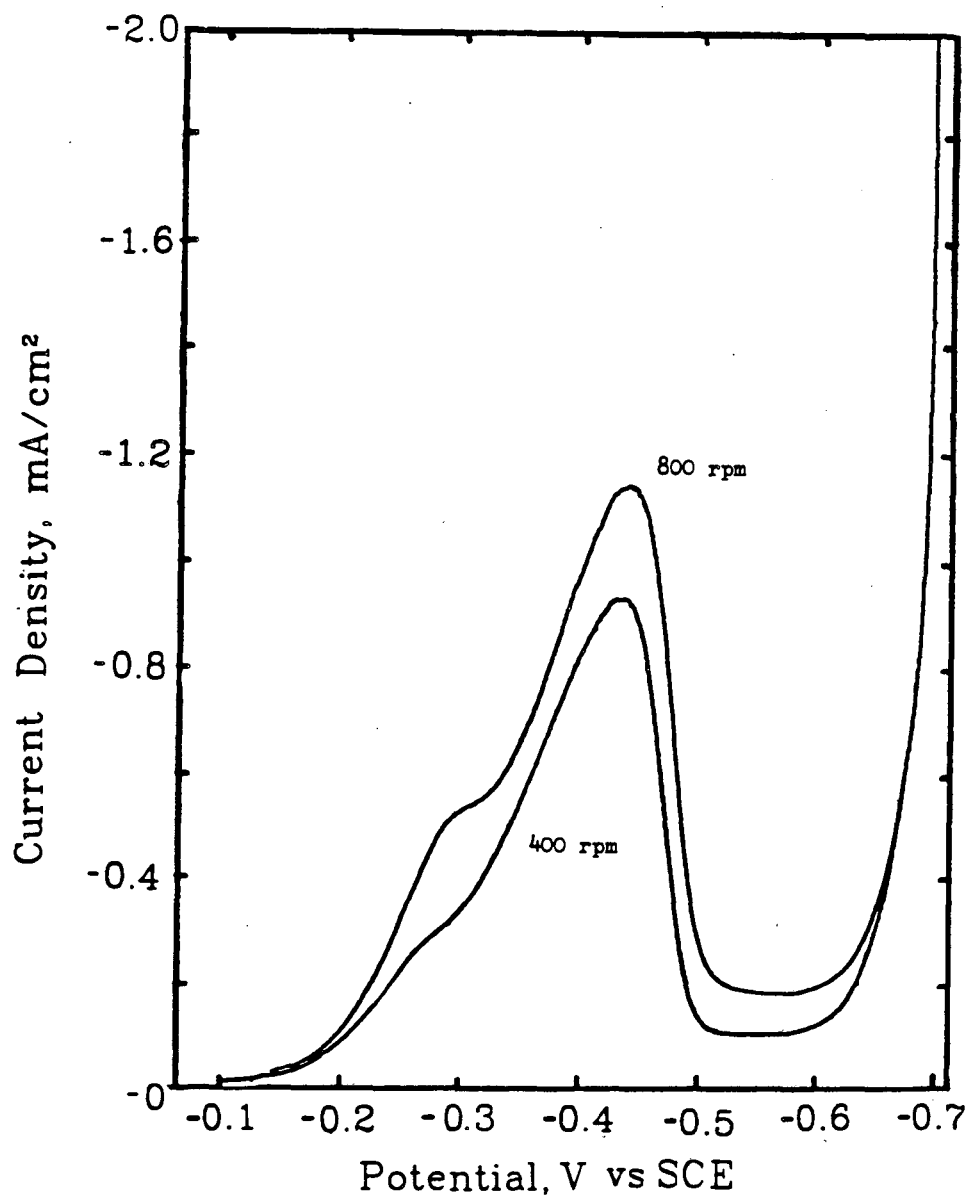
Figure 7-8. Cathodic current density as a function of applied potential in a potential-sweep experiment with a glassy carbon, rotating disk electrode for two different rotation speeds (conditions as in Figure 7-4 except the rotation rate).
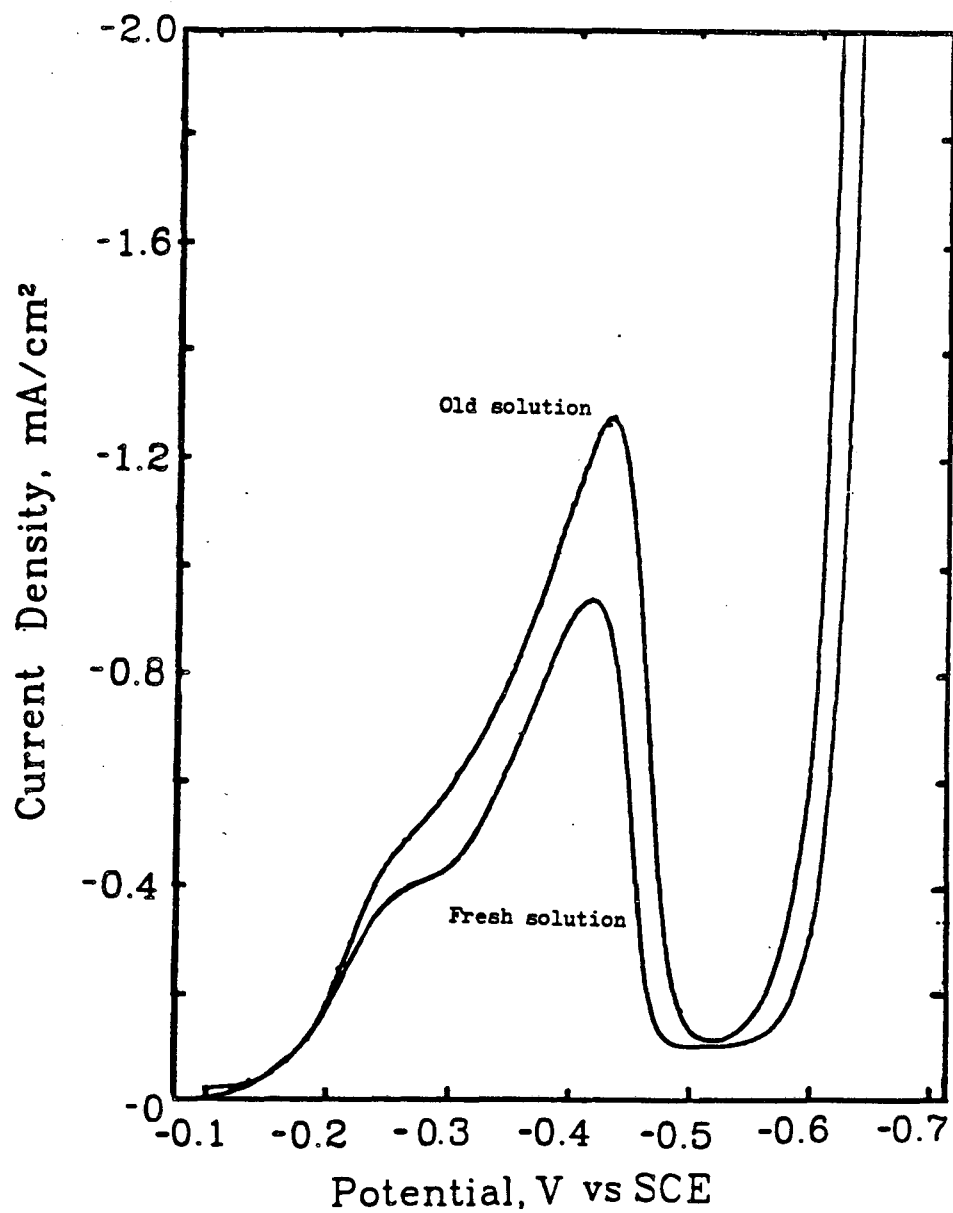
Figure 7-9. Cathodic current density as a function of applied potential in a potential-sweep experiment with a glassy carbon, electrode with fresh electrolyte and old electrolyte (Conditions as in Figure 7-4 except that the disk rotation rate was 600 rpm).
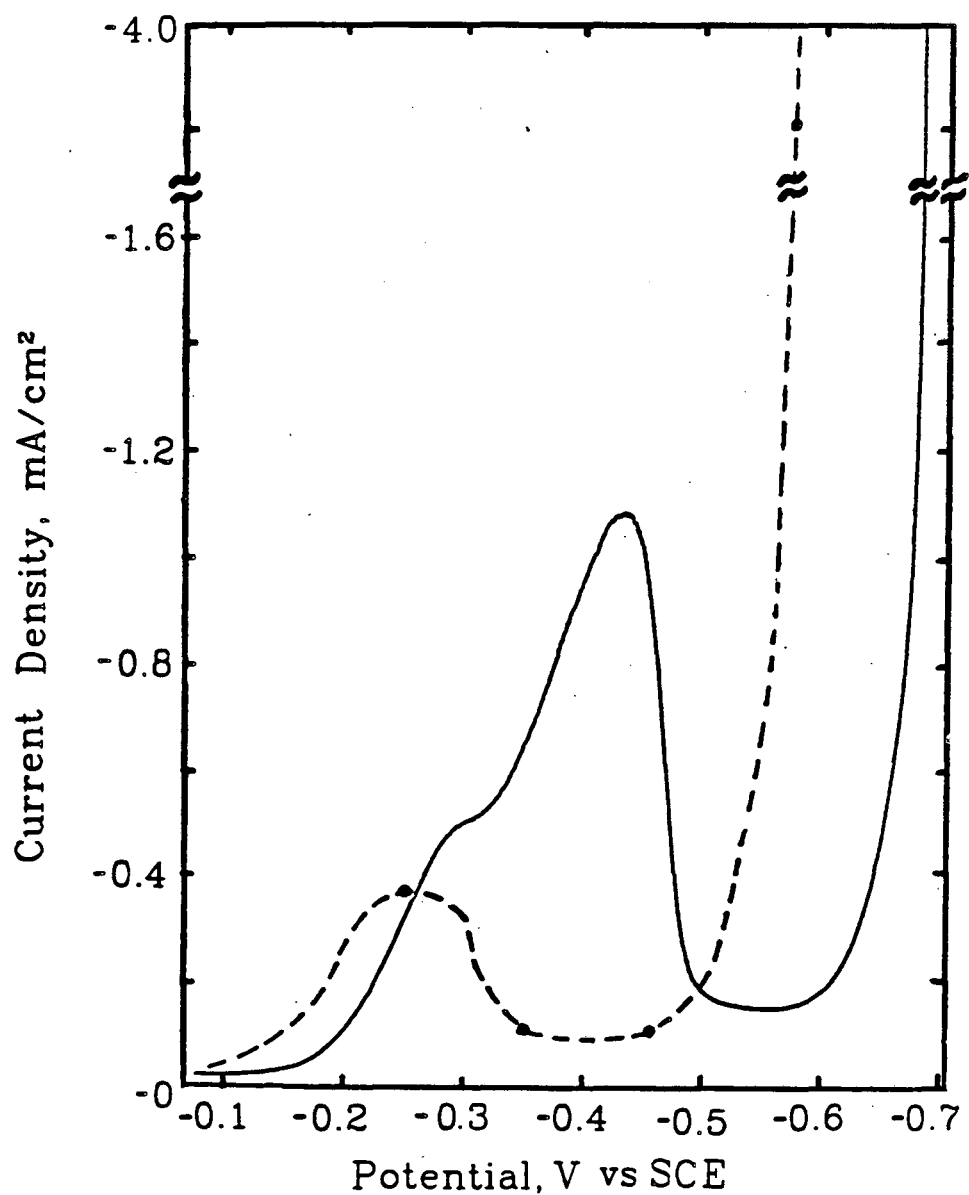
Figure 7-10. Cathodic current density as a function of applied potential in a potential-sweep experiment (solid line) and in five potential-step experiments (dashed line) at the same conditions as in Figure 7-4.
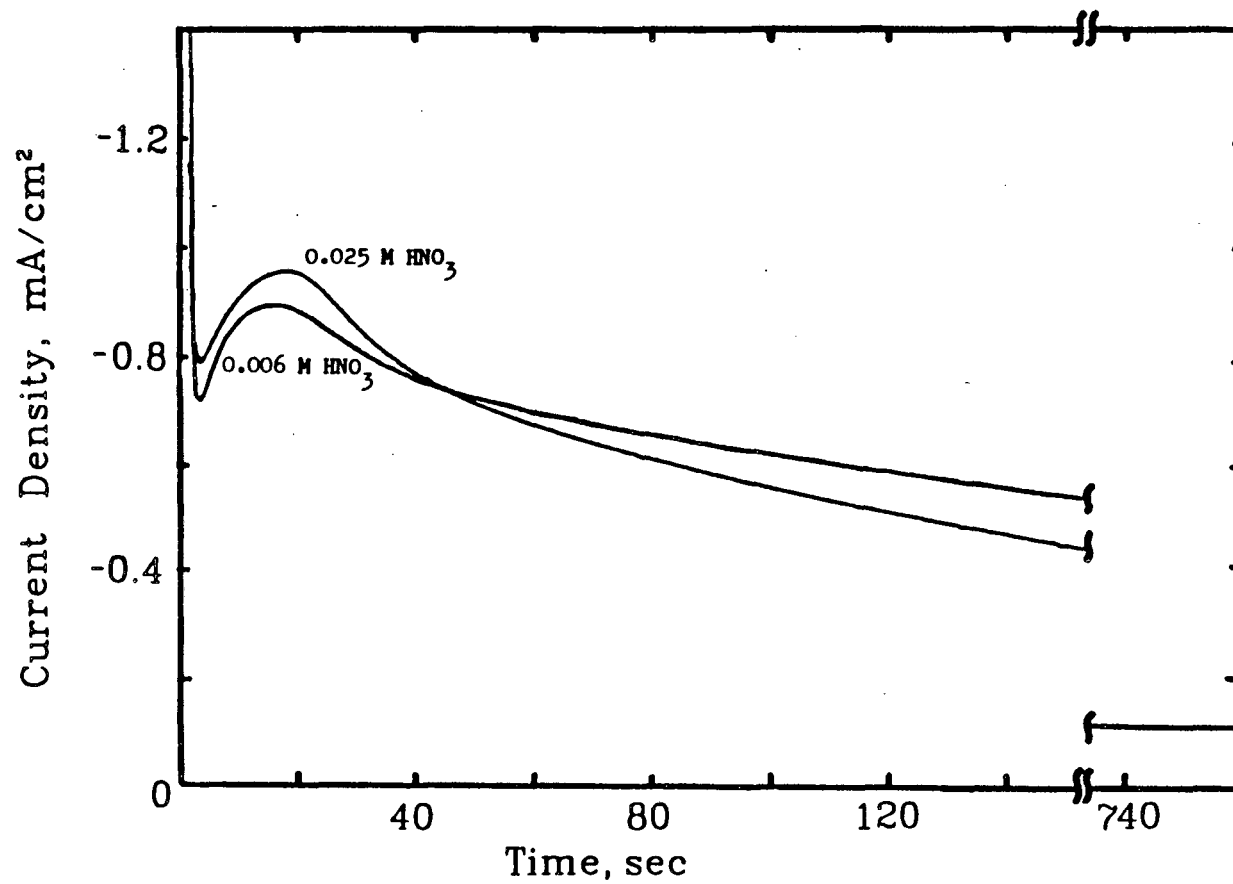
Figure 7-11. Cathodic current density as a function of time in a potential-step experiment with a glassy carbon, rotating disk electrode for two concentrations of HNO_3 (800 rpm, -0.35 V versus SCE, 2.56 M $Ni(NO_3)_2$).

After four experiments (each with fresh electrolyte), the result shown in Figure 7-12 is observed if the electrode is not polished. Qualitatively, the same behavior is observed; however, the time scales are shifted. It is interesting that approximately the same steady-state currents are reached. Thus, the transient behavior of the system is dependent on the state of the electrode surface.

The effect of increasing the acid concentration on the current response in a potential-step experiment is shown in Figures 7-11 and 7-13 for 2.56 and 0.25 M $Ni(NO_3)_2$ solutions, respectively. For the 2.56 M $Ni(NO_3)_2$ solution, a steady current response ($\approx$ -0.12 mA/cm^2) is obtained in both cases after approximately 700 seconds. If Figure 7-11 is compared to Figure 7-6, it can be seen that the magnitude of the current maximum in the potential-sweep experiment is much more dependent on the acid concentration than that of the maximum in the potential-step experiment.

The response of the X-Y recorder was not fast enough to record the magnitude of the initial current spike. This was measured with an oscilloscope and was observed to be strongly dependent on the bulk acid concentration. The magnitude of the initial current spike in a potential-step experiment (-0.35 V versus SCE, 2.56 M $Ni(NO_3)_2$, 800 rpm) was 78, 22, and 1 mA/cm^2 for 0.025, 0.006, and 3×10^{-5} M HNO_3, respectively. The magnitude of the spike was not sensitive to the bulk concentration of $Ni(NO_3)_2$. The magnitude of the spike (-0.35 V versus SCE, 0.006 M HNO_3, 800 rpm) was observed to be 16.4 and 22.5 mA/cm^2 for 0.25 and 2.56 M $Ni(NO_3)_2$ solutions, respectively. Section 7.4.1 contains a more quantitative discussion of this result.

The result of a potential-step experiment in a solution of low acid concentration is shown in Figure 6-8. In this case, the solution adjacent to the electrode is alkaline enough to cause precipitation of $Ni(OH)_2$. The average current gives the behavior of the maximum in the current response.
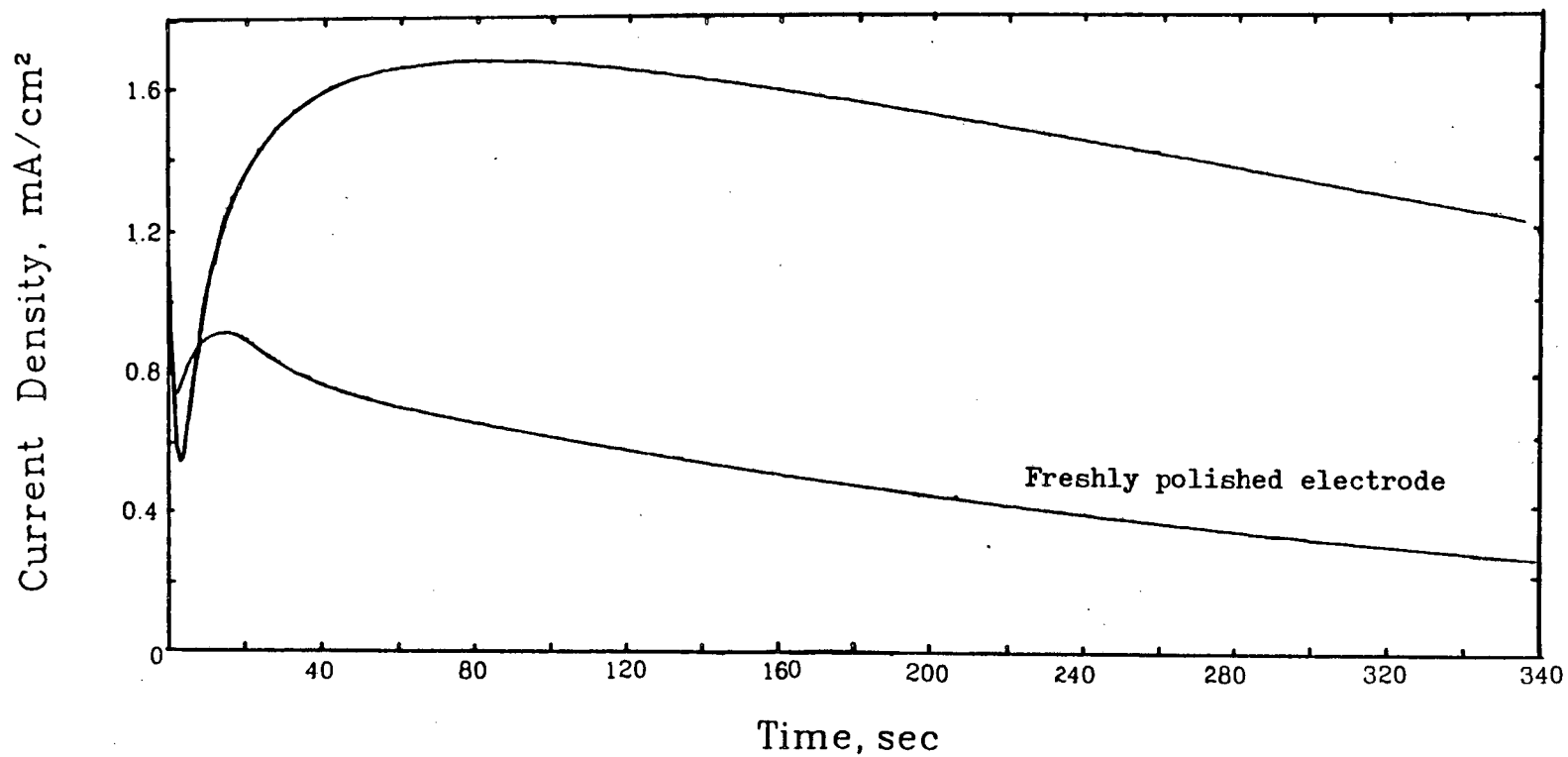
Figure 7-12. Cathodic current density as a function of time in a potential-step experiment with a glassy carbon, rotating disk electrode for a freshly polished electrode and after four experments without polishing (800 rpm, -0.35 V versus SCE, 2.56 M Ni$(NO_3)_2$, 0.006 M HNO_3).
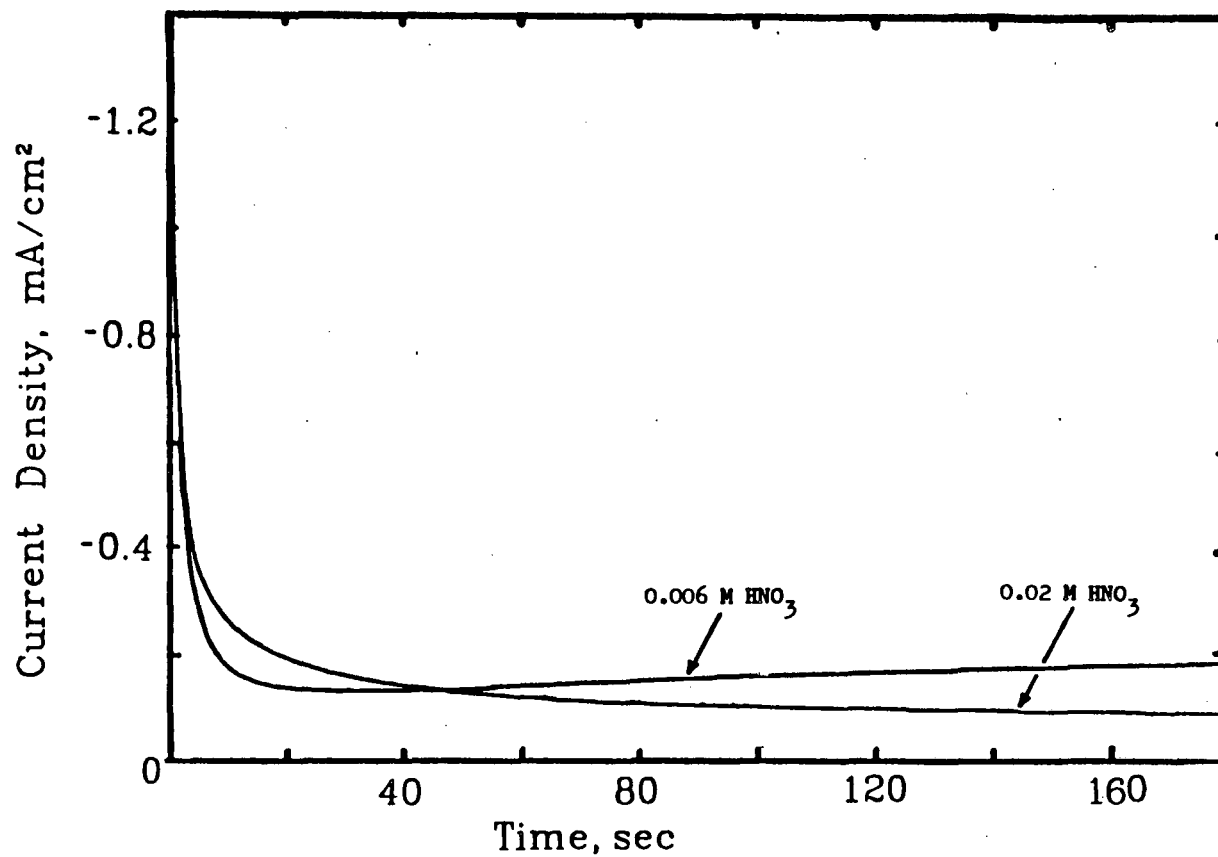
Figure 7-13. Cathodic current density as a function of time in a potential-step experiment with a glassy carbon, rotating disk electrode for two concentrations of HNO_3 (800 rpm, -0.35 V versus SCE, 0.25 M $Ni(NO_3)_2$).

Figure 7-14 shows the effect of decreasing the nickel nitrate concentration on the current response in a potential-step experiment. In Section 7.4.2, a more quantitative explanation is given. It is interesting that decreasing the nickel nitrate concentration by a factor of 10 (from 2.56 M) eliminates the current maximum in a potential-step experiment and decreases the magnitude of the current maximum in the potential-sweep experiment (Figure 7-7).

7.4. Discussion of Results

Zhdanov et al.[55] suggest that the current maximum (Figure 7-1) is associated with the potential of zero charge. That is, the desorption of NO_2^- ion near the potential of zero charge is believed to be responsible for the observed drop in current at approximately -0.4 V versus SCE. Parsons[65] discusses the observation of current maxima for systems in which a non-specifically adsorbed anion is reduced. In Parsons' work, calculations with Frumkin's double-layer theory and experimental results support the conclusion that current maxima associated with non-specifically adsorbed anions near the potential of zero charge should be observed only in very dilute solutions (< 0.1 M). In light of the large concentrations used to study the $Ni(NO_3)_2$ system, we may suspect that the current maxima are not associated with this phenomenon. Parsons, however, gives an example of one case, the reduction of $PtCl_4^{-2}$, in which the current maximum does not vanish at high salt concentrations (1 M KCl). Parsons suggests that strong specific adsorption is responsible for the behavior of the current maximum in this system. Major modifications of simple double-layer theory must be made in order to explain the behavior of reactions occurring in the inner part of the double layer. We have not addressed this, and it should be the subject of further investigations.

We believe that the maxima observed in potential-sweep and potential-step experiments reflect the behavior of the relatively slow nitrate-ion-reduction rate processes. We do not discount the possible effects of strong specific
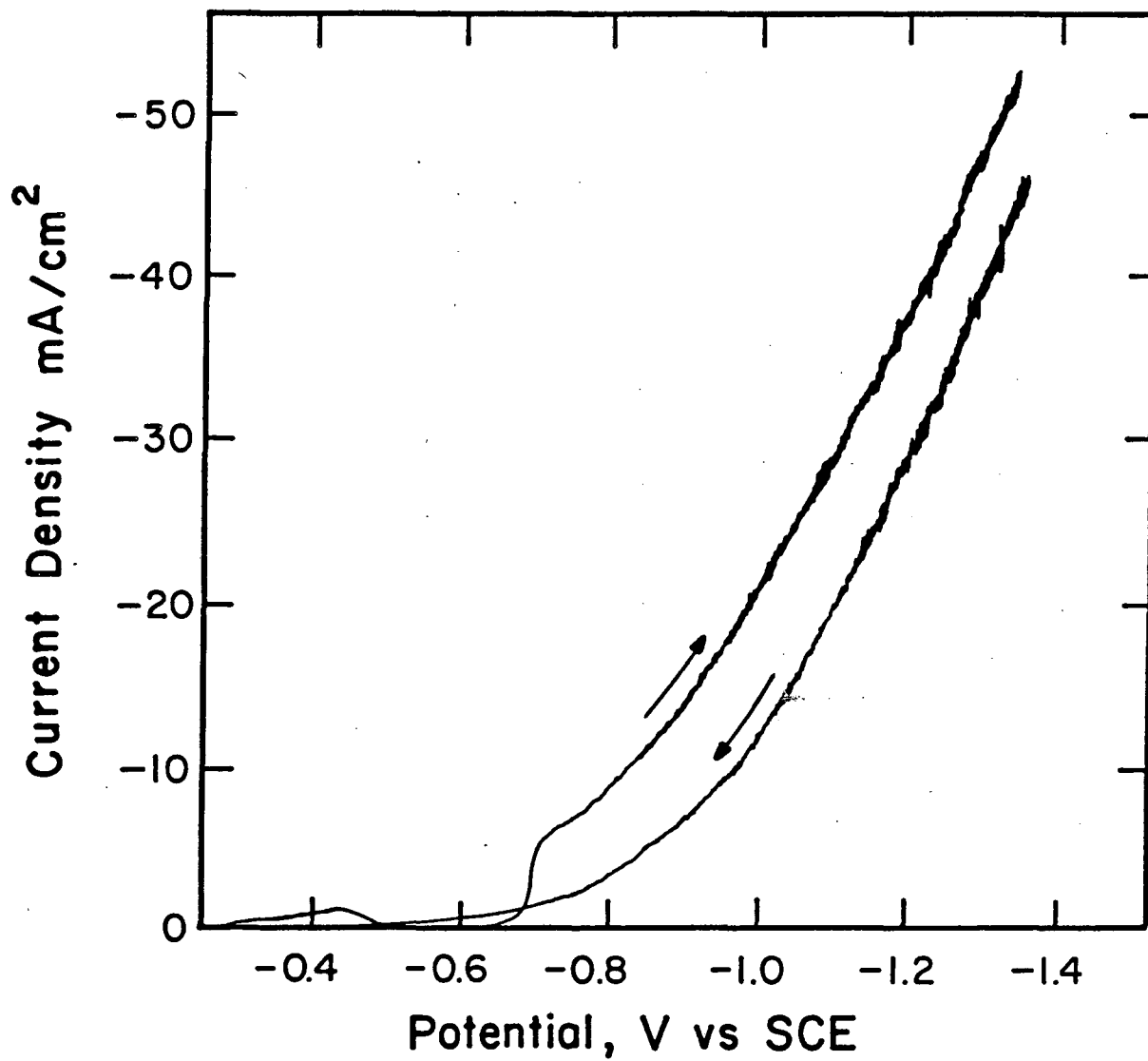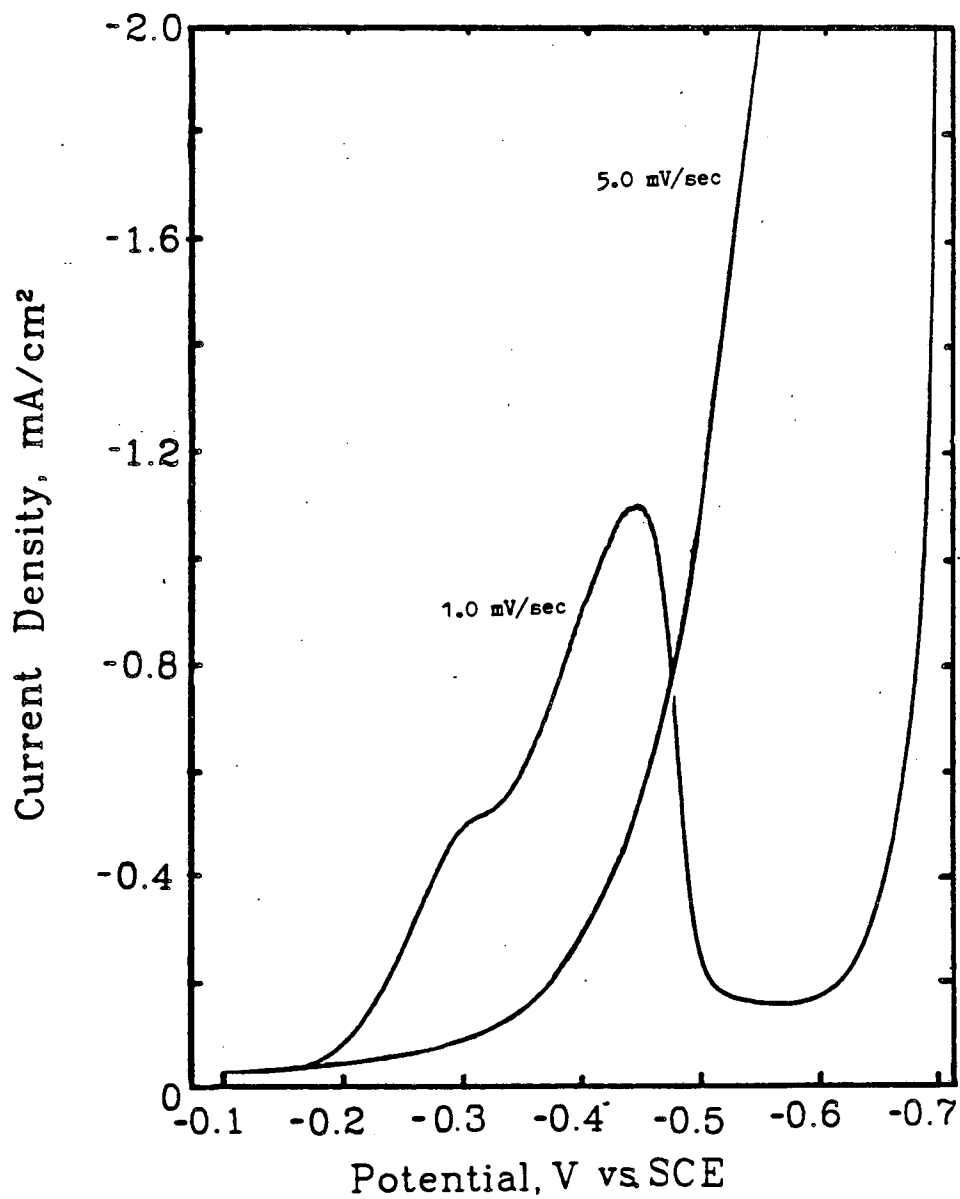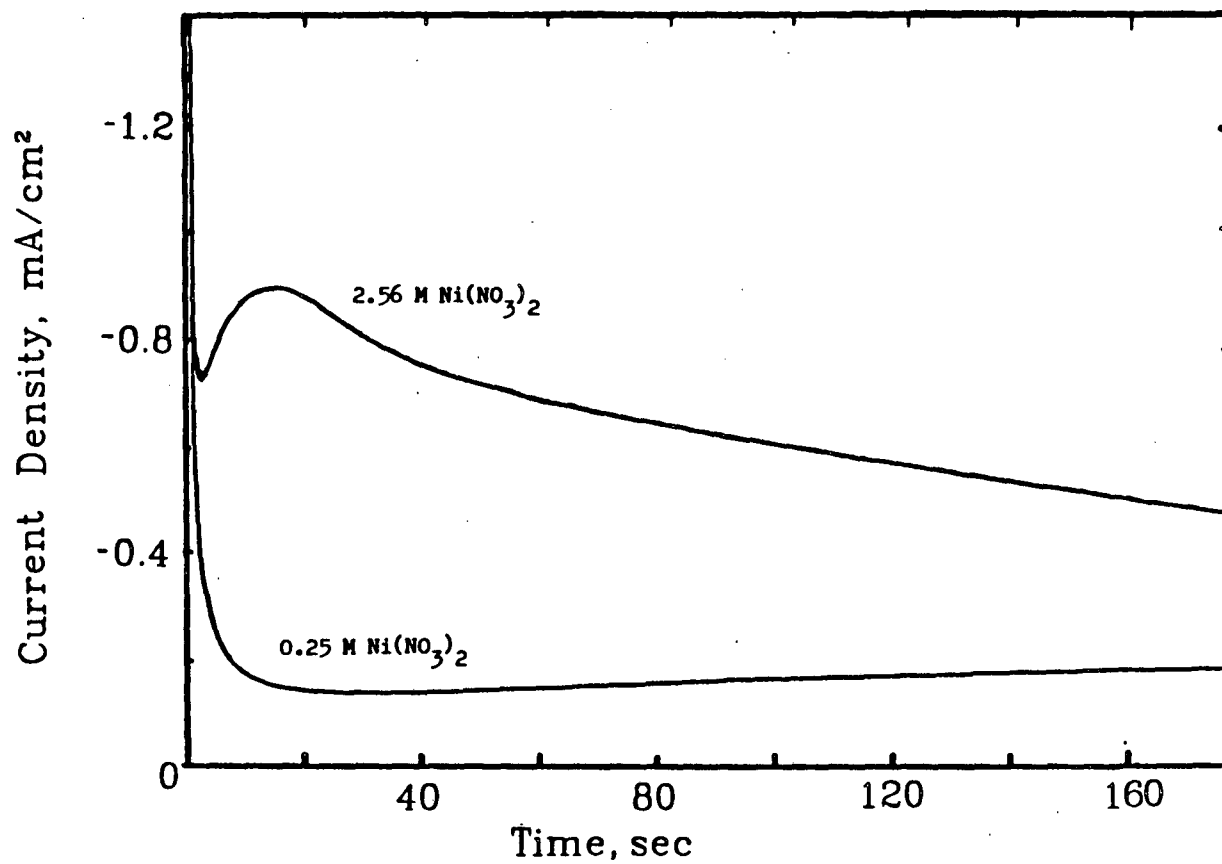
Figure 7-14. Cathodic current density as a function of time in a potential-step experiment with a glassy carbon, rotating disk electrode for two concentrations of $Ni(NO_3)_2$ (800 rpm, -0.35 V versus SCE, 0.006 M HNO_3).

adsorption on the potential in the inner parts of the double-layer; however, we have not included these effects in our calculations. In the next section, we investigate the possible steps in the nitrate-ion-reduction reaction sequence. The electrochemical adsorption of hydrogen ion is discussed in Section 7.4.2. A simple reaction sequence is proposed to explain the experimentally observed effect of decreasing the nitrate ion concentration in potential-step experiments in Section 7.4.3.

7.4.1. Possible Reaction Products and Steps in the Reduction of Nitrate to Nitrite Ion

In order to postulate steps in the nitrate ion reaction sequence, the possible reaction products and adsorption phenomena must be determined. Zhdanov et al.[51] analyze their electrolytic solution after cathodic polarization at -0.3 V versus NHE (pH = 1.0) and find that nitrous acid and ammonia are the only reaction products. Hydrogen evolution and nickel deposition do not occur at these conditions. In 2 M $Ni(NO_3)_2$ solution, the current efficiency for the production of nitrous acid is 74%, and in 0.5 M $Ni(NO_3)_2$ solution, the current efficiency for the production of ammonia is close to 100% (-0.3 V versus NHE). MacArthur[47] measures the amount of $Ni(OH)_2$ produced for a measured amount of coulombs passed and suggests that hydroxylamine may also be a reaction product.

In other work on this system, Zhdanov and Tikhonov[66,67] investigate the adsorption of NO_2^- on nickel and discuss the work of other researchers on the adsorption of NO_3^- and NO_2^- on platinum.

Most researchers cite the importance of electrochemically adsorbed hydrogen in the reduction of nitrate ion. The electrochemical adsorption of hydrogen is relatively well studied because it is an elementary step in the hydrogen evolution reaction on gold and nickel (the slow step is the reaction of

$H^{\bullet}$ with H^+ and an electron to form H_2). In summary, the electrochemical reduction of nitrate ion involves a series of steps involving adsorbed hydrogen and reaction products (NO_2^-, NH_2OH, NH_4^+). For example, the reduction of nitrate ion to nitrous acid may involve the following elementary steps:

$$H^+ + S + e^- \rightarrow H^{\bullet}$$

$$NO_3^- + S \rightarrow NO_3^{-\bullet}$$

$$NO_3^{-\bullet} + H^{\bullet} + e^- \rightarrow NO_2^{-\bullet} + OH^- + S$$

$$NO_2^{-\bullet} \rightarrow NO_2^- + S$$

$$H^+ + OH^- \rightarrow H_2O$$

$$H^+ + NO_2^- \rightarrow HNO_2$$
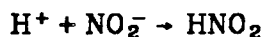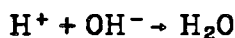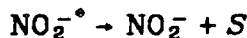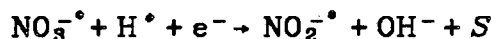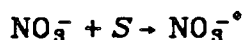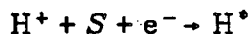
The superscript $^{\bullet}$ refers to an adsorbed species, and S refers to an adsorption site. Hence, the first four elementary steps are interfacial reactions, and the fifth and sixth steps are homogeneous reactions. In Section 7.4.3, we approximate the above mechanism by two reactions (7-1 and 7-2).

7.4.2. The Effect of the Hydrogen Ion Concentration

The bulk acid concentration is observed to influence the magnitude of the initial current spike and to have a small effect on the value of the steady current in a potential-step experiment. If the current spike is observed with an oscilloscope, the tip of the spike is obtained almost instantaneously. The current then decreases from this value over approximately 0.5 seconds. We shall assume that the primary electrochemical process at the start of a potential-step experiment is first order in hydrogen ion.

$$i = nF k_H c_{H^+}$$

With this assumption, is is expected that the magnitude of the initial current

spike is proportional to the bulk acid concentration (at constant potential). As discussed in Section 7.3.2, the magnitude of the current spike is approximately proportional to the acid concentration and less sensitive to the $Ni(NO_3)_2$ concentration. The slight dependency on the $Ni(NO_3)_2$ concentration may indicate that the initial current response includes some contribution from the reduction of nitrate ions.

If the electrochemical reaction of hydrogen ion involves the adsorbed species $H^\bullet$,

$$H^+ + S + e^- \rightarrow H^\bullet,$$
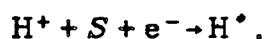
then the decrease in the current may in part be due to the decrease in area available for adsorption. (The current decrease can also be related to the concentration overpotential for the above reaction.)

We may write

$$i = nF k_H c_{H^+}^{sur} (\Gamma_{tot} - \Gamma_{H^\bullet}),$$

to represent the initial current response.

The steady-state current response is observed to be independent of the hydrogen ion concentration. This indicates that the kinetics of the electrochemical reaction involving the hydrogen ion are rapid, relative to the other steps in the reaction sequence. At steady-state, the overall reaction rate is determined by the slow steps in the sequence. In the next section, we examine three important portions of the nitrate-ion-reduction reaction sequence in order to try to explain our experimental results.

7.4.3. A Simple Adsorption Model

A possible explanation for the initial current spike, which occurs within the first few seconds in a potential-step experiment, is given in Section 7.4.2. In this section, a mechanism is proposed for the behavior after the current spike.

A steady-state current response is typically obtained after several hundred seconds, indicating that the system time constants are in the range of 100 to 1000 seconds.

Equations 7-1 through 7-3 are the proposed sequence of reactions.

$$NO_3^- + S \rightarrow NO_3^{-\bullet} \tag{7-1}$$

$$NO_3^{-\bullet} + 3\,H^+ + 2\,e^- \rightarrow HNO_2^\bullet + H_2O \tag{7-2}$$

$$HNO_2^\bullet + 7\,H^+ + 6\,e^- \rightarrow NH_4^+ + 2\,H_2O + S \tag{7-3}$$
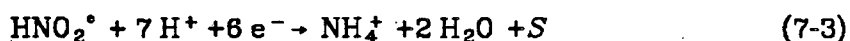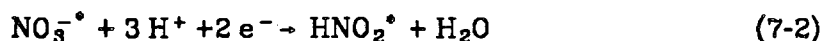
Reactions 2 and 3 are not proposed as elementary steps in the sequence, rather, they are each an overall reaction comprised of a series of elementary steps involving electrochemically adsorbed hydrogen. For example, reactions 1 and 2 represent the simplified mechanism that we propose to capture the salient features of the more detailed reaction sequence outlined in Section 7.4.1. It is assumed that the electrochemical adsorption of hydrogen (Section 7.4.2) is very rapid relative to the reactions in the above sequence and, a constant amount of adsorbed hydrogen Γ_H, is present on the surface of the electrode. The first reaction, the adsorption of nitrate ion, is simple enough to be considered an elementary step. The adsorbed nitrate ions react with hydrogen ions and electrons to form an intermediate species $HNO_2^\bullet$ and water in second reaction. The intermediate reacts with hydrogen ions and electrons to produce NH_4^+ and water in the third reaction.

It is assumed that the second and third reactions are pseudo-first order in the adsorbed nitrate and nitrous acid species. We assume that the concentration of nitrate ion and hydrogen ion near the electrode surface is equal to the bulk concentration of these species. This is not a bad approximation for relatively low current densities and high bulk concentrations. For example, in Chapter 6 we calculate the surface concentration of H^+ and NO_3^- at a current density of -0.195 mA/cm^2, 0.006 M bulk HNO_3, and 2.56 M bulk $Ni(NO_3)_2$, to be

0.0059 M and 5.12 M, respectively.

With the pseudo-first order approximation, we can write the current density expressions,

$$i_2 = -2 \, F \, k_2 \, \Gamma_{NO_3^-\bullet} \tag{7-4}$$

and

$$i_3 = -6 \, F \, k_3 \, \Gamma_{HNO_2^\circ} . \tag{7-5}$$

Material balance equations for the adsorbed nitrate and nitrous acid species are expressed as:

$$\frac{d\Gamma_{NO_3^-\bullet}}{dt} = c_{NO_3^-} k_1 \left(\Gamma_{tot} - \Gamma_{NO_3^-\bullet} - \Gamma_{HNO_2^\circ} - \Gamma_{H\bullet} \right) - k_2 \, \Gamma_{NO_3^-\bullet} \tag{7-6}$$

and

$$\frac{d\Gamma_{HNO_2^\circ}}{dt} = k_2 \Gamma_{NO_3^-\bullet} - k_3 \, \Gamma_{HNO_2^\circ} . \tag{7-7}$$

We define

$$k_1' = k_1 \, c_{NO_3^-} . \tag{7-8}$$

for notational convenience. The quantity Γ_{tot} characterizes the moles of adsorption sites available per unit area of electrode surface. Equations 7-6 and 7-7 are coupled linear differential equations, and simple analytic solutions for $\Gamma_{NO_3^-\bullet}$ and $\Gamma_{HNO_2^\circ}$ can be obtained:

$$\Gamma_{NO_3^-\bullet} = \frac{1}{\tau_+ - \tau_-} \left[\Gamma^o_{NO_3^-\bullet} + \frac{\Gamma^\infty_{NO_3^-\bullet}}{k_3} \tau_- \right] (\tau_+ + k_3) \, e^{\tau_+ t} -$$

$$\frac{1}{\tau_+ - \tau_-} \left[\Gamma^o_{NO_3^-\bullet} + \frac{\Gamma^\infty_{NO_3^-\bullet}}{k_3} \tau_+ \right] (\tau_- + k_3) e^{\tau_- t} + \frac{k_1' k_3 \left(\Gamma_{tot} - \Gamma_{H\bullet} \right)}{k_1' k_2 + k_2 k_3 + k_1' k_3} \tag{7-9}$$

$$\Gamma_{HNO_2^\bullet} = \frac{k_2}{\tau_+ - \tau_-}\left[\Gamma_{NO_3^-\bullet}^o + \frac{\Gamma_{NO_3^-\bullet}^\infty}{k_3}\tau_-\right]e^{\tau_+ t} -$$

$$\frac{k_2}{\tau_+ - \tau_-}\left[\Gamma_{NO_3^-\bullet}^o + \frac{\Gamma_{NO_3^-\bullet}^\infty}{k_3}\tau_+\right]e^{\tau_- t} + \frac{k_1' k_2 (\Gamma_{tot} - \Gamma_{H^\bullet})}{k_1' k_2 + k_2 k_3 + k_1' k_3}. \quad (7\text{-}10)$$

The solutions incorporate the initial conditions: $\Gamma_{HNO_2^\bullet}^o = 0$, and $\Gamma_{NO_3^-\bullet}^o$ and Γ_{tot} are specified. The constant $\Gamma_{NO_3^-\bullet}^\infty$ is given by the last term in Equation 7-9. (The terms with exponentials of time approach zero for large values of time.) Analogously, $\Gamma_{HNO_2^\bullet}^\infty$ is given by the last term in Equation 7-10. These solutions can be substituted into Equations 7-4 and 7-5, which can be added to obtain the total current:

$$\frac{i}{i^\infty} = \frac{i_2 + i_3}{i_2^\infty + i_3^\infty} = 1 + \frac{1}{4(\tau_+ - \tau_-)}\left[\left(\frac{\Gamma_{NO_3^-\bullet}^o}{\Gamma_{NO_3^-\bullet}^\infty} + \frac{\tau_-}{k_3}\right)(\tau_+ + 4 k_3)\, e^{\tau_+ t} -\right.$$

$$\left.\left(\frac{\Gamma_{NO_3^-\bullet}^o}{\Gamma_{NO_3^-\bullet}^\infty} + \frac{\tau_+}{k_3}\right)(\tau_- + 4 k_3)\, e^{\tau_- t}\right]. \quad (7\text{-}11)$$

where

$$\tau_+ = -\tfrac{1}{2}\left[k_1' + k_2 + k_3 + \sqrt{k_1'^2 + k_2^2 + k_3^2 - 2k_1' k_2 - 2k_2 k_3 - 2k_1' k_3}\right], \quad (7\text{-}12)$$

$$\tau_- = -\tfrac{1}{2}\left[k_1' + k_2 + k_3 - \sqrt{k_1'^2 + k_2^2 + k_3^2 - 2k_1' k_2 - 2k_2 k_3 - 2k_1' k_3}\right], \quad (7\text{-}13)$$

and i_2^∞ and i_3^∞ refer to the steady-state current densities for reactions 2 and 3, respectively. The combinations of rate constants, $\frac{1}{\tau_+}$ and $\frac{1}{\tau_-}$, define the time constants of the system. It should be noted that the parameter Γ_{tot} need not be specified for the calculation of the dimensionless current defined by Equation 7-11; instead, the ratio $\dfrac{\Gamma_{NO_3^-\bullet}^o}{\Gamma_{NO_3^-\bullet}^\infty}$ (which is a number between 0 and 1) may be

specified. Also, $\Gamma_{NO_3^-\bullet}^{\infty}$ can be related to $\Gamma_{HNO_2^\bullet}^{\infty}$:

$$\Gamma_{HNO_2^\bullet}^{\infty} = \frac{k_2}{k_3} \Gamma_{NO_3^-\bullet}^{\infty} \qquad (7\text{-}14)$$

if Equation 7-7 is applied as $t \to \infty$.

7.4.2. Comparison of Theoretical and Experimental Results

The mechanism proposed in the previous section represents an attempt to capture some of the salient features of the nitrate reduction reaction with a simplified model. In this section, an explanation of the current maximum observed in potential-step experiments is given in terms of two competing electrochemical reactions involving an adsorbed intermediate.

Equation 7-11 allows us to calculate the time-dependent current response in terms of the three rate constants and $\Gamma_{NO_3^-\bullet}^{o}$. A current maximum is predicted by the model for two sets of parameter combinations. The experimental results depicted in Figure 7-14 allow us to choose the correct set of parameter combinations. That is, when the nitrate concentration is decreased by a factor of ten, the maximum in the current response should be eliminated.

For cases with $k_1' + k_2 \ll k_3$ and $\Gamma_{NO_3^-\bullet}^{o} > \Gamma_{NO_3^-\bullet}^{\infty}$, a current maximum is predicted. It is not possible, however, to eliminate the current maximum by decreasing k_1' by a factor of ten (without changing k_2 and k_3). For parameter sets of this type, the maximum is due to the i_3 component of the current. Initially, i_3 is zero ($\Gamma_{HNO_2^\bullet}^{o} = 0$) and increases to a maximum as the second reaction produces $HNO_2^\bullet$; i_3 then decreases to its steady state current as time proceeds.

Another set of parameters exists that predicts the correct dependence on the nitrate ion concentration and gives a maximum in the current: $k_3 < k_2 < k_1'$. The two cases, high and low nitrate ion concentration, involve eight parameters: three rate constants and $\Gamma_{NO_3^-\bullet}^{\infty}$ for each case. Four of the parameters must be chosen arbitrarily. Equation 7-8 can be used to relate the rate constant k_1'

for the two cases:

$$k'_{1,high} = 10\,k'_{1,low}\,. \tag{7-15}$$

It is also assumed that $k_{2,high} = k_{2,low}$ and $k_{3,high} = k_{3,low}$. In addition, we can also choose to incorporate the constraint that adsorption/desorption equilibrium of the nitrate ion exists initially. In other words, we can expect that there are more nitrate ions adsorbed on the surface initially (before the potential step) in the solution with the high nitrate ion concentration than in the solution with the low nitrate ion concentration. An adsorption rate expression can be equated to a desorption rate expression for each case and combined to yield the following initial condition:

$$\frac{\Gamma^o_{NO_3^- high}}{\Gamma_{tot} - \Gamma^o_{NO_3^- high}} = 10\,\frac{\Gamma^o_{NO_3^- low}}{\Gamma_{tot} - \Gamma^o_{NO_3^- low}}\,. \tag{7-16}$$

Figure 7-15 gives the model results for a case with a high nitrate ion concentration and a case with a 10 times lower nitrate ion concentration. The magnitudes of r_+ and r_- influence the time scales of the simulation. For the case with the high nitrate ion concentration r_+ and r_- are -0.00396 s^{-1} and -0.00124 s^{-1}, respectively. The time to reach a steady-state current for the case with a high concentration of nickel nitrate is reflected by the magnitude of the larger rate constant, $\frac{1}{r_-} = 806$ seconds.

The magnitude of the current response (not shown in Figure 7-15) is dependent on Γ_{tot}. Based on the superficial electrode area and the size of a molecule, Γ_{tot} would be expected to be on the order of 10^{-9} mole/cm^2. A value of Γ_{tot} this large would result in the magnitude of current being two to three orders of magnitude smaller than we observe experimentally. This may indicate that the actual surface area for adsorption is approximately one-thousand times the superficial surface area. The magnitude of the current at infinite time can be matched with the magnitude of the steady current density shown in Figure 7-14
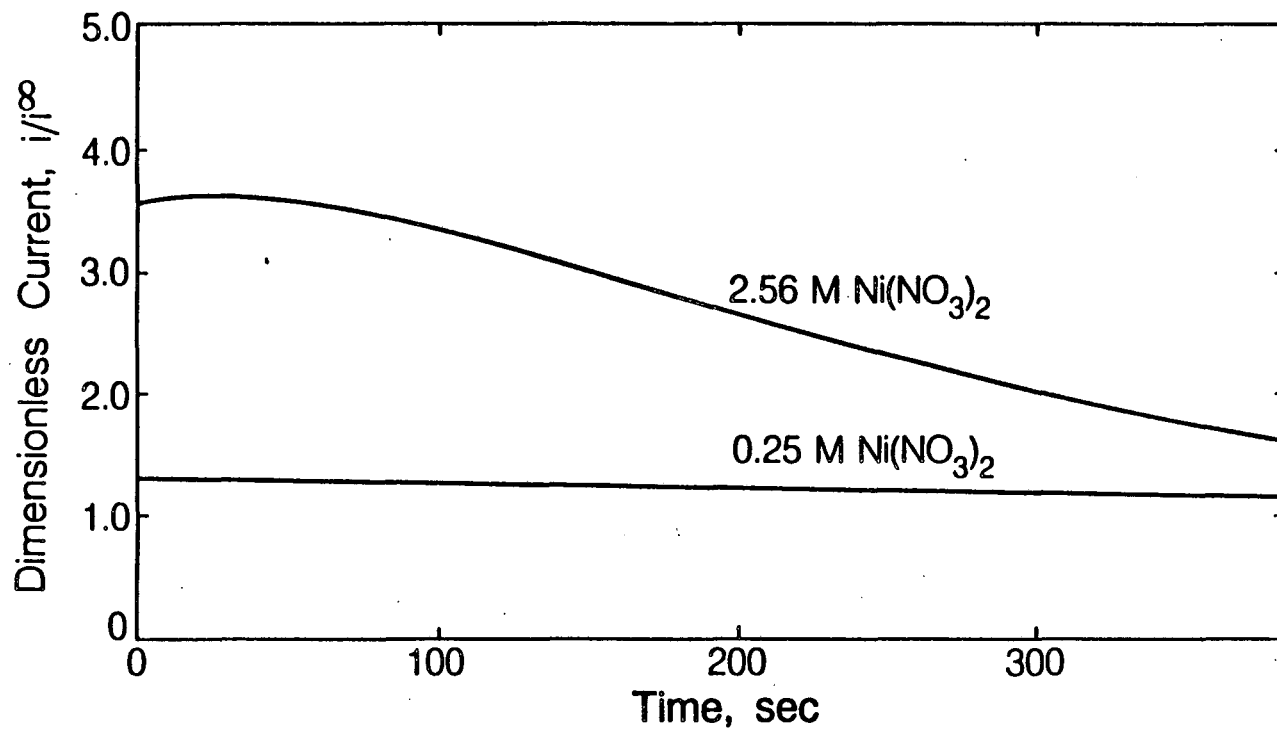
Figure 7-15. Calculated dimensionless current density as a function of time (Equation 7-13) for two concentrations of $Ni(NO_3)_2$ ($k_2 = 0.004$, $k_3 = 0.0001$, $k'_{1,high} = 0.011$, $\dfrac{\Gamma^o_{NO_3^- \cdot high}}{\Gamma_{tot}} = 0.69$, $\Gamma_{H^\cdot} = 0$, and Equations 7-16 and 7-17 for $k'_{1,low}$ and $\dfrac{\Gamma^o_{NO_3^- \cdot low}}{\Gamma_{tot}}$, respectively).

if $\Gamma_{tot} = 1.43 \times 10^{-6}$ mol/cm^2.

Figure 7-16 gives the contributions to the total current by reactions 2 and 3 for the case with the high concentration of nickel nitrate. For this set of parameters, the current maximum is due to the i_2 component of the current. For the first 200 seconds, more than 90% of the total current is due to i_2; however, the i_3 contribution eventually becomes significant. The i_2 contribution accounts for 75% of the total current at steady-state conditions (after $\approx$ 1000 seconds). The maximum in the i_2 current occurs when the derivative of $\Gamma_{NO_3^-\cdot}$ with respect to time (see Equation 7-6) is zero. Initially, the amount of $NO_3^-\cdot$ on the electrode surface increases to a maximum because of the relatively large adsorption rate constant. The current then decreases because the surface area available for NO_3^- adsorption has been depleted. The third reaction is slow, so the $HNO_2^\cdot$ species contributes to the decrease in the area available for adsorption. For the case with the low nitrate ion concentration, the rate of adsorption is low enough that an initial increase in current does not occur. The initial increase in current for the case with the high nitrate ion concentration occurs because $\Gamma_{NO_3^-\cdot}$ increases above $\Gamma^0_{NO_3^-\cdot}$. In summary, this simple model qualitatively fits experimental observations if the third reaction is slow relative to the first and second.

It is interesting to note that the model predicts the steady-state surface coverage of nitrate ion, $\Gamma^\infty_{NO_3^-\cdot}$, to be approximately equal for the case of the high and the low nitrate concentrations. The total current at steady state,

$$i_2^\infty + i_3^\infty = -8F\,k_2\,\Gamma^\infty_{NO_3^-\cdot}\,.$$

is approximately equal for the two cases. Zhdanov et al.[55] observe the steady-state current response in the potential range of -0.25 to -0.35 V versus SCE to be proportional to the nitrate ion concentration (Figure 6-2). We expect that the behavior described in this section applies to the potential range in which the
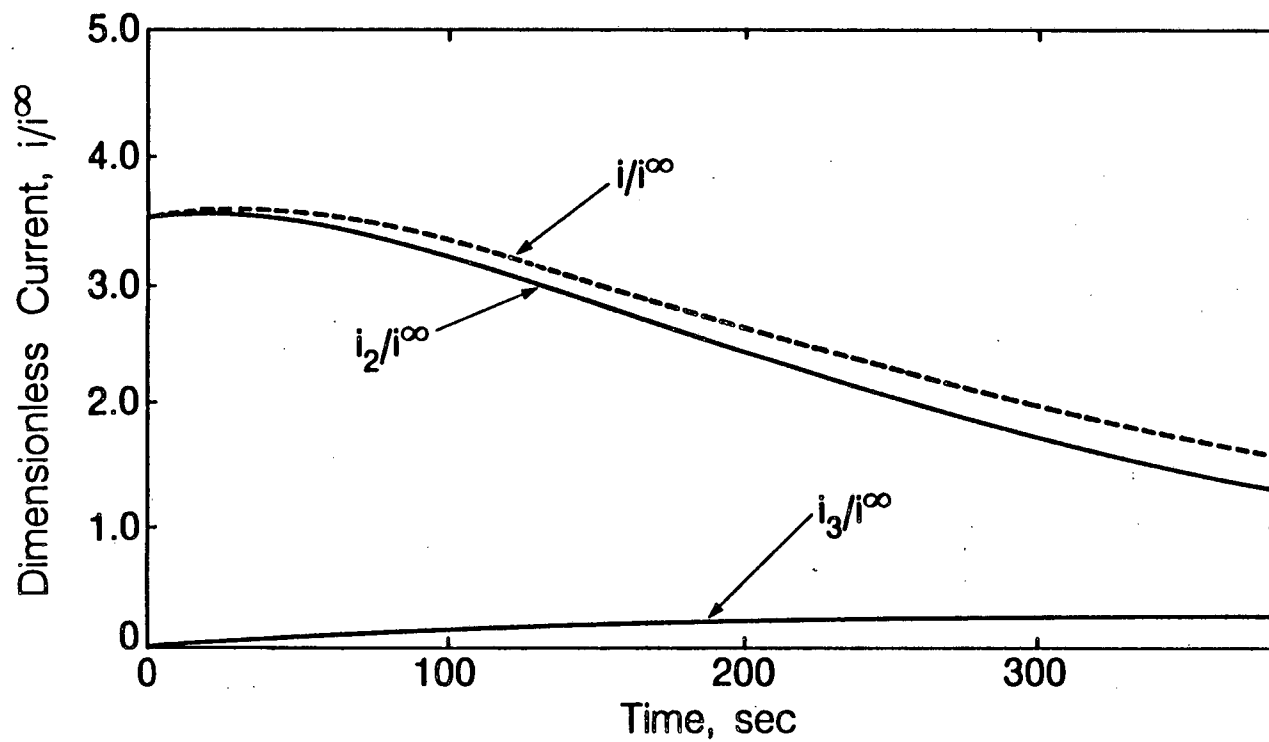
Figure 7-16. Calculated dimensionless components of the current density as a function of time for the case with the high nitrate ion concentration (parameters as in Figure 7-15).

current maximum in a potential-sweep experiment occurs. Zhdanov *et al.* observe the first-order dependency on the nitrate ion concentration in the potential range in which a current maximum is not observed.

7.5. Suggested Further Work

Further work with the nickel nitrate system should include more sophisticated theoretical efforts. An attempt to model the observed behavior in the potential sweep experiments should be made. This will require the consideration of a transient potential source. Strong specific adsorption may influence the behavior of the current maximum in this system. Modifications of simple double-layer theory may be required in order to explain the behavior of reactions occurring in the inner part of the double layer. We have not addressed this and, it should be the subject of further investigations.

Models should include the electrochemical adsorption of hydrogen ion and desorption reactions for $NO_3^{-\bullet}$ and $HNO_2^{\bullet}$. Reactions for the direct reduction of nitrate ion and intermediate reduction products (without species adsorption) should be considered along with homogeneous reactions. Homogeneous reactions should include the acid-base reactions for water, nitrous acid, hydroxylamine, and ammonia. The resulting equations are nonlinear, and the solution will require the use of numerical techniques. The effects of migration and possibly multi-component diffusion should be treated.

7.6. Summary and Conclusions

We have experimentally and theoretically investigated the mechanism for nitrate ion reduction in acidic, nickel nitrate solution. It is postulated that this mechanism involves species adsorption and desorption. A simple adsorption model is proposed to explain some of the observed experimental results. An estimation of the rate constants is made after comparing experimental observations with the model results. Though simple, the proposed model captures

some of the distinguishing features of experimental observations. Development of a more sophisticated model of the system is suggested.

List of Symbols for Chapter 7

c_i	concentration of species i, mol/cm^3
e^-	symbol for an electron
F	Faraday's constant, 96487 C/equiv
i_2, i_3	current densities for reactions 7-2 and 7-3, respectively, A/cm^2
k_1	rate constant for reaction 7-1, cm^3/mol-s
k_1', k_2, k_3	rate constants, s^{-1}
n	number of electrons involved in reaction
r_+, r_-	constants defined by Equations 7-14 and 7-15, respectively, s^{-1}
t	time, s
V	electrode potential, V

Greek

Γ_i	surface concentration of species i, mol/cm^2
Γ_{tot}	surface concentration of sites available for adsorption, mol/cm^2

Subscripts and Superscripts

i	species i
high	high NO_3^- ion concentration
∞	at long times
low	low NO_3^- ion concentration
o	at initial time
sur	at the electrode surface
1, 2, 3	corresponding to reactions 7-1, 7-2, and 7-3
*	adsorbed species

References for Part B

42. A. R. Landgrebe and K. Klunder, *Proceedings of the 27th Power Sources Symposium*, 23 (1976).

43. L. E. Miller, "Eagle Picher's Ni-Cd Plant," *Batteries Today*, 30-32 (Summer, 1981).

44. Y. M. Pozin, *Zhurnal Prikladnoi Khimii*, **35**, 2715-2719, (December, 1962) (English translation: "Cathodic Polarization in Concentrated Solutions of Nitrates," *Journal of Applied Chemistry of the U.S.S.R.* **35**, 12, 2604-2607 (1962).

45. G. W. Briggs and W. F. K. Wynne-Jones, "The Nickel Hydroxide Electrode; the Effects of Aging-I X-Ray Diffraction Study of the Electrode Process," *Electrochimica Acta*, **7**, 241-248 (1962).

46. E. J. McHenry, "Electrochemical Precipitation of $Ni(OH)_2$ into Porous Electrodes," *Electrochemical Technology*, **5**, 275-279 (May-June, 1967).

47. D. M. MacArthur, "Electrochemical Properties of Nickel Hydroxide Electrodes," *Power Sources 3*, Proceedings of the 7th International Symposium, D. H. Collins ed., Oriel Press, Brighton, England, 91-118 (1971).

48. Eagle-Picher Industries, *Annual Report for 1978 on Research, Development and Demonstration of Nickel-Iron Batteries for Electric Vehicle Propulsion*, Contract No. 31-109-38-4292, Argonne National Laboratory Report ANL/OEPM-78-13, (October, 1979).

49. P. Russell, *Corrosion of Iron: The Active - Passive Transition and Sustained Electrochemical Oscillations*, Dissertation, University of California, Berkeley (1984).

50. P. Russell and J. Newman, "Anodic Dissolution of Iron in Acidic Sulfate Electrolytes. Part I. Formation and Growth of a Porous Salt Film," *Journal of the Electrochemical Society*, **133**, 59-69 (January, 1986).

51. V. V. Zhdanov, K. I. Tikhonov, and A. L. Rotinyan, *Zhurnal Prikladnoi Khimii*, **53**, 581-583 (March, 1980) (English translation: "Cathodic Process on a Nickel Electrode in Nickel Nitrate Solutions," *Journal of Applied Chemistry of the U.S.S.R.*, **53**, 465-467 (March, 1980)).

52. C. F. Baes, Jr., and R. F. Mesmer, *The Hydrolysis of Cations*, Wiley-Interscience, (1976).

53. J. Newman, *Electrochemical Systems*, Prentice Hall, Englewood Cliffs, New Jersey (1973).

54. I. A. Cherepkova, V. V. Sysoeva, and N. N. Milyutin, *Zhurnal Prikladnoi Khimii*, **52**, 2503-2507 (November, 1979) (English translation: "Investigation of the Deposition and Electrochemical Properties of Thin Layer Nickel-Oxide Electrodes Obtained by Electrolysis of Nickel Nitrate Solution," *Journal of Applied Chemistry of the U.S.S.R.*, **53**, 2369 (November, 1979)).

55. V. V. Zhdanov, N. A. Chvyrina, K. I. Tikhonov, I. A. Shoshina, and A. L. Roitnyan, *Zhurnal Prikladnoi Khimii*, **53**, 833-836 (April, 1980) (English translation: "Electroreduction of Nitrate Ion at a Nickel Electrode," *Journal of Applied Chemistry of the U.S.S.R.*, **53**, 649-652 (April, 1980)).

56. R. C. Weast, *Handbook of Chemistry and Physics*, 48th Edition, CRC Press, Cleveland, Ohio (1967).

57. T. R. Beck, "Formation of Salt Films during Passivation of Iron," *Journal of the Electrochemical Society*, **129**, 2412-2418 (November, 1982).

58. S. Shibata, "Supersaturation of Oxygen in Acidic Solution in the Vicinity of

an Oxygen-Evolving Platinum Anode," *Electrochimica Acta,* **23,** 619-623 (1978).

59. J. Crank and P. Nicholson, *Proceedings of the Cambridge Philosophical Society,* **43,** 50-67 (1947).

60. A. J. Bard and L. R. Faulkner, *Electrochemical Methods,* John Wiley & Sons, New York (1980).

61. K. Nisancioglu and J. Newman, "Transient Convective Diffusion to a Disk Electrode," *Electroanalytical Chemistry and Interfacial Electrochemistry,* **50,** 23-29 (1974).

62. H. P. Lee, K. Nobe, and A. J. Pearlstein, "Film Formation and Current Oscillations in Electrodissolution of Cu in Acidic Chloride Media, I. Experimental Studies," *Journal of the Electrochemical Society,* **132,** 1031-1037 (May, 1985).

63. A. J. Pearlstein, H. P. Lee, and K. Nobe, "Film Formation and Current Oscillations in Electrodissolution of Cu in Acidic Chloride Media, II. Mathematical Model," *Journal of the Electrochemical Society,* **132,** 2159-2165 (September, 1985).

64. M. Tokuoka and J. Ruzicka, "Polarographic Studies with the Dropping Mercury Cathode.- Part XLII. - The Salt Action in the Electro-reduction of Nitrates," *Collection of Czechoslov. Commun.,* **6,** 339-353 (1934).

65. R. Parsons, "The Structure of the Electrical Double Layer and Its Influence on the Rates of Electrode Reactions," *Advances in Electrochemistry and Electrochemical Engineering,* Paul Delahay, ed. (Interscience Publishers, New York), **1,** 1-64, (1961).

66. V. V. Zhdanov and K. I. Tikhonov, *Zhurnal Prikladnoi Khimii,* **53,** 1056-1058 (May, 1980) (English translation: "Adsorption of Nitrite on a Smooth Nickel Electrode," *Journal of Applied Chemistry of the U.S.S.R.,* **53,** 822-825 (May, 1980)).

67. V. V. Zhdanov and K. I. Tikhonov, *Elektrokhimiya*, **18**, 608-611 (May, 1982) (English translation: "Electroreduction of Nitrite Ion on a Nickel Electrode," *Soviet Electrochemistry*, **18**, 535-538 (May, 1980)).

Appendix A-1

Program EFES: Calculates the thermodynamic, open-circuit potential of a LiAl/FeS cell as a function of temperature and state-of-discharge (see Chapter 1).

```
      PROGRAM EFES(INPUT,OUTPUT)
      COMMON UJO(5),R,F,S1B1(5),S2B1(5),EONSB1(5),DOCCPT(5)
      DIMENSION UTHETA(5),DTTHETA(5),UO(5),DUO(5)
      CALL PARAM
      F=96487.
      R=8.3143
      XA=0.58
      XB=1.-XA
      CALL GAMMA(XA,XB,ACA,ACB)
      PRINT 991
991   FORMAT(* RXN     UTHETA     DTTHETA*)
      DO 10 I=1,5
      UTHETA(I)=UJO(I)+R/F*(S2B1(I)/EONSB1(I)*ACB
     1+(S1B1(I)/EONSB1(I)+1.)*ACA)
      DTTHETA(I)=DOCCPT(I)+R/F*(S2B1(I)/EONSB1(I)*ALOG(1.-XA)
     1+(S1B1(I)/EONSB1(I)+1.)*ALOG(XA))
      PRINT 999, I,UTHETA(I),DTTHETA(I)
10    CONTINUE
      T=768.
      IF(T.GT.0.0) GO TO 99
      XA=0.752
      XC=0.
      XB=1.-XA-XB
15    CALL GAMMA(XA,XB,ACA,ACB)
      PRINT 992,XA,T
 992  FORMAT(* RXN       U         AT XA= *,G12.5,* AND TEMP = *,G12.5)
      DO 20 I=1,5
      U=UTHETA(I)-R/F*(S2B1(I)/EONSB1(I)*ACB
     1+(S1B1(I)/EONSB1(I)+1.)*ACA)
      UO(I)=U
      DOCCP1=DTTHETA(I)-R/F*(S2B1(I)/EONSB1(I)*ALOG(1.-XA-XC)
     1+(S1B1(I)/EONSB1(I)+1.)*ALOG(XA))
      U=U+DOCCP1*T
      PRINT 999, I,U,UO(I),DOCCP1
20    CONTINUE
      IF(XA.GT.0.54  ) STOP
      XA=XA+0.002
      GOTO 15
999   FORMAT(1X,I2,6X,5G17.8)
  99  UTIL=0.0 $ XAO=0.58 $ ELEC=1.0
      ANJMAX=1./26.
      PRINT 203
      ANJ=0.05*ANJMAX
 200  XA=(XAO*ELEC+5.*ANJ)/(ELEC-ANJ) $ XB=1.-XA-XC
      CALL GAMMA(XA,XB,ACA,ACB)
      DO 201 I=1,5
      UO(I)=UTHETA(I)-R/F*(S2B1(I)/EONSB1(I)*ACB
     1+(S1B1(I)/EONSB1(I)+1.)*ACA)
      DUO(I)=DTTHETA(I)-R/F*(S2B1(I)/EONSB1(I)*ALOG(1-XA-XC)
     1+(S1B1(I)/EONSB1(I)+1.)*ALOG(XA))
 201  CONTINUE
```

```
      T1=(UO(2)-UO(1))/(DUO(1)-DUO(2))
      T2=(UO(2)-UO(4))/(DUO(4)-DUO(2))
      U11=3.*ANJ $ ANX=0. $ ANFES=1.-26.*ANJ
      U12=0.5-10.*ANJ
      U22=1.0-23.*ANJ
      PRINT 202, ANJ,XA,U11,T1,U12,T2,U22
202 FORMAT (X,3F7.4,F7.2,F7.4,F7.2,F7.4)
      ANJ=ANJ+0.1*ANJMAX
      IF(ANJ.LT.0.99*ANJMAX) GO TO 200
203 FORMAT (4X,*ANJ*,5X,*XA*,4X,*U11*,5X,*T1*,
    14X,*U12*,5X,*T2*,4X,*U22*)
      PRINT 97 $ T=673.15
 97 FORMAT (4X,*T*,7X,*XA0*,2X,*ELEC*,4X,*UTIL*,4X,*U*)
101 ANJ=UTIL/3. $ IF(UTIL.GT.3./26.) GO TO 102
      IRXN=1 $ GO TO 110
102 ANJ=-(2.*UTIL-1.)/20. $ ANX=(1.-26.*ANJ)/2.
      IF(ANJ.LT.0 .OR. ANX.LT.0.) GO TO 105
     ·IRXN=2 $ GO TO 110
105 ANJ=-2.*(UTIL-1.)/46. $ ANLI2S=1.-26.*ANJ $ IRXN=5
      IF(ANLI2S.GE.0.) GO TO 110
103 ANJ=0. $ ANX=UTIL $ IF(ANFES.LT.0.) GO TO 104
     ·IRXN=3 $ GO TO 110
104 ANX=1.-UTIL $ ANLI2S=UTIL-ANX $ ANJ=0. $ IRXN=4
110 XA=(XA0*ELEC+5.*ANJ)/(ELEC-ANJ) $ XB=1.-XA-XC
      CALL GAMMA(XA,XB,ACA,ACB)
      DO 120 I=1,5
      UO(I)=UTHETA(I)-R/F*(S2B1(I)/EONSB1(I)*ACB
    1+(S1B1(I)/EONSB1(I)+1.)*ACA)
      DUO(I)=DTTHETA(I)-R/F*(S2B1(I)/EONSB1(I)*ALOG(1-XA-XC)
    1+(S1B1(I)/EONSB1(I)+1.)*ALOG(XA))
120 CONTINUE
      T2=(UO(2)-UO(1))/(DUO(1)-DUO(2))
      T1=(UO(2)-UO(4))/(DUO(4)-DUO(2))
      IF(IRXN.EQ.1 .AND. T.GT.T2) GO TO 103
      IF(IRXN.EQ.2 .AND. T.GT.T2) GO TO 103
      IF(IRXN.EQ.2 .AND. T.LT.T1) GO TO 105
      IF(IRXN.EQ.3 .AND. T.LT.T2) GO TO 150
      IF(IRXN.EQ.4 .AND. T.LT.T1) GO TO 160
      IF(IRXN.EQ.5 .AND. T.GT.T1) GO TO 104
130 U=UO(IRXN)+DUO(IRXN)*T
      PRINT 98, T,XA0,ELEC,UTIL,U,IRXN
 98 FORMAT(X,F7.2,3F7.4,F7.4,I4)
      T=T+10. $ IF(T.LT.800.) GO TO 101
      T=673.15
      IF(UTIL.GT.0.90) STOP
      UTILO=UTIL
      IF(ABS(UTILO).LT.0.01) UTIL=0.01
      IF(ABS(UTILO-0.01).LT.0.01) UTIL=0.05
      IF(ABS(UTILO-0.05).LT.0.01) UTIL=0.09
      IF(ABS(UTILO-0.09).LT.0.01) UTIL=0.12
      IF(ABS(UTILO-0.12).LT.0.01) UTIL=0.23
```

```
      IF(ABS(UTILO-0.23).LT.0.01) UTIL=0.37
      IF(ABS(UTILO-0.37).LT.0.01) UTIL=0.51
      IF(ABS(UTILO-0.51).LT.0.01) UTIL=0.77
      IF(ABS(UTILO-0.77).LT.0.01) UTIL=1.0
      GO TO 101
  150 PRINT 151 $ GO TO 130
  151 FORMAT (X,*REACTION 3 DOES NOT MATCH*)
  160 PRINT 161 $ GO TO 130
  161 FORMAT (X,*REACTION 4 DOES NOT MATCH*)
      END
      SUBROUTINE GAMMA(XA,XB,ACA,ACB)
      TBASE=450.+273.15
      ACA=(0.52628*XB-1.2738*XB**2-2.9783*XB**3)*TBASE
      ACB=(-0.52628*XA-5.7413*XA**2+2.9783*XA**3-0.52628*ALOG(XB))
     1*TBASE
      RETURN
      END
      SUBROUTINE PARAM
      COMMON UJO(5),R,F,S1B1(5),S2B1(5),EONSB1(5),DOCCPT(5)
      DO 1 I=1,5
    1 READ 100, UJO(I),DOCCPT(I)
      UJO(1)=-10./3.*UJO(2)+13./3.*UJO(3)
      DOCCPT(1)=-10./3.*DOCCPT(2)+13./3.*DOCCPT(3)
      UJO(5)=20./46.*UJO(2)+26./46.*UJO(4)
      DOCCPT(5)=20./46.*DOCCPT(2)+26./46.*DOCCPT(4)
      DO 2 I=1,5
    2 PRINT 999, UJO(I),DOCCPT(I)
  999 FORMAT(1X,3G12.5)
C
C     RXN 1 FES TO J       RXN 2 J TO X     RXN 3 FES TO X
C
      S1B1(1)=-1.        $   S1B1(2)=-25.   $ S1B1(3)=-2.
      S2B1(1)=-6.        $   S2B1(2)=6.     $ S2B1(3)=0.
      EONSB1(1)=6.       $   EONSB1(2)=20.  $ EONSB1(3)=2.
C
C     RXN 4 X TO LI2S      RXN 5 J TO LI2S
C
      S1B1(4)=-2.        $   S1B1(5)=-51.
      S2B1(4)=0.         $   S2B1(5)=+6.
      EONSB1(4)=2.       $   EONSB1(5)=46.
  100 FORMAT(F10.0,F12.0)
      RETURN
      END
~789
1.769      -0.00068
1.19072    +0.0001753
1.3389     +0.0000133
1.43211    -0.000147
1.3331     -0.00002445
1.769      -0.00068
1.2386     +0.0001753
```

```
1.361      -0.000022
1.4058     -0.0001781
1.3331     -0.00002445
~679
```

Appendix A-2

Program BATRY: Calculates the current, overpotential, and reaction rate distributions for the Lithium(alloy), Iron Sulfide Cell (see Chapters 1, 2, and 5).

Sample Input Data for Program BATRY

```
   81  121  166  2 0 1  3  10193.  0.004D0    0.004D0    0.0047684691D0  0.01
0.5800D0    0.390D0    0.755D0    0.75D0    743.15D0    0.0D0    0.0D0
  0.5D0    0.5D0    0.5D0    2.80D0   16000.D0   2.7D0    1.75D0
12  10 0.000001D0   0.001D0
0.0416D0    1.6929D0    0.000651D0 0.03D0    1.5D0    2.1819D0    1.55D0
  -1.0D0  0.0D0   1.0D0   -2.0D0    0.0D0    2.0D0    0.00000004D0
0.0D0    1.89D0    298.15D0    0.00000825D0
55262130.D0  .0000000004D0  0.50D0    0.58D0  0.450D0  5.00D0
-0.0878D0  2000.0D0  2000.0D0   1.0D0   1.0D0   20.5D0    37.58D0
18.490D0    23.93D0  99.170D0  37.580D0  1900.0D0  100.0D0  .2D0  5.1D0
LINE 1    NJ1,NJ2,NJ, NRESRT,IPHASE,IALLOY,NSTOP, TSTOP,H1,H2,H3,  DELT
LINE 2    XAINIT, EINIT, EINTB, ESEP, TINIT, ECCN, ECCP
LINE 3    GAM, ALPHA, ALPHC, CR1, TGAP, ROA, ROB
LINE 4    IPRINT,MAXITS, CONV, ETAGES
LINE 5    TCD, UJO, DOCCPT, VOVERA, FACTOR, CONADD, RGRID
LINE 6    S1, S3, EONS, S1B, S3B, EONSB, DB
LINE 7    WIDTH, CPMA, TAMB, CHT
LINE 8    EN, DA, CMEAN, XAR, QFMIN, DTCUT
LINE 9    DSEPOT, AIO1, AIO2, AA, AC, VLICL, VKCL
LINE 10   VFE, VFES, VX, VLI2S, SIGFE, SIGFES, SIGX,SIGLIS
```

```
C       PROGRAM BATRY
C       PROGRAM TO FIND CURRENT,OVERPOTENTIAL AND REACTION RATE
C       DISTRIBUTION FOR LI(ALLOY)/IRON SULFIDE BATTERY
C       RELAXATION AND CHARGING
        IMPLICIT DOUBLE PRECISION (A-H,O-Z)
        DIMENSION A(6,6),B(6,6),C(6,401),D(6,13),G(6),X(6,6),Y(6,6),COLD(4
       1,401),DIST(401),V(401),DVX(401),EPKKEP(401),ESUM(401),DIFUSN(401),
       1DDX(401),        CON(401),DCONX(401),EFE(401),
       1DLNAC(401),D2LNAC(401),ZETA(401),DZETAX(401),EPLKEP(401),
       1ZETALD(401),CKEEP(6,401),RBETA(401),ROUTA(401),        EX(401)
       1,RIN(401),RINKEP(401),CPOL(3,401),EFES(401),Q(401)
       1,DVDT(401)        ,XD(401),XDKEEP(401),BIG(6),VSTAR(401),W(401)
       1,NONOFF(401)
       1,        GB(3,1),CJ1(401),CJ2(401),CJ1KEP(401),CJ2KEP(401),SS(4,2),
       1B1(6),B2(6),        SIGINV(401),TALL(6)
       1,ELI2S(401),        NONOF(401)
       1,R1(401),R2(401),RV1(401),RV2(401),EPL(401),EPK(401),DETA(401)
       1,FRAC(401),CJ3KEP(401),Q3(401),CJ3(401)
        EQUIVALENCE (EFES(1),W(1)),(EX(1),RBETA(1)),(ELI2S(1),RIN(1))
       1,(EFE(1),ROUTA(1)),(RINKEP(1),CJ2KEP(1)),(CJ3KEP(1),CJ3(1))
        COMMON A,B,C,D,G,X,Y,N,NJ
        COMMON/P1/V,DVX,DVDT        ,DIFUSN,DDX        ,SIGINV,CON,
       1DCONX,DLNAC,D2LNAC,ZETA,DZETAX        ,FACTOR,T,IX,NJ1,NJ2
       1,EX,EFES,EFE,SIGX,SIGFES,SIGFE,PIN43
        COMMON/P2/R1,R2,RV1,RV2
        COMMON/P3/S,AON,AOP1,AOP2,CJ1,CJ2,EXPAND
        DATA IX,IG,IE,IN,II,IJ/1,2,3,4,5,6/,R,F,TIME/8.3143D0,96487.D0,0./
       1,JCOUNT        /0        /,COEFF/1.0D-11/,CUTOFF/1.0D0/
100     FORMAT(1H1)
102     FORMAT(' CUTOFF VOLTAGE REACHED')
103     FORMAT('0MESH SIZES(H1,H2,H3)'5X'NUMBER OF MESH POINTS'5X'NUMBER O
       1F ITERATIONS'3X'CONVERGENCE CRITERION'4X'TIME(SECS)')
104     FORMAT(1H ,3F7.3,14X,I5,20X,I5,18X,E12.5,F16.6,/)
105     FORMAT(7X'DIST'13X'XA'14X'E'15X'V/J3'10X
       1'I2'11X'J'13X'ETA'13X'J1',/)
109     FORMAT(1H0,'VOL FRAC CURRENT COLLECTOR',/,' IN NEG=',E16.8,4X,
       1'IN POS=',E16.8,/,' U20-U10=',E16.8,'VOLTS',/,' 1ST GUESS FOR ETA=
       1',E16.8,/)
111     FORMAT(3E16.8,I5)
112     FORMAT(1H1,'PARAMETERS FOR SIMULATION OF LI,AL/FES BATTERY'//' NJ1
       1=',I3,4X,'NJ2=',I4,4X,'NJ=',I4,/,' H1=',E13.6,' H2=',E13.6,' H3=',
       1E13.6,/,' DELT(SECS)=',E13.6,4X,'TSTOP=',E13.6,/)
113     FORMAT(1H0,'KINETIC PARAMETERS'/' GAM=',E13.6,5X,'ALPHA=',E13.6,5X
       1,'ALPHC=',E13.6,/,' CR1=',E14.7,/)
114     FORMAT(1H0,'TCD=',E12.5,4X,'V/A=',E12.5,4X,'T(K)=',E12.5,4X,
       1'FACTOR=',E12.5,/)
115     FORMAT(1H0,'S1=',F6.3,4X,'S3=',F6.3,4X,'EONS=',F6.3,4X,/,' S1B=',
       1F6.3,4X,'S3B=',F6.3,4X,'EONSB=',F6.3,/)
116     FORMAT(7E16.8)
117     FORMAT(1H0,6X,'TCD',13X,'TCV',11X,'DPHI2,SEP',7X,'DPHI1,POS',6X,
       1'C(IN,NJ1)',7X,'C(IN,NJ2)',8X,'VOVERA')
```

```
118   FORMAT(8E15.8)
119   FORMAT(1H0,'OCCP(V)=',E13.6,4X,'DOCCPT=',E13.6,/,' RESERVOIR WIDTH
     1=',E13.6,4X,'MEAN CELL HEAT CAPACITY(J/CM2.K)=',E16.8,/,' TAMB=',
     1E15.7,4X,'HTC(W/CM2.K)=',E15.7,/)
120   FORMAT(1H0,'NO. OF LI SPHERES/CM3=',E13.5,4X,'DIF COEFF. IN ALPHA(
     1CM2/SEC)=',E13.5,/,' AVG. CONC OF LI IN ALPHA/CLIASAT  =',E13.5,4
     1X'XAR=',E13.5,/)
121   FORMAT(1H0,'EINIT=',E16.8,4X,'EINITB=',E16.8,4X,'ESEP=',E16.8,/)
122   FORMAT(1H0,'POSITIVE ELECTRODE PARAMETERS',/,' AIO1=',E14.6,'AMP/C
     1M3',4X,'AIO2=',E14.6,4X,/,' ALFA A=',E14.6,4X,'ALFA C=',E14.6,/,
     1' VFE,VFES,VX=',3E16.6,'CM3/MOL',/,' CONFE,CONFES,CONX=',3E16.6,
     1' /OHM/CM',/,' VLI2S(CM3/MOL)=',E16.8,/,' VLICL=',E16.8,4X,'VKCL='
     1,E16.8,/)
124   FORMAT(32HDEL CHANGED DUE TO KINETICS TEST,3E16.8/3E16.8,I6)
125   FORMAT(1H0,'CELL TEMP.(DEG.K)=',EI5.8,X,' HEAT LOSS(W/CM2)=',E16.8
     1,4X,'HEAT GAIN(W/CM2)=',E16.8,/,' HEAT OF PPTE(W/CM2) KCL,LICL=',
     12E16.8)
126   FORMAT(1H0,'JCOUNT=',I2,'FRAC ERR MOLS LI=',E16.8,4X,'F ERR MOLS K
     1=',E16.8,/,' MOLS LI IN S,POS=',E16.8,
     14X,'XASL=',E16.8,4X,'XASK=',E16.8,/,' MOLS LI IN S,NEG=',E18.10,
     1/,' FRAC TOT LI SOL LOST=',E16.8,4X,'CAP NEG=',E16.8,4X,'CAP POS='
     1E16.8,/,'UTILIZATION=',2E21.14)
127   FORMAT(1H ,'NOT CONVERGED AT J=',I3,/,8E15.8,/)
128   FORMAT(1H0,'INTERRUPTER RESISTANCE(OHM.CM2)=',E16.8,/)
129   FORMAT(' AOP1,AOP2=',2E16.8)
130   FORMAT(7E15.8,I5)
132   FORMAT(1H0,6X'DIST'13X'G/Q3'12X'Q'9X'ESUM '8X'RB/EP'12X'ELI2S'10X
     1'RO/EX'8X' CS /EFES',/)
131   FORMAT(1H0,'BARMA,BARMB,CALBET,CLIBET,CLIAS,CLIAM,CALAM,VALA,VLIA,
     1AON,QFMIN,DTCUT,TGAP=',/,5E16.8,/,5E16.8,/,3E16.8,/)
133   FORMAT(1H0,'RGRID=',E16.8,4X,'EXTRA CONDUCTIVITY(/OHM/CM)=',E16.8)
134   FORMAT(1H ,'DELT HALVED',4X,'KEY=',I2)
135   FORMAT(1H0,'NON-CONVERGED SOLN AT',E15.8,' SECS',/)
136   FORMAT(' INITIAL VALUES. SLNO,SLPO,AMTLIO,AMTKO=',/,4E18.9)
137   FORMAT(' PARAMETERS AT REACTION FRONT')
138   FORMAT(' RSUM=',E16.8,4X,'VSUM=',E16.8)
139   FORMAT(' PIN21,PIN22,DFC1,DFC2=',4E16.8)
140   FORMAT(1H ,'QMAXB=',E16.8,4X,'EFINAL=',E16.8,4X,'QMAX=',E16.8,/,
     1' E INTERMEDIATE=',E16.8)
142   FORMAT(2E15.8)
      READ *,NJ1,NJ2,NJ,NRESRT,IPHASE,IALLOY,NSTOP,TSTOP,H1,H2,H3,DELT
      READ *,XAINIT,EINIT,EINITB,ESEP,TINIT,ECCN,ECCP
      READ *,GAM,ALPHA,ALPHC,CR1,TGAP,ROA,ROB
      READ *,IPRINT,MAXITS,CONV,ETAGES
      READ *,TCD,UJO,DOCCPT,VOVERA,FACTOR,CONADD,RGRID
      READ *,S1,S3,EONS,S1B,S3B,EONSB,DB
      READ *,WIDTH,CPMA,TAMB,CHT
      READ *,EN,DA,CMEAN,XAR,QFMIN,DTCUT
      READ *,DSEPOT,AIO1,AIO2,AA,AC,VLICL,VKCL
      READ *,VFE,VFES,VX,VLI2S,SIGFE,SIGFES,SIGX
        CRXNOL=0.0
```

```
               CRXN=0.0
               NTIME=1
               PREPP=1.0D0/3.0D0
           SLNO=0.0
   510     CONTINUE
           HFUSEK=25500.0D0
C              IPHASE IS A PARAMETER USED TO SELECT WHETHER FES OR FES2
C              REACTIONS ARE USED, 1 FOR FES, 0 FOR FES2 , FES=FES2,
C              X=Z, LI2S=X
C              IALLOY IS A PARAMETER USED TO SELECT WHETHER A LIAL OR
C              LI(SI) NEGATIVE ELECTRODE IS USED.  1 FOR LIAL, 0 FOR LISI
C              LI=LI , AL=SI (LI3.25SI->LI2.33SI PLATEAU).
           KEY6=0
           HFUSEL=13400.0
           MAXITS=16
C       IF RESTARTING, READ IN VALUES FROM RESTART FILE
               IF(NRESRT.NE.2)  GO TO 1440
           DO 144 J=1,NJ
           READ (9,145)(C(K,J),K=1,6)
  1181 FORMAT(56HINITIAL VALUES READ IN FOR C(1)/C(2)/C(3)/C(4)/C(5)/C(6)
      1 )
           READ (9,145)EPK(J),EPL(J),RBETA(J),ROUTA(J),RIN(J),Q(J)
           READ (9,145)EFES(J),EX(J),EFE(J),ELI2S(J),CJ1(J),CJ2(J)
           READ (9,145)W(J),DETA(J),ZETA(J),(CPOL(K,J),K=1,3)
             READ (9,145)XD(J),FRAC(J),Q3(J)
             CJ3KEP(J)=0.0D0
   144     CONTINUE
           READ (9,145)TCV,T,VOVERA,XAINIT,DTEMP,TIME
  1440 CONTINUE
   145 FORMAT(6E21.14)
C       EVALUATION OF SOME PARAMETERS USED THROUGHOUT PROGRAM
           EFESO=1.0D0-EINITB-ECCP
           AP1=1.3389D0
           AP2=1.43211D0
           Q1MAX=EFESO*1.0D0*F/VFES
           SLOPEP=0.0D0
           Q2MAX=2.0D0*Q1MAX
           Q3MAX=0.0D0
           IF(IPHASE.EQ.1)GO TO 5100
C       PARAMETERS FOR THE LI(SI) ELECTRODE
           AP1 = 1.4251D0
           AP2 = 1.208771D0
           BP2=0.00065142D0
           AP3=1.3389D0
           BP3=0.0000133D0
           Q1MAX=EFESO*1.5D0*F/VFES
           Q3MQ2=0.5D0-((2.2D0*(4.0D0*0.875D0-2.0D0)/(2.0D0*0.875D0-0.8D0)
      1 )-3.0D0)/2.0D0
           Q3MAX=EFESO*F*Q3MQ2/VFES
           SLOPEP=((AP3-AP2)+T*(BP3-BP2))*VFES/Q3MQ2/EFESO/F
           Q2MAX=(2.0D0-1.5D0-Q3MQ2)*EFESO*F/VFES
```

```
       PRINT 145, SLOPEP,Q3MQ2,Q1MAX,Q2MAX
5100   WTLI=6.939D0
       IF(IALLOY.NE.0)GO TO 151
       CR1=2.8D-3
       WTAL=28.086D0
       XLIAO=0.6997D0
       XALAO=1.0D0-XLIAO
       XLIBO=0.7647D0
       XALBO=1.0D0-XLIBO
       ROLI=0.53D0/WTLI
       ROAL=2.33D0/WTAL
       ROA=(XALAO*WTAL+XLIAO*WTLI)/
    1  (XALAO/ROAL+XLIAO/ROLI)
       ROB=(XALBO*WTAL+XLIBO*WTLI)/
    1  (XALBO/ROAL+XLIBO/ROLI)
       DA=4.9D-5
       DB=7.9D-5
       UJO=UJO+0.133204D0
       GO TO 152
151    WTAL=26.9815D0
       XLIAO=0.1D0
       XALAO=1.0D0-XLIAO
       XLIBO=0.475D0
       XALBO=1.0D0-XLIBO
152  BARMA=XALAO*WTAL+XLIAO*WTLI
     BARMB=XALBO*WTAL+XLIBO*WTLI
     CALBET=XALBO*ROB/BARMB
     CLIBET=XLIBO*ROB/BARMB
     CLIAS=XLIAO*ROA/BARMA
     CLIAM=CMEAN*CLIAS
     VLIA=(BARMB/ROB-XALBO*BARMA/XALAO/ROA)/(XLIBO-XALBO*XLIAO/XALAO)
     VALA=(1.0D0-CLIBET*VLIA)/CALBET
     CALAM=(1.0D0-VLIA*CLIAM)/VALA
     AON=VLIA/F/(1.0D0-CALAM*(CALBET*VALA+CLIBET*VLIA-1.0D0)/(CALBET-
    1CALAM))
     WRITE (7,112)NJ1,NJ2,NJ,H1,H2,H3,DELT,TSTOP
     WRITE (7,121)EINIT,EINITB,ESEP
     WRITE (7,113)GAM,ALPHA,ALPHC,CR1
     WRITE (7,120)EN,DA,CMEAN,XAR
     AIO10=AIO1
     AIO20=AIO2
     WRITE (7,122)AIO1,AIO2,AA,AC,VFE,VFES,VX,SIGFE,SIGFES,SIGX,VLI2S
    1,VLICL,VKCL
     WRITE (7,109)ECCN,ECCP,DSEPOT,ETAGES
     WRITE (7,114)TCD,VOVERA,TINIT,FACTOR
     WRITE (7,115)S1,S3,EONS,S1B,S3B,EONSB
     WRITE (7,119)UJO,DOCCPT,WIDTH,CPMA,TAMB,CHT
     WRITE(7,131)BARMA,BARMB,CALBET,CLIBET,CLIAS,CLIAM,CALAM,VALA,VLIA,
    1AON,QFMIN,DTCUT,TGAP
     NJ1M1=NJ1-1
     NJ2P1=NJ2+1
```

```
        N=5
        JP=N+1
        T1=0.02
        T2=0.1
        T3=0.4
        T4=1.0
        T5=4.0
        T6=10.0
        T7=60.0
        F1=0.02
        F2=0.1
        F3=0.2
        F4=1.0
        F5=2.0
        F6=10.0
        F7=10.0
        S=-0.15
        F8= 60.0
        T8=60.0
        WRITE (7,133)RGRID,CONADD
        T10=T1
        T20=T2
        T30=T3
        T40=T4
        T50=T5
        T60=T6
        T70=T7
        T80=T8
        TOTM=H1*DBLE(NJ1-1)
        TOTS=H2*DBLE(NJ2-NJ1)
        TOTL=TOTM+TOTS+H3*DBLE(NJ-NJ2)
        TLAST=TIME
        IPOLAR=1
        TCADD=0.02
        RF=R/F
        VAL1=RF*S1/EONS
        VAL2=RF*(1.0-S3/EONS)
          ITIME=TIME
          IF(ITIME.EQ.0)T=TINIT
C       T=TINIT
        NJ1P1=NJ1+1
        VAL1B=RF*S1B/EONSB
        VAL2B=RF*(1.0-S3B/EONSB)
    -   ALRA=ALPHA/RF
        ALRC=ALPHC/RF
        ALR1=AA/RF
        ALR2=AC/RF
        NJ2M1=NJ2-1
        ESEPPN=ESEP**FACTOR
        DELT2=DELT/2.0D0
        NJM1=NJ-1
```

```
      IF(IPHASE.NE.0)GO TO 149
C     STOICHIOMETRIES FOR SOLID PHASES IN POSITIVE ELECTRODE REACTIONS
C     1=FE,2=FES,3=X,4=LI2S FOR FES OR 2=FES2,3=Z,4=X FOR FES2
      SS(1,1)=0.0D0
      SS(2,1)=-4.0D0/3.0D0
      SS(3,1)=2.0D0/3.0D0
      SS(4,1)=0.0D0
      SS(1,2)=0.0D0
      SS(2,2)=0.0D0
      SS(3,2)=-2.0D0
      SS(4,2)=4.0D0
      GO TO 150
  149 SS(1,1)=1.0D0
      SS(2,1)=-2.0D0
      SS(3,1)=1.0D0
      SS(4,1)=0.0D0
      SS(1,2)=1.0D0
      SS(2,2)=0.0D0
      SS(3,2)=-1.0D0
      SS(4,2)=2.0D0
  150    AOP1=(SS(3,1)*VX+SS(1,1)*VFE+SS(2,1)*VFES+SS(4,1)*VLI2S)
     1   /EONSB/F
         AOP2=(SS(4,2)*VLI2S+SS(1,2)*VFE+SS(3,2)*VX+SS(2,2)*VFES)
     1   /EONSB/F
         WRITE(7,129)AOP1,AOP2
      PIN1=1.0D0/3.0D0
      PIN4=12.56637D0*EN
      PIN43=PIN4/3.0D0
      PIN21=PIN43*F*(CALBET*VALA+CLIBET*VLIA-CALBET/CALAM)/VLIA
      PIN5=-PIN43/AON
      PIN51=PIN5
      PIN52=PIN5
      DFC1=2.0D0*PIN4*F*DA*CLIAS/(1.0D0+(CLIBET/CLIAM)/((CLIBET/CLIAM)-(
     1CALBET/CALAM)))
      DFC2=PIN4*F*DB*CLIBET
      PIN22=PIN43*(1.0D0-CALAM/CALBET)/AON
      DFC1=PIN4*F*DA*CLIAS/(1.0D0-XLIAO*CMEAN)
      DFC2=PIN4*F*DB*CLIBET/XALBO
      WRITE (7,139)PIN21,PIN22,DFC1,DFC2
      ROINIT=((1.0D0-EINIT-ECCN)/PIN43)**PIN1
      RBINIT=ROINIT
      U1=(CLIBET+(VALA*CALBET-1.0D0)/VLIA)*PIN43
      U2=PIN43/VLIA
      U3=-ROINIT**3*VALA*CALBET/VLIA
      EXPAND=0.0D0
      Y1=-SS(2,1)*VFES/EONSB/F
      Y21=-SS(3,1)*VX/EONSB/F
      Y22=-SS(3,2)*VX/EONSB/F
      Y31=-SS(1,1)*VFE/EONSB/F
      Y32=-SS(1,2)*VFE/EONSB/F
      Y42=-SS(4,2)*VLI2S/EONSB/F
```

```
C       CALCULATION OF ELECTRODE CAPACITIES
        QMAXB=-EFESO*F*EONSB/VFES
           IF(IPHASE.EQ.0)QMAXB=-EFESO*F*4.0D0/VFES
        QMNEG=(1.0D0-EINIT-ECCN)*F*CLIBET
        EFINAL=EINITB+0.5D0*QMAXB*(AOP1+AOP2)
        EINT=0.5D0*(EFINAL+EINITB)
        WRITE (7,140)QMAXB,EFINAL,QMNEG,EINT
        WRITE (7,100)
C       FIRST GUESS FOR UNKNOWN VARIABLES
        EBH2=DEXP(-238.59D0*H3/2.0D0)
        ENH2=DEXP(509.91D0*H1/2.0D0)
        RES=0.0D0
        DO 33 K=1,NJ
           ESUM(K)=1.0D0
        IF(K.LE.NJ1) DIST(K)=H1*DBLE(K-1)/TOTL
        IF(K.GT.NJ1.AND.K.LT.NJ2) DIST(K)=(TOTM+H2*DBLE(K-NJ1))/TOTL
        IF(K.GE.NJ2) DIST(K)=(TOTM+TOTS+H3*DBLE(K-NJ2))/TOTL
C       IF RESTARTING, BRANCH TO STATEMENT 33
           IF(NRESRT.EQ.2)GO TO 33
        FRAC(K)=1.0D0
        C(IX,K)=XAINIT
        C(IG,K)=0.0D0
        ROUTA(K)=0.0D0
        W(K)=0.0D0
        RBETA(K)=0.0D0
        CJ2(K)=0.0D0
        CJ1(K)=0.0D0
        Q(K)=0.0D0
        Q3(K)=0.0D0
        CJ3KEP(K)=0.0D0
        ELI2S(K)=0.0D0
        EFE(K)=0.0D0
        EPK(K)=0.0D0
        EPL(K)=0.0D0
        XD(K)=0.0D0
        ZETA(K)=0.0D0
        DETA(K)=0.0D0
        C(IN,K)=0.0D0
        IF(K.GT.NJ1) GOTO 31
        C(IE,K)=EINIT
        C(IJ,K)=509.91D0*TCD*DEXP(509.91D0*H1*DBLE(K-NJ1))
        ROUTA(K)=ROINIT
        W(K)=1.0D0
        RBETA(K)=RBINIT
        DETA(K)=C(IJ,K)/95669.2D0
        C(II,K)=-C(IJ,K)/509.91D0*ENH2
        CPOL(2,K)=C(IJ,K)*0.02D0/TCD
        CPOL(1,K)=C(II,K)*0.02D0/TCD
        CPOL(3,K)=CPOL(2,K)/95669.2D0
        RIN(K)=RBETA(K)
        C(IN,K)=DETA(K)
```

```
      GOTO 33
31 IF(K.GE.NJ2) GOTO 32
   C(IE,K)=ESEP
   C(II,K)=TCD
   CPOL(1,K)=0.02D0
   CPOL(2,K)=0.0D0
   CPOL(3,K)=0.0D0
   DIST(K)=(TOTM+H2*DBLE(K-NJ1))/TOTL
   C(IJ,K)=0.0D0
   C(IN,K)=0.0D0
   GOTO 33
32 C(IJ,K)=-238.59D0*TCD*DEXP(238.59D0*H3*DBLE(NJ2-K))
   C(IE,K)=EINITB
   C(II,K)=-C(IJ,K)/238.59D0*EBH2
   DETA(K)=C(IJ,K)/45903.0D0
   CPOL(2,K)=C(IJ,K)*0.02D0/TCD
   CPOL(1,K)=C(II,K)*0.02D0/TCD
   CPOL(3,K)=CPOL(2,K)/45903.0D0-DSEPOT
   DIST(K)=(TOTM+TOTS+H3*DBLE(K-NJ2))/TOTL
   EFES(K)=EFESO
   C(IN,K)=DETA(K)-DSEPOT
   CJ1(K)=C(IJ,K)
33    CONTINUE
   IF(NRESRT.NE.2)C(IG,NJ2)=VOVERA
1     DTEMP=0.0
   DELT=0.0D0
   JSPOT=0
2     DO 34 KV=1,NJ
   EPKKEP(KV)=EPK(KV)
   EPLKEP(KV)=EPL(KV)
   XDKEEP(KV)=XD(KV)
   ZETALD(KV)=ZETA(KV)
   CJ1KEP(KV)= CJ1(KV)
   NONOF(KV)=0
   IF(KV.LE.NJ1) RINKEP(KV)=RIN(KV)
   IF(KV.GE.NJ2)CJ2KEP(KV)=CJ2(KV)
   DO 34 L=1,JP
34 CKEEP(L,KV)=C(L,KV)
   IF(IPOLAR.EQ.0) GO TO 30
   DELTMX=DELT
   JSET=0
   NSET=0
   DO 27 J=1,NJ1
   IF(C(IJ,J).LE.0.0) GO TO 25
   DEL =RBETA (J)**3*PIN21/C(IJ,J)*2.0
   IF(DEL.GT.2.0*DELTMX) GO TO 27
   IF(DEL.LE.DELTMX) NONOF(J)=1
   IF(DEL.GT.DELTMX.AND.DELT.GT.0.5*DELTMX) GO TO 26
   IF(DEL.GT.DELT) GO TO 27
   DELT=DEL
   C(IJ,J)=0.0
```

```
      JSET=J
      KSET=1
      GO TO 27
   25 IF(C(IJ,J).EQ.0.0) GO TO 27
      DEL=-Q(J)/C(IJ,J)*2.0
      IF(DEL.GT.2.0*DELTMX) GO TO 27
      IF(DEL.LE.DELTMX) NONOF(J)=2
      IF(DEL.GT.DELTMX.AND.DELT.GT.0.5*DELTMX) GO TO 26
      IF(DEL.GT.DELT) GO TO 27
      DELT=DEL
      C(IJ,J)=0.0
      JSET=J
      KSET=2
      GO TO 27
   26 DELT=0.5*DELT
      JSET=0
   27 IF(NONOF(J).NE.0)WRITE(7,124)DIST(J),DEL,Q(J),CKEEP(IJ,J),RBETA(J)
     1,RINKEP(J),NONOF(J)
C     CALCULATE DEL, THE CHARACTERISTIC TIME FOR DEPLETION OF A REACTANT
      DO 275 J=NJ2,NJ
         IF(IPHASE.EQ.1)GO TO 2691
         Q2=DABS(ELI2S(J)/Y42)-Q3(J)
         IF(Q2.LE.0.0D0)GO TO 2691
         IF(CJ2(J).EQ.CJ3KEP(J))GO TO 2691
         IF((1.0D0-Q2/Q2MAX).LE.1.0D-11)GO TO 2691
         Q2K=(Q2MAX-Q2)+DELTMX*(CJ2(J)-CJ3KEP(J))
         IF(Q2K.LT.0.0D0.AND.Q2K.GT.-1.D-17)Q2K=0.0D0
         IF(Q2K.GE.0.0D0)GO TO 2691
         NON=0
         DEL=-(Q2MAX-Q2)/(CJ2(J)-CJ3KEP(J))*2.0D0
         GO TO 278
 2691 EFESK=EFES(J)+Y1*DELTMX*CJ1(J)
         IF(EFESK.LT.0.0.AND.EFESK.GT.-1.D-17)EFESK=0.0
      IF(EFESK.GE.0.0) GO TO 269
      NON=1
      DEL=-EFES(J)/Y1/CJ1(J)*2.0
      GO TO 278
  269 ELI2SK=ELI2S(J)+Y42*DELTMX*CJ2(J)
         IF(ELI2SK.LT.0.0.AND.ELI2SK.GT.-1.D-17)ELI2SK=0.0
      IF(ELI2SK.GE.0.0) GO TO 271
      NON=2
      DEL=-ELI2S(J)/Y42/CJ2(J)*2.0
      GO TO 278
  271 EXK=EX(J)+DELTMX*(Y21*CJ1(J)+Y22*CJ2(J))
         IF(EXK.LT.0.0.AND.EXK.GT.-1.D-17)EXK=0.0
      IF(EXK.GE.0.0) GO TO275
      IF(EFESK.GT.0.0) GO TO 273
      DEL=-EX(J)/Y22/CJ2(J)*2.0
      NON=3
      GO TO 278
  273 DEL=-EX(J)/Y21/CJ1(J)*2.0
```

```
          NON=4
     278 IF(DEL.LE.DELTMX) NONOF(J)=NON
          IF(DEL.GT.DELTMX .AND. DELT.GT.0.5*DELTMX) GO TO 274
          IF(DEL.GT.DELT) GO TO 275
          DELT=DEL
          JSET=J
          KSET=-NON
          IF(NON.EQ.1 .OR. NON.EQ.4) CJ1(J)=0.0
          IF(NON.EQ.2 .OR. NON.EQ.3) CJ2(J)=0.0
          GO TO 275
     274 DELT=0.5*DELT
          JSET=0
     275 IF(NONOF(J).NE.0)WRITE(7,124)DIST(J),DEL,EFESK,
        1CJ1KEP(J),EXK,CJ2KEP(J),
        1NONOF(J)
             IF(JSET.EQ.0)GO TO 2751
             IF(NONOF(JSET).NE.0)GO TO 2751
             NSET=JSET
             Q2=DABS(ELI2S(NSET)/Y42)-Q3(NSET)
             Q2K=(Q2MAX-Q2)+DELTMX*(CJ2(NSET)-CJ3KEP(NSET))
             JSET=0
             KSET=0
             CJ2(NSET)=0.0D0
             WRITE(7,124)DIST(NSET),DEL,Q2,CJ3KEP(NSET),Q2K,CJ2KEP(NSET),
        1    NONOF(NSET)
    2751 DO 279 J=NJ2,NJ
          IF(J.EQ.JSET) GO TO 279
          IF(NONOF(J).EQ.1) CJ1(J)=CJ1KEP(J)*(1.0-DELT/(-EFES(J)/Y1/CJ1KEP
        1(J)*2.0))
          IF(NONOF(J).EQ.2) CJ2(J)=CJ2KEP(J)*(1.0-DELT/(-ELI2S(J)*2.0/Y42
        1/CJ2KEP(J)))
          IF(NONOF(J).EQ.3) CJ2(J)=CJ2KEP(J)*(1.0-DELT/(-EX(J)/Y22/CJ2KEP(J)
        1*2.0))
          IF(NONOF(J).EQ.4) CJ1(J)=CJ1KEP(J)*(1.0-DELT/(-EX(J)/Y21/CJ1KEP(J)
        1*2.0))
     279 CONTINUE
          DO 24 J=1,NJ1
          IF(J.EQ.JSET) GO TO 24
          IF(NONOF(J).EQ.1) C(IJ,J)=CKEEP(IJ,J)*(1.0-DELT/(RBETA (J)**3
        1*PIN21/CKEEP(IJ,J)*2.0))
          IF(NONOF(J).EQ.2) C(IJ,J)=CKEEP(IJ,J)*(1.-DELT/(-Q(J)/CKEEP(IJ,J)
        1*2.0))
      24 CONTINUE
          KEY5=0
          DTMIN=DELT/20.0
          IF(DTMIN.LT.0.005) DTMIN=0.005
C         SET MAIN ITERATION LOOP COUNTER.INITIALISE ARRAY ELEMENTS
    3     JCOUNT=0
          DENT2=0.5*DELT
          MAXITS=16
          TIME=TIME+DELT
```

```
        T=T+DELT*DTEMP
        IF(DELT.NE.0.0) DTINV=1.0/DELT
        XASL=0.34080-0.0004773*T+0.000001376*T**2
        XASK=0.14615+0.0019117*T-0.000001948*T**2
        TCA=ALRA/T
        TCC=ALRC/T
         TC1=ALR1/T
        TC2=ALR2/T
          NTERR = 1
C       BRANCH TO NORMALIZE THE CURRENT, RETURN IF JCOUNT=0
        GO TO 260
4       JCOUNT=JCOUNT+1
        J=0
        DO 35 I=1,JP
        DO 35 K=1,JP
        X(I,K)=0.0D0
35      Y(I,K)=0.0D0
        JPTERR=0
        NTERR=0
C       CALCULATE PHYSICAL PROPERTIES
        DO 36 MI=1,NJ
        CALL PROPS(MI,C)
        IF(JCOUNT.EQ.1) NONOFF(MI)=0
        IF(IPOLAR.NE.0 .OR. JCOUNT.NE.0) GO TO 36
        IF(MI.GT.NJ1) GO TO 36
        IF(C(IN,MI).LT.0.0) W(MI)=1.1
        IF(C(IN,MI).GE.0.0) W(MI)=0.9
36      CONTINUE
        EFESP=0.0
        EFEP=0.0
        EXPP=0.0
        ELI2SP=0.0
        DSIG1P=0.0
        DSIG2P=0.0
        SIGINV(1)=0.0
        F3N=0.0
        DXOVN=0.0
        BG=0.0
        F3ND=0.0
        FGP=0.0
        HP=H1
        FLUXP=0.0
        DXOVNP=(V(1)-C(IX,1)*DVX(1))/V(1)**2
        F3NP=C(IE,1)**FACTOR*DIFUSN(1)/V(1)
        F3NPD=C(IE,1)**FACTOR*(DDX(1)-DIFUSN(1)*DVX(1)/V(1))/V(1)
5       J=J+1
        AIO1=AIO1O*FRAC(J)
        DSIG1=DSIG1P
        DSIG2=DSIG2P
        AIO2=AIO2O*FRAC(J)
        EFESK=EFESP
```

```
        EXK=EXPP
        ELI2SK=ELI2SP
        DO 37 I=1,JP
        G(I)=0.0D0
        B1(I)=0.0D0
        B2(I)=0.0D0
        TALL(I)=0.0D0
        IF(I.LE.4) COLD(I,J)=C(I,J)
        DO 37 K=1,JP
        A(I,K)=0.0D0
        B(I,K)=0.0D0
   37   D(I,K)=0.0D0
C       CALCULATE DERIVATIVES, COEFFICIENTS A, B, AND D
C       FOR BAND (BASED ON PREVIOUS GUESS)
        H=H2
        IF(J.LE.NJ1) H=H1
        IF(J.GE.NJ2) H=H3
        IF(J.GT.1) A(4,II)=1.0
        IF(J.LT.NJ) B(4,II)=-1.0
        WE=H/4.0D0
        IF(J.EQ.1.OR.J.EQ.NJ) WE=WE/2.0
        IF(J.EQ.NJ1) WE=H1/8.0
        IF(J.EQ.NJ2) WE=H3/8.0
        B(4,IJ)=4.0D0*WE
        IF(J.EQ.NJ1.OR.J.EQ.NJ) B(5,II)=1.0
        IF(J.EQ.NJ) G(5)=-C(II,J)
        IF(J.EQ.NJ1) G(5)=TCD-C(II,J)
        IF(J.EQ.NJ1 .AND.DABS(G(5)).LE.COEFF*DABS(C(II,J))) G(5)=0.0D0
        TALL(4)=DABS(B(4,IJ)*C(IJ,J))
        IF(J.GT.1 .AND. DABS(C(II,J-1)).GT.TALL(4))TALL(4)=DABS(C(II,J-1))
        IF(J.LT.NJ .AND. DABS(C(II,J)).GT.TALL(4)) TALL(4)=DABS(C(II,J))
        G(4)=-4.0D0*WE*C(IJ,J)
        IF(J.GT.1) G(4)=G(4)-C(II,J-1)
        IF(J.LT.NJ) G(4)=G(4)+C(II,J)
        WEP=H/4.0D0
        IF(J+1.EQ.NJ1.OR.J+1.EQ.NJ) WEP=WEP/2.0
        IF(J+1.EQ.NJ2) WEP=H3/8.0
        DYINV=1.0/H
        IF(J.EQ.NJ1) DYINV=1.0/H2
        IF(J.NE.NJ) DXYFD=(XD(J+1)-XD(J))*DYINV
C       KINETIC EQUATION FOR NEGATIVE ELECTRODE G(6), MODEL INCLUDES
C       REACTION AT S/L INTERFACE AND DIFFUSION OF LI IN ALPHA AL.
        ADDJ=DENT2*(C(IJ,J)+CKEEP(IJ,J))
        IF(J.LT.NJ) SIGINV(J+1)=0.0
        IF(J.GT.NJ1) GO TO 45
        KEY=-1
        B(6,IJ)=1.0
        IF(NONOF(J).NE.0) GO TO 46
        IF(Q(J)+ADDJ.LT.0.0) GO TO 8
        IF(Q(J).LE.1.0D-05.AND.C(IN,J).LE.0.0) GO TO 44
        IF(NONOFF(J).GE.3) GO TO 44
```

```
      IF(RBETA(J).LE.1.0D-11.AND.C(IN,J).GE.0.0) GO TO 44
      RINK=RINKEP(J)
      IF(W(J).LE.1.0) GO TO  39
      IF(C(IN,J).LT.0.0) GO TO 38
      W(J)=0.0
      GO TO 40
   38 PIN5=PIN52
      PIN2=PIN22
      DFC=DFC2
      IF(W(J).GT.1.99) RINK=ROUTA(J)
      ROK=(ROUTA(J)**3+ADDJ/PIN52)**PIN1
      KEY=-2
      RIN3=RINK  **3-ADDJ/PIN2
      IF(RIN3.LT.0.0) GO TO 8
      RIN(J)=RIN3**PIN1
      TL=(1.0/RIN(J)  -1.0/ROK)/DFC
      GO TO 41
   39 IF(C(IN,J).GT.0.0) GO TO 40
      W(J)=2.0
      GO TO 38
   40 PIN5=PIN51
      PIN2=PIN21
      DFC=DFC1
      ROK=(ROUTA(J)**3+ADDJ/PIN51)**PIN1
      KEY=-3
      RBETA3=RBETA (J)**3-ADDJ/PIN2
      IF(RBETA3.LT.0.0) GO TO 8
      RBETAK  =RBETA3**PIN1
      RIN(J)=RBETAK
      TL=          (1.0/PIN2+1.0/PIN5)*(Q(J)+ADDJ)/(ROK**2+ROK
     1*RIN(J)+RIN(J)**2)/(DFC*ROK*RIN(J))
   41 SAREA=PIN4*ROK**2
      CR2=DEXP(TCA*C(IN,J))
      CR3=DEXP(-TCC*C(IN,J))
      CR14=CR2-CR3
      EXCHIA=SAREA*CR1*(C(IX,J)/XAR)**GAM
      BIG(2)=CR2
      IF(DABS(CR2).LT.DABS(CR3)) BIG(2)=CR3
      IF(DABS(C(IN,J)).GT.5.0D-04) GOTO 42
      CR14=C(IN,J)*   (TCA+TCC+(TCA**3+TCC**3)*C(IN,J)**2/6.0)
      BIG(2)=CR14
   42 CR15=TL*CR2+1.0/EXCHIA
      CR16=CR15**2
      B(6,IN)=(TCA*TL*CR14*CR2-CR15*(TCA*CR2+TCC*CR3))/CR16
      B(6,IX)=-CR14*GAM/CR16/EXCHIA/C(IX,J)
      B(6,IJ)=1.0+CR14/CR16*DELT/6.0*(CR2/DFC*(1.0/PIN2/RIN(J)**4  +1.0
     1/PIN5/ROK     **4)-2.0/EXCHIA/ROK     **3/PIN5)
      CR5=CR14/CR15
      G(6)=-C(IJ,J)+CR5
      BIG(1)=C(IJ,J)
      BIG(2)=BIG(2)/CR15
```

```
            TAIL=0.0
            DO 43 K=1,2
            IF(TAIL.LT.DABS(BIG(K))) TAIL=DABS(BIG(K))
         43 CONTINUE
            IF(DABS(G(6)).LT.TAIL*COEFF) G(6)=0.0D0
            GO TO 46
         44 B(6,IJ)=1.0
            G(6)=-C(IJ,J)
            GOTO 46
C        KINETIC EQUATIONS FOR POSITIVE ELECTRODE G(6); SIMULTANEOUS
C        REACTIONS, ELECTROCHEMICAL RESISTANCE ONLY
         45 IF(J.LT.NJ2-1) GO TO 44
            IF(J.EQ.NJ) GO TO 284
            EFESP=EFES  (J+1)+Y1*DENT2*(CJ1(J+1)+CJ1KEP(J+1))
            EFEP=EFE    (J+1)+DENT2*(Y31*(CJ1(J+1)+CJ1KEP(J+1))+Y32*(
           1CJ2(J+1)+CJ2KEP(J+1)))
            EXPP=EX     (J+1)+DENT2*(Y21*(CJ1(J+1)+CJ1KEP(J+1))+Y22*(
           1CJ2(J+1)+CJ2KEP(J+1)))
            ELI2SP=ELI2S (J+1)+DENT2*Y42*(CJ2(J+1)+CJ2KEP(J+1))
              IF(EFESP.LT.0.0.AND.EFESP.GT.-1.D-17)EFESP=0.0
              IF(EXPP.LT.0.0.AND.EXPP.GT.-1.D-17)EXPP=0.0
              IF(EFEP.LT.0.0.AND.EFEP.GT.-1.D-17)EFEP=0.0
              IF(ELI2SP.LT.0.0.AND.ELI2SP.GT.-1.D-17)ELI2SP=0.0
C        CALCULATION OF MATRIX CONDUCTIVITY
            CALL         MCOND(SS   ,SIGFE ,SIGX   ,SIGFES,SIGLIS,
           1                   EFESP ,EXPP  ,EFEP   ,ELI2SP,VFES  ,VX    ,
           2                   VFE   ,VLI2S ,DENT2  ,EONSB,F         ,
           3                   SGNVNU,D1NU  ,D2NU   ,
           4                   CONADD)
            SIGINV(J+1) = SGNVNU
            DSIG1P = D1NU
            DSIG2P = D2NU
            IF(J.LT.NJ2) GO TO 44
        284 GB(2,1)=0.0D0
            GB(3,1)=0.0D0
            B(6,IJ)=1.0D0
            G(6)= CJ1(J)+CJ2(J)-C(IJ,J)
            TAIL=0.0D0
            BIG(1)=CJ1(J)
            BIG(2)=CJ2(J)
            BIG(3)=C(IJ,J)
            DO 285 K=1,3
            IF(TAIL.LT.DABS(BIG(K))) TAIL=DABS(BIG(K))
        285 CONTINUE
            IF(DABS(G(6)).LT.TAIL*COEFF) G(6)=0.0D0
            IF(DELT.EQ.0.0) GO TO 287
            IF(J.EQ.JSET) GO TO 297
            IF(NONOF(J).NE.0) GO TO 297
            IF(EFES(J).EQ.0.0 .AND. EFESK.LT.0.0) EFESK=0.0
            IF(ELI2S(J).EQ.0.0 .AND. ELI2SK.LT.0.0) ELI2SK=0.0
            IF(EX(J).EQ.0.0 .AND. EXK.LT.0.0) EXK=0.0
```

```fortran
      IF(ELI2SK.LT.0.0) GO TO 286
      IF(EXK  .GE.0.0.AND.EFESK  .GE.0.0) GO TO 287
  286 KEY=1
      WRITE (7,118)DIST(J),EFESK,EXK,ELI2SK,CJ1(J),CJ2(J),
     1CJ1KEP(J),CJ2KEP(J)
      IF(DELT.GE.10.0.OR.C(IJ,J)*CKEEP(IJ,J).GE.0.0) GO TO 8
      NONOF(J)=5
      IF(CJ1(J).LT.0.0) CJ1(J)=-EFES(J)/DENT2/Y1-CJ1KEP(J)
      IF(CJ1(J).GT.0.0) CJ1(J)=-EX(J)/DENT2/Y21-CJ1KEP(J)
      IF(CJ2(J).LT.0.0) CJ2(J)=-EX(J)/DENT2/Y22-CJ2KEP(J)
      IF(CJ2(J).GT.0.0) CJ2(J)=-ELI2S(J)/DENT2/Y42-CJ2KEP(J)
      C(IJ,J)=CJ1(J)+CJ2(J)
      G(4)=-4.0D0*WE*C(IJ,J)
      IF(J.GT.1) G(4)=G(4)-C(II,J-1)
      IF(J.LT.NJ) G(4)=G(4)+C(II,J)
      GO TO 297
C     KINETICS FOR THE FIRST REACTION, CJ1
  287 ETAS=DETA(J)
      IF(EXK.LE.0.0.AND.ETAS.GT.0.0) GO TO 291
      IF(EFESK  .LE.0.0 .AND. ETAS.LT.0.0) GO TO 291
      CI1=DEXP(TC1*ETAS)
      CI2=DEXP(-TC2*ETAS)
      EXPDIF=CI1-CI2
      AIOXA=AIO1*C(IX,J)
      IF(DABS(ETAS*TC1).GT.4.0D-03) GOTO 289
      EXPDIF=ETAS*((TC1+TC2)*(1.0D0+0.5D0*(TC1-TC2)*ETAS)
     1+(TC1**3+TC2**3)*ETAS**2/6.0D0)
  289 B1(IX)=-AIO1*EXPDIF
      B1(IN)=-AIOXA*(TC1*CI1+TC2*CI2)
      GB(2,1)=-(CJ1(J)+C(IX,J)*B1(IX))
      TAIL=0.0D0
      BIG(1)=CJ1(J)
      BIG(2)=AIOXA*CI1
      BIG(3)=AIOXA*CI2
      DO 290 K=1,3
      IF(TAIL.LT.DABS(BIG(K))) TAIL=DABS(BIG(K))
  290 CONTINUE
      IF(DABS(GB(2,1)).LT.TAIL*COEFF) GB(2,1)=0.0D0
      GO TO 292
  291 GB(2,1)=-CJ1(J)
C     KINETICS FOR THE SECOND REACTION, CJ2 (INCLUDES CJ3 FOR FES2)
  292 IF(ELI2SK  .LE.0.0 .AND. C(IN,J).GT.0.0) GO TO 296
        IF(IPHASE.EQ.0)GO TO 2921
      IF(EXK  .LE.0.0 .AND. C(IN,J).LT.0.0) GO TO 296
 2921   CI1=0.0D0
        CI2=0.0D0
        EXPDIF=0.0D0
        Q2=DABS(ELI2S(J)/Y42)-Q3(J)
        IF(DABS(Q2).GE.Q2MAX.AND.C(IN,J).LT.0.0D0)GO TO 294
        IF((1.0D0-Q2/Q2MAX).LT.1.0D-10.AND.C(IN,J).LT.0.0D0)GO TO 294
        IF(J.EQ.NSET)GO TO 294
```

```
      CI1=DEXP(TC1*C(IN,J))
      CI2=DEXP(-TC2*C(IN,J))
      EXPDIF=CI1-CI2
      IF(DABS(TC1*C(IN,J)).GT.4.0D-03) GOTO 294
      EXPDIF=C(IN,J)*((TC1+TC2)*(1.0D0+0.5D0*(TC1-TC2)*C(IN,J))+(TC1**3+
     1TC2**3)*C(IN,J)**2/6.0D0)
  294 AIOXB=AIO2*C(IX,J)
      IF(IPHASE.EQ.1)GO TO 2941
      ETAS3=C(IN,J)-(SLOPEP*(Q3(J)-DENT2*(C(IJ,J)-(AIOXB*EXPDIF)+
     1 CJ3KEP(J))))
      IF(EXK.LE.0.0D0.AND.ETAS3.LT.0.0D0)GO TO 296
      CI13=DEXP(TC1*ETAS3)
      CI23=DEXP(-TC2*ETAS3)
      EXPDF3=CI13-CI23
      IF(DABS(ETAS3*TC1).GT.4.0D-03) GOTO 2941
      EXPDF3=ETAS3*((TC1+TC2)*(1.0D0+0.5D0*(TC1-TC2)*ETAS3)
     1+(TC1**3+TC2**3)*ETAS3**2/6.0D0)
 2941 B2(IX)=-AIO2*(EXPDIF+EXPDF3-C(IX,J)*SLOPEP*DENT2*EXPDIF*
     1 AIO2*(TC1*CI13+TC2*CI23))
      EXPDIF=EXPDIF+EXPDF3
      B2(IN)=-AIOXB*((CI13*TC1+CI23*TC2)*(1.0D0-SLOPEP*DENT2*AIOXB*
     1 (CI1*TC1+CI2*TC2))+TC1*CI1+TC2*CI2)
      CI1=CI1+CI13
      CI2=CI2+CI23
      B2(IJ)=-SLOPEP*DENT2*AIOXB*(TC1*CI13+TC2*CI23)
      GB(3,1)=-(CJ2(J)-AIOXB*EXPDIF)
      TAIL=0.0D0
      BIG(1)=CJ2(J)
      BIG(2)=AIOXB*CI1
      BIG(3)=AIOXB     *CI2
      DO 295 K=1,3
      IF(TAIL .LT. DABS(BIG(K))) TAIL=DABS(BIG(K))
  295 CONTINUE
      IF(DABS(GB(3,1)).LT.TAIL*COEFF) GB(3,1)=0.0D0
      GOTO 297
  296 GB(3,1)=-CJ2(J)
  297 G(6)=G(6)+GB(2,1)+GB(3,1)
      B(6,IN)=B1(IN)+B2(IN)
      B(6,IX)=B1(IX)+B2(IX)
      B(6,IJ)=B2(IJ)+B(6,IJ)
C     OHMS LAW EQUATION, G(5)
   46 IF(J.EQ.NJ1.OR.J.EQ.NJ) GO TO 311
      IF(J.GT.NJ1.AND.J.LT.NJ2) GO TO 52
      CONJ=CON(J)*C(IE,J)**FACTOR
      CONJP1=CON(J+1)*C(IE,J+1)**FACTOR
      TDLNA2=T*DLNAC(J+1)
      XB2=1.0-C(IX,J+1)
      TDLNA1=T*DLNAC(J)
      XB1=1.0-C(IX,J)
      IF(J.GT.NJ2) GO TO 51
      TER1=(VAL1+VAL2*C(IX,J))/XB1/C(IX,J)
```

```
      F12O=TER1*TDLNA1
      DF12XO=T*D2LNAC(J)*TER1+TDLNA1*(VAL2*C(IX,J)**2-VAL1*(1.0-2.0*
     1C(IX,J)))/((XB1*C(IX,J))**2)
      TER2=(VAL1+VAL2*C(IX,J+1))/XB2/C(IX,J+1)
      F12S=TER2*TDLNA2
      DF12XS=T*D2LNAC(J+1)*TER2+TDLNA2*(VAL2*C(IX,J+1)**2-VAL1*(1.0-2.0*
     1C(IX,J+1)))/((XB2*C(IX,J+1))**2)
   47 CG3=C(II,J)*0.5
      CG8=(F12O+F12S)*DYINV*0.5DO
      B(5,IX)=-CG3*DCONX(J)/CONJ/CON(J)          -CG8+DF12XO*0.5*DXYFD
      D(5,IX)=0.5*DF12XS*DXYFD-CG3*DCONX(J+1)/CONJP1/CON(J+1)+CG8
      DSIG=0.0
      DSIGP=0.0
      IF(CJ1(J).EQ.0.0) GO TO 48
      DSIG=DSIG1
      DSIGP=DSIG1P
   48 IF(CJ2(J).EQ.0.0) GO TO 49
      DSIGP=DSIG2P
      DSIG=DSIG2
   49 B(5,IE)=-CG3*FACTOR/CONJ/C(IE,J)
      D(5,IE) = -CG3*FACTOR/CONJP1/C(IE,J+1)
      B(5,IJ) = .5*(C(II,J) - TCD)*DSIG
      D(5,II)=0.5*(C(II,J)-TCD)*DSIGP*WEP
      B(5,II)=0.5*(1.0/CONJ+1.0/CONJP1+SIGINV(J)+SIGINV(J+1))
      B(5,IN)=DYINV
      D(5,IN)=-DYINV
      BIG(1)=SIGINV(J)*0.5*TCD
      BIG(2)=DYINV*DETA(J+1)
      BIG(3)=0.5*C(II,J)/CONJ
      BIG(4)=0.5*F12S*XD(J)*DYINV
      IF(CONJP1.LT.CONJ) BIG(3)=BIG(3)*CONJ/CONJP1
      G(5)=0.5DO*TCD*(SIGINV(J)+SIGINV(J+1))      -B(5,II)*C(II,J)
     1+DYINV*(DETA(J+1)-DETA(J))+CG8*(XD(J)-XD(J+1))
      B(5,II)=B(5,II)-D(5,II)
      DO  50 K=1,4
      IF(TALL(5).LT.DABS(BIG(K))) TALL(5)=DABS(BIG(K))
   50 CONTINUE
      GO TO 311
C     OHMS LAW EQUATION,POSITIVE ELECTRODE, G(5)
   51 TER1 =(VAL1B+VAL2B*C(IX,J))/XB1/C(IX,J)
      F12O=TER1*TDLNA1
      DF12XO=T*D2LNAC(J)*TER1+TDLNA1*(VAL2B*C(IX,J)**2-VAL1B*(1.0-2.0*
     1C(IX,J)))/((XB1*C(IX,J))**2)
      TER2B=(VAL1B+VAL2B*C(IX,J+1))/XB2/C(IX,J+1)
      F12S=TER2B*TDLNA2
      DF12XS=T*D2LNAC(J+1)*TER2B+TDLNA2*(VAL2B*C(IX,J+1)**2-VAL1B*(1.0-
     12.0*C(IX,J+1)))/((XB2*C(IX,J+1))**2)
      GO TO 47
   52 B(5,IN)=1.0
      G(5)=-C(IN,J)
C     MATERIAL BALANCE EQUATIONS, G(1) AND G(2)
```

```
311 IF(DELT.EQ.0.0) GO TO 329
    F3NM=F3N
    FLUXM=FLUXP
    F3N=F3NP
    F3NMD=F3ND
    F3ND=F3NPD
    FGM=FGP
    HM=HP
    WM=HP
    DXOVNM=DXOVN
    DXOVN=DXOVNP
    BGM=BG
    JE=J
    IF(J.NE.NJ) GO TO 312
    WM=0.375*H3
    FLUXP=0.0
    FGP=0.0
    JE=J-1
    GO TO 315
312 DXOVNP =(V(J+1)-C(IX,J+1)*DVX(J+1))/V(J+1)**2
    F3NP=C(IE,J+1)**FACTOR*DIFUSN(J+1)/V(J+1)
    F3NPD=C(IE,J+1)**FACTOR*(DDX(J+1)-DIFUSN(J+1)*DVX(J+1)/V(J+1))/V(
   1J+1)
    JGP=J
    IF(J.GE.NJ2) JGP=J+1
    IF(J.EQ.1) JE=J+1
    JGM=JGP-1
    IF(J.EQ.1) WM=0.375*H1
    IF(J.EQ.NJ2-1) F3NP=F3NP*(ESEP     /C(IE,J+1))**FACTOR
    IF(J.EQ.NJ2-1) F3NPD=F3NPD*(ESEP/C(IE,J+1))**FACTOR
    IF(J.NE.NJ1) GO TO 313
    JE=J-1
    HP=H2
    WM=0.375*H1
    RAT=(ESEP/C(IE,J))**FACTOR
    F3N=F3N*RAT
    F3ND=F3ND*RAT
    GO TO 314
313 IF(J.NE.NJ2) GO TO 314
    F3N=C(IE,J)**FACTOR*DIFUSN(J)/V(J)
    F3ND =C(IE,J)**FACTOR*(DDX(J)-DIFUSN(J)*DVX(J)/V(J))/V(J)
    JE=JE+1
    HP=H3
    WM=0.375*H3
    JGM=J-1
314 BG=0.25*(C(IX,J+1)+C(IX,J))
    FGP=C(IG,JGP)
    FLUXP=2.0*BG*C(IG,JGP)-0.5*(F3NP+F3N)*(XD(J+1)-XD(J))/HP
315 R1K  =FLUXM-FLUXP+WE/F* C(IJ,J)*4.0
    R2K  =WE*C(IE,J)*(3.0*C(IX,J)/V(J)+C(IX,JE)/V(JE))
   1+WE/VLICL*4.0*EPL(J)
```

```
      RV1K=FGM-FGP+WE*C(IJ,J)/F*4.0
      RV2K  =WE*C(IE,J)*(3.0/V(J)+1.0/V(JE))
     1+WE*4.0*(EPL(J)/VLICL+EPK(J)/VKCL)
      IF(J.EQ.NJ1) RV2K=RV2K+ESEP*H2/8.*(3./V(J)+1./V(J+1))
      IF(J.EQ.NJ2) RV2K=RV2K+ESEP*H2/8.*(3./V(J)+1./V(J-1))+C(IG,J)/V(J)
      IF(J.EQ.NJ1) R2K=R2K+ESEP*H2/8.*(3.*C(IX,J)/V(J)+C(IX,J+1)/V(J+1))
      IF(J.EQ.NJ2) R2K  =R2K  +ESEP*H2/8.*(3.*C(IX,J)/V(J)+C(IX,J-1)/V(J
     1-1))+C(IG,J)*C(IX,J)/V(J)
      RV3=DTINV*(RV2K-RV2(J))
      VDIF=RV3-0.5*(RV1K+RV1(J))
      R3=DTINV*(R2K-R2(J))
      RDIF=R3-0.5*(R1K+R1(J))
      IF(J.GE.NJ2) GO TO 316
      B(1,IG)=BG
      B(2,IG)=0.5
      GO TO 317
  316 IF(J.EQ.NJ) GO TO 318
      D(1,IG)=BG
      D(2,IG)=0.5
  317 D(1,IX)=      0.25*C(IG,JGP)-(F3NP+F3N+F3NPD*(XD(J+1)-XD(J)))/HP/4.
      B(1,IX)=      0.25*C(IG,JGP)+(F3NP+F3N-F3ND*(XD(J+1)-XD(J)))/HP/4.
      IF(J.GE.NJ1.AND.J.LT.NJ2) GO TO 318
      B(1,IE)=B(1,IE)-FACTOR/4.*F3N/HP*(XD(J+1)-XD(J))/C(IE,J)
      D(1,IE)=-0.25*FACTOR /HP   *F3NP*(XD(J+1)-XD(J))/C(IE,J+1)
  318 IF(J.EQ.NJ2) F3N=F3N*(ESEP/C(IE,J))**FACTOR
      IF(J.EQ.NJ2) F3ND=F3ND*(ESEP       /C(IE,J))**FACTOR
      IF(J.EQ.NJ1) F3ND=F3ND*(C(IE,J)/ESEP)**FACTOR
      IF(J.EQ.NJ1) F3N=F3N*(C(IE,J)/ESEP)**FACTOR
      IF(J.LE.NJ2) GO TO 319
      B(1,IG)=-BGM
      B(2,IG)=-0.5
      GO TO 320
  319 IF(J.EQ.1) GO TO 321
      A(1,IG)=-BGM
      A(2,IG)=-0.5
  320 B(1,IX)=B(1,IX)-      0.25*C(IG,JGM)+(F3NM+F3N+F3ND*(XD(J)-XD(J-1)))
     1/HM/4.
      A(1,IX)=(F3NMD*(XD(J)-XD(J-1))-F3NM-F3N)/HM/4.-0.25*C(IG,JGM)
      IF(J.GT.NJ1.AND.J.LE.NJ2) GO TO 321
      A(1,IE)=0.25*FACTOR/HM    *F3NM*(XD(J)-XD(J-1))/C(IE,J-1)
      B(1,IE)=B(1,IE)+FACTOR/4.*F3N/HM*(XD(J)-XD(J-1))/C(IE,J)
  321 B(1,IX)=B(1,IX)+WM*C(IE,J)*DTINV*DXOVN
      B(1,IJ)=-2.0*WE/F
      B(1,IE)=B(1,IE)+WE*(3.0*C(IX,J)/V(J)+C(IX,JE)/V(JE))*DTINV
      B(2,IE)=WE*(3.0/V(J)+1.0/V(JE))*DTINV
      B(2,IJ)=-2.0*WE/F
      B(2,IX)=-WM*DTINV*C(IE,J)*DVX(J)/V(J)**2
      IF(J.NE.1) GO TO 322
      D(1,IX)=D(1,IX)+H1/8.*C(IE,1)*DTINV*DXOVNP
      D(2,IX)=-H1/8.*DTINV*C(IE,J  )*DVX(J+1)/V(J+1)**2
      GO TO 325
```

```
  322 IF(J.NE.NJ) GO TO 323
      A(1,IX)=A(1,IX)+H3/8.*C(IE,NJ   )*DTINV*DXOVNM
      A(2,IX)=-H3/8./DTINV*C(IE,J   )*DVX(J-1)/V(J-1)**2
      GO TO 325
  323 IF(J.NE.NJ1) GO TO 324
      RAT=(ESEP/C(IE,J))**FACTOR
      F3N=F3N*RAT
      F3ND=F3ND*RAT
      A(1,IX)=A(1,IX)+H1/8.*C(IE,J   )*DTINV*DXOVNM
      B(2,IX)=-DTINV*0.375*H2*ESEP*DVX(J)/V(J)**2   +B(2,IX)
      D(2,IX)=-DTINV*H2/8.*ESEP*DVX(J+1)/V(J+1)**2
      A(2,IX)=-H1/8.*DTINV*C(IE,J   )*DVX(J-1)/V(J-1)**2
      D(1,IX)=D(1,IX)+H2/8.*ESEP*DTINV*DXOVNP
      B(1,IX)=B(1,IX)+0.375*H2*ESEP*DTINV*DXOVN
      GO TO 325
  324 IF(J.NE.NJ2) GO TO 325
      RAT=(C(IE,J)/ESEP)**FACTOR
      F3N=F3N*RAT
      F3ND=F3ND*RAT
      B(1,IG)= DTINV*C(IX,J)/V(J)
      B(2,IG)= DTINV/V(J)
      D(2,IX)=-H3/8.*DTINV*C(IE,J   )*DVX(J+1)/V(J+1)**2
      A(1,IX)=A(1,IX)+H2/8.*ESEP*DTINV*DXOVNM
      B(1,IX)=B(1,IX)+DTINV*DXOVN*(0.375*H2*ESEP+ C(IG,J))
      D(1,IX)=D(1,IX)+H3/8.*C(IE,J   )*DTINV*DXOVNP
      A(2,IX)=-DTINV*H2/8.*ESEP*DVX(J-1)/V(J-1)**2
      B(2,IX)=-DTINV*DVX(J)/V(J)**2*(C(IG,J)+H2*0.375*ESEP)+B(2,IX)
  325 G(1)=-RDIF
      G(2)=-VDIF
      IF(EPL(J).GT.0.0.OR.EPK(J).GT.0.0) GO TO 326
C     SOLID PHASE MATERIAL BALANCE, G(3)
C     D(VOID FRACTION)/D(TIME)=AJ.
      B(3,IX)=-C(IJ,J)*DZETAX(J)/2.0
      B(3,IE)=DTINV
      B(3,IJ)=-ZETA(J)/2.0
      BIG(1)=DTINV*CKEEP(IE,J)
      BIG(2)=0.5*ZETALD(J)*CKEEP(IJ,J)
      BIG(3)=B(3,IJ)*C(IJ,J)
      BIG(4)=DTINV*EPLKEP(J)
      BIG(5)=DTINV*EPKKEP(J)
      DO 53 K=1,5
      IF(TALL(3).LT.DABS(BIG(K))) TALL(3)=DABS(BIG(K))
   53 CONTINUE
      G(3)=DTINV*(CKEEP(IE,J)+EPLKEP(J)+EPKKEP(J)-C(IE,J))+BIG(2)-BIG(3)
      GO TO 328
  326 B(3,IX)=1.0
      XANS=XASK
      IF(EPL(J).GT.0.0) XANS=XASL
      G(3)=XANS-C(IX,J)
      IF(EPL(J).EQ.0.0) GO TO 327
      B(1,IE)=B(1,IE)-WE/VLICL*4.0*DTINV
```

```
      B(2,IE)=B(2,IE)-WE/VLICL*4.0*DTINV
      B(1,IJ)=B(1,IJ)+WE/VLICL*4.0*ZETA(J)/2.0
      B(2,IJ)=B(2,IJ)+WE/VLICL*4.0*ZETA(J)/2.0
      B(2,IX)=B(2,IX)+WE/VLICL*4.0*DZETAX(J)*C(IJ,J)/2.0
      B(1,IX)=B(1,IX)+WE/VLICL*4.0*DZETAX(J)*C(IJ,J)/2.0
      GO TO 328
  327 B(2,IE)=B(2,IE)-WE/VKCL *4.0*DTINV
      B(2,IJ)=B(2,IJ)+WE/VKCL *4.0*ZETA(J)/2.0
      B(2,IX)=B(2,IX)+WE/VKCL *4.0*DZETAX(J)*C(IJ,J)/2.0
  328 CONTINUE
      BIG(1)=DTINV*C(IE,J)*C(IX,J)/V(J)*WE*3.0
      BIG(2)=0.25*DYINV *XD(J)*F3N
      BIG(3)=2.0*C(IJ,J)/F*WE
      BIG(5)=4.0*WE*DTINV*EPL(J)/VLICL
      BIG(4)=0.25        *C(IG,J)*C(IX,J)
      DO 54 K=1,5
   54 IF(TALL(1).LT.DABS(BIG(K))) TALL(1)=DABS(BIG(K))
      BIG(1)=DTINV*WE*C(IE,J)*3.0/V(J)
      BIG(2)=0.5*C(IG,J)
      BIG(3)=2.0*WE        *C(IJ,J)/F
      BIG(4)=4.0*WE*EPK(J)*DTINV/VKCL
      BIG(5)=4.0*WE*DTINV*EPL(J)/VLICL
      DO 55 K=1,5
      IF(TALL(2).LT.DABS(BIG(K))) TALL(2)=DABS(BIG(K))
   55 CONTINUE
      GO TO 60
  329 B(1,IX)=1.0
      B(2,IG)=1.0
      B(3,IE)=1.0
      IF(IPOLAR.EQ.0) GO TO 60
      VABAR=V(J)+(1.0-C(IX,J))*DVX(J)
      IF(J-NJ2) 306, 60,308
  306 B(2,IG)=-0.5*(V(J)+V(J+1))
      IF(J.EQ.1) GO TO 309
      A(2,IG)=0.5*(V(J)+V(J-1))
      G(2)=-A(2,IG)*C(IG,J-1)
      GO TO 309
  308 B(2,IG)=0.5*(V(J)+V(J-1))
      IF(J.EQ.NJ) GO TO 309
      D(2,IG)=-0.5*(V(J)+V(J+1))
      G(2)=-D(2,IG)*C(IG,J+1)
  309 B(2,IJ)=(VABAR/F-ZETA(J))*WE*4.0
      B(2,IE)=DVDT(J)*DTEMP/V(J)*WE*4.0
      G(2)=G(2)-B(2,IJ)*C(IJ,J)-B(2,IE)*C(IE,J)-B(2,IG)*C(IG,J)
      IF(J.EQ.NJ1) G(2)=G(2)-      DTEMP/V(J)*H2/2.0*ESEP*DVDT(J)
      TALL(2)=DABS(B(2,IG)*C(IG,J))
      IF(TALL(2).LT.DABS(B(2,IJ)*C(IJ,J))) TALL(2)=DABS(B(2,IJ)*C(IJ,J))
   60 IF((J.GT.NJ1).AND.(J.LT.NJ2)) GO TO 6
C     REMOVAL OF TRANSFER CURRENT
      BINV=1.0/B(6,IJ)
      G(6)      =BINV*G(6)
```

```
      DO 61 MN=1,N
   61 B(6,MN)=BINV*B(6,MN)
      DO 62 L=1,N
      G(L)=G(L)-G(6)     *B(L,IJ)
      IF(TALL(L).LT.DABS(G(6)*B(L,IJ))) TALL(L)=DABS(G(6)*B(L,IJ))
      DO 62 MN=1,N
   62 B(L,MN)=B(L,MN)-B(6,MN)*B(L,IJ)
      NERR=0
      DO  63 JW=1,N
      IF(DABS(G(JW)).LT.TALL(JW)*COEFF) G(JW)=0.0
      IF(G(JW).NE.0.0) NERR=NERR+1
      IF(JW.NE.5.OR.J.NE.NJ1) GO TO 63
      IF(TCD.EQ.0.0. AND .G(JW).NE.0.0) NERR=NERR-1
   63 CONTINUE
      NTERR=NTERR+NERR
      IF(G(4).NE.0.0.AND.JCOUNT.GT.1) WRITE(7,111)DIST(J),G(6),C(IN,J),
     1NONOFF(J)
      IF(IPOLAR.EQ.0 .AND. JCOUNT.LT.9) GO TO 6
      IF(JCOUNT.GE.MAXITS-9.AND.NERR.NE.0)WRITE(7,130)DIST(J),(G(K),K=1,
     1N),C(IN,J),NONOFF(J)
    6 IF(IPOLAR.NE.0) GO TO 64
      B(1,1)=B(4,II)
      B(1,2)=B(4,IN)
      A(1,1)=A(4,II)
      A(1,2)=A(4,IN)
      A(2,1)=A(5,II)
      A(2,2)=A(5,IN)
      D(1,1)=D(4,II)
      D(1,2)=D(4,IN)
      D(2,1)=D(5,II)
      D(2,2)=D(5,IN)
      B(2,1)=B(5,II)
      B(2,2)=B(5,IN)
      G(1)=G(4)
      G(2)=G(5)
      N=2
   64 CALL BAND(J)
      N=5
      IF(J.LT.NJ) GO TO 5
      DO 65 J=1,NJ
      IF(IPOLAR.NE.0) GO TO 65
      C(II,J)=C(1,J)
      C(IN,J)=C(2,J)
      C(1,J)=0.0
      C(2,J)=0.0
      C(3,J)=0.0
   65 CONTINUE
C     REEVALUATION OF MAIN VARIABLES.
      DO 67 J=1,NJ
      XD(J)=XD(J)+C(IX,J)
      C(II,J)=TCD
```

```
      DETA(J)=DETA(J)+      C(IN,J)
      DO 67 K=1,4
   67 C(K,J)=      C(K,J)+COLD(K,J)
      C(II,1)=0.0
      AVILIM=0.0
      DO 443 J=1,NJ1
      IF(C(IN,J)*COLD(IN,J).LT.0.0) NONOFF(J)=NONOFF(J)+1
      IF(C(IN,J)*COLD(IN,J).GT.0.0.AND.NONOFF(J).LT.3) NONOFF(J)=0
      H=H1
      IF(J.EQ.1 .OR. J.EQ.NJ1) H=H/2.0
      IF(J.GT.1) C(II,J)=C(II,J-1)
      IF(NONOF(J).NE.0) GO TO 445
      IF(Q(J).LE.1.0D-05.AND.C(IN,J).LE.0.0) GO TO 444
      IF(NONOFF(J).GE.3) GO TO 444
      IF(RBETA(J).LE.1.0D-11.AND.C(IN,J).GE.0.0) GO TO 444
      DO 442 K5=1,9
      ADDJ=DENT2*(C(IJ,J)+CKEEP(IJ,J))
      RINK=RINKEP(J)
      IF(W(J).LE.1.0) GO TO 439
      IF(C(IN,J).LT.0.0) GO TO438
      W(J)=0.0
      GO TO 440
  438 PIN5=PIN52
      PIN2=PIN22
      DFC=DFC2
      IF(W(J).GT.1.99) RINK=ROUTA(J)
      ROK=(ROUTA(J)**3+ADDJ/PIN52)**PIN1
      RIN3=RINK  **3-ADDJ/PIN2
      IF(RIN3.LT.0.0) GO TO 444
      RIN(J)=RIN3**PIN1
      TL=(1.0/RIN(J)  -1.0/ROK)/DFC
      GO TO 441
  439 IF(C(IN,J).GT.0.0) GO TO 440
      W(J)=2.0
      GO TO 438
  440 PIN5=PIN51
      PIN2=PIN21
      DFC=DFC1
      ROK=(ROUTA(J)**3+ADDJ/PIN51)**PIN1
      RBETA3=RBETA (J)**3-ADDJ/PIN2
      IF(RBETA3.LT.0.0) GO TO 444
      RBETAK  =RBETA3**PIN1
      RIN(J)=RBETAK
      TL=          (1.0/PIN2+1.0/PIN5)*(Q(J)+ADDJ)/(ROK**2+ROK
     1*RIN(J)+RIN(J)**2)/(DFC*ROK*RIN(J))
  441 SAREA=PIN4*ROK**2
      CR2=DEXP(TCA* C(IN,J))
      CR3=DEXP(-TCC*C(IN,J))
      CR14=CR2-CR3
      IF(DABS(C(IN,J)).GT.0.0005) GO TO 437
      CR14=C(IN,J)*(TCA+TCC+(TCA**3+TCC**3)*C(IN,J)**2/6.0)
```

```
437  EXCHIA=SAREA*CR1*(C(IX,J)/XAR)**GAM
     CR15=TL*CR2+1.0/EXCHIA
     CR16=CR15**2
     B(6,IJ)=1.0+CR14/CR16*DELT/6.0*(CR2/DFC*(1.0/PIN2/RIN(J)**4  +1.0
    1/PIN5/ROK      **4)-2.0/EXCHIA/ROK      **3/PIN5)
     C(IJ,J)=C(IJ,J)-(C(IJ,J)-CR14/CR15)/B(6,IJ)
     IF(K5.GT.4.AND.DABS(C(IJ,J)-CR14/CR15).LE.COEFF*DABS(CR14/CR15))
    1GOTO 445
 442 IF(DABS(C(IJ,J)-CR14/CR15).LE.COEFF*DABS(CR14/CR15)*.01) GO TO 445
     WRITE(7,111)DIST(J),C(IJ,J),C(IN,J),NONOFF(J)
     GO TO 445
 444 C(IJ,J)=0.0
 445 IF(TL.LT.1.0D-19) AVILIM=2.0*TCD
     IF(TL.LT.1.0D-19) GO TO 443
     AVILIM=AVILIM+H/TL
 443 C(II,J)=C(II,J)+H*C(IJ,J)
     IF(AVILIM.LT.TCD.AND.IPOLAR.EQ.0) GO TO 98
C    NORMALIZE THE CURRENT DISTRIBUTION IN THE POSITIVE ELECTRODE
 260   KOUNT=0
       POTDF=0.0
       POTREF=0.0
       CURLO=1.0E38
       CURHI=1.0E38
       CUR1=1.0E38
       POT1=0.0
 261   KOUNT = KOUNT+1
     C(II,NJ)=0.0
     DO 298 JB=NJ2,NJ
     J=NJ-JB+NJ2
       C(IN,J)=C(IN,J)+POTDF
       DETA(J)=DETA(J)+POTDF
     AIO1=AIO10*FRAC(J)
     AIO2=AIO20*FRAC(J)
     H=H3
     IF(J.EQ.NJ2 .OR. J.EQ.NJ) H=H/2.0
       IF (J.EQ.JSET) GO TO 293
       CJ1MIN = -DABS(TCD/H)
       IF(DELT.GT.0.0)
    1  CJ1MIN=-0.5*CJ1KEP(J)-EFES(J)/Y1/DELT
       IF(CJ1MIN.GT.0.5*CJ1KEP(J).AND.EFES(J).GT.0.0)
    1  CJ1MIN=CJ1KEP(J)*(1.0+DELT*Y1*CJ1KEP(J)/2.0/EFES(J))
       CJ1MAX = DABS(TCD/H)
       IF(DELT.GT.0.0)
    1  CJ1MAX=-0.5*CJ1KEP(J)-EX(J)/Y21/DELT
       IF(CJ1MAX.LT.0.5*CJ1KEP(J).AND.EX(J).GT.0.0)
    1  CJ1MAX=CJ1KEP(J)*(1.0+DELT*Y21*CJ1KEP(J)/2.0/EX(J))
C    KINETICS, CJ1
     ETAS=DETA(J)
       KEY=9
       IF(DABS(ETAS).GT.2.0)GO TO 8
     CJ1(J)=0.0D0
```

```
       CJ2(J)=0.0D0
       CJ3(J-NJ2M1)=0.0D0
       IF(EFES(J).EQ.0.0 .AND. ETAS.LT.0.0) GO TO 280
       IF(EX(J).EQ.0.0 .AND. ETAS.GT.0.0) GO TO 280
       EXPDIF=ETAS*((TC1+TC2)*(1.0D0+0.5D0*(TC1-TC2)*ETAS)
      1+(TC1**3+TC2**3)*ETAS**2/6.0D0)
       IF(DABS(TC1*ETAS).GT.0.004) EXPDIF=DEXP(TC1*ETAS)-DEXP(-TC2*ETAS)
       CJ1(J)=EXPDIF*AIO1*C(IX,J)
         NONOF(J)=0
         IF(CJ1(J).LE.CJ1MAX) GO TO 262
         CJ1(J)=CJ1MAX
         NONOF(J)=4
 262     IF(CJ1(J).GE.CJ1MIN)GO TO 280
         CJ1(J) = CJ1MIN
         NONOF(J)=1
 280     CJ2MIN=-DABS(TCD/H)
         IF(DELT.GT.0.0)
    1    CJ2MIN=-0.5*CJ2KEP(J)-EX(J)/Y22/DELT
         IF(CJ2MIN.GT.0.5*CJ2KEP(J).AND.EX(J).GT.0.0)
    1    CJ2MIN=CJ2KEP(J)*(1.0+DELT*Y22*CJ2KEP(J)/2.0/EX(J))
         CJ2MAX=DABS(TCD/H)
         IF(DELT.GT.0.0)
    1    CJ2MAX=-0.5*CJ2KEP(J)-ELI2S(J)/Y42/DELT
         IF(CJ2MAX.LT.0.5*CJ2KEP(J).AND.ELI2S(J).GT.0.0)
    1    CJ2MAX=CJ2KEP(J)*(1.0+DELT*Y42*CJ2KEP(J)/2.0/ELI2S(J))
C     KINETICS, CJ2 (INCLUDES CJ3)
       ETAS=C(IN,J)
         KEY=9
         IF(DABS(ETAS).GT.2.0)GO TO 8
         IF(IPHASE.EQ.0)GO TO 2801
       IF(EX(J).EQ.0.0 .AND. ETAS.LT.0.0) GO TO 293
 2801 IF(ELI2S(J).EQ.0.0 .AND. ETAS.GT.0.0) GO TO 293
         Q2=DABS(ELI2S(J)/Y42)-Q3(J)
         IF((1.0D0-Q2/Q2MAX).LT.1.0D-10.AND.ETAS.LT.0.0D0)GO TO 2802
         IF(DABS(Q2).GE.Q2MAX.AND.ETAS.LT.0.0D0)GO TO 2802
         IF(J.EQ.NSET)GO TO 2802
       EXPDIF=ETAS*((TC1+TC2)*(1.0D0+0.5D0*(TC1-TC2)*ETAS)
      1+(TC1**3+TC2**3)*ETAS**2/6.0D0)
       IF(DABS(TC1*ETAS).GT.0.004) EXPDIF=DEXP(TC1*ETAS)-DEXP(-TC2*ETAS)
       CJ2(J)=EXPDIF*AIO2*C(IX,J)
 2802    CALL NRAF(C(IN,J),Q3(J),CJ3KEP(J),TC1,TC2,DENT2,C(IX,J),AIO2,
    1    CCJ3,SLOPEP,ETAS3)
         IF(EX(J).EQ.0.0D0.AND.ETAS3.LT.0.0D0)GO TO 293
         CJ3(J-NJ2M1)=CCJ3
         CJ2(J)=CJ2(J)+CCJ3
         NONOF(J)=0
         IF(CJ2(J).LE.CJ2MAX) GO TO 263
         CJ2(J)=CJ2MAX
         NONOF(J)=2
 263     IF(CJ2(J).GE.CJ2MIN) GO TO 293
         CJ2(J)=CJ2MIN
```

```
      CJ3(J-NJ2M1)=CJ2(J)
      NONOF(J)=3
  293 C(IJ,J)=CJ1(J)+CJ2(J)
      IF(J.EQ.JSET.AND.NONOF(J).EQ.3)CJ3(J-NJ2M1)=CJ2(J)
  298 C(II,J-1)=C(II,J)-H*C(IJ,J)
      CURERR=C(II,NJ2-1)-TCD
      IF(JCOUNT.GT.6.OR.NTERR.EQ.0)GO TO 270
      IF(DABS(CURERR).LT.1.0D-6*DABS(TCD))GO TO 270
      KEY=8
      IF(KOUNT.GT.20)GO TO 8
      IF(DABS(CURERR).LT.DABS(CUR1))GO TO 264
      CUR2=CURERR
      POT2=POTREF
      GO TO 265
  264 CUR2=CUR1
      POT2=POT1
      CUR1=CURERR
      POT1=POTREF
  265 IF(KOUNT.NE.1.AND.CUR2.NE.CUR1)
     1 POTDF=POT1-POTREF-CUR1*(POT2-POT1)/(CUR2-CUR1)
      IF(CUR2.EQ.CUR1.AND.CURERR.GT.0.0)POTDF=0.02
      IF(CUR2.EQ.CUR1.AND.CURERR.LT.0.0)POTDF=-0.02
      IF(POTDF.GT.0.02)POTDF=0.02
      IF(POTDF.LT.-0.02)POTDF=-0.02
      IF(CURERR.GT.0.0.OR.DABS(CURERR).GT.DABS(CURLO))GO TO 266
      IF(KOUNT.EQ.1)POTDF=-1.0D-3
      CURLO=CURERR
      POTLO=POTREF
  266 IF(CURERR.LT.0.0.OR.DABS(CURERR).GT.DABS(CURHI))GO TO 267
      IF(KOUNT.EQ.1)POTDF=1.0D-3
      CURHI=CURERR
      POTHI=POTREF
  267 IF(CURHI.GT.9.0E37.OR.CURLO.GT.9.0E37)GO TO 268
      IF((POTREF+POTDF-POTHI)*(POTREF+POTDF-POTLO).LT.0.0)GO TO 268
      POTDF=0.5*(POTHI+POTLO)-POTREF
  268 POTREF=POTREF+POTDF
      GO TO 261
  270 CONTINUE
      IF(JCOUNT.EQ.0)GO TO 4
C     CALCULATE TOTAL CELL VOLTAGE
      PHI1=0.0
      DO 68 J=1,NJ1M1
   68 PHI1=PHI1+0.5*(SIGINV(J)+SIGINV(J+1))*(C(II,J)-TCD)*H1
      RG=0.0
      DO 69JB=NJ1P1,NJ2M1
      RG=RG+C(II,JB)/CON(JB)/ESEPPN+(VAL1+VAL2*C(IX,JB))*T*DLNAC(JB)*
     1(C(IX,JB+1)-C(IX,JB-1))*0.5/H2/(1.0-C(IX,JB))/C(IX,JB)
   69 CONTINUE
      PHI2=-H2*(RG+.5*(C(II,NJ1)/CON(NJ1)/ESEPPN+(VAL1+VAL2*C(IX,NJ1))*
     1T*DLNAC(NJ1)*(4.0*C(IX,NJ1+1)-3.0*C(IX,NJ1)-C(IX,NJ1+2))*0.5/H2/
     1(1.0-C(IX,NJ1))/
```

```
      1C(IX,NJ1)+C(II,NJ2)/CON(NJ2)/ESEPPN+(VAL1+VAL2*C(IX,NJ2))*T*
      1DLNAC(NJ2)*(-4.0*C(IX,NJ2-1)+3.0*C(IX,NJ2)+C(IX,NJ2-2))*0.5/H2/
      1(1.0-C(IX,NJ2))/C(IX,NJ2)))
       PHI3=0.0
         TCD11 = 0.
         TCD2  = 0.
C      CALCULATE AVERAGE CONCENTRATIONS OF LICL AND KCL
       DO 70 J=NJ2,NJM1
         H = H3
         IF(J.EQ.NJ2)H = H/2.
         TCD11 = TCD11 - CJ1(J)*H
         TCD2  = TCD2  - CJ2(J)*H
   70 PHI3=PHI3+0.5*(SIGINV(J)+SIGINV(J+1))*(C(II,J)-TCD)*H3
         TCD11 = TCD11 - CJ1(NJ)*H3/2.
         TCD2  = TCD2  - CJ2(NJ)*H3/2.
         XAOV=0.
         XAUN=0.
         DO 560 J=1,NJ1
         OVER=H1*C(IE,J)*C(IX,J)/V(J)
         IF(J.EQ.1.OR.J.EQ.NJ1)OVER = OVER/2.
         UNDER = OVER/C(IX,J)
         XAOV = XAOV + OVER
         XAUN = XAUN + UNDER
  560    CONTINUE
         DO 561 J=NJ1,NJ2
         OVER=H2*C(IE,J)*C(IX,J)/V(J)
         IF(J.EQ.NJ1.OR.J.EQ.NJ2)OVER = OVER/2.
         UNDER = OVER/C(IX,J)
         XAOV = XAOV + OVER
         XAUN = XAUN + UNDER
  561    CONTINUE
         DO 562 J=NJ2,NJ
         OVER=H3*C(IE,J)*C(IX,J)/V(J)
         IF(J.EQ.NJ2.OR.J.EQ.NJ)OVER = OVER/2.
         UNDER = OVER/C(IX,J)
         XAOV = XAOV + OVER
         XAUN = XAUN + UNDER
  562    CONTINUE
         XAOV = XAOV + VOVERA*C(IX,NJ2)/V(NJ2)
         XAUN = XAUN + VOVERA/V(NJ2)
         AVGXA = XAOV/XAUN
       PHI4=-TCD*WIDTH/CON(NJ2)
       TCV=PHI1+PHI2+PHI3+PHI4      +UJO+C(IN,NJ2 )-C(IN,NJ1)-RGRID*TCD
C      CALCULATE ENTHALPY OF MIXING TERM FOR THE ENERGY BALANCE, CRXNDT
         CALL CORXN(1,NJ1,V,C,H1,T,AVGXA,CRXN1)
         CALL CORXN(NJ1,NJ2,V,C,H2,T,AVGXA,CRXN2)
         CALL CORXN(NJ2,NJ,V,C,H3,T,AVGXA,CRXN4)
         XA=C(1,NJ2)
         XB=1.-C(1,NJ2)
         TBASE=450.+273.15
       ACA=(0.52628*XB-1.2738*XB**2-2.9783*XB**3)*TBASE/T
```

```
      ACB=(-0.52628*XA-5.7413*XA**2+2.9783*XA**3-0.52628*DLOG(DABS(XB)))
     1*TBASE/T
         XA=AVGXA
         XB=1.-AVGXA
       ACAV=(0.52628*XB-1.2738*XB**2-2.9783*XB**3)*TBASE/T
       ACBAV=(-0.52628*XA-
     15.7413*XA**2+2.9783*XA**3-0.52628*DLOG(DABS(XB)))
     1*TBASE/T
         CRXN3=VOVERA*8.3143*T/V(NJ2)*((ACA-ACAV)*C(1,NJ2)
     1+(1.-C(1,NJ2))*(ACB-ACBAV))
         CRXN=CRXN1+CRXN2+CRXN3+CRXN4
         IF(DELT.NE.0.0)CRXNDT=(CRXN-CRXNOL)/DELT
         CRXNDT = 0.
       IF(IPOLAR.EQ.0) GO TO  7
       IF(DELT.EQ.0.0)
     1DTEMP=0.
C    1  DTEMP=(TCD11*AP1+TCD2*AP2-TCD*TCV-CHT*(T-TAMB))/CPMA
       DO  74 M=1,NJ
       IF(M-NJ2) 71,72,73
   71 VSTAR(M)=0.5*(V(M)+V(M+1))*(C(IG,M)-0.5/F*C(II,M))
       GOTO 74
   72 VSTAR(M)=C(IG,M)
       GO TO 74
   73 VSTAR(M)=0.5*(V(M)+V(M-1))*(C(IG,M)-0.5/F*C(II,M-1))
   74 CONTINUE
C     CALCULATE NEW RESERVOIR VOLUME (CM3/CM2 SEPARATOR)
       VOVERA=C(IG,NJ2)
C     CONSIDER PRECIPITATION OF LICL OR KCL
       DO 333 J=1,NJ
       DEPS=EPKKEP(J)+EPLKEP(J)+CKEEP(IE,J)-C(IE,J)+0.5*DELT *(ZETA(J)
     1*C(IJ,J)+ZETALD(J)*CKEEP(IJ,J))
       IF(EPL(J).LE.0.0) GO TO 330
       EPL(J)=DEPS
       IF(EPL(J).GT.0.0) GO TO 333
       WRITE (7,307)J,EPL(J),C(IX,J)
       C(IX,J)=(C(IE,J)*C(IX,J)+EPL(J))/(C(IE,J)+EPL(J))
       XD(J)=C(IX,J)-XAINIT
       C(IE,J)=C(IE,J)+EPL(J)
       EPL(J)=0.0
       GO TO 333
  307 FORMAT (25HPRECIPITATION CHECK AT J= ,I5, 43HINDICATES A NEGATIVE
     1VALUE OF PRECIPITATE = , F12.6, 22HFOR A MOLE FRACTION OF , F12.6)
  330 IF(EPK(J).LE.0.0) GO TO 331
       EPK(J)=DEPS
       IF(EPK(J).GT.0.0) GO TO 333
       WRITE (7,307)J,EPK(J),C(IX,J)
       C(IX,J)=C(IE,J)*C(IX,J)/(C(IE,J)+EPK(J))
       XD(J)=C(IX,J)-XAINIT
       C(IE,J)=C(IE,J)+EPK(J)
       EPK(J)=0.0
       GO TO 333
```

```
  331 IF(C(IX,J).LT.XASL) GO TO 332
      IF(JCOUNT.NE.3) GO TO 333
      WRITE (7,3077) J,EPL(J),C(IX,J)
      JPTERR=1
 3077 FORMAT ( 30HPRECIPITATION INDICATED AT J= , I5, 11HWITH EPL = ,
     1 F12.6, 9HAND XA = , F12.6)
      EPL(J)=C(IE,J)*(XASL-C(IX,J))/(XASL-1.0)
      XD(J)=XASL-XAINIT
      C(IE,J)=C(IE,J)-EPL(J)
      C(IX,J)=XASL
      GO TO 333
  332 IF(C(IX,J).GT.XASK) GO TO 333
      IF(JCOUNT.NE.3) GO TO 333
      WRITE (7,3078) J,EPK(J),C(IX,J)
      JPTERR=1
 3078 FORMAT ( 30HPRECIPITATION INDICATED AT J= , I15, 11HWITH EPK = ,
     1 F12.6, 9HAND XA = , F12.6)
      EPK(J)=C(IE,J)*(XASK-C(IX,J))/XASK
      XD(J)=XASK-XAINIT
      C(IE,J)=C(IE,J)-EPK(J)
      C(IX,J)=XASK
  333 CONTINUE
      KEY=4
      DO  75 M4=1,NJ
      IF(C(IE,M4).GT.0.0) GOTO 75
      WRITE (7,111),DIST(M4),C(IE,M4),C(IJ,M4),JCOUNT
      GO TO 8
   75 CONTINUE
C     CONVERGENCE TEST.
 7    DO 76 K=1,NJ
      IF(DABS(C(IN,K)-COLD(IN,K)).LT.1.0D-29.AND.TCD.EQ.0.0) GO TO 76
      IF(DABS(C(IN,K)-COLD(IN,K)).GT.CONV*DABS(DETA(K))) GO TO 77
      IF(DABS(C(IN,K)-COLD(IN,K)).GT.CONV*DABS(C(IN,K))) GOTO 77
   76 CONTINUE
      KEY=10
      DO 334 J=NJ2,NJ
      Q2K=DABS(ELI2S(J)/Y42+DENT2*(CJ2(J)+CJ2KEP(J)))
      Q3K=Q3(J)-DENT2*(CJ3(J-NJ2M1)+CJ3KEP(J))
      IF(Q3K.LT.0.0D0)Q3K=0.0D0
      Q2K=Q2K-Q3K
      IF((1.0D0-Q2K/Q2MAX).LT.-1.0D-10)GO TO 8
  334    CONTINUE
      GOTO 10
   77 IF(JCOUNT.GE.7)WRITE(7,127) K,DIST(K),C(IX,K),C(IE,K),VSTAR(K),
     1C(II,K),C(IJ,K),C(IN,K),CJ1(K)
      IF(JCOUNT.LT.MAXITS) GOTO 4
      IF(IPOLAR.NE.0) GO TO 59
      IF(TCD.EQ.0.0.AND.JCOUNT.LT.23)GOTO 4
   59 WRITE (7,135)TIME
      WRITE (7,105)
      WRITE(7,118)(DIST(J),C(IX,J),C(IE,J),VSTAR(J),C(II,J),C(IJ,J),
```

```
        1C(IN,J),CJ1(J),J=    1,NJ )
        KEY=6
C       HALVE TIME STEP
  8     WRITE (7,134)KEY
        JSET=0
        TIME=TIME-DELT
        T=T-DELT*DTEMP
        DELT=0.5*DELT
        IF(KEY.EQ.1.AND.DELT.GE.0.005)
        1GO TO 9
        JSPOT=JSPOT+1
  9     DO  78 M2=1,NJ
           IF(KEY.EQ.5)FRAC(M2)=1.0D0
        IF(KEY.EQ.5.AND.EPKKEP(M2).NE.0.0)FRAC(M2)=
        11.0D0-(EPKKEP(M2)/(CKEEP(IE,M2)+EPKKEP(M2)))**PREPP
        IF(KEY.EQ.5.AND.EPLKEP(M2).NE.0.0)FRAC(M2)=
        11.0D0-(EPLKEP(M2)/(CKEEP(IE,M2)+EPLKEP(M2)))**PREPP
           IF(KEY.EQ.5)Q(M2)=Q(M2)-DENT2*(C(IJ,M2)+CKEEP(IJ,M2))
        XD(M2)=XDKEEP(M2)
        DETA(M2)=CKEEP(IN,M2)
        IF(KEY.NE.-1) GO TO 450
        IF(M2.LT.NJ1.AND.C(IJ,M2).LT.0.0) WRITE (7,118)DIST(M2),C(II,M2),
        1C(IJ,M2),C(IN,M2),Q(M2)
 450    CONTINUE
        NONOF(M2)=0
           ZETA(M2)=ZETALD(M2)
        EPL(M2)=EPLKEP(M2)
        EPK(M2)=EPKKEP(M2)
        IF(M2.GE.NJ2)DETA(M2)=CKEEP(IN,M2)+DSEPOT
        CJ1(M2)=CJ1KEP(M2)
        IF(M2.LE.NJ1) RIN(M2)=RINKEP(M2)
        IF(M2.GE.NJ2)CJ2(M2)=CJ2KEP(M2)
        DO 78 M1=1,JP
  78    C(M1,M2)=CKEEP(M1,M2)
        IF(IPOLAR.EQ.0) GO TO 3
        IF(DELT.LT.DTMIN) GO TO 14
        IF(KEY.EQ.6) KEY6=KEY6+1
        IF(KEY6.EQ.9) GO TO 14
        JCOUNT=0
        GO TO 2
C       CONVERGED SOLUTION - PRINT RESULTS
 10     NERR=0
        DO 435 J=1,NJ1
        IF(NERR.GT.0) GO TO 435
        IF(NONOFF(J).LT.3.OR.C(IN,J).LT.0.0) GO TO 435
        NERR=NERR+1
        NONOFF(J)=0
 435    CONTINUE
        IF(NERR.GT.0) MAXITS=JCOUNT+15
           IF(NERR.GT.0.AND.MAXITS.LT.200) GO TO 4
        IF(JPTERR.NE.0) GO TO 4
```

```
      IF(IPOLAR.EQ.0) GO TO 12
      WRITE(7,103)
1031  FORMAT(13HCONVERGED AT , I4,21HITERATIONS FOR TIME =, G12.6,3HSEC
     1,14HCELL VOLTAGE = G12.6)
      NTIME=NTIME+1
      WRITE(7,104)H1,H2,H3,NJ,JCOUNT,CONV,TIME
      WRITE(7,105)
      JPRINT=1
      DO  80 J=1,NJ
      IF(EPK(J).NE.0.0)FRAC(J)=1.0D0-(EPK(J)/(C(IE,J)+EPK(J)))**PREPP
      IF(EPL(J).NE.0.0)FRAC(J)=1.0D0-(EPL(J)/(C(IE,J)+EPL(J)))**PREPP
      Q(J)=Q    (J)+DENT2*(C(IJ,J)+CKEEP(IJ,J))
      IF(J.EQ.NJ)GOTO 791
      IF(C(IN,J).GT.C(IN,J+1)) GOTO 79
791   IF(J.EQ.1) GOTO 790
      IF(C(IN,J-1).GT.C(IN,J)) GOTO 79
790   IF(J.EQ.JPRINT.OR.J.EQ.NJ) GO TO 79
      IF(J.EQ.NJ1.OR.J.EQ.NJ2) GO TO 79
      IF(EPL(J).EQ.0.0.AND.EPK(J).EQ.0.0) GO TO 80
79    IF(J.GT.(NJ1+NJ2)/2)GO TO 800
      WRITE(7,118)DIST(J),C(IX,J),C(IE,J),VSTAR(J),C(II,J),C(IJ,J)
     1,C(IN,J)
     1,CJ1(J)
      GO TO 801
800   WRITE(7,118)DIST(J),C(IX,J),C(IE,J),CJ3(J-NJ2M1),C(II,J),C(IJ,J)
     1,C(IN,J)
     1,CJ1(J)
801   JPRINT=J+IPRINT
80    CONTINUE
C     STATEMENTS TO PRINT OUT TERMS IN THE OHM'S LAW EQUATION
C     WRITE(7,142)(DIST(J),C(IJ,J),J=NJ2,NJM1)
C     WRITE(7,142)(DIST(J),(DETA(J+1)-DETA(J))/H3/TCD/0.5/
C     1(1.0/(CON(J)*C(IE,J)**FACTOR)+1.0/(CON(J+1)*C(IE,J+1)**FACTOR)+
C     1SIGINV(J)+SIGINV(J+1)),J=NJ2,NJM1)
C     WRITE(7,142)(DIST(J),C(II,J)/TCD
C     1/(1.0+((SIGINV(J)+SIGINV(J+1))/
C     1(1.0/(CON(J)*C(IE,J)**FACTOR)+1.0/(CON(J+1)*C(IE,J+1)**FACTOR))))
C     1,J=NJ2,NJM1)
C     WRITE(7,142)(DIST(J),(C(II,J)/TCD-1.0)/
C     1(1.0+((1.0/(CON(J)*C(IE,J)**FACTOR)
C     1+1.0/(CON(J+1)*C(IE,J+1)**FACTOR))
C     1/(SIGINV(J)+SIGINV(J+1))))
C     1,J=NJ2,NJM1)
C     WRITE(7,142)(DIST(J),(DETA(J+1)-DETA(J))/H3/TCD/0.5/
C     1(1.0/(CON(J)*C(IE,J)**FACTOR)+1.0/(CON(J+1)*C(IE,J+1)**FACTOR)+
C     1SIGINV(J)+SIGINV(J+1))-
C     1C(II,J)/TCD
C     1+(SIGINV(J)+SIGINV(J+1))/
C     1(1.0/(CON(J)*C(IE,J)**FACTOR)+1.0/(CON(J+1)*C(IE,J+1)**FACTOR)+
C     1SIGINV(J)+SIGINV(J+1)),J=NJ2,NJM1)
      IF(TCD.LE.0.0) GO TO 83
```

```
C       CHECK RESULTS
        DO 82 K=NJ2,NJ
        IF(DELT.EQ.0.0D0)CJ3KEP(K)=CJ3(K-NJ2M1)
        IF(C(IJ,K).LE.0.0) GO TO 82
        KEY=5
        IF(CJ2(K-1).LT.0.0.AND.DELT.GT.DTCUT) GOTO 882
        KEY5=KEY5+1
        IF(KEY5.GE.2.OR.DELT.LE.60.0) GO TO 82
    882 WRITE(7,118)(DIST(M),C(IX,M),C(IE,M),C(IG,M),C(II,M),C(IJ,M),
       1C(IN,M),CJ1(M),M=K-1,K+1)
        GO TO 8
     82 CONTINUE
C       CALCULATE PARAMETERS NEEDED AT NEXT TIME STEP
     83 IF(DELT.EQ.0) GO TO 11
        IF(KSET.LT.0) KSET=-KSET
        DO 84 J=1,NJ1
        ADDJ=(C(IJ,J)+CKEEP(IJ,J))*DENT2
        PIN5=PIN51
        DFC=DFC1
        IF(C(IJ,J).GT.0.0) GO TO 81
        DFC=DFC2
        PIN5=PIN52
     81 ROUTA(J)=(ROUTA(J)**3+ADDJ/PIN5)**PIN1
        IF(C(IJ,J).GE.0.0) RBETA(J)=RIN(J)
        ESUM(J)=C(IE,J)+PIN43*ROUTA(J)**3+EPK(J)+EPL(J)+ECCN
        W(J)=1.0-C(IJ,J)*(1.0/RIN(J)   -1.0/ROUTA(J))/DFC
        IF(W(J).LT.0.0) W(J)=0.0
        IF(J.NE.JSET) GO TO 84
        IF(KSET.EQ.2) Q(J)=0.0
        IF(KSET.EQ.1) RBETA(J)=0.0
     84 CONTINUE
C       CALCULATE VOLUME FRACTIONS OF PHASES IN THE POSITIVE ELECTRODE
        DO 299 J=NJ2 ,NJ
        CADD1=CJ1(J)+CJ1KEP(J)
        CADD2=CJ2(J)+CJ2KEP(J)
        EFES(J)=EFES  (J)+Y1 *CADD1*DENT2
           IF(EFES(J).LT.0.0)EFES(J)=0.0D0
        EFE(J)=EFE    (J)+(Y31*CADD1+Y32*CADD2)*DENT2
           IF(EFE(J).LT.0.0)EFE(J)=0.0D0
        ELI2S(J)=ELI2S (J)+Y42*DENT2*CADD2
           IF(ELI2S(J).LT.0.0)ELI2S(J)=0.0D0
        EX(J)=EX    (J)+(Y21*CADD1+Y22*CADD2)*DENT2
           IF(EX(J).LT.0.0)EX(J)=0.0D0
           IF(CJ2(J).EQ.0.0D0)Q3(J)=Q3(J)-DENT2*CJ3KEP(J)
           IF(CJ2(J).EQ.0.0D0.AND.Q3(J).LT.0.0D0)Q3(J)=0.0D0
           IF(CJ2(J).EQ.0.0D0)CJ3KEP(J)=0.0D0
           IF(CJ2(J).EQ.0.0D0)GO TO 2991
    511    FORMAT(1X,I3,7(1X,G14.7))
           Q3(J)=Q3(J)-DENT2*(CJ3(J-NJ2M1)+CJ3KEP(J))
           IF(Q3(J).LT.0.0D0)CJ3(J-NJ2M1)=0.0D0
           IF(Q3(J).LT.0.0D0.OR.ELI2S(J).EQ.0.0D0)Q3(J)=0.0D0
```

```
         CJ3KEP(J)=CJ3(J-NJ2M1)
 2991    CONTINUE
      IF(J.NE.JSET) GO TO 299
      IF(KSET.EQ.1) EFES(J)=0.0D0
      IF(KSET.EQ.2) ELI2S(J)=0.0D0
      IF(KSET.EQ.3 .OR. KSET.EQ.4) EX(J)=0.0D0
      IF(KSET.EQ.4) EFE(J)=0.0D0
        IF(ELI2S(J).EQ.0.0D0)Q3(J)=0.0D0
  299 ESUM(J)=C(IE,J)+EPL(J)+EPK(J)+ELI2S(J)+EFES(J)+EX(J)+EFE(J)+ECCP
C     PRINT MORE RESULTS
 11   DO 87 J=NJ2,NJM1
      IF(CJ1(J).NE.0.0.OR.CJ1(J+1).EQ.0.0) GO TO 86
 85   WRITE(7,137)
      WRITE(7,118)(DIST(K),C(IX,K),C(IE,K),VSTAR(K),C(II,K
     1),C(
     1IJ,K),C(IN,K),CJ1(K),K=J,J+1)
      GO TO 87
 86   IF(CJ2(J).NE.0.0.OR.CJ2(J+1).EQ.0.0) GO TO 87
      GO TO 85
 87   CONTINUE
      WRITE(7,132)
      JPRINT =1
      DO  91 J=1,NJ
      IF(J.EQ.JPRINT.OR.J.EQ.NJ) GO TO 88
      IF(J.EQ.NJ1.OR.J.EQ.NJ2) GO TO 88
      IF(EPL(J).EQ.0.0.AND.EPK(J).EQ.0.0) GO TO 91
 88   IF(J.GT.(NJ1+NJ2)/2)  GO TO 89
      WRITE(7,118)DIST(J),C(IG,J),Q(J),ESUM(J),RIN(J)   ,EPK(J),ROUTA(J),
     1W(J)
      GO TO 90
 89   WRITE(7,118)DIST(J),Q3(J),Q(J),ESUM(J),EPK(J),ELI2S(J),EX(J)
     1,EFES(J)
 90   JPRINT=J+IPRINT
 91   CONTINUE
      DO 94 J=NJ2,NJM1
      IF(CJ1(J).NE.0.0.OR.CJ1(J+1).EQ.0.0) GO TO 93
 92   WRITE(7,137)
      WRITE(7,118)(DIST(K),Q3(K),Q(K),ESUM(K),EPK(K)
     1,ELI2S(K)
     1,EX(K),EFES(K),K=J,J+1)
      GO TO 94
 93   IF(CJ2(J).NE.0.0.OR.CJ2(J+1).EQ.0.0) GO TO 94
      GO TO 92
 94   CONTINUE
C     RESET PARAMETERS AT OLD TIME
C     TEST OF ELECTROLYTE MATERIAL BALANCE
      KEY6=0
      H=H1
      FLUXP=0.0
      FGP=0.0
      RSUM=0.0
```

```
      VSUM=0.0
      F3NP=C(IE,1)**FACTOR*DIFUSN(1)/V(1)
      DIFKCL=0.0
      DIFLCL=0.0
      DO 300 J=1,NJ
      FLUXM=FLUXP
      F3N=F3NP
      FGM=FGP
      IF(DELT.EQ.0.0) GO TO 301
      R1KEP   =R1(J)
      R2KEP   =R2(J)
      RV1KEP=RV1(J)
      RV2KEP=RV2(J)
  301 JE=J
      WE=H/4.0
      IF(J.NE.NJ) GO TO 302
      WE=WE/2.0
      FGP=0.0
      FLUXP=0.0
      JE=J-1
      GO TO 305
  302 F3NP=C(IE,J+1)**FACTOR*DIFUSN(J+1)/V(J+1)
      JGP=J
      IF(J.GE.NJ2) JGP=J+1
      IF(J.EQ.1) JE=J+1
      IF(J.EQ.1) WE=WE/2.0
      IF(J.EQ.NJ2-1) F3NP=F3NP*(C(IE,J)/C(IE,J+1))**FACTOR
      IF(J.NE.NJ1) GO TO 303
      JE=J-1
      WE=H1/8.0
      H=H2
       F3N=F3N*(C(IE,J+1)/C(IE,J))**FACTOR
      GO TO 304
  303 IF(J.NE.NJ2) GO TO 304
      JE=JE+1
      WE=H3/8.0
      H=H3
      F3N=F3N*(C(IE,J)/C(IE,J-1))**FACTOR
  304 FLUXP=0.5*(C(IX,J+1)+C(IX,J))*C(IG,JGP)-0.5*(F3NP+F3N)
     1*(XD(J+1)-XD(J))/H
      FGP=C(IG,JGP)
  305 R1(J)=FLUXM-FLUXP+WE/F*4.0*C(IJ,J)
      R2(J)=WE*C(IE,J)*(3.0*C(IX,J)/V(J)+C(IX,JE)/V(JE))
     1+WE/VLICL*4.0*EPL(J)
      RV1(J)=FGM-FGP+WE/F*4.0*C(IJ,J)
      RV2(J)=WE*C(IE,J)*(3.0/V(J)+1.0/V(JE))
     1+WE*4.0*(EPL(J)/VLICL+EPK(J)/VKCL)
      IF(J.EQ.NJ1) RV2(J)=RV2(J)+ESEP*H2/8.*(3./V(J)+1./V(J+1))
      IF(J.EQ.NJ2) RV2(J)=RV2(J)+ESEP*H2/8.*(3./V(J)+1./V(J-1))+C(IG,J)/
     1V(J)
      IF(J.EQ.NJ1) R2(J)=R2(J)+ESEP*H2/8.*(3.0*C(IX,J)/V(J)+C(IX,J+1)/V(
```

```
     1J+1))
      IF(J.EQ.NJ2) R2(J)=R2(J)+ESEP*H2/8.*(3.*C(IX,J)/V(J)+C(IX,J-1)/V(J
     1-1))+C(IG,J)*C(IX,J)/V(J)
      IF(DELT.EQ.0.0  ) GO TO 300
      R3=(R2(J)-R2KEP)/DELT
     .RDIF=R3-0.5*(R1(J)+R1KEP   )
      RV3=(RV2(J)-RV2KEP)/DELT
      VDIF=RV3-0.5*(RV1(J)+RV1KEP)
      IF(DABS(RDIF).GT.1.0D-11.OR.DABS(VDIF).GT.1.0D-11)WRITE(7,118)
     1,DIST(J)
     1,RDIF,VDIF
      RSUM=RSUM+RDIF
      VSUM=VSUM+VDIF
      IF(J.EQ.NJ) WRITE (7,138)RSUM,VSUM
      IF(DELT.EQ.0.0) GO TO 300
      IF(J.GT.NJ1) GO TO 310
      IF(DABS(EPL(J)-EPLKEP(J)).LT.1.0D-14) GO TO 300
      RU=1.0
      IF(J.EQ.1.OR.J.EQ.NJ1) RU=0.5
      DIFLCL=RU*(EPL(J)-EPLKEP(J))+DIFLCL
  310 IF(J.LT.NJ2) GO TO 300
      IF(DABS(EPK(J)-EPKKEP(J)).LT.1.0D-14) GO TO 300
      RN=1.0
      IF(J.EQ.NJ2.OR.J.EQ.NJ) RN=0.5
      DIFKCL=RN*(EPK(J)-EPKKEP(J))+
     1DIFKCL
  300 CONTINUE
      SLN=0.0D0
      CAPN=0.0D0
      CAPP=0.0D0
      CKCAPP=0.0D0
C     ENERGY BALANCE
      IF(DELT.NE.0.0) DIFKCL=DIFKCL*H3*HFUSEK/VKCL/DELT
      IF(DELT.NE.0.0) DIFLCL=DIFLCL*H1*HFUSEL/VLICL/DELT
      HTLOSS=CHT*(T-TAMB)
        HTGAIN = TCD11*AP1 + TCD2*AP2 -TCD*TCV
        IF(DELT.EQ.0.0)CRXNDT=0.0
      DTEMP=(HTGAIN+DIFKCL+DIFLCL-HTLOSS+CRXNDT)/CPMA
        CRXNOL=CRXN
C     FOR ISOTHERMAL OPERATION, DTEMP=0
      DTEMP=0.
      WRITE(7,125)T,HTLOSS,HTGAIN,DIFKCL,DIFLCL
C     CHECK TOTAL NO. OF MOLS LI AND K, ELECTROLYTE AND SOLID PHASES.
C     CALCULATE UTILIZATION 3 DIFFERENT WAYS, UTIL1, UTIL2, AND UTIL3.
      AMTLI=0.0
      AMTK=0.0
      SOLIDL=0.0
      DO  95 M=1,NJ
      H=H2
      IF(M.LE.NJ1) H=H1
      IF(M.GE.NJ2) H=H3
```

```
      WM=H*C(IE,M)
      IF(M.EQ.1 .OR. M.EQ.NJ) WM=0.375*WM
      IF(M.EQ.NJ1-1 .OR. M.EQ.NJ-1) WM=WM+0.125*H*C(IE,M+1)
      IF(M.EQ.NJ2-1 .OR. M.EQ.NJ1+1) WM=WM+0.125*H2*ESEP
      IF(M.EQ.2 .OR. M.EQ.NJ2+1) WM=WM+0.125*H*C(IE,M-1)
      IF(M.EQ.NJ1) WM=0.375*(H1*C(IE,M)+H2*ESEP)
      IF(M.EQ.NJ2) WM=0.375*(H3*C(IE,M)+H2*ESEP)+C(IG,M)
      IF(M.EQ.NJ1 .OR. M.EQ.NJ2) H=H/2.0
      IF(M.EQ.1 .OR. M.EQ.NJ) H=H/2.0
      IF(M.GE.NJ2) CAPP=CAPP+H*Q(M)
      IF(M.GE.NJ2) Q1=DABS((EFESO-EFES(M))/Y1)
      IF(M.GE.NJ2.AND.Q1.GT.Q1MAX) Q1=Q1MAX
      IF(M.GE.NJ2) QQ3=Q3(M)
      IF(M.GE.NJ2.AND.QQ3.GT.Q3MAX) QQ3=Q3MAX
      IF(M.GE.NJ2) Q2=DABS(ELI2S(M)/Y42)-QQ3
      IF(M.GE.NJ2.AND.Q2.GT.Q2MAX) Q2=Q2MAX
      IF(M.GE.NJ2)CKCAPP=CKCAPP+H*(Q1+Q2+QQ3)
      IF(M.GE.NJ2) SOLIDL=SOLIDL+EONSB*H*(ELI2S(M)*(1.0/SS(4,2)
     1+SS(3,2)/SS(3,1)/SS(4,2))/VLI2S+EX(M)/SS(3,1)/VX)
      AMTLI=AMTLI+WM*C(IX,M)/V(M)+EPL(M)*H/VLICL      .
      IF(M.GT.NJ1) GO TO 95
      CAPN=CAPN+H*Q(M)
      SLN=SLN+H *(U1*RBETA(M)**3+U2*ROUTA(M)**3+U3)
   95 AMTK=AMTK+WM*(1.0-C(IX,M))/V(M)+EPK(M)*H/VKCL
      IF(SLNO.NE.0.0) GO TO 96
      SLNO=SLN
      SLPO=SOLIDL
      AMTLIO=AMTLI
      AMTKO=AMTK
      WRITE (7,136)  SLNO,SLPO,AMTLIO,AMTKO
   96 FAMTLI=AMTLI/AMTLIO-1.0
      FAMTK=AMTK/AMTKO-1.0
      FSL=(SLN+SOLIDL)/(SLNO+SLPO)-1.0
      UTIL1=-TIME*TCD/QMAXB/(NJ-NJ2)/H3
      UTIL2=-CAPP/QMAXB/(NJ-NJ2)/H3
      UTIL3=-CKCAPP/QMAXB/(NJ-NJ2)/H3
      WRITE(7,126)JCOUNT,FAMTLI,FAMTK,SOLIDL,XASL,XASK,SLN,FSL,
     1CAPN,CAPP,UTIL1,UTIL3
      WRITE(7,117)
      WRITE(7,116)TCD,TCV,PHI2,PHI3,C(IN,NJ1),C(IN,NJ2),VOVERA
C     WRITE A RESTART FILE (TAPE 8) EVERY FIVE TIME STEPS
      IF(MOD(NTIME,5).NE.0)GO TO 1422
      DO 1421J=1,NJ
      FRACKEP=1.0D0
      IF(EPKKEP(J).NE.0.0)FRACKEP=
     11.0D0-(EPKKEP(J)/(CKEEP(IE,J)+EPKKEP(J)))**PREPP
      IF(EPLKEP(J).NE.0.0)FRACKEP=
     11.0D0-(EPLKEP(J)/(CKEEP(IE,J)+EPLKEP(J)))**PREPP
      WRITE (8,141)(C(K,J),K=1,6)
      WRITE (8,141)EPK(J),EPL(J),RBETA(J),ROUTA(J),RIN(J),Q(J)
      WRITE (8,141)EFES(J),EX(J),EFE(J),ELI2S(J),CJ1(J),CJ2(J)
```

```
      WRITE (8,141)W(J),DETA(J),ZETA(J),(CPOL(K,J),K=1,3)
        WRITE (8,141)XD(J),FRACKEP,Q3(J)
 1421 CONTINUE
      WRITE (8,141)TCV,T,VOVERA,XAINIT,DTEMP,TIME
        VPLUS=UJO+C(IN,NJ2)+PHI3
        PRINT 130,TIME,UTIL1,VPLUS
      REWIND 8
 1422 CONTINUE
        IF(TCV.LT.CUTOFF)GO TO 15
      IF(TIME.LT.TGAP+TLAST) GO TO 13
C     CALCULATION OF POLARISATION CURVE
      IPOLAR=0
      TCD1=TCD
      TCD=-TCADD
      TLAST=TLAST+TGAP
      DELTSV=DELT
      DELT=0.0
      IF(DABS(TCD1-0.02).GT.1.D-7) GO TO 2
   29 DO 97 J=1,NJ
      CPOL(1,J)=C(II,J)
      CPOL(2,J)=C(IJ,J)
   97 CPOL(3,J)=C(IN,J)
      IF(TCD.GE.0.0) GO TO 30
      GO TO 2
   12 WRITE(7,1241)TCD,TCV,PHI2,PHI3,C(IN,NJ1),C(IN,NJ2),JCOUNT
 1241 FORMAT (24HPOLARIZATION CURVE PRINT , 6E16.8,I6)
      IF(DABS(TCD-0.02).LT.1.D-7) GO TO 29
      IF(TCD.EQ.0.0) GO TO 436
   30 TCD=TCD+TCADD
      IF(DABS(TCD-TCD1).LT.1.0D-7) TCD=TCD+TCADD
      IF(TCD.GE.0.12) GO TO 98
      IF(DABS(TCD-TCD1).LE.0.02) GO TO 9
      IF(TCD.GT.0.041) GO TO 3
      DO 28 J=1,NJ
      C(II,J)=CPOL(1,J)
      C(IN,J)=CPOL(3,J)
      DETA(J)=CPOL(3,J)
      NONOF(J)=0
      IF(J.GE.NJ2) DETA(J)=DETA(J)+DSEPOT
   28 C(IJ,J)=CPOL(2,J)
      GO TO 3
   98 TCD=TCD1
      DELT=DELTSV
      WRITE (7,128)RES
      IPOLAR=1
      DO  99 K=1,NJ
      DETA(K)=CKEEP(IN,K)
      CJ1(K)=CJ1KEP(K)
      IF(K.LE.NJ1 .AND. DETA(K).GE.0.0)W(K)=0.9
      IF(K.LE.NJ1 .AND. DETA(K).LT.0.0) W(K)=1.1
      IF(K.LE.NJ1) RIN(K)=RINKEP(K)
```

```
         IF(K.GE.NJ2) CJ2(K)=CJ2KEP(K)
         IF(K.GE.NJ2) DETA(K)=DETA(K)+DSEPOT
         DO 99 I=4,6
   99    C(I,K)=CKEEP(I,K)
   13    IF(TIME.GE.TSTOP) GO TO 14
         IF(NTIME.GE.NSTOP) STOP
C        RESET TIME STEP.
         IF(DELT.EQ.0.0) DELT=2.0*DELT2
         IF(TIME.GE.T1) DELT=F1
         IF(TIME.GE.T2) DELT=F2
         IF(TIME.GE.T3) DELT=F3
         IF(TIME.GE.T4) DELT=F4
         IF(TIME.GE.T5) DELT=F5
         IF(TIME.GE.T6) DELT=F6
         IF(TIME.GE.T7) DELT=F7
         IF(TIME.GE.T8) DELT=F8
         IF(TIME.GE.120.0) DELT=DTCUT
         IF(JSPOT.EQ.0) GOTO 2
         DELT=DELT/2.0**JSPOT
         JSPOT=JSPOT-1
         IF(DELT.GT.DTMIN) GO TO 2
C        CURRENT INTERRUPTION AND CHARGING
   14    CONTINUE
  141    FORMAT(6E21.14)
         IF(DELT.GE.0.0) STOP
          KEY6=0
         IF(TCD.LE.0.0) STOP
         IF(TCD.EQ.0.0) TCD=-0.020
         IF(TCD.GT.0.0) TSTOP=0.25*TIME
         IF(TCD.GT.0.0) TCD=0.0
         IF(TCD.LT.0.0) GO TO 449
C        CALCULATION OF INTERRUPTER RESISTANCE
  436    RES=0.0
         DO 446 J=2,NJ1M1
  446    RES=RES+H1*SIGINV(J)/(1.0+CON(J)*C(IE,J)**FACTOR*SIGINV(J))
         DO 447 J=NJ1P1,NJ2M1
  447    RES=RES+H2/CON(J)/C(IE,J)**FACTOR
         DO 448 J=NJ2P1,NJM1
  448    RES=RES+H3*SIGINV(J)/(1.0+CON(J)*C(IE,J)**FACTOR*SIGINV(J))
         RES=RES+0.5*(H1*(SIGINV(1)/(1.0+CON(1)*C(IE,1)**FACTOR*SIGINV(1))
        1+SIGINV(NJ1)/(1.0+CON(NJ1)*C(IE,NJ1)**FACTOR*SIGINV(NJ1)))+H2*(1.0
        1/CON(NJ1)/C(IE,NJ1)**FACTOR+1.0/CON(NJ2)/C(IE,NJ2)**FACTOR)+
        1H3*(SIGINV(NJ2)/(1.0+CON(NJ2)*C(IE,NJ2)**FACTOR*SIGINV(NJ2))+
        1SIGINV(NJ)/(1.0+CON(NJ)*C(IE,NJ)**FACTOR*SIGINV(NJ))))
         IF(IPOLAR.EQ.0) GO TO 30
         WRITE(7,128)RES
  449    TSTOP=TSTOP+TIME
         T1=T10+TIME
C        TGAP=600.0
         IF(TCD.LT.0.0) TSTOP=TSTOP+TIME
         T2=T20+TIME
```

```
        T3=T30+TIME
        T4=T40+TIME
        T5=T50+TIME
        T6=T60+TIME
        T7=T70+TIME
        T8=T80+TIME
        GO TO 1
 15     WRITE (7,102)
        GO TO 14
        END
        SUBROUTINE PROPS(J,C)
C       PROGRAM TO CALCULATE PHYSICAL PROPERTIES FOR MATRIX
C       COEFFICIENTS IN MAIN PROGRAM *BATRY*
        IMPLICIT DOUBLE PRECISION (A-H,O-Z)
        DIMENSION V(401),DVX(401),          DVDT(401), DIFUSN(401),
       1DDX(401),CJ1(401),  SIGINV(401),CJ2(401)  ,CON(401),DCONX(401),
       1DLNAC(401),D2LNAC(401),ZETA(401),DZETAX(401)          ,C(6,401)
       1,EX(401),EFES(401),EFE(401),RBFIN(401)
        COMMON/P1/V,DVX,DVDT          ,DIFUSN,DDX          ,SIGINV,CON,
       1DCONX,DLNAC,D2LNAC,ZETA,DZETAX          ,FACTOR,T,IX,NJ1,NJ2
       1,EX,EFES,EFE,SIGX,SIGFES,SIGFE,PIN43
        COMMON/P3/S,AON,AOP1,AOP2,CJ1,CJ2,EXPAND
        XSQD=C(IX,J)**2
C       MOLAR VOLUME OF ELECTROLYTE AND DERIVATIVES WRT XA. RO IN G/CM3
        RODASH=2.1623194-0.00073684*T
        XADASH=0.00147368*T-0.36253409
        U=723.15
        RODASH=2.1623194-0.00073684*U
        XADASH=0.00147368*U-0.36253409
        RO=RODASH+S*(C(IX,J)-XADASH)
        DVDT(J)=0.0
        V(J)=(74.555-32.161*C(IX,J))/RO
        DVX(J)=-(32.161+S*V(J))/RO
C       DIFFUSION COEFFICIENT OF ELECTROLYTE AND DERIVATIVES WRT XA.
C       D IN CM2/SEC
        ACT=DEXP(-1425.76/T)
        DDX(J)=0.0002442*ACT
        DIFUSN(J)=DDX(J)*(C(IX,J)+0.4)
C       ELECTRICAL CONDUCTIVITY IN MHO/CM
        CON(J)=ACT*(18.9803*XSQD-5.017*C(IX,J)+9.0903)
        DCONX(J)=ACT*(37.9606*C(IX,J)-5.017)
C       ACTIVITY COEFFICIENT FOR ELECTROLYTE
        XB=1.0-C(IX,J)
        GAB=1.0+2.0*C(IX,J)
        XB3=XB**3
        THAN=TANH(0.65837*XB3/C(IX,J))
        BIN=1023.84*(THAN**2-1.0)/T/C(IX,J)
        DLNAC(J)=1.0-BIN*GAB*XB**2
        D2LNAC(J)=BIN*XB*(4.0*XSQD+C(IX,J)+1.0-1.31674*THAN*GAB**2*XB3/
       1C(IX,J))/C(IX,J)
        IF(J.GE.NJ2) GOTO 1
```

```
C     NEGATIVE ELECTRODE
C     SOLID MOLAR VOLUMES IN G MOLE/CM3
      ZETA(J)=AON+EXPAND
      DZETAX(J)=0.0
      IF(J.GT.NJ1) ZETA(J)=0.0
      GOTO 2
C     POSITIVE ELECTRODE
   1  CONTINUE
C     SOLID MOLAR VOLUMES IN G MOLE/CM3
      DZETAX(J)=0.0
      AOP=AOP1
      IF(DABS(CJ2(J)).GT.DABS(CJ1(J))) AOP=AOP2
      ZETA(J)=AOP
   2  RETURN
      END
      SUBROUTINE MATINV(N,M,DETERM)
      IMPLICIT DOUBLE PRECISION (A-H,O-Z)
      COMMON A(6,6),B(6,6),C(6,401),D(6,13)
      DIMENSION ID(5)
      DETERM=1.0
      DO 1 I=1,N
   1  ID(I)=0
      DO 18 NN=1,N
      BMAX=1.1
      DO 6 I=1,N
      IF(ID(I).NE.0) GOTO 6
      BNEXT=0.0
      BTRY=0.0
      DO 5 J=1,N
      IF(ID(J).NE.0) GOTO 5
      IF(DABS(B(I,J)).LE.BNEXT) GOTO 5
      BNEXT=DABS(B(I,J))
      IF(BNEXT.LE.BTRY) GOTO 5
      BNEXT=BTRY
      BTRY=DABS(B(I,J))
      JC=J
   5  CONTINUE
      IF(BNEXT.GE.BMAX*BTRY) GOTO 6
      BMAX=BNEXT/BTRY
      IROW=I
      JCOL=JC
   6  CONTINUE
      IF(ID(JC).EQ.0) GOTO 8
      DETERM=0.0
      RETURN
   8  ID(JCOL)=1
      IF(JCOL.EQ.IROW) GOTO 12
      DO 10 J=1,N
      SAVE=B(IROW,J)
      B(IROW,J)=B(JCOL,J)
  10  B(JCOL,J)=SAVE
```

```
       DO 11 K=1,M
       SAVE=D(IROW,K)
       D(IROW,K)=D(JCOL,K)
11     D(JCOL,K)=SAVE
12     F=1.0D0/B(JCOL,JCOL)
       DO 13 J=1,N
13     B(JCOL,J)=B(JCOL,J)*F
       DO 14 K=1,M
14     D(JCOL,K)=D(JCOL,K)*F
       DO 18 I=1,N
       IF(I.EQ.JCOL) GO TO 18
       F=B(I,JCOL)
       DO 16 J=1,N
16     B(I,J)=B(I,J)-F*B(JCOL,J)
       DO 17 K=1,M
17     D(I,K)=D(I,K)-F*D(JCOL,K)
18     CONTINUE
       RETURN
       END
       SUBROUTINE BAND(J)
       IMPLICIT DOUBLE PRECISION (A-H,O-Z)
       DIMENSION E(6,7,401)
       COMMON A(6,6),B(6,6),C(6,401),D(6,13),G(6),X(6,6),Y(6,6),N,NJ
101    FORMAT (15H DETERM=0 AT J=,I4)
       IF (J-2)  1,6,8
  1    NP1 = N + 1
       DO 2 I=1,N
       D(I,2*N+1) = G(I)
       DO 2 L=1,N
       LPN = L + N
  2    D(I,LPN) = X(I,L)
       CALL MATINV(N,2*N+1,DETERM)
       IF (DETERM)  4,3,4
  3    WRITE (7,101) J
  4    DO 5 K=1,N
       E(K,NP1,1) = D(K,2*N+1)
       DO 5 L=1,N
       E(K,L,1) = - D(K,L)
       LPN = L + N
  5    X(K,L) = - D(K,LPN)
       RETURN
  6    DO 7 I=1,N
       DO 7 K=1,N
       DO 7 L=1,N
  7    D(I,K) = D(I,K) + A(I,L)*X(L,K)
  8    IF (J-NJ)  11,9,9
  9    DO 10 I=1,N
       DO 10 L=1,N
       G(I) = G(I) - Y(I,L)*E(L,NP1,J-2)
       DO 10 M=1,N
 10    A(I,L) = A(I,L) + Y(I,M)*E(M,L,J-2)
```

```
   11 DO 12 I=1,N
    . D(I,NP1) = - G(I)
      DO 12 L=1,N
      D(I,NP1) = D(I,NP1) + A(I,L)*E(L,NP1,J-1)
      DO 12 K=1,N
   12 B(I,K) = B(I,K) + A(I,L)*E(L,K,J-1)
      CALL MATINV(N,NP1,DETERM)
      IF (DETERM)  14,13,14
   13 WRITE (7,101) J
   14 DO 15 K=1,N
      DO 15 M=1,NP1
   15 E(K,M,J) = - D(K,M)
      IF (J-NJ)  20,16,16
   16 DO 17 K=1,N
   17 C(K,J) = E(K,NP1,J)
      DO 18 JJ=2,NJ
      M = NJ - JJ + 1
      DO 18 K=1,N
      C(K,M) = E(K,NP1,M)
      DO 18 L=1,N
   18 C(K,M) = C(K,M) + E(K,L,M)*C(L,M+1)
      DO 19 L=1,N
      DO 19 K=1,N
   19 C(K,1) = C(K,1) + X(K,L)*C(L,3)
   20 RETURN
      END
      SUBROUTINE MCOND(SS       ,SIGFE ,SIGX   ,SIGFES,SIGLIS,
     1                 EFESP ,EXPP   ,EFEP   ,ELI2SP,VFES  ,VX       ,
     2                 VFE   ,VLI2S ,DENT2 ,EONSB,F       ,
     3                 SGNVNU,D1NU  ,D2NU  ,
     4                 CONADD)
C     CALCULATE POSITIVE ELECTRODE RESTISTANCE, SIGINV(J)
      IMPLICIT DOUBLE PRECISION (A-H,O-Z)
      DIMENSION SS(4,2)
      SEFESP = EFESP
      SEFEP = EFEP
      SEXPP = EXPP
      SELISP = ELI2SP
      IF(EFEP.LE.0.0)EFEP = 0.0
      IF(EFESP.LE.0.0)EFESP = 0.0
      IF(EXPP.LE.0.0)EXPP = 0.0
      IF(ELI2SP.LE.0.0)ELI2SP = 0.0
      BIGSIG=EXPP*SIGX+ELI2SP*SIGLIS+EFESP*SIGFES+CONADD
      BIGSIG=BIGSIG/(EXPP + ELI2SP + EFESP)
      DSUM1=-3.*SIGFE*EFEP/(2.*SIGFE + BIGSIG)**2
      SUM1NU = 0.0
      SUM2NU = 0.0
      SUM3NU = 0.0
      SUM1NU = EFEP*(SIGFE-BIGSIG)/(2.*SIGFE+BIGSIG)
      SUM1NU = SUM1NU - (1.0 - EFESP - EFEP - EXPP - ELI2SP)
      SUM2NU =((SIGFE - BIGSIG)/(2.*SIGFE + BIGSIG)+1.0)*VFE*SS(1,1)
```

```
      SUM3NU =((SIGFE - BIGSIG)/(2.*SIGFE + BIGSIG)+1.0)*VFE*SS(1,2)
      DBSIG=EXPP*(SIGFES-SIGX)+ELI2SP*(SIGFES-SIGLIS)-CONADD
      DBSIG=DBSIG/(EXPP+ELI2SP+EFESP)**2
      ADDNU=DSUM1*DBSIG+1.+(1.-2.*SUM1NU)*(SUM1NU+1.)*DBSIG/BIGSIG/3.
      SUM2NU = SUM2NU + ADDNU*VFES*SS(2,1)
      DBSIG=EFESP*(SIGX-SIGFES)+ELI2SP*(SIGX-SIGLIS)-CONADD
      DBSIG=DBSIG/(EXPP + ELI2SP + EFESP)**2
      ADDNU=DSUM1*DBSIG+1.+(1.-2.*SUM1NU)*(SUM1NU+1.)*DBSIG/BIGSIG/3.
      SUM2NU = SUM2NU + ADDNU*VX*SS(3,1)
      SUM3NU = SUM3NU + ADDNU*VX*SS(3,2)
      DBSIG=EFESP*(SIGLIS-SIGFES)+EXPP*(SIGLIS-SIGX)-CONADD
      DBSIG=DBSIG/(EXPP + ELI2SP + EFESP)**2
      ADDNU=DSUM1*DBSIG+1.+(1.-2.*SUM1NU)*(SUM1NU+1.)*DBSIG/BIGSIG/3.
      SUM3NU = SUM3NU + ADDNU*VLI2S*SS(4,2)
      SUM2NU = SUM2NU*3.*BIGSIG/(1. -2.*SUM1NU)**2
      SUM3NU = SUM3NU*3.*BIGSIG/(1. -2.*SUM1NU)**2
      SGNVNU = 1.0/(SUM1NU*BIGSIG + BIGSIG)*(1.-2.*SUM1NU)
      D1NU = -DENT2*SGNVNU**2*SUM2NU/EONSB/F
      D2NU = -DENT2*SGNVNU**2*SUM3NU/EONSB/F
      EFESP = SEFESP
      EFEP = SEFEP
      EXPP = SEXPP
      ELI2SP = SELISP
      RETURN
      END
      SUBROUTINE CORXN(NJ2,NJ,V,C,H3,T,AVGXA,D)
C     INTEGRATE CONCENTRATION DISTRIBUTION FOR ENTHALPY-OF-MIXING
C     TERM IN THE ENERGY BALANCE
      IMPLICIT DOUBLE PRECISION (A-H,O-Z)
      DIMENSION C(6,401),V(401)
      TBASE=450.+273.15
      XA=AVGXA
      XB=1.-AVGXA
      ACAV=(0.52628*XB-1.2738*XB**2-2.9783*XB**3)*TBASE/T
      ACBAV=
     1(-0.52628*XA-5.7413*XA**2+2.9783*XA**3-0.52628*DLOG(DABS(XB)))
     1*TBASE/T
      HH=H3
      NLAST=NJ-NJ2+1
      LFLAG=0
      N=NLAST
      SUMODD=0.
      SUMEVE=0.
      IF(((NJ-NJ2)/2)*2.EQ.(NJ-NJ2))LFLAG=1
      IF(LFLAG.EQ.0)NLAST=NJ-NJ2
      DO 50 LL=1,N
      J=NJ2+LL-1
      XA=C(1,J)
      XB=1.-C(1,J)
      ACA=(0.52628*XB-1.2738*XB**2-2.9783*XB**3)*TBASE/T
      ACB=(-0.52628*XA-5.7413*XA**2+2.9783*XA**3-0.52628*DLOG(DABS(XB)))
```

```
1*TBASE/T
      HBARA=8.3143*T*(ACA-ACAV)
      HBARB=8.3143*T*(ACB-ACBAV)
      FUNT=C(3,J)/V(J)*(C(1,J)*HBARA+(1.-C(1,J))*HBARB)
101   FORMAT(1X,4G12.6)
      M=LL/2
      M=M*2
      IF(LL.EQ.NLAST.OR.LL.EQ.1) GOTO 45
     IF(LL.EQ.N.AND.LFLAG.EQ.0) GO TO 45
      IF(M.EQ.LL) SUMEVE=SUMEVE+FUNT
      IF(M.NE.LL) SUMODD=SUMODD+FUNT
45    IF(LL.EQ.1)FUNT1=FUNT
      IF(LL.EQ.NLAST)FUNTN=FUNT
      IF(LL.EQ.NLAST.AND.LFLAG.EQ.0)FUNTN=FUNTN+1.5*FUNT
      IF(LL.EQ.N.AND.LFLAG.EQ.0)FUNTN=FUNTN+1.5*FUNT
50    CONTINUE
15    D=HH/3.*(FUNTN+4.*SUMEVE+2.*SUMODD+FUNT1)
      RETURN
      END
      SUBROUTINE NRAF(CINJ,Q3J,CJ3KEP,TC1,TC2,DENT2,CIXJ,
     1 AIO2,CCJ3,SLOPEP,ETAS)
C     CALCULATE CJ3 IN KINETIC EQUATION
      IMPLICIT DOUBLE PRECISION (A-H,O-Z)
      CCJ3=CJ3KEP
      DO 500 L=1,30
      ETAS=CINJ-(SLOPEP*(Q3J-DENT2*(CCJ3+CJ3KEP)))
      FOFX=AIO2*CIXJ*(DEXP(TC1*ETAS)-DEXP(-TC2*ETAS))-CCJ3
      FPOFX=AIO2*CIXJ*SLOPEP*DENT2*
     1 (DEXP(TC1*ETAS)*TC1+DEXP(-TC2*ETAS)*TC2)-1.D0
      CJ3OL=CCJ3
      CCJ3 = CCJ3 -  (FOFX/FPOFX)
      IF(DABS(CCJ3-CJ3OL).LT.1.0D-13*DABS(CCJ3))GO TO 501
500   CONTINUE
501   IF(DABS(ETAS*TC1).GT.0.004)GO TO 504
      CCJ3=CJ3KEP
      DO 600 L=1,30
      ETAS=CINJ-(SLOPEP*(Q3J-DENT2*(CCJ3+CJ3KEP)))
      FOFX=AIO2*CIXJ*(ETAS*((TC1+TC2)*(1.0D0+0.5D0*
     1 (TC1-TC2)*ETAS)+(TC1**3+TC2**3)*ETAS**2/6.0D0))-CCJ3
      FPOFX=AIO2*CIXJ*SLOPEP*DENT2*
     1 ((TC1+TC2)*(1.0D0+(TC1-TC2)*ETAS)+
     1 (TC1**3+TC2**3)*ETAS**2/3.0D0)-1.0D0
      CJ3OL=CCJ3
      CCJ3 = CCJ3 -  (FOFX/FPOFX)
      IF(DABS(CCJ3-CJ3OL).LT.1.0D-13*DABS(CCJ3))GO TO 504
600   CONTINUE
504   CONTINUE
      EXPDIF=CCJ3/AIO2/CIXJ
      RETURN
      END
```

Appendix A-3

Supplements for Chapter 3:

Choice of the Average Composition for a Multicomponent System

Estimate of the Temperature rise in a Lead-Acid Cell Following

Current Interruption

Energy Equations for LiAl/FeS Cell Model Studies

Relevant Input Data for the LiAl/FeS Cell Model (including the

activity coefficient expression for the LiCl-KCl system)

Choice of the Average Composition

for a Multicomponent System

For a multicomponent phase, the integral in Equation 15 may be written as

$$\int_v \sum_i c\, x_i\, (\overline{H}_i - \overline{H}_i^{avg})\, dv \ . \tag{A-1}$$

In this development it will be assumed that Equation A-1 is a function only of the average composition and that the spatial variation of composition is fixed. If the molar enthalpy is defined as

$$\tilde{H} = \sum_i x_i\, \overline{H}_i \ . \tag{A-2}$$

Equation A-1 may be written as

$$\int_v c\, \left[\, \tilde{H} - \sum_i x_i\, \overline{H}_i^{avg}\, \right] dv \ . \tag{A-3}$$

Equation A-1 can be minimized with respect to the average composition by equating the total differential to zero. Recognizing that the enthalpy is independent of the choice of the average composition we may write

$$d\left[\sum_i \int_v \overline{H}_i^{avg}\, c\, x_i\, dv\, \right] = \sum_i \left(\int_v c\, x_i\, dv\, \right) d\overline{H}_i^{avg} = 0 \ . \tag{A-4}$$

If we multiply and divide each term in Equation A-4 by x_i^{avg},

$$\sum_i \left(\frac{\int_v c\, x_i\, dv}{x_i^{avg}} \right) x_i^{avg}\, d\overline{H}_i^{avg} = 0 \ , \tag{A-5}$$

and compare this to the Gibbs-Duhem equation,

$$\sum_i x_i^{avg} \, d\overline{H}_i^{avg} = 0 \, , \tag{A-6}$$

we see that we can reach the desired extremum by requiring that the bracketed quantity in Equation A-5 be equal to a constant, independent of i.

$$K = \frac{\int_v c \, x_i \, dv}{x_i^{avg}} \, . \tag{A-7}$$

The constant K can be determined by requiring that the values of x_i^{avg} sum to unity:

$$\sum_i x_{i_{avg}} = \frac{\sum_i \int_v c \, x_i \, dv}{K} = 1 \, . \tag{A-8}$$

Then

$$K = \int_v c \, dv \, . \tag{A-9}$$

and the final form for x_i^{avg} is

$$x_i^{avg} = \frac{\int_v c \, x_i \, dv}{\int_v c \, dv} \, . \tag{A-10}$$

Estimate of the Temperature Rise in a Lead-Acid Cell

Following Current Interruption

Prior to discharge, the cell is assumed to have a uniform composition of 5 molal sulfuric acid. It is assumed that one-third of the electrolyte is contained in the cathode space, one-third is in the anode space, and one-third is in the space between the electrodes. It is also assumed that during discharge the concentration of acid in the intermediate space remains unchanged and that the acid concentration throughout each electrode compartment is uniform. Basing the discharge on two Faradays (1 mole PbO_2), one kilogram of sulfuric acid solution, and a transference number of 0.74 for hydrogen ion, we may calculate that the concentration in the cathode space and anode space drops to 1.04 and 2.79 molal, respectively.[27] The initial number of moles of acid and water per mole of PbO_2 (n_s^0) in this example is 60.5. If we regard the cell to be well insulated and there are no phase changes (such as formation of ice crystals), Equation 3-15 may be written as

$$1.15 \frac{dT}{dt} (n_{PbSO_4} \tilde{C}_{P_{PbSO_4}} + n_1 \overline{C_{P_1}^{avg}} + n_2 \overline{C_{P_2}^{avg}}) = \quad \text{(A-11)}$$

$$- \frac{d}{dt} \int_v c [\tilde{H} - (x_1 \overline{H_1^{avg}} + x_2 \overline{H_2^{avg}})] dv.$$

In writing this equation, it is assumed that the heat capacity of the battery support material is 15% of the heat capacity of the reactive material. The integral on the right side is easy to evaluate in this case because the concentration is uniform and the volume is the same in each compartment. The average composition of acid, defined by Equation 3-26, is 2.95 molal. As mentioned earlier, this is the final, uniform concentration after relaxation, and the temperature rise is proportional to the value of the integral when the current is interrupted (8630 J

or 6.5 J/gram of electrolyte). Using the data available in Reference 27 (for 298 K), we calculate the temperature rise to be about 1.6 K. (If we discharge 1.25 moles of PbO_2 in the same amount of electrolyte ($n_e^o = 48.4$), then the concentrations in the cathode and anode space drop to 0.05 and 2.23 molal, respectively, and the temperature will rise 2.9 K as the concentration profiles relax). We recognize that the assumed concentration jumps at the interfaces are artificial and that, realistically, diffusion tends to equalize the concentrations. The estimated temperature rise would be slightly lower if the above effect were taken into account. We must also, however, recognize the effects of non-uniform reaction distribution in porous electrodes and that this will tend to make the concentration distribution non-uniform. Reference 26 gives spatial distributions of concentration and reaction for a one-dimensional model of a lead-acid cell.

Energy Equations for LiAl/FeS Cell Model Studies

Mechanism 1 (The number subscripts refer to the reactions in Table 3-1)

$$\frac{M}{A}\hat{C}_P^m \frac{dT}{dt} = \tag{A-12}$$

$$-h(T - T_A) \qquad\qquad\qquad heat-losses$$

$$+ (i_1a_1 + i_2a_2) - V(i_1 + i_2) \qquad enthalpy-of-reaction$$

$$and\ electrical-work$$

$$+ \frac{d}{dt}\int_0^L \varepsilon RT\left[c_{LiCl}\ln\left(\frac{\gamma_{LiCl}}{\gamma_{LiCl}^{avg}}\right) + c_{KCl}\ln\left(\frac{\gamma_{KCl}}{\gamma_{KCl}^{avg}}\right)\right]dy \qquad mixing$$

$$+ \frac{1}{A}\frac{dn_{KCl_\bullet}}{dt}\left[\Delta\tilde{H}_{KCl_f}^o + RT\ln\gamma_{KCl}^{avg}\right] \qquad KCl-precipitation$$

Mechanism 2

The energy equation for mechanism 2 differs only in the enthalpy-of-reaction and electrical-work term which may be written as

$$+ (i_3a_3 + i_4a_4) - V(i_3 + i_4) \tag{A-13}$$

$$-i_3\frac{RT}{F}\ln\left(\left(\frac{\gamma_{LiCl}^{avg}}{\gamma_{LiCl}^{suf}}\right)^{5/8}\left(\frac{\gamma_{KCl}^{avg}}{\gamma_{KCl}^{suf}}\right)^{-1}\right) - i_4\frac{RT}{F}\ln\left(\left(\frac{\gamma_{LiCl}^{avg}}{\gamma_{LiCl}^{suf}}\right)^{-5/46}\left(\frac{\gamma_{KCl}^{avg}}{\gamma_{KCl}^{suf}}\right)^{3/23}\right).$$

Relevant Input Data for the LiAl/FeS Cell Model

quantity	value	quantity	value
x^0_{LiCl}	0.58(eutectic)	$M\hat{C}^m_p/A$	1.89 J/cm^2-K
$\Delta\tilde{H}^0_{KCl_f}$	26530. J/mol	i	0.0416 A/cm^2
h	8.25×10^{-6} W/cm^2-K	T_A	298.15 K
capacity	835.27 C/cm^2	ϵ^0_{FeS}	0.445

$$T\ln\gamma_{LiCl} = 723.15\,(0.52628x_{KCl} - 1.2738x^2_{KCl} - 2.9783x^3_{KCl})$$

$$T\ln\gamma_{KCl} = 723.15\,(-0.52628x_{LiCl} - 5.7413x^2_{LiCl} + 2.9783x^3_{LiCl} - 0.52628\ln x_{KCl})$$

Appendix A-4

Program EFES2: Calculates the thermodynamic, open-circuit potential of a Li(Öi)/FeS$_2$ cell as a function of temperature and state-of-discharge (see Chapter 4).

```
C         PROGRAM EFES2(INPUT,OUTPUT)
          DIMENSION COEFFP(4),COEFFN(3),AP(4),BP(4),AN(3),BN(3)
          NU = 100
          DU = 1.
          COEFFP(1) = 1.5
          COEFFP(4) = 2.0
          COEFFN(1) = .92
          COEFFN(2) = .62
          COEFFN(3) = 2.1449
          AP(1) = 1.5558
          AP(2) = 1.3867065
          AP(4) = 1.39196
          AP(3) = 1.3425
          BP(4) = -.000147
          BP(1) = .0004785
          BP(2) = .00065142
          BP(3) = 0.0000133
          AN(1) = -.187529
          AN(2) = -.088097
          AN(3) = -.034525
          BN(1) = .0000731
          BN(2) = .0001122
          BN(3) = .0001056
          TK = 625.00
          BETA = 2.5974
C         TEMP STARTS OUT AT TK + 25
          DTK = 25.0
          NT = 4
          DO 1000 I=1,NT
          IRP = 1
          IRN = 1
          COEFP = COEFFP(1)
          COEFN = COEFFN(1)
          UTIL = -2.0
          TK  =   TK + DTK
          TC = TK - 273.15
          FE1MX = -9.24E-5*TC + .916580
          COEFFP(2) = (2.2*(4.*FE1MX-2.)/(2.*FE1MX - .8))-3.
          COEFFP(2) = COEFFP(2)/2.
          COEFFP(3) = .5 - COEFFP(2)
          SLOPEP=ABS(((AP(3)-AP(2))+TC*(BP(3)-BP(2)))/COEFFP(3))
          PRINT 100,TK
          DO 2000 J=1,NU
          UTIL = ABS(UTIL + DU)
          ELECT = 4.0*UTIL/100.
100       FORMAT(G10.3)
          IF(ELECT.LT.COEFP)GO TO 201
          IRP = IRP + 1
          COEFP = COEFP + COEFFP(IRP)
201       EP = AP(IRP) + BP(IRP)*TC
          IF(IRP.NE.3)GO TO 203
```

```
           EP = EP + SLOPEP*(2.-ELECT)
   203     COEK = COEFN*BETA
           IF(ELECT.LT.COEK) GO TO 301
           IRN = IRN + 1
           COEFN = COEFN + COEFFN(IRN)
   301     EN = AN(IRN) + BN(IRN)*TK
           E = EP - EN
           PRINT 101,UTIL,E
   101     FORMAT(2G13.6)
  2000     CONTINUE
  1000     CONTINUE
           END
```

Appendix B-1

Program NIFILM: Calculates the concentration profiles, current density, and nickel hydroxide film formation and growth as a function of time for the cathodic reduction of nickel nitrate, nitric acid solution at a rotating disk electrode (see Chapter 6).

Sample Input Data for Program NIFILM

```
~789
   1    1 52360+1 99400-3 29815+2 10000-0 54000-1 38200-1 10000+0
   0    1 38307-1 20000-021300-26 57002-7 02000-3 33000-2 86200-2
 101 102 60000-2 22392-2
30255-9 75000-6 20000-0              Ni++
76647-9 19000-5-10000-0-10000-0 NO3-
21219-8 52600-5-10000-0              OH-
37574-8 93120-5 10000-0-30000-0 H+
   0    0 10000-1-40000-0-60000-0 40000-0 27000-0 00000-0
   5   25 30000-310000-2039430-11 45650+1 65700-1 10000+1
```

```
      PROGRAM NIFILM(INPUT,OUTPUT,TAPE7,TAPE8)

C         PROGRAM TO COMPUTE NICKEL HYDROXIDE FILM
C         GROWTH FOR THE NICKEL NITRATE, NITRIC ACID SYSTEM
C         USES DEVIATION VARIABLES

      COMMON /B1/A,B,D
     1 /B2/C
     1 /B3/COLD
     1 /B4/G
     1 /B6/CIN,DIF,V,S,Z,U,ZUFODR,CBK
     1 /B7/CSAT,DELTA,RHOF,DT,EQCON,EPO,F,H,HF,N,IFLAG,
     1     IPASS,IHSO4,IH,ISO4,IR,IPHI,IL,JSTIME,JFTIME,JCOUNT,THTIME,
     1     TSTAR,NJ,NJM1,NPRINT,QLF,NJD,NJDP1,NJDM1,HETA,JTIME
     1 /B9/X
     1 /B10/Y,BEGTPAS,OHMADJ,RKAP1,P2,P4,P5,P6,P7
     1 /B12/VFE,RATEKA,RATEKC,OHMIC,CUR,CURPAS,ICONPAS,PH,VPASS,OHMCOR
     1 /B14/III
     1 /B17/CINTR
     1 /B19/XX,XXLONG,CLONG,XXMAX,NLONG
     1 /B20/DELHAT
     1 /B23/CDEV
     1 /B24/T,SQRTT,TOLD,SQRTOLD
     1 /B25/XI,ETA
     1 /B26/ICYCLE
     1 /B27/XMIGF,DF,XMIGS,DS,XNF
     1 /B28/SURMIG,SURDIF,SURFLX
     1 /B29/ALPHAA,ALPHAC,FEN,PI,RZERO,RKAPPA,DIMROT,P3,FA,FC,PHIZRO
     1 /B30/XXTEST
     1 /B31/DELC
     1 /B32/J
     1 /B33/SQRTSAV
     1 /B34/EPSURZ,P,EPSUR
      DIMENSION REF(6),A(6,6),B(6,6),D(6,13),XMIGF(4),DF(4),XMIGS(4),
     1 C(6,202),COLD(6,202),G(6),CDEV(6,202),DS(4),XNF(4),SURMIG(4),
     1 SURDIF(4),SURFLX(4),ETA(202),
     1 DIF(6),Z(6),S(6),CIN(6),V(202),ZUFODR(6),CBK(4),U(6),
     1 X(6,6),Y(6,6),
     1 XI(202),XX(202),XXLONG(202),CLONG(6,202),CINTR(6),
     1 DELC(6,202),RI(202)

      CPIR(J) = (C(IR,J-1) - C(IR,J+1))/2.0
      CPSF(I,J) = -3.0*C(I,J) + 4.0*C(I,J-1) - C(I,J-2)
      XCP(I,J) = (C(I,J-1) - C(I,J+1))/2.0

  301 FORMAT (2I4,7E8.4)
  302 FORMAT (4E8.4,A6)
  201 FORMAT (4HONJ=,I4,5H,  H=,F6.4/
     1 38H SPECIES         U         DIF        Z    S/
     1 (3X,A6,2E10.4,2F5.1))
  202 FORMAT (1H ,*NONLINEARITY DID NOT CONVERGE IN*,I3,* INTERATIONS*)
```

```
203 FORMAT (1H ,*CSAT =*,E10.4,3X,*SSF =*,E10.4,3X,*CMAX =*,E10.4)
204 FORMAT(1H ,*N =*,I3,2X,*IFIXDTF =*,I3,2X,
   1 *NPRINT =*,I3,2X,*STRI =*,E9.3,2X,*EQCON =*,E10.4,2X,
   1 *EPO =*,E10.4,2X,*DELTA =*,E10.4)
205 FORMAT(1H ,*IFIXDTS=*,I3,2X,*VFE=*,E10.4,
   1 *TSLOGO=*,E10.4,2X,*TFLOGO=*,E10.4,2X,*TSPDS=*,E10.4,
   1 *TSPDF=*,E10.4/2X,*NINC=*,I3)
206 FORMAT (1H ,*VALUES OF ZUFODR(I)*/1H ,4(I3,1X,E10.4,2X))
207 FORMAT(1X,*ICYCLE =*,I3,* N=*,I1,* NM1=*,I1,* NJ=*,I3,* NJM1=*,I3)
208 FORMAT (1H ,*INITIALIZATION OF FILM CONCENTRATIONS*)
209 FORMAT (1X,*IF NSHUHN=0 NO SHOEHORN, IF NSHUHN=1 USE SHOEHORN, NSH
   1UHN=*,I1)
210 FORMAT (6(1X,E13.7))
211 FORMAT (1X,*JSTIME=*,I2,* TSLOG=*,E12.6,* DT=*,E12.6,
   1    * TSTAR=*,E12.6,* FIXDTS=*,I1,* FIXDTF=*,I1)
212 FORMAT (1X,*EVERY NPRINT'TH VALUE OF V(J)*)
214 FORMAT (1X,*VALUES OF CLONG AND XXLONG*)
216 FORMAT (1X,*JS*,1X,*JF*,3X,*TFLOG*,7X,*DT*,6X,*TSTAR*,4X,*THTIME*,
   1 3X,*FIXDTS*,1X,*FIXDTF*/
   1 2(1X,I2),4(1X,E9.3),2(3X,I1,3X))
217 FORMAT(1X,*SPECIES*,10X,*MIGF*,15X,*DIFF*,15X,*MIGS*,15X,*DIFS*,
   1 15X,*NFI*)
218 FORMAT(4X,I1,2X,5(1X,E18.12))
219 FORMAT(1X,*SPECIES*,8X,*SURMIG*,13X,*SURDIF*,13X,*SURFLX*)
221 FORMAT (1X,*CONCENTRATIONS AT END OF CYCLE*,I2)
222 FORMAT(1X,*OMEGA=*,E12.6,* NU=*,E12.6,* A=*,E12.6,* R=*,E12.6,
   1 * TEMP=*,E12.6,* ALPHAA=*, E12.6,* ALPHAC=*,E12.6/1X,*RO=*,E12.6,
   1 * RKAPPA=*,E12.6,* N=*,F4.1,* OMEGA RED=*,E12.6,* FA=*,E12.6,
   1 * FC=*,E12.6/1X,*RATEKA=*,E14.8,* RATEKC=*,E14.8,* PASS1=*,F6.3,
   1 * PASS2=*,F7.4,* EQCON=*,E12.6,* BEGTPAS=*,E12.6,* ATEND=*,I1)
223 FORMAT(1X,*OPD=*,F7.4,* OCOR=*,F7.4,* PHIZO=*,F7.4,
   1 * V-PO=*,F7.4,* I(A/CMSQ)=*,E11.4,* VP=*,F7.4,
   1 * TPAS=*,E8.2,* SFT=*,F7.4,* PH=*,F7.4)
224 FORMAT(1X,*IPASS*,1X,*INT JS JF*,4X,*TSTAR*,6X,*THTIME*,5X,
   1 *DELTA*,4X,*OHMIC DROP*,4X,*TPASS*,4X,*EPSILN *,4X,*V-PHIO*,4X,
   1 *I(A/CM SQ)*,1X,*C(FE,NJM1)*,2X,*PH*)
225 FORMAT(2X,I2,3X,I2,1X,2(1X,I2),9(1X,E10.4),F7.4)
227 FORMAT(1X,I3,5(1X,E12.6),1X,E20.14,1X,I1)
228 FORMAT(1X,I3,6(1X,E12.6),1X,E20.14,1X,I1)
229 FORMAT(20I4)
230 FORMAT(6E22.15)
232 FORMAT(1X,*VALUES USED TO RESTART PROGRAM*)
233 FORMAT(1X/1X,*ICYCLE=*,I2,* RTIME(SEC)=*,E12.6,* FREQ(HZ)=*,
   1 E12.6,* T=*,E9.3,* EPSILN=*,E9.3,* SFT(UM)=*,E9.3,* CALKAP*,E9.3
   1 //)
234 FORMAT(6X,*Y1*,12X,*Y2*,11X,*RAT*,10X,*TPAST*,9X,*TIMETH*,8X,
   1 *THTIME*)
235 FORMAT(1X,*CURRENTS EQUAL AT NJD AND NJDP1 UNLESS PRINTED BELOW*)
238 FORMAT(1X,I3,1X,E10.4,1X,I3,1X,E10.4,1X,I3,1X,E10.4,1X,I3,1X,
   1 E10.4,1X,I3,1X,E10.4,1X,I3,1X,E10.4,1X,I3,1X,E10.4,1X,I3,1X,
   1 E10.4)
```

```
239 FORMAT(1X,*LASTCYCLE =*,I3,* IRESTRT=*,I3,* ICONPAS=*,I3)
240 FORMAT(1X,*SURFACE DERIVATIVES OF THE LONG PROFILE*)
241 FORMAT(1X,I3,9(1X,E12.6))
242 FORMAT(2X,*J*,2X,*SUM GRAD C*,7X,*KAPPA*,7X,*TRUOHM*,7X,
   1 *OHMINF*,7X,*DIFCOM*,7X,*TOTALP*,6X,*C(IPHI,J)*,5X,*ETACEQ*)
243 FORMAT(1X,*P6*,E12.6,* P7*,E12.6,* RKAP1*,E12.6,* XXMAX*,E12.6,
   1 * XX(NJM1)*,E12.6)
244 FORMAT(1X,*EPSUR=*,E12.6,* EPFILM=*,E12.6,* ADJCONC=*,E12.6)
245 FORMAT(1X,*P=*,E12.6)
248 FORMAT (1X,*BEGTPAS =*,E12.6)
```

```
C        VARIABLE LIST

C        A        MATRIX ENTRIES USED IN BAND(J)
C        ADISK    HYDRODYNAMIC PARAMETER FOR ROTATING DISK, 0.51023
C        ADJCONC  FACTOR TO REDUCE DIF(I) AND U(I) DUE TO CONCENTRATED
C                 SOLUTION EFFECTS
C        ALPHAA   ANODIC TRANSFER COEFFICIENT
C        ALPHAC   CATHODIC TRANSFER COEFFICIENT
C        ATPASS   ABSOLUTE VALUE OF TPASS USED FOR TIME STEP CONTROL, V
C        B        MATRIX ENTRIES USED IN BAND(J)
C        C        VALUES OF THE UNKNOWNS, MOL/CU CM FOR CONCENTRATIONS,
C                 V FOR POTENTIAL
C        CBEGIN   VALUE OF HYDROXIDE ION CONCENTRATION AT ZERO TIME IN THE
C                 FILM USED FOR TIME STEP CONTROL, MOL/CU CM
C        CBULK    BULK NICKEL NITRATE CONCENTRATION, MOL/CU CM
C        CDEV     DEVIATION VARIABLES WHICH APPROACH ZERO FOR A CONVERGED
C                 SOLUTION
C        CIN      BULK SOLUTION CONCENTRATION VALUES, MOL/CU CM
C        CINTR    TRANSIENT BC CONCENTRATIONS USED AT XI(MAX) DURING
C                 INTIAL STAGES OF FILM FORMATION
C                 THEY ARE INTERPOLATED FROM VALUES OF CLONG
C        CLONG    CONCENTRATION PROFILES AT THE INSTANT JUST BEFORE
C                 FILM PRECIPITATION, MOL/CU CM
C        COLD     CONCENTRATION VALUES AT PREVIOUS TIME STEP, MOL/CU CM
C        CMAX     MAXIMUM HYDROXIDE CONCENTRATION BEFORE PRECIPITATION,
C                 MOL/CU CM
C        CPIR     DERIVATIVE OF HYDROGEN ION CONCENTRATION WITH RESPECT TO
C                 DIMENSIONLESS DISTANCE AT MESH POINT J, MOL/CU CM
C        CPSF     3 POINT FORWARD DIFFERENCE DERIVATIVE WITH RESPECT
C                 TO DIMENSIONLESS DISTANCE AT MESH POINT J, MOL/CU CM
C        CPRSF    DERIVATIVE OF HYDROXIDE ION CONCENTRATION AT
C                 FILM-SOLUTION INTERFACE FROM PRIVIOUS TIME STEP
C                 USED TO TEST FOR CONVERGENCE
C        CRO      NITRATE ION CONCENTRATION AT FILM-SOLUTION INTERFACE
C                 USED TO TEST FOR CONVERGENCE
C        CSAT     HYDROXIDE ION SATURATION CONCENTRATION, MOL/CU CM
C        CTEST    NITRATE ION CONCENTRATION USED TO TEST FOR CONVERGENCE,
C                 MOL/CU CM
C        CUR      CURRENT CALCULATED IN BCNJ SUBROUTINE, A/SQ CM
C        D        COEFFICIENTS USED IN BAND(J)
```

```
C       DDELTA  CHANGE IN DELTA OCCURRING IN A TIME STEP DT
C       DELHAT  DELTA + DDELTA
C       DELTA   DIMENSIONLESS FILM THICKNESS
C       DEPDDEL DERIVATIVE OF EPSLIN WITH RESPECT TO DELHAT
C       DF      DIFFUSION COMPONENT OF FLUX FROM FILM AT INTERFACE
C       DIF     DIFFUSION COEFFICIENTS, CM SQ/S
C       DIMROT  REDUCED ROTATION SPEED, 1/CM
C       DS      DIFFUSION COMPONENT OF FLUX INTO SOLUTION AT INTERFACE
C       DTINT   INTERPOLATED VALUE OF DT AT A-P OR P-A TRANSITION
C       DTLOG   INCREMENT IN THE LOGARITHUM OF THE DIMENSIONLESS TIME
C       DTLOGF  INCREMENT IN THE LOGARITHUM OF THE DIMENSIONLESS TIME
C               USED WHEN THE FILM IS PRESENT
C       DTSET   TIME STEP USED WHEN LOGARITHMIC TIME STEPS HAVE BEEN
C               STOPPED
C       DWRTX   DERIVATIVE OF CONCENTRATION WITH RESPECT TO X
C       EPO     FILM POROSITY
C       EPSUR   SURFACE POROSITY
C       EPSILN  FILM POROSITY
C       EQCON   EQUILIBRIUM CONSTANT, MOL/CU CM
C       ETA     DIMENSIONLESS DISTANCE IN THE FILM
C       F       FARADAY'S CONSTANT, COUL/EQ
C       FA      ALPHAA*F/RGAS/TKELV
C       FC      ALPHAC*F/RGAS/TKELV
C       FEN     EQUIVALENTS PER MOL FOR NITRATE, 2
C       FREEZE  PARAMETER TESTED TO STOP LOGARITHMICALLY INCREASING TIME
C               STEPS
C       G       ERROR VECTOR IN BAND(J)
C       H       MESH INTERVAL IN ELECTROLYTE PHASE
C       HETA    REDUCED MESH INTERVAL IN FILM PHASE
C       HF      MESH INTERVAL IN FILM PHASE
C       IFIXDTF =0 LOGARITHMIC TIME STEP USED WHEN FILM IS PRESENT
C       IFIXDTF =1 LOGARITHMIC TIME STEP NOT USED WHEN FILM IS
C               PRESENT
C       IFIXDTS =0 LOGARITHMIC TIME STEP USED FOR SOLUTION ONLY PROBLEM
C       IFIXDTS =1 LOGARITHMIC TIME STEP NOT USED FOR SOLUTION
C               ONLY PROBLEM
C       IFLAG   =1 SOLUTION ONLY PROBLEM
C       IFLAG   =2 FILM PRESENT
C       INI     INDICATES NI++ ION SPECIES #1
C       IH      INDICATES H+ ION SPECIES #4
C       INO3    INDICATES NO3- ION SPECIES #2
C       IRSP    INDICATES THE NUMBER OF IONIC SPECIES
C       IR      INDICATES FE++ ION SPECIES #4
C       IPHI    INDICATES POTENTIAL UNKNOWN #5
C       IL      INDICATES DDELTA UNKNOWN #6
C       IPASS   =0 ELECTRODE ACTIVE
C       IRESTRT =0 DO NOT RESTART
C       IRESTRT =1 RESTART
C       J       MESH POINT #
C       JCOUNT  ITERATION # FOR CONVERGENCE ON NONLINEARITIES
C       JFTIME  TIME STEP # WITH FILM PRESENT
```

```
C      JSTIME  TIME STEP # DURING CONCENTRATION BUILDUP PROCESS
C      JTIME   TIME STEP # FOR THE ENTIRE PROGRAM
C      LASTCYC LAST CYCLE TO BE CALUCULATED
C      N       NUMBER OF EQUATIONS AND UNKNOWNS
C      NATEND  =0 NOT AT END OF CYCLE WHEN RESTARTING
C      NATEND  =1 AT END OF CYCLE WHEN RESTARTING
C      NINC    MAXIMUM # OF ITERATIONS PERMITTED TO OBTAIN CONVERGENCE
C      NJ      TOTAL NUMBER OF MESH POINTS
C      NJD     MESH POINT AT FILM-SOLUTION INTERFACE
C      NLONG   =0 PRINT OUT PRESENT CONCENTRATION VALUES
C      NLONG   =1 PRINT OUT PRESENT LONG PROFILE CONCENTRATION VALUES
C      NPRINT  CONCENTRATIONS PRINTED AT EVERY NPRINT'TH VALUE OF J
C      NSHUHN  =0 NO SHOEHORN
C      NSHUHN  =1 USE SHOEHORN
C      OHMADJ  PARAMETER TO CONTROL (V - PHIO) JUMP SIZE
C      OHMCOR  OHMIC POTENTIAL DROP IN THE DIFFUSION LAYER
C      OHMIC   OHMIC POTENTIAL DROP IN THE BULK SOLUTION
C      OLDCH   VALUE OF CHECK FROM THE PREVIOUS TIME STEP
C      OLDTP   VALUE OF TPASS FROM THE PREVIOUS TIME STEP
C      OMEGA   ROTATION SPEED RAD/S
C      P       PARAMETER IN CONCENTRATION EFFECT TERM IN BV EQUATION
C      PII     -LOG(C(H+)X1000)
C      P3      (V - PHIO)
C      RATEKA  ANODIC RATE CONSTANT, MOL/CM SQ/S
C      RATEKC  CATHODIC RATE CONSTANT, CM/S
C      RGAS    GAS CONSTANT, JOULE/G-MOL/K
C      RHOF    MOLAR DENSITY OF NICKEL HYDROXIDE FILM, MOL/CU CM
C      RI      CURRENT DENSITY CALCULATED AT THE HALF MESH POINTS
C      RKAPPA  ELECTROLYTE CONDUCTIVITY, MHO/CM
C      RNU     KINEMATIC VISCOSITY, CM SQ/S
C      RTIME   PERIOD OF A CYCLE, S
C      RZERO   RADIUS OF THE DISK ELECTRODE, CM
C      S       STOICHIOMETRIC COEFFICIENT
C      SFT     FILM THICKNESS, MICRONS
C      SQRTT   SQUARE ROOT OF DIMENSIONLESS TIME
C      SSF     SUPERSATURATION FACTOR
C      STRI    IONIC STRENGTH OF NICKEL NITRATE IN THE BULK SOLUTION
C      SURDIF  DIFFUSION COMPONENT OF FLUX AT ELECTRODE SURFACE
C      SURFLX  FLUX OF A GIVEN SPECIES AT ELECTRODE SURFACE
C      SURMIG  MIGRATION COMPONENT OF FLUX AT ELECTRODE SURFACE
C      T       DIMENSIONLESS TIME NOT PERMITTED TO BE > 1
C      TFLOG   LOGARITHM OF THE TIME WHEN THE FILM IS PRESENT
C      TFLOGO  INITIAL VALUE FOR THE LOGARITHM OF TIME WHEN THE
C              FILM IS PRESENT
C      THLOG   INTERPOLATED VALUE OF THE LOGARITHM OF TIME
C      THTIME  DIMENSIONLESS TIME THAT IS SET TO ZERO AT THE BEGINNING
C              OF EACH CYCLE
C      TIMETH  DIMENSIONLESS TIME SPENT IN THE ACTIVE MODE DURING A
C              GIVEN CYCLE
C      TKELV   ABSOLUTE TEMPERATURE, K
C      TOLD    VALUE OF DIMENSIONLESS TIME FROM PREVIOUS TIME STEP
```

```
C     TOTEST   VARIABLE USED TO BE SURE THAT TOLD < 1
C     TPASS    <0 ELECTRODE IS ACTIVE
C              >0 ELECTRODE IS PASSIVE
C     TSLOG    LOGARITHM OF DIMENSIONLESS TIME WHEN FILM IS ABSENT
C     TSLOGO   INITIAL VALUE OF THE LOGARITHM OF THE DIMENSIONLESS TIME
C              THAT IS USED WHEN THE FILM IS ABSENT
C     TSPDS    # OF TIME STEPS PER DECADE WHEN FILM IS ABSENT
C     TSPDF    # OF TIME STEPS PER DECADE WHEN FILM IS PRESENT
C     TSTAR    DIMENSIONLESS TIME SINCE START OF HYDROXIDE ION
C              CONCENTRATION BUILDUP WHEN FILM IS NOT PRESENT
C     U        MOBILITY,
C     VFE      VALUE OF V - NORMAL HYDROGEN ELECTRODE REFERENCE
C              ELECTRODE POTENTIAL
C     XCP      CONCENTRATION DERIVATIVE
C     XI       DIMENSIONLESS VARIABLE IN ELECTROLYTE
C     XMIGF    MIGRATION COMPONENT OF FLUX FROM FILM AT INTERFACE
C     XMIGS    MIGRATION COMPONENT OF FLUX INTO SOLUTION AT INTERFACE
C     XNF      NET FLUX ACCULATING AT THE FILM-SOLUTION INTERFACE.
C     XX       DIMENSIONLESS DISTANCE FROM ELECTRODE
C     XXLONG   DIMENSIONLESS DISTANCE CORRESPONDING TO THE LONG
C              PROFILES
C     Z        CHARGE NUMBER
C     ZUFODR   CHARGE NUMBER*MOBILITY*FARADAY/H+ ION DIFFUSION COEF

      READ 301,LASTCYC,IRESTRT,OMEGA,RNU,TKELV,ALPHAA,ALPHAC,RZERO,
     1          ADJCONC
      READ 301,NSHUHN,ICONPAS,RKAPPA,FEN,RATEKA,RATEKC,CURPAS,BEGTPAS,
     1          PASS2

      F=96487.0
      ADISK=0.51023
      RGAS=8.3143


C     MUST SPECIFY INITIAL VALUES OF CBIG AND TIMETH TO PREVENT
C     WORKING WITH UNDEFINED QUATITIES

      CBIG = 0.010
      TIMETH = 0.033

      READ 301, NJD,NJ,H,RHOF
      IL = 6
      IPHI = 5
      IR = 4
        IRSP = 4
        IH = 4
        IOH = 3
        INO3 = 2
        INI = 1
        IFIX1 = 0
        IFIX2 = 0
      NJDP1 = NJD + 1
```

```
      NJDM1 = NJD - 1
      N = 5
      NM1 = N - 1
      NJM1 = NJ - 1
      QLF = 100.0
      IHSO4 = 1
      ISO4 = 3
      PI = ACOS(-1.0)
      HETA = 1.0/QLF

C     SET CDEV

      DO 9  I = 1,IL
        DO 9 K = 1,202
 9      CDEV(I,K) = 0.0

      PRINT 239,LASTCYC,IRESTRT,ICONPAS
      WRITE(7,239),LASTCYC,IRESTRT,ICONPAS

C       NSHUHN=0  NO SHOEHORN          IRESTRT=0  DO NOT RESTART
C       NSHUHN=1  USE SHOEHORN         IRESTRT=1  RESTART

      PRINT 209,NSHUHN


      READ 302, (U(I),DIF(I),Z(I),S(I),REF(I),I=1,NM1)
      PRINT 201, NJ,H,(REF(I),U(I),DIF(I),Z(I),S(I),I=1,NM1)

C     ADJUST THE KINEMATIC VISCOSITY TO ACCOUNT FOR CONCENTRATED SOLNS
C     ADJUST THE DIFFUSION AND MIGRATION COEFFICIENTS TO ACCOUNT FOR
C     CONCENTRATED SOLUTIONS

      RNU = RNU*ADJCONC

      DO 10  I = 1,IRSP
        DIF(I) = DIF(I)/ADJCONC
 10     U(I) = U(I)/ADJCONC

      PRINT 201, NJ,H,(REF(I),U(I),DIF(I),Z(I),S(I),I=1,NM1)
      WRITE(7,201),NJ,H,(REF(I),U(I),DIF(I),Z(I),S(I),I=1,NM1)
      READ 301,IFIXDTS,IFIXDTF,VFE,TSLOGO,TFLOGO,TSPDS,TSPDF,DELTA
      READ 301,NPRINT,NINC,STRI,EQCON,CSAT,SSF,EPO,PASS1

      EPSURZ = 0.01
        EPSUR = EPO
      P = 0.0
      PSET = 1.75
      OHMADJ = 0.0
      CFEMAX = 0.008
      PRINT 244, EPSUR,EPO,ADJCONC
      WRITE (7,244), EPSUR,EPO,ADJCONC
```

```
      PRINT 245, P
      WRITE (7,245), P

C         IF IRESTRT = 1 READ IN ALL THE VARIABLES REQUIRED TO RESTART

      IF (IRESTRT .NE. 1) GO TO 12
      READ 229,IPASS,JSTIME,IFIXDTS,IFIXDTF,IFLAG,JFTIME,NJ,N,ICYCLE,
     1 NSHUHN,NLONG,NM1,NJM1,JTIME,NATEND
      READ 230,DTSET,DELTA,THTIME,TSTAR,DTLOG,DTLOGF,TFLOG,CBEGIN,RATIO,
     1 T,SQRTT,
     1 TSLOG,((C(I,K),COLD(I,K), K = 1,NJ), I = 1,IL)
      IF((ICYCLE.EQ.1).OR.(IFLAG.EQ.2))READ 230,(XXLONG(K),(CLONG(I,K),
     1 I = 1,IL), K = 1,NJDP1)
      IF((ICYCLE.EQ.1).OR.(IFLAG.EQ.2))READ 230,(CINTR(I), I = 1,IPHI)
      IF(IFLAG.EQ.2) READ 230,PASSOLD,TPASS,PASSMAX,(ETA(K), K = 1,NJ),
     1 TOTEST,OHMADJ,CHECK,OLDTP,OLDCH

         TSPDS = 1.0/DTLOG
         TSCT = INT(TSLOG) + 1.0
         IF(C(IH,NJM1).LT.0.004E-7)IFIX1 = 1
         IF(C(IH,NJM1).LT.0.0009E-7)IFIX2 = 1
      PRINT 204,N,IFIXDTF,NPRINT,STRI,EQCON,EPO,DELTA


      DO 11  J = 1,NJ
 11   CLONG(IPHI,J) = 0.0

      PRINT 232
      NPRINT = 10
      CALL CPRINT
      NPRINT = 100

 12 PRINT 204,N,IFIXDTF,NPRINT,STRI,EQCON,EPO,DELTA

      IF(IFLAG .EQ. 1) DELHAT = 0.0
      DO 13 I = 1,IRSP
 13   ZUFODR(I) = Z(I)*U(I)*F/DIF(IR)

      PRINT 206, (I,ZUFODR(I),  I = 1,IRSP)

      DIMROT = (ADISK*RNU/3.0/DIF(IR))**(1./3.)*SQRT(OMEGA/RNU)
      FA = ALPHAA*F/RGAS/TKELV
      FC = ALPHAC*F/RGAS/TKELV
      PRINT 222, OMEGA,RNU,ADISK,RGAS,TKELV,ALPHAA,ALPHAC,RZERO,
     1 RKAPPA,FEN,DIMROT,FA,FC,RATEKA,RATEKC,PASS1,PASS2,EQCON,BEGTPAS,
     1 NATEND
      WRITE(7,222),OMEGA,RNU,ADISK,RGAS,TKELV,ALPHAA,ALPHAC,RZERO,
     1 RKAPPA,FEN,DIMROT,FA,FC,RATEKA,RATEKC,PASS1,PASS2,EQCON,BEGTPAS,
     1 NATEND
      WRITE(7,224)
```

```
C          CALCULATE MAX CONCENTRATION BEFORE PRECIPITATION OF FILM

           CMAX = CSAT*SSF
           CBULK = 0.00256

           PRINT 203,CSAT,SSF,CMAX

C          USE EQUILIBRIUM CONSTANT (EQCON) AND CBULK TO
C          CALCULATE THE H+, NO3-, AND THE NI++ BULK CONCS.

           PHO = 4.33
C          PHO = 2.2218
           CIN(IH) = 10.**(-PHO)/1000.
           CIN(IOH) = EQCON/CIN(IH)
           CIN(INI) = CBULK
           CIN(INO3) = CIN(IH) - CIN(IOH) + 2.*CIN(INI)
           CBK(INO3) = CIN(INO3)
           CBK(INI)  = CIN(INI)
           CIN(INO3) = 0.0
           CIN(INI) = 0.0
           CBK(IH)   = 0.0
           CBK(IOH)  = 0.0

C          THE UNKNOWNS ARE
C          1 HSO4-   2 H+   3 SO4--   4 FE++   5 POTENTIAL   6 DDELTA

C          SET B.C. AT INFINITY FOR THE POTENTIAL AND DDELTA

           CIN(IPHI) = 0.0
           CIN(IL) = 0.0

           PRINT 205,IFIXDTS,VFE,TSLOGO,TFLOGO,TSPDS,TSPDF,NINC
           WRITE (7,205),IFIXDTS,VFE,TSLOGO,TFLOGO,TSPDS,TSPDF,NINC

           DTLOGF =1./TSPDF
           DTLOG =1./TSPDS

           IF(IRESTRT.EQ.0) GO TO 14

C          IF RESTARTING, DO NOT WANT TO INITIALIZE VARIABLES
C          IF RESTARTING, TEST TO SEE WHETHER FILM IS
C          OR IS NOT PRESENT, AND GO TO THE APPROPRIATE LOCATION

           IF(IFLAG - 1) 17,17,56

        14 ICYCLE = 0
           PRINT 205,IFIXDTS,VFE,TSLOGO,TFLOGO,TSPDS,TSPDF,NINC

C          SET THE INITIAL CONDITIONS FOR BOTH THE PRESENT AND OLD
C          CONCENTRATION VARIABLES
```

```
      DO 15  J = 1,202
        C(IPHI,J) = 0.0
        COLD(IPHI,J) = C(IPHI,J)
        C(IL,J) = 0.0
        COLD(IL,J) = 0.0
             DO 15  I = 1,IRSP
                   C(I,J) = CIN(I)
                   COLD(I,J) = C(I,J)
   15 CONTINUE

C      INITIALIZE SOME OTHER CONTROLLING PARAMETERS

   16 IPASS = 0
      IFIXDTS = 0
      IFIXDTF = 0
      IFLAG = 1
      N = 5
      NM1 = N - 1
      NJ = 102
      NJM1 = NJ - 1
      NLONG = 0
      JTIME = 0
      JSTIME = 0
      JFTIME = 0
      DELTA = 0.0
      THTIME = 0.0
      TSTAR = 0.0
      DTSET = 0.0
      RATIO = 0.1
        TSLOGO = -6.0
        TSPDS = 4.0
        TSCT = TSLOGO + 1.0
      TSLOG = TSLOGO - DTLOG
      TFLOG = TFLOGO - DTLOGF
      T = 0.0

      PRINT 207,ICYCLE,N,NM1,NJ,NJM1

C      ESTABLISH THE DISTANCE VARIABLE, XI

   17 DO 18  K = 1,NJ
   18    XI(K) = H*FLOAT(NJ - K -1)

      DO 19  K = 103,202
        DO 19  I = 1,IL
   19      COLD(I,K) = 0.0

C      THIS LOOP CALCULATES THE BUILDUP OF HYDROXIDE ION CONCENTRATION
C      WHEN NO FILM IS PRESENT.  THIS IS REFERED TO AS PHASE 1
C      IN THE THESIS
```

```
   20 JSTIME = JSTIME + 1

      IF (JSTIME .GE.697) STOP

C         CALCULATE TIME STEP SIZE DT, WITH DT = 0 IF JSTIME = 1
C         FOR IFIXDTS=0 THERE IS AN EXPONENTIAL INCREASE IN TIME STEP SIZE

      IF (JSTIME .EQ. 1) GO TO 22
      IF (IFIXDTS .EQ. 1) GO TO 21
        DTLOG = 1.0/TSPDS
      TSLOG = TSLOG + DTLOG
        IF(TSLOG.GE.TSCT)TSPDS = TSPDS*2.0
        IF(TSLOG.GE.TSCT)TSCT = TSCT + 1.0
      DT = 10.0**TSLOG - 10.0**(TSLOG - DTLOG)
      IF (JSTIME .EQ. 2) DT = 10.0**TSLOG
      GO TO 23
   21 DT = DTSET
      GO TO 24
   22 DT = 0.0
      TOLD = 0.0
      SQRTOLD = 0.0
   23 DTSET = DT/3.
   24 TSTAR = TSTAR + DT

C         T IS NEVER PERMITTED LARGER THAN 1, THIS TIME STRETCHES THE
C         THE VARIABLE XI

      T = T + DT
      IF (T .GT. 1.0) T = 1.0
      SQRTT = SQRT(T)
      IF (JSTIME .GE. 2) TOLD = TSTAR - DT
      IF (TOLD .GT. 1.0) TOLD = 1.0
      IF (JSTIME .GE. 2) SQRTOLD = SQRT(TOLD)
      PRINT 211, JSTIME,TSLOG,DT,TSTAR,IFIXDTS,IFIXDTF

C         SET VELOCITY PROFILE FOR THE ROTATING DISK

      DO 25  J = 1,NJ
   25   V(J) = 3.0*T*XI(J)**2

C         IF JSTIME > 1 CALCULATE THE VALUE OF XX FROM XI

      IF (JSTIME - 1) 26,26,28

   26 DO 27  I = 1,NJ
   27   XX(I) = 0.0
      GO TO 30

   28 DO 29  I = 1,NJ
   29   XX(I) = XI(I)*SQRTT
```

```
30 XXMAX = XX(1)

C        ASSIGN MAKES THE CORRECT CHOICE FOR THE BOUNDARY CONDITION
C        AT XI = XIMAX, USING CONCENTRATIONS AT XXMAX

   CALL ASSIGN

C        THE PARAMETER CBEGIN IS USED TO CONTROL TIME STEP SIZE

   IF (JSTIME .EQ. 1) CBEGIN = C(IOH,NJD)

   JCOUNT = 0

C        THE JCOUNT LOOP CONVERGES ON NONLINEARITIES

31 JCOUNT = JCOUNT + 1
   J = 0

C        INITIALIZE X AND Y

   DO 32 I = 1,N
            DO 32 K = 1,N
                        Y(I,K) = 0.0
32                      X(I,K) = 0.0

33 J = J + 1
C
C        INITIALIZE G,A,B, AND D
C
   DO 34  I = 1,N
      G(I) = 0.0
               DO 34  K = 1,N
                       A(I,K) = 0.0
                       B(I,K) = 0.0
34                     D(I,K) = 0.0

   IF (J - 1)  35,35,36

C        SET B.C. AT J=1, XI = XIMAX

35 CALL BC1
   CALL BAND
   GO TO 33

36 IF (J - NJ)  37,38,38

C        SET COEFFICIENTS FOR 1<J<NJ

37 CALL COEF
   CALL BAND
   GO TO 33
```

```
C         SET B.C. AT J = NJ , XI = 0

   38 CALL BCNJ
      CRO = C(INO3,NJM1)
        CROOH=C(IOH,NJM1)

C         THE ERROR IN EACH EQUATION (G(I)) MAY BE PRINTED TO MONITOR
C         CONVERGENCE

C         IF(JSTIME .LE. 14) PRINT 227,(JCOUNT,(G(I), I = 1,N),CRO)

      CALL BAND

C         AFTER THE DEVIATION VARIABLES ARE COMPUTED, THE UPDATED VALUES
C         OF THE VARIABLES ARE OBTAINED BY ADDING THE DEVIATIONS TO THE
C         PREVIOUS VALUES

      DO 39  I = 1,N
        DO 39  K = 1,NJ
   39     C(I,K) = C(I,K) + CDEV(I,K)

C         DON'T ALLOW ANY CONCENTRATION TO GO NEGATIVE

      DO 40  I = 1,IRSP
        DO 40  K = 2,NJM1
        IF(I.EQ.INO3)GO TO 40
        IF(I.EQ.INI)GO TO 40
          IF(C(I,K) .LE. 0.0) C(I,K) = 1.0E-20
   40 CONTINUE
      CTEST = C(INO3,NJM1)
        CTESTOH=C(IOH,NJM1)
      IF(JSTIME.EQ.1) CTEST = CBK(INO3)

C         TEST THE SURFACE CONCENTRATION FOR CONVERGENCE

      IF (ABS(CRO - C(INO3,NJM1)) .LE. 1.0E-8*ABS(CTEST))GO TO 41

C         IF NOT CONVERGED RETURN TO JCOUNT LOOP UNLESS JCOUNT=NINC
C         IN WHICH CASE WE GIVE UP

      IF (JCOUNT .LE. NINC) GO TO 31
      PRINT 202,JCOUNT
      PRINT 223,OHMIC,OHMCOR,C(IPHI,NJM1),P3,CUR
      CALL CPRINT
      STOP

   41 CALL UPDATE

      GO TO 504
      PRINT 242
```

```
      TRUOHM = 0.0
      OHMINF = 0.0
      DIFCOM = 0.0

      DO 502  J = 2,NJM1

         SUM1 = 0.0
         SUM2 = 0.0

         DO 503  I = 1,IRSP
            SUM1 = SUM1 + Z(I)*DIF(I)*CP(I)
503         SUM2 = SUM2 + Z(I)**2*U(I)*(C(I,J)+CBK(I))
      DIMCUR = -F**2*CP(IPHI)*SUM2 - F*SUM1

         SUM1 = SUM1*F
         SUM2 = SUM2*F**2

         TRUOHM = TRUOHM + DIMCUR/SUM2
         OHMINF = OHMINF + DIMCUR/RKAP1
         DIFCOM = DIFCOM + SUM1/SUM2
         TOTALP = TRUOHM + DIFCOM
         ETACEQ = TOTALP - OHMINF

         PRINT 241,J,SUM1,SUM2,TRUOHM,OHMINF,
     1        DIFCOM,TOTALP,C(IPHI,J),ETACEQ,DIMCUR
  502 CONTINUE
  504 CONTINUE
C     IF(MOD(JSTIME,4) .EQ. 0) NPRINT = 10
      NPRINT = 10
      DO 500 I=1,IRSP,1
  500 PRINT 218,I,SURMIG(I),SURDIF(I),SURFLX(I)
      PRINT 223,OHMIC,OHMCOR,C(IPHI,NJM1),P3,CUR
      PH = -ALOG10(1000.0*C(IH,NJM1))
      EPSLN = EPSILN(DELHAT)
      WRITE(7,225),IPASS,JCOUNT,JSTIME,JFTIME,TSTAR,THTIME,DELTA,OHMIC,
     1 TPASS,EPSUR,P3,CUR,C(INO3,NJM1),PH
      IF(JSTIME .EQ. 18) NPRINT = 10
      CALL CPRINT
      NPRINT = 100


C        IF C IS APPROACHING CMAX, SET THE TIME STEP SIZE

C     IF((C(IOH,NJD)-CBEGIN)/(CMAX-CBEGIN).GE. 0.7) IFIXDTS = 1
C     IF((C(IOH,NJD)-CBEGIN)/(CMAX-CBEGIN)-RATIO.LT.0.15)DTSET=1.5*DTSET
C     IF((C(IOH,NJD)-CBEGIN)/(CMAX-CBEGIN)-RATIO.GT.0.25)DTSET=DTSET/3.0
      RATIO = (C(IOH,NJD)-CBEGIN)/(CMAX-CBEGIN)
         IF(C(IH,NJM1).LT.0.15E-7)IFIXDTS=1
         IF(C(IH,NJM1).LT.0.003E-7)IFIX1=IFIX1 + 1
         IF(IFIX1.EQ.1)DTSET=DTSET/5.
         IF(C(IH,NJM1).LT.0.0006E-7)IFIX2=IFIX2 + 1
         IF(IFIX2.EQ.1)DTSET=DTSET/5.
```

```
C       EVERY 4TH TIME STEP WRITE EVERYTHING TO TAPE 8 IN CASE A RESTART
C       IS NEEDED

        IF(MOD(JSTIME,5).NE.0) GO TO 42

        NATEND = 0
          DTLOG = 1.0/TSPDS
        WRITE(8,229),IPASS,JSTIME,IFIXDTS,IFIXDTF,IFLAG,JFTIME,NJ,N,
     1  ICYCLE,NSHUHN,NLONG,NM1,NJM1,JTIME,NATEND
        WRITE(8,230),DTSET,DELTA,THTIME,TSTAR,DTLOG,DTLOGF,TFLOG,CBEGIN,
     1  RATIO,T,SQRTT,
     1  TSLOG,((C(I,K),COLD(I,K), K = 1,NJ), I = 1,IL)
        IF(ICYCLE.EQ.1) WRITE(8,230),(XXLONG(K),(CLONG(I,K),
     1  I = 1,IL), K = 1,NJDP1)
        IF(ICYCLE.EQ.1) WRITE(8,230),(CINTR(I), I = 1,IPHI)
        REWIND 8

C       TEST TO SEE IF C(IOH,NJM1) > CMAX, IF SO FORM FILM

   42 IF (C(IOH,NJM1) - CMAX)  20,43,43

C       PRINT OUT THE DERIVATIVES WITH RESPECT TO X

   43 J = NJM1
      PRINT 240
      DO 45  I = 1,IL
        DWRPTX = CP(I)/H
   45    PRINT 218,I,DWRPTX

C       CALCULATE DIMENSIONLESS CURRENT

      J = 3
      SUM1 = 0.0
      SUM2 = 0.0

      DO 47  I = 1,IRSP
        SUM1 = SUM1 + Z(I)**2*U(I)*(C(I,J) + CBK(I))
   47    SUM2 = SUM2 + Z(I)*DIF(I)*CP(I)

      DIMCUR = -F**2*CP(IPHI)*SUM1 - F*SUM2

      PRINT 242

      TRUOHM = 0.0
      OHMINF = 0.0
      DIFCOM = 0.0

      DO 50  J = 2,NJM1

        SUM1 = 0.0
        SUM2 = 0.0
```

```
      DO 49  I = 1,IRSP
          SUM1 = SUM1 + Z(I)*DIF(I)*CP(I)
49        SUM2 = SUM2 + Z(I)**2*U(I)*(C(I,J) + CBK(I))

      SUM1 = SUM1*F
      SUM2 = SUM2*F**2

      TRUOHM = TRUOHM + DIMCUR/SUM2
      OHMINF = OHMINF + DIMCUR/RKAP1
      DIFCOM = DIFCOM + SUM1/SUM2
      TOTALP = TRUOHM + DIFCOM
      ETACEQ = TOTALP - OHMINF

      IF(MOD(J+4,5) .EQ. 0) PRINT 241,J,SUM1,SUM2,TRUOHM,OHMINF,
    1     DIFCOM,TOTALP,C(IPHI,J),ETACEQ
50 CONTINUE

      PRINT 243,P6,P7,RKAP1,XXMAX,XX(NJM1)

C     SAVE PROFILES AT C(FE,NJM1) > CMAX, CALL THEM CLONG

      DO 53 J = 1,NJDP1
        XXLONG(J) = XX(J)
          DO 53 I = 1,IL
              CLONG(I,J) = C(I,J)
53            IF(I .EQ. IPHI) CLONG(I,J) = 0.0

C     T IS RESET TO START THE FILM FORMATION PROCESS

      SQRTSAV = SQRTT
      T = 0.0
      SQRTT = SQRT(T)
      TOTEST = 0.0

C     T VARIABLE USED TO STRETCH LENGTH VARIABLE, ALWAYS < 1.0
C     TOTEST VARIABLE USED TO BE SURE THAT TOLD IS ALWAYS < 1.0

54 PRINT 214
      NPRINT = 5
      NLONG = 1
      CALL CPRINT
      NPRINT = 100
      NLONG = 0

      IF(ICYCLE .GE. 1) GO TO 59

C     GO TO THE ZERO TIME FORMULATION OF THE EQUATIONS

      NJ = 202
      NJM1 = NJ - 1
      N = 6
```

```
      NM1 = N - 1

C        ERROR FUCTION SOLUTION GIVES FIRST GUESS FOR FILM THICKNESS

      C(IL,NJD)=2.*(CLONG(IOH,NJD) - CSAT)/SQRT(PI)/(1.- EPSILN(DELHAT))
     1 /RHOF
      C(IOH,NJD) = CSAT

C        SET CONCENTATIONS TO THEIR VALUE AT THE FILM SOLUTION INTERFACE
C        THIS MAKES CONVERGENCE EASIER FOR THE ZERO TIME FORMULATION

      DO 55 K = 1,NJ
          ETA(K) = FLOAT(NJM1 - K)/FLOAT(NJM1 - NJD)
              DO 55 I = 1,IL
 55           C(I,K) = C(I,NJD)

 56 DO 57  K = 1,NJDP1
 57   XI(K) = H*FLOAT(NJD - K)

      PRINT 208
      IFLAG = 2
      HF = (DELTA + C(IL,10))*HETA
      CALL CPRINT

C        SET VELOCITY IN FILM EQUAL TO ZERO

      DO 58  K  = NJDP1,NJ
 58   V(K) = 0.0

      IF (NATEND .EQ. 1) GO TO 59
      IF (IRESTRT .EQ. 1) GO TO 60

 59 PRINT 207,ICYCLE,N,NM1,NJ,NJM1

      THTIME = 0.0
      TFLOG = TFLOGO
      IFIXDTF = 0
      JFTIME = 0
      IPASS = 0

C        THIS LOOP IS USED WHEN THE FILM IS PRESENT

 60 JFTIME = JFTIME + 1
      JTIME = JTIME + 1

      IF(JTIME .GE. 3) P = PSET
      IF(JFTIME .GE. 2) OLDTP = TPASS
      IF(JFTIME .GE. 2) OLDCH = CHECK
C        IF ((JFTIME .EQ. 3) .AND. (IPASS .EQ. 1)) STOP
      IF (JFTIME .EQ.2) STOP
```

```
C          CALCULATE PH AND VPASS AT THE GIVEN VALUE OF PH

           PH = -ALOG10(1000.0*C(IH,NJM1))
           VPASS = PASS1 - PASS2*PH

C          CALCULATE DT, WITH DT = 0 IF JTIME = 1

           IF (JTIME .EQ. 1) GO TO 62
           IF(JTIME.EQ.2) TFLOG = -10.25
           IF(JTIME.EQ.2) DTLOGF = 1./4.
             IF(JTIME.GE.20) IFIXDTF = 1
           IF (IFIXDTF .EQ. 1) GO TO 61
           TFLOG = TFLOG + DTLOGF
           DT = 10.0**TFLOG - 10.0**(TFLOG - DTLOGF)
           IF (JTIME .EQ. 2) DT = 10.0**TFLOG
           GO TO 63
        61 DT = DTSET
           DT=0.1E-6
           GO TO 64
        62 DT = 0.0
           TOLD = 0.0
           SQRTOLD = 0.0
        63 DTSET = DT/3.
        64 TSTAR = TSTAR + DT
           TOTEST = TOTEST + DT
           THTIME = THTIME + DT
           T = T + DT
           IF(T .GT. 1.0) T = 1.0

C          T NEVER GREATER THAN 1 SO THAT XX IS NEVER LARGER THAN 6

           SQRTT = SQRT(T)
           IF (JTIME .GE. 2) TOLD = TOTEST - DT
           IF (TOLD .GT. 1.0) TOLD = 1.0
           IF (JTIME .GE. 2) SQRTOLD = SQRT(TOLD)
           PRINT 216, JSTIME,JFTIME,TFLOG,DT,TSTAR,THTIME,IFIXDTS,IFIXDTF

C          SET VELOCITY PROFILE FOR THE ROTATING DISK

           DO 65  J = 1,NJD
             V(J) = 3.0*T*XI(J)**2
        65   XX(J) = XI(J)*SQRTT

C       PRINT 212
C       PRINT 210,(V(J), J = 1,NJ,NPRINT)

           XXMAX = XX(1)

C          ASSIGN WILL ESTABLISH THE CORRECT BOUNDARY CONDITION AT
C          XI = INFINITY.  THE BOUNDARY CONDITIONS ARE LINEARLY
C          INTERPOLATED FROM CLONG IF XXMAX < XXLONG(1)
```

```
C        THE B.C. IS SET EQUAL TO CIN IF XXMAX > XXLONG(1)

      CALL ASSIGN

C  *   START LOOP THAT CONVERGES ON THE NONLINEARITY

      JCOUNT = 0
   66 JCOUNT = JCOUNT + 1
      HF = (DELTA + C(IL,10))*HETA
      DELHAT = DELTA + C(IL,10)

      J = 0

C        INITIALIZE X AND Y

      DO 67 I = 1,N
        DO 67 K = 1,N
              X(I,K) = 0.0
   67         Y(I,K) = 0.0

   68 J = J + 1

C        INITIALIZE A,B,D,G

      DO 69  I = 1,N
        G(I) = 0.0
        DO 69  K = 1,N
              A(I,K) = 0.0
              B(I,K) = 0.0
   69         D(I,K) = 0.0

      IF (J - NJD) 70,75,71

C        GOVERNING EQUATION #6, DC(6)/DXI = 0 FOR THE SOLUTION

   70 B(6,IL) = 1.0
      D(6,IL) = -1.0
      GO TO 73

C        GOVERNING EQUATION #6, DC(6)/DXI = 0 FOR THE FILM

   71 B(6,IL) = 1.0
      A(6,IL) = -1.0
      GO TO 76

   72 CALL BC1
      CALL BAND
      GO TO 68

   73 IF (J - 1) 72,72,74
```

```
C           SET COEFFICIENTS FOR 1<J<NJD AND NJD<J<NJ

   74 CALL COEF
      CALL BAND
      GO TO 68

C           SET COEFFICIENTS FOR NJD

   75 CALL COEFNJD
      CALL BAND
      GO TO 68

C           TEST FOR J = NJ

   76 IF (J - NJ) 74,77,77

C           SET BC AT THE ELECTRODE SURFACE

   77 CALL BCNJ

      CRO = C(IOH,NJM1)
C     CRO = C(INO3,NJM1)
      CPRSF = CPSF(IOH,NJD)

C           MAY PRINT OUT ERRORS IN EACH EQUATION TO MONITOR CONVERGENCE

      IF(JFTIME .GE. 1) PRINT 228,(JCOUNT,(G(I), I = 1,N),CPRSF)

      CALL BAND

C           IF SHOEHORN IS BEING USED,
C           CHECK TO BE SURE THAT THE DEVIATION IN ANY VARIABLE
C           IS NO GREATER THAT 90% OF THE VALUE OF THAT VARIABLE.
C           IF THE DEVIATION IS LARGER THAN THIS VALUE, SET IT EQUAL TO
C           0.9 OF THE ORIGINAL VALUE

      IF (NSHUHN .EQ. 0) GO TO 83

      FACTOR = 0.9
      IF(JCOUNT .GT. 4) FACTOR = 2.0
      DO 82  I = 1,N
        DO 82 K = 1,NJ
          IF(ABS(CDEV(I,K)) - FACTOR*ABS(C(I,K))) 82,82,78
   78     IF(CDEV(I,K)) 79,79,80
   79     SIGN = -1.0
          GO TO 81
   80     SIGN = 1.0
   81     CDEV(I,K) = SIGN*FACTOR*ABS(C(I,K))
   82 CONTINUE

C           AFTER THE DEVIATION VARIABLES ARE COMPUTED, THE UPDATED VALUES
```

```
C        OF THE VARIABLES ARE OBTAINED BY ADDING THE DEVIATIONS TO THE
C        OLD VALUES

   83 DO 84  I = 1,N
         DO 84  K = 1,NJ
   84        C(I,K) = C(I,K) + CDEV(I,K)

C     IF(JFTIME.LE.4)PRINT 228,(JCOUNT,(CDEV(I,NJM1),I=1,N),C(IOH,NJM1))

C        DON'T ALLOW HYDROGEN CONCENTRATION TO GO NEGATIVE

         DO 85  K = 2,NJM1
   85    IF(C(IH,K) .LE. 0.0) C(IH,K) = 1.0E-20

C        TEST FOR CONVERGENCE WITH CONCENTRATION AND DERIVATIVE

         IF ((ABS(CPRSF-CPSF(IOH,NJD)).LE.1.0E-8*ABS(CPSF(IOH,NJD))) .AND.
     1   (ABS(CRO-C(IOH,NJM1)).LE.1.0E-8*ABS(C(IOH,NJM1)))) GO TO 88

C        IF NOT CONVERGED RETURN TO THE JCOUNT LOOP UNLESS JCOUNT=NINC
C        IN WHICH CASE WE PRINT OUT THE MISERY AND PUNT

         IF (JCOUNT - NINC) 66,87,87

   87 PRINT 202,JCOUNT
      PRINT 223,OHMIC,OHMCOR,C(IPHI,NJM1),P3,CUR
      NPRINT = 10
      CALL CPRINT
      STOP

C        UPDATE CONCENTRATIONS

   88 CALL UPDATE
      DELTA = DELTA + C(IL,10)

      IF(C(IH,NJM1) .GT. 0.0) GO TO 89

      NPRINT = 10
      CALL CPRINT
      NPRINT = 100

   89 PH = -ALOG10(1000.0*C(IH,NJM1))
      VPASS = PASS1 - PASS2*PH
      TPASS = P3 - VPASS
      SFT = DELTA*SQRTT/DIMROT*10000.0
      PRINT 223,OHMIC,OHMCOR,PHIZRO,P3,CUR,VPASS,TPASS,SFT,PH
      EPSLN = EPSILN(DELHAT)
      WRITE(7,225),IPASS,JCOUNT,JSTINE,JFTIME,TSTAR,THTIME,DELTA,OHMIC,
     1   TPASS,EPSUR,P3,CUR,C(IOH,NJM1),PH
      IF (JTIME .LE. 3) NPRINT = 10
      IF (MOD(JFTIME,5) .EQ. 0) NPRINT = 10
```

```
      CALL CPRINT
      NPRINT = 100


C      CALCULATE THE CURRENT DENSITY AT EACH HALF MESH POINT AND PRINT
C      RI(J) IS THE CURRENT BETWEEN J-1 AND J

      IF(DT .EQ. 0.0) GO TO 95

      DO 92  J = 2,NJD
        SUM1 = 0.0
        SUM2 = 0.0

          DO 91  I = 1,IRSP
               SUM1 = SUM1 + Z(I)**2*U(I)*(CBARF(I)+CBK(I))
   91          SUM2 = SUM2 + Z(I)*DIF(I)*CPFOR(I)

   92   RI(J) = (-F**2*CPFOR(IPHI)*SUM1 - F*SUM2)*DIMROT/SQRTT/H

      DO 94  J = NJDP1,NJ
        SUM1 = 0.0
        SUM2 = 0.0

          DO 93  I = 1,IRSP
               SUM1 = SUM1 + Z(I)**2*U(I)*(CBARF(I)+CBK(I))
   93          SUM2 = SUM2 + Z(I)*DIF(I)*CPFOR(I)

   94   RI(J) = EPSILN(DELHAT)*(-F**2*CPFOR(IPHI)*SUM1 - F*SUM2)
     1                              *DIMROT/DELTA/SQRTT/HETA

      EPSLN = EPSILN(DELHAT)
      PRINT 238, (J,RI(J),  J = 50,NJ,100)
      PRINT 244,EPSUR,EPSLN

C      EVERY 3RD TIME STEP PRINT OUT THE FLUX COMPONENTS AT THE
C      INTERFACE

      IF (MOD(JFTIME,3) .NE. 0) GO TO 98

   95 PRINT 217

      DO 96  I = 1,IRSP,1
   96 PRINT 218,I,XMIGF(I),DF(I),XMIGS(I),DS(I),XNF(I)

      PRINT 219

      DO 97  I = 1,IRSP,1
   97 PRINT 218,I,SURMIG(I),SURDIF(I),SURFLX(I)

C      FOR JTIME = 1 WANT TO CHANGE THE VALUE OF C60 USED AS THE
C      FIRST GUESS ON THE NEXT TIME STEP. ONLY EXPECT DELHAT TO
```

```
C       CHANGE A SMALL AMOUNT, SO SET C(IL,J) EQUAL TO -.1* ITS PREVIOUS
C       VALUE

   98 IF(JTIME .NE. 1) GO TO 100

      DO 99  K = 1,NJ
   99  C(IL,K) = -0.0001*C(IL,K)

  100 IF(JFTIME .NE. 2) GO TO 101

      PASSMAX = ABS(TPASS)
      PASSOLD = PASSMAX

  101 IF(JFTIME .LE. 2) GO TO 60
      ATPASS = ABS(TPASS)
      FREEZE = 0.35
      CHECK = ATPASS/PASSMAX
      IF((C(IOH,NJM1)/CFEMAX.GT. 0.85) .AND. (IPASS .EQ. 0)) IFIXDTF = 1


C       EVERY 4TH TIME STEP WRITE TO DISK FOR RESTART PURPOSES

      IF(MOD(JFTIME,4).NE.0) GO TO 104

      NATEND = 0
      WRITE(8,229),IPASS,JSTIME,IFIXDTS,IFIXDTF,IFLAG,JFTIME,NJ,N,
     1  ICYCLE,NSHUHN,NLONG,NM1,NJM1,JTIME,NATEND
      WRITE(8,230),DTSET,DELTA,THTIME,TSTAR,DTLOG,DTLOGF,TFLOG,CBEGIN,
     1  RATIO,T,SQRTT,
     1  TSLOG,((C(I,K),COLD(I,K), K = 1,NJ), I = 1,N)
      WRITE(8,230),(XXLONG(K),(CLONG(I,K),I = 1,N), K = 1,NJDP1)
      WRITE(8,230),(CINTR(I), I = 1,IPHI)
      WRITE(8,230),PASSOLD,TPASS,PASSMAX,(ETA(K),K = 1,NJ),TOTEST,OHMADJ
     1  ,CHECK,OLDTP,OLDCH
      REWIND 8

  104 IF (IPASS) 112,105,112

  105 IF (TPASS) 60,60,60
  112 CONTINUE
      STOP
      END
CCCCCCCCCCCCCCCCCCCCCCCCCCCCCCCCCCCCCCCCCCCCCCCCCCCCCCCCCCCCCCCCCCCCCCCCCC

      SUBROUTINE ASSIGN
      COMMON /B2/C
     1 /B6/CIN,DIF,V,S,Z,U,ZUFODR,CBK
     1 /B7/CSAT,DELTA,RHOF,DT,EQCON,EPO,F,H,HF,N,IFLAG,
     1     IPASS,IHSO4,IH,ISO4,IR,IPHI,IL,JSTIME,JFTIME,JCOUNT,THTIME,
     1     TSTAR,NJ,NJM1,NPRINT,QLF,NJD,NJD*1,NJDM1,HETA,JTIME
     1 /B17/CINTR
```

```
      1 /B19/XX,XXLONG,CLONG,XXMAX,NLONG
      1 /B26/ICYCLE
      1 /B30/XXTEST
       DIMENSION C(6,202),XX(202),XXLONG(202),CLONG(6,202),
      1  CIN(6),DIF(6),V(202),S(6),Z(6),ZUFODR(6),CINTR(6),U(6),CBK(4)

       TWEEK = 1.0E-14

C       TEST TO SEE IF IN PHASE 1, CONCENTRATION BUILDUP, FILM
C       ABSENT

       IF(ICYCLE) 10,10,13
   10 IF(IFLAG .EQ. 2) GO TO 13

C       SET THE BOUNDARY CONDITION EQUAL TO CIN FOR PHASE 1
C       AND WHENEVER XXMAX IS GREATER THAN OR EQUAL TO XXLONG(1)

   11 XXTEST = XXMAX

       DO 12 I = 1,N
   12   CINTR(I) = CIN(I)

       RETURN

C       IF XXMAX > XXLONG(1) SET CINTR = CIN

   13 IF ((XXMAX + TWEEK) .GE. XXLONG(1)) GO TO 11

C       XXMAX WILL BE LESS THAN XXLONG SHORTLY AFTER INITIAL
C       FILM PRECIPITATION.
C       INTERPOLATE ON THE CLONG PROFILE TO FIND THE VALUE OF THE
C       BC'S WHEN XI = XI(MAX) AT THE LOCATION CORRESPONDING TO XXMAX

       XXTEST = XXLONG(1)

C       FIND OUT WHICH TWO VALUES OF XXLONG XXMAX IS BETWEEN

       DO 14  K = 1,NJD
          KOUT = K
          IF((XXLONG(K).GE.XXMAX).AND.(XXLONG(K+1).LT.XXMAX)) GO TO 15
   14 CONTINUE

C       WE NOW INTERPOLATE THE DISTANCE BETWEEN XXLONG(K) AND (K+1)

   15 RAT = (XXMAX-XXLONG(KOUT+1))/(XXLONG(KOUT)-XXLONG(KOUT+1))
       CAT = 1.0 - RAT

C       DO LOOP 16 LINEARLY INTERPOLATES BETWEEN CLONG(KOUT+1) AND
C       CLONG(KOUT) TO DETERMINE CINTR FOR THE NEXT INTERATION

       DO 16 I = 1,IPHI
```

```
16    CINTR(I) = CLONG(I,KOUT)*RAT + CLONG(I,KOUT+1)*CAT

      RETURN
      END
```

CCCCCCCCCCCCCCCCCCCCCCCCCCCCCCCCCCCCCCCCCCCCCCCCCCCCCCCCCCCCCCCCCCCCCCCCC

```
      SUBROUTINE BAND
      COMMON /B1/A,B,D
     1 /B4/G
     1 /B7/CSAT,DELTA,RHOF,DT,EQCON,EPO,F,H,HF,N,IFLAG,
     1     IPASS,IHSO4,IH,ISO4,IR,IPHI,IL,JSTIME,JFTIME,JCOUNT,THTIME,
     1     TSTAR,NJ,NJM1,NPRINT,QLF,NJD,NJDP1,NJDM1,HETA,JTIME
     1 /B9/X
     1 /B10/Y,BEGTPAS,OHMADJ,RKAP1,P2,P4,P5,P6,P7
     1 /B23/C
     1 /B32/J
      DIMENSION A(6,6),B(6,6),D(6,13),
     1  C(6,202),G(6),
     1  X(6,6),Y(6,6),E(6,7,202)
  101 FORMAT (15HODETERM=0 AT J=,I4)
      IF (J-2)  1,6,8
    1 NP1= N + 1
      DO 2 I=1,N
      D(I,2*N+1)= G(I)
      DO 2 L=1,N
      LPN= L + N
    2 D(I,LPN)= X(I,L)
      CALL MATINV (N,2*N+1,DETERM)
      IF (DETERM)  4,3,4
    3 PRINT 101, J
    4 DO 5 K=1,N
      E(K,NP1,1)= D(K,2*N+1)
      DO 5 L=1,N
      E(K,L,1)= - D(K,L)
      LPN= L + N
    5 X(K,L)= - D(K,LPN)
      RETURN
    6 DO 7 I=1,N
      DO 7 K=1,N
      DO 7 L=1,N
    7 D(I,K)= D(I,K) + A(I,L)*X(L,K)
    8 IF (J-NJ)  11,9,9
    9 DO 10 I=1,N
      DO 10 L=1,N
      G(I)= G(I) - Y(I,L)*E(L,NP1,J-2)
      DO 10 M=1,N
   10 A(I,L)= A(I,L) + Y(I,M)*E(M,L,J-2)
   11 DO 12 I=1,N
      D(I,NP1)= - G(I)
      DO 12 L=1,N
```

```
      D(I,NP1)= D(I,NP1) + A(I,L)*E(L,NP1,J-1)
      DO 12 K=1,N
 12   B(I,K)= B(I,K) + A(I,L)*E(L,K,J-1)
      CALL MATINV (N,NP1   ,DETERM)
      IF (DETERM)  14,13,14
 13   PRINT 101, J
 14   DO 15 K=1,N
      DO 15 M=1,NP1
 15   E(K,M,J)= - D(K,M)
      IF (J-NJ)  20,16,16
 16   DO 17 K=1,N
 17   C(K,J)= E(K,NP1,J)
      DO 18 JJ=2,NJ
      M= NJ - JJ + 1
      DO 18 K=1,N
      C(K,M)= E(K,NP1,M)
      DO 18 L=1,N
 18   C(K,M)= C(K,M) + E(K,L,M)*C(L,M+1)
      DO 19 L=1,N
      DO 19 K=1,N
 19   C(K,1)= C(K,1) + X(K,L)*C(L,3)
 20   RETURN
      END

      SUBROUTINE MATINV(N,M,DETERM)
      COMMON /B1/A,B,D
      DIMENSION A(6,6),B(6,6),D(6,13),ID(6)
      DETERM=1.0
      DO 1 I=1,N
 1    ID(I)=0
      DO 18 NN=1,N
      BMAX=1.1
      DO 6 I=1,N
      IF(ID(I).NE.0) GOTO 6
      BNEXT=0.0
      BTRY=0.0
      DO 5 J=1,N
      IF(ID(J).NE.0) GOTO 5
      IF(ABS(B(I,J)).LE.BNEXT) GOTO 5
      BNEXT=ABS(B(I,J))
      IF(BNEXT.LE.BTRY) GOTO 5
      BNEXT=BTRY
      BTRY=ABS(B(I,J))
      JC=J
 5    CONTINUE
      IF(BNEXT.GE.BMAX*BTRY) GOTO 6
      BMAX=BNEXT/BTRY
      IROW=I
      JCOL=JC
 6    CONTINUE
      IF(ID(JC).EQ.0) GOTO 8
```

```
      DETERM=0.0
      RETURN
    8 ID(JCOL)=1
      IF(JCOL.EQ.IROW) GOTO 12
      DO 10 J=1,N
      SAVE=B(IROW,J)
      B(IROW,J)=B(JCOL,J)
   10 B(JCOL,J)=SAVE
      DO 11 K=1,M
      SAVE=D(IROW,K)
      D(IROW,K)=D(JCOL,K)
   11 D(JCOL,K)=SAVE
   12 F=1.0/B(JCOL,JCOL)
      DO 13 J=1,N
   13 B(JCOL,J)=B(JCOL,J)*F
      DO 14 K=1,M
   14 D(JCOL,K)=D(JCOL,K)*F
      DO 18 I=1,N
      IF(I.EQ.JCOL) GO TO 18
      F=B(I,JCOL)
      DO 16 J=1,N
   16 B(I,J)=B(I,J)-F*B(JCOL,J)
      DO 17 K=1,M
   17 D(I,K)=D(I,K)-F*D(JCOL,K).
   18 CONTINUE
      RETURN
      END


      SUBROUTINE BC1
      COMMON /B1/A,B,D
     1 /B2/C
     1 /B4/G
     1 /B6/CIN,DIF,V,S,Z,U,ZUFODR,CBK
     1 /B7/CSAT,DELTA,RHOF,DT,EQCON,EPO,F,H,HF,N,IFLAG,
     1     IPASS,IHSO4,IH,ISO4,IR,IPHI,IL,JSTIME,JFTIME,JCOUNT,THTIME,
     1     TSTAR,NJ,NJM1,NPRINT,QLF,NJD,NJDP1,NJDM1,HETA,JTIME
     1 /B9/X
     1 /B17/CINTR
      DIMENSION A(6,6),B(6,6),D(6,13),G(6),C(6,202),U(6),
     1 DIF(6),Z(6),S(6),CIN(6),V(202),ZUFODR(6),X(6,6),CINTR(6),CBK(4)

C     B.C. IN SOLUTION AT XIMAX
C     SEE SUBROUTINE ASSIGN FOR THE SELECTION OF CINTR


      B(1,IHSO4) = 1.0
      G(1) = CINTR(IHSO4) - C(IHSO4,1)

      B(2,IR) = 1.0
      G(2) = CINTR(IR) - C(IR,1)
```

```
      B(3,IPHI) = 1.0
      G(3) = CINTR(IPHI) - C(IPHI,1)

         IOH = 3
         IRSP = 4
      B(4,IH) = C(IOH,1)
      B(4,IOH) = C(IH,1)
      G(4) = -C(IH,1)*C(IOH,1) + EQCON

      SUM = 0.0

      DO 10  I = 1,IRSP
         B(5,I) = Z(I)
   10    SUM = SUM - Z(I)*(C(I,1) + CBK(I))

      G(5) = SUM

      RETURN
      END

CCCCCCCCCCCCCCCCCCCCCCCCCCCCCCCCCCCCCCCCCCCCCCCCCCCCCCCCCCCCCCCCCCCCCCCCC

      SUBROUTINE BCNJ
      COMMON /B1/A,B,D
     1 /B2/C
     1 /B3/COLD
     1 /B4/G
     1 /B6/CIN,DIF,V,S,Z,U,ZUFODR,CBK
     1 /B7/CSAT,DELTA,RHOF,DT,EQCON,EPO,F,H,HF,N,IFLAG,
     1      IPASS,IHSO4,IH,ISO4,IR,IPHI,IL,JSTIME,JFTIME,JCOUNT,THTIME,
     1      TSTAR,NJ,NJM1,NPRINT,QLF,NJD,NJDP1,NJDM1,HETA,JTIME
     1 /B10/Y,BEGTPAS,OHMADJ,RKAP1,P2,P4,P5,P6,P7
     1 /B12/VFE,RATEKA,RATEKC,OHMIC,CUR,CURPAS,
     1   ICONPAS,PH,VPASS,OHMCOR
     1 /B19/XX,XXLONG,CLONG,XXMAX,NLONG
     1 /B20/DELHAT
     1 /B24/T,SQRTT,TOLD,SQRTOLD
     1 /B25/XI,ETA
     1 /B28/SURMIG,SURDIF,SURFLX
     1 /B29/ALPHAA,ALPHAC,FEN,PI,RZERO,RKAPPA,DIMROT,P3,FA,FC,PHIZRO
     1 /B30/XXTEST
     1 /B32/J
     1 /B33/SQRTSAV
     1 /B34/EPSURZ,P,EPSUR
      DIMENSION A(6,6),B(6,6),D(6,13),C(6,202),COLD(6,202),G(6),U(6),
     1   DIF(6),Z(6),S(6),CIN(6),V(202),ZUFODR(6),Y(6,6),XI(202),
     1   ETA(202),SURMIG(4),SURDIF(4),SURFLX(4),XX(202),XXLONG(202),
     1   CLONG(6,202),CBK(4)

      XCP(I,J) = (C(I,J-1) - C(I,J+1))/2.0
```

```
200 FORMAT (1H ,*VALUES OF G(I) FROM BCNJ AFTER STATEMENT 22*)
201 FORMAT (9(1X,E12.6))
202 FORMAT (1X,5X,*P3*,11X,*P7*,11X,*P8*,11X,*PHI*,10X,*PP*,11X,
   1 *C(IR)*,8X,*Q1*,11X,*Q2*,11X,*FAP3*)
203 FORMAT (1X,*P8 .LT. 0 VALUES OF P2,P7,P8,P9,FAP3,FCP3*,6(1X,E9.3))
204 FORMAT (1X,*JCOUNT,ALPHA,SLOPE,CUR,CUR2,G(4),C(IH),PH*,I3,
   1 7(1X,E9.3))
205 FORMAT (2X,*J*,5X,*S1OKAP*,8X,*DIFCOM*,9X,*ODROP*)
206 FORMAT (1X,*KSAV=*,I3,* IPASS=*,I3,* DELTA=*,E12.6,* DDELTA=*,
   1 E12.6,* DELHAT=*,E12.6,* ODROP=*,E12.6,* DIFCOM=*,E12.6)

      IRSP = 4
      IOH = 3
      IH = 4
      INI = 1
      INO3 = 2
C     CALCULATE BOUNDARY CONDITIONS AT ELECTRODE SURFACE

      PP = XCP(IPHI,NJM1)

C     FLUX CONDITIONS; #1 3 N(NO3-) = N(H+)-N(OH-)   #2 N(NI++) = 0

      LOOPEND = 2

      Y(1,IPHI) = (-ZUFODR(IH)*C(IH,NJM1)+ZUFODR(IOH)*C(IOH,NJM1)
   1            +3.*ZUFODR(INO3)*(C(INO3,NJM1)+CBK(INO3)))/2.0
      B(1,IPHI) = -Y(1,IPHI)
      Y(1,IH) = -DIF(IH)/DIF(IR)/2.0
      B(1,IH) = -Y(1,IH)
      Y(1,INO3) = 3.*DIF(INO3)/DIF(IR)/2.0
      B(1,INO3) = -Y(1,INO3)
      Y(1,IOH) = DIF(IOH)/DIF(IR)/2.0
      B(1,IOH) = -Y(1,IOH)
      A(1,IH) = -ZUFODR(IH)*PP
      A(1,INO3) = 3.*ZUFODR(INO3)*PP
      A(1,IOH) = ZUFODR(IOH)*PP
      G(1) = ( ZUFODR(IH)*C(IH,NJM1) -ZUFODR(IOH)*C(IOH,NJM1)
   1        -3.*ZUFODR(INO3)*(C(INO3,NJM1)+CBK(INO3)))*PP
   1        + ( DIF(IH)*XCP(IH,NJM1) -DIF(IOH)*XCP(IOH,NJM1)
   1        -3.*DIF(INO3)*XCP(INO3,NJM1))/DIF(IR)

      Y(2,IPHI) = (-ZUFODR(INI)*(C(INI,NJM1)+CBK(INI)))/2.0
      B(2,IPHI) = -Y(2,IPHI)
      Y(2,INI) = -DIF(INI)/DIF(IR)/2.0
      B(2,INI) = -Y(2,INI)
      A(2,INI) = -ZUFODR(INI)*PP
      G(2) = ( ZUFODR(INI)*(C(INI,NJM1)+CBK(INI)))*PP
   1        + (DIF(INI)*XCP(INI,NJM1) )/DIF(IR)
C     EQUATION #3; EQUILIBRIUM AT THE IMAGE POINT

      B(3,IH) = C(IOH,J)
```

```
      B(3,IOH) = C(IH,J)
      G(3) = -C(IH,J)*C(IOH,J) + EQCON


C        CALCULATE CONDUCTIVITY AT INFINITY

      SUM = 0.0

      DO 12  I = 1,IRSP
   12    SUM = SUM + Z(I)**2*U(I)*(C(I,1)+CBK(I))

      RKAP1 = F**2*SUM

C        TEST TO SEE IF WE ARE WORKING ON PHASE 1 ONLY OR FILM
C        INCLUDED PROBLEM

      IF (IFLAG - 1) 14,13,14

C        EQUATION 4; PHASE 1 CONCENTRATION BUILDUP
C        N(NO3-) = (BUTLER-VOLMER)/NF

   13 P6 = 0.0
      CUR = 0.0
      Q1 = ZUFODR(INO3)*(C(INO3,NJM1)+CBK(INO3))*PP*DIF(IR)/DIF(INO3)
      Q2 = XCP(INO3,NJM1)
      IF(T .NE. 0.0) CUR = DIMROT*FEN*F*DIF(INO3)/SQRTT/H*(-Q1 - Q2)
      IF(T .NE. 0.0)  P6 = DIMROT*FEN*F*DIF(INO3)/H/SQRTT
      P4 = PI*RZERO/4.0/RKAPPA
      P5 = XXMAX/DIMROT/(RKAP1)
      P7 = -Q1 - Q2
      IF((JSTIME.EQ.1).OR.((JSTIME.EQ.2).AND.(JCOUNT.EQ.1)))P7 =-1.E-13
      P1 = P6*(P4 - P5)
      P2 = SQRTT*H/DIMROT/DIF(INO3)
      OHMIC = P6*P4*P7

C        P5*P6*P7 CORRECTS FOR THE OHMIC COMPONENT IN C(IPHI,NJM1)

      OHMCOR = P5*P6*P7
      PHIZRO = C(IPHI,NJM1) - OHMCOR
      P3 = VFE - PHIZRO - OHMIC
      FAP3 = FA*P3
      FCP3 = FC*P3
      IF(FAP3.GT.300.0) FAP3 = 300.0
      IF(FCP3.LT.-300.0) FCP3 = -300.0
      P9 = RATEKA*EXP(FAP3)-RATEKC*(C(INO3,NJM1)+CBK(INO3))*EXP(-FCP3)
      P8 = P2/P7*P9
      IF(P8 .LE. 0.0) PRINT 203,P2,P7,P9,FAP3,FCP3
      IF(P8 .LE. 0.0) P8 = 1.0
      CIR = C(INO3,NJM1)+CBK(INO3)
C     PRINT 202
C     PRINT 201,P3,P7,P8,C(IPHI,NJM1),PP,CIR,Q1,Q2,FCP3
```

```
      G(4) = -ALOG(P8)

      P4PHI = ZUFODR(INO3)*DIF(IR)/DIF(INO3)*CIR*(1./P7
     1   + P1/P9*(RATEKA*EXP(FAP3)*FA + RATEKC*CIR*EXP(-FCP3)*FC))

      P4IR = 1./P7
     1   + P1/P9*(RATEKA*EXP(FAP3)*FA + RATEKC*CIR*EXP(-FCP3)*FC)

      E4IR = ZUFODR(INO3)*DIF(IR)/DIF(INO3)*PP/P7
     1+1./P9*(RATEKA*EXP(FAP3)*FA*P1*ZUFODR(INO3)*DIF(IR)/DIF(INO3)*PP
     1-RATEKC*EXP(-FCP3)*(1.
     1-CIR*FC*P1*ZUFODR(INO3)*DIF(IR)/DIF(INO3)*PP))

      E4PHI = -1./P9
     1          *(RATEKA*EXP(FAP3)*FA + RATEKC*CIR*EXP(-FCP3)*FC)

      Y(4,IPHI) = P4PHI/2.0
      B(4,IPHI) = -Y(4,IPHI)
      Y(4,INO3) = P4IR/2.0
      B(4,INO3) = -Y(4,INO3)
      A(4,INO3) =  E4IR
      A(4,IPHI) = E4PHI

      GO TO 18

   14 IF (IPASS) 17,15,17

   15 P6 = 0.0
      CIR = C(INO3,NJM1) + CBK(INO3)
      CUR = 0.0
      IF(T .NE. 0.0) CUR = DIMROT*FEN*F*DIF(INO3)*EPSILN(DELHAT)/SQRTT
     1    /HETA/DELHAT*
     1    (-ZUFODR(INO3)*
     1    CIR*DIF(IR)/DIF(INO3)*PP-XCP(INO3,NJM1))
      IF (T .NE. 0.0) P6 =DIMROT*FEN*F*DIF(INO3)*EPSILN(DELHAT)/SQRTT
     1    /HETA

C        CALCULATE DIFFUSION POTENTIAL AND INTEGRAL OF 1/KAPPA FOR
C        X=XI(MAX)*SQRTT < X < XXLONG(1) IF X=XI(MAX)*SQRTT < XXLONG(1)


   27 IF (JCOUNT .GE. 2) GO TO 21

      ODROP = 0.0
      DIFCOM = 0.0
      S1OKAP = 0.0


C        IF STRETCHED PROFILE IS FURTHER FROM THE  ELECTRODE THAN THE
C        LONG PROFILE ALL THIS IS UNNECESSARY

      IF(XXMAX .GE. XXLONG(1)) GO TO 21
```

```
      DO 22  K = 2,NJDM1
        KSAV = K

C       ONLY COMPUTE FOR REGION NOT INCLUDED IN XI REGION

        IF(XXLONG(K) .LT. XXMAX) GO TO 25
        SUM1 = 0.0
        SUM2 = 0.0

          DO 23  I = 1,IRSP
              SUM1 = SUM1 + Z(I)*DIF(I)*(CLONG(I,K-1)-CLONG(I,K+1))/2.
   23         SUM2 = SUM2 + Z(I)**2*U(I)*(CLONG(I,K) + CBK(I))

        SUM1 = SUM1*F
        SUM2 = SUM2*F**2

        S1OKAP = S1OKAP + 1./SUM2
        DIFCOM = DIFCOM + SUM1/SUM2

C       IF(MOD(K+4,5) .EQ. 0) PRINT 206, K,S1OKAP,DIFCOM
   22 CONTINUE

   25   ODROP = S1OKAP*(XXLONG(1)-XXLONG(K))/DIMROT/FLOAT(KSAV)
        PRINT 206,KSAV,IPASS,DELTA,C(IL,10),DELHAT,ODROP,DIFCOM

   21 IF(IPASS .EQ. 1) GO TO 26
        P4 = PI*RZERO/4.0/RKAPPA + ODROP

        DIST = XXMAX
        IF (XXLONG(1) .GT. XXMAX) DIST = XXLONG(1)
        P5 = DIST/DIMROT/(RKAPPA)
        Q1 = ZUFODR(INO3)*CIR*PP*DIF(IR)/DIF(INO3)
        Q2 = XCP(INO3,NJM1)
        P7 = - Q1 - Q2
        IF(P7 .GE. 0.0) P7 =-1.E-19
        IF(JCOUNT.EQ.1.AND.JTIME.EQ.2) P7 =-1.E-19
        P1 = P6*(P4 - P5)

        P2 = HETA*SQRTT*EPSUR/DIF(INO3)/DIMROT/EPSILN(DELHAT)
        DO 508 L=1,6
        OHMIC = P6*P4*P7/DELHAT

C       P5*P6*P7 CORRECTS FOR THE OHMIC COMPONENT IN C(IPHI,NJM1)

        OHMCOR = P5*P6*P7/DELHAT
        PHIZRO = C(IPHI,NJM1) - OHMCOR
        P3 = VFE - PHIZRO - OHMIC - DIFCOM
        FAP3 = FA*P3
        FCP3 = FC*P3
          FOFX=P7 + P2*DELHAT*RATEKC*CIR*EXP(-FC*P3)
```

```
            FPOFX=1 + P2*DELHAT*RATEKC*CIR*EXP(-FC*P3)*FC*P1/DELHAT
            P7 = P7 -  (FOFX/FPOFX)
  508 CONTINUE
            P7G = P7
            P7 = -Q1 -Q2
        IF(SQRTT.EQ.0.0)P7=-1.E-14
        IF(SQRTT.EQ.0.0)P7G=-1.E-14
        IF(FAP3.GT.300.0) FAP3 = 300.0
        IF(FCP3.LT.-300.0) FCP3 = -300.0
        P9 = RATEKA*EXP(FAP3) - RATEKC*CIR*EXP(-FCP3)
        P8 = DELHAT*P2/P7G*P9
        IF(P8 .LE. 0.0) PRINT 203,P2,P7,P8,P9,FAP3,FCP3
        IF(P8 .LE. 0.0) P8 = 1.1
        PRINT 202
        PRINT 201,P3,P7,P8,C(IPHI,NJM1),PP,CIR,Q1,Q2,FCP3
        PRINT 206,KSAV,IPASS,DELTA,C(IL,10),DELHAT,ODROP,DIFCOM
C   KINETIC EQUATION
        GO TO 509
        P4PHI = ZUFODR(INO3)*DIF(IR)/DIF(INO3)*CIR*(1.0/P7 +
      1 (RATEKA*EXP(FAP3)*FA + RATEKC*CIR*EXP(-FCP3)*FC)*P1/P9/DELHAT)

        P4IR = 1.0/P7
       1 + (RATEKA*EXP(FAP3)*FA + RATEKC*CIR*EXP(-FCP3)*FC)*P1/P9/DELHAT

        E4IR = ZUFODR(INO3)*DIF(IR)/DIF(INO3)*PP/P7
      1 + 1.0/P9*(RATEKA*EXP(FAP3)*FA*P1/DELHAT*ZUFODR(INO3)
      1 *PP*DIF(IR)/DIF(INO3)
      1 - RATEKC*EXP(-FCP3)
      1 *(1.-CIR*FC*P1/DELHAT*ZUFODR(INO3)*DIF(IR)/DIF(INO3)*PP))

        E4PHI = -1./P9*(RATEKA*EXP(FAP3)*FA + RATEKC*CIR*EXP(-FCP3)*FC)

        SQTTST = SQRTT
        IF (SQRTT .LE. 0.0) SQTTST = 1.0

        E4IL = 1.0/DELHAT +
      1 (RATEKA*EXP(FAP3)*FA+RATEKC*CIR*EXP(-FCP3)*FC)*
      1 (P1*P7/P9/DELHAT**2 + (P5 -P4)*(P7/P9/DELHAT*DIMROT*FEN*F
      1 *DIF(INO3)/SQTTST/HETA*DEPDDEL(DELHAT)))
  509   CONTINUE
        E4IR = ZUFODR(INO3)*DIF(IR)/DIF(INO3)*PP
        E4IL = 0.
        P4IR = 1.0
        P4PHI = ZUFODR(INO3)*DIF(IR)/DIF(INO3)*CIR
        E4PHI = 0.
        B(4,IL) = 0.0
        IF (T .NE. 0.0) GO TO 16

        P4PHI = 1.0
        P4IR = 0.0
        E4IL = 0.0
```

```
      B(4,IL) = 0.0
      E4IR = 0.0
      E4PHI = 0.0
      P8 = 1.0

   16 Y(4,IPHI) = P4PHI/2.0
      B(4,IPHI) = -Y(4,IPHI)
      Y(4,INO3) = P4IR/2.0
      B(4,INO3) =  -Y(4,INO3)
      A(4,INO3) = E4IR
      A(4,IL) = E4IL
      A(4,IPHI) = E4PHI

      G(4) = P7 - P7G

      GO TO 18

   17 GAMMA = DIMROT*FEN*F*DIF(IR)/SQRTT/HETA
      BBB = -0.0908
      BPRIME = BBB*ALOG(10.0)
      ALPHA = EXP(BPRIME)
      BETA = 1000.0
      SLOPE = -0.3578

      CUR = DIMROT*FEN*F*DIF(IR)/SQRTT/HETA/DELHAT
     1                          *(-ZUFODR(IR)*C(IR,NJM1)*PP - XCP(IR,NJM1))
      CUR2 = CURPAS
      IF (ICONPAS .EQ. 0) CUR2 = ALPHA*(C(IH,NJM1)*BETA)**(-SLOPE)
      P6 = DIMROT*FEN*F*DIF(IR)*EPSILN(DELHAT)/SQRTT/HETA

      GO TO 27

   26 P4 = PI*RZERO/4.0/RKAPPA + ODROP
      DIST = XXMAX
      IF (XXLONG(1) .GT. XXMAX) DIST = XXLONG(1)
      P5 = DIST/DIMROT/RKAPPA
      Q1 = ZUFODR(IR)*C(IR,NJM1)*PP
      Q2 = XCP(IR,NJM1)
      P7 = - Q1 - Q2
      P1 = P6*(P4 - P5)
      P2 = HETA*SQRTT/DIF(IR)/EPSILN(DELHAT)/DIMROT

   C     P5*P6*P7 CORRECTS FOR THE OHMIC COMPONENT IN C(IPHI,NJM1)

      OHMCOR = P5*P6*P7/DELHAT
      PHIZRO = C(IPHI,NJM1) - OHMCOR

      IF(JFTIME.EQ.1) OHMADJ = VFE - PHIZRO - P6*P4*P7/DELHAT - VPASS
     1                                     - DIFCOM - BEGTPAS

      OHMIC = P6*P4*P7/DELHAT + OHMADJ
```

```
      P3 = VFE - PHIZRO - OHMIC - DIFCOM

      P4PHI = -GAMMA/DELHAT*ZUFODR(IR)*C(IR,NJM1)
      P4IR = -GAMMA/DELHAT
      E4IH = 0.0
      IF (ICONPAS .EQ. 0)
     1          E4IH = ALPHA*BETA*SLOPE*(BETA*C(IH,NJM1))**(-SLOPE-1.)
      E4IR = -GAMMA/DELHAT*ZUFODR(IR)*PP
      E4IL = -GAMMA/DELHAT**2*P7

      Y(4,IPHI) = P4PHI/2.0
      B(4,IPHI) = -Y(4,IPHI)
      Y(4,IR) = P4IR/2.0
      B(4,IR) = -Y(4,IR)
      A(4,IR) = E4IR
      A(4,IL) = E4IL
      A(4,IH) = E4IH
      G(4) = CUR2 - CUR

C        SET EQUATION 5 ELECTRONEUTRALITY FOR THE IMAGE POINT

   18 SUM = 0.0

      DO 19  I = 1,IRSP
         B(5,I) = Z(I)
   19    SUM = SUM - Z(I)*(C(I,J)+CBK(I))

      G(5) = SUM

C        CALCULATE THE FLUX COMPONENTS AT THE ELECTRODE SURFACE

      DO 20  I = 1,IRSP
         SURMIG(I) = -EPSILN(DELHAT)
     1   *ZUFODR(I)*(C(I,NJM1)+CBK(I))*XCP(IPHI,NJM1)
         SURDIF(I) = -EPSILN(DELHAT)*DIF(I)/DIF(IR)*XCP(I,NJM1)
   20    SURFLX(I) = SURMIG(I) + SURDIF(I)

      RETURN
      END

CCCCCCCCCCCCCCCCCCCCCCCCCCCCCCCCCCCCCCCCCCCCCCCCCCCCCCCCCCCCCCCCCCCCCCCC

      FUNCTION EPSILN(DELHAT)
      COMMON
     1 /B7/CSAT,DELTA,RHOF,DT,EQCON,EPO,F,H,HF,N,IFLAG,
     1     IPASS,IHSO4,IH,ISO4,IR,IPHI,IL,JSTIME,JFTIME,JCOUNT,THTIME,
     1     TSTAR,NJ,NJM1,NPRINT,QLF,NJD,NJDP1,NJDM1,HETA,JTIME
     1 /B24/T,SQRTT,TOLD,SQRTOLD

C        CALCULATE POROSITY AS A DECRESING FUNCTION OF FILM THICKNESS
C        LATER WANT TO CALL 0.070 A VARIABLE SO IT CAN BE CHANGED WITH
```

```
C         CHANGES IN OMEGA

C         EPZRO = 0.75
C         DSQTT = 0.06
C         EPSILN = EPO + (EPZRO - EPO)*(1. - SQRTT*DELHAT/DSQTT)
C         IF (SQRTT*DELHAT .GT. DSQTT) EPSILN = EPO
          EPSILN = EPO
          RETURN
          END


CCCCCCCCCCCCCCCCCCCCCCCCCCCCCCCCCCCCCCCCCCCCCCCCCCCCCCCCCCCCCCCCCCCCCCCC

          FUNCTION DEPDDEL(DELHAT)
          COMMON
        1 /B7/CSAT,DELTA,RHOF,DT,EQCON,EPO,F,H,HF,N,IFLAG,
        1     IPASS,IHSO4,IH,ISO4,IR,IPHI,IL,JSTIME,JFTIME,JCOUNT,THTIME,
        1     TSTAR,NJ,NJM1,NPRINT,QLF,NJD,NJDP1,NJDM1,HETA,JTIME
        1 /B24/T,SQRTT,TOLD,SQRTOLD

C         CALCULATE DERIVATIVE OF EPSILN WITH RESPECT TO DELHAT

C         EPZRO = 0.75
C         DSQTT = 0.06
C         DEPDDEL = -(EPZRO - EPO)*SQRTT/DSQTT
C         IF (SQRTT*DELHAT .GT. DSQTT) DEPDDEL = 0.0
          DEPDDEL = 0.0

          RETURN
          END


CCCCCCCCCCCCCCCCCCCCCCCCCCCCCCCCCCCCCCCCCCCCCCCCCCCCCCCCCCCCCCCCCCCCCCCC

          FUNCTION CP(I)
          COMMON /B2/C
        1 /B7/CSAT,DELTA,RHOF,DT,EQCON,EPO,F,H,HF,N,IFLAG,
        1     IPASS,IHSO4,IH,ISO4,IR,IPHI,IL,JSTIME,JFTIME,JCOUNT,THTIME,
        1     TSTAR,NJ,NJM1,NPRINT,QLF,NJD,NJDP1,NJDM1,HETA,JTIME
        1 /B32/J
          DIMENSION  C(6,202)

C         CALCULATE DERIVATIVE OF SPECIES I AT POSITION J

          CP = (C(I,J-1) - C(I,J+1))/2.0
          RETURN
          END


CCCCCCCCCCCCCCCCCCCCCCCCCCCCCCCCCCCCCCCCCCCCCCCCCCCCCCCCCCCCCCCCCCCCCCCC

          FUNCTION CPP(I)
          COMMON /B2/C
        1 /B7/CSAT,DELTA,RHOF,DT,EQCON,EPO,F,H,HF,N,IFLAG,
```

```
1      IPASS,IHSO4,IH,ISO4,IR,IPHI,IL,JSTIME,JFTIME,JCOUNT,THTIME,
1      TSTAR,NJ,NJM1,NPRINT,QLF,NJD,NJDP1,NJDM1,HETA,JTIME
1 /B32/J
  DIMENSION  C(6,202)
```

```
C      CALCULATE SECOND DERIVATIVE OF SPECIES I AT POSITION J
```

```
  CPP = C(I,J-1) - 2.0*C(I,J) + C(I,J+1)
  RETURN
  END
```

CCCCCCCCCCCCCCCCCCCCCCCCCCCCCCCCCCCCCCCCCCCCCCCCCCCCCCCCCCCCCCCCCCCCCCCC

```
  FUNCTION CPOLD(I)
  COMMON /B3/COLD
1 /B7/CSAT,DELTA,RHOF,DT,EQCON,EPO,F,H,HF,N,IFLAG,
1      IPASS,IHSO4,IH,ISO4,IR,IPHI,IL,JSTIME,JFTIME,JCOUNT,THTIME,
1      TSTAR,NJ,NJM1,NPRINT,QLF,NJD,NJDP1,NJDM1,HETA,JTIME
1 /B32/J
  DIMENSION COLD(6,202)
```

```
C      CALCULATE DERIVATIVE OF OLD SPECIES I AT POSITION J
```

```
  CPOLD = (COLD(I,J-1) - COLD(I,J+1))/2.0
  RETURN
  END
```

CCCCCCCCCCCCCCCCCCCCCCCCCCCCCCCCCCCCCCCCCCCCCCCCCCCCCCCCCCCCCCCCCCCCCCCC

```
  FUNCTION CPPOLD(I)
  COMMON  /B3/COLD
1 /B7/CSAT,DELTA,RHOF,DT,EQCON,EPO,F,H,HF,N,IFLAG,
1      IPASS,IHSO4,IH,ISO4,IR,IPHI,IL,JSTIME,JFTIME,JCOUNT,THTIME,
1      TSTAR,NJ,NJM1,NPRINT,QLF,NJD,NJDP1,NJDM1,HETA,JTIME
1 /B32/J
  DIMENSION  COLD(6,202)
```

```
C      CALCULATE SECOND DERIVATIVE OF OLD SPECIES I AT POSITION J
```

```
  CPPOLD = COLD(I,J-1) - 2.0*COLD(I,J) + COLD(I,J+1)
  RETURN
  END
```

CCCCCCCCCCCCCCCCCCCCCCCCCCCCCCCCCCCCCCCCCCCCCCCCCCCCCCCCCCCCCCCCCCCCCCCC

```
  FUNCTION CPBACK(I)
  COMMON /B2/C
1 /B7/CSAT,DELTA,RHOF,DT,EQCON,EPO,F,H,HF,N,IFLAG,
1      IPASS,IHSO4,IH,ISO4,IR,IPHI,IL,JSTIME,JFTIME,JCOUNT,THTIME,
1      TSTAR,NJ,NJM1,NPRINT,QLF,NJD,NJDP1,NJDM1,HETA,JTIME
1 /B32/J
```

```
      DIMENSION C(6,202)

C        CALCULATE DERIVATIVE OF SPECIES I WITH BACKWARD DIFFERENCE

      CPBACK = C(I,J) - C(I,J+1)
      RETURN
      END

CCCCCCCCCCCCCCCCCCCCCCCCCCCCCCCCCCCCCCCCCCCCCCCCCCCCCCCCCCCCCCCCCCCCCCC

      FUNCTION CPBACKO(I)
      COMMON /B3/COLD
     1 /B7/CSAT,DELTA,RHOF,DT,EQCON,EPO,F,H,HF,N,IFLAG,
     1      IPASS,IHSO4,IH,ISO4,IR,IPHI,IL,JSTIME,JFTIME,JCOUNT,THTIME,
     1      TSTAR,NJ,NJM1,NPRINT,QLF,NJD,NJDP1,NJDM1,HETA,JTIME
     1 /B32/J
      DIMENSION COLD(6,202)

C        CALCULATE DERIVATIVE OF OLD SPECIES I WITH BACKWARD DIFFERENCE

      CPBACKO = COLD(I,J) - COLD(I,J+1)
      RETURN
      END

CCCCCCCCCCCCCCCCCCCCCCCCCCCCCCCCCCCCCCCCCCCCCCCCCCCCCCCCCCCCCCCCCCCCCCC

      FUNCTION CPFOR(I)
      COMMON /B2/C
     1 /B7/CSAT,DELTA,RHOF,DT,EQCON,EPO,F,H,HF,N,IFLAG,
     1      IPASS,IHSO4,IH,ISO4,IR,IPHI,IL,JSTIME,JFTIME,JCOUNT,THTIME,
     1      TSTAR,NJ,NJM1,NPRINT,QLF,NJD,NJDP1,NJDM1,HETA,JTIME
     1 /B32/J
      DIMENSION C(6,202)

C        CALCULATE DERIVATIVE OF SPECIES I WITH FORWARD DIFFERENCE

      CPFOR = C(I,J-1) - C(I,J)
      RETURN
      END

CCCCCCCCCCCCCCCCCCCCCCCCCCCCCCCCCCCCCCCCCCCCCCCCCCCCCCCCCCCCCCCCCCCCCCC

      FUNCTION CPFORO(I)
      COMMON /B3/COLD
     1 /B7/CSAT,DELTA,RHOF,DT,EQCON,EPO,F,H,HF,N,IFLAG,
     1      IPASS,IHSO4,IH,ISO4,IR,IPHI,IL,JSTIME,JFTIME,JCOUNT,THTIME,
     1      TSTAR,NJ,NJM1,NPRINT,QLF,NJD,NJDP1,NJDM1,HETA,JTIME
     1 /B32/J
      DIMENSION COLD(6,202)

C        CALCULATE DERIVATIVE OF OLD SPECIES I WITH FORWARD DIFFERENCE
```

```
      CPFORO = COLD(I,J-1) - COLD(I,J)
      RETURN
      END

CCCCCCCCCCCCCCCCCCCCCCCCCCCCCCCCCCCCCCCCCCCCCCCCCCCCCCCCCCCCCCCCCCCCCCC

      FUNCTION CBARF(I)
      COMMON /B2/C
     1 /B7/CSAT,DELTA,RHOF,DT,EQCON,EPO,F,H,HF,N,IFLAG,
     1     IPASS,IHSO4,IH,ISO4,IR,IPHI,IL,JSTIME,JFTIME,JCOUNT,THTIME,
     1     TSTAR,NJ,NJM1,NPRINT,QLF,NJD,NJDP1,NJDM1,HETA,JTIME
     1 /B32/J
      DIMENSION C(6,202)

C     AVG CONCENTRATION BETWEEN POINTS J AND J-1, FORWARD DIRECTION

      CBARF = (C(I,J) + C(I,J-1))/2.0
      RETURN
      END

CCCCCCCCCCCCCCCCCCCCCCCCCCCCCCCCCCCCCCCCCCCCCCCCCCCCCCCCCCCCCCCCCCCCCCC

      FUNCTION CBARFO(I)
      COMMON /B3/COLD
     1 /B7/CSAT,DELTA,RHOF,DT,EQCON,EPO,F,H,HF,N,IFLAG,
     1     IPASS,IHSO4,IH,ISO4,IR,IPHI,IL,JSTIME,JFTIME,JCOUNT,THTIME,
     1     TSTAR,NJ,NJM1,NPRINT,QLF,NJD,NJDP1,NJDM1,HETA,JTIME
     1 /B32/J
      DIMENSION COLD(6,202)

C     OLD AVG CONCENTRATION BETWEEN POINTS J AND J-1,FORWARD DIRECTION

   10 CBARFO = (COLD(I,J) + COLD(I,J-1))/2.0
      RETURN
      END

CCCCCCCCCCCCCCCCCCCCCCCCCCCCCCCCCCCCCCCCCCCCCCCCCCCCCCCCCCCCCCCCCCCCCCC

      FUNCTION CBARB(I)
      COMMON /B2/C
     1 /B7/CSAT,RHOF,DT,EQCON,EPO,F,H,HF,N,IFLAG,
     1     IPASS,IHSO4,IH,ISO4,IR,IPHI,IL,JSTIME,JFTIME,JCOUNT,THTIME,
     1     TSTAR,NJ,NJM1,NPRINT,QLF,NJD,NJDP1,NJDM1,HETA,JTIME
     1 /B32/J
      DIMENSION C(6,202)

C     AVG CONCENTRATION BETWEEN POINTS J AND J+1, BACKWARD DIRECTION

      CBARB = (C(I,J) + C(I,J+1))/2.0
      RETURN
      END
```

```
CCCCCCCCCCCCCCCCCCCCCCCCCCCCCCCCCCCCCCCCCCCCCCCCCCCCCCCCCCCCCCCCCC

      FUNCTION CBARBO(I)
      COMMON /B3/COLD
     1 /B7/CSAT,DELTA,RHOF,DT,EQCON,EPO,F,H,HF,N,IFLAG,
     1     IPASS,IHSO4,IH,ISO4,IR,IPHI,IL,JSTIME,JFTIME,JCOUNT,THTIME,
     1     TSTAR,NJ,NJM1,NPRINT,QLF,NJD,NJDP1,NJDM1,HETA,JTIME
     1 /B32/J                           .
      DIMENSION COLD(6,202)

C        OLD AVG CONC. BETWEEN POINTS J AND J+1, BACKWARD DIRECTION

      CBARBO = (COLD(I,J) + COLD(I,J+1))/2.0
      RETURN
      END

CCCCCCCCCCCCCCCCCCCCCCCCCCCCCCCCCCCCCCCCCCCCCCCCCCCCCCCCCCCCCCCCCC

      SUBROUTINE COEF
      COMMON /B1/A,B,D
     1 /B2/C
     1 /B3/COLD
     1 /B4/G
     1 /B6/CIN,DIF,V,S,Z,U,ZUFODR,CBK
     1 /B7/CSAT,DELTA,RHOF,DT,EQCON,EPO,F,H,HF,N,IFLAG,
     1     IPASS,IHSO4,IH,ISO4,IR,IPHI,IL,JSTIME,JFTIME,JCOUNT,THTIME,
     1     TSTAR,NJ,NJM1,NPRINT,QLF,NJD,NJDP1,NJDM1,HETA,JTIME
     1 /B12/VFE,RATEKA,RATEKC,OHMIC,CUR,CURPAS,ICONPAS,PH,VPASS,OHMCOR
     1 /B20/DELHAT
     1 /B24/T,SQRTT,TOLD,SQRTOLD
     1 /B25/XI,ETA
     1 /B29/ALPHAA,ALPHAC,FEN,PI,RZERO,RKAPPA,DIMROT,P3,FA,FC,PHIZRO
     1 /B32/J

      DIMENSION A(6,6),B(6,6),D(6,13),C(6,202),COLD(6,202),G(6),XI(202),
     1 DIF(6),Z(6),S(6),CIN(6),V(202),ZUFODR(6),ETA(202),U(6),CBK(4)

C        COMPUTE COEFFICIENTS OF THE GOVERNING EQUATIONS IN THE
C        INTERIOR OF EACH REGION

  200 FORMAT(1X,I3,1X,6(1X,E12.6))
  201 FORMAT(1X,*JSTIME,JFTIME,JCOUNT,TERM,TERM1,TERM2,TERM3*/1X,
     1 3(2X,I2),4(2X,E9.3))

C        CALCULATE THE OLD VELOCITY PROFILE

      VOLD(J) = 3.*XI(J)**2*(T - DT)

C        PROGRAM CHARGE CONSERVATION EQUATION RELATING CURRENT DENSITY
C        AT HALF MESH POINT BETWEEN NJM1 AND NJ-2 TO THE CURRENT DENSITY
C        AT NJM1 ONLY WHEN J = NJM1
```

```
            IOH = 3
            INI = 1
            IH = 4
            INO3 = 2
            IRSP = 4
      IF((J .NE. NJM1) .OR. (DT .EQ. 0.0)) GO TO 11

      SUM1 = 0.0
      SUM2 = 0.0
      SUM3 = 0.0

      DO 10  I = 1,IRSP
        SUM1 = SUM1 + Z(I)**2*U(I)*(CBARF(I)+CBK(I))
        SUM2 = SUM2 + Z(I)**2*U(I)*(C(I,NJM1)+CBK(I))
        SUM3 = SUM3 + Z(I)*DIF(I)*(C(I,J-1)/2.0 - C(I,J) + C(I,J+1)/2.0)
        A(2,I) = -F**2*CPFOR(IPHI)*Z(I)**2*U(I)/2.0 - F*Z(I)*DIF(I)/2.0
        B(2,I) = F**2*Z(I)**2*U(I)*(CP(IPHI) - CPFOR(IPHI)/2.0)
     1            + F*Z(I)*DIF(I)
   10   D(2,I) = -F*Z(I)*DIF(I)/2.0

      A(2,IPHI) =  F**2*(SUM2/2.0 - SUM1)
      B(2,IPHI) =  F**2*SUM1
      D(2,IPHI) = -F**2*SUM2/2.0

      G(2) = F**2*(CPFOR(IPHI)*SUM1 - CP(IPHI)*SUM2) + F*SUM3

   11 LOOPEND = 1

C       DECIDE IF FILM IS PRESENT (IFLAG=2) OR NOT (=1)
C       IF FILM IS PRESENT MUST DECIDE IF J IS IN FILM OR SOLUTION
C       IF FILM IS ABSENT MAY GO DIRECTLY TO SOLUTION COEFFICIENTS

      IF (IFLAG - 1) 14,14,13
   13 IF (J - NJD) 14,14,21

C       COEFFICIENTS FOR THE SOLUTION PHASE ONLY

   14 PP = CP(IPHI)
      IF (T .NE. 0.0) PPOLD = CPOLD(IPHI)
      PPP = CPP(IPHI)
      IF (T .NE. 0.0) PPPOLD = CPPOLD(IPHI)
      HSQ = H**2

C       IF LOOPEND=1, THIS IS SUMMATION MATERIAL BALANCE EQUATION 1.
C       THIS IS SUMMATION MATERIAL BALANCE EQUATIONS 1 AND 2 IF
C       LOOPEND=2.
C       ONLY HAVE ONE SUMMATION EQUATION IF CURRENT IS CARRIED
C       EXPLICITLY (WHICH IT IS IF LOOPEND = 1, AS ABOVE).

      GO TO 501
      DO 15  K = 1,LOOPEND
```

```
      I = 3
      AK1=DIF(2)/DIF(IR)
      AKI=-DIF(I)/DIF(IR)
      AKP=0.0

      TERM=0.0
C
      IF (IFLAG .EQ. 1) TERM =  H/2.*XI(J)
C
      IF (IFLAG .EQ. 2) TERM =  H/2.*(XI(J) + DELHAT)
      IF (T .GT. 0.999) TERM = 0.0
      IF (JTIME .GE. 2) TERM=TERM + 2.*H*T/DT*(DELHAT - DELTA)

      BK1= V(J)*H*SQRTT + TERM
      BKI= V(J)*H*SQRTT + TERM
      BKP=0.0

      TERM = 0.0
      IF ((JTIME.GE.2).OR.((IFLAG.EQ.1).AND.(JSTIME.GE.2)))
     1                                        TERM=-2.*HSQ*T/DT
      DK1= TERM
      DKI= TERM

      TERM = 0.0
      IF (JTIME .GE. 2) TERM=2.*H*T*(CP(2) - CP(I))/DT
      DK6=H/2.*(CP(2) - CP(I)) + TERM

      IF (IFLAG.EQ.1) DK6 = 0.0

      A(K,2)=AK1 + BK1/2. + ZUFODR(2)/2.0*CPFOR(5)
      D(K,2)=AK1 - BK1/2. - ZUFODR(2)/2.0*CPBACK(5)
      B(K,2)=-2.*AK1 + DK1 + ZUFODR(2)/2.0*(CPFOR(5) - CPBACK(5))
      A(K,I)=AKI + BKI/2. - ZUFODR(I)/2.0*CPFOR(5)
      D(K,I)=AKI - BKI/2. + ZUFODR(I)/2.0*CPBACK(5)
      B(K,I)=-2.*AKI + DKI - ZUFODR(I)/2.0*(CPFOR(5) - CPBACK(5))
      A(K,IPHI)=AKP + BKP/2. + ZUFODR(2)*CBARF(2) - ZUFODR(I)*CBARF(I)
      D(K,IPHI)=AKP - BKP/2. + ZUFODR(2)*CBARB(2) - ZUFODR(I)*CBARB(I)
      B(K,IPHI)=-2.*AKP -ZUFODR(2)*(CBARF(2) + CBARB(2))
     1                  +ZUFODR(I)*(CBARF(I) + CBARB(I))
      B(K,IL)=DK6

      FKOLD=0.0
      IF ((JTIME.GE.2).OR.((IFLAG.EQ.1).AND.(JSTIME.GE.2)))
     1 FKOLD = ZUFODR(2)*(CBARFO(2)*CPFORO(5) - CBARBO(2)*CPBACKO(5))
     1       - ZUFODR(I)*(CBARFO(I)*CPFORO(5) - CBARBO(I)*CPBACKO(5))
     1         + VOLD(J)*H*SQRTOLD*(CPOLD(2) - CPOLD(I))
     1         + (DIF(2)*CPPOLD(2) - DIF(I)*CPPOLD(I))/DIF(IR)

      TERM2 = 0.0
      TERM = 0.0
      IF (JTIME .GE. 2) TERM2=-2.*H*T*(DELHAT-DELTA)*(CP(2)-CP(I))/DT
```

```
      IF ((JTIME.GE.2).OR.((IFLAG.EQ.1).AND.(JSTIME.GE.2)))
     1     TERM=2.*HSQ*T*(C(2,J) - COLD(2,J) - C(I,J) + COLD(I,J))/DT

      TERM = TERM + TERM2

      TERM1=0.0
      TERM3=0.0

C
      IF ((IFLAG .EQ. 1) .AND. (JSTIME .GE. 2))
     1     TERM1= XI(J)*(CPOLD(2) - CPOLD(I))
C
      IF (JTIME .GE. 2)
     1     TERM1=(XI(J) + DELTA)*(CPOLD(2) - CPOLD(I))
      IF (T .GT. 0.999) TERM1 = 0.0
C
      IF (IFLAG .EQ. 1) TERM3= XI(J)*(CP(2) - CP(I))
C
      IF (IFLAG .EQ. 2) TERM3=(XI(J) + DELHAT)*(CP(2) - CP(I))
      IF (T .GT. 0.999) TERM3 = 0.0

      G(K)=-H/2.*(TERM3 + TERM1)
     1      - ZUFODR(2)*(CBARF(2)*CPFOR(5) - CBARB(2)*CPBACK(5))
     1      + ZUFODR(I)*(CBARF(I)*CPFOR(5) - CBARB(I)*CPBACK(5))
     1      - V(J)*H*SQRTT*(CP(2) - CP(I))
     1      - (DIF(2)*CPP(2) - DIF(I)*CPP(I))/DIF(IR) - FKOLD
     1      + TERM
   15 CONTINUE
  501 CONTINUE

C     CHARGE CONSERVATION IS NOT SET IF LOOPEND=2, THAT IS WHEN
C     BOTH SUMMATION MATERIAL BALANCES ARE USED.
C     CHARGE CONSERVATION HAS ALREADY BEEN SET IN DO LOOP 10
C     ABOVE IF J=NJM1.

      IF (LOOPEND .EQ. 2) GO TO 18
      IF (J .EQ. NJM1) GO TO 18

C     IF ONLY ONE SUMMATION MATERIAL BALANCE EQUATION IS USED,
C     PROGRAM IN THE CHARGE CONSERVATION EQUATION EXPLICITLY, #2

      SUM1 = 0.0
      SUM2 = 0.0
      SUM3 = 0.0
      SUM4 = 0.0

      DO 16  I = 1,IRSP
         SUM1 = SUM1 + Z(I)**2*U(I)*(CBARF(I)+CBK(I))
         SUM2 = SUM2 + Z(I)*DIF(I)*CPFOR(I)
         SUM3 = SUM3 + Z(I)**2*U(I)*(CBARB(I)+CBK(I))
   16    SUM4 = SUM4 + Z(I)*DIF(I)*CPBACK(I)
```

```
      RIJF = -F**2*CPFOR(IPHI)*SUM1 - F*SUM2
      RIJB = -F**2*CPBACK(IPHI)*SUM3 - F*SUM4

      A(2,IPHI) = -F**2*SUM1
      D(2,IPHI) = -F**2*SUM3
      B(2,IPHI) = -A(2,IPHI) - D(2,IPHI)

      DO 17  I = 1,IRSP
        TERM1 = F**2*CPFOR(IPHI)*Z(I)**2*U(I)/2.0
        TERM2 = F*Z(I)*DIF(I)
        TERM3 = F**2*CPBACK(IPHI)*Z(I)**2*U(I)/2.0

        A(2,I) = -TERM1 - TERM2
        D(2,I) =  TERM3 - TERM2
   17   B(2,I) = -TERM1 + TERM3 + 2.0*TERM2

      G(2) = -RIJF + RIJB

C       MATERIAL BALANCE FOR NICKEL SPECIES, EQUATION 1

   18 A3R=DIF(INI)/DIF(IR)
      A3P=0.0

      TERM = 0.0

C
      IF (IFLAG .EQ. 1) TERM =  H/2.*XI(J)
C
      IF (IFLAG .EQ. 2) TERM =  H/2.*(XI(J) + DELHAT)
      IF (T .GT. 0.999) TERM = 0.0
      IF (JTIME .GE. 2) TERM=TERM + 2.*H*T/DT*(DELHAT - DELTA)

      B3R= V(J)*H*SQRTT + TERM

      TERM = 0.0
      IF ((JTIME.GE.2).OR.((IFLAG.EQ.1).AND.(JSTIME.GE.2)))
     1                                        TERM=-2.*HSQ*T/DT

      D3R= TERM
      B3P=0.0

      TERM = 0.0
      IF (JTIME .GE. 2) TERM=2.*H*T*CP(INI)/DT
      D3IL=H/2.*CP(INI) + TERM

      IF(IFLAG .EQ. 1) D3IL = 0.0
      A(1,INI)=A3R + B3R/2. + ZUFODR(INI)/2.0*CPFOR(5)
      D(1,INI)=A3R - B3R/2. - ZUFODR(INI)/2.0*CPBACK(5)
      B(1,INI)=-2.*A3R + D3R + ZUFODR(INI)/2.0*(CPFOR(5) - CPBACK(5))

      A(1,IPHI)=A3P + B3P/2. + ZUFODR(INI)*(CBARF(INI)+CBK(INI))
```

```
      D(1,IPHI)=A3P - B3P/2. + ZUFODR(INI)*(CBARB(INI)+CBK(INI))
      B(1,IPHI)=-2.*A3P-ZUFODR(INI)*(CBARF(INI)+CBARB(INI)+2.*CBK(INI))

      B(1,IL)=D3IL

      F3OLD=0.0

      IF ((JTIME.GE.2).OR.((IFLAG.EQ.1).AND.(JSTIME.GE.2)))
     1 F3OLD=ZUFODR(INI)*((CBARFO(INI)+CBK(INI))*CPFORO(5)
     1 -(CBARBO(INI)+CBK(INI))*CPBACKO(5))
     1     + VOLD(J)*H*SQRTOLD*CPOLD(INI) + CPPOLD(INI)*DIF(INI)/DIF(IR)

      TERM2 = 0.0
      TERM = 0.0

      IF (JTIME .GE. 2) TERM2= -2.*H*T*CP(INI)*(DELHAT - DELTA)/DT
      IF ((JTIME.GE.2).OR.((IFLAG.EQ.1).AND.(JSTIME.GE.2)))
     1                   TERM=2.*HSQ*T*(C(INI,J) - COLD(INI,J))/DT

      TERM = TERM + TERM2

      TERM1=0.0
      TERM3 = 0.0
C
      IF ((IFLAG. EQ. 1) .AND. (JSTIME .GE. 2))
     1                   TERM1= XI(J)*CPOLD(INI)
C
      IF (JTIME .GE. 2) TERM1=(XI(J) + DELTA)*CPOLD(INI)
      IF (T .GT. 0.999) TERM1 = 0.0
C
      IF (IFLAG.EQ.1) TERM3 = XI(J)*CP(INI)
C
      IF (IFLAG.EQ.2) TERM3 = (XI(J) + DELHAT)*CP(INI)
      IF (T .GT. 0.999) TERM3 = 0.0

      G(1)=-H/2.*(TERM3 + TERM1)
     1-ZUFODR(INI)*((CBARF(INI)+CBK(INI))*CPFOR(5) -
     1(CBARB(INI)+CBK(INI))*CPBACK(5))
     1  -H*V(J)*SQRTT*CP(INI) - CPP(INI)*DIF(INI)/DIF(IR)- F3OLD + TERM

C     MATERIAL BALANCE FOR NITRATE SPECIES, EQUATION 3

      A3R=DIF(INO3)/DIF(IR)
      A3P=0.0

      TERM = 0.0

C
      IF (IFLAG .EQ. 1) TERM =  H/2.*XI(J)
C
      IF (IFLAG .EQ. 2) TERM =  H/2.*(XI(J) + DELHAT)
```

```
      IF (T .GT. 0.999) TERM = 0.0
      IF (JTIME .GE. 2) TERM=TERM + 2.*H*T/DT*(DELHAT - DELTA)

      B3R= V(J)*H*SQRTT + TERM

      TERM = 0.0
      IF ((JTIME.GE.2).OR.((IFLAG.EQ.1).AND.(JSTIME.GE.2)))
     1                                              TERM=-2.*HSQ*T/DT

      D3R= TERM
      B3P=0.0

      TERM = 0.0
      IF (JTIME .GE. 2) TERM=2.*H*T*CP(INO3)/DT
      D3IL=H/2.*CP(INO3) + TERM

      IF(IFLAG .EQ. 1) D3IL = 0.0
      A(3,INO3)=A3R + B3R/2. + ZUFODR(INO3)/2.0*CPFOR(5)
      D(3,INO3)=A3R - B3R/2. - ZUFODR(INO3)/2.0*CPBACK(5)
      B(3,INO3)=-2.*A3R + D3R + ZUFODR(INO3)/2.0*(CPFOR(5) - CPBACK(5))

      A(3,IPHI)=A3P + B3P/2. + ZUFODR(INO3)*(CBARF(INO3)+CBK(INO3))
      D(3,IPHI)=A3P - B3P/2. + ZUFODR(INO3)*(CBARB(INO3)+CBK(INO3))
      B(3,IPHI)=-2.*A3P - ZUFODR(INO3)*
     1(CBARF(INO3) + CBARB(INO3)+ 2.*CBK(INO3))

      B(3,IL)=D3IL

      F3OLD=0.0

      IF ((JTIME.GE.2).OR.((IFLAG.EQ.1).AND.(JSTIME.GE.2)))
     1 F3OLD=ZUFODR(INO3)*((CBARFO(INO3)+CBK(INO3))*CPFORO(5) -
     1   (CBARBO(INO3)+CBK(INO3))*CPBACKO(5))
     1   + VOLD(J)*H*SQRTOLD*CPOLD(INO3) + CPPOLD(INO3)*DIF(INO3)/DIF(IR)

      TERM2 = 0.0
      TERM = 0.0

      IF (JTIME .GE. 2) TERM2= -2.*H*T*CP(INO3)*(DELHAT - DELTA)/DT
      IF ((JTIME.GE.2).OR.((IFLAG.EQ.1).AND.(JSTIME.GE.2)))
     1                    TERM=2.*HSQ*T*(C(INO3,J) - COLD(INO3,J))/DT

      TERM = TERM + TERM2

      TERM1=0.0
      TERM3 = 0.0
C
      IF ((IFLAG. EQ. 1) .AND. (JSTIME .GE. 2))
     1                    TERM1= XI(J)*CPOLD(INO3)
C
      IF (JTIME .GE. 2) TERM1=(XI(J) + DELTA)*CPOLD(INO3)
```

```
      IF (T .GT. 0.999) TERM1 = 0.0
C
      IF (IFLAG.EQ.1) TERM3 = XI(J)*CP(INO3)
C
      IF (IFLAG.EQ.2) TERM3 = (XI(J) + DELHAT)*CP(INO3)
      IF (T .GT. 0.999) TERM3 = 0.0

      G(3)=-H/2.*(TERM3 + TERM1)
     1 -ZUFODR(INO3)
     1 *((CBARF(INO3)+CBK(INO3))
     1 *CPFOR(5)-(CBARB(INO3)+CBK(INO3))*CPBACK(5))
     1 -H*V(J)*SQRTT*CP(INO3)-CPP(INO3)*DIF(INO3)/DIF(IR)- F3OLD + TERM

C     EQUATION 4; EQUILIBRIUM

   19 B(4,IH) = C(IOH,J)
      B(4,IOH) = C(IH,J)
      G(4) = -C(IH,J)*C(IOH,J) + EQCON

C     EQUATION 5; ELECTRONEUTRALITY

      SUM = 0.0

      DO 20  I = 1,IRSP
        B(5,I) = Z(I)
   20   SUM = SUM - Z(I)*(C(I,J)+CBK(I))

      G(5) = SUM

C     MAY WANT TO PRINT ERROR TERMS TO MONITOR CONVERGENCE

C     IF(MOD(J-1,10).EQ. 0)
C    1  PRINT 200,J,(G(I), I = 1,6)

      RETURN

C     COEFFICIENTS IN THE FILM

   21 IF (DT .EQ. 0.0) GO TO 26
      PP = CP(IPHI)
      PPOLD = CPOLD(IPHI)
      PPP = CPP(IPHI)
      PPPOLD = CPPOLD(IPHI)

C    - THIS IS SUMMATION MATERIAL EQUATION #1 IF THE CHARGE
C      CONSERVATION EQUATION IS PROGRAMMED EXPLICITLY (LOOPEND=1).
C      THESE ARE EQUATIONS 1 AND 2; THE SUMMATION MATERIAL BALANCES
C      IF THE CHARGE TRANSFER EQUATION IS NOT EXPLICITLY SPECIFIED.

      GO TO 503
      DO 22  K = 1,LOOPEND
```

```
      I = K + 1
      AKPHI=0.0
      AK1=DIF(1)/DIF(IR)
      AKI=DIF(I)/DIF(IR)

      BKPHI=0.0
      BK1= ETA(J)*HETA/DT*(T*DELHAT**2 - TOLD*DELTA**2)
      BKI= ETA(J)*HETA/DT*(T*DELHAT**2 - TOLD*DELTA**2)

      DK1= -2.*HETA**2*T*DELHAT**2/DT
      DKI= -2.*HETA**2*T*DELHAT**2/DT
      DKIL=2.*ETA(J)*HETA/DT*T*DELHAT*(CP(1) + CP(I))
     1   -4.*HETA**2/DT*T*DELHAT*(C(1,J)-COLD(1,J)+C(I,J)-COLD(I,J))
      GK=-(ZUFODR(1)*(CBARFO(1)*CPFORO(5) - CBARBO(1)*CPBACKO(5))
     1      +ZUFODR(I)*(CBARFO(I)*CPFORO(5) - CBARBO(I)*CPBACKO(5))
     1     +(DIF(1)*CPPOLD(1)+DIF(I)*CPPOLD(I))/DIF(IR))
     1     -ZUFODR(1)*(CBARF(1)*CPFOR(5) - CBARB(1)*CPBACK(5))
     1     -ZUFODR(I)*(CBARF(I)*CPFOR(5) - CBARB(I)*CPBACK(5))
     1     -(DIF(1)*CPP(1) + DIF(I)*CPP(I))/DIF(IR)
     1     -ETA(J)*HETA/DT*(T*DELHAT**2 - TOLD*DELTA**2)*(CP(1) + CP(I))
     1     +2.*HETA**2/DT*T*DELHAT**2
     1                  *(C(1,J) - COLD(1,J) + C(I,J) - COLD(I,J))

      A(K,IPHI)=AKPHI+BKPHI/2.0+ZUFODR(1)*CBARF(1)+ZUFODR(I)*CBARF(I)
      D(K,IPHI)=AKPHI-BKPHI/2.0+ZUFODR(1)*CBARB(1)+ZUFODR(I)*CBARB(I)
      B(K,IPHI) = -2.*AKPHI - ZUFODR(1)*(CBARF(1) + CBARB(1))
     1                  - ZUFODR(I)*(CBARF(I) + CBARB(I))
      A(K,1) = AK1 + BK1/2.0 + ZUFODR(1)/2.0*CPFOR(5)
      D(K,1) = AK1 - BK1/2.0 - ZUFODR(1)/2.0*CPBACK(5)
      A(K,I) = AKI + BKI/2.0 + ZUFODR(I)/2.0*CPFOR(5)
      D(K,I) = AKI - BKI/2.0 - ZUFODR(I)/2.0*CPBACK(5)
      B(K,1) = -2.*AK1 + DK1 + ZUFODR(1)/2.0*(CPFOR(5) - CPBACK(5))
      B(K,I) = -2.*AKI + DKI + ZUFODR(I)/2.0*(CPFOR(5) - CPBACK(5))
      B(K,IL) = DKIL
      G(K) = GK
   22 CONTINUE
  503 CONTINUE
C     PROGRAM CHARGE CONSERVATION ONLY WHEN LOOPEND=1 AND J .NE. NJM1

      IF (LOOPEND .EQ. 2) GO TO 25
      IF (J .EQ. NJM1) GO TO 25

C     PROGRAM IN THE CURRENT EQUATION EXPLICITLY EQUATION 2

      SUM1 = 0.0
      SUM2 = 0.0
      SUM3 = 0.0
      SUM4 = 0.0

      DO 23 I = 1,IRSP
        SUM1 = SUM1 + Z(I)**2*U(I)*(CBARF(I)+CBK(I))
```

```
      SUM2 = SUM2 + Z(I)*DIF(I)*CPFOR(I)
      SUM3 = SUM3 + Z(I)**2*U(I)*(CBARB(I)+CBK(I))
23    SUM4 = SUM4 + Z(I)*DIF(I)*CPBACK(I)

   RIJF = -F**2*CPFOR(IPHI)*SUM1 - F*SUM2
   RIJB = -F**2*CPBACK(IPHI)*SUM3 - F*SUM4

   A(2,IPHI) = -F**2*SUM1
   D(2,IPHI) = -F**2*SUM3
   B(2,IPHI) = -A(2,IPHI) - D(2,IPHI)

   DO 24  I = 1,IRSP
     TERM1 = F**2*CPFOR(IPHI)*Z(I)**2*U(I)/2.0
     TERM2 = F*Z(I)*DIF(I)
     TERM3 = F**2*CPBACK(IPHI)*Z(I)**2*U(I)/2.0

     A(2,I) = -TERM1 - TERM2
     D(2,I) =  TERM3 - TERM2
24   B(2,I) = -TERM1 + TERM3 + 2.0*TERM2

   G(2) = -RIJF + RIJB

C      EQUATION 3; MATERIAL BALANCE FOR NITRATE

25 A3PHI=0.0
   A3IR=DIF(INO3)/DIF(IR)
   B3IR= ETA(J)*HETA/DT*(T*DELHAT**2 - TOLD*DELTA**2)
   B3PHI=0.0
   D3IR= -2.*HETA**2/DT*T*DELHAT**2
   D3IL=2.*ETA(J)*HETA/DT*T*DELHAT*CP(INO3)
 1    -4.*HETA**2/DT*T*DELHAT*(C(INO3,J)-COLD(INO3,J))
   G3=-(ZUFODR(INO3)*((CBARFO(INO3)+CBK(INO3))*CPFORO(5) -
 1  (CBARBO(INO3)+CBK(INO3))*
 1  CPBACKO(5))+CPPOLD(INO3)*DIF(INO3)/DIF(IR))
 1  -ZUFODR(INO3)*((CBARF(INO3)+CBK(INO3))*CPFOR(5) -
 1   (CBARB(INO3)+CBK(INO3))*CPBACK(5)) -
 1CPP(INO3)*A3IR-ETA(J)*HETA/DT*(T*DELHAT**2-TOLD*DELTA**2)*CP(INO3)
 1  +2.*HETA**2/DT*T*DELHAT**2*(C(INO3,J)-COLD(INO3,J))

   A(3,IPHI) = A3PHI+B3PHI/2.0+ZUFODR(INO3)*(CBARF(INO3)+CBK(INO3))
   D(3,IPHI) = A3PHI-B3PHI/2.0+ZUFODR(INO3)*(CBARB(INO3)+CBK(INO3))
   B(3,IPHI) = -2.*A3PHI - ZUFODR(INO3)*
 1(CBARF(INO3) + CBARB(INO3) + 2.*CBK(INO3))
   A(3,INO3) = A3IR + B3IR/2.0 + ZUFODR(INO3)/2.0*CPFOR(5)
   D(3,INO3) = A3IR - B3IR/2.0 - ZUFODR(INO3)/2.0*CPBACK(5)
   B(3,INO3)=-2.*A3IR+D3IR+ZUFODR(INO3)/2.0*(CPFOR(5) - CPBACK(5))
   B(3,IL) = D3IL
   G(3) = G3


C      MATERIAL BALANCE FOR NICKEL SPECIES EQUATION 1
```

```
      A3PHI=0.0
      A3IR=DIF(INI)/DIF(IR)
      B3IR= ETA(J)*HETA/DT*(T*DELHAT**2 - TOLD*DELTA**2)
      B3PHI=0.0
      D3IR= -2.*HETA**2/DT*T*DELHAT**2
      D3IL=2.*ETA(J)*HETA/DT*T*DELHAT*CP(INI)
     1    -4.*HETA**2/DT*T*DELHAT*(C(INI,J)-COLD(INI,J))
      G3=-(ZUFODR(INI)*((CBARFO(INI)+CBK(INI))*CPFORO(5)
     1 - (CBARBO(INI)+CBK(INI))*CPBACKO(5))
     1 +CPPOLD(INI)*A3IR)
     1 -ZUFODR(INI)*((CBARF(INI)+CBK(INI))*CPFOR(5) -
     1  (CBARB(INI)+CBK(INI))*CPBACK(5)) -
     1 CPP(INI)*A3IR-ETA(J)*HETA/DT*(T*DELHAT**2-TOLD*DELTA**2)*CP(INI)
     1 +2.*HETA**2/DT*T*DELHAT**2*(C(INI,J)-COLD(INI,J))

      A(1,IPHI)=A3PHI+B3PHI/2.0 +ZUFODR(INI)*(CBARF(INI)+CBK(INI))
      D(1,IPHI)=A3PHI-B3PHI/2.0 +ZUFODR(INI)*(CBARB(INI)+CBK(INI))
      B(1,IPHI)=-2.*A3PHI
     1-ZUFODR(INI)*(CBARF(INI)+CBARB(INI)+2.*CBK(INI))
      A(1,INI) = A3IR + B3IR/2.0 + ZUFODR(INI)/2.0*CPFOR(5)
      D(1,INI) = A3IR - B3IR/2.0 - ZUFODR(INI)/2.0*CPBACK(5)
      B(1,INI) = -2.*A3IR+D3IR +ZUFODR(INI)/2.0*(CPFOR(5) - CPBACK(5))
      B(1,IL) = D3IL
      G(1) = G3

      GO TO 19

C     COEFICIENTS FOR THE CONSTANT CONCENTRATION EQUATIONS IN THE
C     FILM FOR THE ZERO TIME SOLUTION

   26 B(1,INI) = 1.0
      A(1,INI) = -1.0
      B(2,INO3) = 1.0
      A(2,INO3) = -1.0
C     IF(JCOUNT.EQ.1) CINO3 = C(INO3,J)
C     B(2,INO3) = 1.0
C     G(2) = CINO3 - C(INO3,J)
      B(3,IPHI) = 1.0
      A(3,IPHI) = -1.0

      GO TO 19

      END

CCCCCCCCCCCCCCCCCCCCCCCCCCCCCCCCCCCCCCCCCCCCCCCCCCCCCCCCCCCCCCCCCCCCCCCCCC

      SUBROUTINE COEFNJD
      COMMON /B1/A,B,D
     1 /B2/C
     1 /B3/COLD
     1 /B4/G
```

```
      1 /B6/CIN,DIF,V,S,Z,U,ZUFODR,CBK
      1 /B7/CSAT,DELTA,RHOF,DT,EQCON,EPO,F,H,HF,N,IFLAG,
      1      IPASS,IHSO4,IH,ISO4,IR,IPHI,IL,JSTIME,JFTIME,JCOUNT,THTIME,
      1      TSTAR,NJ,NJM1,NPRINT,QLF,NJD,NJDP1,NJDM1,HETA,JTIME
      1 /B20/DELHAT
      1 /B24/T,SQRTT,TOLD,SQRTOLD
      1 /B27/XMIGF,DF,XMIGS,DS,XNF
      1 /B32/J
       DIMENSION A(6,6),B(6,6),D(6,13),C(6,202),COLD(6,202),G(6),U(6),
      1 DIF(6),Z(6),S(6),CIN(6),V(202),ZUFODR(6),
      1 XMIGF(4),DF(4),XMIGS(4),XNF(4),DS(4),CBK(4)

  200 FORMAT(1X,I3,1X,6(1X,E12.6))

C         PROGRAM IN FLUX CONDITIONS AT THE FILM-SOLUTION INTERFACE

C         INTITIALIZE A,B,D, AND G
          IOH = 3
          INI=1
          IH=4
          INO3=2
          IRSP = 4

      DO 10  I = 1,N
        G(I) = 0.0
          DO 10  K = 1,N
                A(I,K) = 0.0
                B(I,K) = 0.0
   10           D(I,K) = 0.0

C         ESTABLISH VARIABLES FOR THE DIFFUSION AND MIGRATION
C         COMPONENTS OF THE FLUXES IN BOTH SOLUTION AND
C         FILM PHASES.
C         ALSO CALCULATE THE NET FLUX OF EACH SPECIES ARRIVING
C         AT THE INTERFACE.


      DO 11  I = 1,IRSP
        XMIGF(I)=-EPSILN(DELHAT)*H*ZUFODR(I)*(CBARB(I)+CBK(I))*CPBACK(5)
        DF(I) = -EPSILN(DELHAT)*H*DIF(I)/DIF(IR)*CPBACK(I)
        XMIGS(I) = -HETA*DELHAT*ZUFODR(I)*(CBARF(I)+CBK(I))*CPFOR(5)
        DS(I) = -HETA*DELHAT*DIF(I)/DIF(IR)*CPFOR(I)
   11   XNF(I) = XMIGF(I) + DF(I) - XMIGS(I) - DS(I)

C         RELATIONSHIP #1; 2*NET FLUX(NI++) =-NET FLUX(H+)+NET FLUX(OH-)

      A(1,IPHI) = DELHAT*HETA*(2.*ZUFODR(INI)*(CBARF(INI)+CBK(INI))
      1   - ZUFODR(IOH)*CBARF(IOH) + ZUFODR(IH)*CBARF(IH))
       D(1,IPHI) = EPSILN(DELHAT)*H*(2.*ZUFODR(INI)*(CBARB(INI)+CBK(INI))
      1   - ZUFODR(IOH)*CBARB(IOH) + ZUFODR(IH)*CBARB(IH))
       B(1,IPHI)= EPSILN(DELHAT)*H*(-2.*ZUFODR(INI)*(CBARB(INI)+CBK(INI))
```

```
1  + ZUFODR(IOH)*CBARB(IOH) - ZUFODR(IH)*CBARB(IH))
1        + DELHAT*HETA*(-2.*ZUFODR(INI)*(CBARF(INI)+CBK(INI))
1  + ZUFODR(IOH)*CBARF(IOH) - ZUFODR(IH)*CBARF(IH))

 A(1,INI)=
1DELHAT*HETA*2.*(ZUFODR(INI)*CPFOR(5)/2.+DIF(INI)/DIF(IR))
 A(1,IOH) = -DELHAT*HETA*(ZUFODR(IOH)*CPFOR(5)/2.+DIF(IOH)/DIF(IR))
 A(1,IH) = DELHAT*HETA*(ZUFODR(IH)*CPFOR(5)/2.0 + DIF(IH)/DIF(IR))

 D(1,INI)=
1-EPSILN(DELHAT)*H*2.*(ZUFODR(INI)*CPBACK(5)/2.0-DIF(INI)/DIF(IR))
 D(1,IOH) = +EPSILN(DELHAT)*H*(ZUFODR(IOH)*CPBACK(5)/2.0
1  - DIF(IOH)/DIF(IR))
 D(1,IH) = -EPSILN(DELHAT)*H*(ZUFODR(IH)*CPBACK(5)/2.0
1  - DIF(IH)/DIF(IR))

 B(1,INI) = 2.*ZUFODR(INI)*(-EPSILN(DELHAT)*H*CPBACK(5)
1  + DELHAT*HETA*CPFOR(5))/2.
1  - (DELHAT*HETA + EPSILN(DELHAT)*H)*2.*DIF(INI)/DIF(IR)
 B(1,IOH) = ZUFODR(IOH)*(+EPSILN(DELHAT)*H*CPBACK(5)
1  - DELHAT*HETA*CPFOR(5))/2.
1          + (DELHAT*HETA + EPSILN(DELHAT)*H)*DIF(IOH)/DIF(IR)
 B(1,IH) = ZUFODR(IH)*(-EPSILN(DELHAT)*H*CPBACK(5)
1  + DELHAT*HETA*CPFOR(5))/2.
1          - (DELHAT*HETA + EPSILN(DELHAT)*H)*DIF(IH)/DIF(IR)

 B(1,IL) = ((2.*DIF(INI)*CPFOR(INI) - DIF(IOH)*CPFOR(IOH)
1   +DIF(IH)*CPFOR(IH))/
1   DIF(IR)+CPFOR(5)*(2.*ZUFODR(INI)*(CBARF(INI)+CBK(INI))
1   - ZUFODR(IOH)*CBARF(IOH) + ZUFODR(IH)*CBARF(IH)))*HETA
1   -H*DEPDDEL(DELHAT)*(CPBACK(IPHI)*
1   (2.*ZUFODR(INI)
1   *(CBARF(INI)+CBK(INI))
1   -ZUFODR(IOH)*CBARF(IOH)+ZUFODR(IH)*CBARF(IH))
1   +(2.*DIF(INI)*CPBACK(INI)-DIF(IOH)*CPBACK(IOH)+DIF(IH)*
1   CPBACK(IH))/DIF(IR))

 G(1) =-2.*XNF(INI) + XNF(IOH) - XNF(IH)

C     RELATIONSHIP #2; CURRENT DENSITY IS CONTINUOUS ACROSS THE
C     INTERFACE

 SUM1 = 0.0
 SUM2 = 0.0
 SUM3 = 0.0
 SUM4 = 0.0

 PARAM = EPSILN(DELHAT)*H/HETA

 DO 12  I = 1,IRSP
   SUM1 = SUM1 + Z(I)**2*U(I)*(CBARF(I)+CBK(I))
```

```
      SUM2 = SUM2 + Z(I)*DIF(I)*CPFOR(I)
      SUM3 = SUM3 + Z(I)**2*U(I)*(CBARB(I)+CBK(I))
12    SUM4 = SUM4 + Z(I)*DIF(I)*CPBACK(I)

   RIJF = -F**2*CPFOR(IPHI)*SUM1 - F*SUM2
   RIJB = -F**2*CPBACK(IPHI)*SUM3 - F*SUM4

   A(2,IPHI) = -F**2*SUM1
   D(2,IPHI) = -F**2*SUM3*PARAM/DELHAT
   B(2,IPHI) = -A(2,IPHI) - D(2,IPHI)

   DO 13  I = 1,IRSP
     TERM1 = F**2*CPFOR(IPHI)*Z(I)**2*U(I)/2.0
     TERM2 = F*Z(I)*DIF(I)
     TERM3 = F**2*CPBACK(IPHI)*Z(I)**2*U(I)/2.0*PARAM/DELHAT
     TERM4 = F*Z(I)*DIF(I)*PARAM/DELHAT


   A(2,I) = -TERM1 - TERM2
   D(2,I) =  TERM3 - TERM4
13 B(2,I) = -TERM1 + TERM3 + TERM2 + TERM4

   B(2,IL) = RIJB*H/HETA*(EPSILN(DELHAT)/DELHAT**2
  1 - DEPDDEL(DELHAT)/DELHAT)

   G(2) = -RIJF + RIJB*PARAM/DELHAT

C     RELATIONSHIP #3; C(OH-) = CSAT

   B(3,IOH) = 1.0
   G(3) = CSAT - C(IOH,NJD)

C     RELATIONSHIP #4; EQUILIBRIUM

   B(4,IH) = C(IOH,J)
   B(4,IOH) = C(IH,J)
   G(4) = -C(IH,J)*C(IOH,J) + EQCON

C     RELATIONSHIP #5; ELECTRONEUTRALITY

   SUM = 0.0

   DO 14  I = 1,IRSP
     B(5,I) = Z(I)
14   SUM = SUM - Z(I)*(C(I,J)+CBK(I))

   G(5) = SUM

C     RELATIONSHIP #6; C(IL,NJD) = NET FLUX(NI++)*DT/(1-EPSILN)/RHOF

   A(6,IPHI) = DELHAT
```

```
     1*HETA*ZUFODR(INI)*DIF(IR)/DIF(INI)*(CBARF(INI) +CBK(INI))
      D(6,IPHI)=EPSILN(DELHAT)
     1*H*ZUFODR(INI)*DIF(IR)/DIF(INI)*(CBARB(INI)+CBK(INI))
      B(6,IPHI)=-ZUFODR(INI)*DIF(IR)/DIF(INI)*(EPSILN(DELHAT)*H
     1 *(CBARB(INI)+CBK(INI)) + DELHAT*HETA*(CBARF(INI)+CBK(INI)))

      A(6,INI)=
     1DELHAT*HETA*(ZUFODR(INI)*DIF(IR)/DIF(INI)*CPFOR(5)/2.0+1.)
      D(6,INI) =
     1-EPSILN(DELHAT)*H*(ZUFODR(INI)*DIF(IR)/DIF(INI)*CPBACK(5)/2.-1.)
      B(6,INI) =
     1 ZUFODR(INI)*DIF(IR)/DIF(INI)/2.*(-EPSILN(DELHAT)*H*CPBACK(5)
     1    +DELHAT*HETA*CPFOR(5))
     1           - (DELHAT*HETA + EPSILN(DELHAT)*H)

C     USE SPECIAL FORMULATION AT ZERO TIME

      IF (DT .EQ. 0.0) GO TO 15

      B(6,IL)=(CPFOR(INI)
     1+ZUFODR(INI)*DIF(IR)/DIF(INI)*(CBARF(INI)+CBK(INI))*CPFOR(5))*HETA
     1    -H*DEPDDEL(DELHAT)
     1    *(ZUFODR(INI)*DIF(IR)/DIF(INI)*
     1    (CBARB(INI)+CBK(INI))*CPBACK(5) + CPBACK(INI))
     1    -H*RHOF*HETA*((1.0 - EPSILN(DELHAT))*(T*DELHAT/DT + DELHAT)
     1    -DEPDDEL(DELHAT)*(T/2.*(DELHAT**2 - DELTA**2)/DT
     1    + DELHAT**2/2.))


      TERM= HETA*H*(1.0 - EPSILN(DELHAT))*RHOF
     1   *(T/2.*(DELHAT**2 - DELTA**2)/DT + DELHAT**2/2.)

      GO TO 16

   15 GAMMA = H*HETA*RHOF*(1.- EPSILN(DELHAT))/2.0
      TERM=GAMMA*DELHAT**2

      B(6,IL) = (CPFOR(INI)
     1    +ZUFODR(INI)*
     1    DIF(IR)/DIF(INI)*(CBARF(INI)+CBK(INI))*CPFOR(5))*HETA
     1    -H*DEPDDEL(DELHAT)
     1    *(ZUFODR(INI)*DIF(IR)/DIF(INI)
     1    *(CBARB(INI)+CBK(INI))*CPBACK(5) + CPBACK(INI))
     1    -H*HETA*RHOF*((1. - EPSILN(DELHAT))*DELHAT
     1    -DEPDDEL(DELHAT)*DELHAT**2/2.)

   16 G(6) = -XNF(INI)*DIF(IR)/DIF(INI) + TERM

      IF(MOD(J-1,10).EQ. 0) PRINT 200,J,(G(I), I = 1,N)
C     IF(JFTIME .EQ. 31) PRINT 200,J,(G(I), I = 1,N)
```

```
      RETURN
      END

CCCCCCCCCCCCCCCCCCCCCCCCCCCCCCCCCCCCCCCCCCCCCCCCCCCCCCCCCCCCCCCCCCCCCCCCCC

      SUBROUTINE CPRINT
      COMMON  /B2/C
     1 /B6/CIN,DIF,V,S,Z,U,ZUFODR,CBK
     1 /B7/CSAT,DELTA,RHOF,DT,EQCON,EPO,F,H,HF,N,IFLAG,
     1     IPASS,IHSO4,IH,ISO4,IR,IPHI,IL,JSTIME,JFTIME,JCOUNT,THTIME,
     1     TSTAR,NJ,NJM1,NPRINT,QLF,NJD,NJDP1,NJDM1,HETA,JTIME
     1 /B19/XX,XXLONG,CLONG,XXMAX,NLONG
     1 /B24/T,SQRTT,TOLD,SQRTOLD
     1 /B25/XI,ETA
      DIMENSION
     1  C(6,202),XI(202),XX(202),XXLONG(202),CLONG(6,202),ETA(202),
     1  DIF(6),Z(6),S(6),CIN(6),V(202),ZUFODR(6),THICK(202),HOLDX(202),
     1  HOLDC(6,202),U(6),CBK(4)

C       PRINTS OUT VALUES OF THE CONCENTRATIONS

      CP(I,J) = (C(I,J-1) - C(I,J+1))/2.0
      CPP(I,J) = C(I,J-1) -2.0*C(I,J) + C(I,J+1)

  200 FORMAT(1X/1X,*JCOUNT =*,I3,5X,*IFLAG =*,I3,5X,
     1    *IPASS =*,I3,* JTIME=*,I4/1H ,*TSTAR =*,E10.4,5X,*THTIME = *,
     1 .  E10.4,5X,*JSTIME =*,I3,5X,*JFTIME= *,I3,4X,*DT=*,E10.4,4X,*N=*,
     1    I2,4X,*NM1=*,I2,* T=*,E12.6)
  201 FORMAT (1H ,1X,*J*,10X,*NI++(J)*,7X,*NO3-(J)*,8X,*OH-(J)*,14X,
     1    *H+(J)*,8X,*PHI(J)*,6X,*XI*,9X,*XX*)
  204 FORMAT (1H ,1X,*J*,10X,*NI++(J)*,7X,*NO3-(J)*,8X,*OH-(J)*,14X,
     1    *H+(J)*,8X,*PHI(J)*,6X,*ETA*,2X,*(DELTA)(SQRTT)*)
  202 FORMAT (1H ,I3,1X,E16.10,1X,E16.10,1X,E16.10,1X,E16.10,1X,E10.4
     1    ,1X,E10.4,1X,E10.4)
  203 FORMAT (1X,*DELTA=*,E12.6,*FILM THICKNESS*,E20.14,* C6=*,
     1  E14.8)

      NM1 = N - 1
      PRINT 200, JCOUNT,IFLAG,IPASS,JTIME,TSTAR,THTIME,JSTIME,JFTIME,
     1 DT,N,NM1,T

      IF (NLONG .NE. 1) GO TO 11

C       IF NLONG = 1 PRINT OUT THE LONG PROFILES

      DO 10  K = 1,NJD
        HOLDX(K) = XX(K)
        XX(K) = XXLONG(K)
        DO 10 I = 1,N
          HOLDC(I,K) = C(I,K)
   10     C(I,K) = CLONG(I,K)
```

```
C         ESTABLISH VALUES OF XI AND XX FOR BOTH THE FILM AND THE
C         SOLUTION PHASES

   11 DO 13  J = 1,NJ
         IF ((IFLAG .EQ. 2) .AND. (J .GE. NJD)) GO TO 12
         THICK(J) = 0.0
         GO TO 13
   12    THICK(J) = ETA(J)*DELTA*SQRTT
   13 CONTINUE

      PRINT 201
         PRINT 202,((J,(C(I,J), I = 1,5),XI(J),XX(J)),
     1                          J = 1,NJD,NPRINT)
         PRINT 202,((J,(C(I,J), I = 1,5),XI(J),XX(J)),
     1                          J =81,NJD,1)
      IF (IFLAG.EQ.2) PRINT 204
      IF (IFLAG.EQ.2) PRINT 202,((J,(C(I,J), I = 1,5),ETA(J),THICK(J)),
     1                       J = NJD,NJ,NPRINT)
      IF(IFLAG.EQ.2) PRINT 203, DELTA,THICK(NJD),C(IL,10)
      IF (NLONG .NE. 1) RETURN

      DO 14  K = 1,NJD
        XX(K) = HOLDX(K)
          DO 14  I = 1,N
   14        C(I,K) = HOLDC(I,K)

      RETURN
      END

CCCCCCCCCCCCCCCCCCCCCCCCCCCCCCCCCCCCCCCCCCCCCCCCCCCCCCCCCCCCCCCCCCCCCCCC

      SUBROUTINE UPDATE
      COMMON  /B2/C /B3/COLD
     1 /B7/CSAT,DELTA,RHOF,DT,EQCON,EPO,F,H,HF,N,IFLAG,
     1      IPASS,IHSO4,IH,ISO4,IR,IPHI,IL,JSTIME,JFTIME,JCOUNT,THTIME,
     1      TSTAR,NJ,NJM1,NPRINT,QLF,NJD,NJDP1,NJDM1,HETA,JTIME
     1 /B31/DELC
      DIMENSION   C(6,202),COLD(6,202),DELC(6,202)

C     UPDATE SETS COLD = C AFTER A CONVERGED SOLUTION IS FOUND
C     DELC IS USED FOR INTERPOLATION PURPOSES

      DO 10  I = 1,N
         DO 10  J = 1,NJ
            DELC(I,J) = C(I,J) - COLD(I,J)
   10       COLD(I,J) = C(I,J)

      HF = DELTA*HETA
      RETURN
      END
```